Cave Art as Installation Art: Analysis of the Human-Art-Wall Triad in Three Cantabrian Caves, and Embedded Interactivity in the Image-Making and Image-Viewing process.

SAKAMOTO, TAKASHI

Takashi Sakamoto

Cave Art as Installation Art: Analysis of the Human-Art-Wall Triad in Three Cantabrian Caves, and Embedded Interactivity in the Image-Making and Image-Viewing process.

Abstract

Why were caves selected as places for art in the Palaeolithic? The question has not yet been explained. Previously, I attempted to answer it in part by examining cave art from the perspective of *installation art* whose aim is to provide us with different multisensory experiences to those of quotidian life. As a result, this theory of contemporary art led to a theory, *cave art as installation art*, which denotes an interactive nature between humans and a cave's physical environment. In this thesis I develop this theory through the provision of concrete observations obtained from fieldwork in decorated caves. I investigate 54 images from three caves (Covalanas, El Pendo, El Castillo) in Cantabria, Spain, focusing on the interactivities of cave art during the production and post-production (viewing) phases. The environmental factor concerned is the condition of the cave's wall, with which humans were able to interact creatively. The data collected comprises three categories, each of which testifies to a different type of interactivity: integration of natural lines with art; topographic conditions of the art area; and distortion of images due to its background topography. These categories reflect how the wall's features are incorporated into images, and how those features generated further interactivity in the post-production phase. As I am primarily concerned with the physical condition of the cave wall, I adopted digital photogrammetry to reconstruct 3D models of the 54 analysed images, which enabled me to analyse their topographic information in detail. The data were subsequently sorted statistically in terms of the three data categories. Consequently, the study suggests that Palaeolithic artists intentionally used walls' specific conditions to enhance the processes of image-making and image-viewing. A mutual relationship between an actor and an artistic medium inevitably redraws our concept of cave art to an interconnection between environment, art, and human.

Cave Art as Installation Art: Analysis of the Human-Art-Wall Triad in Three Cantabrian Caves, and Embedded Interactivity in the Image-Making and Image-Viewing process.

Takashi Sakamoto

PhD Thesis

Archaeology Department

Durham University

2019

Contents

Acknowledgement

I would like to express my sincere appreciation to Professor Paul Pettitt and Professor Mark White, my research supervisors, for their enthusiastic encouragement and useful advice on my research. I also would like to thank Dr Roberto Ontañón (IIPC: Instituto Internacional de Investigaciones Prehistóricas de Cantabria) for kindly providing me with access to sites of cave art. My grateful thanks are also extended to Dr Andy Needham (York University) for his assistance to acquire the skill of 3D modelling. Moreover, I wish to thank my colleagues for their intellectual support to my research: Stephany Leluschko, Lisa-Elen Meyering, Aaron Rawlinson, Blanca Ochoa, Izzy Wisher, and Barbara Oosterwijk. Also, I must thank my friends, especially Hiroya Akaike, who provided me with a hint for the idea of cave-installation art. Finally, my family has to be received my very great gratitude for their priceless assist. Thank you so much, my father, mother, sister, brother. Finally, I would like to send my best thankfulness to Gessica Martini, my fiancé, for her spiritual support during the last five years of PhD project.

List of Tables

List of Figures

Figure 2.6a-c: Examples of shadow-light interaction. 2.6a (top left) is an image of bison in the Salon Noir at Niaux, France. The topography of the wall forms its dorsal line, and the shadow recreates the volume of bison. It is imaginable that the image would be harder to be seen once the shadow vanishes by changing a position of the light. 2.6b (top right) is an image of an ibex with two heads from Pair-non-Pair cave, Dordogne, France. As the position of the light is changed, the ibex seems to shift gradually from a head-down to head-up position. 2.6c (bottom left) illustrates the movement of a horse: five superimposed horses in different postures in La Marche cave, Dordogne, France. The fluid motion of which increases under the moving light. (2.6a: after Lewis-Williams 2002: Figure 17 and 18, 2.6b: after Wachtel 1993: Figure 6, 2.6c: after Azema and Rivere 2012: Figure 3).

Figure 2.7: Single static viewpoint in Spanish Levantine art and plural viewpoints in Upper Palaeolithic cave art. Due to the existence of multiple horizontal axes in this single panel of the cave art, viewers are required to change their viewing position (after Boado and Romero 1993: Figure 4).

Figure 2.8ab: An example of anamorphic image and the mechanism. 8a shows a red cow with a black head in Lascaux cave, Dordogne, France. The red cow is depicted on a complex shaped high wall, but the image keeps perfect proportion and appears realistic when it is looked up to from a lower position (above). However, once the picture is viewed from the same height, the proportion is disturbed (bottom). 8b illustrates the optical mechanism of anamorphosis in cave art. Although an actual image in distortion is depicted on the cave surface A-B, the anamorphic image with proper form is seen on the imaginary surface of A-B. Therefore, images will appear to float over the surrounding topography of the wall.

Figure 2.9: Six parts of animal contour (Head, Dorsal, Tail, Buttock, Limbs, and Ventral). Use of natural lines for outlining images (integration) is a well-known artistic method in Palaeolithic parietal art. The number of integration is counted by body section in this analysis.

Figure 2.10: The list of natural lines. Narrow, long depressions running on the cave's surface are assessed as Groove (1), and peak lines of sharply elevated surface are defined as Ridge (2). Edges of rocks or cracks which generate an acute elevational gap against their surrounding regions are treated as Edge (3-4); lines formed along blunt concave or convex features are also classified as Edge (5). In the cases where the boundary of different the medium's surficial conditions (e.g. smooth and porous surface) appears as a line, I classified them as Border (6: Normals filter is applied because this type is less distinctive than the others). Valley lines are formed between two adjacent convexities (7).

Figure 2.11ab: Sections of the animal body. Images are firstly divided into seven body parts (Head, Neck-shoulder, Mid torso, Thigh, Tail, and Frontal and Back leg: see 2.10a), and then Neck-shoulder, Mid torso, Thigh are further divided by Dorsal, central and Ventral area (2.10b). Thus, each image contains 13 body parts.

Figure 2.12: These five images illustrate how the cross-sectional layer passes a model (seen vertically). By inputting parameters, the cross-sectional layer (the grey layer in the figures) gradually proceeds towards a model (1-2). Accordingly, the 3D model starts passing through the layer from its highest area in elevation (2-3) and its lowest at the end (4-5).

Figure 2.13: Images illustrating different elevation levels. By horizontally applying a cross-section layer to a 3D model in Photoshop, the difference in elevation level by region is objectively documentable. Since body parts which passed the layer change their colour into bright, areas of bright colour denote higher elevation than that remains dark.

Figure 2.14: I selected horizontal edges (a-b) and vertical edges (c-d) in each model and set models in the position where each combination of edges pass the layer simultaneously. In doing so, the baseline can be set accurately horizontally with the model.

Figure 2.15a-d: The mechanism of how topography distorts the appearance of an image. As convex surface hides concave area when a picture is viewed from either side, an unseen area is generated (grey zone in 15b and 15c). Because the visible surface (red line in above three figures) changes, images appear significantly different. Meanwhile, even if one views images on a flat surface from different viewpoints, the viewer only perceives a slight distortion caused by the perspective (15d).

Figure 2.16: Sections of the animal body. Images are divided into six body parts (Head, Neck-shoulder, Mid torso, Thigh, Tail, and limbs). The number of distortion is counted by body section in this analysis.

Figure 2.17: An example of rotating a 3D model. Angles are inputted along y-axis so that models rotate horizontally. The rotation simulates how images are distorted by topography while a viewer moves side to side of them. Still images are recorded from different angles as shown in the above figures, and those stills are gathered and combined along a timeline to be an animation. Based on the animation data, this study observed and described the process of constant distortion in detail.

Figure 2.18: a 3D model seen from the front (A), seen from the left (B), and a 2D model seen from the left (C). I assessed a deformation when the outline of body parts is apparently deformed (twisted, bent, contracted: A-B). I also compared the difference in appearance between an image on 3D and 2D surface (B-C) to isolate the distortions caused by topographic intervention from those simply by principle of perspective.

Figure3.1: A plan of Covalanas cave. Although there are two galleries, the straight passage is the subject of this case study (after Romanillo et al. 1990: Figure 2).

Figure 3.2: The detailed plan of the area where examined 18 images are found. Each of all images is given a unique code (after Romanillo et al. 1990: Figure 3).

Figure 3.3: Seven reconstructed models and the number of photographic images used for the reconstruction. In total, 18 images are located in these panels. Blue squares on the panel represent the camera position of each photograph.

Figure 3.4: A1, outline red deer facing left.

Figure 3.5: The integrated part of A1. Images are highlighted by digital filter: Hue/Saturation (left), Normals (right). The outline of the belly is drawn along a borderline separating the smooth surface from the porous surface.

Figure 3.6: A1 (1/100 scale) seen from the vertical position. As the whole image forms a concave shape like a bowl, the elevation at both ends is high, while it is the lowest at the mid-torso.

Figure 3.7: These images illustrate the depth of A1. When the cross-section layer passes the surface of A1, the colour of the surface changes; dark regions denote lower elevation than coloured parts. Images 1 - 3 are for 0.1mm - 86.1mm, 4 - 6 for 86.2mm - 129.2mm, 7 - 9 for 129.3mm - 166.1mm, and 10 - 12 for 166.2mm - 203mm.

Figure 3.8: A1 on the 3D surface (left) and 2D surface (right) seen from y-60°. The image on the 3D panel is significantly distorted at its neck and head, but these parts stretch straight on the flat wall.

Figure 3.9: When the image is seen from the direct position, there is a space between the buttock and belly (picture on the left). However, once the viewpoint moves to the right, this space disappears, and the outline of the buttock connects to the ventral line.

Figure 3.10: A2, outline red deer facing left. The ventral body is not provided.

Figure 3.11: A2 (1/100 scale) seen from the vertical position. As the whole image forms a bowl-like concave shape, the elevation is highest at both ends, while the lowest surface is found in the middle part.

Figure 3.12: These nine images illustrate the depth of A2. When the cross-section layer passes the surface of A2, the colour of the surface changes; dark regions denote lower elevation than coloured parts. Images 1 - 3 are for 0.1mm - 16.3mm, 4 - 6 for 16.4mm - 32.7, and 7 - 9 for 32.8 - 49mm.

Figure 3.13: A3, red deer facing left but looking back. All body parts are given except the tail.

Figure 3.14: An example of integration in A3. From the root of the neck to the whole posterior dorsal is outlined along a horizontal ridge running horizontally. The artist of this image may have determined the entire picture of A3 based on this ridgeline.
Figure 3.15: A3 (1/200 scale) seen from the vertical position. The highest elevation is found on the head, while the lowest is on the frontal legs.

Figure 3.16: These 15 images illustrate the depth of A3. When the cross-section layer passes the surface of A2, the colour of the surface changes; dark regions denote lower elevation than coloured parts. Images 1 - 3 are for 0.1mm - 50.3mm, 4 - 6 for 50.4mm - 70.5, and 7 - 9 for 70.6 - 90.6mm, 10 -12 for 90.7mm - 110.6mm, and 13 -15 for 110.7mm - 146mm.

Figure 3.17: A3 on the 3D surface (left) and 2D surface (right) seen from y-70°. The image drawn on the 3D panel is significantly distorted at its neck and mid-torso, but such deformations are absent in the image drawn on the flat wall. These interventions on A3's appearance are due to multiple topographic conditions rather than a single topography.

Figure 3.18: A5, outline deer facing right. All body parts are given except the tail.

Figure 3.19: A5 and the natural pattern of the wall behind the image. Although noticeable natural lines are absent, there is a number of subtle edge lines. The contour of the cervical dorsal partly overlaps with one of those edges.

Figure 3.20: A5 (1/100 scale) seen from the vertical position. The highest elevation is found on the tip of the ears, while the lowest is on the frontal leg.

Figure 3.21: These ten images illustrate the depth of A5. When the cross-section layer passes the surface of A5, the colour of the surface changes; dark regions denote lower elevation than coloured parts. Images1-3 are for 0.1mm - 10.2mm, 4 and 5 for 10.3mm - 16mm, 6 and 7 for 16.1mm - 21.8mm, 8 and 9 are for 21.9mm - 26.2mm, and 10 for 26.3mm - 32mm.

Figure 3.22: A5 on the 3D surface (left) and the 2D surface (right) seen from y70°. There are no significant differences, but the image on the 3D panel appears thinner at its neck and head.

Figure 3.23: A6, outline red deer facing right. The ventral body is absent. The dorsal line of A7 horizontally crosses the neck of A6.

Figure 3.24: A6 (1/200 scale) seen from the vertical position. The highest elevation is found on the tip of the ears while the lowest is on the dorsal thigh.

Figure 3.25: These six images illustrate the depth of A6. When the cross-section layer passes the surface, the colour of the surface changes; dark regions denote lower elevation than coloured parts. Images 1 and 2 are for 16.1mm - 26.7mm, 3 and 4 for 26.8mm - 37.3mm, and 5 and 6 for 37.4mm - 48mm.

Figure 3.26: A7, outline red deer. As only the dorsal line and V-shape ears are visible, the figure appears as a line rather than body.

Figure 3.27: A7 (1/200 scale) seen from the vertical position. The wall forms an overall convex shape. The highest elevation is found on the middle dorsal, while the lowest is on the tip of the ears and the thigh.

Figure 3.28: These nine images illustrate the depth of A7. When the cross-section layer passes the surface of A7, the colour of the surface changes; dark regions denote lower elevation than coloured parts. Images 1-3 are for 0.1mm - 6.5mm, 3 and 4 for 6.6mm - 12.9mm, and 5 and 6 for 13mm - 19.4mm.

Figure 3.29: A8, outline red deer facing left. The whole body except the forelimbs and tail is depicted. The presence of the image is generally weak as the density of the outlining dots is low (digital filter applied).

Figure 3.30: An example of integration in A8. A thick groove line running just under the image is utilised as a part of the ventral line.

Figure 3.31: Another example of the integration in A8. The buttock is outlined along with an edge line. The curve of the buttock coincides with that of the edge line.

Figure 3.32: A8 (1/200 scale) seen from the vertical position. The highest elevation is found on the neck-shoulder while the lowest is on the hind limbs.

Figure 3.33: These eight images illustrate the topographic depth of A6. When the cross-section layer passes the surface of A9, the colour of the surface changes; dark regions denote lower elevation than coloured parts. Images 1 and 2 are for 0.1mm -12mm, 3 and 4 for 12.1mm - 24mm, 5 and 6 for 24.1mm - 36mm, and 7 and 8 for 36.1mm - 48mm.

Figure 3.34: A8 on the 3D surface (left) and the 2D surface (right) seen from y-70°. The dots that constitute the dorsal line become partly invisible because they are hidden by a raised wall, while the dots are still visible in the image drawn on the flat surface. Although this is only a slight difference, the neck becomes shorter than in the 2D simulation.

Figure 3.35: A8 on the 3D surface (left) and the 2D surface (right) seen from y70°. Although multiple convex surfaces distort the posterior body, both hind limbs are noticeably deformed as their direction changes. However, the legs on the 2D surface receive no topographic intervention.

Figure 3.36: A9, outline red deer facing left. The whole body except the tail is depicted. This is one of the most outstanding images in Convalanas cave (digital filter applied).

Figure 3.37: the example of integration in A9. A ridge which runs obliquely is integrated into the outline of the frontal neck. This natural line becomes noticeable especially when the image is viewed from the right.

Figure 3.38: A9 (1/200) scale seen from the vertical direction. The highest elevation is found in the head and limbs while the lowest is in the ventral middle.

Figure 3.39: These ten images illustrate the depth of A9. When the cross-section layer passes the surface of A9, the colour of the surface changes; dark regions denote lower elevation than coloured parts. Images 1 and 2 are for 0.1mm - 15.2mm, 3 and 4 for 15.3mm - 35.4mm, 5 and 6 for 35.5mm - 55.6mm, 7 and 8 for 55.7mm - 75.8mm, and 9 and 10 for 75.9mm - 96mm.

Figure 3.40: A9 on the 3D surface (left) and 2D surface (right) seen from y-70°. The image is markedly deformed due to the convexity above the neck and head and the concave in the mid-torso. The distortion is noticeable when it is compared to A9 on the 2D panel.

Figure 3.41: A10, outline red deer facing left. The ventral body is absent. A run-off on the cave wall blurs the muzzle.

Figure 3.42: A10 (1/100 scale) seen from the vertical position. The highest elevation is found in the muzzle and the buttock, while the lowest is in the central mid-torso.

Figure 3.43: These six images illustrate the depth of A10. When the cross-section layer passes the surface of A10, the colour of the surface changes; dark regions denote lower elevation than coloured parts. Images 1 and 2 are for 0.1mm - 22mm, 3 for 22.1mm - 27.5mm, 4 for 27.6mm - 33mm, 5 for 33.1mm - 38.5mm, and 6 for 38.6mm - 44mm.

Figure 3.44: A10 on the 3D surface (left) and the 2D surface (right) seen from y70°. Since the elevation of the dorsal-neck is lower than the mid-torso and the mid-torso is lower than the thigh, the lower areas are hidden by the higher parts when viewed from the right. Consequently, the neck and the mid-torso appear to shrink remarkably. This contraction seems as if A10 is raising its head. The extent of the distortion is significant once compared to A10 on the 2D surface.

Figure 3.45: A11, outline horse facing left (digital filter applied). The image is maintained in a remarkably good condition. Although the frontal limbs are missing, the rest of the body parts, even also mane, are provided.

Figure 3.46: A11 (1/100 scale) seen from the vertical position. The highest elevation is found on the hind limbs, while the lowest is on the dorsal thigh.

Figure 3.47: These nine images illustrate the depth of A11. When the cross-section layer passes the surface of A11, the colour of the surface changes; dark regions denote lower elevation than coloured parts. Images 1 - 3 are for 0.1mm - 48mm, 4 - 6 for 48.1mm - 89.1mm, 7 - 9 for 89.2mm - 137mm.

Figure 3.48: A11 on 3D surface (left) and the 2D surface (right) seen from y-70°. As a large convexity on the mid-torso conceals the entire thigh, the body is perceived significantly shrunk. Meanwhile, the image on the 2D wall also appears contracted, but its extent is not as significant as on the 3D surface.

Figure 3.49: A11 on 3D surface (left) and the 2D surface (right) seen from y70°. As a large convexity on the mid-torso emphasises, the posterior body appears more substantial on the 3D surface than on 2D. On the other hand, the anterior becomes contracted because of the low elevation of the region. The extent of this contraction is somewhat limited on the flat surface.

Figure 3.50: A13, outlined red deer facing upward (digital filter applied). The ventral body is absent.

Figure 3.51: A13 (1/100 scale) seen from the vertical position. The highest elevation is found on the thigh, while the lowest is on the chin.

Figure 3.52: These nine images illustrate the depth of A13. When the cross-section layer passes the surface of A13, the colour of the surface changes; dark regions denote lower elevation than coloured parts. Images 1 - 3 are for 2.4mm - 9.1mm, 4 - 6 for 9.2mm - 16mm, 7 - 9 for 16.1mm - 22.9mm.

Figure 3.53: A14, outline red deer facing right (digital filter applied). The ventral body is absent. Locating left to the face of the large horse (A11), this deer is arranged as if confronting the horse.

Figure 3 54: An example of integration on A14. The dorsal line is outlined along with an edge line which forms along with the convex immediately above the image.

Figure 3.55: A14 (1/100 scale) seen from the vertical position. The highest elevation is found on both edges of the image (the thigh and muzzle), while the lowest is on the right ear.

Figure 3.56: These eight images illustrate the depth of A14. When the cross-section layer passes the surface of A14, the colour of the surface changes; dark regions denote lower elevation than coloured parts. Images 1 and 2 are for 0.1mm to 2.8mm, 3 and 4 for 2.9mm to 5.5mm, 5 and 6 for 5.6mm to 8.3mm, and 7 and 8 for 8.4mm to 11mm.

Figure 3.57: B1, an image of reindeer facing left (digital filter applied). As the whole body except the tail is provided, this is the largest picture among all left in Covalanas cave. The condition of the preservation is also remarkably well.

Figure 3.58: An example of integration on B1. The tip of the muzzle is outlined along with an edge of a rocky surface, although its extent is limited.

Figure 3.59: B1 (1/50 scale) seen from the vertical position. The highest elevation is found on the horns, while the lowest is on the frontal limb.

Figure 3.60: These eight images illustrate the topographic depth of B1. When the cross-section layer passes the surface of B1, the colour of the surface changes; dark regions denote lower elevation than coloured parts. Images 1 and 2 are for 0.1mm - 74.8mm, 3 and 4 for 74.9mm - 106.9mm, 5 and 6 for 107mm - 139mm, and 7 and 8 for 139.1mm - 171mm.

Figure 3.61: B4, outline red deer facing left. Although the ventral body and hind limb are not clear, these parts are also provided and once visible. There is a trace of modern graffiti on the frontal limb.

Figure 3.62: An example of integration on B4. There are two parallel grooves on the panel. They already form the basic shape of the posterior body. One of this line (upper) is mostly shared with the dorsal line, although the ventral line does not entirely overlap on the other groove (lower).

Figure 3.63: A unique sample of possible integration. Although a ridge seems irrelevant to any outlines of the face, it perfectly overlaps with the contour of the frontal neck once B4 is viewed from the left.

Figure 3.64: B4 (1/20 scale) seen from the vertical position. The highest elevation is found on the tip of the ear, while the lowest is on the dorsal thigh.

Figure 3.65: These 12 images illustrate the depth of B4. When the cross-section layer passes the surface of B4, the colour of the surface changes; dark regions denote lower elevation than coloured parts. Images 1 - 3 are for 0.1mm - 22.5mm, 4 - 6 for 22.6mm - 33.7mm, 7 - 9 for 33.8mm - 44.9mm, and 10 - 12 for 45.0mm - 56.2mm.

Figure 3.66: B4 on the 3D surface (left) and the 2D surface (right) seen from y-60°. The neck on the 3D panel is compressed by the multiple topographic features and appears lifted upwards as if the deer is raising its neck. On the other hand, the neck on the flat surface remains stretched straight.

Figure 3.67: B4 on the 3D surface (left) and the 2D surface (right) seen from y70°. Distortion occurs on three regions in the anterior body: the straight outline of the front neck is deformed into a zigzag line; both ears are bent forward; the muzzle goes unseen. These deformations are specific to B4 on the 3D surface because such phenomena do not occur on the 2D surface.

Figure 3.68: B5, outline red deer facing left. All body parts are provided except the tail. Because the density of the dots that constitute the ventral and buttock is lower than the rest of the body, the presence of those regions is also weaker.

Figure 3.69: Example of integration on B5. The posterior dorsal is perfectly integrated into a noticeable ridge. The topography of the region has its shape which is already reminiscent of the whole posterior body, but the other outlines (the buttock and ventral line) are not integrated into natural lines.

Figure 3.70: B5 (1/20 scale) seen from the vertical position. The highest elevation is found on the ears, while the lowest is on the frontal leg.

Figure 3.71: These four images illustrate the depth of B5. When the cross-section layer passes the surface of B5, the colour of the surface changes; dark regions denote lower elevation than coloured parts. Image 1 is for 0.1mm - 41mm, 2 for 41.1mm - 49.3mm, 3 for 49.4mm - 57.5mm, and 4 for 57.6mm - 73.9mm.

Figure 3.72: B5 on the 3D surface (left) and the 2D surface (right) seen from y-70°. The neck on the 3D panel appears greatly elongated as the convex shoulder hides the dorsal mid-torso. This distortion is absent in B5 on a 2D surface.

Figure 3.73: C1, outline red deer facing right. All body parts are provided except the tail. The unique arrangement of the frontal leg features C1. The condition of the image is remarkably good as the vividness of the red colour still survives until present.

Figure 3.74: An example of integration on C1. The wall is raised immediately below the image, generating an elevational gap. The belly is outlined along the edge of the convex surface.

Figure 3.75: C1 (1/100 scale) seen from the vertical position. The highest elevation is found on the hind limb, while the lowest is on the head.

Figure 3.76: These six images illustrate the depth of C1. When the cross-section layer passes the surface of C1, the colour of the surface changes; dark regions denote lower elevation than coloured parts. Images 1 and 2 are for 0.1mm - 30mm, 3 for 30.1mm - 36mm, 4 for 36.1mm - 42mm, and 5 and 6 for 42.1mm - 54mm.

Figure 3.77: C2, outline red deer facing left (digital filter applied). Located immediately right to C1, the shape is also identical to the previous deer. The figure is subject to decay despite thick outlined body.

Figure 3.78: Example of integration on C2. The wall forms a sizeable convex topography which produces edge lines along the elevational gap. The outline of the croup and the buttock overlaps on the top and right edge of the topography.

Figure 3.79: C2 (1/100 scale) seen from the vertical position. The highest elevation is found on the dorsal thigh, while the lowest is on the ears and hind leg.

Figure 3.80: These eight images illustrate the depth of C2. When the cross-section layer passes the surface of C2, the colour of the surface changes; dark regions denote lower elevation than coloured parts. Images 1and 2 are for 0.1mm - 29.3mm, 3 and 4 for 29.4mm - 37.6mm, 5 and 6 for 37.7mm - 46mm, and 7 and 8 for 46.1mm - 54.4mm.

Figure 3.81: C2 on the 3D surface (left) and the 2D surface (right) seen from y-70°. In the image depicted on the 3D wall, the contour of the thigh is thinner and appears deformed as the line tilts inward. These distortions are attributed to the high elevation of the thigh.

Figure 3.82: C2 on the 3D surface (left) and the 2D surface (right) seen from y70°. The presence of the posterior becomes immense much more than the image on the 2D surface. Due to this distortion, the deer appears raising the posterior.

Figure 3.83: D1, outlined red deer facing left (digital filter is applied). All body parts are provided. D1 is one of the well-preserved figures in Covalanas cave as its vivid red still survives until today. The frontal limb extends upward, even to the inside the body. This fill-in part does divide not only the neck and the posterior but also rough surface (right) and smooth surface (left).

Figure 3.84: D1 (1/100 scale), seen from the vertical direction. The highest elevation is found on the central thigh, while the lowest is on the ventral neck.

Figure 3.85: These eight images illustrate the topographic depth of D1. When the cross-section layer passes the surface of D1, the colour of the surface changes; dark regions denote lower elevation than coloured parts. Images 1 and 2 are for 0.1mm - 26mm, 3 and 4 for 26.1mm - 40.9mm, 5 and 6 for 41mm - 55.7mm, and 7 and 8 for 55.8mm - 70.6mm.

Figure 3.86: D1 on the 3D surface (left) and the 2D surface (right) seen from y-60°. The image drawn on the 3D panel is significantly distorted at its neck and head, but in D1 on the 2D surface, these parts stretch straight. This is because of the topography whose elevation gradually grows higher from the neck to the muzzle.

Figure 3.87: The number of integrations by body part (H: Head, D: Dorsal, Ta: Tail, B: Buttock, L: Limbs, and V: Ventral). Integration mostly likely occurs on the dorsal line (8 images) and then ventral line (5). No sample is detected from the limbs and the tail.

Figure 3.88: The number of images by the frequency of integration (Inte = Integration, Inte 0: 7 images, Inte 1: 6, Inte 2: 4, and Inte 3: 1). The case with plural integrations on a single image is rare.

Figure 3.89: Among 6 images with single integration, all cases occurs either on the dorsal (4 images) or the ventral line (2).

Figure 3.90: The number of combinations of integrated body parts. Integration occurs on D-V and D-B in 2 images. Values for other combinations are 1 (H-D, H-B, and B-V). Integration on the buttock can appear together with that on any other contour parts, but contrarily the ventral line has no combination with any other contours except the buttock.

Figure 3.91: The number of the topographic condition by body part. Medium level and low level tend to be found on the neck-shoulder and middle part respectively, while the head and thigh is likely located on the wall of higher elevation. Therefore, the general shape of the wall is a plate-like concave. The extra elevation levels are confirmed only on the head and limbs.

Figure 3.92: The number of the topographic condition by body part. The data is simplified as the three divisions in Ns, M, and T are integrated. Even so, the graph shows the same trend as demonstrated in Figure 3.91.

Figure 3.93: The average elevation level of each body part is quantified (H: 62 points, Ns: 53, M: 48, T: 59, FL: 18, HL: 34, and Ta: 2). The elevation reflects high if the numerical value is high, and on the contrary, the depth is deeper if the numerical value is low. Therefore, it is clear that the head and thigh are more likely to be placed on higher elevation.

Figure 3.94: The line graph shows the elevation level by body part, as a result, there are roughly six patterns in the shape of the wall: Pattern 1 (P1) is overall concavity; Pattern 2 (P2) is overall slope; Pattern 3 (P3) is overall convexity; Pattern 4 (P4) is zigzag; Pattern 5 (P5) is partial concavity; Pattern 6 (P6) is partial slope. Among these six patterns, P1 is the most popular topography (P1: 5 images, P2: 3, P3: 2, P4: 3, P5: 3, and P6: 2).

Figure 3.95: The number of images by the frequency of distortion (Dis = Distortion). Distortion is confirmed in 11 images (Dis2: 6, Dis3: 4, and Dis5: 1). All of them are subject of plural distortions. All in all, distorting an image by topography is not rare, and in some images, their appearance is severely deformed as the viewing angle changes.

Figure 3.96: The number of distortion by body part (H: Head, Ns: Neck-shoulder, M: Mid-torso, T: Thigh, L: Limbs, and Ta: Tail). Distortion more likely occurs in the anterior body (Head: 7 images, and Neck: 8). Meanwhile, the mid-torso (4) and leg (4) is rarely deformed, and no distortion is confirmed at the tail.

Figure 4.1: Site plan of El Pendo cave. Although the entire area is approx. 150 m, the large chamber constitutes the almost half of the cave.

Figure 4.2: The Frieze of the Pictures (8.5m width x 3.5m height). 17 images are depicted on this limited area.

Figure 4.3: The Frieze and a total of 17 images. This case study selected 11 images (N1, N2, N4, N5, N7, N8, N12, N13, N14, N16, and N17).

Figure 4.4: A reconstructed model and camera positions (shown in the figure as blue rectangles).

Figure 4.5: A model looked up from x30° angle. This angle simulates the appearance of an image viewed from a lower position.

Figure 4.6: N1, outline red deer facing left (digital filter is applied). The head and neck are painted. This image is located on the highest position (approx. 4m) among 11 images.

Figure 4.7: A detailed illustration of N1 (Barquin 2001). The location of the natural lines is clearly illustrated. The cervical dorsal and the under-neck are integrated with grooves.

Figure 4.8: N1 (1/50 scale) seen from the vertical position. The highest elevation is found on the head, while the lowest is on the tip of the hind limb.

Figure 4.9: These eight images illustrate the depth of N1. When the cross-section layer passes the surface of N1, the colour of the surface changes; dark regions denote lower elevation than coloured parts. Images 1-3 are for 0.1mm - 23.3mm, 4-6 for 23.4mm - 46.7mm, and 7-8 for 46.8mm - 70mm.

Figure 4.10: N1 on the 3D surface (left) and 2D surface (right) seen from y80°. The length of the neck on the 3D wall is significantly shortened because the convex surface on the shoulder overlaps and hides the neck. Meanwhile, the neck on the 2D wall is visible.

Figure 4.11: N2, outline red deer facing left (digital filter is applied). The image is in excellent condition so viewers can easily see it.

Figure 4.12: Examples of integration. N2 (left) and its highlighted topography (right). The dorsal line is integrated with the groove and edge which separate the panel from another rock plate (indicated by the white circle). The buttock is also placed along the right edge of the wall (indicated by the blue the circle). The "h" pattern on the panel already appears the basic form of a quadruped mammal. Meanwhile, the front neck is outlined along the ridge that extends from the bottom of the chest to the upper left obliquely (indicated by the red circle).

Figure 4.13: N2 (1/40 scale) seen from the vertical position. The highest elevation is found on the under-neck, while the lowest is on the ventral middle.

Figure 4.14: These eight images illustrate the depth of N2. When the cross-section layer passes the surface of N2, the colour of the surface changes; dark regions denote lower elevation than coloured parts. Images1 and 2 are for 0.1mm - 21.5mm, 3 and 4 for 21.6mm - 42.9mm, 5 and 6 for 43mm - 64.4mm, and 7 and 8 for 64.5mm - 85.9mm.

Figure 4.15: N2 on the 3D surface (left) and 2D surface (right) seen from y-60°. The sharply elevated wall along the front neck overlaps on the entire cervical dorsal, and the head appears detached from the body. The image on the 2D wall is not distorted in this way, but the anterior body is merely stretched.

Figure 4.16: N2 on the 3D surface (left) and 2D surface (right) seen from y60°. The muzzle goes unseen, and the rock along which the buttock is placed emphasises the 3D volume of the body. On the other hand, N2 on the 2D surface is stretched merely to the right.

Figure 4.17: N4, outline caprid facing left (digital filter is applied). This image is located on the lowest position of all pictorial samples in El Pendo cave. Although the contour is not salient, all body part is fully outlined by natural lines.

Figure 4.18: Examples of integration. N4 (left) and its highlighted topography (right). Edges are integrated into the posterior dorsal, the buttock (see the red circle) and the back leg (see the right side of the black circle). The use of various types of natural line is also seen in other body parts: muzzle (edge:see the white circle), frontal limbs (groove), belly (valley: see the centre of the black circle), and cervical dorsal (valley). Overall, the original shape of the wall already appears the shape of N4.

Figure 4.19: N4 (1/20 scale) seen from the vertical position. The highest elevation is found on the ventral mid-torso, while the lowest is on the tip of the hind limb.

Figure 4.20: These eight images illustrate the depth of N4. When the cross-section layer passes the surface of N4, the colour of the surface changes; dark regions denote lower elevation than coloured parts. Images1 and 2 are for 0.1mm - 12.7mm, 3 and 4 for 12.8mm - 25.3mm, 5 and 6 for 25.4mm and 38mm, and 7 and 8 for 38.1mm - 76mm.

Figure 4.21: N4 on the 3D surface (left) and 2D surface (right) seen from y60°. The face is located on an inclined surface which can be seen clearly from the left but mostly invisible from the right.

Figure 4.22: N5, outline red deer facing right (digital filter is applied). The condition is remarkably good, although N5 is the smallest of all images in El Pendo.

Figure 4.23: N5(left) and its highlighted topography (right). The rock where N5 is located already has a basic shape of N5. However, the image's outline does not perfectly overlap on the pre-existing pattern, as if the artists intentionally avoided to do so. Instead, the dorsal line, buttock, and tail are integrated with a ridge (indicated by the red circle).

Figure 4.24: N5 (1/30 scale) seen from the vertical position. The highest elevation is found on the ventral neck, while the lowest is on the tip of the ear.

Figure 4.25: These seven images illustrate the depth of N5. When the cross-section layer passes the surface of N5, the colour of the surface changes; dark regions denote lower elevation than coloured parts. Image1 is for 0.1mm - 2.6mm, 2 and 3 are for 2.7mm - 7.8mm, 4 and 5 for 7.9mm - 13mm, and 6-7 for 13.1mm - 20.8mm.

Figure 4.26: N5 seen from y60° (left) and y-60°(right). When viewers stand on the right, the shoulder hides the mid-torso and thigh. The body is therefore perceived to be shorter. At the same time, the neck appears longer and thinner because the convex surface under the neck pushes the neck upward and narrows the width. When N5 is viewed from the left, the head becomes much smaller as the section is placed on a concave surface.

Figure 4.27: N7, complete image of red deer facing right (digital filter is applied). N7 is located in the centre of the frieze, with the largest size of all 11 images (125cm).

Figure 4.28: N7 (left) and its highlighted topography (right). N7 is located on the panel with innumerable fractures. These fractures generate grooves and edges. The contour of the image is integrated with those natural lines at the ventral (see the white and black circle), the buttock (see the blue circle), and the dorsal (see the red circle). Natural line is also utilised as the border between the fill-in and non-fill-in part inside the body.

Figure 4.29: N7 (1/100 scale) seen from the vertical position. The highest elevation is found on the tip of the ears, while the lowest is on the dorsal mid-torso.

Figure 4.30: These eight images illustrate the depth of N7. When the cross-section layer passes the surface of N7, the colour of the surface changes; dark regions denote lower elevation than coloured parts. Images 1 and 2 are for 0.1mm -25.6mm, 3 and 4 for 25.7mm - 51.3mm, 5 and 6 for 51.4mm - 76.9mm, and 7 and 8 for 77mm - 102.6mm.

Figure 4.31: N7 on the 3D surface (left) and 2D surface (right) seen from y70°. The neck is particularly deformed by the raised surface which is located on the right to the shoulder. This topographic feature pushes the outline of the chest inward and forces the neck to stretch. On the other hand, such a distortion is absent in the image on the 2D surface where the body sustains its original appearance.

Figure 4.32: N8, incomplete image of a horse facing left (digital filter is applied). N8 is located on the centre of the Frieze, immediately right to N7. It is assumed that this image, together with N7, constitutes a unified theme.

Figure 4.33: Examples of the integration. N8 (left) and its highlighted topography (right). The dorsal line is integrated with a deep groove on its cervical area and then continues along an edge of a convex surface (see the black circle). The front neck and lower jaw are also outlined, following the curve of a valley line (see the white circle).

Figure 4.34: N8 (1/100 scale) seen from the vertical position. The highest elevation is found on the frontal leg, while the lowest is on the dorsal mid-torso.

Figure 4.35: These 12 images illustrate the depth of N8. When the cross-section layer passes the surface of N8, the colour of the surface changes; dark regions denote lower elevation than coloured parts. Images 1-3 are for 0.1mm - 24mm, 4-6 for 24.1mm - 40mm, 7-9 for 40.1mm - 56mm, and 10-12 for 56.1mm - 72mm.

Figure 4.36: N8 seen from y0° (left) and y-70°(right). The body proportion between the anterior and posterior is noticeably disturbed by the topography as the viewing angle decreases.

Figure 4.37: N12 (above), outlined image of unknown quadruped animal facing right (digital filter is applied). The head and ventral side are missing. It is depicted immediately above N13.
Figure 4.38: Examples of the integration in N12. The white circle shows that the valley between two convex is integrated into the cervical dorsal. On the other hand, the black circle indicates the possible integration; the part in which outline is absent appears to adopt the edge line of a rock, and this edge naturally merges into the dorsal line.
Figure 4.39: N12 (1/40 scale seen from the vertical direction). The highest elevation is found on the front neck, while the lowest is on the dorsal mid-torso.

Figure 4.40: These ten images illustrate the depth of N12. When the cross-section layer passes the surface of N12, the colour of the surface changes; dark regions denote lower elevation than coloured parts. Images 1-3 are for 0.1mm - 43.8mm, 4-6 for 43.9mm - 87.7mm, and 7-10 for 87.8mm - 126mm.

Figure 4.41: An example of distortion in N12. Above three images are N12 seen from y0°(left), y40°(centre) and y60° (right). The convex wall under the neck gradually narrows the neck as viewing angle increase, and finally both outlines of the front neck and cervical dorsal perfectly overlap at y60°.

Figure 4.42: N13 (below), outlined red deer facing right. The ventral side of the body is absent. It is placed immediately below N12.

Figure 4.43: Examples of integration in N13. The rocky surface generates a large number of edges, grooves, and ridgelines. N13 maximises those lines in order to outline its body as the integration is found on the multiple locations: the facial area, front neck and posterior dorsal.

Figure 4.44: N13 (1/20 scale) seen from the vertical position. The highest elevation is found on the muzzle, while the lowest is on the dorsal mid-torso.

Figure 4.45: These eight images illustrate the depth of N13. When the cross-section layer passes the surface of N13, the colour of the surface changes; dark regions denote lower elevation than coloured parts. Images 1 and 2 are for 0.1mm - 13.9mm, 3 and 4 for 14mm - 19.5mm, 5 and 6 for 19.6mm - 25.1mm, and 7 and 8 for 25.2mm - 30.6mm.

Figure 4.46: N14, image of a quadrupedal animal facing right. Despite its stunning presence, the species is not discernible due to the absence of its head.

Figure 4.47: Examples of integration. N14 (left) and its highlighted topography (right). The red circle on the images suggests the integrated section of the ventral line. Most of the belly is provided along the edge which lies horizontally. The black circle shows the contour of the buttock and the croup is exactly fixed to an edge of the wall of half-square shape. Meanwhile, one of the hind legs is drawn along a groove (see the white circle).

Figure 4.48: N14 (1/50 scale) seen from the vertical position. The highest elevation is found on the hind leg, while the lowest is on the ventral neck.

Figure 4.49: These 12 images illustrate the depth of N14. When the cross-section layer passes the surface of N14, the colour of the surface changes; dark regions denote lower elevation than coloured parts. Images1-3 are for 0.1mm - 54.4mm, 4-6 for 54.5mm - 81.7mm, 7-9 for 81.8mm - 108.9mm, and 10-12 for 109mm - 136.1mm.

Figure 4.50: N14 seen from y-70° (left), y0°(middle), and y70°(right). This shows significant distortion because of topographic features. Especially, the shape of the thigh and mid-torso is remarkably deformed because the position of the hind legs constantly slides side to side. Apart from distortion to these parts, the appearance of the neck and forelimbs also changes: the neck appears stretched when the image is viewed from right; the interval between forelimbs gradually narrows, and the right limb vanishes at y-70°.
Figure 4.51: N16, image of a deer facing left. Although its head appears somewhat blurred due to decay, the deer still possesses strong presence.

Figure 4.52: N16 (left) and its highlighted topography (right). Natural lines are integrated into most of the dorsal (see the white circle), buttock (see the black circle), and ventral line (see the red circle). As the wall itself already appears the basic form of N16, the artist took full advantage of this condition.

Figure 4.53: N16 (1/30 scale) seen from the vertical position. The highest elevation is found on the hind leg, while the lowest is on the ventral mid-torso and frontal limb.

Figure 4.54: These 12 images illustrate the topographic depth of N16. When the cross-section layer passes the surface of N16, the colour of the surface changes; dark regions denote lower elevation than coloured parts. Images1-3 are for 0.1mm - 93.6mm, 4-6 for 93.7mm - 129.2mm, 7-9 for 129.3mm - 164.9mm, and 10-12 for 165mm - 200.5mm.

Figure 4.55: N16 on the 3D surface (above) and 2D surface (below) seen from y-60° (left) and y60° (right). The combination of the concave and convex surface distorts the deer dramatically as a viewpoint sifts side to side. In contrast, significant distortions do not occur on N16 on the 2D surface (below left and below right).

Figure 4.56: N17, image of red deer facing right (digital filter is applied). This deer is located on the rightmost of the Frieze of Pictures. As it is fixed in back-to-back position against N16, these two images are depicted in a symmetrical composition.

Figure 4.57: N17 (1/60 scale) seen from the vertical position. The highest elevation is found on the ear, while the lowest is on the frontal limb.

Figure 4.58: These 12 images illustrate the depth of N17. When the cross-section layer passes the surface of N17, the colour of the surface changes; dark regions denote lower elevation than coloured parts. Images 1-3 are for 0.1mm - 49.2mm, 4-6 for 49.3mm - 98.4mm, 7-9 for 98.5mm -147.6mm, and 10-12 for 147.7mm - 237mm.

Figure 4.59: N17 on 3D surface (left) and 2D surface (right) seen from y-80°. The mid-torso and thigh appear thinner because the central area overlaps the dorsal region. The convex topography on the left frontal limb also overlaps on the other leg. Meanwhile, the anterior part sustains a certain proportion because the massive convex on the forefront body constantly displays the part towards the viewer on the left. These changes are never detected in the 2D simulation.

Figure 4.60: N17 on the 3D surface (left) and 2D surface (right) seen from y50°. The combination of the concave and convex surface distorts the deer dramatically. Especially, the distortion on the neck is significant as it narrows its width. The hind leg also appears bent backwards. The extent of the topographic intervention is visualised once compared to N17 on the 2D surface.

Figure 4.61: The number of images with integration by body part (H: Head, D: Dorsal, Ta: Tail, B: Buttock, L: Limbs, and V: Ventral). Integration mostly likely occurs on the dorsal line (10 images) and then ventral line (9). Especially, almost all images (10 out of 11 images) utilise natural lines for outlining the dorsal line. By contrast, limbs (2) and the tail (1) were not preferred sections for integration.

Figure 4.62: The number of images by the frequency of integration (Inte = Integration). In El Pendo cave, multiple integrations are a significantly common phenomenon as 9 images contain at least 2 integrated body parts. Particularly, the number of images with 3 integrated parts and 4 integrated parts are high (each case contains 4 images). This is attributable to the fractured wall surface where innumerable natural lines are available for integration.

Figure 4.63: The number of combinations of integrated body sections. Despite the high value for the combination of the dorsal and ventral line (9 images), this result is understood given the high occurrence of integration for these body sections. Meanwhile, the result for the head and buttock is only once in spite of relatively high occurrences for them (4 and 5 images, respectively). That seems as if the palaeo-artist intended to avoid simultaneous integration on these two parts.

Figure 4.64: The number of images by body part regarding elevation level (H: Head, Ns: Neck-shoulder, M: Mid-torso, T: Thigh, FL: Front Leg, HL: Hind Leg, Ta: Tail. D, C, and V, refer to Dorsal, Central, and Ventral, respectively). Certain trends are visible in the graph: High elevation tends to be placed on the head (6 images); Medium level is more likely found on the main body (Ns: 7-4, M: 6-3, T: 5-3); the elevation for the mid-torso (7-3) and limbs are more likely low (FL: 4, and HL: 4); Extra elevation level is mostly allocated to limbs (FL: 3, and HL: 4). However, some images are not complete figure as the head, thigh, limbs or tails are missing, while all images contain the neck-shoulder and mid-torso. Therefore, this result is not obtained from images in the same condition.

Figure 4.65: A simplified graph of the topographic condition for 11 images by body part. Although the nine main body parts are integrated into the three parts (Ns, M, T), the result still reflects the trends seen in Figure 4.64.

Figure 4.66: A graph of the total elevation point by body section (H: 31 points, Ns: 35, M: 30, T: 33, FL: 21, HL: 29, and Ta: 5). The elevation reflects high if the point is high, while the depth is deeper if the point is low.

Figure 4.67: A simplified graph based on 8 images. Unlike the previous result, the values of Medium level for Neck-shoulder, Mid-torso, and Thigh remarkably drop (4, 4, and 3, respectively), but instead the value of High for Thigh increases (4).

Figure 4.68: A graph of total elevation point by body part based on eight images (H: 27 points, Ns: 24, M: 22, T: 27, FL: 14, HL: 19, and Ta: 5). Unlike the previous result, points for Head and Thigh are higher than Neck-shoulder and Mid-torso. That means examined images are generally found on an overall concave. This result is the same as the case of Covalanas.

Figure 4.69: Numerically visualised topography patterns. 5 patterns are detected in El Pendo: Overall concavity (P1), Overall slope (P2), Overall convexity (P3), Zigzag (P4), and Partial concavity (P5). Above all, P1 is the most popular type, with 3 images (N7, N16, and N17), followed by P5 (N2 and N13). On the other hand, the other types contain only 1 image respectively (P2: N1, P3: N4, P4: N5).

Figure 4.70: The number of images by the frequency of distortion (Dis = Distortion). All images are subject of distortion in El Pendo cave (Dis0: 0 image, Dis1: 3, Dis2: 2, Dis3: 2, Dis4: 3, and Dis5: 1). Multiple deformations are significantly common as 8 images contain at least 2 distorted body parts. This fact signifies the active role of the topography to distort images.

Figure 4.71: The number of images with distortion by body part (H: Head, Ns: Neck-shoulder, M: Mid-torso, T: Thigh, L: Limbs, and Ta: Tail). Distortion intensively occurs in the neck, with 10 images. The limbs are the second preferred section, with 7 images. The mid-torso has the lowest value as only 3 images contains distorted mid-torso.

Figure 5.1: A site plan of El Castillo cave. The cave is the largest of the Monte Castillo caves, constituting five large halls called Room A, B, C, D and the final room. The interior is divided into East and West area; Room A-D are located in the east part, whereas the Final Room is in the west. These sections are connected by a long corridor called Gallery of Discs, and some other small chambers (Room of Tectiforms, Hands Gallery and Hands Ceiling) are situated in the north part of Room A.

Figure 5.2: The images analysed here and their location. In total, 25 images were selected for the study, based on their visibility and accessibility. These samples are distributed in 6 different regions throughout the cave. However, the most of them (19 images) is located in the north side of Room A which is covered by the red oval over the cave plan.
Figure 5.3: 11 images on Polychrome Panel. These images include five bison (PB1-PB5), three deer (PD1-PD3, two horses (PH1 and PH2), and one unknown quadruped animal (PU1). This panel contains the largest number of samples in this case study. The surface is smooth on the right side of the panel, while the wall severely undulates on the left.

Figure 5.4: An image of Aurochs located in Diverticulum of Room A. Although the picture is somewhat blurred due to weather, the figure is visible to naked eyes. This Aurochs is treated as DA1.

Figure 5.5: Five images on Ceiling of hands (CB1-CB5). This ceiling contains over 320 graphics and 40 hand stencils, which signifies the importance of this place for the practice of cave art in El Castillo.

Figure 5.6: Two horses (EH1-EH2) and one deer (ED1) in Entrance of Hands Gallery. These images are fixed on different walls: EH1 is located on a wall of the north-end, whereas EH2 and ED1 are placed as a pair on an undulating ceiling. The distance between those panels is approximately 200 cm. EH1 is a complete figure, while the posterior is absent in EH2 and ED1.

Figure 5.7: GM1, an image of a mammoth located on the wall in the west of the gallery of discs.

Figure 5.8: Four images in Room B. BMB1 is a hybrid image of human and bison. BU1 is an unknown quadruped mammal whose head is absent, and BB1 and BB2 are bison. These samples are collected from three different regions in Room B; BMB1 is located on a stalagmite pillar which forms at the north area; BU1 is placed on the wall on the south; BB1 and BB2 are fixed in the passage connecting Room B to Room C.

Figure 5.9: Nine reconstructed 3D models. Blue squares represent camera positions. The total number of photographic data for the reconstruction of each model is following: 558 for Polychrome panel (1), 373 for Ceiling of hands (2), 66 for Entrance of hands gallery (3: EH1), 81 for Entrance of hands gallery (4: EH2 and ED1), 47 for Diverticulum (5), 81 for Room B (6: RMB1), 83 for Room B (7: RB1 and RB2), and 58 for Room B (8: RU1), and 39 for Gallery of disks (9).

Figure 5.10: PB1, outline bison facing left. While the image is clear in its posterior area, its anterior is somewhat ambiguous. PB1 contains an unnatural depiction: one of its frontal leg abnormally long and extends forward.

Figure 5.11: Examples of integration. The posterior dorsal line overlaps on the edge of a convex surface (see the blue circle). The buttock (see the white circle) and the tip of the tail (see the black circle) are also integrated with grooves.

Figure 5.12: PB1 (1/40 scale) seen from the vertical position. The highest elevation is found on the tip of the frontal leg, while the lowest is on the central shoulder and tail.

Figure 5.13: These ten images illustrate the depth of PB1. When the cross-section layer passes the surface of PB1, the colour of the surface changes; dark regions denote lower elevation than coloured parts. Images 1-3 are for 0.1mm - 22.1mm, 4-6 for 22.2mm - 47.8mm, and 7-10 for 47.9mm - 73.6mm.

Figure 5.14: PB1 on the 3D surface (left) and 2D surface (right) seen from y70°. The length of the mid-torso on the 3D wall is significantly shortened because the convexed thigh hides the part. Meanwhile, such deformation is absent in the 2D simulation

Figure 5.15: PB2, image of bison facing to the upper right. Despite that the face and limbs are relatively well conserved, most of the body parts appear unclear. Five images (three hand-stencils and two deer) are superimposed on PB2. Such a high density of images generates a chaotic impression.

Figure 5.16: Examples of integration. The head is outlined by an edge (from its top to the muzzle) and by a ridge (from the muzzle to the jaw).

Figure 5.17: PB2 (1/10 scale) seen from the vertical position. The highest elevation is found on the ventral thigh, while the lowest is on the tip of the muzzle.

Figure 5.18: These ten images illustrate the depth of PB2. When the cross-section layer passes the surface of PB2, the colour of the surface changes; dark regions denote lower elevation than coloured parts. Images 1 and 2 are for 0.1mm - 30.9mm, 3 and 4 for 31mm and 46.4mm, 5 and 6 for 46.5mm - 61.9mm, 7 and 8 for 62mm - 77.3mm, and 9 and 10 for 77.4mm - 116mm.

Figure 5.19: PB2 seen from y0°(left) and y-70° (right). While the hind limbs are visible when PB2 is viewed from y0° (the legs are in the red circle), the convexed ventral thigh hides the makes the limbs unseen at y70°.

Figure 5.20: PB3, image of bison facing to the upper right (digital filter is applied). Most of the body parts are unclear due to severe decay. The yellow colour is visible on the anterior body. Also, a hand stencil and a geometric sign are superposed on the dorsal mid-torso.

Figure 5.21: Examples of integration in PB3. The dorsal is integrated with an edge and a groove. On the left to the bison, the surface elevates and creates an edge which is partially used for the posterior dorsal (indicated in the black circle). Meanwhile, a zigzag groove is used for a part of the anterior dorsal line (shown in the white circle).

Figure 5.22: PB3 (1/10 scale) seen from the vertical position. The highest elevation is found on the ventral neck-shoulder, while the lowest is on the central neck-shoulder.

Figure 5.23: These ten images illustrate the depth of PB3. When the cross-section layer passes the surface of PB3, the colour of the surface changes; dark regions denote lower elevation than coloured parts. Images 1-3 are for 0.1mm - 32.8mm, 4-6 for 32.9 - 65.6mm, and 7-10 for 65.7mm - 105mm.

Figure 5.24: PB3 seen from y0°(left) and y-60° (right). Distortion occurs on the dorsal mid-torso and head. As for the dorsal mid-torso, when viewers see the image from the left, the area appears moving upward, shortening its outline. This is because the convex surface on the body hides the mid-torso. Similarly, the distortion on the head is caused by the convex neck-shoulder: as the head is concealed by the neck-shoulder, the part appears contracted at y-60°.

Figure 5.25: PB4, image of bison facing to the lower left (digital filter is applied). The outline of most of the body parts is unclear due to severe decay. However, the red colour is visible on the anterior body. PB4 is located on a rock in front of the polychrome panel.

Figure 5.26: Examples of integration in PB4 (indicated by black lines). Natural lines are utilised for the outline in five sections: grooves are used for the posterior dorsal, buttock and ventral, edges are used for the cervical dorsal and head. Also, a ridge is integrated into the hind limb.

Figure 5.27: PB4 (1/30 scale) seen from the vertical position. The highest elevation is found on the hind limbs, while the lowest is on the central mid-torso.

Figure 5.28: These 12 images illustrate the depth of PB4. When the cross-section layer passes the surface of PB4, the colour of the surface changes; dark regions denote lower elevation than coloured parts. Images 1-3 are for 0.1mm - 89.1mm, 4-6 for 89.2mm - 152.7mm, 7-9 for 152.8mm - 216.4mm, and 10-12 for 216.5mm - 280mm.

Figure 5.29: PB4 seen from y40°(left), y0° (centre), and y-60° (right). Distortion occurs on multiple body parts: The thigh, hind limbs, mid-torso, neck-shoulder, and head. The convex posterior distorts the thigh and hind limbs; this convex hides the buttock area once PB4 is viewed from the left (y-60°), while two hind legs partly overlap each other viewed from the right. The mid-torso, neck-shoulder and head are located on outer-edges of overall concave, and these parts are also largely distorted by the topography.

Figure 5.30: PB5, outline bison. This bison is incomplete as only limited sections (the head, cervical dorsal, and frontal) are provided. PB5 contains superimposition with two other images (PU1 and PD3) on its dorsal middle area.

Figure 5.31: Examples of integration in PB5 (indicated by the red line and the black line). Ridges are utilised for the dorsal line, while grooves are substituted for the ventral line. Because these natural lines continue even after the contour disappear, the body of PB5 appears enlarged.

Figure 5.32: PB5 (1/200 scale) seen from the vertical position. The highest elevation is found on the dorsal mid-torso, while the lowest is on the ventral neck.

Figure 5.33: These six images illustrate the depth of PB5. When the cross-section layer passes the surface of PB5, the colour of the surface changes; dark regions denote lower elevation than coloured parts. Image 1 is for 0.1mm - 22.3mm, 2 for 22.4mm - 33.4mm, 3 for 33.5mm - 44.6mm, 4 for between 44.6mm - 55.7mm, and 5 and 6 for 55.8mm - 156mm.

Figure 5.34: PD1, outline red deer (digital filter is applied). Partly superimposed on PB2, the posterior body is somewhat ambiguous; however, PD1 contains the hind legs and thigh.

Figure 5.35: PD1 (1/10 scale) seen from the vertical position. The highest elevation is found on the frontal limb, ventral neck, and dorsal thigh, while the lowest is on the ventral mid-torso.

Figure 5.36: These six images illustrate the depth of PD1. When the cross-section layer passes the surface of PD1, the colour of the surface changes; dark regions denote lower elevation than coloured parts. Images 1 and 2 are for 0.1mm - 7.6mm, 3 and 4 for 7.7mm - 15.3mm, and 5 and 6 for 15.4mm and 22.9mm.

Figure 5.37: PD2, outline red deer (a digital filter is applied). Located immediately on the right to PD1 and partly superimposed on PB2, this image is considerably blurred due to severe decay. Especially, the ventral area is hardly confirmable even through a digital filter.

Figure 5.38: PD2 (1/10 scale) seen from the vertical position. The highest elevation is found on the dorsal thigh and ear, while the lowest is on the frontal limb.

Figure 5.39: These 12 images illustrate the depth of PD2. When the cross-section layer passes the surface of PD2, the colour of the surface changes; dark regions denote lower elevation than coloured parts. Images 1 and 2 are for 0.1mm - 4mm, 3 and 4 for 4.1mm - 10mm, 5 and 6 for 10.1mm - 16mm, 7 and 8 for 16.1mm - 22mm, and 9 and 10 for 22.1mm - 28mm.

Figure 5.40: PD3, outline red deer. The ventral line is absent. The dorsal line is also used for the muzzle of PU1. The buttock is disproportionally long. This buttock is drawn on the body of PB5.

Figure 5.41: PD3 (1/200 scale) seen from the vertical position. The highest elevation is found on the dorsal thigh, while the lowest is on the central thigh.

Figure 5.42: These eight images illustrate the depth of PD2. When the cross-section layer passes the surface of PD2, the colour of the surface changes; dark regions denote lower elevation than coloured parts. Image 1 is for 0.1mm - 1.5mm, 2 and 3 for 1.6mm - 4.5mm, 4 and 5 for between 4.6mm -7.5mm, 6 and 7 for 7.6mm-10.5mm, and 8 for 10.6mm - 12mm.

Figure 5.43: PU1, outline image of an unknown herbivore. Only the face is provided. PU1 shares its outline with PD3 and PB5: the line of the upper muzzle is also used for the dorsal line of PD3, while the tip of the muzzle is a part of the dorsal line of PB5.

Figure 5.44: PH1, outline face of a horse. Although the only facial part is provided, the face has the details (eye, mouth, nostril).

Figure 5.45: An example of integration in PH1. The lower part of the muzzle is drawn on two independent grooves.

Figure 5.46: PH2, outline horse. Located on the leftmost of Polychrome Panel, this horse is the largest figure of all samples in El Castillo (188cm). All body parts are provided. Because four projectiles are depicted on its body, PH2 is associated with a practice of the hunting magic.

Figure 5.47: PH2 (1/400 scale) seen from the vertical position. The highest elevation is found on the tail, head, and dorsal mid-torso, while the lowest is on the frontal limb.

Figure 5.48: These eight images illustrate the depth of PH2. When the cross-section layer passes the surface of PH2, the colour of the surface changes; dark regions denote lower elevation than coloured parts. Images 1 and 2 are for 0.1mm - 22.2mm, 3 and 4 for 22.3mm - 44.4mm, 5 and 6 for 44.5mm - 66.7mm, and 7 and 8 for 66.8mm - 100mm.

Figure 5.49: CB1, outline bison facing right (digital filter is applied). Although the image is subject of severe decay, its entire body is meticulously drawn.
Figure 5.50: Examples of integration in CB1. A thin groove is utilised for the outline of the buttock (indicated by a black line in the left picture). The tip of the tail is also drawn along a groove (indicated by a red line).

Figure 5.51: CB1 (1/10 scale) seen from the vertical position. The highest elevation is found on the tip of the frontal leg, while the lowest is on the central body.

Figure 5.52: These ten images illustrate the depth of CB1. When the cross-section layer passes the surface of CB1, the colour of the surface changes; dark regions denote lower elevation than coloured parts. Images 1 and 2 are for 0.1mm - 34.4mm, 3 and 4 for 34.5mm - 47.2mm, 5 and 6 for 47.3mm - 60.1mm, and 7 and 8 for 60.2mm - 73mm.

Figure 5.53: CB1 seen from y-70°(left), y0° (centre), and y70° (right). Distortion occurs on the head, neck-shoulder, thigh, and limb: the cervical dorsal and head appears noticeably contracted as the angle increases to y70; the dorsal thigh is pulled upward as the viewing position moves to the left (y-70°); both frontal and back leg appear bending their directions between y-70°and y70°. The overall concave surface causes these distortions.

Figure 5.54: CB2, outline bison facing left (digital filter is applied). Due to severe conservation condition, the image is hardly recognisable to viewers. The ventral side is missing.

Figure 5.55: An example of integration in CB2. The dorsal line is drawn along the edge of a concave surface.

Figure 5.56: CB2 (1/10 scale) seen from the vertical position. The highest elevation is found on the central shoulder and tip of the horn, while the lowest is on the ventral thigh.

Figure 5.57: These six images illustrate the depth of CB2. When the cross-section layer passes the surface of CB2, the colour of the surface changes; dark regions denote lower elevation than coloured parts. Images 1 and 2 are for 0.1mm - 4.7mm, 3 and 4 for 4.8mm - 9.3mm, and 5 and 6 for 9.4mm - 14mm.

Figure 5.58: CB3, outline bison facing right (digital filter is applied). Provided with the entire body, CB3 is in the best condition of all the other pictures on the ceiling. The outline becomes ambiguous in the anterior. There are lines which extend from the head.

Figure 5.59: Examples of integration in CB3. A thin horizontal groove runs along the posterior dorsal line and the root of the tail.

Figure 5.60: CB3 (1/10) scale seen from the vertical position. The highest elevation is found on the tail, while the lowest is on the central neck-shoulder.

Figure 5.61: These eight images illustrate the depth of CB3. When the cross-section layer passes the surface of CB3, the colour of the surface changes; dark regions denote lower elevation than coloured parts. Images1-3 are for 0.1mm - 18.4mm, 4 and 5 for 18.5mm and 30.6mm, and 6-8 for 30.7mm - 49mm.

Figure 5.62: CB3 on the 3D surface (left) and 2D surface (right) seen from y70°. While the body is significantly contracted on the 3D surface, CB3 sustains its general proportion on the flat surface. This is because the wall is elevated in the ventral shoulder area.

Figure 5.63: CB4, outline bison facing right (digital filter is applied). The condition of the image is good. CB4 is depicted schematically, with three oblique lines portraying the frontal neck. Additionally, a superimposition with a hand-stencil is found on the belly and frontal neck.

Figure 5.64: CB4 (1/60 scale) seen from the vertical position. The highest elevation is found on the tip of the hind leg, while the lowest is on the central mid-torso.

Figure 5.65: These nine images illustrate the depth of CB4. When the cross-section layer passes the surface of CB4, the colour of the surface changes; dark regions denote lower elevation than coloured parts. Images1-3 are for 0.1mm - 23.3mm, 4-6 for 23.4mm - 46.6mm, and 7-9 for 46.7mm - 66mm.

Figure 5.66: CB5, outline bison facing left (digital filter is applied). The condition of the image is relatively good. There are red pigments on CB5: some of them appear signs, while the red colour on the dorsal mid-torso might be a cloud part of a hand-stencil.

Figure 5.67: CB5 (1/30 scale) seen from the vertical position. The highest elevation is found on the tip of the tail and central mid-torso, while the lowest is on the dorsal neck.

Figure 5.68: These six images illustrate the topographic depth of CB5. When the cross-section layer passes the surface of CB5, the colour of the surface changes; dark regions denote lower elevation than coloured parts. Images 1 and 2 are for 0.1mm - 7.5mm, 3 and 4 for 7.6mm - 12.5 mm, and 5 and 6 for 12.6mm - 20mm.

Figure 5.69: EH1, outline horse facing left (digital filter is applied). According to Marc Groenen, this is a hybrid species of a horse and an aurochs because ears are much longer and resemble the horns of a bovid.

Figure 5.70: A unique example of integration in EH1. A conspicuous ridge runs obliquely above the image (indicated in the black circle on the left picture)). On this ridge, the posterior dorsal and upper part of the buttock are outlined. Once viewed from the right, the ridge seems a half arch which turns to be a natural dorsal line (indicated in the black on the right picture), and this curve naturally merges to the outline of the buttock and hind leg.

Figure 5.71: EH1 (1/30 scale) seen from the vertical position. The highest elevation is found on the tip of the ears, while the lowest is on the central mid-torso.

Figure 5.72: These eight images illustrate the depth of EH1. When the cross-section layer passes the surface of EH1, the colour of the surface changes; dark regions denote lower elevation than coloured parts. Images 1 and 2 are for 0.1mm - 35.6mm, 3 and 4 for 35.7mm - 53.4mm, 5 and 6 for 53.5mm - 71.3mm, and 7 and 8 for 71.4mm - 89.1mm.

Figure 5.73: EH1 seen from y-70°(left), and y0° (right). The head and neck are significantly distorted when viewed from the left due to the convex topography on these body sections. The leaning wall also enhances the extent of the distortion.

Figure 5.74: EH2, outline horse facing right. The image is provided only with the anterior body. Although the used colour is yellow, a part of the dorsal line appears red. Also, two parallel lines are left inward from the frontal neck.

Figure 5.75: An example of integration in EH2. A ridgeline on the convex ceiling is used for a part of the ventral line.

Figure 5.76: EH2 (1/30 scale) seen from the vertical position. The highest elevation is found on the ventral mid-torso, while the lowest is on the dorsal mid-torso.
Figure 5.77: These ten images illustrate the topographic depth of EH2. When the cross-section layer passes the surface of EH2, the colour of the surface changes; dark regions denote lower elevation than coloured parts. Images 1 and 2 are for 0.1mm - 24.2mm, 3 and 4 for 24.3mm - 48.4mm, 5 and 6 for 48.5mm - 72.6mm, 7 and 8 for 72.7mm - 96.8mm, and 9 and 10 for 96.9mm - 129mm.

Figure 5.78: EH2 on the 3D surface (left) and 2D surface (right) seen from y70°. The muzzle appears considerably longer in the 3D simulation than in the 2D simulation.

Figure 5.79: ED1, outline red deer facing right. This is an incomplete image as it only contains the anterior body. ED1 is located immediately above EH2.
Figure 5.80: An example of integration in ED1. A thin groove is located on the tip of the muzzle connecting the upper and the lower jaw.

Figure 5.81: ED1 (1/50 scale) seen from the vertical position. The highest elevation is found on the tip of the ears, while the lowest is on the muzzle and dorsal mid-torso.

Figure 5.82: These six images illustrate the depth of ED1. When the cross-section layer passes the surface of ED1, the colour of the surface changes; dark regions denote lower elevation than coloured parts. Images1 and 2 are for 0.1mm - 11.7mm, 3 for 11.8mm - 13.2mm, 4 for 13.3mm - 14.6mm, 5 for 14.7mm -16.1mm, and 6 for 16.2mm - 19mm.

Figure 5.83: DA1, outline aurochs facing right. DA1 is under severe decay as the contour has gone somewhat unclear in some parts.

Figure 5.84: Examples of integration in CB2. The forehead is outlined along with a steep edge (as indicated by the white oval). The ventral line also partly corresponds to an edge line (black oval).

Figure 5.85: DA1 (1/100 scale) seen from the vertical position. The highest elevation is found on the hind limb, while the lowest is on the central mid-torso.

Figure 5.86: These eight images illustrate the topographic depth of DA1. When the cross-section layer passes the surface of DA1, the colour of the surface changes; dark regions denote lower elevation than coloured parts. Images1 and 2 are for 0.1mm - 7.3mm, 3 and 4 for 7.4mm - 14.5mm, 5 and 6 for 14.6mm - 21.8mm, and 7 and 8 for 21.9mm - 29mm.

Figure 5.87: BBM1, image of a human-bison hybrid. Vertically fixed on a stalagmite pillar, all body parts are provided. As well as painting, the artist of BBM1 also executed a remarkable engraving skill on the feet.

Figure 5.88: These two pictures represent BBM1 (right) and its topographic condition (left). Bison-man is located on a convex surface whose appearance is already reminiscent of its basic form. The contour is drawn along the edge of this elevated wall.

Figure 5.89: BBM1 (1/20 scale) seen from the vertical position. The highest elevation is found on the central mid-torso, while the lowest is on the head.

Figure 5.90: These 12 images illustrate the depth of BBM1. When the cross-section layer passes the surface of BBM1, the colour of the surface changes; dark regions denote lower elevation than coloured parts. Images 1-3 are for 0.1mm - 23.4mm, 4-6 for 23.5mm - 46.8mm, 7-9 for 46.9mm - 70.2mm, and 10-12 for 70.3mm - 156mm.

Figure 5.91: BBM1 viewed from y0° (left) and y-70° (right). Because of its sculptural quality, the image appears considerably different as viewing angle changes. In particular, the distortion on the hind leg is noteworthy: when the viewpoint moves to the left, the limb gradually bends backwards. This change is due to the convex surface on the calf and feet. Because of this distortion, BBM1 constantly appears folding and stretching its hind legs within the angle range between y-70° and y0°.

Figure 5.92: BU1, outline quadruped mammal facing right. Entire body except the head is provided; because the neck is attached to a calcite plate which vertically develops from the wall, BU1 appears as if beheaded by the plate.

Figure 5.93: Examples of integration in BU1. An edge of a large convex surface is used for outlining the buttock (see the black circle), while a deep groove corresponds to the ventral line. This groove extends to the further right, as if depicting the missing forelimbs (see the white circle).

Figure 5.94: BU1 (1/40 scale) seen from the vertical position. The highest elevation is found on the tail, while the lowest is on the ventral neck.

Figure 5.95: These 12 images illustrate the depth of BU1. When the cross-section layer passes the surface of BU1, the colour of the surface changes; dark regions denote lower elevation than coloured parts. Images 1-3 are for 0.1mm - 97mm, 4-6 for 98mm - 114mm, 7-9 for 105mm -130mm, and 10-12 for 131mm - 146mm.

Figure 5.96: BU1 viewed from y-70° (left), y0° (centre), and y40° (right). The shape of the thigh significantly changes as the viewing position moves.

Figure 5.97: BB1, outline bison facing right. The image is well-preserved, although the outline is somewhat ambiguous at the anterior ventral.

Figure 5.98: BB1 (left) and highlighted topographic images (centre and right). The original pattern of the wall is already a reminiscent of BB1 as the dorsal, hind leg, and ventral line mostly relies on natural lines.

Figure 5.99: BB1 (1/200 scale) seen from the vertical position. The highest elevation is found on the hind leg, while the lowest is on the ventral middle.

Figure 5.100: These 12 images illustrate the depth of BB1. When the cross-section layer passes the surface of BB1, the colour of the surface changes; dark regions denote lower elevation than coloured parts. Images 1-3 are for 0.1mm - 48.9mm, 4-6 for 49mm - 97.9mm, 7-9 for 98mm - 146.8mm, and 10-12 for 146.9mm - 195.9mm.

Figure 5.101: BB1 on the 3D surface (left) and 2D surface (right), viewed from y60°. Pushed inward by the elevated surface, the anterior body appears significantly contracted. In contrast, BB1 on the 2D surface maintains its body proportion unchanged.

Figure 5.102: BB2, outline bison facing right. Located immediately on the left to BB1, all body parts are provided. As the wall behind the image is cleaned and abraded, it is considered that the artist of BB2 carefully prepared before carrying out the image-making.

Figure 5.103: BB2 (left) and highlighted topographic images (right). The groove which is integrated into the dorsal line of BB1 obliquely crosses the head of BB2, and the horn is drawn along this groove. There is also an edge line extending obliquely to the left at the upper part of the head, and this line corresponds to the anterior dorsal line. This edge disappears at the centre of the dorsal area, but instead, a ridge which forms by the peak of the convex surface substitutes the posterior dorsal line (see the red circle).

Figure 5.104: BB2 (1/200 scale) seen from the vertical position. The highest elevation is found on the middle dorsal, while the lowest is on the horn.

Figure 5.105: These eight images illustrate the depth of BB2. When the cross-section layer passes the surface of BB2, the colour of the surface changes; dark regions denote lower elevation than coloured parts. Images 1 and 2 are for 0.1mm - 17.2mm, 3-5 for 17.3mm - 38.7mm, and 6-8 for 38.8mm - 60.2mm.

Figure 5.106: BB2 on the 3D surface (left) and 2D surface (right), viewed from y70°. The elevated wall on the mid-torso hides the thigh and causes a significant contraction. At the same time, the anterior part appears by far enlarged. Such a distortion is absent in BB2 on the 2D wall.

Figure 5.107: GM1, outline mammoth facing left (digital filter is applied). It is originally executed in red, although the colour has altered into somewhat darker.
Figure 5.108: GM1 (1/100 scale) seen from the vertical position. The highest elevation is found on the central mid-torso, while the lowest is on the tip of the frontal leg.

Figure 5.109: These six images illustrate the depth of GM1. When the cross-section layer passes the surface of GM1, the colour of the surface changes; dark regions denote lower elevation than coloured parts. Image 1 is for 0.1mm - 2.7mm, 2 for 2.8mm - 5.3mm, 3 for 5.4mm - 8mm, 4 for 8.1mm - 10.7mm, and 5 and 6 for 10.8mm - 48mm.

Figure 5.110: The number of images by the frequency of integration (Inte = Integration). In El Castillo cave, plural integrations occur in 12 images which accounts for nearly a half of all examined pictures (Inte 0: 7 images, Inte 1: 6, Inte 2: 4, and Inte 3: 5, Inte 4: 1,

Inte 5: 1, and Inte 6: 1). Given this number, it can be said that integration is a common artistic method in the cave. Especially, the condition of the wall is responsible for the multiple integrations as images with more than 3 integrations are located on the wall where natural lines are abundant.

Figure 5.111: The number of integrations by body part (H: Head, D: Dorsal, Ta: Tail, B: Buttock, L: Limbs, and V: Ventral). Integration mostly likely occurs on the dorsal line and then ventral line (12 and 9 images, respectively). On the other hand, limbs (4) and the tail (4) are not preferred for integration. This result conforms to the other two caves.

Figure 5.112: The frequency of combinations of body parts among images with multiple integrations. The combination of the dorsal and ventral line appears most frequently (7 images), and all the other frequent combinations also include integration either into the dorsal or ventral line (H-D: 6, H-V: 5, B-D: 4, and B-V: 4). This result reflects the general result of the predominant body section for integration.

Figure 5.113: These two graphs show the number of images by body part regarding elevation level (H: Head, Ns: Neck-shoulder, M: Mid-torso, T: Thigh, FL: Front Leg, HL: Hind Leg, Ta: Tail. D, C, and V, refer to Dorsal, Central, and Ventral, respectively). The left graph includes sub-divisions in the neck-shoulder, mid-torso, thigh, while in the right graph those divisions are united. Nevertheless, these two graphs are almost identical. Unlike the other two caves where High level concentrates on the head and where Medium and Low levels are likely placed on the shoulder and mid-torso, the distribution of elevation levels is more complicated in El Castillo. On the other hand, Extra levels are exclusively located on the legs (FL: 3 images, and HL: 6) and tail (1) in all cases except 1 case on the thigh. In particular, the rate for the hind legs with Extra levels is high as 4 images contain the limb on Extra High and 2 images on Extra Low.

Figure 5.114: A simplified graph regarding the topographic condition by body part based on 19 images. Values for Medium and Low level grow in the neck-shoulder (8 and 9 images,respectively) and mid-torso (8 and 7 images, respectively), although the thigh still has the highest value in Medium level (11). At the same time, the value for the head in Low level is reduced (7). In consequence, the result shows a similar trend to that in Covalanas and El Pendo.

Figure 5.115: A graph of total elevation point by body part based on 19 images (H: 55 points, Ns: 50, M: 51, T: 59). Generally, the elevation of the head and thigh is higher than both Neck-shoulder and mid-torso, meaning that the general shape of the topography is overall concavity.

Figure 5.116: The numerically-visualised shapes of images. 6 patterns are detected from 19 images. The most common patterns of the topography are P1 and P5 as each pattern contains 5 images. The next common pattern is P2 and P6, with 3 images respectively. Meanwhile, P3 and P4 are not preferred patterns as only 2 images and 1 image belong to P3 and P4 respectively. The fact that concave surface is the predominant topographic type conforms to the general shape of topography.

Figure 5.117: The number of images by the frequency of distortion (Dis = Distortion). 12 images are subject of distortion in El Castillo (Dis0: 13 image, Dis1: 6, Dis2: 1, Dis3: 0, Dis4: 4, and Dis5: 1) Overall, images with distinguishable distortion are relatively rare in the cave, compared to the other cases. Multiple distortions in a single image are also less common.

Figure 5.118: The number of distortion by body part (H: Head, Ns: Neck-shoulder, M: Mid-torso, T: Thigh, L: Leg and, Ta: Tail). Distortion most frequently occurs on the head (7 images) and the limb (7). Topography less likely deforms the neck-shoulder and middle part as only 5 and 4 distortions are found respectively.

Figure 6.1: The number of integration by body part (H: Head, D: Dorsal, Ta: Tail, B: Buttock, L: Limbs, and V: Ventral). Integration most likely occurs on the dorsal line (30 images) and then ventral line (23). Buttock and Head are also relatively popular (15 and 13, respectively). On the other hand, the limbs (6) and tail (5) are not preferred parts for integration.

Figure 6.2: The frequency of simultaneous integration with other body parts. The dorsal line and ventral line are the most popular combination (13). Integration into the head and buttock are in most case accompanied by that into the dorsal or ventral line (H-D: 10, H-V: 9, D-V: 14, BD: 11, and B-V: 9).

Figure 6.3: The number of full and partial integration by body section. Large integration mostly occurs in the dorsal (21 times) and ventral area (15 times). This result might reflect an optimised way of image-making: the use of longer natural lines can determine the more detailed shape of an animal image. One can better imagine a complete form of images in advance of image-making with natural lines which are available for full dorsal or\and ventral integration.

Figure 6.4: Different levels of fragmentation of images. When subjects have more visual cues, the perception will be easier. (After Snodgrass and Feenan 1990).

Figure 6.5: The number of integrated natural lines by type. Edges are the most popular type of integration (46 cases). Grooves are applied for the outline in 35 cases, whereas the ridgeline is the third popular type (10 cases). Border (1 case in Covalanas) and valley lines (3 cases in El Pendo) were detected not as a universal type but as a site-specific example.

Figure 6.6: The number of images regarding elevation levels and corresponding body parts, based on 45 images (H: Head, Ns: Neck-shoulder, M: Mid-torso, and T: Thigh. Limbs and Tail are eliminated). There is a clear tendency as the head and thigh are more frequently placed on a higher elevation (19 images and 16 images, respectively) than the neck-shoulder and middle part (7 and 6, respectively).

Figure 6.7: The generalised model of the topographic condition (H: 144, Ns: 127, M: 121, and T: 145). Higher points denote higher elevation. Based on the topographic data of 45 images, the general topography in the three studied caves is overall concavity.

Figure 6.8: The number of images regarding elevation levels and corresponding body parts, based on 54 images (the limbs and tail are included). The legs tend to be located on Extra elevation levels at a much higher frequency (19 images) than the rest of the body parts (H:4, Ns:0, M:0, T: 3, and Ta: 1).

Figure 6.9: Briefly visualised topographic condition of images. Six patterns are detected from 45 images. The most common pattern is P1, with 13 images. The next common pattern is P5 (ten images) and then P2 (seven images). Meanwhile, P3, P4 and P6 contain five images respectively. Thus, the surface with a concave feature is the predominant topographic type. This fact conforms to the general shape of the topography seen in Figure 6.7.

Figure 6.10: A merit of using an overall concave surface. When a viewer sees an image on a flat surface from the front, the image, although limited extent, is inevitably distorted at its both sides; due to the imbalance in the distance between the viewpoint, the centre of the surface, and the edges of the surface, the centre area appears larger than the sides. In contrast, when images on a moderate concave surface are viewed, the imbalance is cleared as the topography forms a distance between the viewpoint and the centre, and, as a result, viewers can experience less distorted images. (After Ahn et al. 2014)

Figure 6.11: A different degree of distortion caused by viewing from different distances. Closer viewing-distance causes more noticeable distortion as the inequality in the distance between the viewpoint, the edges of the wall and the centre is larger than a distant viewpoint.

Figure 6.12: Illustration of viewing an image on an overall concavity (left) and overall convexity (right) from the same distance. The concavity equalises the distance of viewpoint-centre (A-c) and that of viewpoint-edges (A-a and A-b), while the convexity emphasises the inequality in the distance between viewpoint-centre (B-f) and viewpoint edge (B-d and B-e). Therefore, the image on the convexity appears noticeably distorted.

Figure 6.13: Illustration of viewing an image on an overall concavity (left) and overall convexity (right). The image on the concavity can be viewed from a much wider viewing range than one on the convexity. It means that the viewers can select a viewpoint from a broader range to see images on a concavity without unseen areas, whereas viewers have to stay around the front area in the case of the convexity. This wide viewing range potentially allows accommodating multiple viewers.

Figure 6.14: Another merit of using P1 topography. Since both edges of overall concave surface elevate, these edges are more likely to face viewers when images are viewed from sides. On the other hand, an acute angle forms between the surface and a viewer in the case of the flat surface because the wall does not face viewers standing on sides. The use of the overall concave might have had merit to reduce a chance that images were unnoticed.

Figure 6.15: The number of images by the frequency of distortion (Dis = Distortion). A total of 33 images are distorted in the three caves, which accounts for 61% of the whole samples. Particularly, the number of images with more than two distorted body parts is 25 (Dis2: 9, Dis3: 7, Dis4: 5, and Dis6: 4), nearly 50% of all, and the appearance of these images are subjected to a remarkable deformation.

Figure 6.16: The number of distortions by body part. Distortions mostly occur on the head (20 cases), neck-shoulder (22), and legs (18). On the other hand, the thigh (15) and mid-torso (12) were less frequently deformed. Meanwhile, no distortion was found on the tail.

Figure 6.17: Examples of unusual integration (EH1 and B4). Despite their normal appearance when being viewed from the direct position, natural lines which exist irrespectively around/on the images (see circled areas) turn into a part of the outline once viewpoint moves to a side. These lines can be an obstacle for viewers, and potentially the artists could have avoided this composition if they had aimed them to view only from the front.

Figure 6.18: The correlation between topography types and the frequency of distortion. Distortion most frequently occurs to images on P1 (92 per cent: 12/13). However, the ratio for other topography type is between 60 and 30 per cent.

Figure 6.19: The number of images, detected distortions, and the average number of distortion per image by topography type. The number of distortion for P1 images are significantly higher than images of other topography types. In average, almost three distortions are detected from each image of P1 (2.9: see the line graph), while values for the other types are less than 1.1.

Figure 6.20: These images show a mechanism of how viewing from different positions distorts images on an overall concave surface. When viewing point is taken in front of the wall, both edges of an image are equally captured in sight (A). However, once the viewpoint moves to the left, that balance collapses, and the body part depicted on the

left side will be distorted remarkably due to the interference by the elevated surface. On the other hand, since the body part is drawn on the right area of the wall faces the viewer, the part maintains its original shape (B). Similarly, when the viewpoint is taken on the right, the image deforms greatly on the right side, while the left side sustains a relatively stable shape (C). If the image were placed on a flat surface, the opposite edge would always fail to face a viewer standing either on the left or right. Therefore, an acute angle would form between the viewpoint and the surface, and images would appear shrunk at the opposite side to the viewer (D).

Figure 6.21: Mechanism of how A1 (Covalanas) is deformed by viewing different viewpoints. Since A1 is located on an overall concave surface, the head and neck-shoulder maintain their original shape even if the viewpoint moves to the right (y60°), while the thigh is deformed largely. In contrast, once the viewpoint moves to the left (y-60°), the thigh recovers its original shape, whereas the head and neck are deformed to a great extent. This phenomenon is unique to the overall concave surface and does not occur on a flat medium.

Figure 6.22: Viewers can deliberately change the appearance of the head and neck of A1 by moving between y0° and y-60°. The deformation process is perceived as an animation as if deer shaking its head side to side.

Figure 6.23: An example of distortion caused by placing an image on a high position (e.g. N7 in El Pendo). N7, even on a 2D surface, appears largely deformed when it is viewed from lower right (x-30°, y70°), and the extent is conspicuous compared to the same image seen from the same height. The neck appears to expand and contract in motion as viewers move between the front (y0°) and right (y70°), and viewers potentially can manipulate the shape of N7.

Introduction

European Upper Palaeolithic cave art constitutes some of the greatest cultural heritage of *Homo sapiens*. Although a recent discovery also confirmed the artistic capability of Neanderthals who left non-figurative images at least 64000 BP (Hoffman et al. 2018), Upper Palaeolithic humans had practised this art tradition for at least 25,000 years from somewhere before 40,000 to at least 15,000 BP (Bahn and Vertut 1997, Lewis-Williams 2002, Bahn 2016). Since the formal recognition of the art's authenticity and research into its nature began in the late 19th century, scholars have been engaged with the enigma of this lost art tradition, and still our understandings are often overturned whenever a new decorated cave is discovered.

Cave art accounts for at least three-quarters of human art history (Pettitt 2016), and its appearance is generally considered to be the result of the emergence of a fully 'modern' mind. Essentially, its primary characteristic is the naturalistic depiction of large animals on cave walls and ceilings –at least from the Mid Upper Palaeolithic (~30,000 BP) - mainly in southern France and northern Spain, although with outliers elsewhere in those countries, and in Italy, Germany, the Czech Republic, the United Kingdom and in Russia (Bahn 2018). Although our modern senses prefer paintings containing dynamic landscapes with a watery place and blue skies (Dutton 2009), cave art still attracts present-day audiences, providing a distinct trace of the earlier phases of humanity and questioning our identity as a human species. Unlike images found in Palaeolithic open-air sites in the Iberian peninsula (e.g. Portugal's Foz Côa Valley and Spain's Siega Verde: see Bahn 1995, Baptista 2009, Batarda Fernandes et al. 2017) and in Hunsrück in Germany (Welker 2016), animal images have barely weathered in the caves' protective environments. Such unweathered images still retain their aesthetic potency so strongly that most researchers who enter into caves with masterpieces such as Lascaux for the first time speak of their sense of awe (Clottes 2005). These are clearly creations of artists with exceptional expertise, rarely by the hand of beginners, and display evidence of visual effects on their viewers (Ibid). Given the persistence of cave art, it can be presumed that some form of systematic education for the acquisition of artistic skills existed (Straus 1987).

In addition to sophisticated artistic ability, the fact that enigmatic animal motifs were engraved and painted in deep caves did not prevent artists from making an association between animals and the environmental features of caves. The experience that one could gain in such decorated caves was not merely the receipt of visual information from the art. Instead, a rich variety of the cave's spatial characteristics

necessarily stimulated human auditory, tactile and olfactory senses: namely, the cave environment provided visitors with novel multisensory experiences (Sakamoto 2014).

The multisensory aspect of cave art and its importance to academic research has been pointed out elsewhere (Leroi-Gourhan 1968, Lewis-Williams 2002, White 2003). Despite this, cave art tends to be researched and explored only with regard to its visual characteristics, notably theme and style, and few studies have focused on the relationship between the environmental conditions of caves and the art itself (c.f. Groenen 2000; Pettitt 2016). The primary reason for this can be attributed to the very nature of vision: unlike sound and smell, visual information can be easily recorded (simply scratching a cave wall or the ground constitutes a direct trace of an activity), and it can, therefore, be readily observed. It inevitably follows that research questions will be based only on visual aspects; which allows researchers to make associations between parietal art and portable art concerning theme and style, and thus to generate broader descriptive, chronological and distributional perspective.

Regarding cave art simply as visual information, however, can only lead us to an insufficient understanding of the nature of the earliest known art and its long-term evolution. Such a view fails to address an old question; why were areas of deep caves, away from quotidian living spaces, selected as places for art in the first place? Archaeologists agree that cave mouths have been universally used for dwellings throughout prehistory. Cave entrances were the location of actual living areas while the use of darker zones of caves for inhabitation was rare due to the inconvenience that the absence of natural light causes (Straus 1990, Moyes 2012, and Bahn 2016). However, most works of cave art are found in such inconvenient, dark zones. This site selection must have been deliberate: humans during the Upper Palaeolithic preferred the interior of caves for depicting images despite there often being plenty of free space in the mouths of caves where there would be more light for either image-making or seeing an image (Pettitt 2016). Accordingly, researchers, presuming an inherent link between cave art and the deeper spaces of caves, have sought the reason why Palaeolithic artists produced art in such remote locations.

In my master's dissertation (Sakamoto 2014), I attempted to answer the question by examining the multisensorial nature of cave art from the perspective of installation art, whose aim is to provide us with different multisensory experiences to those of quotidian life. By so doing I argued that the novel environment of caves enhances viewers' multisensorial engagement, and that cave art is not mere visual information but largely concerns "interaction" for both its production and appreciation. Namely, the novel constraints of caves, such as the morphology of their surface, and the play of darkness and shadows are responsible for the creation of certain types of images, and cave art itself can be considered as an interactive device where viewers can leave a direct

influence of themselves on the art. I coined the term 'cave art as installation art' in order to refer to the site-specific, multisensorial, and interactive nature of cave art. This led to a new understanding, which can address the reason why caves were chosen: site-specific ways of bodily engagement with art must have had a particular meaning/role and so might have also been a part of the entire art unit, unless otherwise locating art in easily-accessible places such as open-air sites and rock-shelters is more reasonable than entering to the deep interior of caves. Thus, under the perspective of cave-installation art, environmental components are better accounted for opening the way to study unrecognised points of interactions between Palaeolithic people and parietal art.

The aim of this thesis, in a broad sense, is to develop the fledgling theory of cave-installation art much further. As it stands, the theory developed in the MA project remained only abstract, lacking the necessary provision of concrete observations obtained from first-hand fieldwork in the decorated caves themselves. The initial idea was built upon a foundation of elements gathered from previous research, notably (Boado and Romero 1993, Groenen 2000, and Azema and Rivère 2012). Therefore, in order to understand in an actual context what sort of interactive factors had driven Palaeolithic artists in their image-making and image-viewing, it is necessary to investigate decorated caves with a clear focus on interactivity. The purpose of this thesis, therefore, is to examine formally the possibly interactivities in the production and post-production (viewing) phases of cave art through fieldwork, and to elucidate specifically what these were, how frequent they were, whether they were shared inter-site, and whether one might conclude that any specific 'rules' were being followed in this regard.

In considering 'interactivity', the critically important factor in the design of this thesis was the selection of appropriate images for study and the development of an appropriate methodology for the objective investigation of the issue. Although cave art consists of various forms of such interactivities, many of them will not be 'visible' or understandable to modern eyes (e.g. sound and odour), nor readily observable even if they are primarily of a visual nature. Given the limited constraints of a PhD thesis, it is impossible to explore the entirety of possible interactive elements. As this is the first formal research to my knowledge into the interactivity of cave art, I consider only the basic, observable/quantifiable elements as my highest priority. Accordingly, I chose interactivities mediated by the condition of the cave wall due to its readily observable nature. The cave wall is generally considered to be one of the essential characteristics of cave art, as its interrelation with visual works is repeatedly referred to by archaeologists over time. Natural features on the surface tend to be fundamental ingredients for completing images (e.g. Alcalde del Río et al. 1912, Breuil 1985, Leroi-Gourhan 1992, Groenen 2000, Hodgson 2000 and 2003, and Petitt 2016); and cave wall constantly

intervenes the appearance of images as its undulation causes distortion (Leroi-Gourhan 1965, Groenen 2000, Aujoulat 2005, Azema 2008, and Sakamoto 2014).

Based on the essentiality of the cave surface, I selected three data categories for examination: the integration of natural lines into the image; the topographic conditions of images; and topographic distortion of images. The first category relates to how natural lines are integrated into images' outlines, while topographic condition denotes a close examination of the elevational gap within the outlined area of images to learn how convex and concave surfaces are located on images. Although these two categories refer to how Palaeolithic artists interacted with the cave's wall in the *production* phase, the last category pertains by contrast to a direct interaction between viewers and images in the *post-production* phase. Because undulating walls can deform images no matter when the viewpoint changes, such an ever-changing appearance can encourage viewers' participation as they can actively 'manipulate' the image by moving from one viewpoint to another. I consider this aspect as a form of interactivity. By examining these three categories, I aim to detect whether or not there were specific conditions (or rules) that induced interaction in image-making and/or image- viewing. In order to secure objectively scientific validity, I needed to develop an empirical methodology. As I will describe in detail in a later chapter, I used digital photogrammetry to create 3D models of the images selected for analysis, and subsequently analysed these using Digital Image Processing (DIP) software. The analysis mainly involves the detection of natural lines, the quantification of different elevational levels, and quantification of the deformation of images. Detected features were then statistically managed by their locations, and finally explored with the aim of discerning whether any trends are visible, based on the notion that statistically demonstrable tendencies should reflect signs of an *unrevealed intention* testifying preferences and and regulations about the caves, walls, and the art created there upon.

In terms of the specific interactivities, I needed to explore exactly how the wall's condition contributed to site-specificity, i.e. whether relatively unique characteristics determined relatively unique responses to it. However, as I argue in Chapter 2, because multisensorial properties of the environment of caves are interwoven with each other (White 2003), one cannot separate them. Environmental novelties (such as reduced vision, silence, and undulating floors) together with the cave wall may always enhance interactions with cave art both directly and indirectly. Given the interconnectivity of spatial elements, studying human-wall relations should not fail to address the significance of the site-specificity of caves.

As for the case studies, I performed fieldwork in three caves in Cantabria, Spain: Covalanas, El Pendo and El Castillo. These sites are closely distributed within a geographic area of ~50 kilometres diameter and are believed to have been occupied by

groups sharing the same artistic characteristics. Common artistic features such as outlining by red dots and the predominance of a specific motif (red deer) are widely found in caves in the region (e.g. La Pasiega, La Haza, Covalanas and El Pendo etc..), suggesting the fact that images in these caves were produced by only a limited number of artists, known as 'Ramales school' (Apellaniz 1978 and Straus 1987). Although limited hunter bands might have occupied these caves, the development of the cave differs remarkably site by site: Covalanas is a narrow corridor-like hollow, whereas El Pendo is an enormous chamber with a high ceiling. El Castillo consists of multiple halls and passages connecting them. Aside from their accessibility (availability for study) the reason I selected these caves was to detect whether or not their relatively different internal structures had an impact on the artistic interactions with them. Additionally, the different archaeological features of each of the three sites provides further contrast. El Castillo was inhabited continuously by humans during the course of the Upper Palaeolithic (and at least occasionally beforehand), with an abundance of indications that it served as a crucial site for seasonal aggregation (Conkey 1980). By contrast, Covalanas has shown no evidence for human occupation per se, suggesting that humans used it only for artistic activity (Bahn 2007, 152). Accordingly, the socio-cultural difference in each cave also stimulates further discussion on whether the result yields noticeable differences between caves.

The thesis consists of six chapters. The first is dedicated to reviewing the wider intellectual context of my objectives, before explaining how the research was designed in detail (motivation, examined subjects, methodology, etc.). All research exists base on the accumulation of previous approaches; therefore, everything stands on the shoulder of giants. In the history of research into cave art, interpretations are always changing and have an intellectual influence on each other. Some of them have been rejected over the course of time, some resurrected, and some have achieved the paramount (dogmatic) position in their wider context. Each of those proposed approaches is accompanied by a unique theoretical background and methodology, which possesses both advantages and disadvantages. Archaeologists have evaluated them based on the validity of the applied methodology to reach the most reliable one. Re-visiting the history of research into cave art inevitably reveals the dominant interpretations by time, proposed methodologies, and their issues which are enveloped in methodologies. At the same time, doing so also depicts intellectual struggles of archaeologists to overcome methodological problems.

In the second chapter, I introduce my theoretical background of 'cave art as installation art' and explain how this research is designed. Since the examination of interactions is originated from the discussion in my MA dissertation (Sakamoto 2014), I describe here, although briefly, the core argument so as to provide a clear basis for

understanding the entire scope of the research. In order to do this, I first present the concept of 'installation art' with its definitions and then refer to the reason why I think cave art is interpretable as installation art. Installation art concerns site-specific ways of multisensorial engagement, and thus, I argue, cave art, as a three dimensional phenomenon, can be viewed in this way. Such a view is also profoundly related to the *affordance theory* proposed by James. J. Gibson (1979), which sees the environment and the actor (i.e. any animals) as a single unit; the theory dictates that any actor's actions are reactions to the components of the environment, and therefore that the environment and the actor exist in an interactive relationship and cannot be separated. After setting this theoretical background I list the interactions regarding cave art by environmental factors to demonstrate how the ways of viewers' engagement are diverse.

Additionally, I outline the detailed research plan. As noted above, the core of this thesis is fieldwork in three caves (Covalanas, El Pendo, and El Castillo). In this research, I created 3D models of pictorial samples from these by digital photogrammetry. 3D models were then analysed based on three different perspectives (position of natural lines, topographic conditions, and position of deformations). Because the scientific validity of a research depends on the method both for data collection and following analysis, it is vitally important to design the entire process of fieldwork and post-fieldwork along with appropriate criteria as concrete as possible. Therefore, the adopted methodology will be explained in the latter half of this chapter.

Over the course of the next three chapters, I present each case study, respectively Covalanas, El Pendo, and EL Castillo. As the purpose of the case studies is to report 1) how natural lines are integrated into an outline of images, 2) how topographic features are distributed within images, and 3) how images appear distorted by the topography, the result of analysis on these three categories is primarily described by each examined image. Each cave has its unique context such as location, formation, socio-cultural significance, and research context. Furthermore, depending on the circumstance (e.g. environmental difference in a location between the present and the Palaeolithic caused by erosional processes, excavation or other modifications of the cave interior), conditions for analysis needed to be amended. This sub-information will also be provided in advance of the actual analysis. Obtained data is treated statistically. At the end of each case study, I will also report the statistical results of each of the above data categories so that we can know whether or not there is a statistically noticeable imbalance, which supposedly reflects an intentional act of Palaeolithic humans.

In the final chapter, the results from each case study are united and re-examined in order to ascertain, describe and interpret the overall trends by each data category. At the same time, I will logically interpret any signs appearing in the statistical data and discuss the nature of wall-human interactions embedded in cave art (e.g. how

'deliberate' was their borrowing from cave topography? Can distinct cave assemblages be distinguished along topographic features, or were more general principles in use? Were any specific features prioritised, or was this essentially random?). Based on the theory of installation art and the results obtained, I will attempt to deduce a plausible hypothesis, regarding questions such as what did cave art mean/function to Palaeo-humans? Why did they produce such an enigmatic art? Given the multisensory experience within installation art and the generally-agreed view that images depicted in caves in some way represent the 'cosmology' of Upper Palaeolithic hunter-gatherers, the interpretation of 'cave art as installation art' will inevitably emphasise the experience of cosmology. Therefore, the hypothesis is as follows: unlike the 'inner trip' of supposed shamanic trances (Eliade 1964) and their possible (and untested) effect on art, participants literally enter into a scene of cosmological narrative with their multiple senses. In this way, I will explore the possibility of the hidden nature of cave art as an interactive art.

Chapter 1

A brief history of research into Upper Palaeolithic cave art

> "…So he walked on, but it was a long way. For he was in the main street of the village, and it did not lead to Castle Mount but merely passed close to it before turning aside, as if on purpose, and although it moved no further away from the castle, it came no closer either."
>
> (Franz Kafka. *The Castle.* p11)

The sentence above derives from the unfinished work of Franz Kafka, *The Castle.* In the story, K., the protagonist and a land surveyor, is hired by the county authority in the castle, fails to reach it despite his best attempts. Meanwhile, he is gradually involved in irrelevant events and ultimately loses his enthusiasm for his profession. He can see the castle over there but can never reach it. In a sense this is reminiscent of cave art research: paintings of still vivid quality are still visible on cave walls, but due to the absence of written documents or informants providing clues about the meaning of the art, its function and the reason for the production, we will never reach the truth about its specific meaning, assuming there is 'one' (Lewis-Williams 2002). As many scholars insist, archaeology is an academic discipline whose primary purpose is to reconstruct the most reliable figure of the past through examination of data, evidence, and context (Renfrew and Bahn 1991). However, due to the scarcity of evidence and the technical and methodological difficulties in assessing prehistoric symbolic systems, all approaches seem to fail to achieve a sufficient elucidation. Moreover, the definition of "reliable figure of the past" differs by the perspective from which one 'sees' cave art, causing an incompatibility between competing explanatory models. After all, what we need to accept is a cruel fact against our never-ending curiosity that the perfect theory cannot be constructed.

If so, *what are we doing* when we are researching Upper Palaeolithic cave art, some of the earliest known examples of human art? I will consider this here. I shall briefly review the history of cave art research, particularly in terms of interpretation and methodology. By so doing will illustrate issues in the topic that archaeologists have addressed. This chapter consists of two sections: The first section is to introduce interpretation models that have so far been proposed from the initial recognition of Palaeolitic art in the 1860s to the present; in the second part, I will examine the

methodological issues which repeatedly appeared in the mainstream explanatory theory during the last century, and how others have attempted to avoid them; to highlight these points is crucial for future researches to set a question properly. Absolute 'truth' is unreachable. However, disciplines that have contributed to the history of cave art research deserve to be praised as a great intellectual challenge. Especially, as we will learn, answering different questions allows us to accumulate knowledge about different aspects of cave art. Through this, at least, I believe a better understanding is possible.

1.1 Interpretation of cave art and its history

Cave (or parietal) art forms a major component of the 'art culture' of the European Upper Palaeolithic period, and to date forms one of the oldest traces of human artistic activity. It is widely accepted that after the Upper Palaeolithic- and its art – had begun before 40,000 cal BP, and lasted until its formal end with the Pleistocene-Holocene transition around 11,650 cal BP (Bahn and Vertut 1997, Pettitt 2014). The Upper Palaeolithic is often taken to have been part of behavioural modernity although is likely to be much older and more complex than thought until relatively recently; the recent confirmation of Neanderthals' painting behavour requires us to rethink the figure of the Pleistocene Europe (see Hoffmann et al. 2018). Behavioural modernity denotes greater technological divergence than its preceded periods had ever had (Bahn and Vertut 1997). Cave art is considered as one of the reflections of cultural advance that took place in this very era.

'Decorated' caves concentrate in Franco-Cantabria, quite an extensive area in prehistoric sense. Cave art comprises various subjects and techniques, such as naturalistically painted and engraved images of animals, geometric signs, hand stencils and prints, sculpture, finger flutings (doodling-like lines left by fingers on cave wall of soft clay) and, although relatively rare, anthropomorphic figures (Bahn and Vertut 1997, Clottes and Lewis-Williams 1998, Vialou 1998, White 2003). Animal images are often found in superimposition or apparently associated with depictions of other species or with geometric signs (Bahn and Vertut 1997, Clottes and Lewis-Williams 1998). Above all, despite taphonomic processes presumably destroying what was originally a rich heritage of art in the open air (Straus 1990), they are abundant in the deep interiors of caves (Pettitt 2016). This enigmatic setting of cave art is rarely seen in rock art cultures in other regions or periods, where art tends instead to be found in rockshelters (Clottes and Lewis-Williams 1998).

Over 150 years, archaeologists have studied cave art with the objective of providing a universal explanation for its symbolic meaning and function. This has produced a small number of 'umbrella theories' that purport to 'explain' the art as a monolithic whole. It is no surprise that such historical attempts have failed given the significantly long chronological period over which it developed. Figure 1.1 illustrates major interpretation types hitherto proposed to 'explain' cave art, and the intellectual and methodological background that justifies the theory. We can see the number of interpretative models increases over time, and they tend to parallel broader intellectual trends of the time. For instance, the 19th century was the era in which European supremacy refused to recognize intelligence and humanity among hunter-gathers. This extreme prejudice saw an improvement during the first half of the 20th century, first through an improved accumulation of ethnographic knowledge and then through the emergence of structuralist perspectives; subsequently, interpretations were then attempted by postmodernists and cognitive scientists from and after the 1980s. Accordingly, cave art, beyond being a fitting a subject for anthropology and archaeology, often serves resource for other intellectual disciplines. This trend is outstanding particularly today where cognitive and brain science confidently joins the research. Keeping this in mind, I will introduce the brief history of interpretation of cave art.

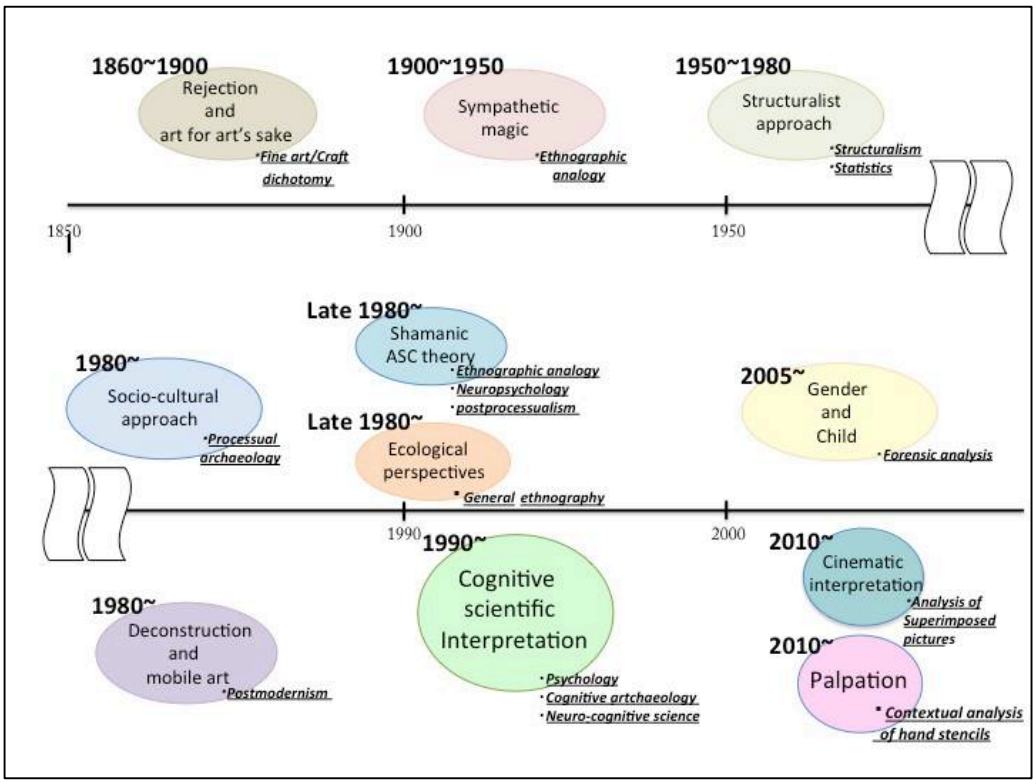

Figure 1.1: Proposed interpretations of Upper Palaeolithic cave art from the 1860s to the present. Each model has its own unique methodological/intellectual background which justifies the validity of the model.

1860~1980s

In the first phase of cave art research archaeologists were skeptical as to the authenticity of the few examples of cave art that were then known (Bahn and Vertut 1997, Lewis-Williams 2002). This was largely due to the dominant idea that denied Palaeolithic people a highly developed cognitive ability, at least enough to produce art (Clottes and Lewis Williams 1998, Palacio-Perez 2010). This attitude is particularly reflected in the reaction to the Altamira discovery of 1879: Because the discovered polychrome paintings in the cave apparently held aesthetic potency, archaeologists of that time dismissed this stunning parietal art as a fake, which denotes that it was not a topic worthy of consideration in the 19th century (Beltran 1998, Abadia 2006). At the start of the 20th century the situation changed; undeniable examples had now been discovered and researchers saw in the wealth of ethnographic information reaching them about 'primitive art' that 'sympathetic magic' explained the newly emerged canon of Palaeolithic art (Ucko and Rosenfeld 1967, Bahn and Vertut 1997; Lewis-Williams 2002). This theory, underpinned in particular by ethnography from Australia, attributed cave art to ceremonial magic activity such as one seen among culture of Australian hunter-gatherers with the goal of survival at its core (Reinach 1903), and had been in the paramount position in research for almost 50 years (Bahn and Vertut 1997; Lewis-Williams 2002; Palacio-Perez 2010). The early second half of the 20th saw the dominance of 'structuralist' approaches, which rejected sympathetic magic and ethnographic analogy. Instead, leading scholars of this time such as André Leroi-Gourhan (e.g. 1968 a, 1968 b, 1986) and Annette Laming-Emperaire (1959), under the structuralist ideology, treated cave art as a complicated symbolic system that allocated different symbolic significance to different images and different areas of the cave's interior, and the idea being that these would be visible to statistical survey (Leroi-Gourhan 1968 b, 1986).

1980s~1990s

From 1980 onwards, a number of interpretations were forwarded. With the growing influence of processualism in Palaeolithic archaeology, 'decorated' caves were interpreted as the backdrop to hunter-gatherer seasonal aggregation sites (Straus 1976, Conkey 1980, Bicho et al 2007). Aggregation is 'a collection of people present in a public setting' (Darvill 2002, 5). In hunter-gather context, this communal activity is accompanied with extensive ceremonial events which might have functioned both to ease territorial conflict between communities and to strengthen social ties (Gamble 1982, Jochim 1983 Straus 2009). Conkey (1980), for example, based upon the significance in the number and diversity of mobile art discovered in Altamira, argued that Altamira

was one of the most important aggregation sites for Upper Palaeolithic hunter-gatherers. Apart from this, 'postmodernism' had impact on archaeology in two ways: First, a deconstructive view encouraged archaeologists to spotlight the value of minorities; secondly, post-processualism saw the pursuit of individual agency in the past as an active participant in the meaning of archaeological symbols, both of which had been ignored by processual archaeology as unreachable. An example of the former is the revision of mobile art led by Margaret Conkey (e.g. 1987, 2001, 2010). To Conkey and others, 'cave art' constituted a misuse of the term "art" which lead archaeologists mistakenly to view this as an example of human magnificence while at the same time devalue portable art, despite the fact that the latter are often more informative about the embeddedness of art in the Upper Palaeolithic and quotidian activities (Conkey 1987, 2010). Also, the Shamanic ASC (Altered State of Consciousness) theory proposed by Lewis-Williams and colleagues is salient here (Lewis-Williams and Dawson 1988, Clottes and Lewis-Williams 1998, Lewis-Williams 2002). This theory highlighted the altered states of conscious of individual 'shamans' (In shamanic culture shaman is believed to possess a power to negotiate with supernatural existence and to cure members of community by entering 'trance') and attempted to ascribe the meaning/function of paintings to such individuals (Lewis-Williams and Dawson 1988). The theory stimulated strong and frank debate, to which I shall return later. In addition to the postmodern trend, interpretation from ecological perspectives was also proposed by Mithen (1988). This explanation concerned the general ecological knowledge necessary for food procurement activity of hunter-gatherers, and, illustrated how animal paintings in cave art could represent and transmit such knowledge. Mithen claimed this art culture was a trace of information transmission from generation to generation (1988), which followed a notion proposed by Pfeiffer (1982) that sees cave art was used for children's education.

1990s~

During the 1990's, interpretation of cave art relative to human cognitive capacity emerged, and researchers began to describe the cognitive states required to produce the art based upon evolutionary psychology, cognitive and neurological science, from the point of view that cave art was informative about the *origin* of art. While most of these approaches treat the images as evidence of the emergence of the 'cultural modernity' of our species (e.g. Helverson 1992, Humphrey 1998, Mithen 1999, Anderson 2013), Hodgson (e.g. 2000, 2003, 2006 , and 2008) discusses the mechanism of the production and possible functional advantage of art for survival, proposing his hypothesis as a counter-argument to the Altered States of Consciousness (ASC) theory. Mainstream

interpretations disappear from 2000 onwards, and attempts to establish a single universal law that explains cave art cease to exist. Instead, archaeologists sought other, more specific ways to view cave art or focused on specific types of images and suggested explanations limited to that specific art type. In the former case, Marc Azema (e.g. Azema 2008, 2015, and Azema and Rivere 2012) examined animal images in French caves based upon animal ethology and anatomy. Consequently, this ethological approach revealed that almost half of images known in French cave art were depicted in poses that represent certain actions, i.e. movement, and Azema proposed a hypothesis that cave art expressed specificially *interactions* between wild animals. Later, Pettitt et al. (2014) found that hand stencils are more likely to have been created on convex walls rather than flat, as if their creators 'palpated' the shape of the wall, and these researchers associated this result with the importance of the sense of touch in such dark environments. Azema and Rivere (2012) examined superimposed animal images, arguing that their production was aimed at obtaining the optical illusion of a motion picture. These recent approaches tend to emphasise the dynamic interaction between the human and the cave environment, which leads cave art research to a new and significant phase. Other attempts have been made to identify females and adolescents among Palaeolithic artists based on the forensic (i.e. morphometrical analysis of hand stencils and finger flutings, based on apparent metrical differences between male and female fingers (Sharpe and Van Gelder 2006, Snow 2006, Bednarik 2008, Van Gelder and Sharpe 2009).

1.2 Methodological Issues

Erroneous theories

Theories can be envisaged as a box with an entrance and an exit. If one inputs a particular phenomenon into the box, a particular result will emerge, the nature of which will depend upon the nature of the theory. In hard science the output can be a mathematical formula, and in social science it is an explicit explanatory text. Because the interpretation of cave art is an unquantifiable practice, art theory belongs to the latter.

A phenomenon and an output are mediated by a theory in equal proportion. In hard science, it is relatively easy to test the *accuracy* of a theory, since whether or not a phenomenon is properly reconstructed from a theoretically deduced explanation is *empirically falsifiable*. However, in archaeology, this procedure to prove the credibility of a theory is often difficult or impossible, due to the intangible nature of the past (Lewis-Williams 2002); those very phenomena that are to be explained are themselves abstract concepts, and are thus *unconfirmable*. For this reason, a theory explaining the past needs

rationale to justify its use: historically, ancestral spiritual cosmologies (such as the bible) served as this rationale (Trigger 1989). Processual archaeology therefore required ethnoarchaeological fieldwork as a tool to reinforce explanation (Ascher 1961, Binford 1967, Sabloff 2013); postprocessualism used theoretical deconstruction to deny 'modernistic' views of the past and focused, for example, on the value of minors (Hodder 1986, Bintliff 1991, Vanpool and Vanpool 1999). As a recent trend, cognitive approaches draw on evolutionary psychology and neuroscience in order to reveal evolutionary processes underlying our cognition, attributing our cognitive functions to evolutionary advantage (e.g., Orians and Heewagen 1992, Segal 1994, Mithen 1999, Hodgson 2003 and 2006). Thus, each broad paradigm employs its own methodology in order to secure and present the tenability of their authenticity of explanation, and as a scientific principle, the logic that composes a theory has to maintain consistency.

However, even this theory box does not necessarily always generate reliable results: if a phenomenon being input is untreatable within the intellectual framework which governs a theory, no result will be obtained; and if the theory contains internal errors in logic, the explanation will likely be incorrect. In cave art research the epitome of the former case is found in the rejection of archaeological authenticity of the earliest discovered examples of parietal art in the 19th century. At this time the views of hunter-gatherers were widely rejected as the prevailing view was that they were primitive and savage and did not have enough cognitive capacity to produce art (Clottes and Lewis Williams 1998, Palacio-Perez 2010). The discovery of portable art in several European caves, however, provoked a dilemma. Consequently, archaeologists at first tried to understand portable art, applying the theoretical dichotomy of fine and craft art (Abadia 2006); fine art is a concept that formed during and after enlightenment era, and denotes a praise of the authenticity of human imagination and creativity involving painting, sculpture, music and poetry. Craft art, by contrast, represents a dull reproduction of items of quotidian use, such as pottery, jewelry and embroidery (Woodmansee 1994, Shiner 2001 and Abadia 2006). However, in 1879, the discovery of paintings in Altamira Cave (Cantabria, Spain), which clearly display significant aesthetic potency, was far beyond the limit of intellectual framework of archaeologists at the time. It was therefore inevitable that they judged the parietal art to be fake, a work of a modern forger (Beltran 1998).

In this section I will consider the latter case where the procedure to prove the credibility of a theory is not straightforward. Although parietal art was a central problem for palaeolithic art research in the late 19th century, specialists in early 20th century began discussions with ethnographic knowledge as a crucial aid to interpretation. However, this practice at the same time generated persistent errors in the field. Two types of errors can be identified: an error in *the premise of* the *theory* and in

the way to *prove the validity* of theory. In the former case, the flaw in theory is attributed to a false scientific reasoning and misuse of ethnographic analogy. The other is found in the selection of suitable evidence of a hypothesis, and the subjectivity involved in interpretation, which is considered as a scientifically inappropriate procedure for the research. This section mainly focuses on this issue and on efforts that have been proposed in order to avoid the error. At first, it is necessary to discuss the sympathetic magic interpretation as it contains methodological issues that emerge in theories in the later period.

1.3 Sympathetic Magic: an origin of methodological issues

In the early 20th century, ethnography had come to form the essential intellectual reference for cave art research that would prevail for over half a century (Bahn and Vertut 1997; Lewis-Williams 2002; Palacio-Perez 2010). 'Ethnographic analogy' especially became a mainstream of methodology. Ethnographic records about certain hunter-gatherer groups would therefore form *examples* that would be used (directly) to *explain* Upper Palaeolithic art. "sympathetic magic" in particular, which could be observed in central Australia (Spencer and Gillen 1899, cited in Bahn and Vertut 1997: 171) was seen as a perfect explanatory model of cave art. This magical activity is based upon a belief which recognizes an identical or causal relationship between representing *images* and represented *subjects*; the purpose of this magic (usually referred to today as 'volt magic') is to cause effects on real life by depicting animals and interacting with those images. In this idea possession of an image of an animal, for example, can empower its holder with the attributive potency of the animal species (Bahn and Vertut 1997, Lewis-Williams 2002). This association also naturally leads to a causal relation of action: a certain action performed on a representation (such as striking a prey animal) may bring about a similar (caused) effect on the actual subject represented (e.g. power in the hunt).

Based on such perspectives, cave art came to be ascribed to three specific types of sympathetic magic: fertility, hunting, and destruction (Clottes and Lewis-Williams 1998). Fertility magic is performed in the light of an underlying desire for the fertility/fecundity (i.e. success) of resources critical for survival, i.e. prey animals. The rationale is that by depicting two images of same animal taxon, the creator aspired for abundant procreation of the species and thus avoided the dangers of starvation. With this interpretation, superimposed animal images could be interpreted as scenes of copulation, the very act of creation and a symbol of fertility. Hunting magic was practiced in order that real hunting will be successful through the magical injuring of the images with spears or arrows, or by depicting incomplete images that functioned-

by their incompleteness - to reduce the power of target animals. Destruction magic basically derived from the same idea but was applied to hostile (non-prey) animals such as bears and felines (Bahn and Vertut 1997, Lewis-Williams 2002) and, perhaps, other humans. With this view, deliberate damage of images was interpreted as evidence of deliberate attack, and in addition geometric symbols on animal images interpreted as tools for hunting; claviforms (club-shaped signs), for example, were seen as throwing spears, and tectiforms ('hut' shaped signs) were seen as traps (ibid.).

Thus, sympathetic magic, explaining the purpose, function, and symbolic meaning of cave art using ethnographic references, portrayed the dynamic nature of the past, and the explanatory model seems to have satisfied the great majority of archaeologists. Consequently, the approach enjoyed its main prosperity during the first half of the last century. However, researchers began having a skeptical attitude toward the scientific validity of the approach. The main reason for the doubt is attributed to the logical reasoning underlying the sympathetic magic approach. Supporters of the theory had a belief on the human in the past in this way: a) palaeolithic hunters were hunter-gatherers; b) recent hunter-gatherers practice magical rituals; c) therefore, palaeolithic hunters must have practiced such rituals. That is the basic archaeological reasoning underlying the sympathetic magic approach, and hence, in short, what supporters for the model did is essentially to seek the evidence to reinforce their arguments with the assistance of ethnographic analogy. Doubt was cast on the validity of their logic; particularly on the premise which supporters of the theory believed to validate the analogical use of the Australian recent ethnographic record onto the deep past of Palaeolithic art in Europe.

Issue 1: Misuse of ethnographic analogy

The fundamental issue relates to the false premise of the deductive reasoning deployed in this period. Over time it came to be thought that this model contained a critical error at its root; the misuse of the ethnographic analogy that formed the justification of a magical interpretation in the first place. In short, it came to be seen that Australian ethnography cannot be applied to Palaeolithic parietal art because not all observable hunter-gatherers can be shown to practice sympathetic magic; it cannot, therefore, be said to have been universal, and consequently cave art may have represented something completely different. The premise of sympathetic magic may simply be erroneous, therefore, and the argument is not deductively valid. Nevertheless, archaeologists continued to rely on ethnographic analogy. Usually, analogy possesses a value only when it is already understood that different analogized systems all followed the same law (Layton 1992). In this case, even if it cannot be

demonstrated that cave art did relate to sympathetic magic, supporters of this model would still deal with it as such; in other words, they used ethnographic analogy as an explanation, despite the fact that no evidence exists that European Palaeolithic groups and Late Holocene Austrarian Arunta groups shared an identical cultural system. Binford (1967) warned that such misuse of analogy would lead researchers to an intellectual dead-end, because when analogy is only *applied* to explanation, intellectual activities pursuing truth would be 'complete'. Overall, the sympathetic magic interpretation used analogy directly to provide answers, and as such could not develop intellectually or lead to further theories.

Issue 2: Selection of evidence

The error discussed above is an example of the error of the logical underpinning of the theory itself. Skepticism extended even to the way that archaeological explanation was undertaken by sympathetic magic theorists. Accordingly, two issues were drawn under a spotlight and then intensively discussed. One is associated with the nature of selection of pertinent evidence. As was mentioned earlier, cave art researchers in the first half of the 20th century, particularly the supporters of hunting magic, 'studied' animal images bearing apparent scars or geometric signs, and attributed them to hunting magic. The number of examples of cave art that are relevant here, however, is very low comparable to the widest known canon of cave art as a whole. For instance, the proportion of animal images depicted with geometric symbols is less than 15 percent (Clottes and Lewis-Williams 1998: according to White 2003 around 10 percent). This amount is too small to formulate any generalizations. Researchers, nevertheless, ignored this large gap and thus applied a miniscule amount of 'evidence' to a universal explanation of cave art. It is no surprise, therefore, that this interpretation was exposed to severe criticism.

Issue 3: Subjectivity in interpretation

The final issue is related to the subjective nature of the interpretation of images. With fertility magic, for example, one often cannot precisely establish the sex of specific animal depictions. One might subjectively define an image of a horse as male on some grounds, but on others it could be seen as female. How can one tell? Similarly, it is impossible for us to discern what sort of weapon a certain type of geometric sign might represent with regard to hunting magic, assuming it even does represent a weapon. Naturally, such subjective differences ruin the objectivity of research, which in turn can

be harmful for the integrity of archaeological research as a scientific discipline. An experiment conducted by Layton (1991) highlights this issue well. Three students were asked to copy a panel from Hornos de la Peña cave (Cantabria, Spain) of which Breuil (1911, cited in Layton 1991) also reproduced. The students had never seen Breuil's tracing before. Three types of light sources, a fat-fueled lamp (as close to the Palaeolithic condition as possible), an acetylene lamp (as close to Breuil's condition as possible) and an electric fluorescent light (aimed at an ideal condition to see the images) were used. Each student was instructed to reproduce the images under each lighting condition. The students' results (Figure 2a to 2c) were then compared to the drawings of Breuil – considered to be one of the finest recorders of cave art - (Figure 2d) and to a tracing (Figure 2e) which was drawn under electric light in a previous study and which, according to Layton, is the most unbiased. Consequently, it was demonstrated that no single reproduction is the same, even though the lighting condition is taken into consideration. This result illustrates a lack of objectivity even in the straightforward act of faithful reproduction, which weakens the credibility of evidence itself that this interpretation relies on.

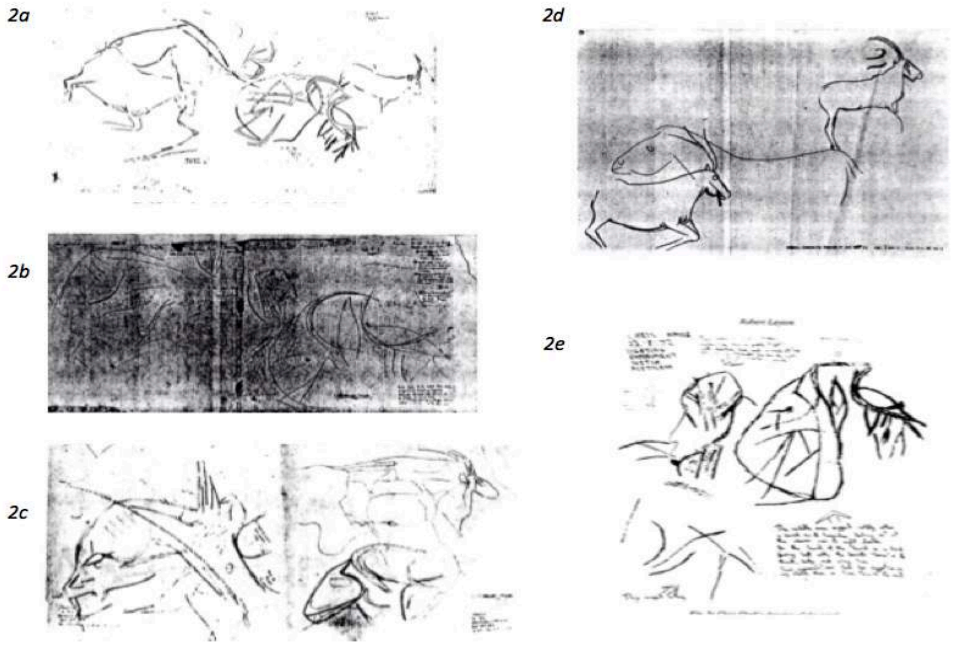

Figure 1.2a-e: Five different tracings of images on same panel in Hornos de la Pena cave (Layton 1991, 27-29). They well reflect the issue that evidence selected by one interpreter may differ considerably with another's view.

1.4 Treatment of these three issues and failure

Cave art research between the 1950~1990s essentially reflects the history of attempts by archaeologists to establish an effective interpretation that successfully overcame or avoided the problem of subjectivity. Sociocultural approaches (the explanation that saw decorated caves as the backdrop to aggregation sites) and deconstructive approaches (one emphasizing the cultural significance of portable art) did not deal with such issues, as their scope belongs to another dimension. The ecological perspective of Mithen (1988) drew on the universality of information gathering among all modern hunter-gathers, which could reasonably be seen to apply to the Upper Palaeolithic, but it actually does not *explain* cave art; instead it simply states that the art contains information about its subjects and may therefore have had some didactic use. Far more influential, however, were the structuralist perspectives (e.g. (Leroi-Gourhan 1968a, 1968b, 1986, and Laming-Emperaire 1959) and the ASC theory (e.g. Lewis-Williams and Dawson 1988, Lewis-Williams 2002) because of their outstanding interpretations of cave art inferred by their unique methodologies. Each approach had a special treatment to the issues of sympathetic magic and aimed to establish the universal explanation.

Structuralist perspectives

In the mid-twentieth century, the traditional ethnographic approaches had begun to stall, for the reasons discussed above. A new approach was introduced by archaeologists such as André Leroi-Gourhan (e.g. 1968a, 1968b, 1986) and Annette Laming-Emperaire (e.g. 1959). These were intellectually underpinned by structuralism, a fresh philosophical idea of the day, pioneered by Claude Levi-Straus, and dominant in Parisian academia (Layton 1992). They opened a new phase of understanding of Palaeolithic art. Leroi-Gourhan and Laming-Emperaire viewed cave art as complicated compositions (that is, comprised of many interrelated parts), comprising separate images which, far from being isolated, were created and *meaningfully linked* in formal relationships with other images. Thus all images within a certain decorated cave (or sanctuary to use Leroi-Gourhan's term) were meaningfully linked as a conceptual whole, and, so proponents argued, through the elucidation of such meanings and relationships, the concealed meaning of the art could be recaptured. Thus, scholars came to treat each decorated cave as a single work, containing different symbolic significance of different parts of the cave interior.

The major characteristics of this approach were a rejection of ethnographic analogy, and its replacement by statistical analysis. In this sense, structuralist approaches can be seen as an example of the processual approaches that were taking root more widely in archaeology. With such approaches, one could arguably maintain objectivity in research, emphasizing a scientific authenticity that previous interpretations had failed to achieve. It is perhaps no surprise that quantified and statistical approaches to the themes of cave art are still popular (e.g. Sauvet and Wlodarczyk 1992, 2008, Layton 2000, Sauvet et al. 2013, Pettitt et al. 2014). Leroi-Gourhan and Laming-Emperaire grounded their methodology in the statistical analysis of directly observed art, quantifying the number of images of each animal taxon, and the frequency of each taxa in the cave's 'set' as a whole. It was thus objectively revealed that horse and bison are the most predominantly depicted taxa (in the caves studied) and that it was likely that the two would be depicted together (Leroi-Gourhan 1968). By modern standards the number of caves which were used to establish this 'rule' were limited (66, in relation to >500 decorated caves known in Europe today), although its *general* conclusions were confirmed by an extensive study in Franco-Cantabrian caves much more recently (Sauvet and Wlodarczyk 2008). This is significant: it demonstrates that 'themes' in cave art were not simply random but followed strict (grammatical) rules.

Problems surfaced when Leroi-Gourhan and Laming-Emperaire attempted to explain the *symbolic meaning* of their data. Again, subjectivity in interpretation emerged. As structuralism assumes that meanings are understood in terms of binary opposition (e.g. darkness-light, death-life, and sun-moon: Lewis-Williams 2002), they applied binary structures to cave art, concluding that the underlying structure of meaning behind the artistic binary patterning related to the centrality of maleness-femaleness in Upper Palaeolithic society. As gendered human images were known to have been created Palaeolithic societies by this time (e.g. the Mid Upper Palaeolithic 'Venus' figurines – although it should be apparent that these should have no relevance for cave art of the Early or Late Upper Palaeolithic), they hypothesized that the male/female dichotomy should be reflected in parietal art. Following this they divided images into male or female, apparently on a purely arbitrary basis: if one cannot actually tell if a specific depiction is male or female, how can one ever hope to tell which broad faunal taxa 'represent' maleness and which femaleness? Leroi-Gourhan arbitrarily allocated horse to maleness and bison to femaleness, whereas Laming-Emperaire supposed that bison represented maleness and that horse was femaleness (Bahn and Vertut 1997, Lewis-Williams 2002). Sadly, such guesswork merely added a subjective gloss to an otherwise objective enterprise. It took us no nearer to understanding the mechanics of cave art.

ASC (Altered State of Consciousness) theory

As the structuralist paradigm gave way, Lewis-Williams and Dowson (1988) proposed that the creation of Upper Palaeolithic art related to altered states of consciousness and associated 'shamanistic' activity such as that seen among South African San and North American Coso. According to Bahn and Vertut (1997), shamanism is a type of belief system, in which (animal) spirits endow specific individuals with spiritual power, who then journey between this and other worlds to sort out their group's problems. In such beliefs certain animal species can be worshiped as 'helpers', and shamans (a Tungus word meaning 'raised (or enlightened) ones') directly utilize the power of these helpers to cure ills and solve problems through the medium of trance. Using examples from the last one or two centuries, Lewis-Williams and Dowson argued that Upper Palaeolithic cave art was a product of similar shamanic activity, since geometric signs were commonly depicted in the shamanic art of recent San and Coso and thus denoted a shared meaning with Palaeolithic art.

Key concepts of this theory are "entoptic phenomena" and the "ASC (Altered State of Consciousness)" experienced by shamans in trance. Entoptic Phenomena are created in the human optical nervous system and experienced as geometric shapes such as 'zigzags', 'grids', 'dots', 'spirals' and 'catenary curves' (ibid. 202). The authors argue that, due to their similar brains and neurological structure, palaeolithic individuals must have experienced the same entoptic phenomena, and thus 'seen the same figures' as present day humans do. According to Lewis-Williams and Dowson (1988) San

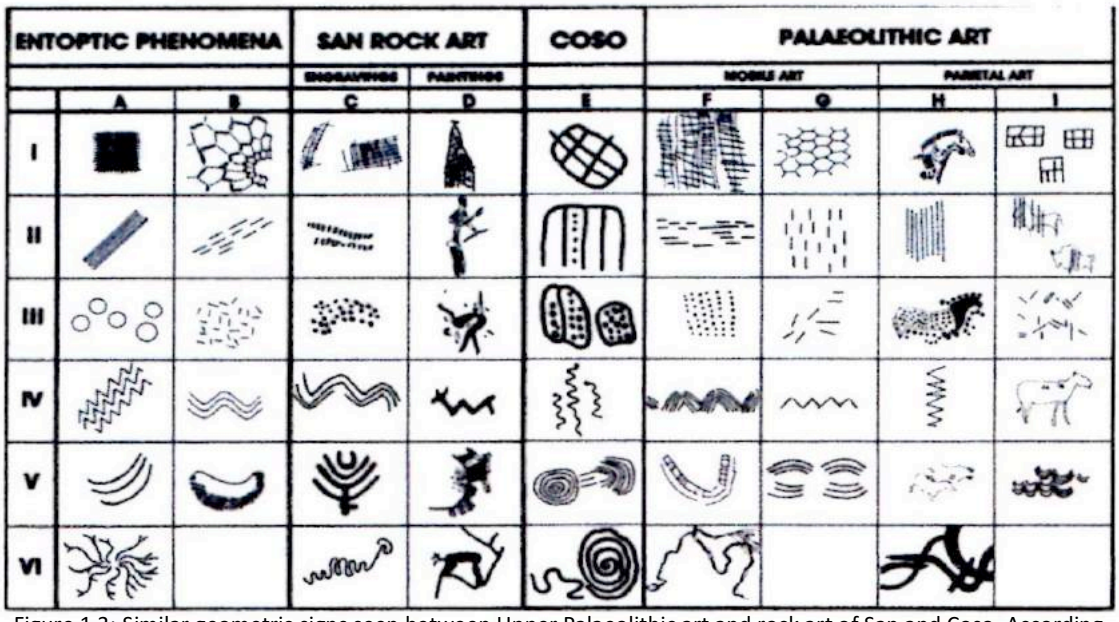

Figure 1.3: Similar geometric signs seen between Upper Palaeolithic art and rock art of San and Coso. According to Lewis-Williams and Dowson, this commonality is attributed to entoptic phenomena (Lewis-Williams and Dawson 1988, 206-207).

ethnography reveals that a shaman undergoes three phases of trance during ASC, through which the entoptic phenomena evolve from simple patterns to complex figures that latterly involve representational images of animals or humans. Based on this, the authors suggest that San and Coso rock art actually depicts this experience, and that this can be compared to Upper Palaeolithic art. Finally, they concluded that cave art is a product of shamanic culture due to the correspondence between images (*Figure* 1.3). ASC theory presupposes that such cultural characteristics will emerge in the art's contents, in other words, as structuralists assumed a hidden grammar underlies artistic expression, Lewis-Williams and Dawson expected that if two the cultural systems behind the art are identical, the contents will be also identical.

The conventional problems raised with sympathetic magic again also appear. They, under the unconfirmed hypothesis that Palaeolithic culture was attributable to shamanism (misuse of analogy), purposively select images suitable to their theory (selection of evidence), despite the criterion to judge the similarity between images is matter of subjectivity (subjective interpretation). In fact, they were well aware of these traditional issues. However, because Lewis-Williams and his colleagues wished to understand the "meaning" of art, ethnographic analogy was seen to be invaluable (Clottes and Lewis-Williams 1996). But for the analogy to maintain its value, it must be shown that the different systems examined in the analogy correspond to the same law. How can one do this objectively? For this reason, Lewis-Williams and Dowson relied on the neurological universality between Palaeolithic and modern minds as revealed by neuropsychological discoveries (Layton 1992). Such generalisations based on human anatomy cannot, however, explain the existence of rock art in non-shamanic cultures, or of the lack of rock art in shamanic ones (Bahn and Helvenston 2002); some non-shamanic hunter-gatherer societies simply do not report ASCs or shamanic beliefs, and thus cognitive universality does not necessarily equate with cultural universality. The rationale that the authors asked for securing the universality of theory was thus known to be dubious, and ASC theory, being exposed to a large number of criticisms, induced discussions which lasted throughout the 1990s.

1.5Methodology: From 1990s onwards

Most of the problems noted above relate to the ambition of archaeologists to pursue the meaning of cave art through the medium of ethnographic reference. As a reaction to this traditional attitude, later researchers directed their study to methods that did not deal with ethnography and broad 'meaning'. It has also been suggested that cave art may not have fallen into any categories of existing belief system reported

among hunter-gatherers (Layton 2000, Sauvet et al. 2009). Accordingly, treating cave art from ethnographical perspective itself has become doubtful (Pettitt 2016).

Under such circumstances, some researchers, unlike conventional studies which pursued a single universal explanation in particular cultural terms, reject this point, and instead demonstrate methodologically diversified attempts: one is to interpret cave art on an individual case-by-case approach (e.g. Sharpe and Van Gelder 2006, Azema and Rivere 2012, Pettitt et al 2014); one carefully set objective criterion to assess subjective matters (e.g. Azema 2006, 2008*);* meanwhile some treat cave art from unconventional perspectives (e.g. cognitive approach: Helverson 1992, Mithen 1999, Anderson 2013, Hodgson 2003, 2006, 2008). I will illustrate the methodological feature of each approach below.

Case-by-case study

Researchers for the former overcome the methodological issues noted above by looking at specific image types (superimposed images, hand-stencils or finger-flutings) and employing objective methodologies such as statistics, experimental replication, and forensic analysis, which bolster the plausibility of their approach. For example, Pettitt et al. (2014) statistically demonstrated the fact that hand-stencils were more likely located on concave and convex part of cave wall in El Castillo and La Garma caves (Spain) and associates this result with examination behaviour of the topography of cave wall by palaeolithic humans and with heightened sense of touch in a dark environment; Azema and Rivere (2012) associate 53 superimposed animal images in 12 French caves with successive drawings that produces modern technique of animation, visualising with films how they actually appear in motion; forensic analysis by Sharpe and Van Gelder (2006) involves experiments to obtain modern samples of the average length between index and ring finger by age and sex, and statistically apply the sampled data to a case (finger flutings) of upper Palaeolithic cave art. What is highlighted by these approaches are objectively confirmable facts which ethnographic analogy has failed to yield. Although explanations proposed by these approaches are only valid to the specific art type, they are not necessarily incompatible with each other. An argument whether some pictures appears as motion picture referrers to different dimensions from what Pettitt et al (2014) argue on hand-stencils. Meanwhile, Sharpe and Van Gelder (2006) are more interested in the question, *who were cave artists?* It is true these approaches do not reach a global explanation of cave art as one that previous mainstream studies aimed. However, as in archaeological discipline is generally believed that 'multiple lines of evidence improve an argument' (Fogeline 2007, 608), multi-dimensionality of facts proposed by each case-by-case study rather enriches our understanding.

Ethological approach

In the latter case, researchers depart from unique intellectual bases for cave art. One is the ethological approach led by Marc Azema, and the other is the neuro-cognitive approach. Regarding the question, *whether or not animal images are static?* Azema (e.g. 2006, 2008) attempts to read a message from postures of the animal figures. In this study he first collected ethological and anatomical data expressed by observing contemporary large mammals so that it can be used to define or express a certain action (e.g. bellowing trotting, eating etc.). Azema then applied the resulting data to 4634 animal figures (assessable figures were reduced to 3763). As a result, the study showed nearly half (41.1%)of total figures represent a specific action (although there is a slight fluctuation in percentages by a motif (in total 21 categories), almost half of the images for each motif are associated with an action). At the same time, because there is not a salient deviation in either chronological or regional distribution, it was also suggested that depicting animated images had been one of the prevailing concerns of upper Palaeolithic artists. Based upon these finds, Azema hypothesised that cave art had depicted eventual "interactions" between wild animals (such as seasonality of mating, migration and hunting by carnivores), and that the primary aim of cave art is narrative of such scenes. To assess actions by a specific posture of an animal image must involves a qualitative analysis, that means to some extent the assessment cannot be free from subjectivity as illustrated in issue 3. However, Azema carefully avoided falling into this previous failure. To reduce the potential methodological risk he adopted 'axes of reference' of (Azema 2008, 123) which are direct lines connecting starting points of the major animal movement (head, neck, shoulder, knee, hock, tail) and therefore representing the simplest body structure of the quadruped mammal; once setting a form by axes as a basic immobile (or neutral) posture, any deformations in the form based on the animal anatomical structure is understood as actions; therefore taking account of this as reference, assessing actions from postures of animal figures of cave art heightens its objectivity.

Neuro-cognitive approach

On the other hand, others regard cave art as a resource containing clues about human cognitive evolution, such as in the cognitive-neurological approach, where psychological and neurological evidence is applied to the examination of cave art, superseding ethnographic references. For instance, Helverson (1992), argued from the perspective of perceptual psychology that Palaeolithic humans first of all needed to

perceive and depict outlines of form correctly for further development of artistic skill and that is why in cave art images that comprise *contours* are abundant (approximately 90 per cent); Mithen (1999), discussing anthropomorphic figures, considered that in order to create an imaginative creature a cognitive passage where fictional and non-fictional thought can interchange was necessary, and insisted on the importance of linguistic development in the Upper Palaeolithic that facilitated this; Anderson (2013), describing a neural pathway activated by artistic activity, claimed that cave art holds significance for human cognitive development, interweaving vision, with language and emotional state.

The work of Hodgson (e.g. 2003, 2006, 2008) is noteworthy above all others, as he attempts to answer the traditional question about the production of art and its function. What Hodgson argues essentially relates to two things: geometric signs, and incomplete and superimposed animal images. In terms of the former, he proposes 'resonance theory' (Hodgson 2006: 32): In neuroscience it is generally agreed that the brain's primary visual cortex processes the most basic form of visual information (such as geometric shapes), but producing a large amount of geometric signs and seeing them could cause information overload within the brain area that induces an excitation as if one were exposed to an optical form of art (*Figure* 1.4). In this vein, Hodgson explains that further geometric figures were created *deliberately* in order to stimulate excitation. With the latter he suggests that the art production might have been a practice to enhance the ability to distinguish animal figures from the topography of the cave wall; being able to distinguish quickly the shape of prey animals would of course be essential for hunter-gatherer survival. For this interpretation, Hodgson borrows two principles from evolutionary psychology: that humans have evolved hunting animals (and thus through their evolution, animals have been strongly engaged with the human mind).

Figure 1.4*:* dots in cave art (left) and an example of contemporary optical art (right). Hodgson argues the reason for the production of the prehistoric signs is associated with an excitation induced by information overload within the primary visual cortex of the brain that processes the most basic form of visual information such as geometric shape.

Secondly, shapes or lines that resemble the contours of animals can function as "a sign of stimuli" and therefore cause "fixed action pattern" from humans; that is to say, the human mind will interpret (and identify) animal taxa from natural lines that resemble their outline, and respond accordingly. In this context, the human brain would therefore identify prey animals among the complicated topography of cave walls. Thus, the generation of cave images relates to the fundamental properties of the human brain. At this point, Hodgson, deliberately contrasts his work to Lewis-Williams's ASC theory which eagerly sought the way to apply ethnography to universal human neuronal principles but tried to secure universality at the expense of ethnographic aspects. Hodgson (2008) refined his theory based upon the cognitive principle and attempted to provide a more valid explanatory model that refers to emotional arousal and socio-cultural facts as well as evolutionary essentials. His aim concentrates on proposing a scientifically objective and reliable theory which can accommodate a broad range of issues rather than pursuing specific meaning of cave art (2006). Thus, the study by Hodgson deals with the brain as the absolute universal system that defines human action regardless of time and place, and proposed new interpretation while avoiding the dilemma that emerged from the use of ethnographic analogy and the issues accompanied with it.

Summary

In this way cave art study after the 1990s experienced significant diversification both in terms of the motivation for research and of the methodology deployed. Consequently, researchers concentrated their efforts on describing facts and probable interpretations only in cases where those facts could directly concern questions, rather than on unreachable meaning. Ethnographic analogy is no longer a central methodological concern among recent researchers of cave art. What is important is that current research enterprise essentially address different intellectual dimensions, and obtained facts are essentially compatible with each other. Such multi-dimensional facts can cope with the broad range of research questions, which in consequence leads us closer to the universal understanding of cave art, although these approaches cannot refer to cave art in the specifically cultural terms that concerned archaeologists for more than 80 years.

Conclusion

In over 150 years of research, Palaeolithic archaeologists have invested a great deal of effort (and passion) trying to reveal what cave art 'is'. Some have focus on its

symbolic meaning, while others have enquired about the reasons for its production. One could also address the function of cave art, or the question as to whether it conveyed any kind of an advantage to survival. Thus, researchers have introduced a number of interpretative models from widely different perspectives. Such efforts have not necessarily come to fruition, however, because of methodological limitations. I have highlighted in this paper what I believe to be the three key theoretical issues that limited research over the last century or more: the misuse of analogy, the subjective selection of evidence, and subjectivity in interpretation. These issues began to appear as early as the use of sympathetic magic, although partly, were perpetuated by the Structuralist approach, and fully revived in ASC theory.

Daniel (1950) mentioned that misuse of ethnographic analogy in archaeology was led by an uncontrollable aspiration for clarifying more concrete narratives than ones that we could even know from written records; it illustrates the dynamism of social change and values in society, at the expense of scientific rigour and authenticity. Because of this, researchers ignored problems and by so-doing came to establish complicated but ultimately erroneous theories. I have also covered recent methodological trends: whereas some archaeologists look into a specific image type, others carefully adopt a method to maximize scientific authenticity. Furthermore, approach to cave art from cognitive-evolutionally perspective became a substantial alternative to the conventional cave art sturdy. What is significant is that research no longer pursues ethnographic explanations in any cases; yet they still they make remarkable contributions to our understanding to cave art, providing new notions that any researchers in 20th century failed to see.

Our discipline will never reach a conclusion about the *specific nature or meaning of cave art,* due to the absence of written records or other informants which could directly tell us the truth. Specific studies are, however, elucidated in as objective grounds as possible, ways in which specific examples of art – specific caves, specific forms – functioned. Elements of decision-making can be established, all adding to a growing nuanced understanding of cave art's parameters. The aims and objectives of this thesis arise from such a concern with contextualizing methodological analysis of cave art. Looking back to the first point of its history - when the authenticity of cave art was rejected – the research community has come a long way. That, I believe, at least secures the value of cave art study. K. *cannot* reach the castle. Nevertheless, the story forms through events with villagers. They tell us little about the castle, but nevertheless, readers cannot stop turning the pages. Cave art study is something like this.

Chapter 2

Theory, and Methodology

> "And there were other rocks that were like animals, creeping, horrible animals, putting out their tongues, and others were like words that I could not say, and others like dead people lying on the grass. I went on among them, though they frightened me, and my heart was full of wicked songs that they put into it; and I wanted to make faces and twist myself about in the way they did, and I went on and on a long way till at last I liked the rocks, and they didn't frighten me any more"
>
> (Arthur Machen, *The white people)*

In the previous chapter, I reviewed the history of research into cave art. Since the official recognition of its authenticity in the 19th century, archaeologists have discussed topics such as the process of its production, its purpose, and the meaning behind cave art, mostly focusing on ethnographic and cognitive perspectives. Meanwhile, the environmental properties of the caves themselves have hardly been examined, given archaeologists' preference for the former, despite the fact that novel spatial conditions could potentially illustrate the reason why this art tradition was created specifically in caves. As Moyes et al. (2017) note, in existing studies, caves tend to be treated only as a passive medium for artists to draw pictures upon; such an attitude toward the cave's environment is found even in Lewis- Williams's shamanism theory. This situation has, however, been gradually changing from the 2000s, and a small number of researchers have considered the production process and ways to view cave art in relation to its environmental context. Studies by Hodgson (superimposed images: 2000, 2003, and 2006) and Pettitt (hand stencils: 2014) ultimately concern interactions between humans and the morphology of the wall in the dark conditions of the cave interior; Azema's 'cave-as-cinema' view (Azema and Revere 2012) demonstrates the possibility of a viewing *interaction* as viewers are able to cause an animation effect on superimposed images by changing the position of their light source and/or their viewing stance. The view on interactivity extends even further at a macro level: Pastoors and Weniger (2011) claim that the production of cave art required organizational involvement of the community, based on the visibility range obtained by a candle-sized light source, and based on investigation of spatial management in three caves (Bedeilhac, Fontanet, and Le Portel, all in France). All these studies suggest that the unique environment of caves is far from irrelevant or incidental to the artistic activity, and

highlight the site-specific and interactive nature of cave art. They form the rationale of a new interpretative era, in which the objectives of this thesis are firmly set.

In my master's thesis (Sakamoto 2014), I explored such an interactivity from the perspective of *affordance theory* introduced by Gibson (1979) and *installation art* which is an expression format in contemporary art. 'Affordance' is an idea that any possible actions an animal can take in an environment are actually defined by its environmental features and by the physical-cognitive capacity of an animal species (e.g. if there is a bridge across a river, one can walk on the bridge; if not, one has to walk or swim across). From the perspective of affordance theory, caves cannot simply be passive natural cavities but active agents governing human physical-cognitive conditions (Moyes et al. 2017). In this sense, human 'action' blurs into human-cave 'interactions'. On the other hand, installation art governs an artistic environment which consists of novel multisensory stimuli so as to enhance viewers' bodily engagement with it (Bishop 2005). As the artwork itself forms the surrounding environment, viewers (i.e. those individuals who are installed in it) are actively allowed to interact with its environmental components. In spite of the similarity between the concepts of affordance and installation art, they do not share the same intellectual origin; Gibson proposed the affordance theory from the academic context of visual perception (Gibson 1979), while installation art developed alongside the postmodern artistic movement (Ran 2012). Both approaches share a critical assumption, however: that the environment and human individuals form an unseparable, singular unit. This concept is significantly useful for the study of cave art, providing as it does a framework for addressing the site-specificity of a particular cave environment. The notion of installation art in particular offers us crucial insights on cave art since examples of modern installation artwork can been treated as anaologous to cave art in terms of interaction.

Based on these key concepts, I argued that caves' spatial constrains can induce multisensorial responses from viewers both at the physical and cognitive level, and such bodily engagements were involved in producing and viewing the art, i.e. interacting with it. I also classified various interactions reported by previous researchers along two different phases (human-cave interaction and human-artwork interaction). Human-cave interaction denotes the basic interactivity between a human and the cave's environmental properties, which is the pre-condition for any activities of humans in caves including image-making. On the other hand, human-artwork interactions mean interactive relations between humans and images which are mediated by spatial factors. Based on those arguments, I concluded that cave art was indeed highly site specific and interactive; put it into another way, cave art eventually functions as installation art. Therefore, its essence would never be understood without considering such site-specific interactions.

This is how the idea of "cave art as installation art" originated. Before explaining the details of the methodology of data collection and analysis, I would like to briefly describe the idea of cave-installation art in order to portray the overall picture of this research.

2.1 What is installation art?

Installation art is a format of expression in contemporary art which developed with the postmodernism movement (Ran 2012). In this discipline, artists construct a unique environment which viewers can explore. The central feature of installation art is to force viewers to *interact* with an artistically constructed space; while conventional fine art requires audiences to be a passive recipient of visual information transmitted from artworks such as paintings and sculptures, installation art rejects such a one-way relationship (Reiss 1999, Bishop 2005). Precisely, as Bishop (2005, 6) expresses, installation art presupposes an *embodied* viewer whose sense of touch, smell and sound are as heightened as their sense of vision.' For this purpose, artists aim to establish an environment full of elements that may enhance one's multi-sensory experience, and, importantly, in order to experience an installation work, viewers need to physically walk into it, i.e. become installed within it (Reiss 1999). This is the most salient contrast to conventional art, wherein one walks around paintings or statues admiring them visually. Once a viewer enters into a work, however, he/she is no longer a passive recipient/consumer of the art, but becomes an active participant: the viewer becomes a part of the art itself. In short, installation art comprises novel multisensory-environments which change viewers into explorers by forcing them to interact with their special components; artists carefully incorporate these components so that they effectively 'afford' viewers specific actions/experience. In addition, installation art does not allow any single point to dominate the view of the entire space, or a single viewpoint within the environment. Because of this, a viewpoint is never fixed, but instead constantly assumes different characters(Ibid.). Thus, multiple viewpoints in combination with multisensory experience highlight the temporality and ephemerality of installation art.

Although a significant number of installation art works has been produced, elements that enhance interaction and one's multisensory experience are simple and easily describable. In *Installation art,* considered to be one of the most comprehensive guides for this art format today, Claire Bishop (2005) analyses the nature of installation art. According to Bishop, the elements to engage audiences with installation art are as follows:

- Setting a novel scene in which audiences should find their own presence anomalous (e.g. *Pyramid* by Paul Thek, figure 2.1a: Ibid, 30);

- Building a unique topographic feature which forces audiences into using full-body movement (e.g. *Walking in Venus Blue Cave* by Ernest Neto, figure 2.1b: Ibid, 65);

- Manipulating illumination or auditory setting in order to heighten one's sense of immersion (e.g. *Dhatu 2009* by James Turrell, figure 2.1c: Ibid, 85); and

- Attaching devices with which audiences can creatively interact in the environment (e.g. *Words* by Allan Kaprow, figure 2.1d: Ibid, 24).

Installation art is therefore defined by the interaction of these four components, and environments with any of these features can be defined as installation art. In this thesis, these interactive categories will be concisely treated as Novel scene, Bodily engagement, Immersion, and Creative interaction.

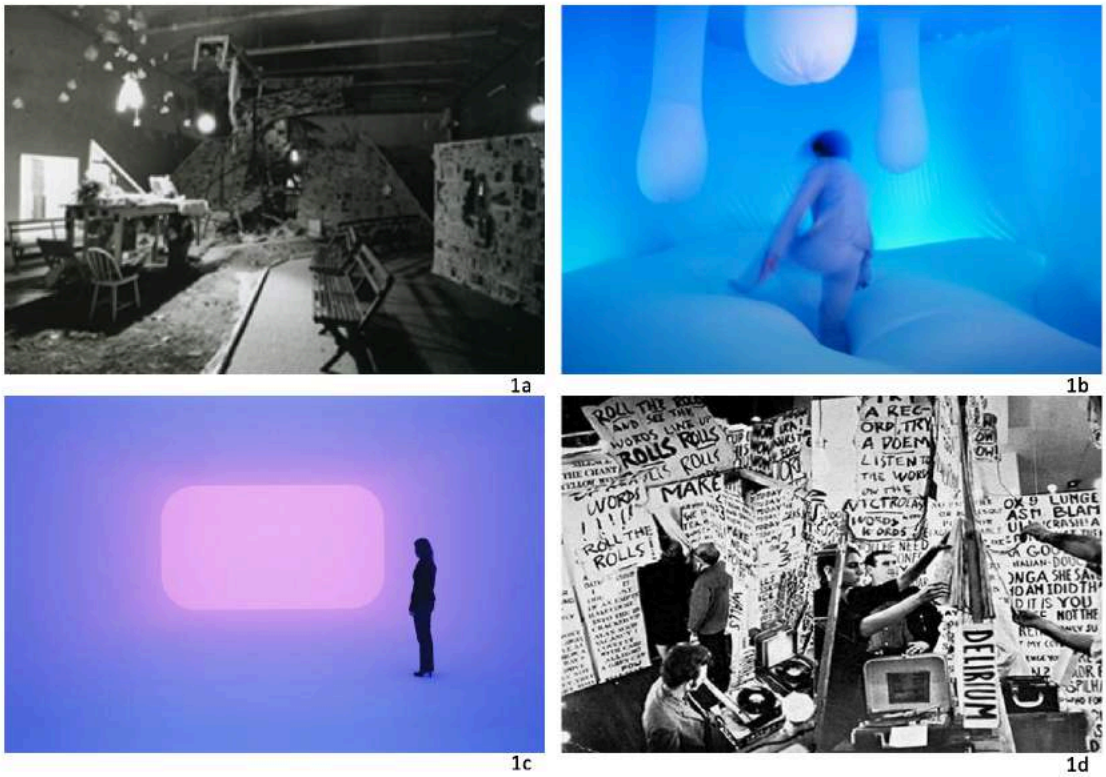

Figure 2.1a-d: Examples of installation art by type. 1a (top left) is Paul Thek's work in 1971, Pyramid/A Work in Progress. By constructing a novel scene, audiences enter into a surreal environment where they could find an anomalous presence of themselves. 1b (top right) is Walking in Venus Blue Cave by Ernest Neto (2001). This work is built with a unique topographic feature which encourages a full-body interaction. 1c (bottom left) is Dhatu by James Turrell (2009). Audiences experience a sense of immersion in dimly lit space. 1d (bottom right) is Allan Kaprow's work (1962), Words. As viewers are allowed to write any words on provided papers and put them on the wall in the room, they can creatively interact with the work.

2.2 Installation art: theoretical application for cave art

Human-cave interaction

Based on the definition and engaging elements described above, I discussed the plausibility of using installation-art perspectives for understanding Palaeolithic cave art (Sakamoto 2014). Although there are also interactivities which the visual content of cave art itself offers, the interactive relation between humans and caves is a precondition of any activities. Various spatial properties of caves have a significant impact both on human physical and cognitive state. Basic environmental features of caves that are compatible with those of installation works are as follows: Topography, visual and auditory conditions. These components can fall into the categories of Novel scene, Bodily engagement, and Immersion. Below is a brief summary of one's basic actions and cognitive condition through interaction with caves.

- Mirror-like environment (Novel scene): a visual effect of flowstones (stalagmites and stalactites) and water pools.

The very nature of the physical environment of caves is outstanding: the presence of pooled water which reflects the cave ceiling, and numerous stalagmites (growing up) and stalactites (growing down) creates a unique, unusual environment where everything can appear upside down (Till 2014). The illusory effect could further be exaggerated with the reflection of those calcite flowstones on still pools of water

2a 2b

Figure 2.2ab: Mirror-like environment of caves and installation works. 2a (left) is inside of Chauvet cave. Numerous stalactites and stalagmites can easily create the illusion that everything appears upside down and disorientate one's sense of balance. 2b (right) is Ubiquitous Site, Ryoanji in Nagi, Japan, by Arakawa and Gins (1994). The mirror-like-environment easily hampers visitors' spatial orientation.

(Figure 2.2a). According to Keane (2013) such a mirror-like-environment easily hampers visitors' spatial orientation (example work; *Ryoanji in Nagi* by Shusaku Arakawa and Madeline Gins: Ibid., *figure 2.2b*); accordingly, visitors in caves can also lose the sense of their proper positioning, i.e. can become disorientated. In quotidian life in the Upper Palaeolithic such disorienting upside down architectures did not exist; the cave environment, by contrast, must have strongly drawn attention from their explorers and stimulated questions such as *where am I*? or *where is here?* Particularly in low light.

• Unique topography (Bodily engagement): unusual use of body

As many researchers have argued (e.g. White 2003, Pettitt et al. 2014), navigating inside caves is not an easy task, and even shallow caves could present difficulties or dangers due to their slippery, unpredictable topography. Even speleologists with modern equipment can, and, do die in caves (Waltham 2014). An explorer needs to pay constant attention to such undulating floors and walls in order to navigate properly, and an unusual use of the body is often required so as to keep one's balance. Such a condition naturally heightens one's awareness of the surrounding to avoid any accidents and injuries. As the shape of the cave wall unpredictably alters inward and outward, space can occasionally become so narrow that visitors must twist their body, stooping, extending, crawling or climbing in order to progress (Pastoors and Weniger 2011). As reported by Bacci and Pavani (2014), such actions generally cause dizziness in space (e.g. *Sequence* by Richard Serra: ibid, Figure 2.3*).* Thus, humans are embodied and installed into the environment by an 'overall multisensory-motor experience' (Bacci and Pavani 2014: 26).

Figure 2.3: A sculptural installation work, 'Sequence' by Richard Serra in 2006. This work also challenges the ordinary body use of participants.

- Visual condition (Immersive): darkness, light, and heightened non-visual senses

In deep caves, permanent darkness envelops everything. As long as this is the primary condition of a cave's environment, human actions are governed by darkness, and therefore the use of artificial light sources is essential to obtain visibility (Moyes 2012, Pettitt et al. 2017). Unlike modern electric lighting, however, the light sources available during the Upper Palaeolithic was stone lamps or torches fueled by animal fat (de Beaune 1987), which provided only candle size illumination (Delluc and Delluc 2009). With such a limited illumination, the visible area around the light source is profoundly limited (approximately ~4 m diameter: Pastoors and Weniger 2011). As stated in the report of an installation project, *Storr* by Nacionale Vite Actia (Morris 2011), in such a place with low visibility, one's sense of hearing, texture, and olfaction are noticeably heightened, substituting for reduced visual sense. Consequently, one's awareness became so sensitive that one responds even to the softest of noises, the smallest feeling of touch and subtlest odour. Accordingly, one cannot help being extremely 'attentive' (ibid, 322). This super-attentive mode maximises the chances to identify dangers or opportunities correctly (Aglioti and Pazzaglia 2010, Levent and Pacual-Leone 2013).

- Auditory condition (Immersive): cognitive state and possible action in silence

Deep caves are in most cases profoundly silent places. In such acoustic conditions, even very low levels of sound become accentuated, such as footsteps and the sound of dripping water (Till 2014). Human auditory sense naturally become sensitive to the sounds, especially those which are not made by themselves, resulting in a further, deepened awareness of surroundings. At the same time, one could hear the sound of own heartbeat in such a total silence (Sontag 1969), which leads to an augmentation of self-awareness. Apart from silence, once a certain level of sound is made, the strong acoustic resonance of caves considerably exaggerates noise. Reznikoff (e.g. 1995, 2008, and 2014) suggests that Upper Palaeolithic cave visitors must have utilized the resonance to measure distance as part of their exploration: since the interior of a cave is entirely dark one could use resonance and their voice (particularly a *mm* or *um* sound) as a form of sonar navigation (this sonar navigation is known as echolocation: see Arnott and Alain 2013, 98).

Summary

To sum up, caves are filled with multisensory-novel properties and anyone staying in the environment is constantly exposed to such unusual stimuli. As a result, we have to physically respond to them using various novel actions (e.g. unusual body use, light use, and echolocation), and simultaneously the mode of our cognition is altered into another mode which is called by Moyes et al. (2017) "alternative mental states of reality" or, in short, "alternative reality" (Sakamoto 2014, 83). From the point of affordance, these actions and cognitive alteration are considered as reactions to the environmental constraints of caves, and therefore humans and caves are interactive. Given this point, we are no longer able to treat caves as only a passive medium. This nature is compatible with the definition of installation art; or more directly, caves themselves eventually function as installation art. Thus, caves inevitably enhance interactions, providing with site-specific multisensory experience, and importantly, this environmental setting was the absolute condition for Palaeolithic humans either to produce or view cave art.

Human-cave-art interaction

As was mentioned in the introduction, a growing number of researches dealing with interactivity about cave art has been published since 2000 onwards (e.g. Groenen 2000, Hodgson 2000, 2003, 2006, Azema and Rivere 2012, Petiitt et al. 2014, Petiitt 2016, and Pettitt et al. 2017). In these publications the description of a correlation between human and art mediated by environmental condition is universally clear. From the point of the theory of installation art, interactive relations documented in previous studies mainly fall into the creative interaction type, where participants can cause a direct influence on artworks, while some elements of images can install humans into the space by altering their awareness of images and by encouraging them to take a specific viewing action. I will now describe a brief summary of human-cave art interaction.

- Seeking (Creative interaction)

As a widely known fact, Palaeolithic artists utilized the configuration of the cave wall as part of their created compositions, typically reading (=identifying) the cave's topography as part of an animal's figure and subsequently embellishing the figure from this starting point (e.g. Bahn and Vertut 1997, Lewis-Williams 2002, Hodgson 2003, 2006, Pettitt 2016: see example Figure 2.4). Imagining a particular (animal) image in irrelevant natural features is known as "apophenia" in psychology, although as

Figure 2.4: Bison in Bernifal cave, Dordogne, France. Topographic features of a wide area of cave wall are integrated into the single figure.

noted in chapter 1, Hodgson (2003) refers to this as "sign stimuli" and "fixed action pattern". The precise definition of this phenomenon is "the experience of seeing meaningful patterns or connections in random data" (Petchkovsky 2008, 247): certain forms of cloud, for example, can be interpreted as a figure of Jesus Christ; or we could incorrectly perceive mountains on Mars as a human face (Figure 2.5). Due to apophenia, the natural configuration of cave wall can appear as animal figures. Based on this idea, Hodgson concluded that the evolutionarily advantageous ability to distinguish a real animal figure from its background as quickly as possible provided Palaeolithic hunters with a cognitive predisposition for interpreting natural shapes as the animals on which they were dependent for survival, and hence the opportunity in caves to 'trip' this ability. Thus, in Hodgson's view, images partly integrated with the cave wall represent the interaction that came about out of this cognitive feature. Moreover, there is a number of incomplete, superimposed, or difficult-to-distinguish outlines of animal in cave art. Given his theory, distinguishing such an unclear animal form from the other numerous animal-like shapes on the wall is also considered to be interaction.

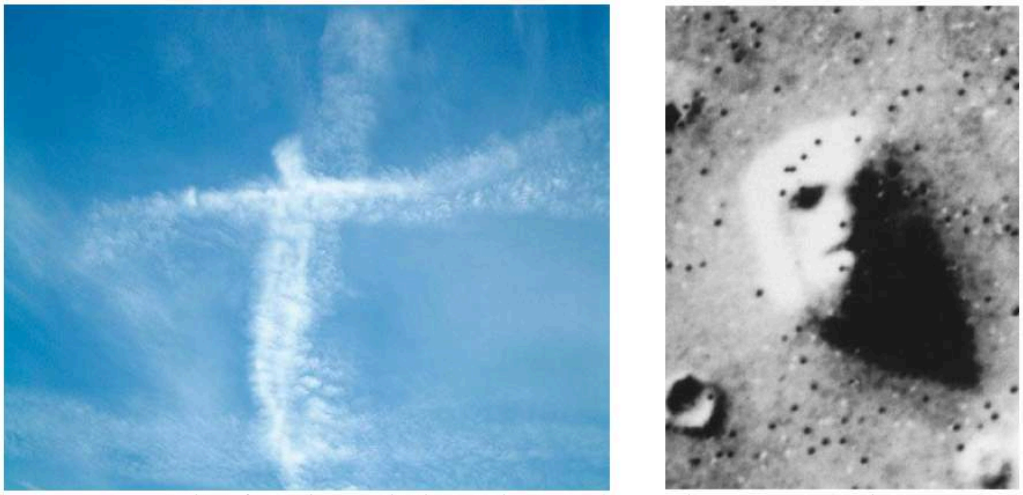

Figure 2.5: Examples of apophenia. The human brain tends to make an association between an ambiguous visual stimulus and a familiar thing. For example, we can see a figure of crucified Jesus in the cloud (left) or a face on the surface of Mars (right).

• Light-shadow interaction (Creative interaction and Bodily engagement)

Using light and shadow is considered as one of the most engaging methods of viewer participation in installation art (Steinkamp 2009 and Jacucci et al. 2009). In caves, artificial lights were not only critical to safe navigation, but also had the advantage of mobility: one can move the position of stone lamps or torches and hence control the direction of light and shadow. This simple principle enables viewers to manipulate the appearance of artworks by changing the position of the light (Wachtel 1993, Ramos et al. 1999, and Azema and Rivere 2012). For instance, a bison in Niaux whose dorsal line corresponds a natural ridge will disappear once it is projected by light from the right (Figure 2.6a); and an ibex in Pair-non-Pair with two heads facing different direction respectively (Figure 2.6b) and five superimposed horses in La Marche (Figure 2.6c) will appear animated when one alternately casts shadows on a part of their superimpositions by a moving light source (Azema and Rivere 2012). Thus, the use of artificial light - more importantly simulating its effects - provides us with a crucial clue about participation in cave art.

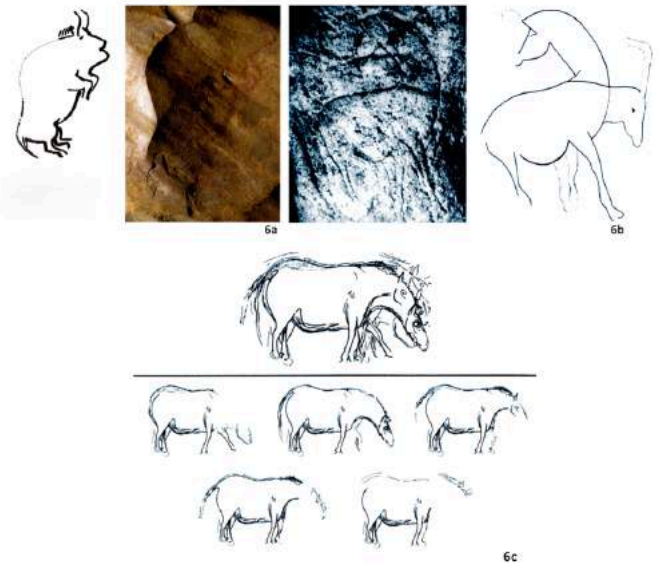

Figure 2.6a-c: Examples of shadow-light interaction. 2.6a (top left) is an image of bison in the Salon Noir at Niaux, France. The topography of the wall forms its dorsal line, and the shadow recreates the volume of bison. It is imaginable that the image would be harder to be seen once the shadow vanishes by changing a position of the light. 2.6b (top right) is an image of an ibex with two heads from Pair-non-Pair cave, Dordogne, France. As the position of the light is changed, the ibex seems to shift gradually from a head-down to head-up position. 2.6c (bottom left) illustrates the movement of a horse: five superimposed horses in different postures in La Marche cave, Dordogne, France. The fluid motion of which increases under the moving light.

• Viewing action (Bodily engagement)

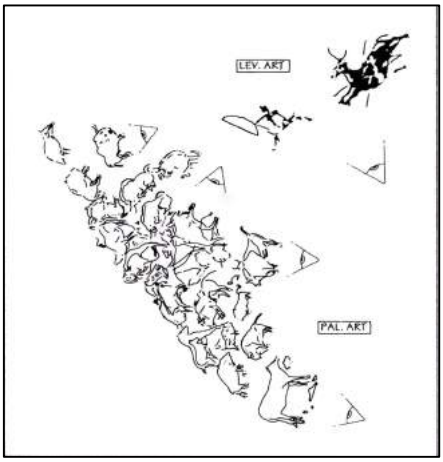

Figure 2.7: Single static viewpoint in Spanish Levantine art and plural viewpoints in Upper Palaeolithic cave art. Due to the existence of multiple horizontal axes in this single panel of the cave art, viewers are required to change their viewing position.

It is well known that images are often found in places which are not easily accessible (Pettitt 2016). In such situations one cannot view artworks simply by passively standing as one would in a modern art gallery; instead, particular viewing actions are required, such as twisting the body, climbing, and crouching down (ibid.). In a unique case, a decorated panel contains multiple viewpoints, which also prompt viewer's participation. According to Boado and Romero (1993), as for the case of the ceiling of polychrome chamber in Altamira, where images are composed in multiple horizontal lines, viewers can choose a viewing point based on each horizontal line by looking up and rotating their body (Figure2.7). Panels in similar composition are found in both Northern Spain (e.g. a horse and a deer in Las Monedas) and France (a horse and three bulls in Lascaux). Accordingly, cave art can afford specific ways of bodily engagement by virtue of its location and composition. In addition to this, anamorphosed images cause further viewing action. Anamorphosis refers to a deliberately distorted image which appears in a proper proportion only once seen from a specific viewpoint (Topper 2000). As will be discussed in detail later, anamorphosed images in cave art (e.g. Figure 2.8a) have been reported by archaeologists (e.g. Groenen 2000, Clottes 2005 and Aujoulat 2005). I illustrated an optical mechanism of anamorphosis in cave art (Sakamoto 2014: Figure 2.8b). A distorted image is depicted on the three-dimensional surface of a cave wall (the curve A-B). But an image in proper proportion must be perceived on an imaginary flat surface (straight line A-B). So an anamorphic image will appear to 'float' over the surrounding topography of the wall. At the same time, the images can seem to be gradually assimilated into the cave wall by changing the viewer's position; in other words, the proportion of images collapse as viewers move. This ever-changing proportion by taking different viewpoints is also considered possible interaction.

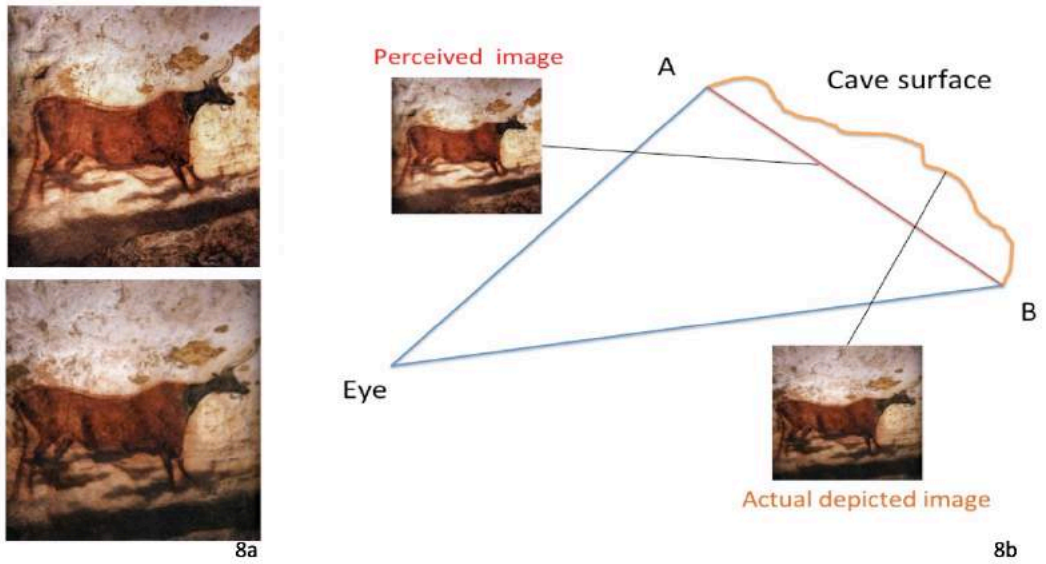

Figure 2.8ab: An example of anamorphic image and the mechanism. 8a shows a red cow with a black head in Lascaux cave, Dordogne, France. The red cow is depicted on a complex shaped high wall, but the image keeps perfect proportion and appears realistic when it is looked up to from a lower position (above). However, once the picture is viewed from the same height, the proportion is disturbed (bottom). 8b illustrates the optical mechanism of anamorphosis in cave art. Although an actual image in distortion is depicted on the cave surface A-B, the anamorphic image with proper form is seen on the imaginary surface of A-B. Therefore, images will appear to float over the surrounding topography of the wall.

- Image size (Novel scene and Immersive)

Large images are often characteristic of cave art (e.g. a bear in Chauvet: 120 cm long; a horse in Niaux: 147 cm; a female bison in Altamira: 164cm; the great black bull in Lascaux: 371 cm; and the two horses of Pech-Merle cave: 400cm). The cave space into which such large images (occasionally larger than the real size of animals) are installed, naturally transforms them into further enigmatic scenes. Furthermore, a large visual stimulus holds a strong capacity to engage between viewers and the space of concern; a larger stimulus is perceived "nearer" than a smaller stimulus, causing arousal from viewers (see Codispoti and De Cesarei 2007). In the low visibility of the cave environment the visual impact of large images on our attention is inevitably significant. Accordingly, large images could also play a major role in the installation of viewers into the environment.

Summary

Given all these interactive aspects, assuming cave art functioned exclusively as one-dimensional visual information seems misleading. The artistic significance of a cave art is far more complex and dynamic than what specialists have previously thought. Crucially, we must remember that the basic multisensorial experience of cave

environment itself is also added to human-art interaction. Novel spatial elements and artistic interactions were accumulated and interconnected with each other, composing the overall interactive nature of cave-installation art. For this reason, the significance of caves as places for art is highlighted. Meanwhile, interactions such as seeking, viewing action, and image size are not necessarily site-specific, because what causes these interactivities are not exclusively found in a cave's environment; in contrast, the light-shadow interaction requires the use of the light source in the cave, and therefore the cave environment directly matters. This point must be considered, regarding other environmental conditions. The morphology of the wall, which enables the seeking and viewing actions, can be found elsewhere, i.e. in rockshelters and open-air sites (valley sites); and large surfaces which can accommodate large images abundantly exist widely in the landscape. However, taking account of the other environmental properties and accompanied responses of humans to all of these properties, any interactions will transform to be site-specific; these activities are performed in already-site-specific condition as I will describe later. All interactive aspects described in both cave-human and art-human relations are listed in Table 2.1.

The environmental conditions of caves are diverse, and each of them do not exist alone. They are interwoven in complicated ways and thus imbue caves with various action possibilities. Taking account of affordances and installation art, we must keep in mind that image-making is one of these entire action possibilities and therefore that images left in caves are but one of the entire aspects of cave-installation art. It is well known that Palaeolithic humans performed diverse activities in decorated caves (Medina-Alcaide et al. 2018). They left burn marks on the cave wall and rock fragments (e.g. Clottes et al. 2005, Ferrier et al. 2014, Medina-Alcaide and Zapata 2015), created indentation marks by their own body parts (Duday and Garcia 1983, Clottes 1983, Clottes et al. 1984), rearranged the geomorphology and built structures (e.g. Arias 2009, Delannoy et al 2012), and left raw materials and bones in fissures and other niches (e.g. Garate et al. 2012, Groenen and Paillet 2014). Although the purpose and meaning of these activities remain unknown, they were afforded by caves' rich environmental novelties. Some may be attributed to ritualistic activity, while others could have been left by chance. In any case, since actors can potentially take various approaches to a single environmental feature (Costall 2006), possible actions can be diverse. In the process of diversification, actors must perceive a new possibility of action only by learning the nature of the medium (Lahlou 2008); and learning is achieved through the exploration of, and interaction with, a specific medium (Alland 1983). These activities testify to the interaction and exploration of caves as media by Palaeolithic humans. These activities were probably enculturated through time, provided specific meanings and interconnected with each other. Image-making was presumably part of such an

Installtion art type	Elements of human-cave interaction	Elements of Human-cave art interaction
Novel scene	• Stalagmites and stalactites make caves as a mirror-like environment (spatial disorientation: Till 2014).	• Image size (arousal: Sakamoto 2014)
Bodily engagement	• Topography of cave floor, wall, and ceiling (crawling, twisting, bending, keeping a balance: White 2003, Pettitt et al. 2014; dizziness: Bacci and Pavani 2014)	• Viewing action (changing viewpoints: Boado and Romero 1993, Sakamoto 2014) • Use of light source (the manipulation of the appearance of images: Wachtel 1993, Azema and Rivere 2012; casting shadows: Groenen 2000)
Immersive	• Darkness (heightened non-visual senses: Morris 2011; use of light source: Groenen 2000, Pettitt et al. in press) • Silence and acoustic resonance (Enhanced awareness of self, and others: Sakamoto 2014; echolocation: Reznikoff 1995, 2008)	• Image size (arousal: Sakamoto 2014)
Creative interaction	• Seeking (distinguishing animal figures from the topography of cave wall: Hodgson 2003, 2006)	• Seeking (distinguishing animal figures from the topography of cave wall: Hodgson 2003, 2006) • Use of light source (the manipulation of the appearance of images: Wachtel 1993, Azema and Rivere 2012; casting shadows: Groenen 2000,)

Table 2.1: Types of installation art and causes of interactions in cave art. Installation art is roughly categorised into four types: Novel scene, Bodily engagement, Immersive, and Creative interaction. This typology is applicable to cave art as environmental elements cause a unique interaction.

enculturation. Cave art was produced in this complex context, and the whole context is enclosed in cave-installation art.

2.3 Methodology:

Selection of interactivity

I outlined above the theoretical framework behind this thesis, in which I will examine human-art interactions in actual settings. As discussed, the spatial novelties constituting cave-installation art vary significantly, including from what elements encourage humans to take specific actions to the conditions that induce phenomenological responses. In this research it is impossible to focus on all aspects at once because designing a research plan on each aspect requires considerably long time, and even if possible, the number of all outputs will be far beyond the limited volume of

this thesis. Therefore, I have selected specific interactions to evaluate. As was already stated in the beginning of this thesis, the to-be-examined elements are:

- Integration of natural lines (production phase)
- Topographic condition (production phase and post-production phase)
- Distortion of images (post-production phase)

The essential condition for selecting interactive aspects is whether or not they can be examined objectively, because doing so will add a firm empirical fact to the abstract idea of "cave art as installation art". Considering this condition, phenomenological aspects was not taken into account in this study due to the difficulty to record factors and due to lack of the proper methodology to assess them. For instance, elements which consist of human-cave interactions are significantly ephemeral, mainly addressing our cognitive state. They are not suitable for objective documentation, therefore. On the other hand, these three interactive factors are objectively observable and cause bodily engagement and creative interaction regarding the production phase and post-production phase of cave art. *Integration of natural lines* reflects a significant interaction in the production phase, and *Topographic condition* concerns both the production and post-production phases. Meanwhile, *Distortion of images* denotes a particular viewing action in the post-production phase.

As for the first and second factors, these interactions are considered to be creative interaction types, especially seeking, from the perspective of cave-installation art, the affordance of natural features on cave walls for subsequent artistic activity, as Palaeolithic artists reacted to the morphology of the cave wall and transformed it as a part of wider experiential activity. I aim to learn through this analysis how natural lines were integrated into the images' outlines and how convex and concave surfaces are located within the outlined area of images. If palaeo-artists sought a specific condition for this way of image-making, detecting such a condition is a major objective of this research. It is generally known that the morphology of cave walls were frequently utilized for completing images; researchers believe that the use of cave wall served as a crucial basis for image-making. The documentation on the image-wall relationship began at the time of Alcalde del Río et al. (1911), and subsequently it has been discussed, for example, by Breuil (1952), Leroi-Gourhan (1992), Ewing (1997), Groenen (2000), and Hodgson (2000, 2003). This use of cave wall morphology has been named "integration" by Ogawa (2005), and it is now a widely recognized -if unquantified - phenomenon. I therefore use this term here.

Distortion of images, on the other hand, concerns the matter of how specific bodily engagement contributed to viewing images. The cave wall is never flat and

constantly undulates, irrespective of the additional influence of light sources on it. Such a topography distorts the appearance of images no matter when or how the viewing angle changes (Azema 2008). Therefore, images of cave art never had a 'fixed' impression on the viewer, but rather continually appears deformed as the viewer moved. Such a constantly changing appearance encouraged the participation of its viewers, who could actively manipulate the image by moving from one viewpoint to another. As noted earlier, distortion is particularly noticeable in anamorphic images (Aujoulat 1985, Surre 1992, Groenen 2000, Aujoulat 2005), and I argued the topographic intervention as an enhancer of viewing interaction in the context cave-installation art (Sakamoto 2014). I will also consider distortion here, and examine the phenomenon closely, in order to ascertain the mutuality of types of distortion and of topography. Since the distortion is caused by topography of the medium, the second category (topographic condition) is also largely related. Through an examination, I also aim to detect signs indicating whether or not certain topographies were intentionally incorporated for causing distortion.

In this way, the cave walls directly interfered with the artistic activity in specific ways in both production and post-production phase. Certainly, I cannot rule out the possibility that some of the phenomena can happen by chance, especially when their extent is not outstanding: for example, the use of undistinguishable topographic features (including natural lines) and non-dynamic distortions. These unremarkable cases, however, are also treated as a sample as there is not a criterion to isolate them from other more suggestive samples. In any case, the collected data should be empirically identifiable and documentable facts; further details will be described later by each category with explanation of the methodology of the data correction and analysis.

The cave wall is, therefore, an essential interactive element for both image-making and viewing images. It induces a creative interaction and also specific viewing actions. However, one might think that above interactive aspects are not exclusive to a specific cave's environment. As was briefly mentioned in the introduction, it seems that, since similar morphology can also be found on rockshelters and open-air sites, these interactivities do not necessarily pertain exclusively to cave-installation art. Even integration is also found in the rock art in the open-air site of Portugal's Côa Valley (Batarda Fernandes et al. 2017). This fact suggests that the integration might have been a fundamental component of Palaeolithic parietal art in general, regardless of its environmental context. Hence, only focusing on interactions with cave wall seems insufficient to discuss the site-specific nature of cave art.

Environmental components are not separable; they are mutually connected. Spatial novelties of caves (darkness, silence, and unusual scene setting and

geomorphology) constantly demand the attention of anyone in the environment; they never cease to affect artists/viewers even if when they are performing specific actions. Also, some spatial conditions, if not directly, have an impact on the three interactions of concern here. For example, in dark spaces where the amount of visual information available to the senses is significantly reduced, the brain creates a false vision because it attempts to process the same amount of information as found in well-illuminated spaces. Because of this feature, humans are more likely to perceive an illusion in a dimly-lit environment (Moyes 2012, and Moyes et al. 2017). Therefore, as Hodgson (2008) argues, caves are a particularly ideal settings for humans to see figures of animals in the pattern of the wall. Such a dark environment is also a suitable setting for perceiving images in motion. Dobrez (2013) has noted how our brains preferentially perceive movement rather than shape or colour: motion is processed in the dorsal signalling stream, and its processing speed is faster than that of ventral pathway which is responsible for perception of colour and shape. Given this specific quality of the human brain and the above relation between darkness and illusion, in caves, viewers perceive a constant deformation of images while moving from viewpoint to viewpoint. Thus, environmental elements constantly interfere with any activities in caves, and therefore, even if I isolate only the cave wall as a subject for examination, it will not be irrelevant to the significance of cave-installation art.

Fieldwork and analysis

Fieldwork was undertaken in Covalanas, El Pendo and El Castillo caves (Cantabria, Spain). I selected 54 images from these three caves for in-depth recording and analysis. For the examination, non-figurative motifs were not subjected to analysis; I only considered figurative images. This is because, as Azema (2008, 118) stated, 'contrary to abstract motifs whose graphic construction relates to concepts which escape us, the animal images are directly relatable to natural science.' In other words, even if we include non-figurative depictions in the analyses, ultimately we will never identify what the signs refer to , or even their general orientation. By contrast, from animal figures we can at least obtain information about movement, direction, species and often behaviour. This point is relevant to what I have studied. In order to select images for analysis, I considered conditions of accessibility and visibility; for the latter reason, engravings and severely weathered images were also excluded from the sample list.

Based on these conditions, I finally chose 54 images (Covalanas 18 images; El Pendo 11 images; El Castillo 25 images). Of these, deer is the most predominant motif (27 images), followed by Bison (12 images), Horse (6 images), unidentified herbivore (4

images), aurochs (2 images), caprid (1 image), mammoth 1 image), and an anthropomorph (1 image). Specific details of these samples will be described in each of the following case studies.

This sampling strategy inevitably introduces a bias; selecting images based on visibility might cause a methodological issue (selection of evidence: see Chapter 1, p51) because in doing so I potentially chose samples so they can fit my hypothesis, despite that there might be falsifiable cases among non-selected images. As for this point, I must admit that the analysis of the 54 images might not correctly represent reality. However, since this study focuses on the image-viewing process, the condition where images are clearly visible is the most desirable. In other words, if samples which lost their visibility cannot be visualised even by digital filters, it is impossible to perform the analysis itself. Furthermore, this research aims to examine only an aspect of cave art in the three caves and to discuss its significance; I do not intend to claim a universal theory which is applicable to hundreds of sites of cave art in Upper Palaeolithic Europe as previous researchers attempted based on selected evidence. Therefore, the introduced bias by the sampling will not be misleading.

Apart from the selection bias, I also need to mention a taphonomic issue. As cave art has survived for a significantly long time, no images are free from the taphonomic process of the cave's surface. Therefore, all images are more or less altered, or perhaps some of them might have completely vanished; namely, what we see today is not the same as it was in Upper Palaeolithic. However, the selected 54 images are well conserved, and the alteration of the appearance does not affect the result of the analysis negatively.

These 54 images are not chronologically coherent. Images in Covalanas and El Pendo are believed to be contemporaneous (Straus et al. 2002), but their age of production remains uncertain: Ochoa and Garcia-Diez (2015) suggest the significantly wide range of the chronology from Aurignacian to late Magdalenian. Examined samples in El Castillo are also chronologically diverse; although not all images are dated, some of the red paints are attributed to Solutrean or earlier (Garcia-Diez et al. 2015) while some of the black images to Magdalenian (Valladas et al. 2001). I will describe the detail later in the case-study chapters. Due to such a chronological uncertainty, sampled images appear to us as if they are culturally monolithic even though they might have represented the dynamism of the cultural change and therefore carried different cultural significance by period. If each image were accurately dated and so if I could see them in chronological order, I would also be able to observe the presence/absence of the interactivity in association with the chronological difference. However, since the chronology is unclear, this thesis has to examine these 54 samples as a cultural monolith, and the result will not reflect such a detail of the cultural change. Even so, the

chronological uncertainty is not harmful because at this stage I aim to inspect least elements about the interactivity of cave art (e.g. did intentional interactivities exist? and if so, were there any rules?). This thesis, as a first-time approach from the theory of the installation art, addresses these basic questions to highlight the interactivity as a fundamental feature of cave art. Therefore, chronological uncertainty does not affect the result.

Data collection: Photogrammetry

For the analyses, I produced a 3D model for each image, using digital photogrammetry, so that all interactive elements could be digitally and objectively examined during post-fieldwork analysis. Photogrammetry is 'the science of obtaining reliable information about the properties and surfaces of objects without physical contact with objects, and of measuring and interpreting this information' (Schenk 2005, 3). In short, it is a method to reconstruct a 3D model from the overlapping of photographs of a subject taken from different angles. I will describe the specific nature of this method below.

Historically, in the field of rock art study, three recording methods have been adopted; drawing, tracing, and photography (Chandler and Fryer 2005). The former two are rather traditional, with both advantages and disadvantages; for example, tools required for drawing are simply a pen and a paper, and it is easy to perform even in the dark environment but is subjective and far less accurate than the other two methods; tracing is more accurate than drawing, but the procedure is invasive as a recorder directly rub engravings onto paper (ibid.). Photography is considered to be the most universal recording method, since technological development made the photographic procedure easier and quicker. In addition to this, the recent advance of digital photographic techniques allows DIP (Digital Image Processing) in software such as Photoshop, which in consequence provides incomparable benefits such as visualizing of invisible traces to the naked eye and enables further detailed analysis. The application of the digital photogrammetry for recording rock art is based on the context of such a technological advance.

The essential element of a 3D model is a cloud of points which form the shape of an object in 3 dimensional computational space. Based on these point clouds, meshing between points (to form a triangular mesh) and texturing follows to complete the 3D modeling (Lerma et al. 2010, Chodoronek 2015). Point clouds themselves are usually insufficient for the analysis of the external surface of an object, so further coordination (meshing and texturing) are necessary to enable the analysis of morphology of the 3D surface (Ibid).

At present, two techniques are well known for 3D modeling; laser scanning and photogrammetry. Lerma et al. (2010) describe the advantages and disadvantages of each. Laser scanning is a technique that directly gathers the surface data of objects as point clouds by means of an irradiating laser pulse that measures the distance between the sampling point and objects of concern. Due to the direct way that the 3D surface is reconstructed by laser scanning it is more accurate than photogrammetry. On the other hand, laser scanner is expensive, and the time required to undertake it is relatively lengthy. With regard to photogrammetry, the resulting model has less accuracy, especially when the external surface of an object is complicated. This is because the technique calculates (but does not gather) the position of points based on the metric information recorded in digital photographs. It is therefore an *estimate* rather than a measurement. However, digital photogrammetry is significantly cost-effective, and the time required to undertake it is much shorter than laser scanning.

Recent advances in photogrammetric techniques are, however, closing the distance between the two. A 3D imagining technique called Structure-from-Motion (SfM) has particularly had a revolutionary impact on photogrammetry. Although SfM shares the same principles with conventional photogrammetric methods (both rely on the overlapping of objects in sample images), it does not require the manual input of parameters such as scene geometry, camera position or orientation. All of these processes are, instead, digitally simulated. SfM software automatically calculates and triangulates the position of feature points, identifies the position of the camera, and reconstructs a 3D mesh and even the texture of a model in 3D coordinate (computational) space simply from overlapping images (Westoby et al. 2012). It is true that the scale is initially absent in generated models due to the lack of the procedure inputting numerical parameters about spatial relation, yet the scale of the model can be added subsequent to the completion of the model. The accuracy and reliability of SfM as applied to archaeological practice has been characterised by many researchers (e.g. Kersten and Lindstaedt 2012, Koutsoudis et al. 2013, Katz and Friess 2014). These studies compare the ability of different digital photogrammetry algorithm/software, focusing on a number of varied objects possessing unique surface features (e.g. human crania - Katz and Friess 2014; a Cycladic female figurine - Koutsoudis et al. 2013). Consequently, it has been confirmed that archaeological validity of 3D model constructed by photogrammetry is equivalent to that of 3D scanners; although the quality of models varies by software type. All, however, are within an acceptable range (Kersten and Lindstaedt 2012).

In sites such as Palaeolithic art caves, the time available for fieldwork is often significantly limited due to issues of conservation and access. Digital photogrammetry, by which one can obtain the data necessarily for 3D visualization relatively quickly, is

a more suitable method than laser scanning. Furthermore, from the point of "repairability" of the equipment involved, photogrammetry is considered to be more usable method in caves: during an archaeological project the camera and its parts, tripod and lights are easily fixable or replaceable at far lower cost, while fragile laser scanners may need to be repaired in a specialist laboratory. in addition, given that the price of scanners which is commonly used for archaeological purpose is no less than 3000 dollars (Porter et al. 2016), photogrammetry can be purchased at low cost. These points might significantly affect 3D documentation, especially during fieldwork where mechanical troubles in the scanner could ruin the project itself (Ibid).

For this reason, I adopted digital photogrammetry for the 3D imaging on which the analyses were based. In order to collect photo-data from each of the selected images I used a digital camera (Canon 1200D with a lens EFS 18-55mm) and a tripod. Flash lights were also utilized in places where electric lights were not installed. In order to reconstruct the 3D models, I used the SfM photogrammetry software *Agisoft Photoscan* (standard endition). Photoscan has been utilised for archaeological research in various contexts (e.g. rock art, Plisson and Zotkina 2015; underwater, McCarthy and Benjamin 2014; museums, Nabil and Saleh 2014), and the accuracy of its reconstructed models has been proven to be highly reliable (e.g. Kersten and Lindstaedt 2012, Koutsoudis et al. 2013). During the first step of data processing (producing sparse clouds) with of Photoscan, users can select quality settings from lowest, low, medium, high to ultrahigh. Higher quality requires a longer time processing time and more spec in a computer to process the data, but such "high" level quality is always desirable for academic recording in order to maximise the accuracy of the model (Chodoronek 2015). During the next step, dense point clouds are generated, during which the same quality settings are used, as is the photo alignment process. In this research, all 3D models were produced in the high level of quality resolution. However, some models needed to downsize their quality to medium because a consumer-level computer frequently cannot complete data-processing in high or ultrahigh levels because the amount of the data to be processed for 3D modeling require considerable computational capacity (ibid.). As will be examined in each subsequent case study chapter, however, the accuracy of the generated models is certainly acceptable for addressing the research questions of this thesis. Westoby et al. (2012) note that sampling the higher number of images for 3D visualization will lead to a better result at the expense of a longer time for data processing. Models of medium quality involve a sufficient number of sample photographs to secure a high degree of accuracy. In addition, Photoscan also contains an additional program for calibration of a camera lens which generates certain parameters once necessary photo data taken by the lens is applied to the program. These parameters are used to equalize the distortion caused by lens. By inputting such

parameters into the setting of Photoscan, I was able to generate models with an increased accuracy.

In order to secure the validity of the 3D analysis, generated 3D models must be accurate and so correctly scaled. Normally, when a 3D model is reconstructed by digital photogrammetry, GCPs (Ground Control Points) or scale bars are also photographed together with targets so that the model is given the actual dimensions in a virtual coordinate space either after or during generating the model. However, in most case of cave art research, we are not allowed to touch the wall, and hence scale bars cannot be directly attached to the wall. Chodoronek, in his MA dissertation (2015), examine the accuracy of a photogrammetric model generated by Agisoft Photoscan without using scale bars. One of the methods introduced in Chodoronek's work seems suitable for this case study. That is to compare numeric gaps between physical measurements obtained from actual fieldwork and virtual measurements in the 3D model. Along with this methodology, the accuracy of the model was reviewed by the following processes: First, the model was outputted in DAE file to scale on Meshlab, a free online software (Photoscan standard edition is not capable of scaling); Second, the physical measurement of arbitrarily selected image was applied to the same image in the model on this software to generate a scaled model; Third, images in the scaled model were individually measured; and last, obtained virtual measurements were compared to physical measurements. I expressed the difference in length (cm) and percentage (%); percentage is obtained by difference (cm)/physical measurement (cm). Scaling process on Meshlab is automatic. Once a physical measurement is applied, the program scales the model based on the inputted value. The result of the assessment will be demonstrated in each case study.

Analysis: procedure

Once 3D models were generated and their accuracy assessed, they were exported to Photoshop (Version CC 2015.5) with which further analysis was conducted. In order for Photoshop to read the 3D data, the models were outputted in PLY format. Details of the performed analysis and its procedure are to be described below by each category of the interaction type.

Integration of natural lines

Integration is a crucial indicator of an interaction between humans and cave walls at the production stage. Artists did not only rely on their own imagination but also 'borrowed' from pre-exiting natural lines in order to complete outline images. Inspiration derived from these lines could act as a starting point for image-making.

Integration seems a basic method by which to produce cave art. However, whether or not artists followed certain rules during integrating process is unknown, although it is briefly mentioned that integration is mostly found in the cervico-dorsal line (Hodgson and Pettitt 2018, White et al. 2017). How 'deliberate' was their borrowing from cave topography? Were any specific features prioritised, or was this essentially random? Was the borrowing simple or complex? The aims of this interaction category is to address these questions. For this purpose, I statistically examined the correlation between the body parts of animal figures and natural lines. If natural lines have been intensively integrated into a particular body part, this suggests that integration was not a random action, but instead can be seen as an established means of communication between humans and caves where decision-making was a constant.

For the analysis, each single animal image was first divided into six body parts (Head, Dorsal, Buttock, Tail, Ventral, and Limbs: see Figure 2.9). Each of these parts were examined for each image on the 3D model so as to detect integration of the image section with natural lines. At this time, if necessary, various digital filters were applied on Photoshop in order to best visualize the integration part in more detail and enhance the analysis. The digital filters applied were Hue/Saturation, Normals, and Displaying triangulated meshes. Hue/Saturation filter allows to adjust the intensity of colours and lightness, by so doing highlight specific features on an image. Normals filter displays RGB condition of all polygonal surfaces of a 3D object, which is defined by the orientation of each surface in 3D coordinate space. As a result, the depth of the object appears clearer. Triangulate mesh is a concentration of lines connecting point clouds. Since those lines are located on a 3D surface, the topographic condition of an object will be more visible if they are displayed. Furthermore, the confirmed integration was then

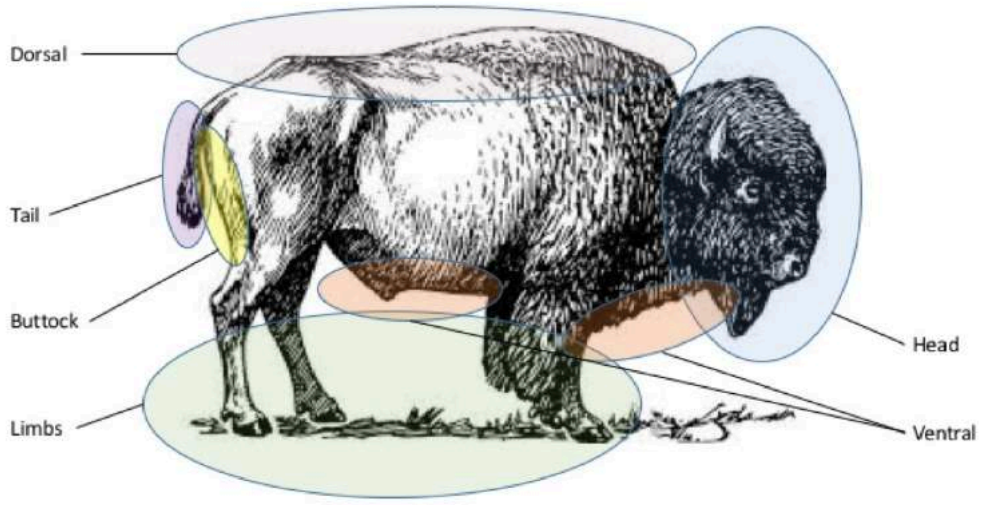

Figure 2.9: Six parts of animal contour (Head, Dorsal, Tail, Buttock, Limbs, and Ventral). Use of natural lines for outlining images (integration) is a well-known artistic method in Palaeolithic parietal art. The number of integration is counted by body section in this analysis.

quantified by body part for each image in order to create a statistical basis for analysis. When integrations were detected in multiple body parts of a single image, all of them were quantified. However, in the case where two or more integrations were observed within a *single* body part, the number of integrations was marked as a total of 1. Based on the resulting statistical data, I examined whether it demonstrates a particular trend in the frequency of integration by body part so as to consider the following questions: were specific body parts more amenable to integration than others? Did this differ by animal taxon? Did it differ by technique of integration (e.g. convex versus concave; cracks versus ridges)? Finally, the data from each cave was compared, i.e. at a site by site level. Can distinct cave assemblages be distinguished along these lines, or were more general principles in use? If a noticeable tendency is detected by statistically scrutinising the relationship between integration and its location, the trend indicates a certain reason which led to the specific use of natural lines; if there is such a rule for this very method of image-making, it must be revealed for further understanding of the production of cave art.

One must be attentive regarding how to treat various types of integration. The term "Integration" might denote that the outline directly overlaps on a pre-existing line. However, Palaeolithic artists did not always use natural features in the same way. In some cases, natural lines are certainly associated with the outline, although not perfectly overlapped (i.e. parallel lines). In this study, I treated direct integration as "Direct" and the latter case as "Offset". Also, the size of integration might be different; while a certain extent of a body section can be integrated in some images, an integrated area can be considerably limited in some occasions. I labelled the former integration type as "Full" and the other case as "Partial". Therefore, a sample of integration must be Direct or Offset, and Full or Partial. In this thesis, I equally treated all of these different types as integration but counted them along with these labels.

I judged the types of natural lines based on morphological characteristics. Narrow and long depressions running on the cave's surface are assessed as Groove (Figure 2.10, 1), and peak lines of sharply elevated surface are defined as Ridge (2). On the other hand, edges of rocks or cracks which generate an acute elevational gap against their surrounding regions are treated as Edge (3-4); lines formed along blunt concave or convex features are also classified as Edge (5). In the cases where the boundary of different the medium's surficial conditions (e.g. smooth and porous surface) appears as a line, I classified them as Border (6: Normals filter is applied because this type is less distinctive than the others). The last type is valley: lines formed between two adjacent convexities (7). Although other types of natural lines potentially exist on the cave wall (e.g. a train of natural holes which appear as a line), but the studied images are integrated with these five types.

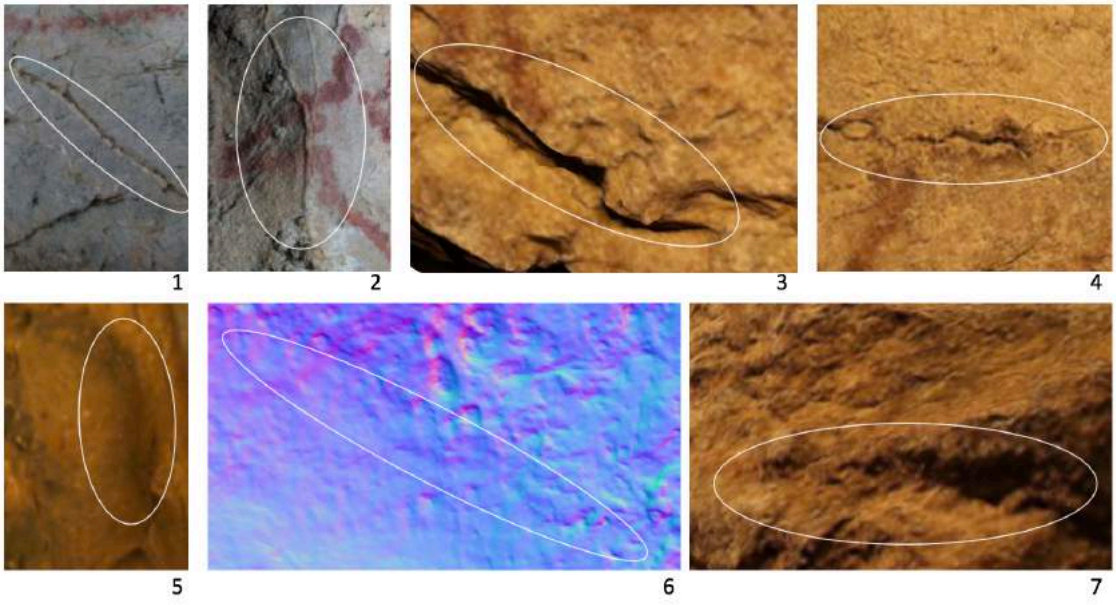

Figure 2.10: the list of natural lines. Narrow, long depressions running on the cave's surface are assessed as Groove (1), and peak lines of sharply elevated surface are defined as Ridge (2). Edges of rocks or cracks which generate an acute elevational gap against their surrounding regions are treated as Edge (3-4); lines formed along blunt concave or convex features are also classified as Edge (5). In the cases where the boundary of different the medium's surficial conditions (e.g. smooth and porous surface) appears as a line, I classified them as Border (6: Normals filter is applied because this type is less distinctive than the others). Valley lines are formed between two adjacent convexities (7).

Topographic condition

Cave walls are of course never perfectly flat. Their surfaces constantly undulate, generating *differences in elevation* location to location. Such an undulating topography is a basic premise of the medium on which the cave art is depicted.

To our modern sense - familiar with paintings typically produced on a flat surface - drawing a picture on an undulating surface seems unnatural, given that its purpose is to effectively transmit visual information. Such notions may well be anachronistic for Palaeolithic art, however, especially undulating topographic surfaces so ubiquitously formed the canvas for image making. This aspect is well described by Pettitt et al. (2014), who examined the relation between hand-stencils and topography in the La Garma and El Castillo cave, revealing that stencils were more likely deliberately created on topographic features such as convex and concave surface rather than flat areas (which were available in these caves but remained unmarked). In this category, inspired by the contextual analysis of these authors, I assessed elevation levels of the wall by body part of animal images to assess whether or not there is a specific relation between topographic condition and graphics.

In order to undertake this, I express the topographic elevation of each of the 13 body parts in three levels (High, Medium, Low). Initially, images were divided into

seven parts (Head, Neck-shoulder, Mid torso, Thigh, Frontal leg, Back leg, and Tail: see Figure 2.11a); the neck and shoulders were treated as the same unit, because the distinction of these parts is not conspicuous in certain animal species (for example, the division of the neck and the shoulder is clear in deer, while it is hard to tell the distinction in bison). Therefore, this study dealt with those parts as single section. Furthermore, the neck-shoulder, the middle area, and the thigh were further divided into three along the dorsal, the central, and the ventral area (Figure 2.11b). This treatment marks a more accurate distribution of the elevation level: originally each of these parts occupy a large area, and when there is a noticeable elevational difference in a limited area of the body part (e.g. a noticeable convex on the ventral area), if it is not divided into three the situation cannot be described accurately. Thus, each image was divided into 13 sections in total.

The division is determined based on the best estimation. Usually, the body shape of depicted animal images is diverse significantly, even though they possess a basic quadruped form; some images are provided with the disproportionally large mid-torso, whereas some have the considerably small thigh. Therefore, a single criterion cannot be applied to such a different form of images.

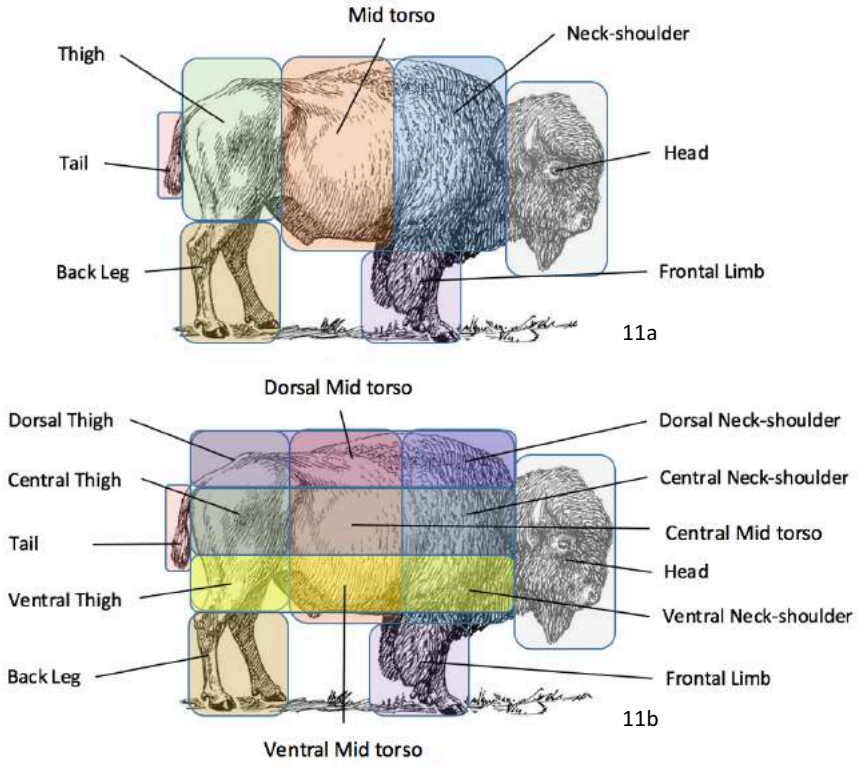

Figure 2.11ab: Sections of the animal body. Images are firstly divided into seven body parts (Head, Neck-shoulder, Mid torso, Thigh, Tail, and Frontal and Back leg: see 2.10a), and then Neck-shoulder, Mid torso, Thigh are further divided by Dorsal, central and Ventral area (2.10b). Thus, each image contains 13 body parts

Following this, images on the 3D model were extracted along their contour, and their topographic condition was assessed by each body part. To examine the elevational level of topography, I set a cross-section layer horizontally with 3D models in Photoshop and moved the layer so that the models passed through it. A cross-sectional layer can be placed anywhere in the digital 3D coordination space. By entering a specific parameter, the position of the layer can be manipulated; for example, by inputting parameters from 1 to 3, the layer gradually moves towards a model; see Figure 2.12 which illustrates how the cross-sectional layer passes a model (seen vertically). Accordingly, a 3D model starts passing through the layer from its highest area in elevation (2-3) and its lowest at the end (4-5). Figure 2.13 shows this process seen from the front. Once a surface passes the layer, the colour of the surface changes from dim to bright, and so places in bright colour reflect higher elevation than darker area. To generate this dim-bright effect, I applied the Normals filter to the body areas which are passed by the layer. Although the bright colour is different by region (see

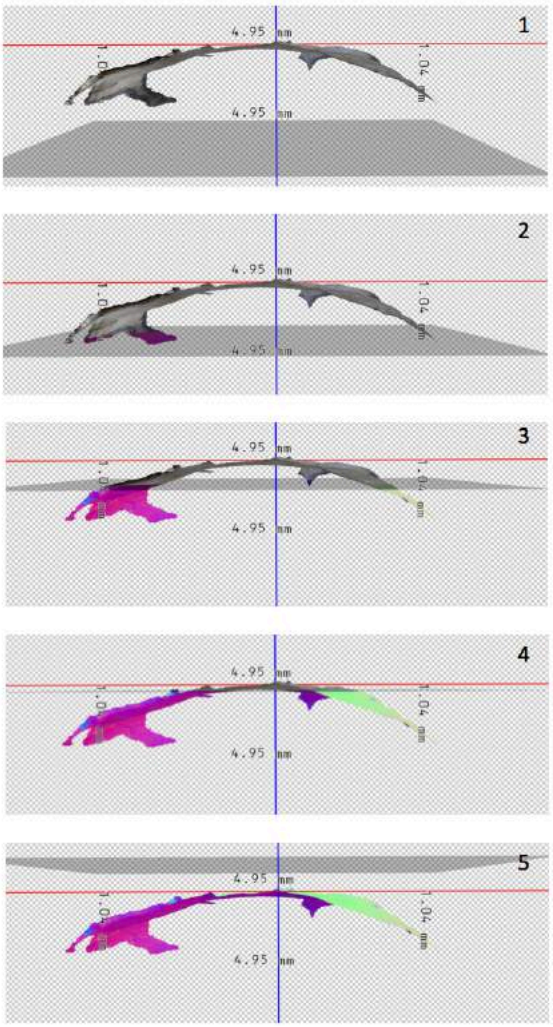

Figure 2.12: These five images illustrates how the cross-sectional layer passes a model (seen vertically). By inputting parameters, the cross-sectional layer (the grey layer in the figures) gradually proceeds towards a model (1-2). Accordingly, the 3D model starts passing through the layer from its highest area in elevation (2-3) and its lowest at the end (4-5).

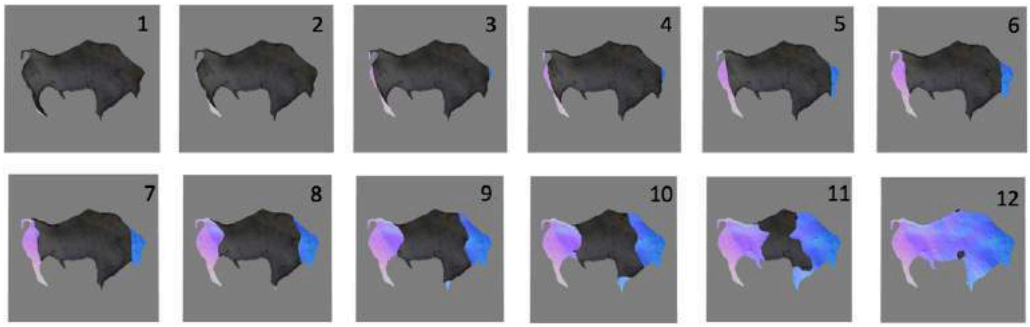

Figure 2.13: Images illustrating different elevation levels. By horizontally applying a cross-section layer to a 3D model in Photoshop, the difference in elevation level by region is objectively documentable. Since body parts which passed the layer change their colour into bright, areas of bright colour denote higher elevation than that remains dark.

Figure 2.12-13), this difference does not cause any problems to the analysis because, as the function of the Normals filter, it merely reflects RGB condition highlighted by the different orientation of each polygonal surfaces of a 3D object. In order to analyse the topographic condition accurately, the baseline must be set horizontally with models. For this reason, I selected horizontal edges (see Figure 2.14, a-b) and vertical edges (c-d) in each model and set models in the position where each combination of edges pass the layer simultaneously (see Figure 2.13, 2-3 for horizontal edges, and 12 for vertical edges). Accordingly, the baseline a-b and c-d parallel to the cross-sectional layer, and so the models do.

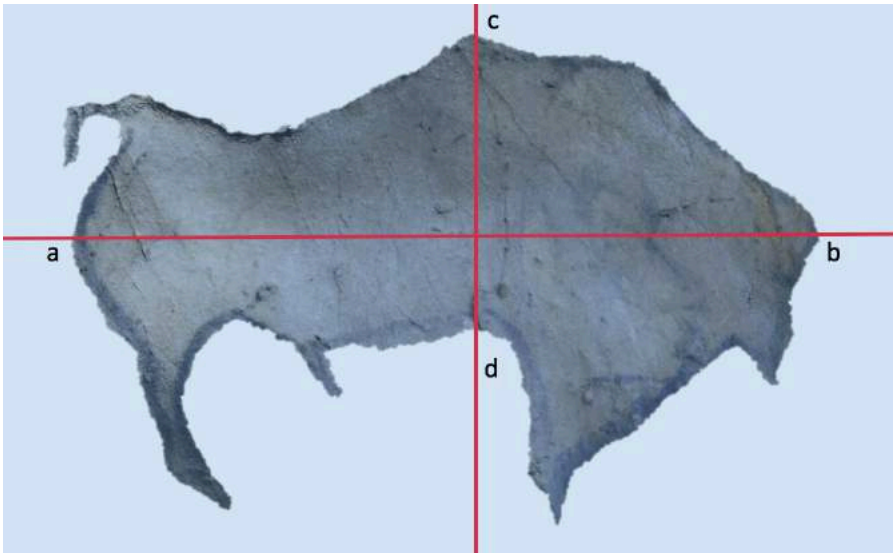

Figure 2.14: I selected horizontal edges (a-b) and vertical edges (c-d) in each model and set models in the position where each combination of edges pass the layer simultaneously. In doing so, the baseline can be set accurately horizontally with the model.

I set the Elevation levels based on the range of the inputted parameter because it represents the depth of the elevation of 3D models. For example, if passing begins at parameter 1 and ends at 9, the process can be divided into three stages (e.g. parameters 1-3, 4-6, and 7-9). At this time, when the body parts are evenly distributed between parameters 1 and 9, the part passing through the layer during 1 - 3 is set as High, the part between 4 and 6 is as Medium, and the part between 7 and 9 is as Low. The elevation level of a body part was defined when more than half of the part passed the layer at a particular level. In the case where all body parts are defined within the limited range of all parameters (for example, 13 parts are defined their level within the range 4-6, but the total range is 9), this limited range is divided into three levels (e.g. 4: High, 5: Medium, and 6: Low).

Although I stated "More than half" of a body section, whether or not a detected area reaches the significant extent relies on the subjective assessment. The above-explained methodology is still under development, so a method to judge objectively the

extent of detection is still absent. Therefore, the judgement cannot be free from a subjectivity, but decisions to be made must be the best estimation.

This is a novel method, devised for the thesis, the aim of which is to express the elevation of the topography at three levels. Body parts were occasionally located on the wall at remarkably high or low elevation. For example, in a figure with a total range of 20, most of its head is located in the range 1-8; if the other body parts are located in the remaining 9-20, 1-8 is set as Extra High and 9-20 was divided into three to determine the elevation level (9-12: High, 13-16: Medium, 14-20; Low). Similarly, when the elevation of a certain body part is remarkably low, the level is determined as Extra Low in the same way. Furthermore, when one image contains both Extra High and Extra Low elevations, the range where the majority of body parts are located is divided into three, and the other ranges are set as Extra High and Extra Low; when the range is 20 where 1-6 and 16-20 are set as Extra High and Extra Low respectively, 7-9 is set as High, 10-12 as Medium, and 13-15 as Low.

The elevation levels obtained for each body part was numerically expressed by coded points of 1 to 5 (Extra High: 5, High: 4, Medium: 3, Low: 2, Extra Low: 1). The resulting data table thus codes for the topographic composition of each image. In this phase the division of the dorsal, the central, and the ventral regions was united in order to simplify the data. Therefore, component parts of the neck-shoulder, the middle, and the thigh were treated as a single body part. To determine the elevation level of those united parts, I calculated the average value based on the elevation point of each component area (1-5); if the average value contains a fraction (for example 2.7 or 4.3 etc.) the number obtained by rounding was defined as the elevation level (e.g. 2.7≈3, or 4.3≈4). The generated data table was subsequently used to ascertain whether a strong correlation exists between a specific body part and a specific topographic condition.

Additionally, I also produced a line graph for each image representing the topographic condition of the main body (head, neck-shoulder, middle, and thigh), based on the quantified elevation level. As a result, the topographic conditions of each image can be visualized fairly simply, enabling a quick 'eye balling' of the figures' basic topography. Patterns detected by this coding and visualisation were analysed and will be described in the next case study chapter. Patterns were statistically managed in order to identify the most frequent topographic pattern. Finally, I compared and integrated the data obtained from each of these caves and verified whether there is a common tendency within or between them.

Distortion on images

As I discussed in the theoretical background to this research, 'cave art as installation art' treats anamorphosis as a form of interactivity. In anamorphic images the degree of image deformation is significantly large when they are viewed from different angles. This plurality of viewpoints might have been an enhancer of an interaction in the post-production phase, involving a deliberate bodily engagement of viewers. In fact, this plurality is not limited purely to anamorphosis; any images which are depicted on undulating surfaces constantly change their appearance as a viewpoint moves because visible and invisible areas on the image also change due to the surface of the uneven wall. Figures 15a-c illustrate how topography distorts an image. If a viewer stands in front of the 3D surface, there are no unseen areas, i.e. the viewer sees all aspects of the figure's surface (Figure 2.15a); the viewer can see the image without distortion. However, once the viewer moves to the left, the protruding region at the figure's centre hides much of the concave area to its right, foreshortening it and therefore distorting the appearance of the image significantly (Figure 2.15b). Similarly, if the viewpoint moves to the right, then the convex wall hides part of the concave area to the left. Accordingly, the visible area changes once more (Figure 2.15c). The perceived image will now be noticeably different from the image seen from the left. If one views images on a flat surface, one will not experience such a distortion. The viewer only perceives a slight distortion caused by the perspective when he/she sees the image from different viewing positions, but fundamentally their shapes will appear relatively uniform (Figure 2.15d). In this way, the topography of a cave wall wields a great influence on the appearance of the image as viewpoints change. The purpose of the analysis in this category is ultimately to detect signs of *intentional use* of such distortion as the basis of an interaction. Because the viewing action based on distortion on the image still remains hypothetical, my reason for undertaking this is that if I am able to detect such a

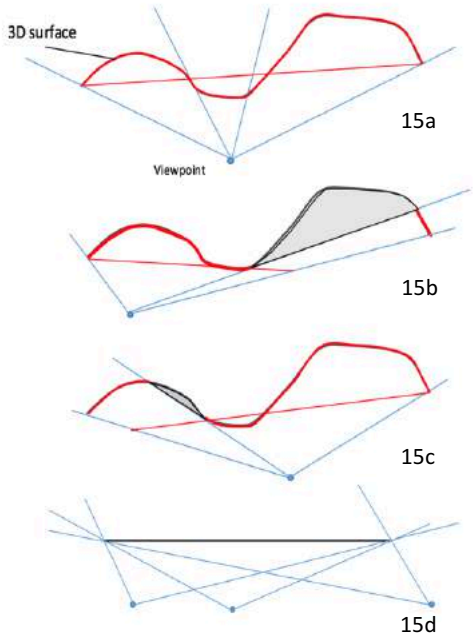

Figure 2.15a-d: The mechanism of how topography distorts the appearance of an image. As convex surface hides concave area when a picture is viewed from either side, an unseen area is generated (grey zone in 15b and 15c). Because the visible surface (red line in above three figures) changes, images appear significantly different. Meanwhile, even if one views images on a flat surface from different viewpoints, the viewer only perceives a slight distortion caused by the perspective (15d).

form of intentional interactional distortion, the result will considerably bolster the notion that at least some Palaeolithic cave art was an interactive device.

This study assumes that the intention is visible in the frequency of distortion by body part, and if distortion intensively occurs in a specific body part. To analyse this, images were first divided into six body parts (Head, Neck-shoulder, Mid torso, Thigh, Leg, and Tail: see Figure 2.16). Secondly, 3D models were viewed from different angles in Photoshop in order to confirm body sections which were remarkably distorted. As the previous topography section, the assessment relies on the best estimation. Once a remarkable distortion was detected, it was counted by body part. After all of this examination, a data table was generated. Whenever I was able to confirm a deformation, I describe in detail specifically how the topography causes the deformation in association with the obtained data about the cave's topographic condition.

In this analysis, it is necessary to code, compare and present differences in the appearance of images when they are viewed from multiple viewpoints. For this purpose, I produced animation movies for each of the subject images in order to simulate the active process of the deformation by a moving viewer. I did this by horizontally rotating the 3D models. This simulation is equivalent to the situation where a viewer moves around an image. The procedure for creating movies is straightforward: a still image was captured as parameters for angle in Y-axis increase (e.g. 0°, 10°, 20°, 30°, 40°…), and those still images were united altogether to animate the rotation (Figure 2.17). In order to reconstruct situations as close as possible to their Palaeolithic reality, I took into account the height of each image from the cave floor (in all these caves probably a relatively accurate estimation of their height in the Palaeolithic as little has changed, but

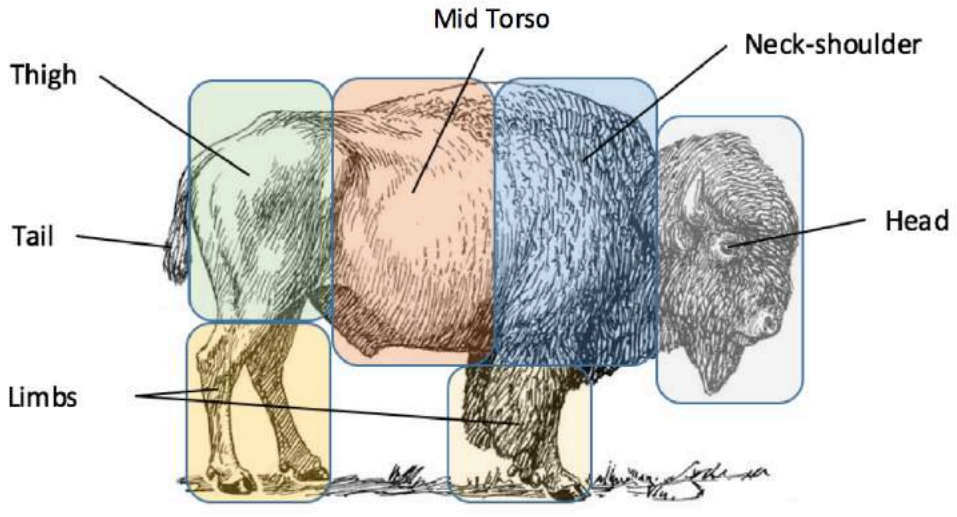

Figure 2.16: Sections of the animal body. Images are divided into six body parts (Head, Neck-shoulder, Mid torso, Thigh, Tail, and limbs). The number of distortion is counted by body section in this analysis.

in any case for the purposes of this analysis a consistent bench mark). For images located at high levels, their 3D models were tilted in the X-axis based on their heights so as to simulate how those images appear when viewers looked up to capture them in their sight (e.g. I set the angle as X10° or X20°. As the X angle increases, the viewing angle grows sharper). The degree of horizontal rotation of each 3D model was set, based on the condition of the location in which where the image was fixed; when an image was invisible by viewing from the right in its actual setting, the same situation was reconstructed by limiting the rotation of the 3D model. By such simulation I compared the appearance of images viewed from the front and sides in order to detect an outstanding deformation. At that time, I assessed a deformation when the outline of body parts is apparently deformed (twisted, bent, contracted: Figure 2.18, see A-B). Additionally, I performed an experiment for images drawn on a flat surface; I rotated images simultaneously fixed on 2D surface in 3D computational space by the same procedure as the above 3D simulation, and compared the difference in appearance between the two (Figure 2.18, B-C). By such a comparative analysis I aimed to isolate the distortions caused by topographic

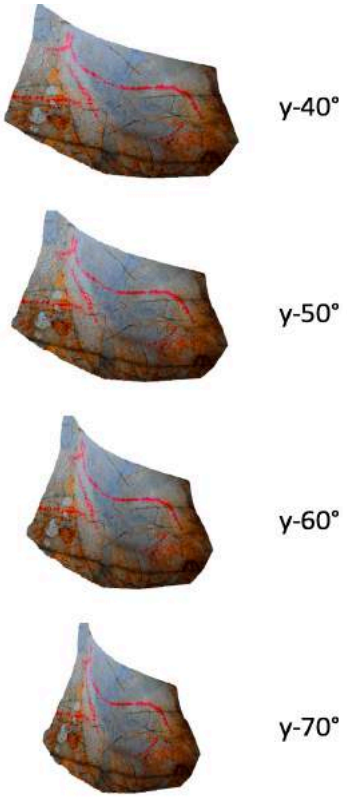

Figure 2.17: An example of rotating a 3D model. Angles are inputted along y-axis so that models rotate horizontally. The rotation simulates how images are distorted by topography while a viewer moves side to side of them. Still images are recorded from different angles as shown in the above figures, and those stills are gathered and combined along a timeline to be an animation. Based on the animation data, this study observed and described the process of constant distortion in detail.

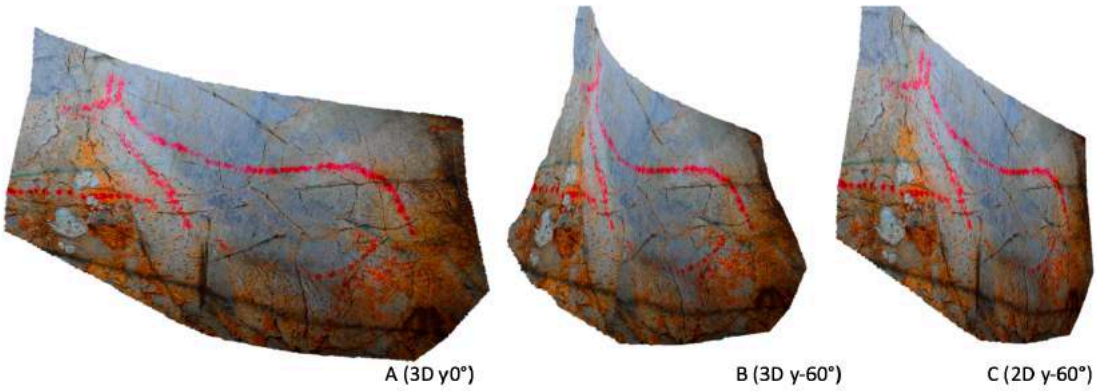

Figure 2.18: a 3D model seen from the front (A), seen from the left (B), and a 2D model seen from the left (C). I assessed a deformation when the outline of body parts is apparently deformed (twisted, bent, contracted: A-B). I also compared the difference in appearance between an image on 3D and 2D surface (B-C) to isolate the distortions caused by topographic intervention from those simply by principle of perspective.

intervention from those simply by principle of perspective. Generally, images, regardless of the shapes of their surface, are subjected to distortion to some extent by being viewed from the sides; for instance, if a viewer stands on the right, the right part of the image appears elongated while the other part seems contracted, opposite phenomenon occurs when the viewer moves to the left. Comparing these two simulations enables to focus on distortions of topographic-cause and lead to further refinement of observations. Therefore, when images are viewed from sides, 1) if the outline of their body parts appears noticeably different from that of frontal view on 3D medium, and 2) if those deformed contours are also not identical to that of images seen from the same angle but fixed on 2D medium, I marked them as presence of deformation.

Summary

This study, beginning with the theories of affordance and installation art, interprets Palaeolithic cave art as a multisensorial interactive environment. On the grounds of this view, I selected three types of interactivities to examine through fieldwork in three caves in Northern Spain (Covalanas, El Pendo, and El Castillo): Integration of natural lines, Topographic condition, and Distortion on images. The cave wall forms the essential medium where artworks of cave art were placed and thus seems the appropriate subject for this first formal examination into the interactivities of cave-installation art, given its significant influence on both producing and viewing art. As I have discussed so far, the methodologies I employ mainly constitute coded observations and 3D manipulation of images, aimed at detecting indicators of any specific rules behind interactivities: whether integration was performed according to specific rules or completely at random; whether Palaeolithic artists preferred a certain topographic type as a canvas for their images or whether they left depictions regardless of the shape of the wall; whether Palaeolithic artists were aware of the distortion of images and deliberately utilised a plurality of viewpoints for further viewing-interaction or whether distortion is merely distortion and no more than that. I rationalise that if meaningful results on these points can be demonstrated, we can consider them to be empirical and objective facts which would reinforce the basis of the cave-installation art theory.

To test the significance of the obtained statistical data, I performed Chi-square test. Chi-square test is a statistical method commonly used to assess the probability of association between variables by comparing observed values to theoretically expected values obtained under the null hypothesis (for example, if four topographic types are detected among 54 images, 13.5 (54/4) is the expected value of each type because the number should be evenly distributed if the null hypothesis is “there is no preferential

use of specific topography"). The test returns probability-value (p-value) between 1 and 0, and p-value below 0.05 normally rejects the null hypothesis (from the above-example, $p<0.05$ means that the obtained data likely shows a preferential use of specific topographies). As Chi-square test is not suitable to small samples, I performed Chi-square test to the united data of the three case studies.

Considering the adoption of this empirical approach, this research represents a significant departure from the conventional ethnographic approach to understanding cave art, which I outlined in a previous chapter.

In the next chapter, I will detail the case studies and examine the 3D data which was obtained from fieldwork. Each case study will introduce further information of the subject images and present specific details about the data correction employed (e.g. camera positions, the number of photographic images used for generating 3D models). In addition, the detailed setting of the simulation for detecting distortions are also described. In some cases, depending on the actual environmental conditions, some simulations required amendments (e.g. tilting angles in X-axis), which are also noted. After discussing these relevant conditions, I present a case-by-case analysis, beginning with Covalanas cave.

Chapter 3

Case study 1: Covalanas cave

3.1 General Information

Site

Covalanas cave is located in the municipality of Ramales de la Victoria, Cantabria. The Calera river runs through the region, forming a valley in Mount Pando. The cave developed on the right bank, on the south West side of the river, at 320m above sea level. The municipality of Ramales de la Victoria is located southernmost part of Cantabria which is close to the boundary of the province of Vizcaya. Although it is a small town with a population of about 3000, it enjoys popularity for a large concentration of Palaeolithic cave with artistic images; as well as Covalanas, 9 caves (Arco A, Arco B, Arco C, Pondra, Morro del Horidillo, La Haza, Sotarriza, Cullalvera, El Miron) are located in proximity to the town. As graphics left in these caves are very similar both in style and presumed date, it is believed that they also share their social meaning within the same graphic territory (Garcia-Diez and Torre 2007). The limestone in the area is highly soluble, and such a geological condition contributes to such a high density of caves.

The cave was discovered in 1903 by H. Alcalde del Rio and L. Sierra on 11th September (2 days after La Haza) who also discovered the Palaeolithic art of El Castillo cave in the same year, and it was the first Palaeolithic art cave found after the eventual recognition of the authenticity of Palaeolithic art in Altamira cave. Several excavations have been carried out at the entrance to the cave in the early 1900s, 1950 and 1956, but none yielded any fruitful archaeology. The findings are only a limited amounts of lithic fragments and faunal remains (bear, deer and wild boar: Moure Romanillo et al. 1990) which are now conserved in the Museum of Prehistory and Archaeology at Santander (Bischoff et al. 2012). This fact indicates that Covalanas cave was not attractive to human occupation during the Upper Palaeolithic, but was used for a purely artistic purpose. Instead, El Miron cave, which is located only 30m below Covalanas, is considered as the residential and seasonal aggregation site due to abundant archaeological records (Morales and Straus 2000).

The region consists of rivers and their accompanying valleys (e.g. Calera, Gándara, Vega, Asón, and Carrenza). Palaeolithic hunter-gatherers took advantage of this geographic condition as a focal point of their survival strategy, with regards to communication: the area lies at the confluence of Calera, Gándara and Vega, which are accessible from anywhere of these valleys; and Asón valley forms as a direct route to a

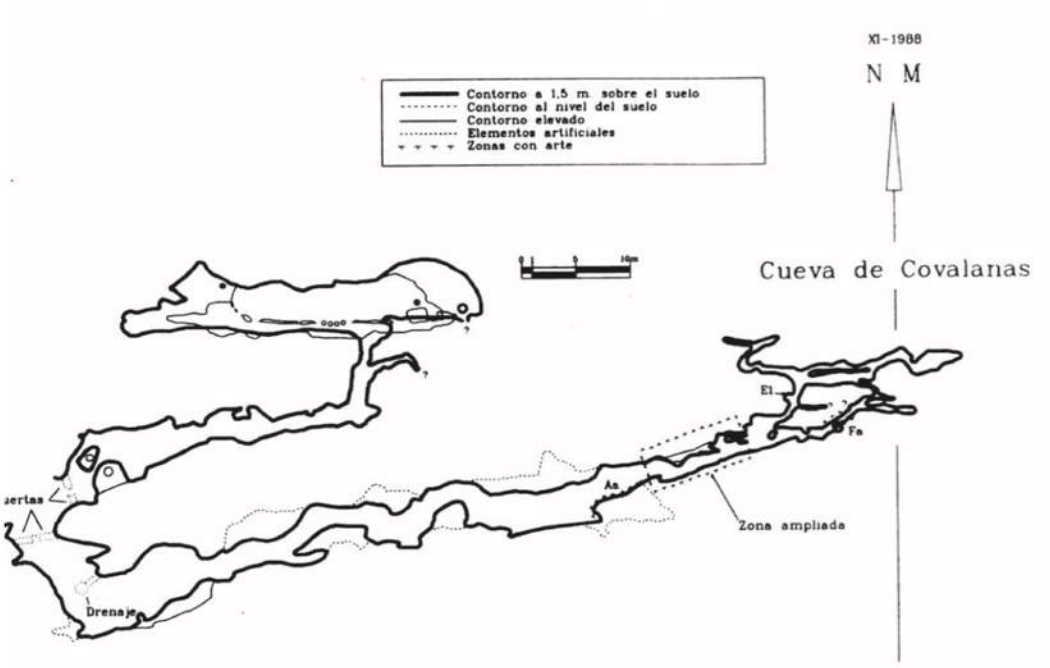

Figure 3.1: A plan of Covalanas cave. Although there are two galleries, the straight passage is the subject of this case study (after Romanillo et al. 1990: Figure 2).

coastal area (Morales and Straus 2000). Particularly this accessibility signifies the different importance of El Miron cave as an aggregation cave and Covalanas cave as a place for art.

The cave is divided into two area at its entrance, and this separation forms two parallel running galleries; the one on the left extending ~40m, and the right hand one a straight passage ~100m long (Figure 3.1). The cavity on the right contains pictures of stunning quality and therefore is the subject of this case study. The width of this gallery varies within 3-5m until 60m from the entrance, and it narrows until 1-2m after this point; especially after 70m the width further narrows. There are not salient speleothems and large stalagmites/stalactites in the gallery, and visitors can easily travel until the deepest area.

Images

The cave contains a total of 23 figurative images (19 deer, two horses, one aurochs, one possible zoomorphic figure) and geometric signs (four rectangles, one trapeze, one diamond shape, and a number of small lines and dots: Bischoff et al. 2012). Because of its dominant motif of the cave, Covalanas is known as 'the cave of red deer' (Ibid.). These images cluster between 60 and 90m along the passage; and all figurative images cluster in an even tighter area between 60-65m, where the gallery suddenly

narrows conspicuously. This confined area contains a further narrow conduit next to the main corridor, and images are also located on this conduit. Although the majority of images are found in the limited zone, red dots also repetitively appear on the left-side wall at the point of about 40m from the entrance and are distributed within a few meters. In addition, non-figurative black lines are located at random in this area. However, these black lines are dated to the medieval era (Maidagán 2010).

Red pigment was used for all images, which have been created by finger painting in the form of red dots. The artist/s of Covalanas cave created outlines of animals by superimposing these dots. As well as this unique drawing technique, 'V-shaped' ears of the deer are characteristic the art of Covalanas cave, and are shared among images in caves of Cantabrian region (e.g. El Pendo, Arenaza, and La Pasiega, which are so-called 'Group of the Ramales School': Barquin et al. 1998, 89). The wide distribution of similar painting style and technique allows us to presume an interaction between Upper Palaeolithic hunter groups even in long distance (e.g. there is approximately 40 km distance between La Pasiega and Covalanas).

Modern graffiti were once found on the wall throughout the cave. Today, most of the graffiti disappears after a cleaning programme. That was destructive enough to damage on the cave surface, and even some of the images were damaged (Moure Romanillo et al. 1990).

As for the age of the images, no reliable result of absolute dating has hitherto been established. Their age is therefore presumed on the basis of stylistic dating (Alcalde del Rio 1911,) and by the association with the few archaeological artefacts recovered in the excavations (Garcia-Diez and Ochoa 2012). Accordingly, its possible age falls in a broad timeframe between Aurignacian and Solutrean (Garcia-Diez et al. 2012); a recent review (Ochoa and Garcia-Diez 2015) suggests the possibility of the chronological range can be even widened, to include the late Magdalenian (approx. 17000 BP). However, it is usually considered to belong to the Solutrean period (Straus et al. 2002) in addition to La Pasiega and El Pendo due to their stylistic similarity.

Archaeologists have studied the set of the images in Covalanas at two distinct times: they were first examined by H. Alcalde del Río, H. Breuil and L. Sierra during the 1900s and the detail of the study was published *in Les Cavernes de la Région Cantabrique* (1911); this was subsequently updated in the early 1990s by A. Moure Romanillo, M. R. González Morales, and C. González Sainz (Moure Romanillo et al. 1990, 1991). The first work presented general perspectives on the images, involving the description of their detail as well as the cave plan, evaluation of their chronology, and interpretation of the depicted species. However, the knowledge provided by this early study is considerably inaccurate, regarding all aspects: descriptions were made by subjective assessment, and therefore systematic analysis was absent (Maidagan 2010); the interpretation was also

incorrect for some images (ibid.); and the cave plan generated was inaccurate (Moure Romanillo et al. 1990). For these reasons, the 1990s work focused on correcting these points and updated the previous documentation, presenting further accurate, detailed descriptions of images regarding technical execution, thematic, stylistic analysis. Although only recently Madagan (2010) re-examined the images by digital analysis and submitted more detailed information, above studies provide us with the basic knowledge of the pictures in Covalanas, all in all.

3.2 Methodology

Pictures to study

Although there is a total of 23 figurative images known in the cave, I examine 18 here. Five images are not clear enough for the analysis, and in one case, the shape is not reminiscent of that of a quadruped even though it is interpreted as deer. To treat the images, this study adopts the way to manage the images practiced in the work of Moure Romanillo et al. (1990): these authors divide the images into four groups on the basis of their location (pictures on the right walls are called A, on the left are B, on the right wall of the conduit part which is located behind the main collider are C, and on the left of this conduit as D). Also, they provide the images with the number as "A1" and "B5". The number is assigned in order from the entrance unless the exception of the images C1-2 (in this case the hind on the left is allocated the code C1 despite that it is farther from the entrance than the other hind on the right of the panel). Figure 3.2 shows the detailed plan of the area where the studied images are located and the distribution of the pictures with code in the area. The 18 images to be examined in this chapter are as follows: A1 (red deer), A2, (red deer), A3 (red deer), A5 (red deer), A6 (red deer), A7 (red deer), A8 (red deer), A9(red deer), A10 (red deer), A11, (horse), A13 (red deer), A14 (red deer), B1 (reindeer), B4 (red deer), B5 (red deer), C1 (red deer), C2 (red deer), and D1 (red deer).

These 18 images are distributed on seven independent panels. A1 and A2 are located on the panel closest to the entrance. They are horizontally juxtaposed within 151 cm (this width is measured from the backend of A1 to the frontend of A2). The next panel is where B1 is depicted. This panel is located nearby A1-2 but on the other side of

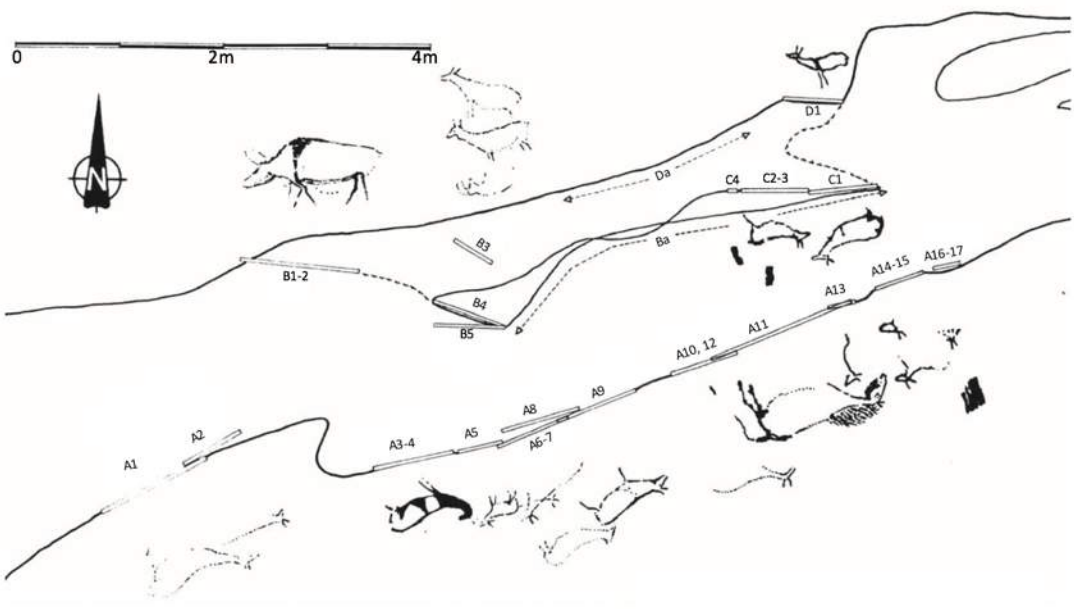

Figure 3.2: The detailed plan of the area where examined 18 images are found. Each of all images is given a unique code (after Romanillo et al. 1990: Figure 3).

the corridor. Another panel is found next to the panel of B1. This wall contains B4 and B5 in vertical juxtaposition within the width of approximately 100cm. The next two panels are located on the right wall of the corridor. The first panel possesses the highest number of images to be examined (A3, A5, A6, A7, A8, and A9), and these six images are placed within the area of 250 cm (the measurement is obtained between the right-end of A3 and the left-end of A9). The other panel is the most extensive of all panels, with the approximate length of 300m (from the right-end of A10 to the left-end of A14), and A10, A11, A13, and A14 are drawn on this panel. The remaining two panels are situated on the conduit behind the main corridor. This part is accessible from the wall in front of the previous panel, and panel C and D are located on the left and the right side of the wall of the conduit respectively. Panel C contains two deer (C1 and C2) facing each other within the width of 150cm, while there is only a single image (D1) on the other panel.

3D model

In this case study, a 3D model was created for each of these seven panels. The total number of photographs which was used for the reconstruction of each model is 126 (A1-2), 82 (B1), 81 (B4-5), 141 (A3-9), 176 (A10-14), 77 (C1-2), and 50 (D1). Figure 3.3 lists the all reconstructed models and their camera positions.

As artificial electric light was not installed inside the cave a flash light was used to generate enough visibility for the photoshoot. Once the models were reconstructed,

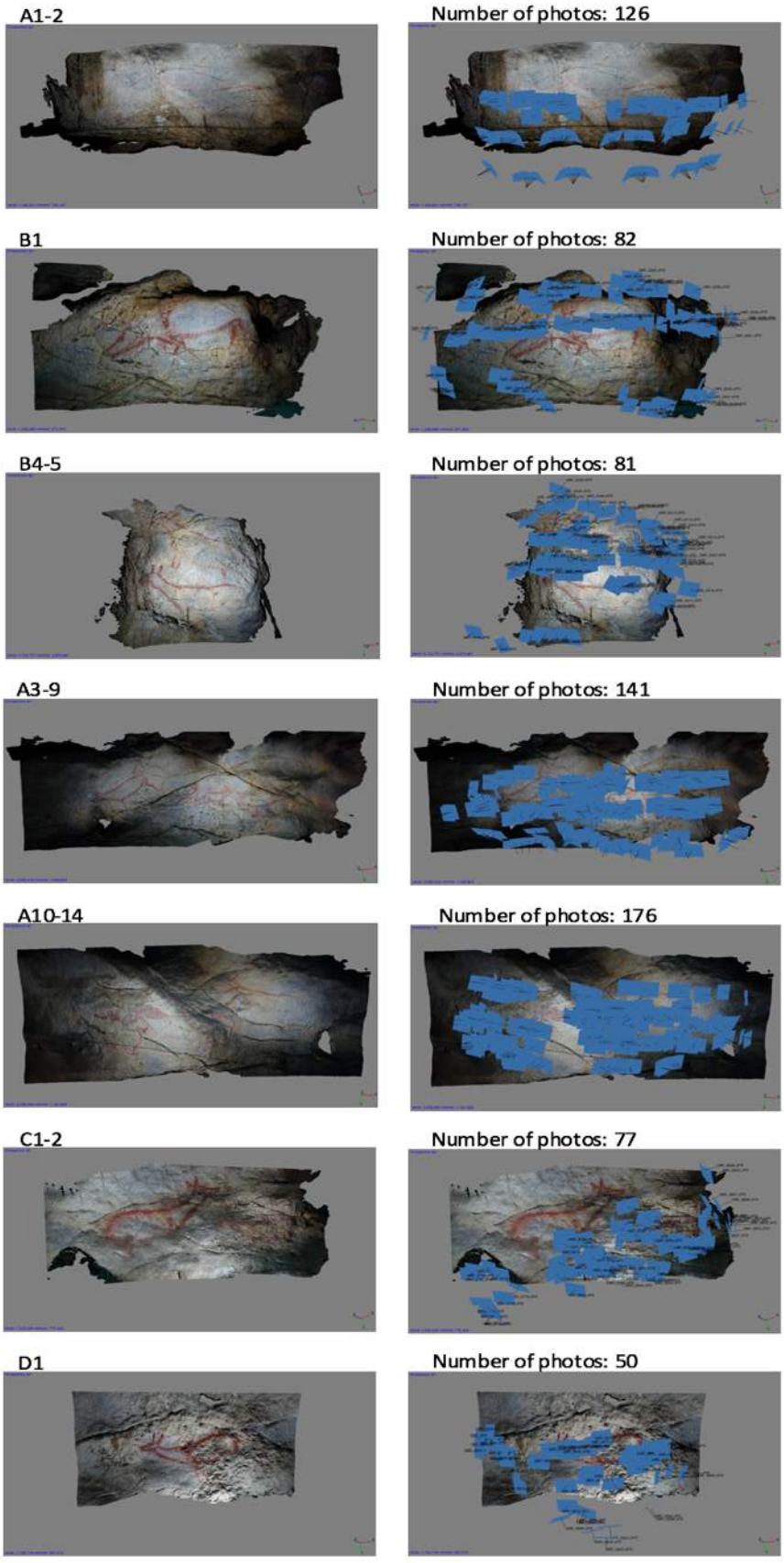

Figure 3.3: Seven reconstructed models and the number of photographic images used for the reconstruction. In total, 18 images are located in these panels. Blue squares on the panel represent the camera position of each photograph.

each image was respectively extracted from the 3D panel and exported in PLY format for a further analysis on Photoshop. Regarding two panels (A3-9 and A10-14), the processed data size is considerably large, so it was necessary to reduce the quality level from high to middle in order to properly operate the software due to an insufficient spec of the computer which processed the data. Nevertheless, as will be referred later, the accuracy of the model possesses enough reliability, despite lowering the quality.

The models generated were scaled and their accuracy assessed by following the procedure described in the last chapter. Arbitrarily selected images to scale models are A2, B2, B3, A3, A10, C2, and D1. As for the case where only a single image appears in the panel (B1 and D2), the upper muzzle was used to compare the difference between the physical and the virtual measurement. The measurement of the muzzle for both images is provided by Moure Romanillo et al. (1990). The result is shown in Table 3.1 below.

Consequently, the difference between the physical and virtual length for any images are within the range of 2.6 cm; the largest ratio of the difference is approx. 5% (A14: Difference (cm)/Physical length = 0.457). Basically, a physical measurement

Images	Physical length (cm)	Virtual length (cm)	Difference (cm)	Difference (%)
A1 (Red deer)	119	121.3	2.3	2
A2 (Red deer)	77	77	0	0
A3 (Red deer)	74	74	0	0
A5 (Red deer)	43	43.1	0.1	0.2
A6 (Red deer)	76	75.5	0.5	0.7
A7 (Red deer)	35	36.3	1.3	4
A8 (Red deer)	77	78.3	1.3	2
A9 (Red deer)	78	79.2	1.2	2
A10 (Red deer)	84	84	0	0
A11 (Horse)	122	119.4	2.6	2
A13 (Red deer)	16	15.6	0.4	3
A14 (Red deer)	35	36.6	1.6	5
B1 (Reindeer)	122 25(frontal)	122 25.8	0 0.8	0 3
B4 (Red deer)	88	88	0	0
B5 (Red deer)	85	85.3	0.3	0.3
C1 (Red deer)	90	90	0	0
C2 (Red deer)	67	67.8	1.8	3
D1 (Red deer)	64 10(frontal)	64 9.6	0 0.4	0 4

Table 3.1: The differences between the physical measurements and virtual measurements obtained in scaled models. The difference is less than 2.6 cm in all the pictures, which means that the reconstructed 3D models are sufficiently accurate.

suggests only an approximate value in its nature; a perfectly correct measurement cannot be obtained (Chodoronek 2015). This fact is especially a matter for a fieldwork regarding cave art. To avoid any damages on the artistic remains, archaeologists have to gather measurements without touching samples, and so it is inevitable that some degree of error occurs in the data: for example, the measurements of the images of Covalanas cave given by Romanillo et al. (1990) and Maidagán (2010) constantly show a marginal difference (1 – 3 cm). Therefore, the above-detected differences should be acceptable level as it is impossible to rule out any errors. Thus, generated seven models are accurate enough to be used for pictorial analysis in this case study. In addition, in some models, a green line or meshes appear on the wall. Those are protection nets covering each panel; however, they are assimilated into the topography of the model because their visibility is too marginal to be reconstructed as a 3D entity. Therefore, these nets appear simply a configuration on the model and do not affect the reconstructed topographic condition.

Simulation

As stated in the previous chapter, 3D models were rotated along the Y-axis to simulate how the topography of the wall distorts the appearance of images. The range of the rotation is summarised in Table 3.2. Also, each image is provided with a fixed angle in the X-axis, depending on its position. Although most images are placed on the location where viewers do not need to look up (x0°), several samples (A8, A10, B5, C1, and D1) are placed on a high position. X-axis for those images is set between x10° and x20°. For

Image	Horizontal Rotation (Y-axis)	Fixed angle (X-axis)
A1 (Red deer)	130° (left limit -70°, front 0°, right limit 60°)	10°
A2 (Red deer)	130° (-70°, 0°, 60°)	0°
A3 (Red deer)	130° (-70°, 0°, 60°)	0°
A5 (Red deer)	140° (-70°, 0°, 70°)	0°
A6 (Red deer)	140° (-70°, 0°, 70°)	0°
A7 (Red deer)	120° (-60°, 0° 60°)	0°
A8 (Red deer)	140° (-70°, 0°, 70°)	10°
A9 (Red deer)	150° (-70°, 0°, 80°)	0°
A10 (Red deer)	130° (-60°, 0°, 70°)	10°
A11 (Horse)	140° (-70°, 0°, 70°)	0°
A13 (Red deer)	150° (-70°, 0°, 80°)	0°
A14 (Red deer)	140° (-70°, 0°, 70°)	0°
B1 (Reindeer)	110° (-60°, 0°, 50°)	0°
B4 (Red deer)	150° (-80°, 0°, 70°)	0°
B5 (Red deer)	140° (-70°, 0°, 70°)	10°
C1 (Red deer)	140° (-70°, 0°, 70°)	10°
C2 (Red deer)	140° (-70°, 0°, 70°)	0°
D1 (Red deer)	140° (-60°, 0°, 80°)	20°

Table 3.2: The range of the horizontal angle for each image. Horizontal rotation simulates how the appearance of images changes when the viewer moves side to side. On the other hand, the fixed angle represents a degree at which a viewer looks up the image according to the height of the image.

the pictures with a relatively low height (A3, A5, A6, A7, A11, A13, and A14), the fixed angle is also given at 0°, which means the viewpoint is set at the same height as these images' height. As for viewing these images, even though viewers can freely choose their posture (crouching down or looking down) on their own, the simulation aims to reconstruct a view obtained by a viewer crouching down while looking forward. That is because rotating panels without a tilt in X-axis enables us to analyse the distortion more visibly. Therefore, their fixed angle is set at 0°. As the floor of the studied area remains intact and is supposed to be the same height as in the Palaeolithic (Moure Romanillo 1990), the measurements of the height of all images obtained from the fieldwork can be applied to the determination of the angle. The condition of the simulation for rotating the 2D models was also performed in the above setting.

3.3 Analysis of images

Deer (A1)

General Description

An outline red deer (*Cervus elaphus*) facing left, executed in a red finger dot line (Figure 3.4). The deer appears incomplete as only the head, under the neck and dorsal-buttock line are visible. However, the figure is in fact given its entire ventral line and the hind leg which have gone ambiguous to naked eyes today, and the lost part resurrects once a digital filter is applied (Hue/Saturation). All in all, the most visible area is the outline of the upper buttock, while the contours of the anterior, especially head, is somewhat blurred. Even so, the V-shaped ears and the long muzzle is clearly confirmable; otherwise, the head does not have details (eyes and mouth). Once the dotted line depicts the outstanding V-shape ears, the contours continue horizontally to the right as it slightly curves and then turns downward outlining the buttock. In this area, the visibility is lost, and the hind limb is almost invisible. Meanwhile, the face line continues from the muzzle obliquely to lower right portraying the under-neck. This line turns horizontally and extends further right, which is the outline of the belly. The length of the image is 119 cm, and the width is 48 cm. A1 is located on the height of 159 cm (shoulder) from the nearest floor.

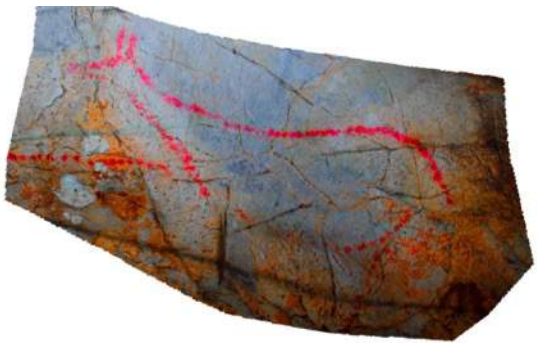

Figure 3.4: A1, outline red deer facing left (digital filter is applied).

Integration of natural lines

On the wall where A1 is located a large number of natural lines exist. Most of them are grooves, but there are also ridges. In addition to these lines, there is one point which needs be noted. The surface of this wall is generally smooth, but on the lower side, it becomes porous. The boundary between this porous part and the smooth surface is clearly visible as a natural line, and significantly, almost all of the belly line is outlined along this boundary line (Figure 3.5).

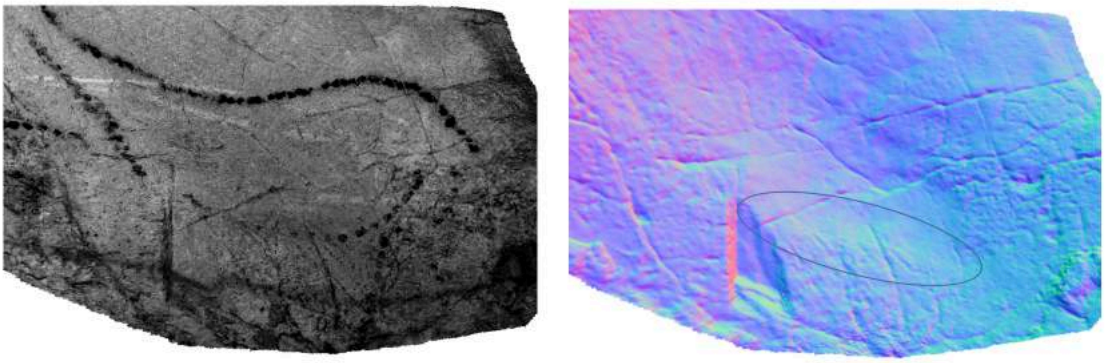

Figure 3.5: The integrated part of A1. Images are highlighted by digital filter: Hue/Saturation (left), Normals (right). The outline of the belly is drawn along a borderline separating the smooth surface from the porous surface.

Another compelling case is detected between the lower neck and the belly: in this region, the surface forms steep concavity, both edges of which appear as cliffs due to the elevational gap, and because these two edges lie vertically in a particular length, they seem as if frontal legs of A1. Although the truth for this case is unidentifiable (its appearance might be entirely coincidental and therefore not intentional), the shape of the legs by the two edges is closely identical to that of images in Covalanas (A3, A5, and D1). This sample is not counted as integration in this case study.

Topographic condition

Although the topography of this wall is moderate, the area on which the image is located forms a large concavity. Almost the entire body of the deer is located on this feature; the hind limb is not included in the analysis because of its lack of clarity. The body parts on the highest elevation are the head and the thigh; since this concaved wall is bowl-like shape, outer-edges are more elevated than inside the bowl. On the other hand, the central and ventral middle is placed on the bottom of the concave. The depth of the image is approximately 203mm, with the muzzle and the ventral thigh as the highest and the central middle as the lowest point (the model is at 1/100 scale: Figure 3.6). However, the head and the thigh comprise nearly half of this range (0.1-86.1mm) because the elevation of these areas are notably higher than the rest of the body.

Therefore, this level is treated as the extra high. The elevation is divided into three levels in the rest of the range between 86.2mm and 203mm (high: 86.2-129.2mm, medium: 129.3-166.1mm, low: 166.2-203mm). Although all body parts except the head and the thigh are located within this range, the defined part as high level are absent for this image because the area fails to includes the majority of any body parts.

Figure 3.6: A1 (1/100 scale) seen from the vertical position. As the whole image forms a concave shape like a bowl, the elevation at both ends is high, while it is the lowest at the mid-torso.

The wall begins recessing on the very tip of the muzzle and the thigh, and it gradually lowers elevation (0.1-86.1mm: see Figure 3.7, 1-3). The elevation is still reduced gradually toward the bottom as it extends from the head and the thigh, covering a part of the neck and the right side of the middle (86.2-129.2mm: 4-6). However, the detected areas are too limited to categorise the body parts as high elevation level as mentioned above. Between 129.3-166.1mm (7-9), the elevation becomes the medium level, and then the neck-shoulder is defined as this level. In the

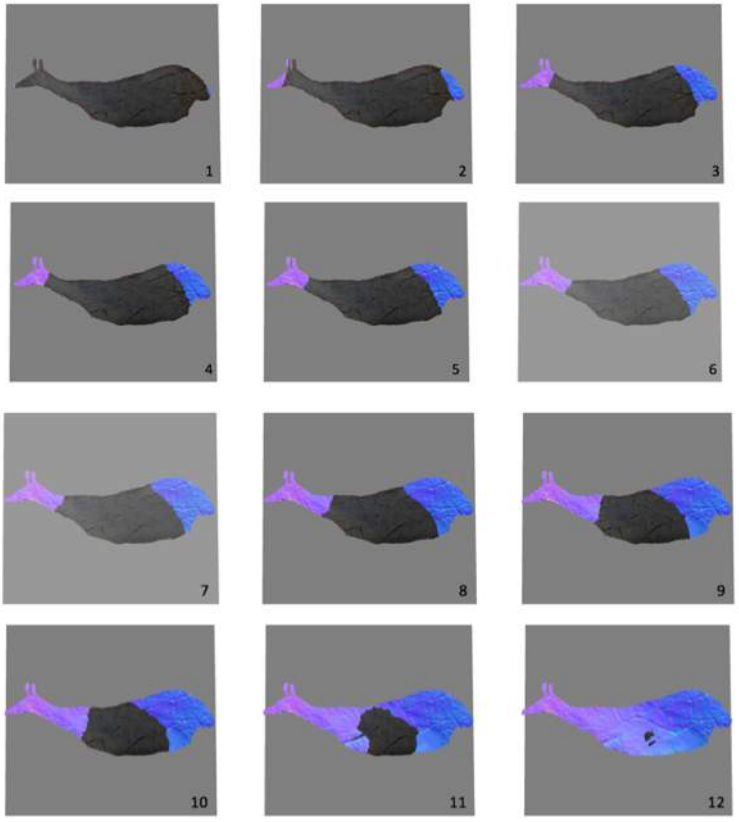

Figure 3.7: These images illustrate the depth of A1. When the cross-section layer passes the surface of A1, the colour of the surface changes; dark regions denote lower elevation than coloured parts. Images 1 - 3 are for 0.1mm - 86.1mm, 4 - 6 for 86.2mm - 129.2mm, 7 - 9 for 129.3mm - 166.1mm, and 10 - 12 for 166.2mm - 203mm.

meantime, the entire middle part is fixed on the zone of low elevation (166.2-203mm: 10-12). Although the elevation still varies by the region in the middle (dorsal side is higher than central and ventral), this area appears relatively flat. In contrast, the surface rises sharply on the right to the belly where the thigh is depicted.

Distortion on images: (Horizontal rotation x0°, y-60° to y60°)

This panel forms an overall concave as was mentioned above, and this topographic condition dramatically affects the appearance of the image when it is viewed from different viewing points. In particular, a remarkable distortion occurs on the neck and the head which are located on the surface of higher elevation. The rise on the wall gradually bends the outline of the cervical dorsal upward as it narrows the width of the neck when the viewing angle decreases (at y-60°: Figure 3.8). At the same time, the shape of the facial area goes horizontally shrunk as the interval of the ears almost vanishes. Especially this deformation is salient when the viewing angle is between -60° and -20°. This distortion causes a significant difference in the appearance of A1 compared to the image on the 2D surface; as for the image on the 3D surface the anterior becomes smaller, while it seems much larger on the 2D surface (Figure 3.8).

Figure 3.8: A1 on the 3D surface (left) and 2D surface (right) seen from y-60°. The image on the 3D panel is significantly distorted at its neck and head, but these parts stretch straight on the flat wall.

The image is also deformed once it is viewed from the right: although the contour of the right end of the ventral where the rear leg is supposed to exist is not perfectly attached to that of the buttock, this blank space gradually narrows from the viewing angle of 40° and disappears completely at 60° (Figure 3.9). That is because the convex surface on the right to A1 bents the outline of the buttock inward; the curve line at the dorsal to the buttock becomes considerably acute due to this topographic

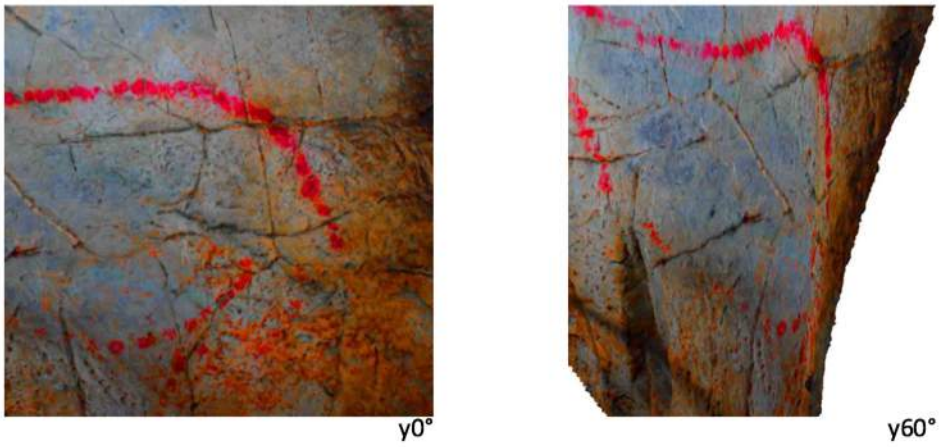

Figure 3.9: When the image is seen from the direct position, there is a space between the buttock and belly (picture on the left). However, once the viewpoint moves to the right, this space disappears, and the outline of the buttock connects to the ventral line.

intervention. Simultaneously, the anterior maintains its proportion even in this viewing angle as the wall of the area faces to the viewer. Therefore, A1 sustains its proportion at a certain level. This intervention does not occur for the anterior of the image on the 2D surface as it becomes noticeably smaller.

Deer (A2)

General description

An outline red deer facing left, located on the right to A1 but slightly lower position (Figure 3.10). This is an incomplete figure as only the head and the dorsal part are provided. Executed in a dotted red line, the head with noticeable V-shaped ears is visible; otherwise, the elements of the face (mouth and eyes) are absent. Although the provided body parts are limited, the face is well outlined including its protruded muzzle. The dotted line appears extending from the lower jaw to the right; however, it suddenly disappears immediately after the jaw. On the other hand, the contour of the dorsal continues horizontally to the right, but the line ends before portraying the buttock, and so the whole figure of this deer cannot be fully assumed. All parts of the ventral area are absent. The size of the image is 77 cm, and it is located at a height of 161 cm (dorsal) from the nearest floor.

Figure 3.10: A2, outlined red deer facing left. The ventral body is not provided.

Integration of natural lines

On the wall where A2 is located a large number of natural lines exist. Most of them are grooves, but there are also numerous edge lines due to the rough surface. However, none of these pre-existing lines is utilised for any contours of the deer. Despite that a long horizontal groove paralleling to the dorsal line appears overlapping at the right-end, they are not perfectly superimposed. Meanwhile, short grooves cross the face, but none of them seems integrated into the outline neither. Thus, A2 is placed on the panel independently from the natural pattern of the wall.

Topographic condition

First of all, the central and ventral sections are absent in A2. Unlike the previous image, no conspicuous topographic feature exists on the panel. Although the surface is finely undulating, the elevation is relatively homogeneous. Nevertheless, the surface for A2 appears, if not as a bowl, as a plate; the outer-edges are high in elevation, whereas the centre is low. The total depth is 49mm (the model is at 1/100 scale: Figure 3.11). The highest points are located on the head, precisely the tip of the ears, and the rightmost of the thigh. On the other hand, the lowest point is found on the dorsal middle. As was already noted above, the elevation level is homogeneously distributed within the range (high: 0.1-16.3mm, medium: 16.4mm-32.7mm, low: 32.8-49mm). There is no extra high and low elevation area.

Figure 3.11: A2 (1/100 scale) seen from the vertical position. As the whole image forms a bowl-like concave shape, the elevation is highest at both ends, while the lowest surface is found in the middle part.

The high area begins from both peripheries of the image. These sections gradually extend inward as they slightly decrease the elevation and finally cover the upper head and a part of the thigh (0.1-16.3mm: see Figure 3.12, 1-3). However, none of these body parts is assessed as the high level because these high-elevation areas are considerably limited. The elevation becomes the medium as the areas keep further extending inward, and this is where the all provided body parts are located except the mid-torso (16.4mm-32.7mm: 4-6); although the head and neck-shoulder partially remain undetected, most of these sections are fell in the medium level. Finally, the mid-torso is the lowest part of A2 (32.8mm- 49mm: 7-9). Thus, this deer is fixed on a moderate overall concave topography.

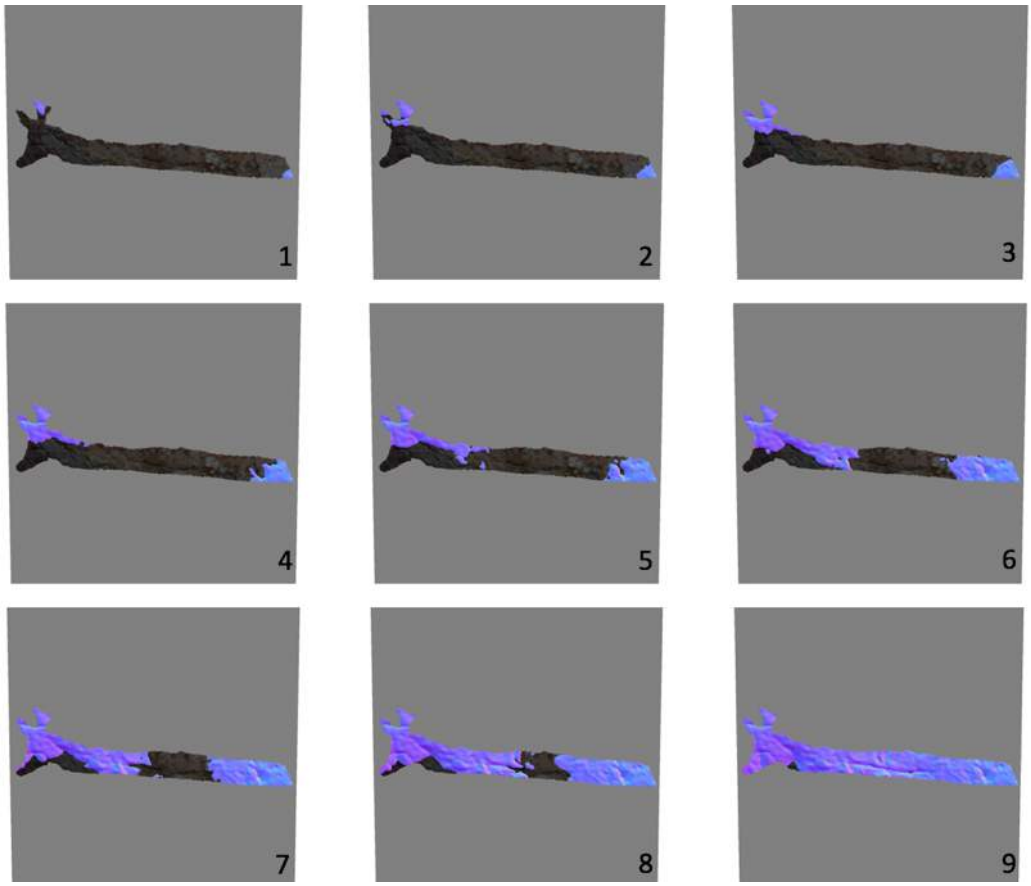

Figure 3.12: These nine images illustrate the depth of A2. When the cross-section layer passes the surface of A2, the colour of the surface changes; dark regions denote lower elevation than coloured parts. Images 1 - 3 are for 0.1mm - 16.3mm, 4 - 6 for 16.4mm - 32.7, and 7 - 9 for 32.8 - 49mm.

Distortion on images (horizontal rotation, x0°, y-60° to 60°)

Overall, significant distortions are not detected on A2, despite the fact that the image is fixed on a plate-like shape of the wall. This is probably attributed to two facts: it is because only the head and dorsal are depicted, and therefore no noticeable distortion occurs within the visible area; the other reason is that the topographic condition itself is not conspicuous in the given area. A subtle gap in elevation generates a slight deformation such as contraction\expansion of the length of the dorsal line by seeing the image from side to side. However, these transformations are not remarkable, and mainly there are no significant differences in appearances between A2 on the 3D and 2D surface.

Deer (A3)

General description

An outline red deer located to the rightmost part of the panel (Figure 3.13). A3 is a complete image outlined in red (only the tail is missing), although the frontal and hind limbs appear ambiguous due to erosion; these parts become visible to some degree once a digital filter (Hue/Saturation) is applied. According to Moure Romanillo et al. (1990), A3 is the most complex image regarding its composition of the posture and the artistic quality: unlike all the rest of the pictorial samples in Covalanas cave, the head and the body are oriented oppositely so that the deer appears turning back. As for the pictorial aspect, the image also has fill-in parts in its body. The area from the face to the neck is fully painted in vivid red, and the fill-in also appears in the mid-torso. On the right to this painted region, where the thigh is located, again only the outline is given. The face has no detail but is provided with V-shaped ears, although the left of which has gone slightly invisible. The contour is drawn in a streamline; in particular, the curve of the dorsal to the buttock and that of the belly are well expressed. The length of A3 is 79 cm, and it is located on a height of 106 cm (belly) from the nearest floor.

Figure 3.13: A3, deer facing left but looking back. All body parts are given except the tail.

Integration of natural lines

The wall where A3 is located is not especially rough although porous, and conspicuous natural lines are not present; only one distinguishable groove runs vertically, crossing the neck, and a small number of edges and ridges occasionally exists. However, the significant integration is confirmed in this deer. Figure 3.14 illustrates the topography of the panel, and it is visible that a long ridgeline, although subtle, runs horizontally. A part of the cervical dorsal and the full posterior dorsal are outlined along this line. There are also a few other ridges on this wall, and they are reminiscent of the contour of the buttock and ventral. However, there is no apparent overlap between the outlines and those ridges; nevertheless, those patterns might have inspired the artist of this image.

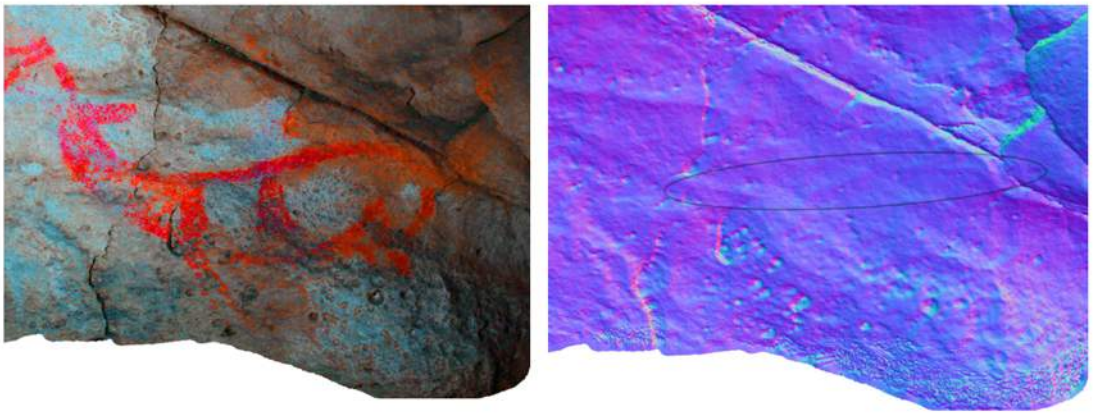

Figure 3.14: An example of integration in A3. From the root of the neck to the whole posterior dorsal is outlined along a horizontal ridge running horizontally. The artist of this image may have determined the entire picture of A3 based on this ridgeline.

Topographic condition

This wall undulates significantly and therefore generates areas of differring elevation level. The total range of the elevation is 146mm (the model is at 1/200 scale: Figure 3.15). However, the range within which the elevation level of most body parts are defined is limited between 50.4mm and 110.6mm (high:50.4-70.5mm, medium 70.6-90.6mm, and low: 90.7-110.6mm). The outside of that range is the extra high and extra low (0-50.3mm and 110.6-146mm) as there are body parts fixed within these extra levels.

Figure 3.15: A3 (1/200 scale) seen from the vertical position. The highest elevation is found on the head, while the lowest is on the frontal legs.

The detection began from the ears. The area gradually extends and covers the entire head, although lowering its elevation (0.1-50.3mm: see Figure 3.16, 1-3). Thus the head is located in the extra-high elevation. Between the range 50.4mm and 70.5mm, the high area continues downward from the head to the neck; however, the newly detected area is limited, and therefore it is not assessed as the high level. On the other hand, the dorsal thigh is fixed on a convex surface, and over half of the part passed the layer by a depth of 70.5mm (4-6). In the medium level, the highlighted regions further expand from both anterior and posterior; nearly a half of the neck-shoulder and the almost whole thigh are located on this moderate level (70.6-90.6mm: 7-9). At the same time, the hind leg is also fixed on this level. Accordingly, the entire mid-torso and a part of the neck-shoulder, and the frontal legs are placed on areas of lower elevation; especially the

ventral shoulder is the lowest among main body (90.7-110.6mm: 10-12). The frontal limbs gradually decrease its elevation from their roots, and the detection finally reaches the lowest point at the tip of the limb of the frontal left. (110.6-146mm: 13-15).

Distortion on images (horizontal rotation, x0°, y-70° to y60°)

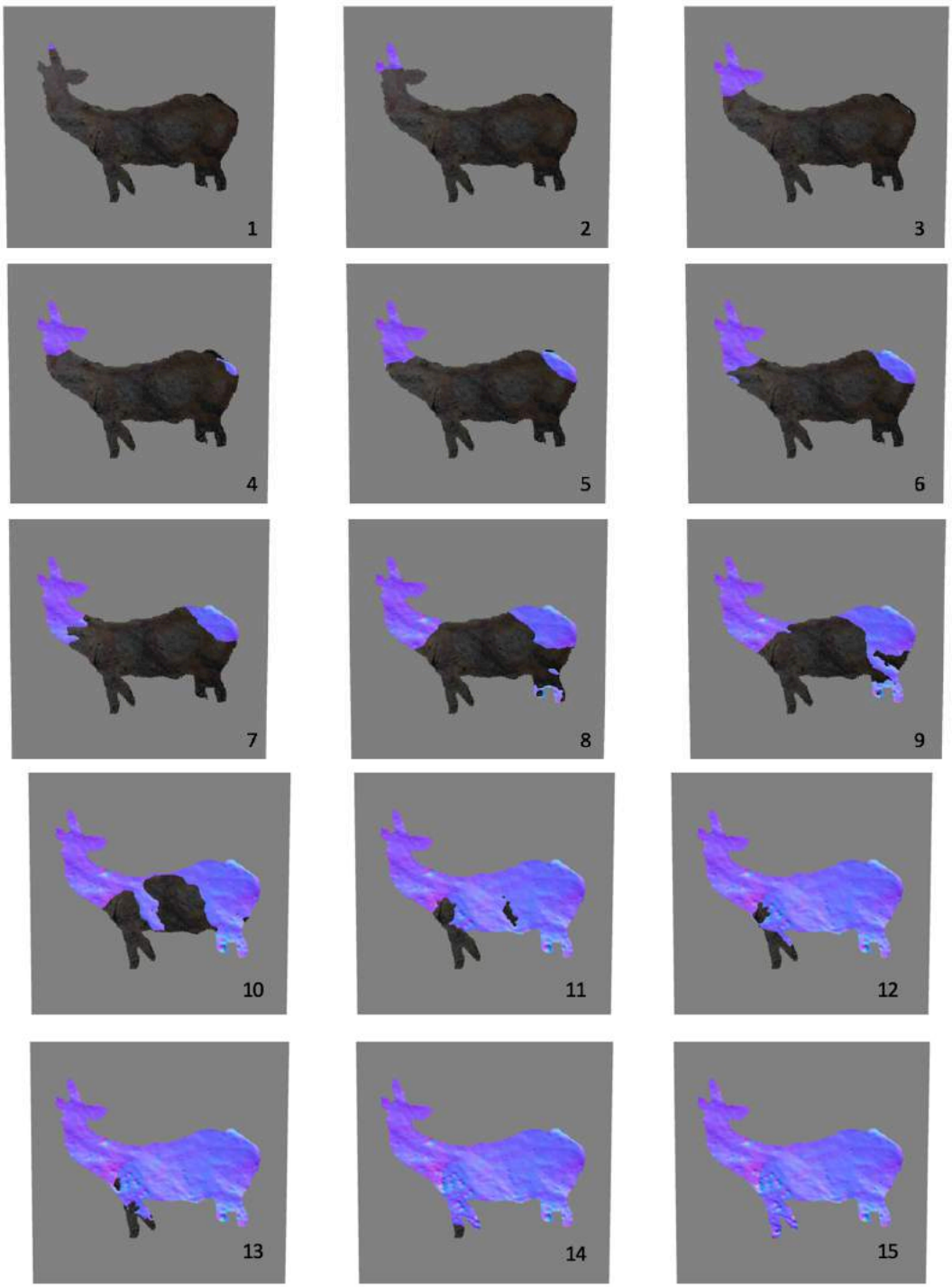

Figure 3.16: These 15 images illustrate the depth of A3. When the cross-section layer passes the surface of A2, the colour of the surface changes; dark regions denote lower elevation than coloured parts. Images 1 - 3 are for 0.1mm - 50.3mm, 4 - 6 for 50.4mm - 70.5, and 7 - 9 for 70.6 - 90.6mm, 10 -12 for 90.7mm - 110.6mm, and 13 -15 for 110.7mm - 146mm.

As the wall behind A3 highly undulates, such a topographic condition profoundly interferes the appearance of the image. Especially, the distortions are noticeable on the anterior part when the deer is seen from the left. As the viewing angle decreases, the overall width of the neck goes thinner (y-70°: Figure 3.17). This phenomenon is also detected in the 2D simulation; the neck is shrunk homogenously on the 2D surface. However, the extent and the way of the deformation is significantly different. The responsible factors for this distortion are the topographic condition on and around the neck: there is a concave on the neck which is immediately accompanied by a convex surface on its left, and this convexity gradually hides that concave area as the viewing point moves to the left. Consequently, the outline of the under-neck appears being pushed inward. At the same time, this convex wall on the left to the neck also pushes the chest inward, and therefore the neck appears further thinner.

Figure 3.17: A3 on the 3D surface (left) and 2D surface (right) seen from y-70°. The image drawn on the 3D panel is significantly distorted at its neck and mid-torso, but such deformations are absent in the image drawn on the flat wall. These interventions on A3's appearance are due to multiple topographic conditions rather than a single topography.

Aside from this, another deformation also occurs in the neck: the deer appears to be raising its neck further upwards. This distortion is also caused by several topographic factors. Along the cervical line, the wall rises, and the ridge of this elevated part substitutes the actual contour once the image is seen from the left. Along the cervical line, the wall rises, and the ridge of this elevated part substitutes the actual contour once the image is seen from the left. This substituting line appears extending upward sharply. Moreover, because the elevation on the dorsal middle area is lower than the dorsal neck, the substituting line (higher elevation) partly covers the line of the middle dorsal (lower elevation). Accordingly, the dorsal line appears shorter. Due to these factors altogether, the neck appears raising further upward as if the deer sees the further backward. Although the distortion occurs when the image is seen from the left,

the extent of the distortion reaches a maximum within the viewing range between y-70° and y-50°.

Meanwhile, a deformation also occurs in the middle part. Although the fill-in part appears clearly when viewed from the direct position, the painted area gradually narrows as the viewpoint moves to the left, and it is significantly contracted by y-70°. As a result, the whole body appears shrunk. That is due to the overall concave topography of A3; because the belly is located on an area of lower elevation than the neck, the neck-shoulder overlaps and hides the mid-torso. This deformation is most notably recognised when the viewpoint moves between y-70° and -30°.

Deer (A5)

General description

An outline red deer facing right, located immediately left to A3 (Figure 3.18). This deer appears standing still, while raising its muzzle as if bellowing or sniffing. The whole body except the tail is outlined in red dots. As it is in a well-preserved condition, the appearance of the entire body is still vivid, and therefore, viewers can see A5 easily. The contour of the muzzle, limbs (frontal and hind) and buttock is slightly blurred in comparison with the outline of the rest of the body. The face has no detail, but the V-shape ears are clearly visible. After the thin neck is outlined, the contour depicts the well-proportioned body. The spatial arrangement of the hind legs creates a perspective between them. The length of the image is 45cm, and it is located on a height of 135 cm (belly) from the nearest floor.

Figure 3.18: A5, outline red deer facing right. All body parts are given except the tail.

Integration of natural lines

Although no natural lines of any note are present on on the surface where A5 is located, this wall forms a complicated natural pattern by its undulating topography. This topographic irregularity produces a large number of edges along elevation gaps,

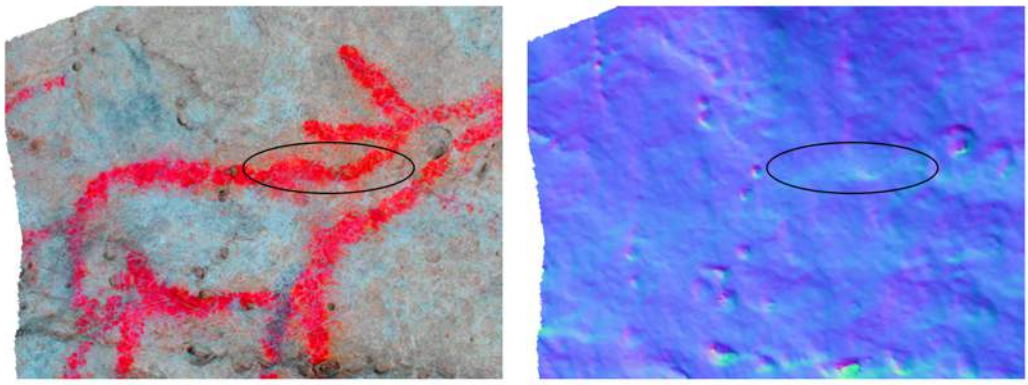

Figure 3.19: A5 and the natural pattern of the wall behind the image. Although noticeable natural lines are absent, there is a number of subtle edge lines. The contour of the cervical dorsal partly overlaps with one of those edges.

and the dorsal line is partly superimposed on one of such edge lines. Figure 3.19 demonstrates A5 and its topography, and it is visible that the cervical dorsal, although not entirely, is outlined along an edge. Apart from this integration, no other effective use of natural patterns is detected. Despite a horizontal groove running under the ventral line, it merely crosses the contour of the limbs. Thus A5 has integration only on the part of dorsal.

Topographic condition

A5 does not contain salient topographic features within its body. However, the undulation of the wall generates the elevational gaps. The total depth is 32mm (the model is at 1/100 scale: Figure 3.20) as the highest elevation found on the hind leg, and the lowest point is located on the frontal leg. The range within which the elevation level of most body parts are defined is limited between 10.3mm and 26.2mm (high:10.3-16mm, medium 16.1-21.8mm, and low: 21.9-26.2mm). The range between 0.1mm and 10.2mm contains the significant extent of the hind limb, and therefore there is an extra level in A5.

Figure 3.20: A5 (1/100 scale) seen from the vertical position. The highest elevation is found on the tip of the ears, while the lowest is on the frontal leg.

As the most elevated part of A5 is the left hind-leg. This area gradually extends upward, covering the other side of the back leg. By the depth of 10.2 mm, more than the half of the hind legs pass the cross-section layer, and the body section is defined as the extra high (Figure 3.21, 1-3). As the cross-section layer proceeds, the area continues extending from the hind limb to the ventral thigh, and simultaneously the detection also

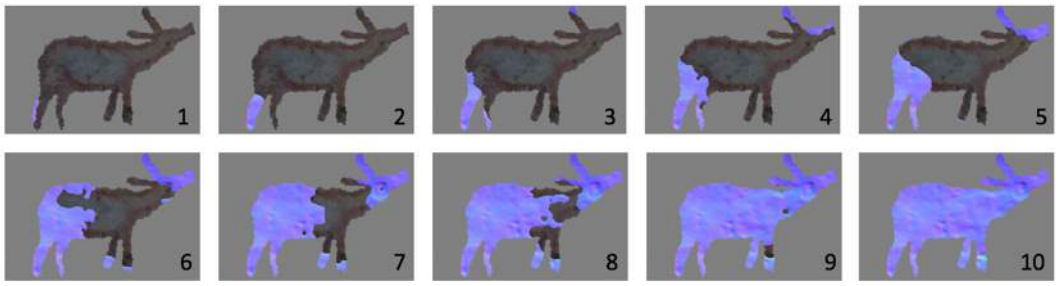

Figure 3.21: These ten images illustrate the depth of A5. When the cross-section layer passes the surface of A5, the colour of the surface changes; dark regions denote lower elevation than coloured parts. Images1-3 are for 0.1mm - 10.2mm, 4 and 5 for 10.3mm - 16mm, 6 and 7 for 16.1mm - 21.8mm, 8 and 9 are for 21.9mm - 26.2mm, and 10 for 26.3mm - 32mm.

starts on the head. These areas are mostly detected by 16mm and defined as high elevation level (4-5). During the next phase, the detected zone spreads inward from both anterior and posterior. However, the extent of the detection from the head is limited as only an insignificant part of the neck passes the layer. In contrast, the layer detected the dorsal-central thigh and the almost entire mid-torso, and hence these parts are assessed as the medium. (16.1-21.8mm: 6-7). The entire neck-shoulder and the frontal legs are fixed on the surface of the low elevation level (21.9-26.2mm: 8-9). Particularly, the surface of the limbs is concaved, and it needs further 5.8mm to be fully detected (10).

Distortion on images (horizontal rotation, x0°, y-70° to y70°)

Due to the gentle topography, no significant distortions are detected. However, A5 is deformed as the viewing point shifts. The body part which is most remarkably distorted is the head and the neck. Because the muzzle and the neck are located on a convex wall, this topographic setting interferes with their appearance once the viewing point is taken from the right. The convexity of the neck narrows its width, while the other convexity at the tip of muzzle pushes this part upward. Overall, it appears that

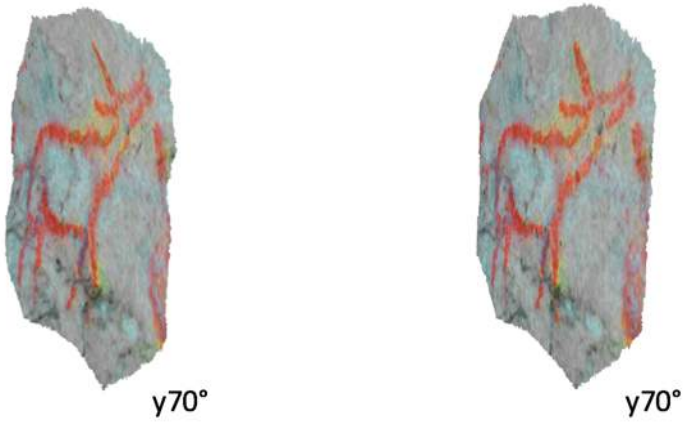

Figure 3.22: A5 on the 3D surface (left) and the 2D surface (right) seen from y70°. There are no significant differences, but the image on the 3D panel appears thinner at its neck and head.

the deer raises its neck and head, and these parts become smaller, compared to A5 in 2D simulation (Figure 3.22). At this time, the right ear appears thinner because the elevated wall interrupts the sight. This deformation most noticeably occurs when the viewing angle is taken between y50° and y70°. Apart from these examples, there are no other outstanding distortions in A5.

Deer (A6)

General description

An outline red deer facing right, executed in red finger dot (Figure 3.23). This deer is incomplete as the body on the ventral side is missing. The depicted sections are not homogeneously visible because the intensity of the colour varies. All in all, the contour of the anterior dorsal, the ears, and the under-neck appears vivid. On the other hand, most of the face and posterior dorsal and buttock are somewhat ambiguous. The face does not contain the detail; however, its V-shaped ears are confirmable. A6 is located immediately on the left to A5. Also, this image has an overlap with another deer (A7); the dorsal line of A7 horizontally crosses the neck of A6. According to Moure Romanillo et al. (1990), the upper part of the body is affected by the cleansing in the modern time, which somewhat blurs the appearance of the contour. The length of the image is 76 cm, and it is located on a height of 118 cm (buttock) from the nearest floor.

Figure 3.23: A6, outlined deer facing right. The ventral body is absent. The dorsal line of A7 horizontally crosses the neck of A6.

Integration of natural line

On the wall where A6 is depicted remarkable natural lines are mostly absent. Although a deep groove horizontally runs above the dorsal line, the line is irrelevant to integration. Other sorts of natural lines (edges, cracks and ridges) also do not appear. On such a pattern-less surface, the image is outlined without support from any natural features.

Topographic condition

Overall, remarkable topographic features are absent from the wall. However, the level of the elevation differs by parts of the body. The total depth is 48mm (the model is at1/200 scale: Figure 24). The range within which the elevation level of most body parts are defined is limited between 16.1mm and 48mm (high: 16.1-26.7mm, medium: 26.8-37.3mm, and low: 37.4-48mm). The highest point is the tip of ears, while the lowest is found on the dorsal thigh.

Figure 3.24 A6 (1/200 scale) seen from the vertical position. The highest elevation is found on the tip of the ears while the lowest is on the dorsal thigh.

The detection of the topography begins at both ears, and the detected regions extend downward (0.1-16mm). However, none of the body sections is located within this depth range. Between 16.1mm and 26.7mm, the head is assessed as the high elevation as over half of the part passes the cross-section layer (see Figure 3.25, 1-2). As the layor proceeds further, the region around the head continues extending to the left, while it lowers the elevation. The dorsal-central neck is mostly detected at a depth of 37.3mm (3-4) and evaluated as the medium. A part of the mid-torso also elevates as high as the neck-shoulder, but it cannot be assessed as the medium because the extent is limited. Therefore, the entire thigh and most of the mid-torso are located on the low-level surface (37.4-48mm: 5-6). All in all, the whole body of A6 is moderately undulating, but the posterior appears flat.

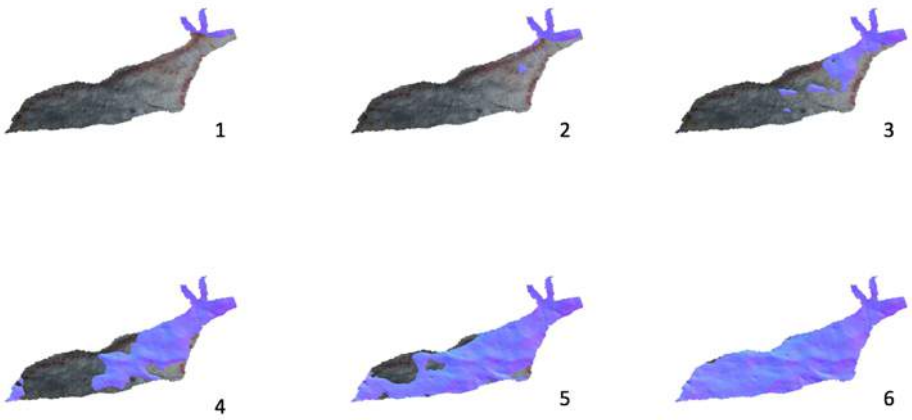

Figure 3.25: These six images illustrate the depth of A6. When the cross-section layer passes the surface, the colour of the surface changes; dark regions denote lower elevation than coloured parts. Images 1 and 2 are for 16.1mm - 26.7mm, 3 and 4 for 26.8mm - 37.3mm, and 5 and 6 for 37.4mm - 48mm.

Distortion on images (horizontal rotation, x0°, y-70° to y70°)

The simulation does not demonstrate any remarkable distortions. There is also no conspicuous difference in the appearance between the image on the 3D and 2D surface. The absence of deformation might be due to the image's incomplete body and the relatively flat surface.

Deer (A7)

General description

An outline red deer facing left, located to the left of A5 and overlapping with A6 (Figure 3.26). A7 contains only V-shaped ears and its dorsal line. Because of its incompleteness, the image appears as a line rather than a figure. The contour is executed in red dots; the ears and the rightmost of the posterior are the most visible as the dots concentrate more here than in its other parts. Most of the body, particularly the face, is affected by the cleaning (Moure Romanillo et al. 1990). The length of the image is 35 cm, and it is located at a height of 120cm from the nearest floor.

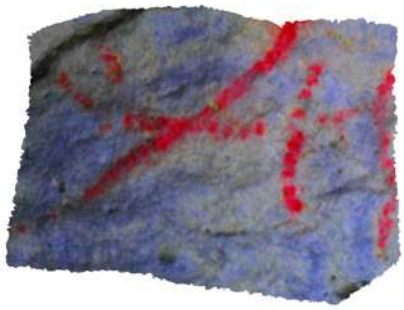

Figure 3.26: A7, outline image of red deer. As only the dorsal line and V-shape ears are visible, the figure appears as a line rather than body.

Integration of natural lines

On the wall where A7 is depicted remarkable natural lines are mostly absent. Although a deep groove horizontally runs under the outline of the dorsal line, the line is irrelevant to integration. Other sorts of natural lines (edges, cracks and ridges) also do not appear. On such a pattern-less surface, A7 is outlined without support from any natural features.

Topographic condition

A7 is depicted on an overall moderate convexity, although only the head and the dorsal side of the body is provided. The total depth is 28mm (the model is at 1/200 scale: Figure 3.27). However, the range within which the elevation level of the most body parts are defined is limited between 0.1mm and 19.4mm (high:0.1-6.5mm, medium 6.6-12.9mm, and low: 13-19.4mm). The range between 19.5mm and 28mm is applied to the tip of the ears and the right edge of the thigh.

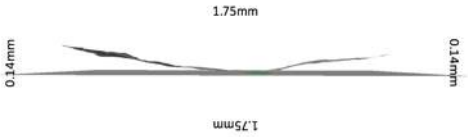

Figure 3.27: A7 (1/200 scale) seen from the vertical position. The wall forms an overall convex shape. The highest elevation is found on the middle dorsal, while the lowest is on the tip of the ears and the thigh.

The high elevation of this topography corresponds to the mid-torso. Detection gradually expands from the section towards the right and left (0.1-6.5mm: see Figure 3.28, 1-3). During the next phase, the neck is mostly detected and assessed as the medium level (6.6-12.9mm: 4-6). The expansion also continues to the right, and the topography of the thigh passes the cross-section layer by 19.4mm, meaning that the

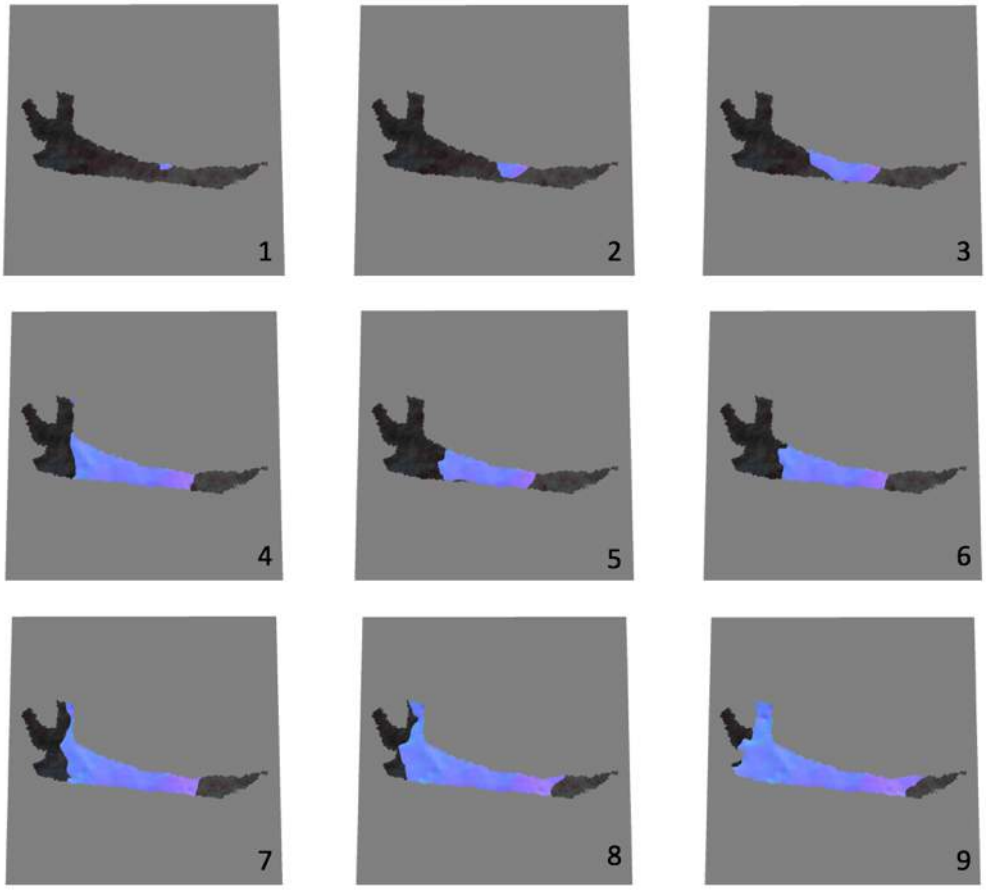

Figure 3.28: These nine images illustrate the depth of A7. When the cross-section layer passes the surface of A7, the colour of the surface changes; dark regions denote lower elevation than coloured parts. Images 1-3 are for 0.1mm - 6.5mm, 3 and 4 for 6.6mm - 12.9mm, and 5 and 6 for 13mm - 19.4mm.

body section is located in the low elevation range (13-19.4mm: 7-9). At this time, the cross-section layer also detects the head, and hence it is assessed as the low-level elevation. The elevation of both edges of A7 is further lower, but this area accounts for only a marginal proportion of the head and the thigh.

Distortion on images (horizontal rotation, x0°, y-60° to y60°)

The simulation does not demonstrate any remarkable distortions. There is also no conspicuous difference in the appearance between the image on the 3D and 2D surface. The absence of deformation might be due to the image's incomplete body and the relatively flat surface.

Deer (A8)

General description

An outline red deer facing left, located above A6 and A7 (Figure 3.29). This deer is an almost complete figure; only its tail and forelimbs are absent. The overall presence of A8 is weaker than the other images on the same panel because the red dots which outline the image are sparse. The face lacks details as the mouth and eyes are not provided. A8 is fixed in a slightly oblique position. The length of the image is 77cm, and it is located on a height of 178cm (belly) from the nearest floor, which is the highest position in this panel.

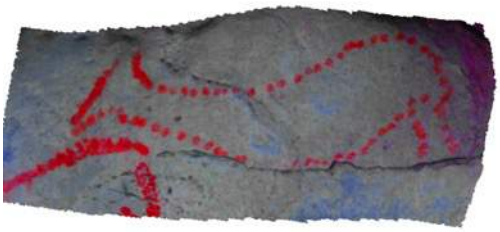

Figure 3.29: A8, outline deer facing left. The whole body except the forelimbs and tail is depicted. The presence of the image is generally weak as the density of the outlining dots is low (digital filter applied).

Integration of natural lines

The wall contains two conspicuous natural lines. One of these is an edge line formed by an elevational gap, traversing the body of the deer semi-vertically from the upper left. However, this natural pattern is not used for integration. The other line is a deep, thick groove which runs immediately under A8. This groove is integrated into a part of the ventral line. Figure 3.30 illustrates the

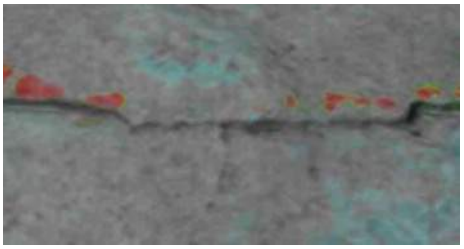

Figure 3.30: An example of integration in A8. A thick groove line running just under the image is utilised as a part of the ventral line.

integrated section of the ventral contour, and it is clear that the outline of sparse dots is not provided along the groove, but in turn, the groove itself becomes the outline.

Additionally, another integration is found on the buttock. There is an edge line on the upper posterior area caused by a slight elevation gap (Figure 3.31). This edge lies as it curves downward, and the curvy outline of the buttock is partly drawn along it. Apart from these examples, no more integration is confirmed.

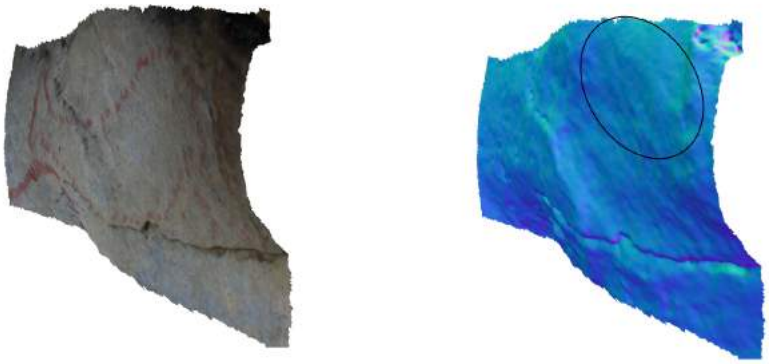

Figure 3.31: Another example of the integration in A8. The buttock is outlined along with an edge line. The curve of the buttock coincides with that of the edge line.

Topographic condition

This panel does not contain any salient topographic features except for a small convexity on the shoulder, but the surface is somewhat undulating, and therefore the elevation differs by region. The total depth is 66mm (the model is at 1/200 scale: Figure 3.32). The range within which the most body parts are defined their elevation level is limited as it happens between 12.1mm and 48mm (high:12.1-24mm, medium 24.1-36mm, and low: 36.1-48mm). Ranges between 0mm and 12mm and between 48.1m and 66mm are the highest and the lowest region, but none of the body sections belongs to these extra elevation levels.

Figure 3.32: A8 (1/200 scale) seen from the vertical position. The highest elevation is found on the neck-shoulder while the lowest is on the hind limbs.

The highest elevation corresponds to the convexity on the central neck-shoulder as the detection begins from the region and then gradually spreads (0.1-12mm: see Figure 3.33, 1-2). However, the detected area fails to cover neither the majority of the central nor ventral neck-shoulder. This convex, although lowering the elevation, further extends and includes almost all the neck-shoulder at the high elevation level (12.1-24mm: 3-4). At the same time, the high elevation area is detected at the ventral thigh.

Even though nearly half of the face belongs to the high level, it is assessed as the medium level because the area which passes the cross-section layer reaches its majority between 24.1mm and 36mm (5-6). The dorsal-central thigh is also placed in the medium level. The parts left on the low-level surface are the entire mid-torso and the hind leg as well as a part of the head (36.1-48mm: 7-8). Although the elevation is almost homogenous in the middle, it is slightly higher in the centre as the surface rises. The lowest area is the hind legs as the elevation decreases toward the feet.

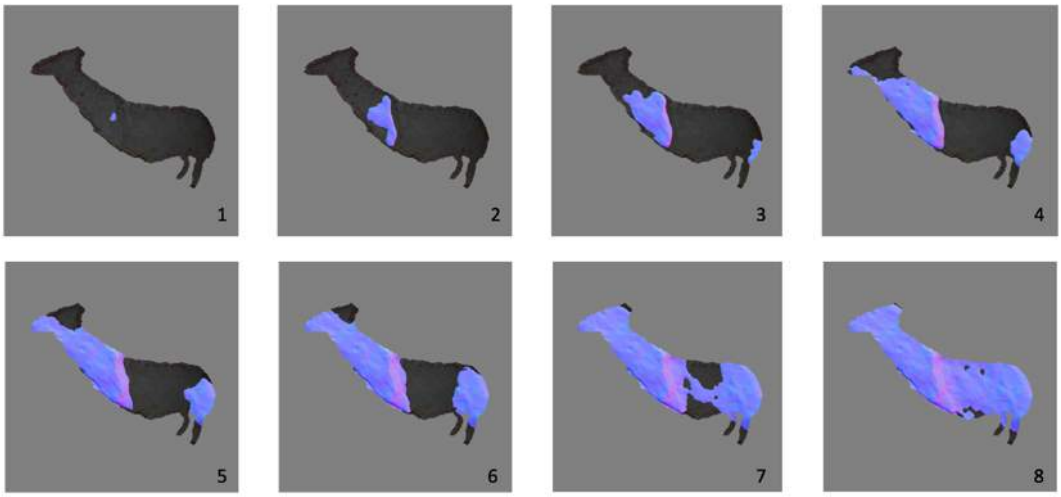

Figure 3.33: These eight images illustrate the topographic depth of A6. When the cross-section layer passes the surface of A9, the colour of the surface changes; dark regions denote lower elevation than coloured parts. Images 1 and 2 are for 0.1mm -12mm, 3 and 4 for 12.1mm - 24mm, 5 and 6 for 24.1mm - 36mm, and 7 and 8 for 36.1mm - 48mm.

Distortion on images (horizontal rotation, x10°, y-70° to y70°)

The simulation demonstrates distortions on the image, although their extent is not remarkable. When the viewing point moves towards the left, the image appears almost identical to one on the 2D wall; however, a deformation occurs at the middle of the dorsal line. The two dots, which are located on the right to the convexity of the neck-shoulder, gradually go unseen as they are hidden by the elevated surface (y70°: Figure 3.34). By contrast, these dots are visible even if seen from the same angle in the 2D simulation. Once the two simulations are compared, the cervical-dorsal area of A8 appears more shortened on the 3D surface. This contraction recovers conspicuously as soon as the viewpoint moves to the direct position (y0°). This shrink-stretch movement is most noticeably perceived when the viewing angle is between y-70° and y-40°.

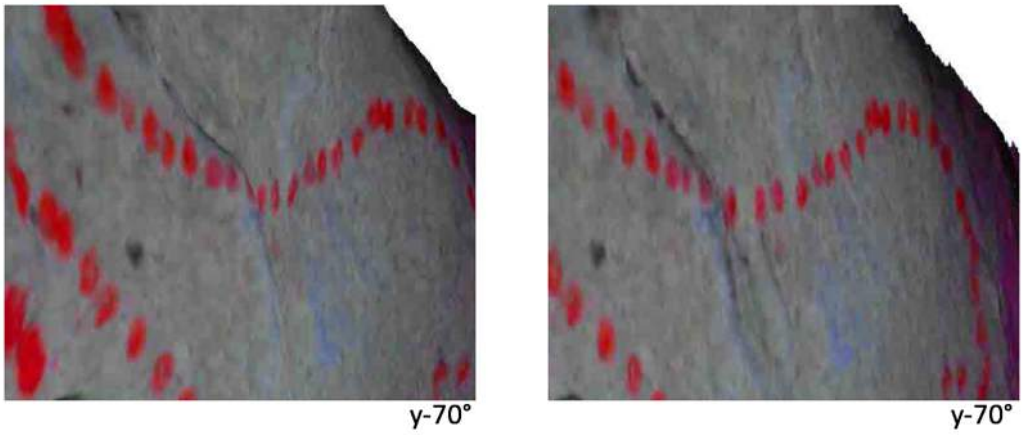

Figure 3.34: A8 on the 3D surface (left) and the 2D surface (right) seen from y-70°. The dots that constitute the dorsal line become partly invisible because they are hidden by a raised wall, while the dots are still visible in the image drawn on the flat surface. Although this is only a slight difference, the neck becomes shorter than in the 2D simulation.

Meanwhile, A8 is also distorted when the viewpoint is taken to the right. Because the wall on the buttock and the root of the hind limbs rises, this convex topography deforms the outline of those body parts. Figure 3.35 shows A8 viewed from y70°. The contour from the buttock to the right hind leg appears bent inward by the convex surface. Also, the rise on the limbs, although not significant, distorts the belly by pushing it inward. Consequently, the entire posterior part appears raised further upward. This deformation becomes the most remarkable between y60° and y70°. That deformation is unique to the 3D setting as such a phenomenon is absent in the 2D simulation.

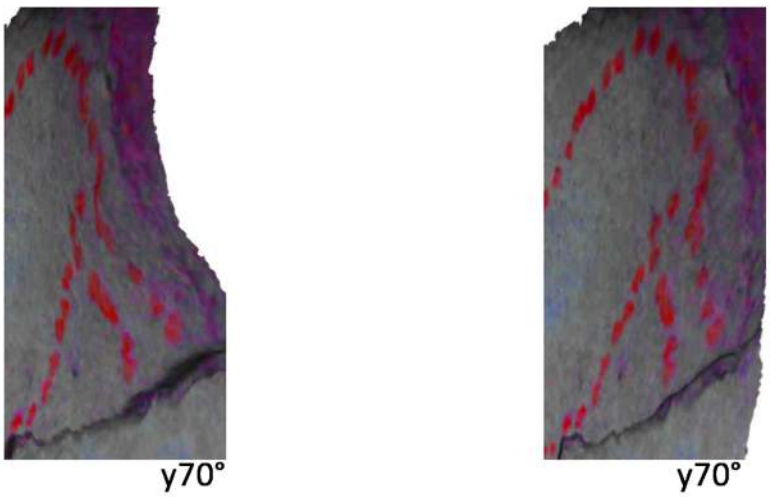

Figure 3.35: A8 on the 3D surface (left) and the 2D surface (right) seen from y70°. Although multiple convex surfaces distort the posterior body, both hind limbs are noticeably deformed as their direction changes. However, the legs on the 2D surface receive no topographic intervention.

Deer (A9)

General description

An outline red deer facing left, located at the leftmost side of the panel (Figure 3.36). The complete body minus the tail is fixed slightly in an oblique position, as with the previous deer. A9 is well-preserved, and its strong presence remains vivid. The outline is executed by both dot painting and single stroke. The stroke appears intermittent because the pigment was not diluted enough. Therefore, the colour did not spread homogeneously on the limestone surface, and the outline still resembles a trail of dots (Moure Romanillo 1990). The head is provided with an eye and V-shaped ears; the eye itself is expressed by a single dot. Additionally, several dots are left on the body. There are also traces of scraping on the head, torso, and croup. However, these removed surface is not the palaeolithic origin, but a result of a destructive work to clean the modern graffiti (Ibid). The length of the image is 78 cm, and it is located on a height of 153 cm (belly) from the nearest floor.

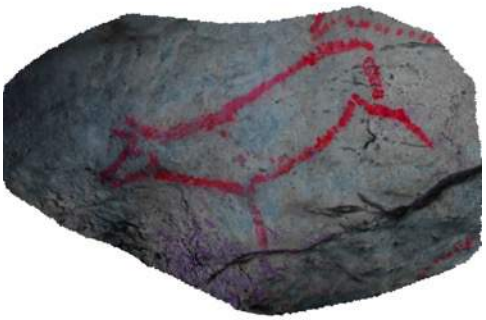

Figure 3.36: A9, outline red deer facing left. The whole body except the tail is depicted. This is one of the most outstanding images in Convalanas cave (digital filter applied).

Integration of natural line

The wall on which A9 is depicted contains a large number of natural lines. These lines vary regarding the size and the type (groove, edge and ridge) However, most of such lines are located around the deer; for example, the most remarkable edge on this panel obliquely lies below the image, which appears as the ground line for A9 and creates an impression as if a deer is ascending a slope. Short grooves are also intensively found on the thigh. Nevertheless, these grooves are not utilised for any contours of A9. The integration is confirmed on the ventral line. On the left side of the image, the topography turns to be complicated and generates noticeable elevational gaps. In such an undulating surface, a ridgeline runs semi-vertically, and the contour of the under-neck is drawn along this ridge (Figure 3.37). Apart from this example, apparent integration is absent.

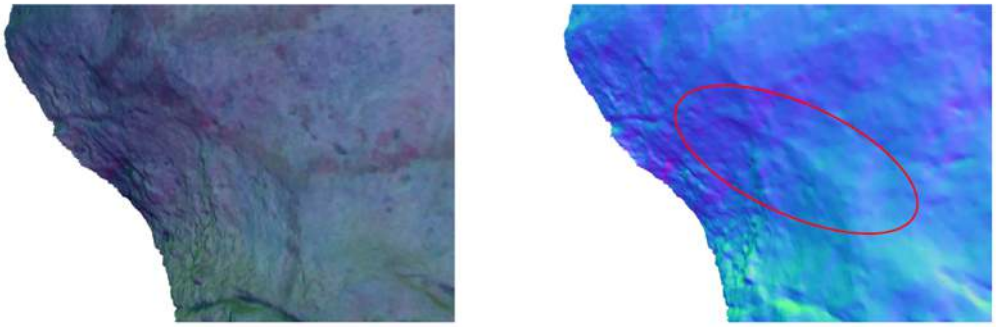

Figure 3.37: The example of integration in A9. A ridge which runs obliquely is integrated into the outline of the frontal neck. This natural line becomes noticeable especially when the image is viewed from the right.

Topographic condition

A9 is placed on a highly undulating surface, which generates a noticeable elevation gap between the body sections. The total depth is 96mm (the model is at 1/200 scale: Figure 3.38). The range within which the elevation level of the most body parts are defined is limited between 15.3mm and 75.8mm (high: 15.3-35.4mm, medium: 35.5-55.6mm, and low: 55.7-75.8mm). Some body parts are located out of the above range, meaning that there is the extra high (0.1-15.2mm) and the extra low level (75.9-96mm) for A9.

Figure 3.38: A9 (1/200) scale seen from the vertical direction. The highest elevation is found in the head and limbs while the lowest is in the ventral mid-torso.

The highest elevation is detected on the head and both frontal and hind foot. While the elevated area at the legs does not extend significantly, the major extent of the head passes the cross-section layer between the ranges of 0.1mm and 15.2mm (see Figure 3.39, 1-2). The high-elevation surface continues spreading as it lowers the elevation, and the dorsal neck-shoulder and the frontal limb are located on this level (15.3-35.4mm: 3-4). The hind leg has not been defined yet because most of the section is not detected. The medium level is between 35.5 and 55.6mm (5-6), and the central-ventral neck-shoulder, the hind limb, and the dorsal thigh are detected within this level. Therefore undetected sections (the whole mid-torso and central-ventral thigh) is defined as a lower elevation. However, the elevation still varies; dorsal-central mid-torso and central-ventral thigh are detected at the low level, whereas the ventral mid-

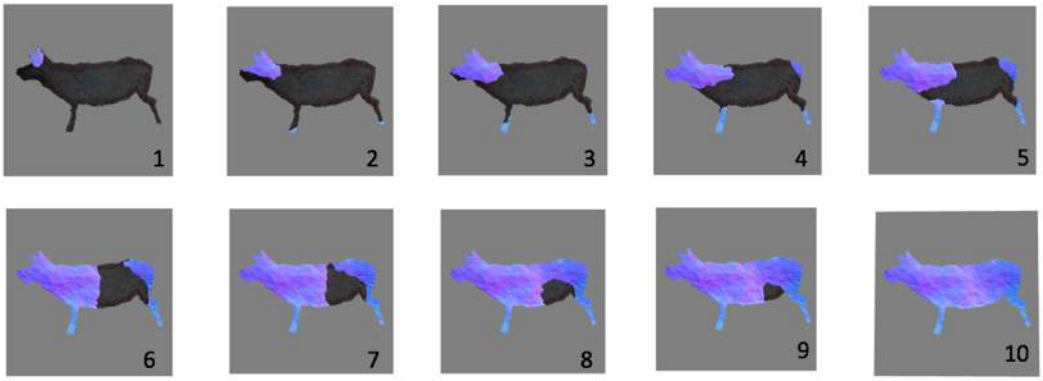

Figure 3.39: These ten images illustrate the depth of A9. When the cross-section layer passes the surface of A9, the colour of the surface changes; dark regions denote lower elevation than coloured parts. Images 1 and 2 are for 0.1mm - 15.2mm, 3 and 4 for 15.3mm - 35.4mm, 5 and 6 for 35.5mm - 55.6mm, 7 and 8 for 55.7mm - 75.8mm, and 9 and 10 for 75.9mm - 96mm.

torso is placed in a further lower concave (55.7-75.8mm: 7-8). That is the deepest point of A9, which finally passes the layer at a depth of 96mm (9-10).

Distortion on images (horizontal rotation, x0°, y-70° to y80°)

Due to A9's dynamic topographic condition, profound distortions constantly occur in all body parts of the image whenever the viewing angle changes. Generally, when the viewing position moves to a side, an image on a 2D medium appears shrunk inward both from the anterior and posterior because of the perspective. However, the shrinkage of A9 on the 3D setting is not identical to the distortion in the 2D image because the combination of the large convex (the head and cervical area) and the large concave (the mid-torso) interferes the appearance of A9 destructively. In consequence, the image is severely distorted (Figure 3.40): as the viewing angle decreases from 0°, both dorsal and ventral line gradually appear bent upward at the posterior; at the same time, the buttock is pushed inward as it is located on a concave surface, and this

Figure 3.40: A9 on the 3D surface (left) and 2D surface (right) seen from y-70°. The image is markedly deformed due to the convexity above the neck and head and the concave in the mid-torso. The distortion is noticeable when it is compared to A9 on the 2D panel.

distortion also contributes to the further rise of the posterior body; moreover, the convex on the head pushes the anterior section to the front. This combination of deformations generates a particular form of dynamism: all in all, the deforming process of A9 which is perceived between y0° and y-70° appears as if a deer is dynamically kicking the ground.

When the viewing point moves to the right, the topographic condition also affects A9's appearance. While the image on the 2D surface merely shrinks as the angle increase from 0°, A9 on this topography sustains its length even at y80°. That is because the convex on the anterior constantly shows its surface to the viewer and because the concaved posterior emphasises the presence of the mid-torso and thigh. Apart from the main body, both frontal and hind limbs are also deformed: these limbs are hidden by the noticeably elevated wall on the right to the buttock as the viewing position moves to the right. Both legs start disappearing from y40° and go completely unseen at y80°. During this process, the legs also appear bending forward and backwards. Thus, A9 is remarkably deformed at any time when viewing position moves and seems no fixed form.

Deer (A10)

General description

An outline red deer facing left, located on the upper right part of the panel (Figure 3.41). A10 is provided with the contour of the head, dorsal, buttock and under-neck. The under-neck and the buttock appear somewhat ambiguous at their edge due to cleaning to remove grafiti. Executed techniques are overlapping dots and simple dots. The head is the most visible of all the body parts; above all, V-shape ears are still noticeable, and a single dot depicts an eye. The muzzle somewhat loses visibility because of runoff on the cave surface. From the head, the contour continues to the obliquely downward right, depicting the dorsal and under-neck. The presence is stronger in the anterior than the posterior; outlining dots more concentrate in the anterior as they overlap each other, whereas dots in the posterior are sparse. The length of the image is 84 cm, and it is located on a height of 178 cm (under-neck) from the nearest floor.

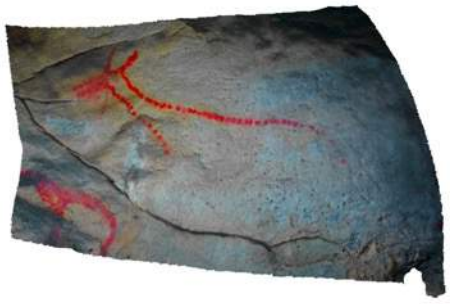

Figure 3.41: A10, outline red deer facing left. The ventral body is absent. A run-off on the cave wall blurs the muzzle.

Integration of natural lines

The wall on which A10 is fixed is very smooth, and natural lines are almost completely absent. Three major grooves are running above, in front of, and under the image, none of them overlaps A10's outline. The surface is occasionally undulating, and this topography creates edge lines around the neck. However, the ventral neck is drawn regardless of those edges. Overall, integrations are not confirmed on any parts of the contour, which means the artist of A10 produced this image without the assistance of the natural patterns of the wall.

Topographic condition

Because of the absence of the ventral body, only the head and dorsal-central body are considered for the analysis. Overall, no significant topographic features exist on this panel. However, it is not completely flat as the wall forms an overall concavity. As the shape of the wall itself appears as a plate, the elevation of the outer-edges are the highest. The total depth is 44mm (the model is at 1/100 scale: Figure 3.42). The range within which the elevation level of all body sections are defined is limited between 22.1mm and 38.5mm (high:22.1-27.5mm, medium: 27.6-33mm, and low: 33.1-38.5mm).

Figure 3.42: A10 (1/100 scale) seen from the vertical position. The highest elevation is found in the muzzle and the buttock, while the lowest is in the central mid-torso.

First of all, the cross-section layer detected the highest elevation at the muzzle and the rightmost of the thigh (0.1-22mm: see Figure 3.43, 1-2). These areas gradually

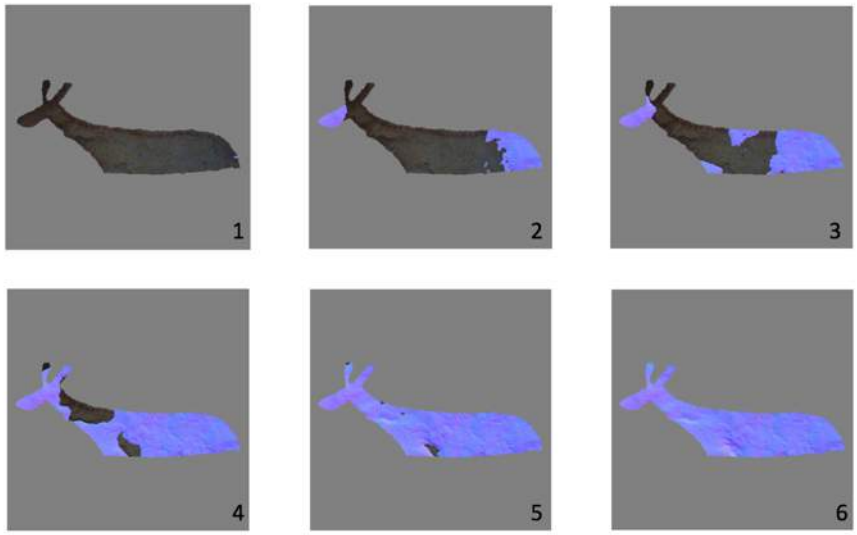

Figure 3.43: These six images illustrate the depth of A10. When the cross-section layer passes the surface of A10, the colour of the surface changes; dark regions denote lower elevation than coloured parts. Images 1 and 2 are for 0.1mm - 22mm, 3 for 22.1mm - 27.5mm, 4 for 27.6mm - 33mm, 5 for 33.1mm - 38.5mm, and 6 for 38.6mm - 44mm.

extend inward and finally covers the majority of the head and the dorsal-central thigh (22.1-27.5mm: 3). Between 27.6mm and 33mm, the detection continues, defining the dorsal-central middle and the central neck-shoulder as the medium (4). The rest of the body (the dorsal neck-shoulder and a part of the central mid-torso) is detected by the cross-section layer at 33.1mm afterwards (5). The elevation of the central shoulder is the lowest as it finally passes the layer at a depth of 44mm (6).

Distortion on images (horizontal rotation, x10°, y-60° to y70°)

Although significant distortions cannot be identified, the topography deforms A10 especially when the viewing point is taken to its right. As described in the previous section, its elevation is lower in the dorsal neck and middle but higher in the thigh, and this topographic setting gradually but noticeably shorten the body as the angle increases (y70°: Figure 3.44). That is is because the convexity on the posterior hides the concave neck-shoulder and middle part. This topographic intervention is distinguishable, compared to the image in the 2D simulation. A10 repeatedly shrinks and stretches when the viewing point moves between y10° and y70°.

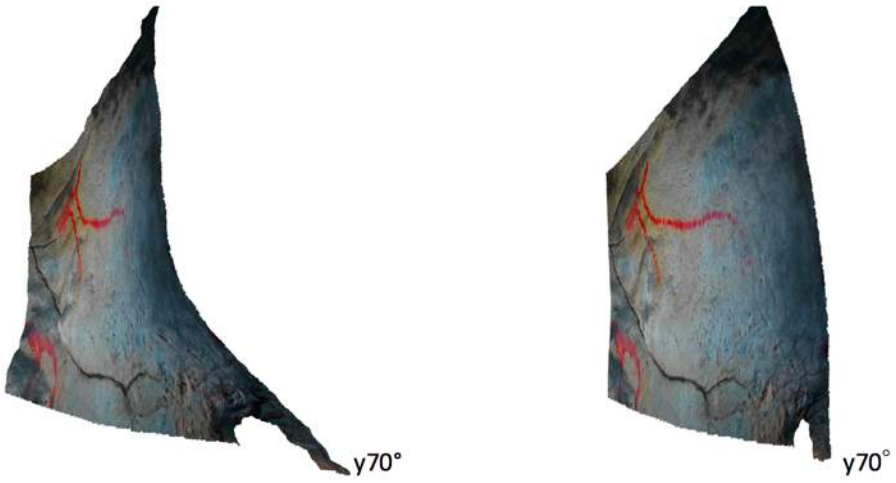

Figure 3.44: A10 on the 3D surface (left) and the 2D surface (right) seen from y70°. Since the elevation of the dorsal-neck is lower than the mid-torso and the mid-torso is lower than the thigh, the lower areas are hidden by the higher parts when viewed from the right. Consequently, the neck and the mid-torso appear to shrink remarkably. This contraction seems as if A10 is raising its head. The extent of the distortion is significant once compared to A10 on the 2D surface.

Horse (A11)

General description

An outline equid facing left (Figure 3.45). Located on the lower left part of A10, A11 contains all body parts except its frontal limb. This horse is significantly detailed and well-preserved. The face is also elaborate: the mouth is depicted as two lines in the muzzle; the eye is provided as a combination of a line and dots; the robustness of the jaw is well-expressed. Furthermore, there is a trace of the V-shaped ears (Moure Romanillo 1990). The head is outlined by the stroke, not by a train of dots. A11 also contains the mane, and this hair part is depicted by a concentration of dots. As the cervical line continues to the posterior, the contour is drawn by sparse dots which somewhat weaken the presence of the mid-dorsal area. However, the croup, buttock, and tail are painted in robust red with a fill-in on the upper part of the thigh. The hind limbs are also elaborated as a hoof is provided with each of them. The size of the image is 122 cm, and it is located on a height of 116 cm (belly) from the nearest floor.

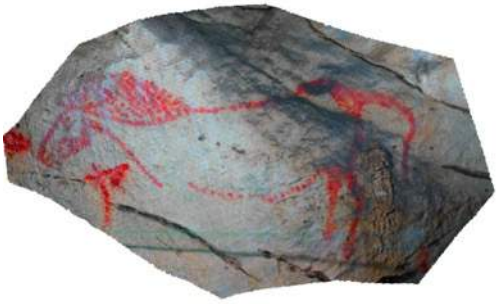

Figure 3.45: A11, outline horse facing left (digital filter applied). The image is maintained in a remarkably good condition. Although the frontal limbs are missing, the rest of the body parts, even also mane, are provided.

Integration of natural lines

Overall, integration is not observable on any parts of the contour. Because the wall on A11's anterior body is smooth, no conspicuous natural lines are found in the region. There are edges and grooves on the posterior where the condition of the wall turns to be rough, but none of them is integrated into any outlines of the horse. Therefore, A11 is depicted regardless of the natural pattern.

Topographic condition

A sizeable convexity characterises the wall of A11. Because this raised wall divides the horse into two parts at the centre of the image, a significant elevational gap forms between the body sections. The total depth is 137mm (the model is at 1/100 scale: Figure 3.46). The highest

Figure 3.46: A11 (1/100 scale) seen from the vertical position. The highest elevation is found on the hind limbs, while the lowest is on the dorsal thigh.

elevation is located at the tip of the hind limbs, while the lowest elevation is found at the dorsal thigh. Even though the elevation gap is profound, the three elevation levels are homogeneously distributed within the depth (high:0-48mm, medium: 48.1-89.1mm, and low: 89.2-137mm). Therefore, there is neither the extra high nor extra low level.

The tips of the hind limbs are first detected, and then the central-ventral middle (0.1mm-20.6mm: see Figure 3.47, 1-2). As the cross-section layer moves, these areas expand and cover the whole mid-torso and the limbs (20.7-48mm: 2-3). The layer further detects the surface as the medium level: the detected region continues expanding outwards and covers the entire neck-shoulder and the ventral thigh (48.1-89.1mm: 4-6). The remaining sections are the head, dorsal-central thigh, and tail (89.2-137mm: 7-9), and they are therefore assessed as low level. The expansion of the coloured region is persistent and finally includes the whole body. The area of the lowest elevation is found on the dorsal thigh.

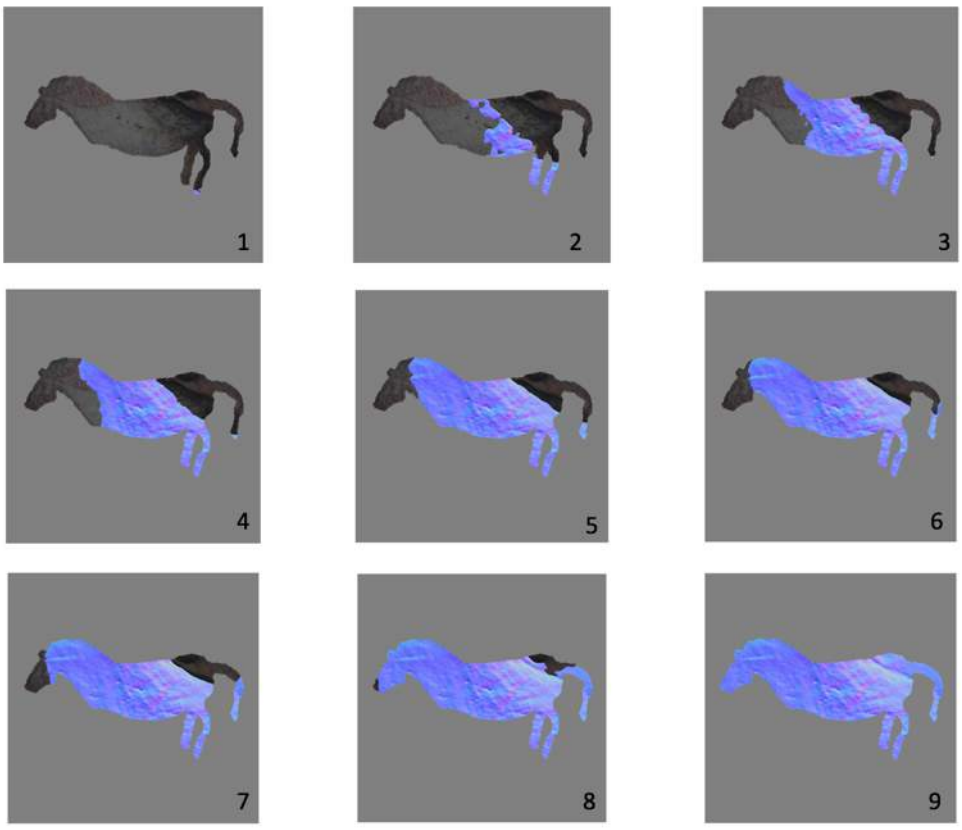

Figure 3.47*:* These nine images illustrate the depth of A11. When the cross-section layer passes the surface of A11, the colour of the surface changes; dark regions denote lower elevation than coloured parts. Images 1 - 3 are for 0.1mm - 48mm, 4 - 6 for 48.1mm - 89.1mm, 7 - 9 for 89.2mm - 137mm.

Distortion on images (horizontal rotation, x0°, y-70° to y70°)

As a large convexity is located in the centre of the body, this topographic feature distorts A11. In particular, the deformation is the most salient when the viewpoint is taken on the left. The convex surface is large enough to hide the almost entire posterior at y-70° (Figure 3.48) but instead highlight the presence of the anterior. At this time, an edge of this convexity substitutes the outline of the buttock, and the entire body appears significantly shrunk; however, the image still sustains the basic form of a quadruped animal because the tail and hind legs are still visible. This distortion is most noticeably perceived when the viewing angle is between y-30° and y-70°. In contrast, the image in the 2D simulation shrinks homogenously.

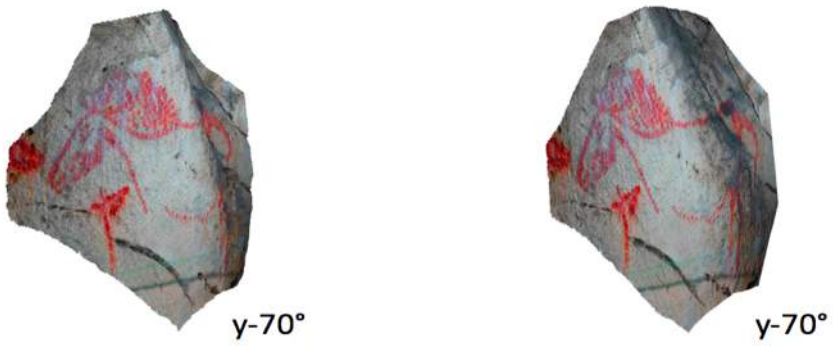

Figure 3.48: A11 on 3D surface (left) and the 2D surface (right) seen from y-70°. As a large convexity on the mid-torso conceals the entire thigh, the body is perceived significantly shrunk. Meanwhile, the image on the 2D wall also appears contracted, but its extent is not as significant as on the 3D surface.

Meanwhile, when A11 is viewed from the right, the image appears more massive than that on the 2D wall due to the convex (y70°: Figure 3.49). Nevertheless, the anterior body saliently shrinks as the viewing angle increases from y0°, and the extent of the contraction is also more significant than the 2D simulation. The low elevation of the anterior causes this visual effect; the area appears away from the viewer. The range of the angle where the distortion is most outstanding is between y40° and y70°.

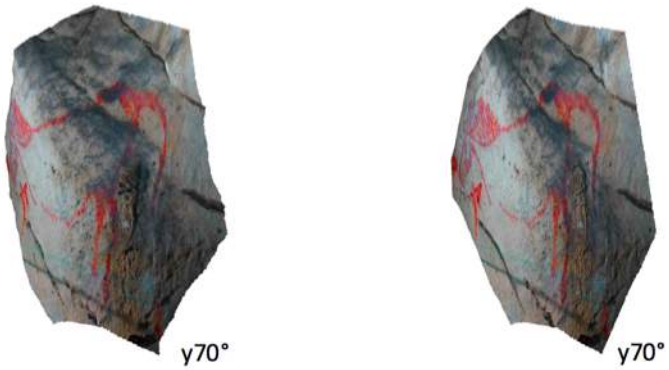

Figure 3.49: A11 on 3D surface (left) and the 2D surface (right) seen from y70°. As a large convexity on the mid-torso emphasises, the posterior body appears more substantial on the 3D surface than on 2D. On the other hand, the anterior becomes contracted because of the low elevation of the region. The extent of this contraction is somewhat limited on the flat surface.

Deer (A13)

General description

An outline red deer, fixed vertically (Figure 3.50). A13 is incomplete as the entire ventral body is missing. This deer is located on immediately below the face of the previous horse. The contour is well-preserved. Although the detail of the face is absent, the V-shaped ears are attached to the head. The technique used is the single stroke and dot painting. The face and cervical line are vivid, while it goes weaker in the middle dorsal area. However, the image regains the vividness at the posterior. The length of the image is 40 cm, and it is located on a height of 87 cm (posterior) from the nearest floor.

Figure 3.50: A13, an outline red deer facing upward (digital filter applied). The ventral body is absent.

Integration of natural lines

The wall on which A13 is located is considerably smooth, and therefore natural lines are mostly absent. Two noticeable grooves lie around the image; however, they are not utilised for the outlines. There is a small dent on the muzzle which then generates a short edge, but this line is also not integrated into the contour of the face. Overall, integrations are not confirmed on any parts of the outline.

Topographic condition

Because A13 is an incomplete image, only the dorsal body is taken into account for this analysis. Even though there is no significant topographic feature on the surface, the surface slightly rises at the face and thigh. The total depth is 32mm (the model is at 1/100 scale: Figure 3.51). However, all the body parts are defined their elevation level between 2.4mm and 22.9mm (high: 2.4-9.1mm, medium: 9.2-16mm, and low: 16.1-22.9mm). There are no extra levels for A13.

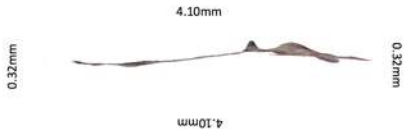

Figure 3.51: A13 (1/100 scale) seen from the vertical position. The highest elevation is found on the thigh, while the lowest is on the chin.

First of all, the surface of the thigh partly passes the cross-section layer (0.1-2.3mm), and then the area gradually extends and covers the dorsal thigh (2.4-9.1mm: 1-3, see Figure 3.52). At the same time, the muzzle and the ears are also detected. As the cross-section layer proceeds, these regions further spread over the head and the dorsal mid-torso (9.2-16mm: 4-6). Finally, almost all the dorsal neck passes the layer between 16.1mm and 22.9mm (7-9), and therefore this body part is defined as the low-level elevation. Especially the area immediately next to chin is deep and does not pass the layer until 32mm.

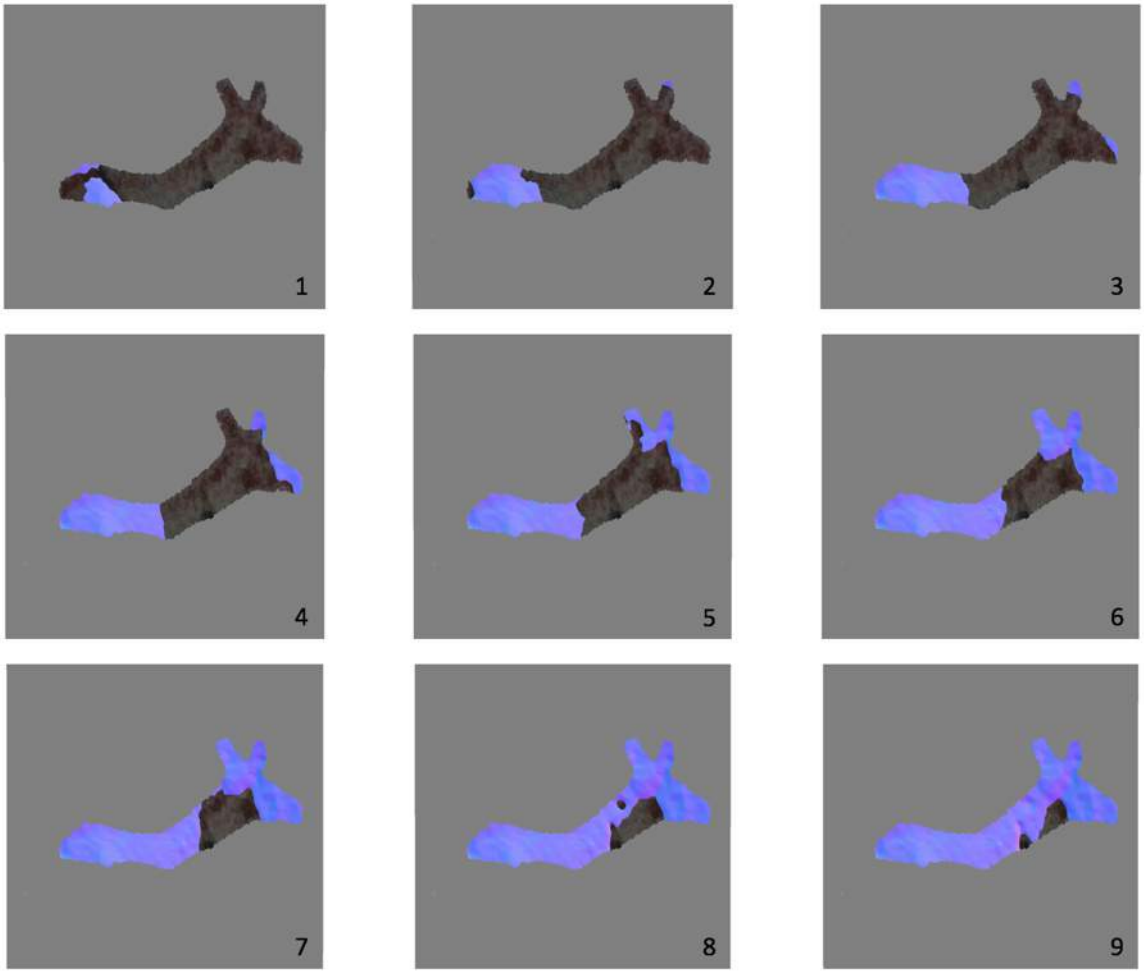

Figure 3.52: These nine images illustrate the depth of A13. When the cross-section layer passes the surface of A13, the colour of the surface changes; dark regions denote lower elevation than coloured parts. Images 1 - 3 are for 2.4mm - 9.1mm, 4 - 6 for 9.2mm - 16mm, 7 - 9 for 16.1mm - 22.9mm.

Distortion on images (horizontal rotation, x0°, y-70° to y80°)

The simulation does not demonstrate any remarkable distortions There is also no conspicuous difference in the appearance between the image on the 3D and 2D surface. The absence of deformation is attributed to the image's incomplete body and a lack of conspicuous topographic features.

Deer (A14)

General description

An outline image of a red deer facing right (Figure 3.53). Located to the left of A11, A14 is positioned as if it is confronting the horse. As the image is incomplete, only the head and the dorsal line is provided. The dorsal line extends from the cervical area towards the posterior, but the contour becomes somewhat ambiguous at the buttock because calcite runoff blurs the part. In addition, there are two coloured areas: a thin red line under the face and a red spot under the posterior dorsal. However, whether or not they are relevant to A14 is unknown. The length of the image is 45 cm, and it is located on a height of 113 cm (dorsal) form the nearest floor.

Figure 3.53: A14, outline red deer facing right (digital filter applied). The ventral body is absent. Locating left to the face of the large horse (A11), this deer is arranged as if confronting the horse).

Integration of natural lines

Integration is confirmed on the dorsal line. A14 is located below a convex surface generating an edge along its underside. The almost entire dorsal line is drawn along this edge (Figure 3.54). Although this is the only case of the integration for A14, a groove horizontally runs under the image appears as if it substitutes the absent ventral line. However, whether or not this is also a sample of integration is unknown.

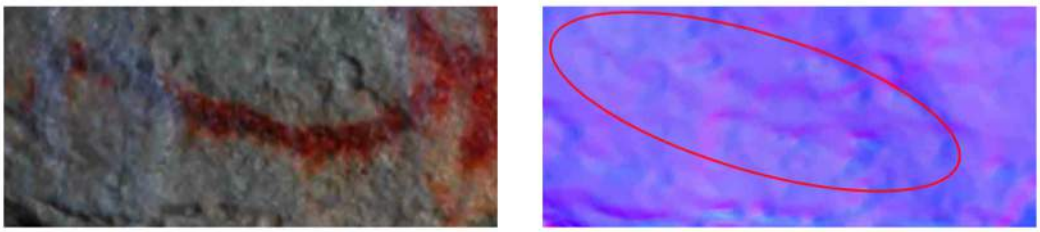

Figure 3 54: An example of integration on A14. The dorsal line is outlined along with the edge line of the convex immediately above the image.

Topographic condition

As A14 is an incomplete image, only the dorsal body is taken into account for this analysis. Although salient topographic features are absent, the surface is slightly depressed at the mid-torso and the face. The total depth is 11mm (the model is at 1/100 scale: Figure 3.55). The highest point is found in the face and dorsal thigh, while the lowest is placed in the dorsal neck. The elevation level of all body parts are defined between 0mm and 8.3mm (high:0.1-2.8mm, medium: 2.9-5.5mm, and low: 5.6-8.3mm). There are no extra levels for A14.

Figure 3.55: A14 (1/100 scale) seen from the vertical position. The highest elevation is found on both edges of the image (the thigh and muzzle), while the lowest is on the right ear.

First, the cross-section layer detects both edges of the image: the head and the thigh. Although the area on the face does not extend greatly, over the half of the thigh passes the layer by a depth of 2.8mm, and therefore the section is defined as the high elevation (see Figure 3.56, 1-2). Simultaneously, the surface of the neck also starts being detected. These detected areas continue expanding and cover the entire thigh and the neck within the range of the medium level; however, the majority of the face still remains undetected (2.9-5.5mm: 3-4). The elevation of the head and dorsal mid-torso are finally defined as the low level between 5.6mm and 8.3mm (5-6). The right ear is located on a slightly deeper surface, and it passes the layer completely at a depth of 11mm (7-8).

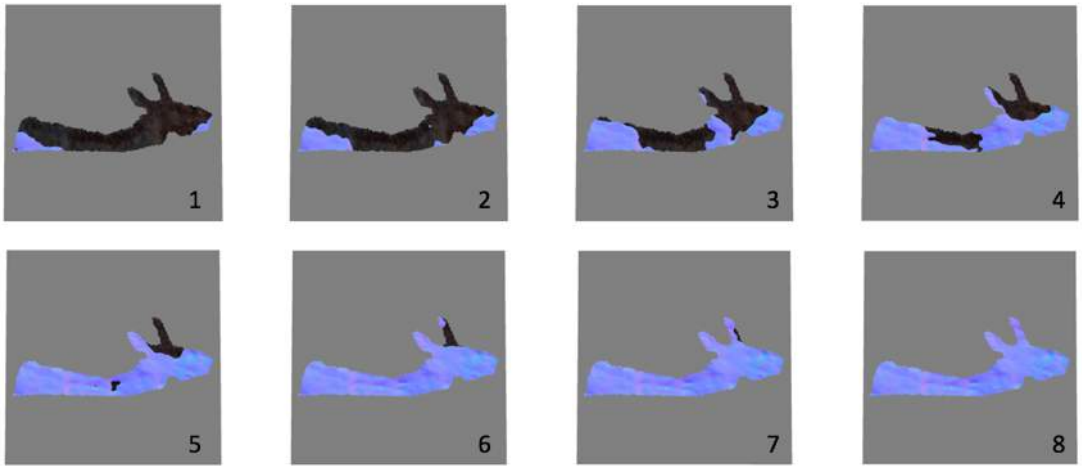

Figure 3.56*:* These eight images illustrate the depth of A14. When the cross-section layer passes the surface of A14, the colour of the surface changes; dark regions denote lower elevation than coloured parts. Images 1 and 2 are for 0.1mm to 2.8mm, 3 and 4 for 2.9mm to 5.5mm, 5 and 6 for 5.6mm to 8.3mm, and 7 and 8 for 8.4mm to 11mm.

Distortion on images (horizontal rotation, x0°, y-70° to y70°)

The simulation of A14 does not demonstrate any remarkable distortions. There is also no conspicuous difference in the appearance between the image on the 3D and 2D surface. The absence of deformation is attributed to the incomplete body of the image and relatively flat topography.

Reindeer (B1)

General description

An image of a reindeer facing left (Figure 3.57). All body parts are provided except the tail. The overlapping red dots form its thick outline, which contributes to the strong presence of B1. The head contains an eye and the two antlers, and the long muzzle is well-expressed. From the back-head, the contour, although occasionally blurred, extends to upper left and then continues toward right horizontally along the edge of the rock. This edge is also utilised for outlining the buttock. A fill-in area is placed on the shoulder as it gradually narrows from the dorsal to the ventral. Apart from these pictorial elements, two other dotted lines are superimposed on B1: one is overlaps on the lower jaw, while the other is drawn along the belly line. Moure Romanillo et al. (1990) interpreted these superimposed lines as an animal image (in the paper it is given a code as "B2"). B1 is the largest image in Covalanas cave, with the length of 135cm, and it is located at a height of 135 cm (belly) from the nearest floor.

Figure 3.57: B1, an image of reindeer facing left (digital filter applied). As the whole body except the tail is provided, this is the largest picture among all left in Covalanas cave. The condition of the preservation is also remarkably well.

Integration of natural lines

As noted above, B1 contains integrated body parts: the shape of the upper edge of the panel already represents the entire contour of the dorsal and buttock (see Figure 3.57). Apart from these parts, the outline does not have support from natural lines in the main body. However, another integration is found in the head. Generally, the wall where B1 is depicted is smooth, but it becomes considerably rough and rocky in the

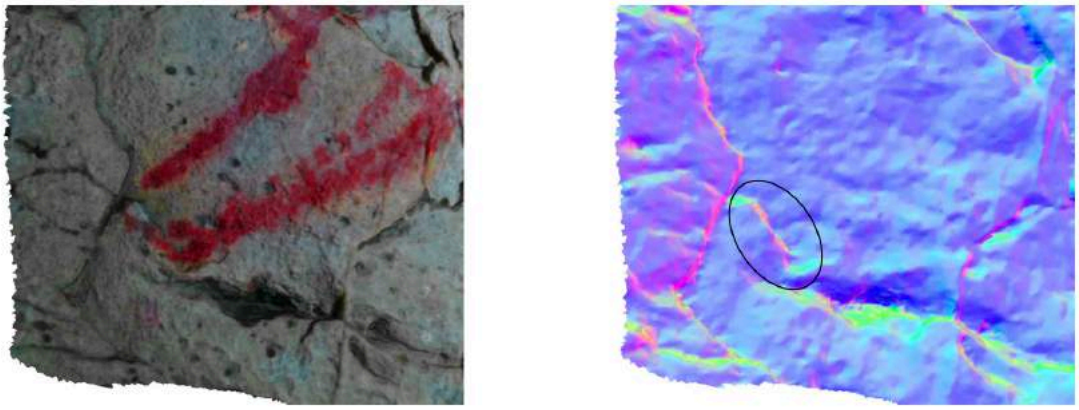

Figure 3.58: The example of integration on B1. The tip of the muzzle is outlined along with an edge of a rocky surface, although its extent is limited.

facial area. Integration, although offset, is confirmed on the tip of the muzzle: the outline of the muzzle is drawn along the short edge formed by an elevational gap of a rocky surface (Figure 3.58).

Topographic condition

Overall, this wall is not particularly undulating. However, the elevation varies by body parts, and especially the elevation is high on the peripheral body parts. The highest point in elevation is found on the tip of both antlers, whereas the lowest is located on the frontal limb. The total depth is 171mm (the model is at 1/50 scale: Figure 3.59). Antlers and hind legs are particularly high as the wall above those regions rise noticeably, accounting for over a third of all range (0.1-74.8mm: 1-2, see Figure 3.60). The rest of the body parts are distributed within the range between 74.9mm and 171mm (high: 74.9-106.9mm, medium: 107-139mm, and low:139.1-171mm).

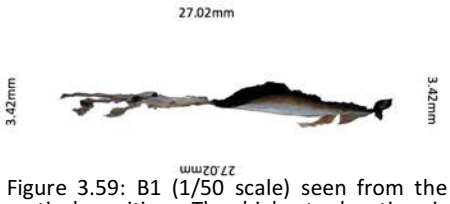

Figure 3.59: B1 (1/50 scale) seen from the vertical position. The highest elevation is found on the horns, while the lowest is on the frontal limb.

Althought the topographic condition of B1 varies,the main body is relatively flat. The horn and hind limb are the highest (see Figure 3.60, 1-2), and these detected areas spread as they gradually lower the elevation and cover the dorsal neck, the central and ventral mid-torso, and whole thigh (74.9-106.9mm: 3-4). These sections are marked as the high level. As the cross-section layer proceeds, the central-ventral neck-shoulder and dorsal mid-torso are defined as the medium level between 107mm and 139mm (5-6). Even though the head is also located on the medium elevation on its upper side, the area does not account for the major extent of the body part. Thus, the elevation level of

the head is assessed as low (139.1-171mm: 7-8). The major part of the frontal leg is also fixed on this level. on this level.

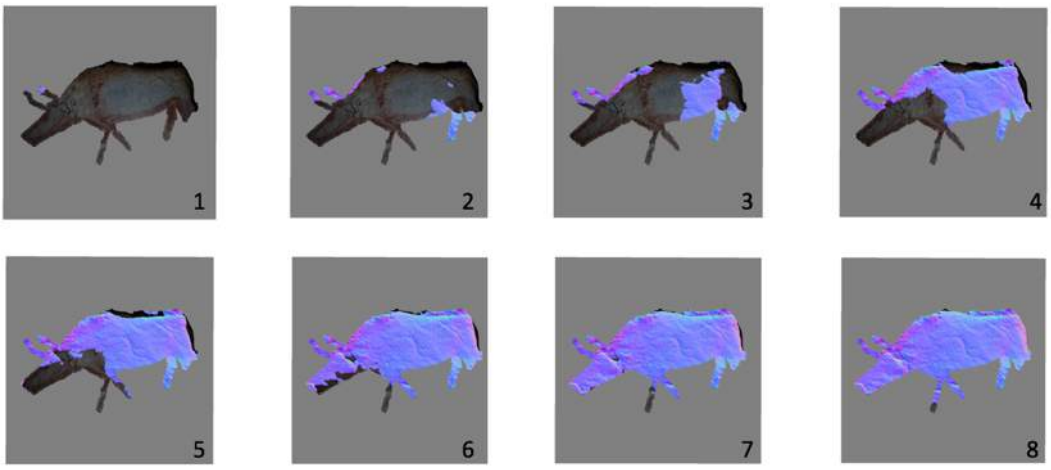

Figure 3.60: These eight images illustrate the topographic depth of B1. When the cross-section layer passes the surface of B1, the colour of the surface changes; dark regions denote lower elevation than coloured parts. Images 1 and 2 are for 0.1mm - 74.8mm, 3 and 4 for 74.9mm - 106.9mm, 5 and 6 for 107mm - 139mm, and 7 and 8 for 139.1mm - 171mm.

Distortion on images (horizontal rotation, x0, y-60° to y50°)

Significant distortions are not detected from most of the body parts. Only hind limbs where the wall most noticeably elevates appear deformed when the viewpoint moves; the left-hind leg seems always bent between y-60° and y50°, while the body section on the 2D surface sustains itself unchanged. The ventral area is also seemingly deformed; however, the extent is not distinguishable. Thus, the topography does not saliently intervene the appearance of B1.

Deer (B4)

Genera description

An outline red deer facing left (Figure 3.61). Although B4 appears incomplete as the buttock and the hind legs have largely disappeared, although they were once visible (Moure Romanillo et al. 1990). Through the digital filter, the contour of the posterior body can be partly resurrected but mostly remain invisible. The outline is executed by red dots. The density of dots differs by area, and therefore, the intensity

Figure 3.61: B4, outline red deer facing left. Although the ventral body and the hind limb are not clear, these parts are also provided and once visible. There is a trace of modern graffiti on the frontal limb.

of the B4's presence is not homogenous. The head contains two ears (but not the typical V-shaped) and an eye. The contour extends from the face to under-neck, and the colour abruptly loses its vividness at the root of the frontal leg. Instead, a black line is superimposed with the limbs' contour. This black line is attributed to the vandalism in modern times. The length of B4 is 85 cm, and it is located at a height of 136 cm (belly) from the nearest floor.

Integration of natural lines

This wall contains a number of grooves, ridges, and edges. Even though most of them are irrelevant to the reindeer's outline, two horizontal parallel grooves are integrated. Figure 3.62 is a detailed image of this surface, and these two groves already form the basic shape of the posterior body of B4. One of this line (upper) is short but shared with the dorsal line at the middle area. On the other hand, as for the case of the ventral, both natural and artificial lines are not perfectly overlapped; the ventral line is drawn slightly off from the natural groove; the contour gradually goes away as it continues to the right. Even so, the width of the outlined body and that of space between these natural grooves appears identical, and therefore this pre-existing pattern, although not entirely integrated into the outlines, might have stimulated the imagination of the Palaeolithic artist.

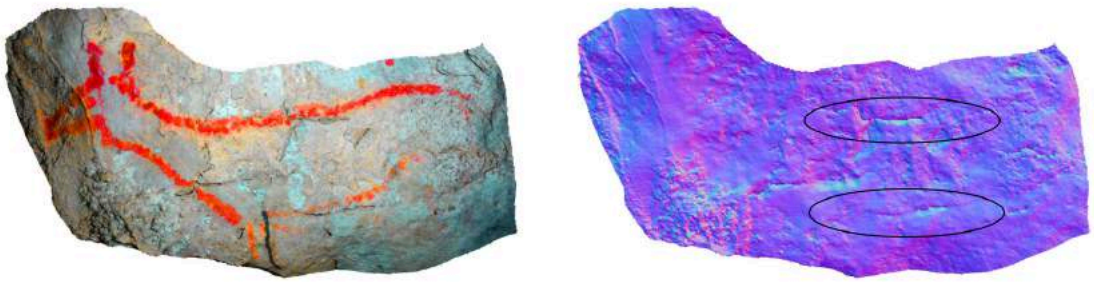

Figure 3.62: An example of integration on B4. There are two parallel grooves on the panel. They already form the basic shape of the posterior body. One of this line (upper) is mostly shared with the dorsal line, although the ventral line does not entirely overlap on the other groove (lower).

Apart from these examples, another potential use of the natural lines is found in the facial region. On the face, immediately left to the eye, a calcite ridge runs vertically. Although this line seems irrelevant to any contours of B4, it perfectly overlaps with the under-neck once it is viewed from the left (Figure 3.63). Admittedly, whether or not this positioning is intentional is not provable. However, this example suggests a possibility of the existence of multiple viewpoints.

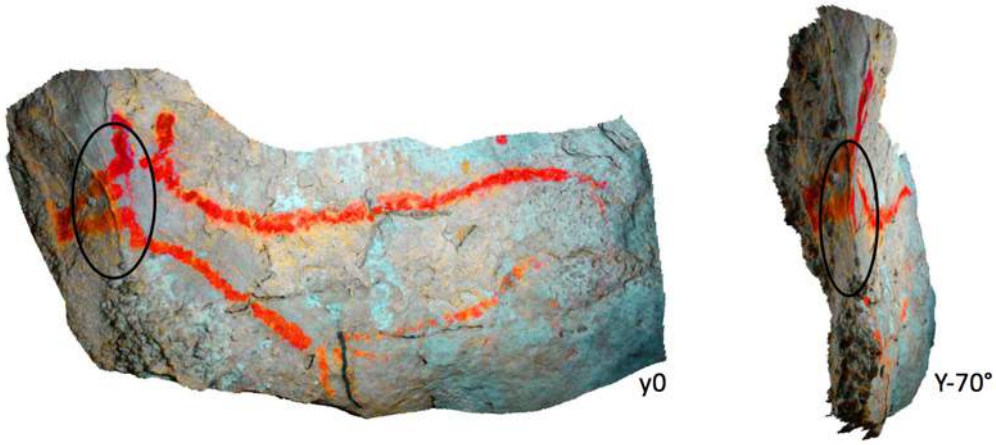

Figure 3.63: A unique sample of possible integration. Although a ridge seems irrelevant to any outlines of the face, it perfectly overlaps with the contour of the frontal neck once B4 is viewed from the left.

Topographic condition

The panel is partly rocky and porous. Therefore, the body of the reindeer undulates, although if not remarkably. The highest point is located on the frontal limb, while the lowest is found on the dorsal thigh. The total depth is 67.4mm (the model is at 1/20 scale: Figure 3.64), but most of the body parts are defined their elevation levels between 22.6mm and 56.2mm (high: 22.6-33.7mm, medium: 33.8-44.9mm, low: 45.0-56.2mm). Because there is a body part whose elevation level is defined within the range between 0.1mm and 22.5.5mm, B4 contains the extra high level.

Figure 3.64: B4 (1/20 scale) seen from the vertical position. The highest elevation is found on the tip of the ear, while the lowest is on the dorsal thigh.

Detection starts from the tip of the ears. The detected area covers most of the head between 0.1mm and 22.5.5mm (see Figure 3.65, 1-3). Therefore, the head is defined as the extra-high level. The tip of both limbs is also highly elevated. Because the wall rises on the ventral side, the high elevation areas expand from the lower body. Both legs are located on this level, but the expansion to the mid-torso and thigh is limited.

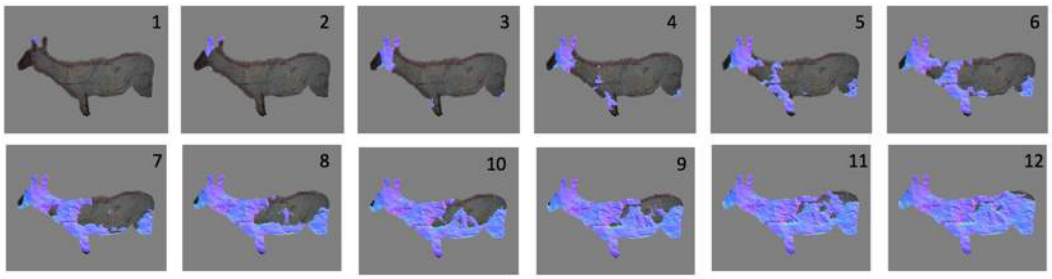

Figure 3.65: These 12 images illustrate the depth of B4. When the cross-section layer passes the surface of B4, the colour of the surface changes; dark regions denote lower elevation than coloured parts. Images 1 - 3 are for 0.1mm - 22.5mm, 4 - 6 for 22.6mm - 33.7mm, 7 - 9 for 33.8mm - 44.9mm, and 10 - 12 for 45.0mm - 56.2mm.

Meanwhile, the ventral-dorsal neck-shoulder is also fell into the high level (22.6-33.7mm: 4-6). As for the medium level (33.8-44.9mm), the detected region continue spreading from the ventral side, including the central neck-shoulder, ventral-central mid-torso, and ventral thigh (7-9). The dorsal mid-torso and the central-dorsal thigh are located on the low elevation level. (45.0-56.2mm: 7-8).

Distortion on images (horizontal rotation, x0°, y-70° to y80°)

The undulating surface noticeably distorts B4. In particular, deformation is significant in the anterior side. As the viewing angle decreases, the neck and the head appears pushed backwards as if the reindeer raises its neck straight (y-60°: Figure 3.66). This is due to the convex topography in the head hides the neck; moreover, because the muzzle which is located on the low elevation level constantly shows its surface to viewers on the left, the part sustains a certain proportion unlike B4 on a 2D surface. Factors responsible for this distortion are not only the topography but also the calcite ridge vertically crossing the face. This natural line gradually approaches to the contour of the under-neck as the viewing angle shift to the left, and it perfectly overlaps on the outline (y-70°). At this time, the distance between the neck and the ridge disappears, and this integration adds further dynamism to the deformation process. This distortion is most noticeable as the viewing angle is taken between y-70° and y-30°.

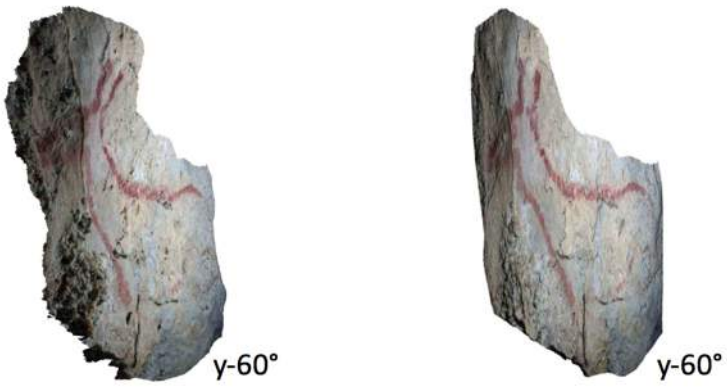

Figure 3.66: B4 on the 3D surface (left) and the 2D surface (right) seen from y-60°. The neck on the 3D panel is compressed by the multiple topographic features and appears lifted upwards as if the deer is raising its neck. On the other hand, the neck on the flat surface remains stretched straight.

The anterior of B4 is also distorted by viewing it from the right. The undulation of the surface gradually bends the outline of the under-neck at two regions, although the contour appears straight when B4 is seen from the left and the direct position (y70°: Figure 3.67). This distortion is most noticeable when the viewing point shifts within the

range between 0° and 80°. Additionally, the raised wall on the ears disturbs their orientation. The ears appear extending backwards when seen from the left, while they gradually bend forward as the viewing points shift to the right (y80°: Figure 3.67). These deformations are specific to the simulation of the 3D surface. Simultaneously, the muzzle gradually goes unseen once viewed from the right. This invisibility of the facial part provides the image with a sculptural quality.

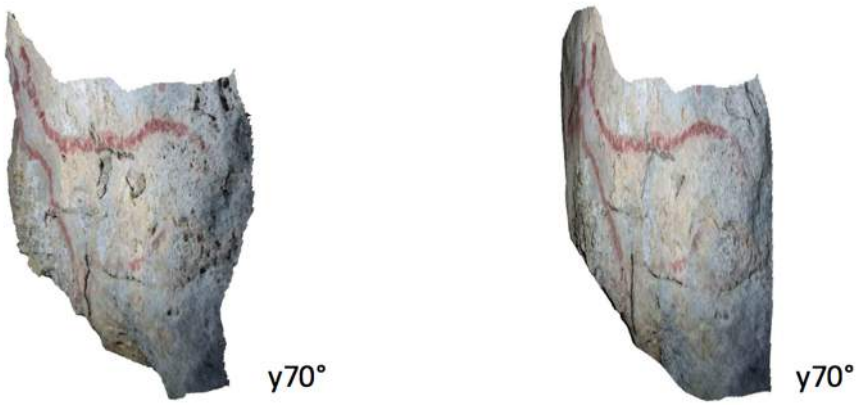

Figure 3.67: B4 on the 3D surface (left) and the 2D surface (right) seen from y70°. Distortion occurs on three regions in the anterior body: the straight outline of the front neck is deformed into a zigzag line; both ears are bent forward; the muzzle goes unseen. These deformations are specific to B4 on the 3D surface because such phenomena do not occur on the 2D surface.

Deer (B5)

General description

An outline red deer facing left (Figure 3.68). All body parts except the tail are provided. The executed technique is dot painting similar to other images in Covalanas cave. Although the detail of the face is absent, the V-shape ears are clearly visible. Outlining dots are more dense at the head, dorsal, buttock, and under-neck, while the density of dots is lower at the belly and limbs. The length of the B5 is 84 cm, and it is located on a height of 166 cm (belly) from the nearest floor.

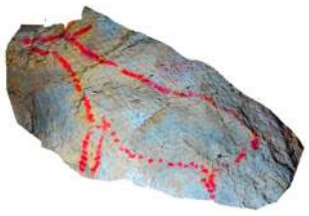

Figure 3.68: B5, outline red deer facing left. All body parts are provided except the tail. Because the density of the dots that constitute the ventral and buttock is lower than the rest of the body, the presence of those regions is also weaker.

Integration of natural lines

The rough surface of this wall creates a number of natural lines. They are mostly edge lines, grooves and ridges. However, the outline of B5 is mostly independent of these pre-existing patterns. Even so, the posterior-dorsal part is outlined along with a ridgeline (Figure 3.69).

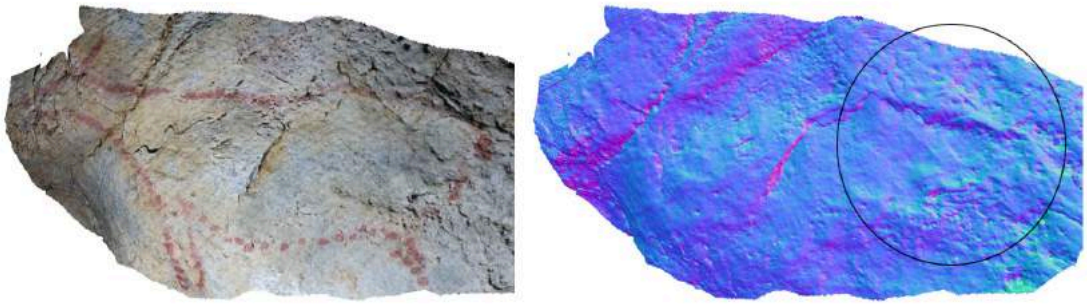

Figure 3.69: Example of integration on B5. The posterior dorsal is perfectly integrated into a noticeable ridge. The topography of the region has its shape which is already reminiscent of the whole posterior body, but the other outlines (the buttock and ventral line) are not integrated into natural lines.

Topographic condition

This wall undulates as different rock plates merge, causing an elevation gap. Moreover, there is a noticeable topographic feature on the shoulder. These elements profoundly affect the topographic condition of B5. Overall, the total depth is 115mm (the model is at 1/20 scale: Figure 3.70). The range within which the elevation level of the most body parts are defined is limited between 41.1mm and 73.9mm (high:41.1-49.3mm, medium 49.4-57.5mm, and low: 57.6-73.9mm). There are body sections located within the ranges between 0.1 and 41mm and between 74 and 115mm. Therefore, B5 contains both extra-high and extra-low level.

Figure 3.70: B5 (1/20 scale) seen from the vertical position. The highest elevation is found on the ears, while the lowest is on the frontal leg.

The most convex part of B5 is the ears, and this highly elevated area expands to more than half area of the head and a part of the dorsal neck (0.1-41mm: see Figure 3.71, 1). Additionally, the convex on the shoulder is also partly included within this range (the extra-high level). These extra high areas further extend during the next phase, covering most of the dorsal neck and ventral shoulder (41.1-49.3mm: 2). In the medium

level elevation, nearly all the body parts are placed as the detected area covers the central neck, almost the entire mid-torso and the ventral thigh (49.4-57.5mm: 3). Meanwhile, the sections which belong to the low elevation level are the hind leg, dorsal and central thigh; in particular, the elevation below the ridge outlining the croup is low (57.6-73.9mm: 4). At this point, the frontal leg remains undetected, which means the elevation level of this part is significantly lower than any other regions in this wall. As it is fully detected at 115mm, the leg is defined as the extra-low level. Thus, the body of B5 is never flat but rather dynamically undulating.

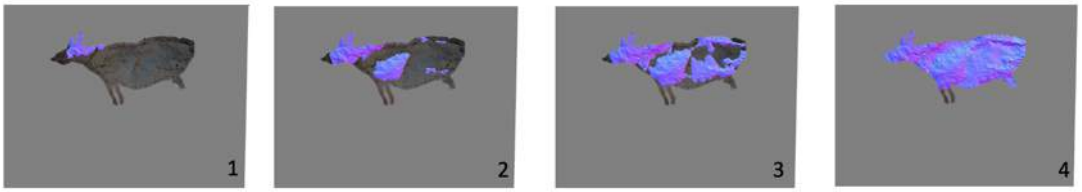

Figure 3.71: These four images illustrate the depth of B5. When the cross-section layer passes the surface of B5, the colour of the surface changes; dark regions denote lower elevation than coloured parts. Image 1 is for 0.1mm - 41mm, 2 for 41.1mm - 49.3mm, 3 for 49.4mm - 57.5mm, and 4 for 57.6mm - 73.9mm.

Distortion on images (horizontal rotation, x10°, y-70° to 70°)

Overall, the unique topographic condition of this wall greatly affects the appearance of B5. Above all, the most significant deformation is detected on the neck. Figure 3.72 compares the same image on the 3D and 2D surface seen from y-70°, and the shape of these images are considerably different. This deformation is caused by the complex topographic condition. Even though the wall rises at the central torso, the elevation of the dorsal neck and dorsal mid-torso is saliently lower. Therefore, when the view point moves to the left, these low areas go unseen as they are hidden by the convex in the central shoulder and torso. Moreover, because this convex hides the lower

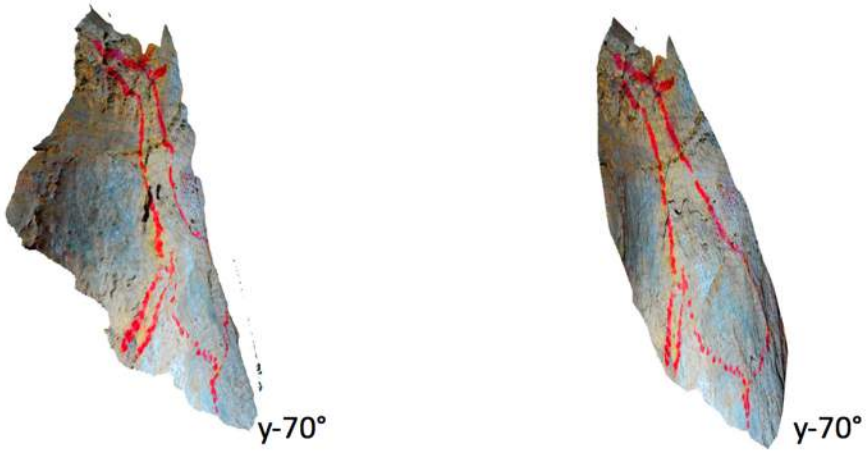

Figure 3.72: B5 on the 3D surface (left) and the 2D surface (right) seen from y-70°. The neck on the 3D panel appears greatly elongated as the convex shoulder hides the dorsal mid-torso. This distortion is absent in B5 on a 2D surface.

elevation area of the posterior body, B5 appears significantly shrunk. At this time, the contour of the mid-torso turns to be the root of the cervical line, and therefore, the neck appears considerably longer. Further to this, the convex wall on which the face and a part of the neck are located also contributes to the severe distortion: this raised surface narrows the width of the neck and bends the contour. These distortions are most significantly perceived between -70° and -50°.

Meanwhile, distortion also occurs when the viewing position moves to the right. The major convexity on the shoulder and mid-torso bends the outline of the breast area outwards. As a result, the contour of the under-neck is deformed to be zigzag. Furthermore, a concave surface in the muzzle distorts the face; as the viewpoint shifts to the right, the head can be captured in sight until y20°, but the muzzle gradually goes unseen between the angle of y30° and y70°. This deformation causes sort of a visual effect such as a deer shaking its head side to side between the range (y30° to y70°). In the 2D simulation, these distortions are not confirmed.

The unique topography of B5 also interferes the appearance of the image's frontal and hind limb. Because the legs are located on the low elevation surface, their appearance remarkably changes as they constantly bend forward and backwards; apparently, such deformed limbs are a specific phenomenon to the 3D setting. This phenomenon is perceived within the whole range of the viewing angle, but most noticeably between y0° and y60°. Thus, B5 never has a fixed appearance.

Deer (C1)

General description

An outline red deer facing right (Figure 3.73). C1 is a complete figure as only the tail is absent. This image is placed as if it is confronting the other deer (C2) on this panel. Its preservation state is remarkably good as the red pigment is still vivid, although the contour has gone slightly ambiguous in the buttock and ventral. The outline is executed by juxtaposing dots in a very precise manner so that the intensity of the colour appears homogenous. The head part is provided with an outstanding V-shaped ears and an eye. Both frontal and hind leg are also presented. However, the positional arrangement of the frontal limb is so unique that no other images in Covalanas conform to the same fashion: this limb originates from the shoulder, a spot inside of the bodies outline. Even

Figure 3.73C1, an outline red deer facing right. All body parts are provided except the tail. The unique arrangement of the frontal leg features C1. The condition of the image is remarkably good as the vividness of the red colour still survives until present.

though it extends downward as a single line, it disappears before protruding from the ventral line. The interpretation of this treatment has not been established yet (Moure Romanillo 1990). The length of the image is 90 cm, and it is located on a height of 150 cm (belly) from the nearest floor.

Integration of natural lines

The wall on which C1 is depicted contains a large number of natural lines. They are mostly grooves, some of which are outstandingly visible. The most noticeable line is one running horizontally immediately above the image. This line, although not directly integrated into the C1's contour, parallels to the dorsal and crosses the head. At the left of the panel, this natural line merges with another groove which runs along an edge line. The belly line of C1 is drawn along this edge (Figure 3.74). The shape formed by these two natural lines are a reminiscence of the shape the deer's body, and it might have been a case that this pre-existing pattern provides the artist of this image with support for image-making, even though the outline does not perfectly correspond to these grooves. Apart from the integration on the ventral line, C1 does not borrow any support from the wall.

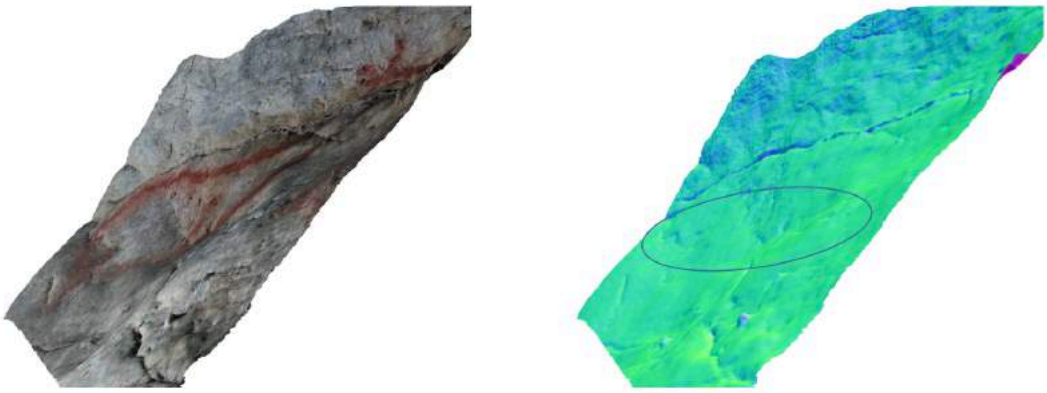

Figure 3.74: An example of integration on C1. The wall is raised immediately below the image, generating an elevational gap. The belly is outlined along the edge of the convex surface.

Topographic condition

The topography of this panel is calm as there are not any conspicuous features on and around the image. Therefore, C1 appears mostly flat. However, the elevation, although slightly, differs by region. The total depth is 60mm (the model is at 1/100 scale: Figure 3.75). The range within which the elevation level of the most body

Figure 3.75: C1 (1/100 scale) seen from the vertical position. The highest elevation is found on the hind limb, while the lowest is on the head.

parts are defined is limited between 30.1mm and 54mm (high: 30.1-36mm, medium: 36.1-42mm, low: 42.1-54mm). There is a body section whose major area is located on the range between 0.1 and 30mm, and therefore, C1 contains the elevation of the extra-high level.

Overall, the elevation is higher in the ventral than in the dorsal side. The cross-section layer first detects the tip of the hind limb, and the highlighted area spreads, covering the whole limb as well as a part of the ventral buttock, ventral neck and muzzle (0-30mm: see Figure 3.76, 1-2). Between 30.1mm and 36mm, the detected area extends to the entire edge of the ventral body. This region includes the ventral thigh, defining it as the high elevation (3). At the medium level (36.1-42mm: 4), the area dramatically spreads over nearly half of the body, including the central thigh and the central-ventral neck-shoulder. The rest of the body (the head, dorsal neck, entire mid-torso, and dorsal thigh) is fell into the low elevation level (42.1-54mm: 5-6). Among them, the elevation of the ears is particularly deep as the detection of the area completes at a depth of 60mm.

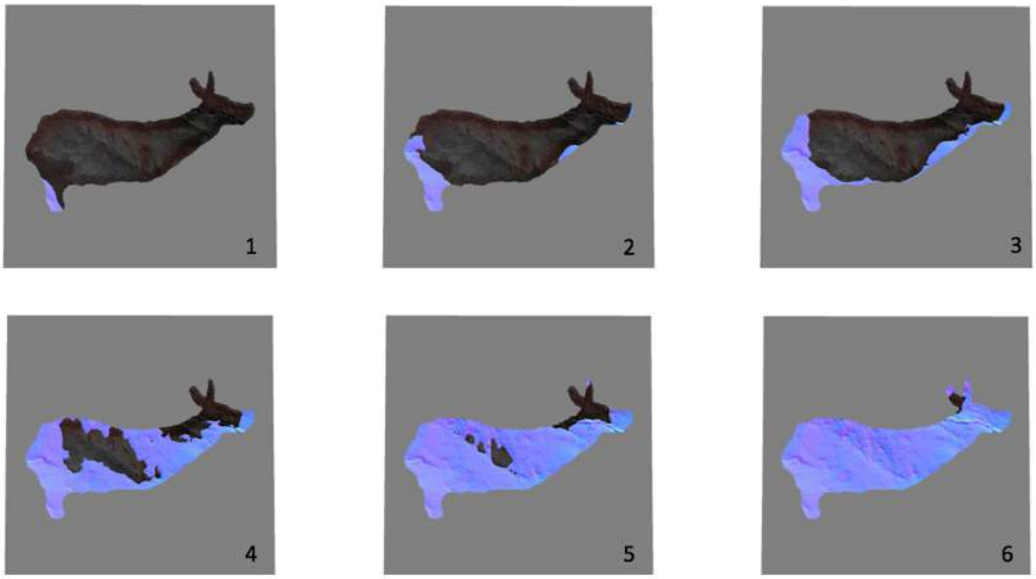

Figure 3.76: These six images illustrate the depth of C1. When the cross-section layer passes the surface of C1, the colour of the surface changes; dark regions denote lower elevation than coloured parts. Images 1 and 2 are for 0.1mm - 30mm, 3 for 30.1mm - 36mm, 4 for 36.1mm - 42mm, and 5 and 6 for 42.1mm - 54mm.

Distortion on images (horizontal rotation, x10°, y-70° to y70°)

The simulation does not demonstrate any remarkable distortions There is also no conspicuous difference in the appearance between the image on the 3D and 2D surface. The absence of deformation is attributed to a lack of conspicuous topographic features.

Deer (C2)

General description:

An outline red deer facing left (Figure 3.77). C2 is located on the right of C1. The figure is mostly complete, but its front limb and tail are missing. The contour is thick especially at the posterior dorsal and buttock because the dots which constitute the line meticulously overlap. The head contains no elements except its V-shaped ears; however, an eye is provided as a dot, according to Moure Romanillo et al. (1990). The dorsal line continues from the head to the right as its width gradually becomes thicker, and then turns downward to depict the buttock. This line merges to the contour of the hind leg. The robust back leg is drawn backwards as if a deer is running and kicking the ground. The ventral line is outlined from the neck downward, and then it continues to the right horizontally (belly). Several spots of the red pigment are also detected on the body (the shoulder and the thigh). The size of the image is 67 cm, and it is located on a height of 145 cm from the nearest floor.

Figure 3.77: C2, outline red deer facing left (digital filter applied). Located immediately right to C1, the shape is also identical to the previous deer. The figure is subject to decay despite thick outlined body.

Integration of natural lines

The surface on which C2 is depicted is considerably rough, generating a complicated natural configuration. Such a wall contains a large number of natural lines. The type of the line varies as it includes grooves, ridges, and edges. Although some of them exist on C2's body or cross the outline, integration occurs only limited parts of the body: the dorsal line and buttock. The most noticeable integration is found on the posterior dorsal area. Immediately above the right-end of the dorsal, the wall rises

Figure 3.78: Example of integration on C2. The wall forms a sizeable convex topography which produces edge lines along the elevational gap. The outline of the croup and the buttock overlaps on the top and right edge of the topography.

sharply, and hence it forms an edge line. The line of the croup and the middle dorsal area is drawn along this edge (Figure 3.78). Meanwhile, the buttock is also outlined along the edge running the right-end of the large convex. (see Figure 3.78). Apart from these integrations, the contour is drawn regardless of natural lines.

Topographic condition

This panel contains a large convexity on its right as well as a minor undulation. This topography generates a noticeable elevational gap by region. The total depth is 67mm (the model is at 1/100 scale: Figure 3.79). The range within which the elevation level of most of the body parts are defined is limited between 29.4mm and 54.4.mm (high: 29.4-37.6mm, medium: 37.7-46.0mm, and low:46.1-54.4mm). The ranges outside this range are applied to the dorsal thigh (0.1-29.3mm) and ears and the hind leg (54.5-67mm). The whole dorsal thigh belongs to the extra-high elevation level because its range is disproportionally large, while the areas of the lowest elevation are considerably limited and do not include the majority of any body parts. Therefore, there is no extra-low level for C2.

Figure 3.79: C2 (1/100 scale) seen from the vertical position. The highest elevation is found on the dorsal thigh, while the lowest is on the ears and hind leg.

The elevation is first detected on the edge of the dorsal thigh where the large convexity is located. The detection of this elevated area continues, expanding downward and covering the almost all dorsal thigh and a part of the central thigh (0.1-29.3: see Figure 3.80, 1-2). During the next phase which is defined as the high level, no significant detection occurs yet. Simply, the elevated area from the dorsal thigh continues expanding downward and covers the central-ventral thigh as it gradually lowers its elevation (29.4-37.6mm: 3-4). At the same time, the tip of the hind leg also passes the cross-section layer. The rest of the whole body except the leg is detected at the medium level between 37.7mm and 46mm (5-6). The head and neck are first detected, and then the almost entire mid-torso passes the layer during the medium elevation level. Because these parts are located in the same elevation level, C2 appears mostly flat in its anterior body. Meanwhile, the hind leg remains undetected. Although the leg is placed in the low level (46.1-54.4mm: 7-8), the part is fully detected at a depth of 67mm.

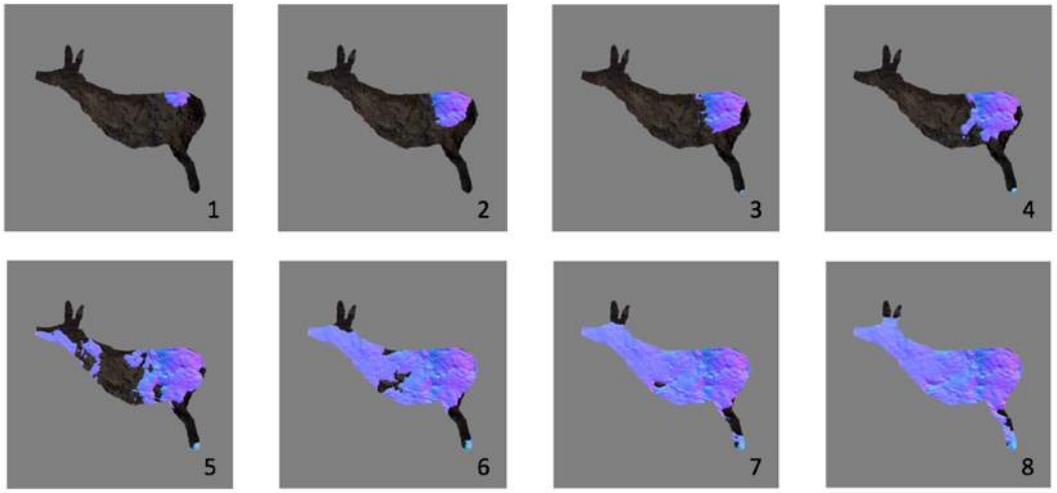

Figure 3.80: These eight images illustrate the depth of C2. When the cross-section layer passes the surface of C2, the colour of the surface changes; dark regions denote lower elevation than coloured parts. Images 1and 2 are for 0.1mm - 29.3mm, 3 and 4 for 29.4mm - 37.6mm, 5 and 6 for 37.7mm - 46mm, and 7 and 8 for 46.1mm - 54.4mm

Distortion on images (horizontal rotation, x10°, y-70° to y70°)

The sizeable convex surface on the thigh is a noticeable feature of C2. That topographic condition distorts the appearance of C2, especially the posterior, as the viewing position moves side to side. When the degree of the angle decreases, the outline of the buttock gradually becomes thinner because the elevated thigh hides its contour (y-70°: Figure 3.81). Moreover, the outline of the buttock appears pushed inwards; that causes a noticeable contraction at the root of the hind leg. This is due to the lower elevation of the ventral thigh. At the same time, the back leg also appears thinner due to the uneven topographic condition in the part. Because the elevation is higher on the left side of the leg, this elevated surface hides its right side where the elevation is lower. These deformations are absent in the 2D simulation (see Figure 3.81). These distortions are most likely perceived between y-70° and y-40°.

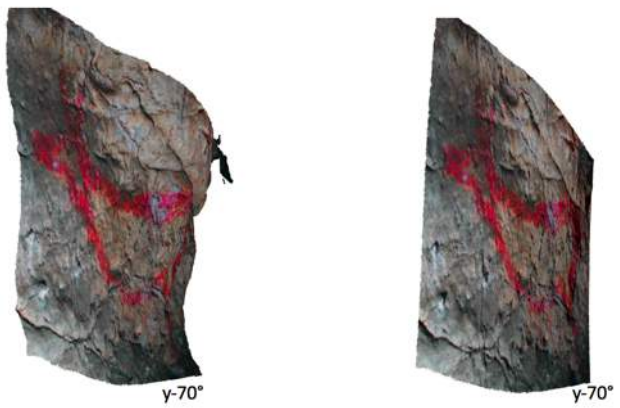

Figure 3.81C2 on the 3D surface (left) and the 2D surface (right) seen from y-70°. In the image depicted on the 3D wall, the contour of the thigh is thinner and appears deformed as the line tilts inward. These distortions are attributed to the high elevation of the thigh.

Meanwhile, the presence of the posterior is highlighted once the viewing position moves to the right; the robustness of the outline of the buttock and the hind limb appears clearer. The section on which distortion is especially salient is the dorsal-buttock. The area is gradually raised upward, strengthening its presence, and consequently the posterior becomes significantly large in comparison with the anterior, causing a bent in the dorsal line (y70°: Figure 3.82). The viewing range where this distortion is most recognisable is between y50° and y70°.

Figure 3.82: C2 on the 3D surface (left) and the 2D surface (right) seen from y70°. The presence of the posterior becomes immense much more than the image on the 2D surface. Due to this distortion, the deer appears raising the posterior.

Deer (D1)

General description

An outline red deer facing left (Figure 3.83). The deer is preserved in a remarkably good condition. The outline is executed by overlapping dots. D1 is a complete figure including the tail. The head contains the V-shaped ears and an eye. The contour of the muzzle extends inward beyond that of the under-neck until the cervical line. Two frontal limbs are provided as a thin vertical line. On the other hand, the hind leg appears absent, but the part is depicted as a small protuberance. Also, D1 contains a fill-in part on the shoulder. From the root of the frontal limbs to the dorsal line, there is a painted area which as if

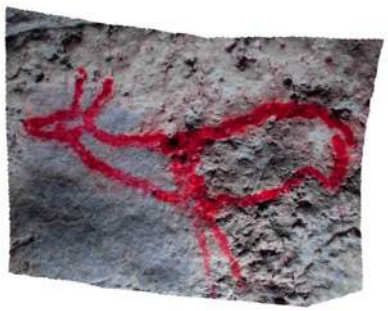

Figure 3.83: D1, outline red deer facing left (digital filter is applied). All body parts are provided. D1 is one of the well-preserved figures in Covalanas cave as its vivid red still survives until today. The frontal limb extends upward, even to the inside the body. This fill-in part does divide not only the neck and the posterior but also rough surface (right) and smooth surface (left).

separates the head and neck (the left side) from the main body (the right side). The condition of the surface is different between those two sides; the wall is smooth on the left, while considerably rough on the right. The size of the image is 65 cm, and it is located at a height of 210 cm (belly).

The integration of natural lines

Conspicuous natural lines are absent on this wall. There are only ambiguous edges due to an elevation gap on the right of the panel. However, none of them is integrated into any contour of the deer. Despite that the fill-in part is painted along the boundary which separates a smooth surface from a rough one, this is not considered as an integration. Therefore, D1 is outlined without any assists of the natural configuration of the cave wall.

The topographic condition

Generally, noticeable topographic features are not found on this wall; however, the surface forms a bowl-shape concave. The depth of D1 is approximately 78mm (the model is at 1/100 scale: Figure 3.84). The range within which the elevation level of most of the body parts are defined is limited between 26.1mm and 70.6mm (high: 26.1-40.9mm, medium: 41-55.7mm, and low: 55.8-70.6mm). The ranges outside this range are applied to the central thigh (0-26mm) and the ventral neck (70.7-78mm). While the central thigh belongs to the extra-high level because its range is disproportionally large, the area of the lowest elevation does not include the majority of the ventral neck. Therefore, there is no extra-low level for this image.

Figure 3.84: D1 (1/100 scale), seen from the vertical direction. The highest elevation is found on the central thigh, while the lowest is on the ventral neck.

The elevation is first detected on a part of the buttock and ears. As for the thigh, the detection continues based on the above area, expanding downward and inward, and it covers over half of the central thigh (0-26mm: see Figure 3.85, 1-2). Simultaneously, the elevated area of the face (muzzle and ears) also passes the cross-section layer, but the extent is limited. During the next level, areas which passed the layer further expands inward from both edges of the image and covers the entire thigh and most of the face (26.1-40.9mm: 3-4). As the cross-section layer proceeds, the regions of medium elevation level are revealed: the whole mid-torso belongs to this level as well as the

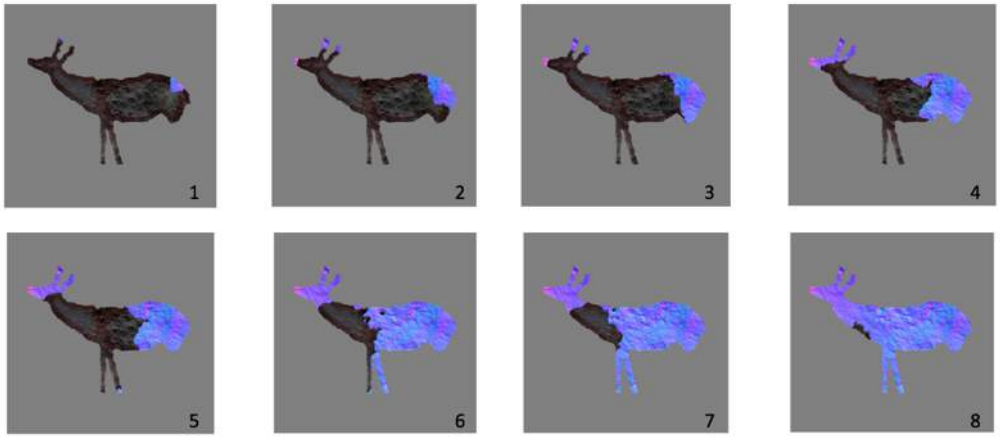

Figure 3.85: These eight images illustrate the topographic depth of D1. When the cross-section layer passes the surface of D1, the colour of the surface changes; dark regions denote lower elevation than coloured parts. Images 1 and 2 are for 0.1mm - 26mm, 3 and 4 for 26.1mm - 40.9mm, 5 and 6 for 41mm - 55.7mm, and 7 and 8 for 55.8mm - 70.6mm.

frontal legs (41-55.7mm: 5-6). The expansion of the highlighted area also continues from the head to the neck. However, the extent is considerably limited as the elevation gap between the head and neck is large. The topographic condition for the neck is defined as the low level during the next phase (55.8-70.6mm: 7-8). The surface is detected from the dorsal to the ventral, as the rest of the leg also entirely passes the layer. Although a part of the ventral neck-shoulder is the deepest, the region is finally detected at a depth of 78mm.

Distortion on images (horizontal rotation, x20°, y-60° to y80°)

As the whole body of D1 is located on a large concave surface, both the right and left edge of the image are significantly distorted once it is viewed from a side. Particularly, a remarkable distortion occurs on the neck and the head which are located on the surface of higher elevation. The elevated surface gradually bends the neck upward when the viewing angle decreases (y-60°: Figure 3.86). At the same time, the shape of the facial area horizontally shrinks; by being pushed inwards by the convex wall, the muzzle vanishes from the sight at y-60°. On the other hand, the posterior body sustains a similar proportion because the elevated edge of the thigh constantly faces the viewer. This stability in the shape of the posterior highlights the deformation of the anterior. Especially this deformation is salient when the viewing angle is between y-60° and y0°. Within this angle range, the deer appears shaking its head and neck up and down. D1 in the 2D simulation does not show such a way of distortion.

Figure 3.86: D1 on the 3D surface (left) and the 2D surface (right) seen from y-60°. The image drawn on the 3D panel is significantly distorted at its neck and head, but in D1 on the 2D surface, these parts stretch straight. This is because of the topography whose elevation gradually grows higher from the neck to the muzzle.

The image is also deformed once it is seen from the right: while the deer on 2D surface loses its clarity of appearance by simple inward contraction from both left and right side, the image on 3D medium sustains its clarity in all body parts at y80°. Particularly, the anterior clearly appears because the curve of the concave wall constantly shows the part to viewers on the right. As for the posterior, all contours are distorted by the topography: because the elevation is higher at the right end, the body on this area sustains the detailed curves in contours unlike in 2D surface. In particular, the deformation on the dorsal thigh which is caused by the rise of the wall on the region allows the image to maintain a certain proportion. This effect most likely appears between 60° and 80°.

3.4 Results

Integration of natural lines

In this case study, a total of 18 pictorial samples were analysed, among which integration was observed in 11 (A1, A3, A5, A8, A9, A14, B1, B4, B5, C1, and C2). Figure 3.87 illustrates the frequency of the integration by body section. The most popular area for integration is the dorsal line, with eight pictures (A3, A5, A14, B1, B4, B5, C1, and C2). The ventral part is next in importance as integration is found in five images (A1, A8, A9, B4, and C1). Although the use of natural lines in the buttock and head is not as frequent as the above body sections, integration is confirmed in three images at their buttock (A8, B1, and C2) and one image in its head (B1). No integrations are detected in the legs and the tail.

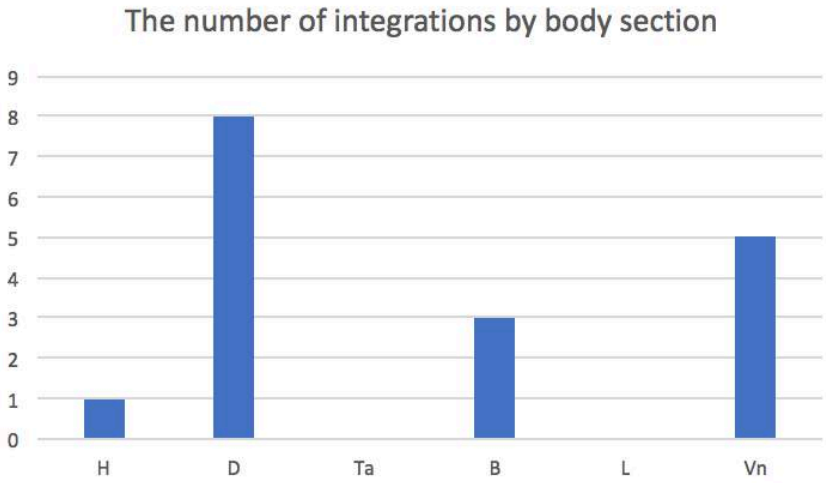

Figure 3.87: The number of integrations by body part (H: Head, D: Dorsal, Ta: Tail, B: Buttock, L: Limbs, and V: Ventral). Integration mostly likely occurs on the dorsal line and then ventral line. No sample is detected from the limbs and the tail.

Meanwhile, samples with several integrations are relatively rare, as in most cases integration occcurs in only a single section (six images: A1, A3, A5, A9, A14, B5, see Figure 3.88); there are four images where natural lines are integrated into two body sections (A8, B4, C1 and C2), while only one image contains three integrations (B1). Among the six images with a single integration, the integrated sections are the dorsal (A3, A5, A14, and B5) and ventral line (A1 and A9). Integration does not occur in the head or the buttock alone, despite a number of natural lines which can have been integrated into the head and buttock. Integration on these sections are always accompanied with that on the dorsal or the ventral line (see Figure 3.89). Therefore, Integration into the dorsal and ventral was somehow preferred by the ice-age artist of Covalanas more than into the head and buttock.

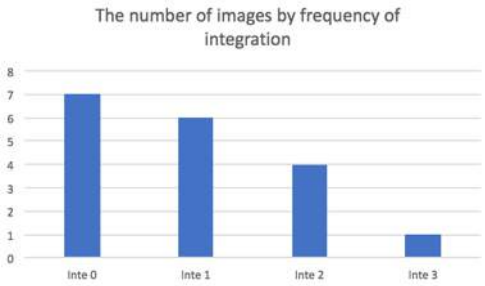

Figure 3.88: The number of images by the frequency of integration (Inte = Integration, Inte 0: 7 images, Inte 1: 6, Inte 2: 4, and Inte 3: 1). The case with plural integrations on a single image is rare.

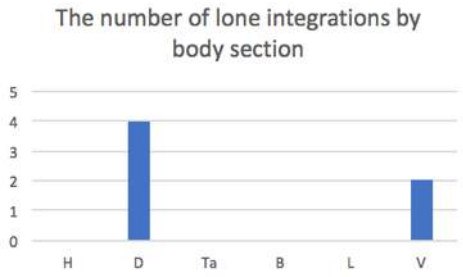

Figure 3.89: Among 6 images with single integration, all cases occurs either on the dorsal or the ventral line (H: Head, D: Dorsal, Ta: Tail, B: Buttock, L: Limbs, and V: Ventral).

As for the combination of integrated sections among images with multiple integrations (A8, B1, B4, C1 and C2), integrations simultaneously happen to the head and the dorsal in one image (see Figure 3.90). The ventral line and buttock are also integrated at the same time in one image. The other combinations (the dorsal and buttock, and the dorsal and ventral line) occur in two images. Even though this result suggests that the buttock can be combined with either the dorsal or ventral, the total number of the samples are too small to discuss any meaningful trend about combinations.

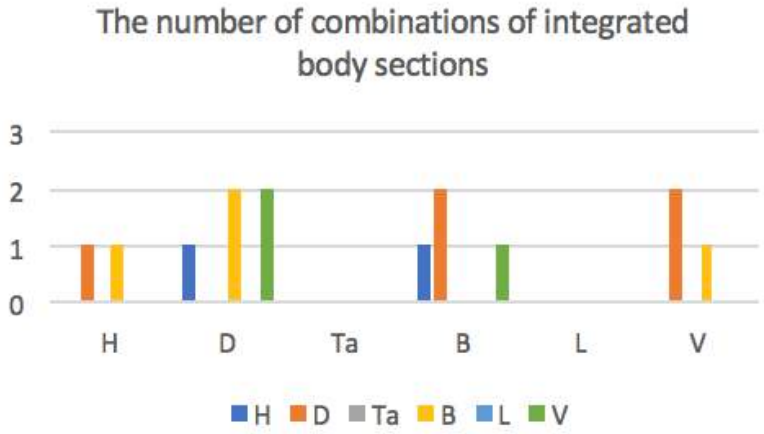

Figure 3.90: The number of combinations of integrated body parts. Integration occurs on D-V and D-B in 2 images. Values for other combinations are 1 (H-D, H-B, and B-V). Integration on the buttock can appear together with that on any other contour parts, but contrarily the ventral line has no combination with any other contours except the buttock.

Topographic Condition

Regarding the analysis of the topographic condition, this study first divided each image into 13 sections and secondly assessed the elevation level by body section (Extra High, High, Medium, Low, and Extra Low). As a result, a certain tendency is detected. Figure 3.91 shows the frequency of elevation levels by body section. According to this, the higher levels (Extra High and High) are more likely located on the head, thigh and limbs than on the neck-shoulder and mid-torso; especially, no extra-high level is found on the torso area.

By contrast, the number of the medium level is markedly higher in the neck-shoulder than any other body part (DNs: 11 images, CNs: 10 images, VNs: 8 images), and the frequency of the low elevation level is the highest in the central part of the body (DM: nine images, CM: eight images, VM: five images). Meanwhile, regarding the extra-low level, it does not appear in any body parts other than the forelegs (two images). Accordingly, the elevation tends to be lower on the neck-shoulder and the mid-torso than on the head and the thigh.

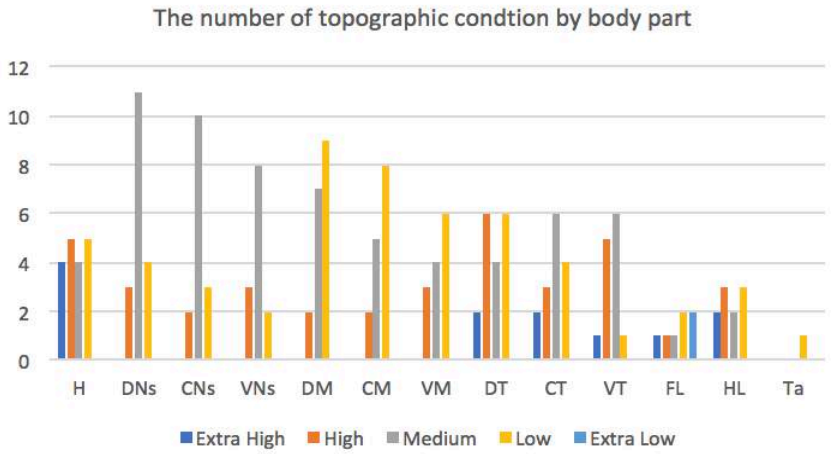

Figure 3.91: The number of the topographic condition by body part (H: Head, Ns: Neck-shoulder, M: Mid-torso, T: Thigh, FL: Front Leg, HL: Hind Leg, Ta: Tail. D, C, and V, refer to Dorsal, Central, and Ventral, respectively). Medium level and low level tend to be found on the neck-shoulder (Medium: 8-11 images) and middle part (Low: 6-9 images) respectively, while the head and thigh is likely located on the wall of higher elevation (Head: 9 images, 8-5 images). Therefore, the general shape of the wall is a plate-like concave. The extra elevation levels are confirmed only on the head and limbs.

To generalise from this result and handle the overall tendency in the topographic condition, I united the divisions of the neck-shoulder, mid-torso, and thigh to generate simplified data (for the procedure see Chapter 2). This simplification allowed me to calculate the sum of the elevation points by body section. Based on this sum, the overall topographic condition can be generalised. Figure 3.92 demonstrates the simplified data. According to this graph, the trend indicated by the above original graph is maintained. Figure 3.93 shows a generalised topographic condition. In this generalised data, the higher numerical value represents the higher elevation. Consequently, it is numerically clear that the surface on the head (62 points) and the thigh (59 points) is higher in elevation than the neck-shoulder (53 points) and mid-torso (48 points). Namely, 18 images in Covalanas cave are apt to be drawn on an overall concave wall.

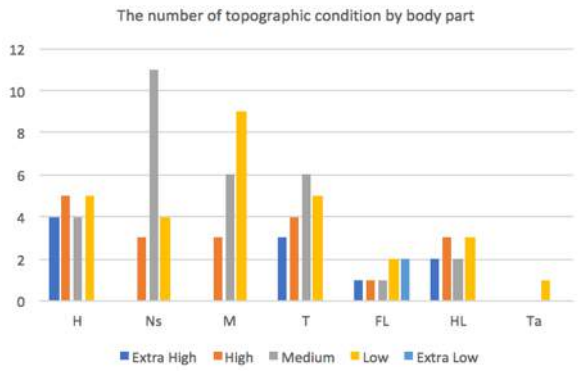

Figure 3.92: The number of the topographic condition by body part (H: Head, Ns: Neck-shoulder, M: Mid-torso, FL: Front Leg, HL: Hind Leg, and Ta: Tail). The data is simplified as the three divisions in Ns, M, and T are integrated. Even so, the graph shows the same trend as demonstrated in Figure 3.91: Higher elevation in H and T, while lower elevation in Ns and M.

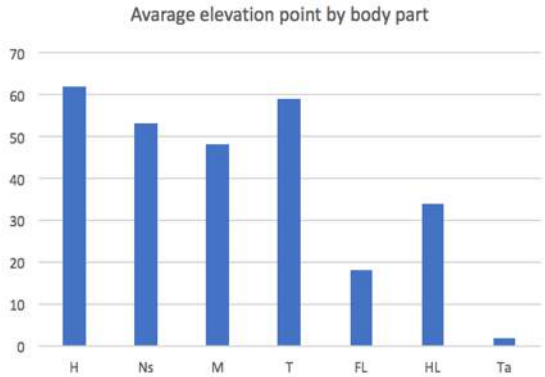

Figure 3.93: The average elevation level of each body part is quantified (H: Head, Ns: Neck-shoulder, M: Mid-torso, FL: Front Leg, HL: Hind Leg, and Ta: Tail). The elevation reflects high if the numerical value is high, and on the contrary, the depth is deeper if the numerical value is low. Therefore, it is clear that the head and thigh are more likely to be placed on higher elevation.

This trend is more concretely demonstrated by examining the topographic condition of each image. The simplified topographic condition is visualised as a line graph. Consequently, roughly six patterns of topography are detected (Figure 3.94). Those patterns and their definitions are described below:

- Pattern 1 (P1): Overall concavity. The elevation of both neck-shoulder and mid-torso is lower than that of both head and thigh.

- Pattern 2 (P2): Overall slope. The elevation of both neck-shoulder and mid-torso is lower than either head or thigh but higher either head or thigh. At the same time, the elevation does not fluctuate between these four body parts.

- Pattern 3 (P3): Overall Convexity. The elevation of both neck-shoulder and mid-torso are higher than that of both head and thigh.

- Pattern 4 (P4): Zigzag: The elevation constantly fluctuates between these four body parts.

- Pattern 5 (P5): Partial concavity: The elevation of either neck-shoulder or mid-torso is lower than that of both head and thigh.

- Pattern 6 (P6): Partial slope: The elevation of both or either neck-shoulder or mid-torso is same as that of either head or thigh but at the same time higher or lower than either head or thigh.

As a result, five images conform to P1 (A1, A3, A5, A10, and D1). On the other hand, three images are fell into P2 type (B1, B4, B5). P3 contains two images (A7 and A11), and the images belong to P4 are A8, A14, and C1. While three images (A2, A9, and A13) are categorised as P5, two images (A6 and C2) are labelled as P6 type. As is shown in Figure 3.94, overall concavity is the most popular topographic type in Covalanas.

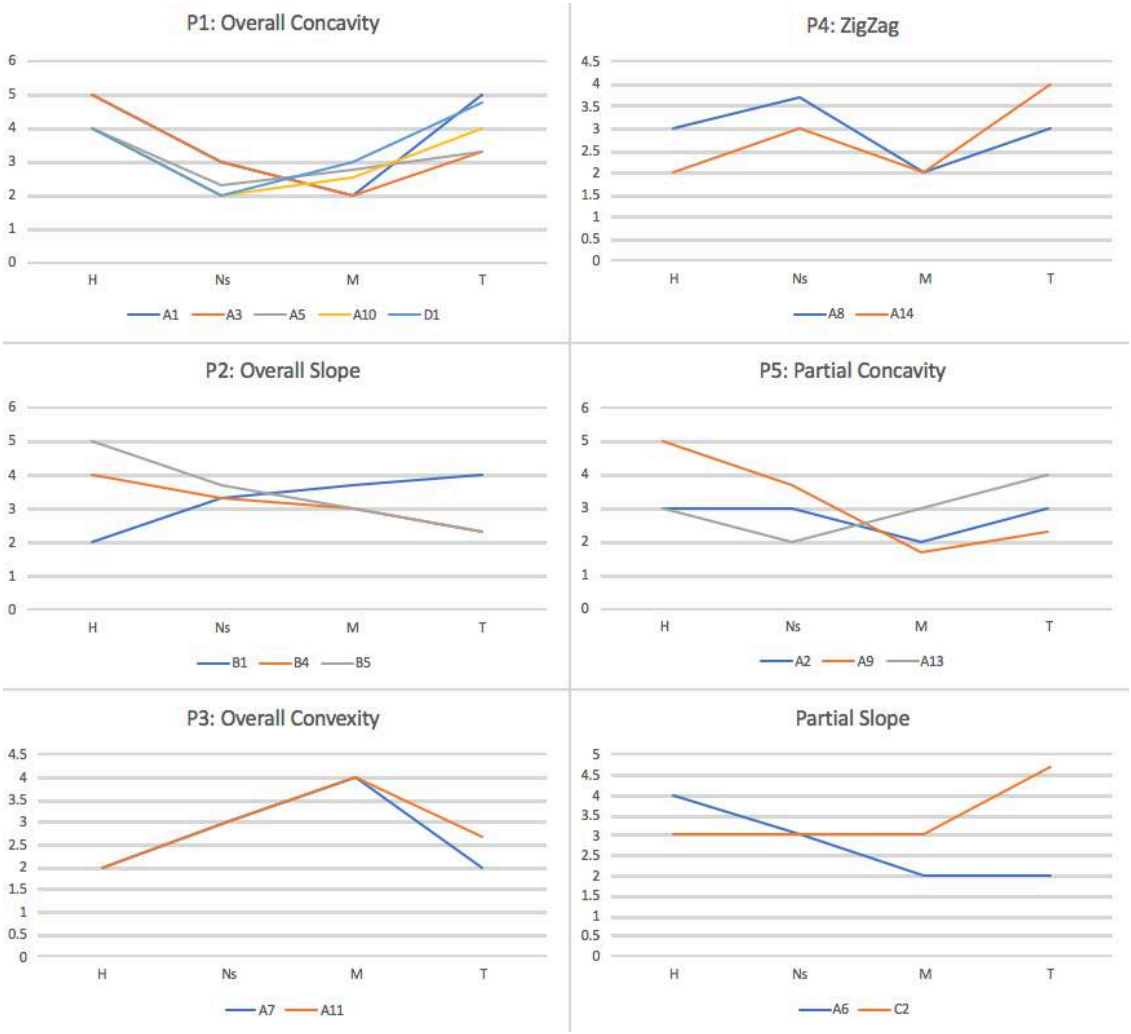

Figure 3.94: The line graph shows the elevation level by body part, as a result, there are roughly six patterns in the shape of the wall: Pattern 1 (P1) is overall concavity; Pattern 2 (P2) is overall slope; Pattern 3 (P3) is overall convexity; Pattern 4 (P4) is zigzag; Pattern 5 (P5) is partial concavity; Pattern 6 (P6) is partial slope. Among these six patterns, P1 is the most popular topography (P1: 5 images, P2: 3, P3: 2, P4: 3, P5: 3, and P6: 2).

Distortion on images

With regard to distortion on images, remarkable examples were detected on 11 images (A1, A3, A5, A8, A9, A10, A11, B4, B5, C2, and D1). This number accounts for >60% of all analysed images in Covalanas (Figure 3.95). Significantly, all of these 11 images contain multiple distortions as two body parts are deformed in six images (A3, A5, A10, A11, B4, and C2) and three parts in four images (A1, A8, B5 and D1). Above all, A9 most dynamically changes its appearance, with five deformed sections. Among images with no distortion, most of them (A2, A6, A8, A13, A14) are incomplete, lacking multiple body parts, and the outline defining the appearance of their entire body is unclear. Therefore, it is difficult to identify the deformation. If these had been complete figures, distortion might have also been detected in them.

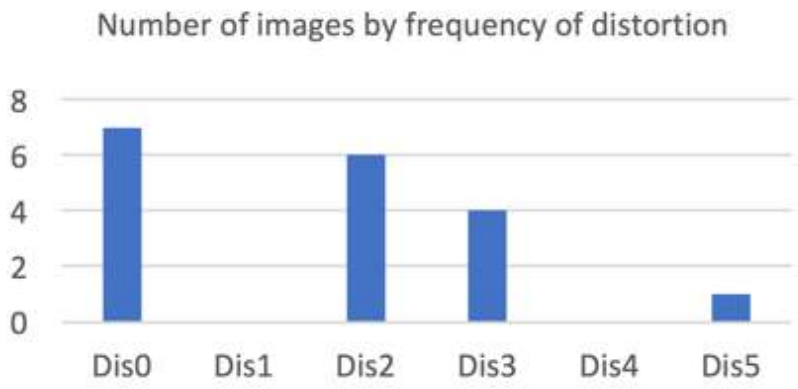

Figure 3.95: The number of images by the frequency of distortion (Dis = Distortion). Distortion is confirmed in 11 images (Dis2: 6, Dis3: 4, and Dis5: 1). All of them are subject of plural distortions. All in all, distorting an image by topography is not rare, and in some images, their appearance is severely deformed as the viewing angle changes.

Among the body parts, distortion is most frequently confirmed in the neck-shoulder (eight images: see Figure 3.96) and then the head (seven images). Although less often than these regions, distortion also commonly occurs in the thigh (six images). By contrast, distortion less likely occurs in the middle and the legs as each of them contain four images. No distortion is found in the tail. Regarding this result, an inequality between body parts must be taken into account: not all images are equally complete. For example, about the tail, even though no distortions are confirmed, among almost all analysed pictures the tail is absent; only A11 and D1 contains this. Therefore, the value for the tail inevitably marks the lowest result. The limb is also missing in seven images, but it is deformed in four images. this number suggests a higher rate at which distortion occurs (4/11= 0.36) than that in the thigh which are provided with 18 images but deformed in six images (6/18= 0.33); that is, the leg could have also achieved a higher result if all figures have been equally completed. Thus, the detected trend requires consideration.

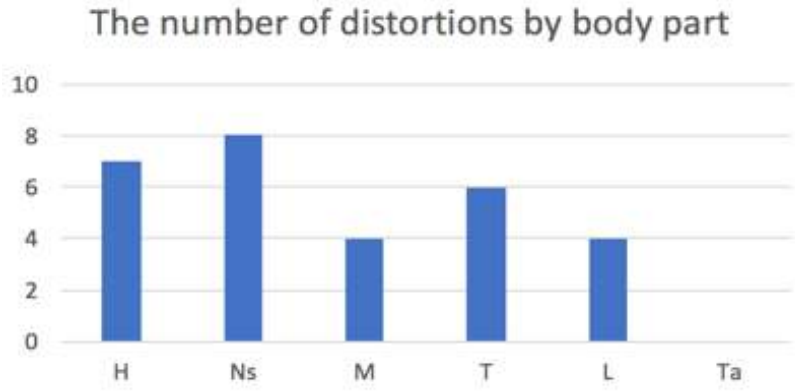

Figure 3.96: The number of distortion by body part (H: Head, Ns: Neck-shoulder, M: Mid-torso, T: Thigh, L: Limbs, and Ta: Tail). Distortion more likely occurs in the anterior body (Head: 7 images, and Neck: 8). Meanwhile, the mid-torso (4) and leg (4) is rarely deformed, and no distortion is confirmed at the tail.

Summary

The collected data demonstrate a particular trend in all of the interaction categories. With regard to integration and topographic condition, the results obtained provide a detailed example of interactivity in the production phase. I will discuss the significance of this in Chapter 6, once all data have been presented. As for the interactivity in the post-production phase, no definitive evidence has been found as to whether or not the distortion was intentionally created. However, the result offers us a specific insight about the distortion (e.g. types of topography causing distortion, and popular locations of deformation). The following is a summary of the analysis results in each category.

- In Covalanas cave, integration of natural lines was confirmed in more than half of the total examined images. Dorsal and Ventral lines are most frequently integrated.

- The neck-shoulder and the mid-torso tend to be placed on a wall with a lower elevation than the head and thigh. Images are, therefore, more likely depicted on a concave surface.

- The extra elevation levels are found only on the head and limbs.

- Six patterns of the underlying topography have been confirmed in Covalanas cave: P1 (Overall concavity), P2 (Overall slope), P3 (Overall convex), P4 (Zigzag), P5 (Partial concavity), and P6 (Partial slope). The most frequent type is P1.

- Distortion has been confirmed in 11 images out of 18. This number suggests the distortion is not a rare phenomenon. All of these 11 images are subject to multiple distortions which can change their appearance to a great extent.

- The body parts where distortion occurs most frequently are the neck-shoulder and the head.

These are the main observations detected in this case study; the case study of Covalanas cave has, therefore, yielded significant information on the specifics of the interactive nature of cave art. All data used to visualise the figures is presented in the appendix. As noted above, I will not discuss the meaning of the above trends further in

this chapter; general trends will be reviewed, discussed, and interpreted based on the all obtained data from the three case studies. Keeping the detected observations from Covalanas in mind, I now move on to the next case study.

Chapter 4

Case study 2: El Pendo Cave

4.1 General information

Site

El Pendo is one of the cavities in Peñajorao mountain (alt. 169m) which is located in Escobedo, a town in the municipality of Camargo. Although the sierra is marked by the environment of the rich indigenous vegetation (e.g. oaks, laurels, hazel), a great wealth of speleological landscape also features the area as Puente Viesgo and Ramales de la Victoria (Garcia-Mondejar 1990). Through the underground of the forest of the mountain, a karstic network system develops several kilometers, and El Pendo cave is the most significant cavity for Paleolithic archaeology in this underground network. An underground river eroded the karstic soil, forming a current large holes as well as repetitions of internal collapses of ceilings. This river now flows a few meters below the current entrance.

The entrance of El Pendo is located on the slope of Aptian limestone cliff, facing South. The interior extends north, with the travelable area of about 150 m (Figure 4.1). Although in the deep part the conduit to explore becomes significantly narrower, a large hall features this cave. After the entrance, as the floor forms an abrupt slope, this immense chamber develops 80 m long, 45 m wide and 25 m high. The newly discovered images are situated on the wall that marks the end of this hall at the point 80m away from the cave mouth.

The cave was brought to light in 1878 by Marcelino Sanz de Sautuola, who also discovered polychrome images on the ceiling of Altamira cave one year later. Since then El Pendo has been researched by archaeologists such as Juan Vilanova, Piera, J. Carballo,

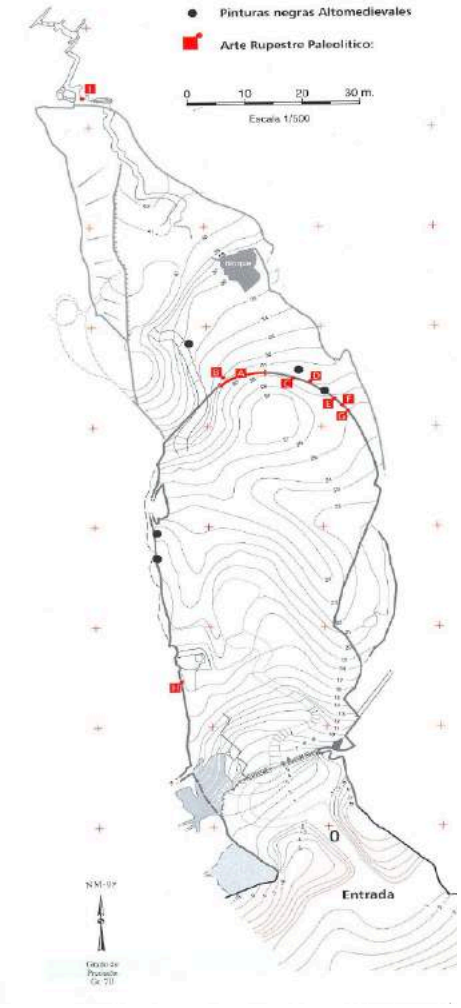

Figure 4.1: Site plan of El Pendo cave. Although the entire area is approx. 150 m, the large chamber constitutes the almost half of the cave.

Martinez Santa-Olalla, and many others. The site was frequently excavated during the late 19th century, which generated rich archaeological records in a stratigraphic sequence. The stratigraphy consisting of 18 layers and 24 different units, testimony a long cultural transitional history of almost 80,000 years from the Middle Palaeolithic to the Middle ages (Barquin et al. 1998). This whole sequence, in addition to that of El Castillo, has been crucial to the development of prehistoric chronology and sedimentology of the region and Europe in general (Hoyos Gomez and Laville 2009). Regarding its archaeological material, various sorts of assemblages (stone or bone tools, portable art and faunal remains) are recovered from throughout Mousterian and Upper Palaeolithic layers (Pike-Tay et al. 1999). The collection of portable art in particular is so large that the site is recognized as a portable art 'sanctuary' cave in Franco-Cantabrian region. Artefacts such as perforated batons, harpoons, perforated sticks, needles and spatulas possess abundance of engravings of animals and signs of great technical quality (e.g. Carballo and Echegaray 1952, Mateos 1982, Sieveking 1991, and Rivero et al, 2014). Moreover, rare animals in parietal art are also represented in the portable objects among them such as snakes, fish or goats in frontal vision (Maestu 1994 and Rivero et al. 2014).

Those who left these rich archaeological remains might have also been responsible for the remains in other caves. A comparative research into the relation between seasonal behaviors of hunter-gatherers and lithic-faunal assemblage among three caves in Cantabria (El Pendo, El Miron, and El Castillo) suggests that the occupation of El Pendo repeatedly happened during Palaeolithic time especially for winter camp, and it is considered that these three caves could be crucial seasonal settlement of limited hunter-gatherer bands (See Pike-tay et al. 1999).

Pictures

24 newly discovered images comprise the wall known as "the Frieze of the Paintings". The panel spans 25 m along the deep end of the massive chamber. Among these 24 images, at least 15 images clearly represent quadruped animals. The Palaeithic artists of them as well as those of Covalanas had an obvious preference of motifs. The majority of the depicted animals is deer, with 11 pictures. Although there is also the presence of other animal species (two unidentified quadrupeds, one caprid, and one horse), the dominant motif is outstanding. Meanwhile 9 non-representations are also left on the frieze, although their presences are marginalized by the stunning quality of animal depictions. The type of the signs varies from a simple dot to scattered lines. Some sigs, due to their shapes, appear that they might have originally been a part of an animal depiction, however nothing on this point can be confirmed because of the poor conservation condition.

In particular, 17 manifestations of both representational (figurative) art and non-figurative 'signs' are fixed on the further limited wall of 8.5 m wide and 3.5 m height where is the leftmost of the entire frieze (Figure 4.2). Significantly, it seems that the positioning of these pictorial contents was thoughtfully organized – i.e. deliberate - as any major overlaps between individual images are absent. In particular, the area with the concentration of 17 images, to some extent, appears symmetrically and synchronically composed by placing the largest deer in its centre, and organizing subsequent images around that. Consequently, it is justifiable to view the panel as a singular pictorial unit.

This unique composition also suggests that we should take account of matters of the spatial limitation. These images are distributed at different heights, and no picture is located below 2 m (the highest position is over 6 m). Considering this height, in advance of image depiction artists must have been required additional labors such as making a tool for working place (e.g. ladder or scaffold) and installing them. Even so, working in such a high place is fundamentally not as comfortable and stable as standing directly on the ground. Nevertheless, the artists treated each images equally, securing same artistic standard (Barquin 2003). After all, we can say that depicting images on such a high wall seems not practical as extra efforts are needed. However, this inconvenient location of images must have necessarily been considered for the composition which features this pictorial device of El pendo probably because the spatial organization itself might have had a certain cultural significance (Ibid.).

The parietal art in El Pendo cave, like Covalanas, shares a number of common traits with the artistic style of Ramales school. Images in El Pendo are stylistically similar to others of the Ramales school, with a feature generally known as 'V-shaped ears'; these images are exclusively executed in red, and as studies indicate by mineral pigments (red ochre) available in the close vicinity of the site (Barquin 2003). The artistic techniques

Figure 4.2: The Frieze of the Pictures (8.5m width x 3.5m height). 17 images are depicted on this limited area.

are the simple dot, overlapping dot, and buffering colour, all of which are principal methods among the caves of Ramales School (see Barquin et al. 1993 Barquin 2001, and Barquin 2003). Moreover, both directly and indirectly generated of the pictorial set is coherent to the dates of parietal art in caves of Ramales school (approx. 20,000 BP: Barquin 2003). These facts indicate the presence of a shared single artistic mode in the region and strongly suggest that El Pendo belonged to this cultural unit.

Because this decorated panel located at the center of the end wall of the large room, it is believed that those images are visible from any points of the chamber even from the cave entrance as long as the cave is lit with basic illumination (Barquin 2003). There is also another possibility with regard to the luminary condition during Palaeolithic time. J. Carballo who intensively studied El Pendo cave during early 20th century, believed that during the winter season when the position of the sun is at its lowest to the South of the cave it might have been able to capture direct sunlight at depth of up to 50 m from the entrance as it is considered the original entrance which collapsed at some time in Holocene was much wider than current mouth (Carballo 1960). If Carballo's claim is true, the frieze could also have been visible without artificial light. Although this point is unprovable, it is worth keeping it in mind.

Previous research and the images selected for study

Since the new discovery of El Pendo's parietal art in 1997, its images have been formally studied by Ramon Montes Barquin and his colleagues who as a result have made three publications so far (Barquin et al. 1998, Barquin 2001, and Barquin 2003). The aim of the first literature published in 1998 was to provide a general description of 16 images in the main panel (the description includes analysis on the location, pictorial style and adopted techniques). Every time new literature was published, new updates were also made; reviewed interpretation of depicted animals, more detailed descriptions, and a further discovery of new images (e.g. the paper published in 1998 referred only 16 images, while the number was up to 24 in the later documents) were added to the ground knowledge of the pictorial set in the cave.

The published literature seems relatively brief, especially when regarding the fact that El Pendo cave is one of the most cited sites for its complete stratigraphy (Barquin et al. 1998). it does, however provide enough fundamental information for this case study. For instance, this chapter adopts the interpretation of painted species and the measurement of each picture which were both addressed in these documents. The latter is particularly crucial reference because the measuring images in El Pendo is a considerably hard task due to the high instability of the floor in front of the frieze. Each measurement is a significant criterion for this case study to inspect the accuracy of a reconstructed 3D model of the panel as will be mentioned later.

After the revision of the first work, Barquin (2001) treats figures by adding them motif number (from N1 to N24). The number initiates from the figure located the leftmost of the frieze and escalates as counting images toward the right in order. The exceptions are N18 (it is fixed on a lower part of the left of the frieze), N15a and N15b (they are located on different positions on the main frieze), and the last figure N24 (this is found on the left wall where is approximately 25 m away from the entrance). These images are located on the wall called "the Frieze of Pictures", an area of 25 m width (figure), with an exception of N24. The all artistic contents and their corresponding motif numbers are the followings: deer (N1), deer (N2), serpentiform sign (N3), goat (N4), deer (N5), deer (N6), deer (N7), horse (N8), oval-shape sign (N9), V-shaped line (N10), red dots (N11), acephalous quadruped animal (N12), deer (N13), acephalous quadruped animal (N14), dot (N15 a), dot (N15 b), deer (N16), deer (N17), two discs (N18), deer (N19), red line (N20), buffered two red lines (N21), deer (N22), deer (N23), and lines (N24). This case study also adopts this motif number for the management of sample figures.

Although there are a total of 24 images in the set, this case study focuses on 11 animal images on the main frieze (N1, N2, N4, N5, N7, N8, N12, N13, N14, N16, and N17: see Figure 4.3) as was stated in the beginning of this chapter. Signs are eliminated from the list because they do not suit the purpose of the analysis. This study also left 4 animal images unexamined; 3 of them are located on the wall several meters away from the panel of images of high concentration, and one is fixed on the studied panel. The reasons for this selection of pictures are firstly the matter of accessibility to the location (the main panel has much easier access than the right part of the frieze) and secondly that of the conservation condition (these eliminated 4 pictures are not clearly visible due

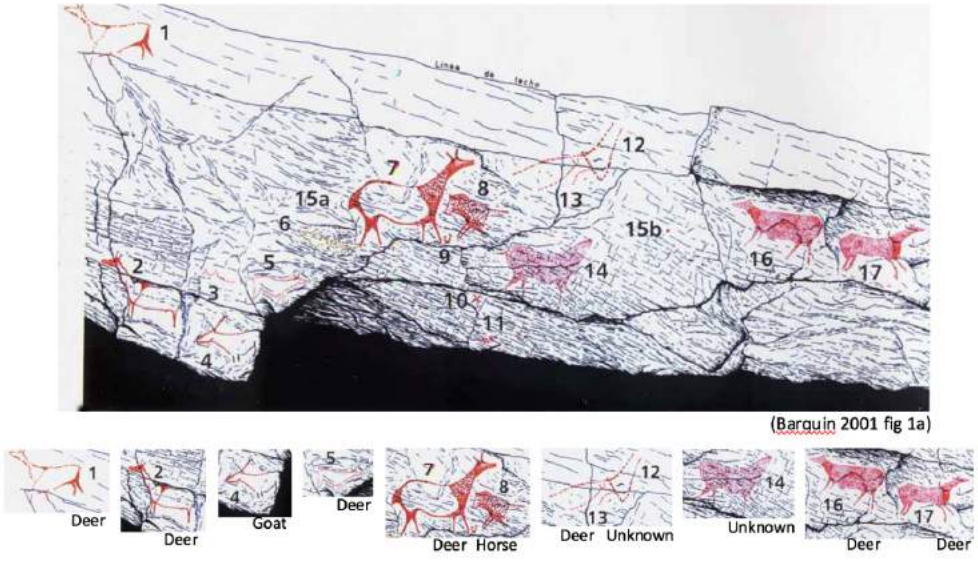

Figure 4.3: The Frieze and a total of 17 images. This case study selected 11 images (N1, N2, N4, N5, N7, N8, N12, N13, N14, N16, and N17.

to the weathering of the wall's surface, so therefore any pictorial analyses are considerably difficult). Additionally, N10 is indeed considered as graphic remains which originally represented a deer (Barquin et al. 1998, and Barquin 2001), but it is also not examined in this chapter because even if the V shape reflects the ears of a deer, the information left to us is too limited to imagine the entire appearance of the motif.

4.2 The frieze and Methodology

The wall to be studied is a large rocky panel, with an approximate length of 880 cm and height of 300-350 cm (Barquin et al. 1998). The 11 pictorial units examined are all found on this wide area from edge to edge, apparently forming a high density of decoration. This painted wall is located on the centre of the end wall of main chamber, which posits in front of the entrance but 80 m away. The height of the panel varies by area but basically becomes narrower toward the right. The bottom of the frieze tends to be collapsed (especially the centre and right areas), and so the wall surface of these areas tilts backward, creating significant gap in elevation between collapsed and non-collapsed surface. Pictures are depicted on the non-collapsed part as if Palaeolithic artists intentionally avoided the collapsed area at the bottom.

It must be noted that the current floor in front of this frieze is not original. The original height of the floor is supposed to have been much lower than that of present day, perhaps as much as 150-200cm lower (Barquin et al. 1998). Boulders fell off from the ceiling and formed the current floor. The level might have varied by location, but at least the height from the original ground for N1-N13 should have been more than 2m high (Barquin 2003).

This fact introduces a degree of imprecision to this case study. As there is no clue which allows us to presume any concrete figures of the original ground around the frieze, it is impossible to examine images in the same setting as in the Palaeolithic. The accumulation of large boulders prevents the identification of the actual viewpoints and specific viewing actions. Moreover, because the experiment with illumination cannot be performed on the actual situation either, to investigate a viewing distance would also produce information that was essentially irrelevant to Palaeolithic time. For this reason, images were analysed based on a single condition; as these pictorial samples are essentially situated on high locations, this study considered that a "looking up" perspective was the basic viewing action, and analysed these 11 images by reconstructing panel that appears from looking up.

Aside from this problem, there are two further matters to take into account: first, that the frieze is essentially visible from anywhere in the large hall; second, that Palaeolithic cave visitors might have been able to view the frieze without the assistance of artificial light. The first issue addresses a fundamental fact which specifies the

topographic feature of El Pendo cave. If this is the case, two aspects need to be considered. First, the images can also be viewed from higher position, as the floor of the chamber continues downward from the entrance. Namely, this fact suggests an additional requirement of a 3D simulation of "looking down at images". Secondly, the frieze is visible from a distance, even from the entrance 80 m away from the decorated wall (Ibid.). In this case, viewers capture in their sight the entire panel, a composition consisting of the sum of images, rather than an individual picture. Accordingly, it is also crucial for the simulation to account for how the topography of the wall intervenes in the appearance of entire composition. However, this first fact pertains, as Barquin (2003) notes, only if the least visibility is secured in the underground environment. Regarding this point, Barquin neither specified how much illumination was required for gaining the basic visibility, nor whether it is achievable by an illumination device (e.g. torch or stone lamp) in the Palaeolithic. Directly speaking, the information that currently we have is too insufficient to take this aspect into the account of this case study. Therefore, the analysis below concentrates on the case of "looking up" at an individual image. Similarly, the second matter is also avoidable. Carballo (1960) believed that original cave mouth might have harnessed a significant amount of natural light which potentially illuminates the area of 50 m from the entrance in a certain season. If this is true, the panel might have been visible without an artificial light from any points of the chamber, therefore. However, the actual luminance level of the cave interior is untestable, and currently we cannot know whether the illumination was unnecessary to Palaeolithic cave visitors to appreciate the artworks. For this reasons, this case study keeps these issues aside but instead concentrates on 3D analysis based on the very basic condition for viewing images as above mentioned.

3D model

A 3D model of the Frieze of the Pictures has been generated from a total of 308 photographs (Figure 4.4). There are lights installed in El Pendo cave which provide enough of a luminance level for image acquisition. Once the model was reconstructed, each image was extracted from the 3D panel and exported in PLY format for a further analysis on Photoshop. The amount of processed data is considerably large, so it was inevitable to reduce the quality level from high to middle in order to properly operate the software due to an insufficient spec of the computer which processed the data. Nevertheless, as will be referred later, the accuracy of the model possesses enough

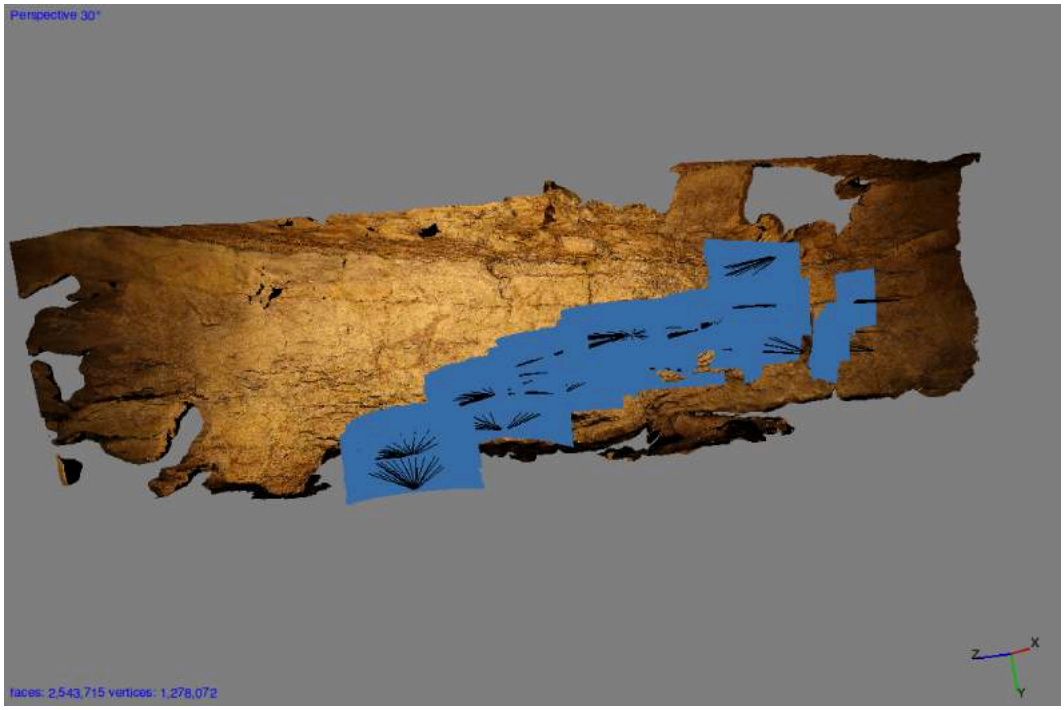

Figure 4.4: A reconstructed model and camera positions (shown in the figure as blue rectangles).

reliability, despite lowering a quality. Meanwhile, there is an issue. Target images are distributed in a wide area, and so some areas can only be photographed from a distance. Because of this inaccessibility, the resolution of some marginal areas (especially top-left part of the panel) is less clear than the central region, which causes visual information in such regions slightly obscured. This result affects the analysis of N1; the detail of the surface, mostly natural lines, on the region is unclear. Therefore, the analysis of N1 partly relies on the detailed illustration listed in the Barquin's publication that was made in 2001.

Generated models were scaled and assessed for their accuracy by following the procedure described in Chapter 2. As for physical measurement, I also used the dimension described in Barquin's paper (2001). The image to scale the model is N8. The result is shown in Table 4.1 below.

Images	Physical Length (cm)	Virtual Length (cm)	Difference (cm)	Difference (%)
N1 (Red deer)	75	72.6	2.4	3
N2 (Red deer)	85	84.7	0.3	0.4
N4 (Caprid)	60	61.6	1.6	3
N5 (Red deer)	48	50.7	2.7	6
N7 (Red deer)	125	124.4	0.6	0.5
N8 (Horse)	64	64	0	0
N12 (Unknown)	96	91.1	4.9	5
N13 (Red deer)	43	41.6	1.4	3
N14 (Unknown)	83	81.3	1.7	2
N16 (Red deer)	70	71	1.0	1
N17 (Red deer)	68	70.3	2.3	3

Table 4.1: Comparisons between physical measurements and virtual measurements. The difference is within the range of ± 3 cm for almost all images, indicating the high accuracy of the model.

Consequently, the difference for 10 pictures out of 11 are within the range of 3 cm; the largest ratio of the difference is approx. 6% (N5: Difference/Physical length = 0.0562). An anomaly is N12, with 4.9 cm gap. Although this result appears large in comparison with that of the rest of graphics, this is probably because of the position where N12 is fixed. The image is located on a considerably high place. This fact together with the instability of the floor makes a measuring activity difficult, and so the physical measurement might slightly be bigger in reality. Given this factor, the difference for N12 is also understandable. Thus, the gaps between physical and virtual measurements seem to be within an acceptable level. Therefore, it can be said that the 3D model of "the Frieze of the Pictures" are accurately reconstructed and suits for the further analysis.

Simulation

3D models were rotated along the Y-axis to simulate how the topography of the wall distorts the appearance of images. For the X-axis, the model is fixed as a preset in the position of X30° which simulates that images are looked up. This is because the original floor in front of the frieze is supposed to be approximately 2m lower than current level (Figure 4.5). The range of the degrees of the angle for each graphic is set so that samples could sustain their basic appearances unless otherwise the over-disruption of images makes graphic analysis difficult. The ranges are summarised in the Table 4.2 below.

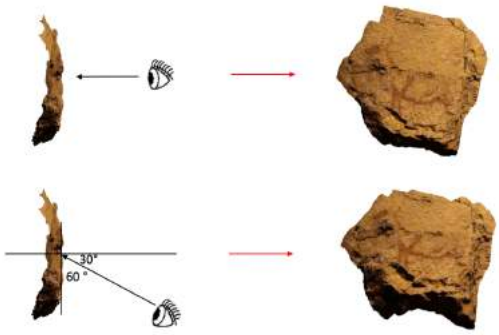

Figure 4.5: A model looked up from x30° angle. This angle simulates the appearance of an image viewed from a lower position.

Image	Horizontal Rotation (Y-axis)	Fixed angle (X-axis)
N1 (Red deer)	140° (left limit -60°, front 0°, right limit 80°)	30°
N2 (Red deer)	130° (-60°, 0°, 70°)	30°
N4 (Caprid)	120° (-60°, 0°, 60°)	30°
N5 (Red deer)	120° (-60°, 0°, 60°)	30°
N7 (Red deer)	140° (-70°, 0°, 70°)	30°
N8 (Horse)	140° (-70°, 0° 70°)	30°
N12 (Unknown)	130° (-70°, 0°, 60°)	30°
N13 (Red deer)	150° (-70°, 0°, 80°)	30°
N14 (Unknown)	130° (-60°, 0°, 70°)	30°
N16 (Red deer)	140° (-70°, 0°, 70°)	30°
N17 (Red deer)	130° (-80°, 0°, 50°)	30°

Table 4.2: Rotating range (Y-axis) and fixed viewing angle from the bottom (X-axis).

In addition to the 3D simulation, an image obtained by converting a 3D model into a 2D image was also rotated in the vertical and horizontal planes in a three-dimensional space, and then the change was compared with the change in the appearance of the image seen when the 3D model was rotated. Normally when a viewpoint is on the right side of an image, the right side of the image appears expands according to the principle of perspective, and in turn, the left side seems shrunk (on the contrary, when the viewpoint is on the left side, the left side appears magnified). I conducted this comparative simulation to distinguish the change of appearance of an image by perspective from the interference by topography accurately. The condition for this 2D simulation is the same as done by the rotation of the 3D model.

4.3 Description and analysis

Deer (N1)

General description

An outline red deer, facing left (Figure 4.6). This image is located on a left edge of the panel and a height of 4m from the bottom of the panel (Barquin et al. 1998). This position is higher than any other images. All body parts are outlined in red; the head and neck are fully painted. There are several coloured spots on the forequarters of the dorsal line (Ibid.). The contours of the belly, thigh and hind legs are executed in a thick line. This figure has not yet been observed in detail because of its hardly-accessible position. It is still partially covered by deposits of dirt (Barquin 2001). N1 is approximately 75 cm long.

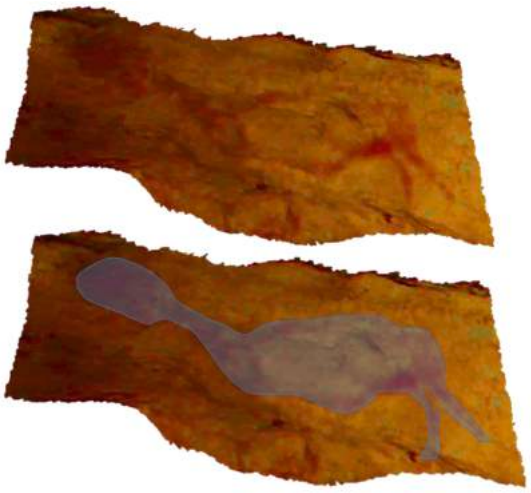

Figure 4.6: N1, outline red deer facing left. The head and neck are painted. This image is located on the highest position (approx. 4m) among 11 images.

Integration of natural lines

Due to N1's position, a 3D model of high resolution could not be generated. Therefore, for the analysis here I used a detailed illustration which is available in a book chapter published in 2001 by Barquin (Figure 4.7). According to this detailed sketch, the surface of this wall is severely fractured; this condition generates the countless number of grooves and edges. Two outlines conspicuously overlap on a natural groove. From the back of the V-shaped ears to the central dorsal, the contour is drawn almost the same shape along a groove. The chest is also depicted along another groove line. Apart from these examples, the outline is independent of any natural lines.

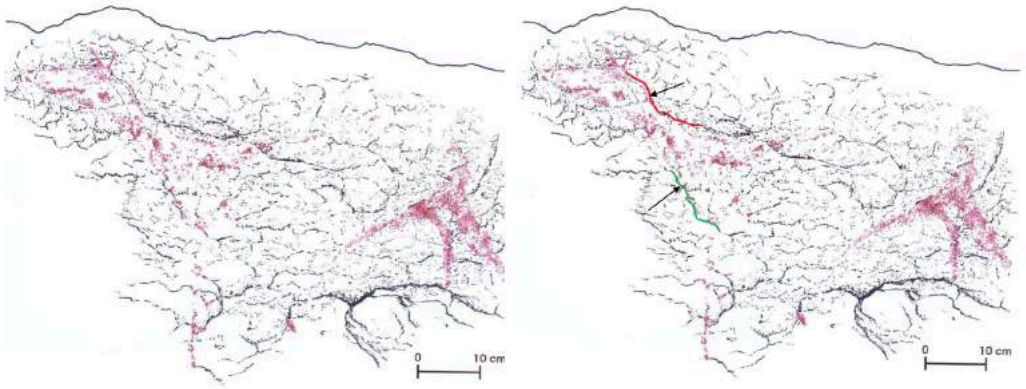

Figure 4.7: A detailed illustration of N1 (Barquin 2001). The location of the natural lines is clearly illustrated. The cervical dorsal and the under-neck are integrated with grooves.

Topographic condition

In this analysis, the frontal leg is excluded because it is almost invisible. Overall, the topographic condition of N1 is gentle, compared to other regions of the panel. Even so, the topography forms convex on the upper side of the head and area between the shoulder and mid-torso. These topographic features, although not conspicuous, are responsible for the moderately rough surface of the deer. The total depth is approximately 84mm (the model is at 1/50 scale: Figure 4.8). The highest point corresponds to the top of the head, while the lowest to the tip of the hind limb. The range within which all body parts are defined their elevation level is between 0.1mm and 70mm (high: 0.1-23.3mm, medium: 23.4-46.7mm, and low: 46.8-70mm). None of the body is assessed in the rest of the depth (70.1-84mm), and there is not the extra low level in N1, therefore.

Figure 4.8: N1 (1/50 scale) seen from the vertical position. The highest elevation is found on the head, while the lowest is on the tip of the hind limb.

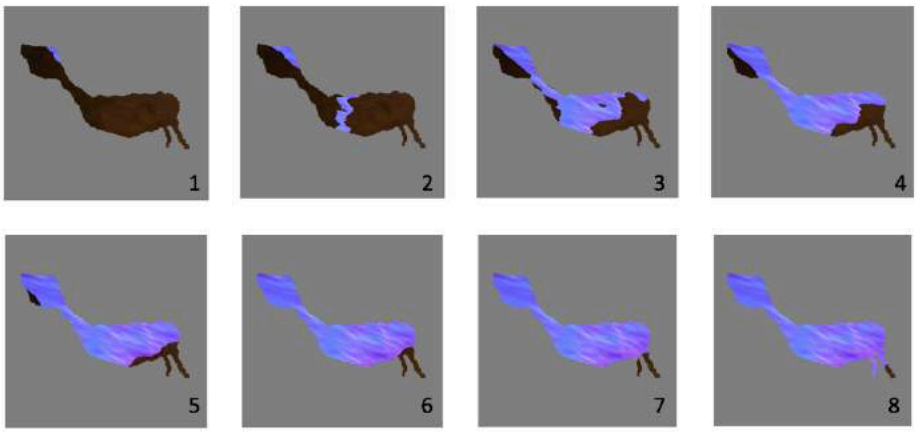

Figure 4.9: These eight images illustrate the depth of N1. When the cross-section layer passes the surface of N1, the colour of the surface changes; dark regions denote lower elevation than coloured parts. Images 1-3 are for 0.1mm - 23.3mm, 4-6 for 23.4mm - 46.7mm, and 7-8 for 46.8mm - 70mm.

The surface is first detected at the top of the head, and the area slightly extends within the range between 0.1 and 9.3mm (see Figure 4.9, 1). After the cross-section layer exceeds 9.4mm, the detection also begins at the shoulder, continuing based on these already-detected areas. Consequently, the head, dorsal-central neck-shoulder, dorsal-central mid-torso are assessed as the high elevation by 23.4mm (2-3). As the layer proceeds, detection further extends and covers the rest of the all body except the hind limbs: the ventral neck-shoulder, ventral mid-torso, and entire thigh are fully detected and assessed as medium (23.4-46.7mm: 4-6). The hind limbs are therefore located in the low elevation level. During the range of this elevation level, the undetected area narrows downward, lowering the elevation toward the tip of both legs. The major part of the limbs passes the layer by 70mm (7-8). At this time, the tip (right) remains undetected. However, this area also entirely passes the layer at 84mm.

Distortion on images (Horizontal movement, x30°, y-60° to y80°)

Apparently, noticeable distortions do not occur when the viewing point shifts to the left, and the appearance remain almost similar to N1 in the 2D simulation. However, the distortion is confirmed as the viewing position is taken on the right. Because the convex shoulder gradually overlaps the neck, the neck goes unseen. In consequence, the length of the neck is saliently shortened (at y80°: Figure 4.10). This deformation is absent on N1 on a 2D wall. This distortion most likely occurs when the viewing angle is between y40° and y80°.

Figure 4.10: N1 on the 3D surface (left) and 2D surface (right) seen from y80°. The length of the neck on the 3D wall is significantly shortened because the convex surface on the shoulder overlaps and hides the neck. Meanwhile, the neck on the 2D wall is visible.

Deer (N2)

General description

On the left bottom of the frieze, a hind is depicted (Figure 4.11). This deer, facing left, is an almost complete figure (only its tail is absent). It is executed with dot painting and colour-wash (Barquin et al. 1998). The face is somewhat obscured and contains no specific detail (the mouth and eyes) except V-shape ears. Although the contour is unclear due to decay in some sections, the cervical, dorsal and ventral lines are still visible. The length is approximately 85 cm.

Figure 4.11 N2, outline red deer facing left (digital filter is applied). The image is in excellent condition so viewers can easily see it.

Integration of natural lines

Among all images in El Pendo cave, N2 contains examples of the most dynamic integration. This deer is depicted on a rock which is separated from another rock above it by a large crack. This crack runs horizontally and generates a deep groove which then transforms to an edge along the contour of the wall. This groove is used for the anterior dorsal line, and the edge is integrated into the posterior dorsal. The edge line turns downward at the right end of the rock, and the buttock corresponds to this vertical edge. Figure 4.12 shows the original shape of the wall. According to this visualisation, the original topography already appears a figure resembling the basic body structure of a quadruped mammal. The natural configuration appears an "h" shape, and the body is outlined along the "h" line. These integrated sections are vital to forming the essential shape of this deer since they constitute almost half of the entire body and determines its

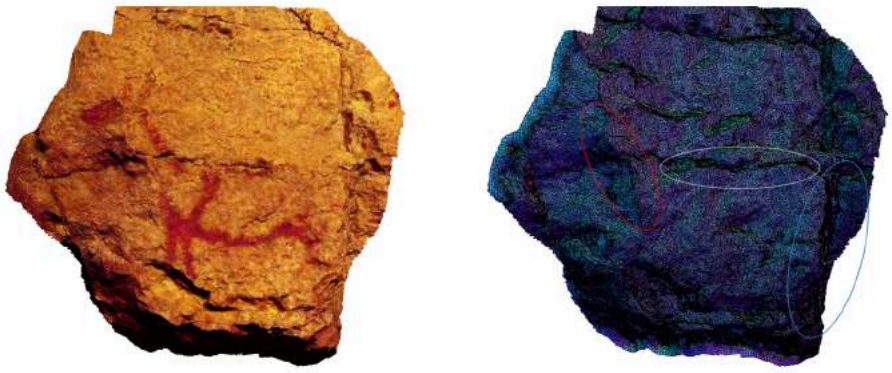

Figure 4.12: Examples of integration. N2 (left) and its highlighted topography (right). The dorsal line is integrated with the groove and edge which separate the panel from another rock plate (indicated by the white circle). The buttock is also placed along the right edge of the wall (indicated by the blue the circle). The "h" pattern on the panel already appears the basic form of a quadruped mammal. Meanwhile, the front neck is outlined along the ridge that extends from the bottom of the chest to the upper left obliquely (indicated by the red circle).

overall appearance; therefore, the artist of N2 relies more on the natural lines than artificial ones.

Apart from the examples above, N2 contains another integrated outline; there is a ridge extending from the bottom of the chest to the upper left obliquely, and the front neck is fixed along with this ridge (see Figure 4.12). In this way, even though the artist outlined some sections (the head, ventral, limbs, and back neck) by himself\herself, N2's basic form is already defined by natural lines.

Topographic condition

N2 is attached to a rectangular rock that remarkably protrudes strikingly from the surrounding walls. The left side of the rock (the left side of N2) is sharply inclined. The right side is not inclined, but it forms a ridge where the buttock is is assigned. Additionally, the torso also undulates noticeably. The total depth is approximately 102mm (the model is at 1/40 scale: Figure 4.13). The highest point is found on the front neck, while the lowest corresponds to the ventral mid-torso. The range within which most body parts are defined their elevation level is between 21.6mm and 85.9mm (high: 21.6-42.9mm, medium: 43-64.4mm, and low: 64.5-85.9mm). None of the significant parts of the body is fixed on the rest of the depth (0.1-21.5mm and 86-102mm), and there are no extra elevation levels, therefore.

Figure 4.13: N2 (1/40 scale) seen from the vertical plane. The highest elevation is found on the under-neck, while the lowest is on the ventral mid-torso.

The surface is first detected at the area immediately below the jaw. This convex wall spreads upward and downward. However, no sections belong to this extra range

(0.1- 21.5mm: see Figure 4.14, 1-2). Between 21.6mm and 42.9mm (3-4), the detected surface further extends, and firstly, the head (at 37.6mm) and then the ventral neck (at 42.9mm) are defined their elevation as high. During the next phase, as the highlighted region further extends, the detection also begins from the posterior side; since the surface slightly undulates on the posterior, the detected area scatters on the thigh and hind limb. However, by a depth of 64.4mm, the dorsal-central neck-shoulder, frontal limb, entire thigh, and hindlimb pass the layer (the medium level: 5-6). The rest of the body is located at the low-level elevation. Although the entire mid-torso remains undetected, the detection continues from the dorsal to the ventral area as the cross-section layer proceeds. The mid-torso is assessed as the low elevation by 85.9mm (7-8). The surface becomes deepest at a part of the ventral mid-torso, but this area is also fully detected at 102mm.

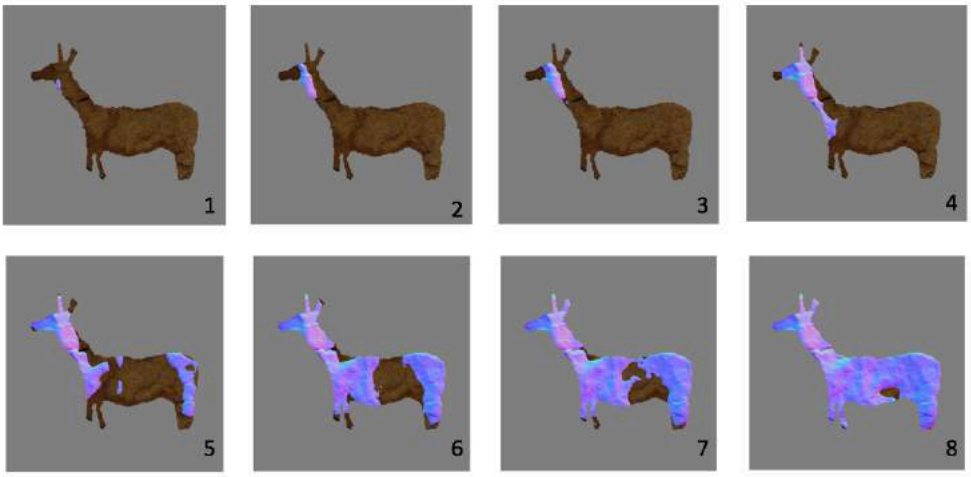

Figure 4.14: These eight images illustrate the depth of N2. When the cross-section layer passes the surface of N2, the colour of the surface changes; dark regions denote lower elevation than coloured parts. Images1 and 2 are for 0.1mm - 21.5mm, 3 and 4 for 21.6mm - 42.9mm, 5 and 6 for 43mm - 64.4mm, and 7 and 8 for 64.5mm - 85.9mm.

Distortion on images (Horizontal movement x30°, y-60° to y70°)

The remarkable transformations are confirmed in the neck and head. The factors responsible for both cases are same: the sharp elevation gap on the left edge of the panel. A semi-vertical ridge along which the front neck is outlined generates two sides, and the elevation is largely lower on the right to this ridge. As the viewing point moves to the left, that ridge gradually overlaps on the cervical dorsal line because the cervical area is lower elevation than the front neck. Consequently, the neck loses its width completely at y-60°, and the head appears as if detached from the body (Figure 4.15). This distortion is perceived within the range between y-50° and y-20°, and such a difference is absent in the 2D simulation.

Figure 4.15: N2 on the 3D surface (left) and 2D surface (right) seen from y-60°. The sharply elevated wall along the front neck overlaps on the entire cervical dorsal, and the head appears detached from the body. The image on the 2D wall is not distorted in this way, but the anterior body is merely stretched.

Meanwhile, the topography also distorts the head when N2 is viewed from the right. Despite the fact that the muzzle appears at y0°, it gradually disappears as the viewing angle increases and completely vanishes at y60° (Figure 4.16). This is because the ridge on the face hides the muzzle. As a result, viewers perceive the head section as a relief. This distortion most likely appears between y30° and y60°, and the image appears as if shaking its head side to side within this range.

Figure 4.16: N2 on the 3D surface (left) and 2D surface (right) seen from y60°. The muzzle goes unseen, and the rock along which the buttock is placed emphasises the 3D volume of the body. On the other hand, N2 on the 2D surface is stretched merely to the right.

When the viewpoint moves to the right, the width of the rock itself also becomes visible. This thick rock corresponds to the thigh and adds a sculptural volume to the image. Additionally, the wavy shape of the dorsal line is further highlighted, increasing the 3D texture. All of these changes in appearance are never detected in the 2D simulation because the flat surface lacks rich topographic features.

Caprid (N4)

General description

An outline caprid facing left (Figure 4.17). Even though all body parts are provided except for the tail, the contour is obscure; above all, the ventral line is hardly visible. Compared to the unclear ventral side, the dorsal and buttock part is more apparent. The caprid has a horn which extends semi-vertically backwards. IT is executed in overlapping dots (Barquin et al. 1998). This graphic is found on the lowest position in the frieze, approximately 20 cm right to N2. Because N4 was closest to viewers standing on the original floor during the Palaeolithic time, the image must have appeared the most clearly among all of the paintings in the panel. The length of N4 is approximately 60 cm.

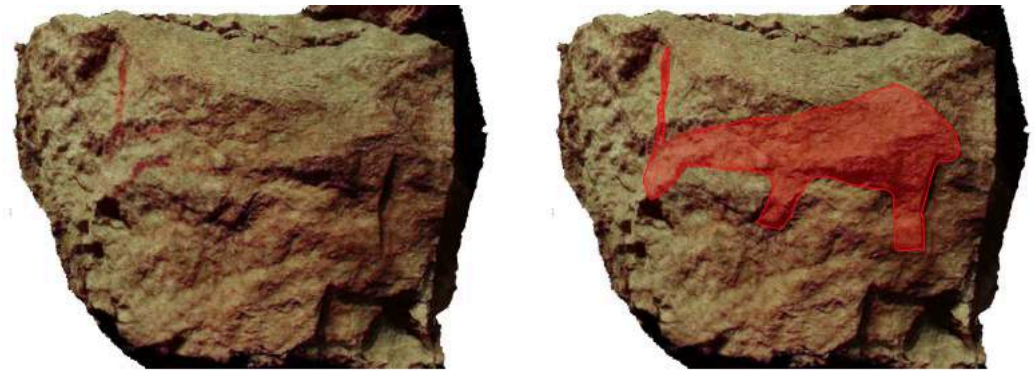

Figure 4.17: N4, outline caprid, facing left. This image is located on the lowest position of all pictorial samples in El Pendo cave. Although the contour is not salient, all body part is fully outlined by natural lines.

Integration of natural lines

N4 also borrows the natural topography for the outlining of most of its body. The form of integration is also similar to the previous image; a horizontal edge of rock is taken as the contour of its posterior dorsal and the buttock (Figure 4.18). This rock edge is also used for the outline of the back leg. Overall, the original shape of the wall itself already represents the appearance of N4.

Integration is also found in other sections: the forelimb is visualised between two short grooves running semi-vertically; the muzzle borrows an edge. Further to these examples, the belly and cervical dorsal line is drawn along a unique type of natural lines: these lines form between convex surfaces as a valley. In this way, most of the body of N4 is outlined by pre-existing lines.

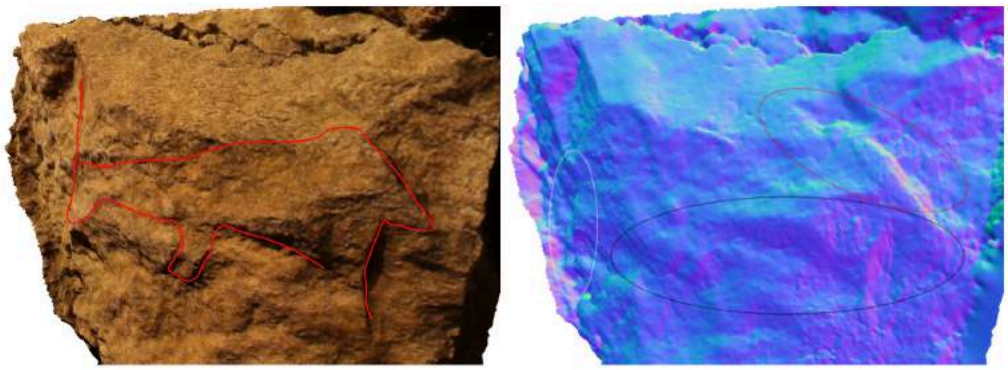

Figure 4.18: Examples of integration. N4 (left) and its highlighted topography (right). Edges are integrated into the posterior dorsal, the buttock (see the red circle) and the back leg (see the right side of the black circle). The use of various types of natural line is also seen in other body parts: muzzle (edge:see the white circle), frontal limbs (groove), belly (valley: see the centre of the black circle), and cervical dorsal (valley). Overall, the original shape of the wall already appears the shape of N4.

Topographic condition

Although this topography forms a relatively gentle arch, its surface is smooth and uniform relative to its highly irregular surroundings. The total depth is approximately 76mm (the model is at 1/20 scale: Figure 4.19). The highest point corresponds to the ventral mid-torso, while the lowest to the tip of the hind limb. The range within which most of the body parts are defined their elevation level is between 0.1mm and 38mm (high: 0.1-12.7mm, medium: 12.8-25.3mm, and low: 25.4-38mm). As the rest of the total range (38.1-76mm) includes a significant extent of the hind leg, there is the extra-low level in N4.

Figure 4.19: N4 (1/20 scale) seen from the vertical position. The highest elevation is found on the ventral mid-torso, while the lowest is on the tip of the hind limb.

The surface is first detected at the ventral/mid-torso as the topography is convex in this region. Subsequently, the dorsal-ventral neck also partly passes the cross-section layer. By 12.7mm, the areas highlighted on Figure 4.20 (1, 2) extend, and the ventral mid-torso is assessed as the high elevation; detection on the dorsal-ventral neck is limited. During the next phase, the major part of the torso is detected by the layer and assessed as the medium elevation; the neck area is fully detected at first, and then the detection continues from the shoulder to the central thigh. Accordingly, the whole neck-shoulder, central mid-torso, central thigh, and frontal leg are defined (12.8-25.3mm: 3-4) in this medium level. Between 25.4mm and 38mm, detection further continues rightward and leftward. As a result, most of the head and dorsal-ventral thigh are assessed as the low level (5-6). The hind limb remains undetected, and the elevation is particularly low: the layer fully detects the surface of the leg at a depth of 76mm (7-8).

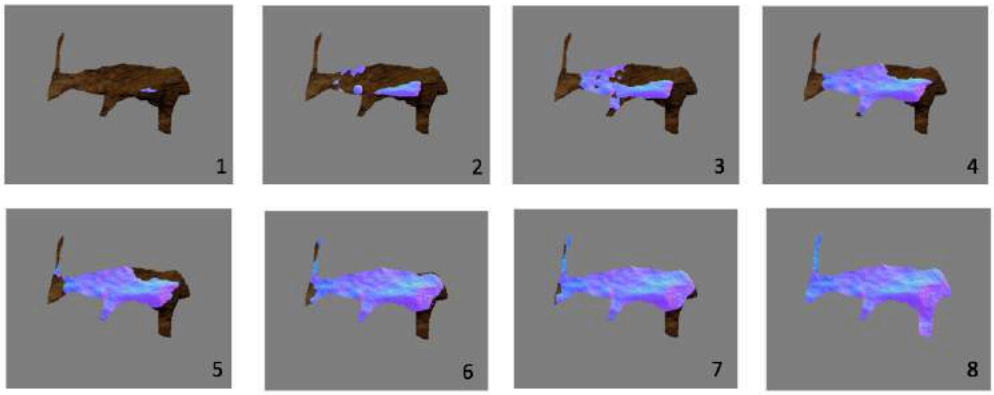

Figure 4.20: These eight images illustrate the depth of N4. When the cross-section layer passes the surface of N4, the colour of the surface changes; dark regions denote lower elevation than coloured parts. Images1 and 2 are for 0.1mm - 12.7mm, 3 and 4 for 12.8mm - 25.3mm, 5 and 6 for 25.4mm and 38mm, and 7 and 8 for 38.1mm - 76mm.

Distortion on images (Horizontal movement, x30°, y-60° to y60°)

N4 seems to move its neck up and down when the viewpoint shifts side to side, although this distortion is also confirmed in the 2D simulation. However, topographic features magnify the extent of this visual illusion: the face is located on an inclined surface which appears clearly from the left but mostly invisible from the right (Figure 4.21). In consequence, the head and neck seem to be pulled to the left edge of the wall as the viewing angle decreases. At the same time, the convex topography on the belly and the thigh sustains N4's overall proportion even though the image is viewed from the left. It means that the body is static, unlike the shrunk head. This contrast between the motionless body and the deformed head and neck further highlights the deformation.

Figure 4.21: N4 on the 3D surface (left) and 2D surface (right) seen from y60°. The face is located on an inclined surface which can be seen clearly from the left but mostly invisible from the right.

There are two other distortions: one occurs on the horn, and the other is on the front leg. There is a convexity immediately right to the horn, and this elevated surface hides the horn when a viewing position is taken to the right (y50° and y60°). Potentially, viewers can manipulate the appearance and disappearance of the horn by moving between y30° and y60°. Another convex surface causes the deformation in the front limb: the leg appears bending inward and outward. This animation occurs while viewers move between (y-60° and y60°).

Deer (N5)

General description

An outline red deer facing right (Figure 4.22). This image is a complete, with the tail and V-shape ears. N5 is well-preserved, so the contour of the entire body is visible without an ambiguity. The figure is located on a rock boss, approximately 40 cm above N4. It is executed by the simple dot technique (Barquin et al. 1998). The rock where N5 is placed slightly protrudes from its surrounding wall, and the image reasonably fits the dimension of the rock; only the rear limb and ears are off from the brink of the rock. This is the smallest figure among all complete animal figures, with the body length of 48cm.

Figure 4.22: N5, outline red deer facing right. The condition is remarkably good, although N5 is the smallest of all images in El Pendo.

Integration of natural lines

As for integration, N5 is a unique sample. There are some distinctive natural lines (grooves and edge) on the area, and they already constitute a basic part of N5. However, this hind is fixed in an offset position as if the artist intentionally avoided direct duplication of the wall's original shape (Figure 4.23). For example, above the dorsal line, there is a groove running horizontally; the dorsal line, the tail, and a part of the buttock are outlined in parallel to this groove as if it imitates the natural line. A similar case is also found for the ventral line. Above the ventral section, there is a horizontal edge. Nevertheless, the ventral line does not overlap on this line but is drawn in parallel to it. Furthermore, this edge, although running horizontally until around the frontal limb, changes its direction upward and then turns to the right. The contour of

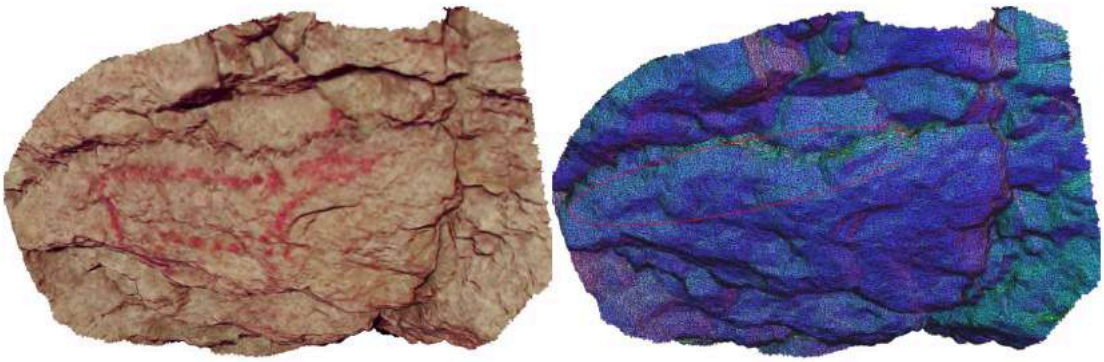

Figure 4.23: N5(left) and its highlighted topography (right). The rock where N5 is located already has a basic shape of N5. However, the image's outline does not perfectly overlap on the pre-existing pattern, as if the artists intentionally avoided to do so. Instead, the dorsal line, buttock, and tail are integrated with a ridge (indicated by the red circle).

the chest and the front neck is executed, again, in parallel to this line, not directly superimposed. In this way, N5 contains unique samples of offset-integration.

Further to this offset integration, N5 also contains even direct integrations. The surface elevates below the groove which parallels to the dorsal line, and a ridge forms along the rise. The ridge runs horizontally, and dorsal line, buttock, and the tail overlap on this line. (see Figure 4.23). In this way, the artist of N5 utilised and incorporated natural lines.

Topographic condition

The wall where N5 is located elevates, adding a 3D volume to the image. This convex surface also defines the overall appearance of N5 as the shape of the surface across the tail, thigh, mid-torso, neck-shoulder, and front leg is already reminiscent of a quadruped animal. Notably, the elevation in the shoulder and forelimb is high as if a rise of the muscles. The total depth is approximately 52mm (the model is at 1/30 scale: Figure 4.24). The highest point corresponds to the ventral neck, while the lowest to the tip of the ear. The range within which all body parts are defined their elevation level is limited between 2.7mm and 20.8mm (high: 2.7-7.8mm, medium: 7.9-13mm, and low: 13.1-20.8mm). None of the body sections belongs to the ranges between 0.1 and 2.6mm and between 20.9 and 52mm. Therefore, there are no extra-elevation levels.

Figure 4.24: N5 (1/30 scale) seen from the vertical position. The highest elevation is found on the ventral neck, while the lowest is on the tip of the ear.

The surface is firstly detected at the front neck between 0.1mm and 2.6mm, although its extent is considerably limited (see Figure 4.25, 1). However, as detection continues, the coloured area extends to the central neck and frontal leg between 2.7mm and 7.8mm. The central-ventral neck-shoulder belongs to the high level; the detected area in the frontal leg does not cover its significant extent (2-3). At the same time, the topography on the ventral thigh also begins detected. During the next phase (7.9-13mm), the detection further continues around the neck and thigh; while in the anterior body almost all sections except the head are assessed (the dorsal neck-shoulder and frontal limb), the detected area in the posterior is not consistent. Nevertheless, more than half of the ventral-central thigh and central mid-torso passes the cross-section layer by 13mm, and they are defined as the middle level (4-5). The head, dorsal-ventral mid-torso, dorsal thigh, tail, and hind leg are fixed in the low elevation. These undetected areas are also fully detected by 20.8mm (6-7).

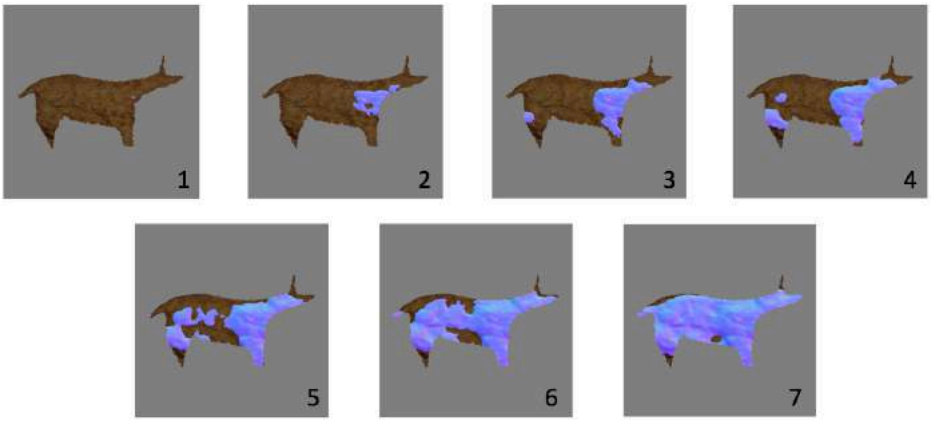

Figure 4.25: These seven images illustrate the depth of N5. When the cross-section layer passes the surface of N5, the colour of the surface changes; dark regions denote lower elevation than coloured parts. Image1 is for 0.1mm - 2.6mm, 2 and 3 are for 2.7mm - 7.8mm, 4 and 5 for 7.9mm - 13mm, and 6-7 for 13.1mm - 20.8mm.

Distortion on images (Horizontal, x30°, y-60° to – y60°)

The most noticeable deformation occurs in the neck. The neck shrinks and extends as a fundamental distortion in both 2D and 3D simulation due to the perspective. However, this movement is emphasised once the topography intervenes. The cause is a combination of multiple topographic factors: the convex in the shoulder and lower-neck, and the concave in the ventral side. The shoulder slightly hides the mid-torso and thigh when seen from the right, significantly deforming the ventral side. As a result, the body is perceived to be shorter than its original state (Figure 4.26 left). At the same time, the convex under the neck pushes the neck upward and narrows its width. Consequently, the neck appears longer and stretched. This distortion is

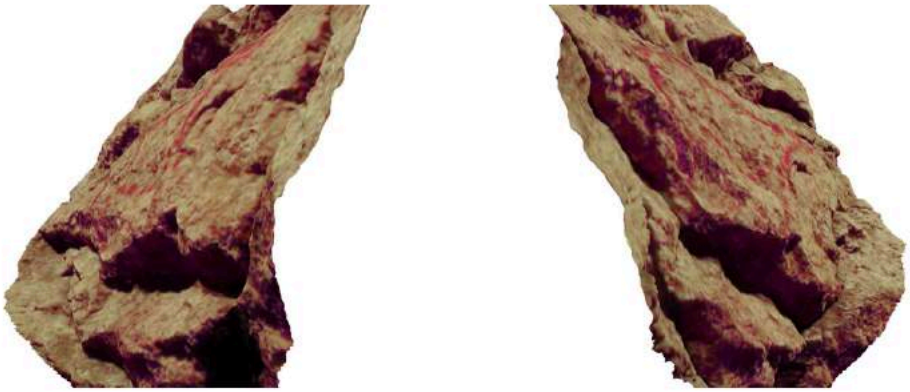

Figure 4.26: N5 seen from y60° (left) and y-60°(right). When viewers stand on the right, the shoulder hides the mid-torso and thigh. So the body is perceived to be shorter. At the same time, the neck appears longer and thinner because the convex surface under the neck pushes the neck upward and narrows the width. When N5 is viewed from the left, the head becomes much smaller as the section is placed on a concave surface.

substantially different from the essential elongation of the neck by perspective. This distortion most likely occurs between y20° and y50°.

Meanwhile, once the viewer takes a viewing point to the left, the head appears significantly smaller (Figure 4.26, right). This is due to a concave surface as well as perspective: the head partly goes unseen as it is fixed in the low elevation area. The size of the head, to some extent, can be manipulated by viewers who move around on the left. In this case, the distortion generates a visual illusion as if the face appears shaking side to side. This distortion most noticeably takes place within the range between y-60° and y-30°.

Aside from the neck and head, the hind leg also deforms. As the limb is fully located on a cliff of the rock, it constantly appears to bend whenever viewing point moves: the leg is attached straight to the thigh at y-60°, while it gradually turns inward as the viewpoint shifts toward the right. Thus, the hind leg never holds a fixed form. Overall, together with the other distortions, N5 is subjected to a significant change in its appearance by viewing from different viewing angles.

Deer (N7)

General description

An image of red deer facing right (Figure 4.27). This is the largest image in El Pend cave, with a length of 125 cm. It predominantly occupies the centre of the frieze. This large deer is a complete image. According to Barquin et al. (1998), three artistic skills are used in its

Figure 4.27: N7, complete image of red deer facing right (Hue/Saturation filter is applied). N7 is located in the centre of the frieze, with the largest size of all 11 images (125cm).

production: simple line, overlapping dots, and colour-wash. The body is depicted in a thick outline, especially its rump, limbs and ventral line. The anterior sections (the shoulder, neck and head) are fully painted in red. Barquin (2001 and 2003) claims that one of the hind legs of N7 overlaps another image (N6) which is unexamined in this case study.

Integration of natural lines

This panel consists of a large number of fractures which generates countless edges and grooves. Most of them are short and horizontal, but occasionally, lines cross N7 vertically or diagonally in some sections (the dorsal shoulder and thigh). Overall, N7 contains integration in the ventral-dorsal line and the buttock. Regarding the ventral line, the thigh is placed on a rock whose shape is already similar to the thigh; the outline is drawn along the contour of this rock from the right hindlimb to the point where the belly begins (Figure 4.28). From the belly to the left foreleg, there is a horizontal edge, and the thick ventral line is provided along the edge. About the buttock, the part is outlined along the outer edge of the thigh-like rock: especially, in the upper part of the buttock there is a deep groove running obliquely, and the contour is executed along the left side of the groove. This rock forms a zigzag edge at the bottom, and the lower buttock is drawn along the meandering edge. As for the dorsal line, there is a large dent in the dorsal part, which causes a significant elevation gap. The dorsal line is outlined along the edge line of the low elevation area.

The natural lines also play another critical role in this image. Although the anterior part (neck, shoulder, and head) is painted in red, the boundary between the painted and the unpainted section is partially defined by natural lines. For example, the red spreading from the dorsal to inside is given along edge lines. Similarly, the red coloured area from the ventral side to the top is also provided along with other edges.

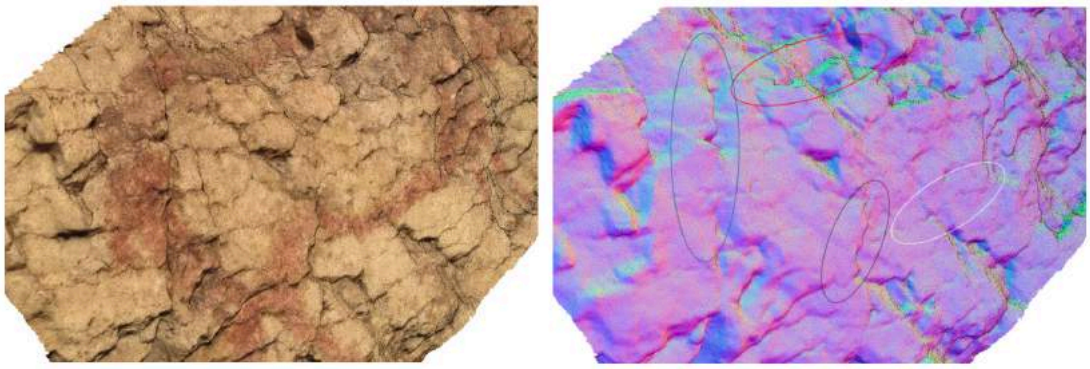

Figure 4.28: N7 (left) and its highlighted topography (right). N7 is located on the panel with innumerable fractures. These fractures generate grooves and edges. The contour of the image is integrated with those natural lines at the ventral (see the white and black circle), the buttock (see the blue circle), and the dorsal (see the red circle). Natural line is also utilised as the border between the fill-in and non-fill-in part inside the body.

These examples suggest that natural patterns are not only integrated for outlining but also for decorating the body.

Topographic condition

Although N7 appears mainly flat, the wall gently undulates. For instance, the elevation is slightly higher at the head and thigh than the rest of the body sections. The total depth is 109mm (the model is at 1/100 scale: Figure 4.29); the highest point corresponds to the ears, while the lowest to the dorsal mid-torso. The range within which all body parts are defined their elevation level is between 25.7mm and 102.6mm (high: 25.7-51.3mm, medium: 51.4-76.9mm, and low: 77-102.6mm). None of the significant extents of body sections is fixed in the other ranges (0.1-25.6mm and 102.7-109mm). Therefore, there are no extra levels in N7.

Figure 4.29: N7 (1/100 scale) seen from the vertical position. The highest elevation is found on the tip of the ears, while the lowest is on the dorsal mid-torso.

The surface is firstly detected at the tip of the right ear. Detection continues from this area, involving the other ear and muzzle as the cross-section layer proceeds from 0.1mm to 25.6mm. However, the extent is considerably limited (see Figure 4.30, 1-2). Simultaneously, detection, although marginally, also begins from the dorsal thigh. The detected area further extends between 25.7mm and 51.3mm, based on the head and thigh. As a result, the head and dorsal-central thigh are assessed as the high level by a depth of 51.3mm (3-4). At the same time, the torso parts regionally pass the layer, but these detected areas scatter due to the fractioned topography. In the medium level (51.4mm-76.9mm), the detected section expands dramatically, assessing the almost

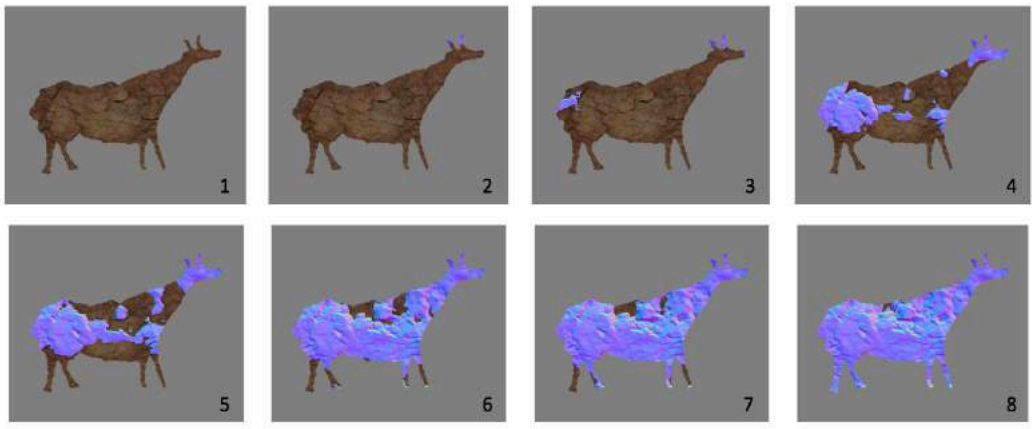

Figure 4.30*:* These eight images illustrate the depth of N7. When the cross-section layer passes the surface of N7, the colour of the surface changes; dark regions denote lower elevation than coloured parts. Images 1 and 2 are for 0.1mm -25.6mm, 3 and 4 for 25.7mm - 51.3mm, 5 and 6 for 51.4mm - 76.9mm, and 7 and 8 for 77mm - 102.6mm.

entire body parts; except the limbs and dorsal mid-torso, all sections are located within this elevation level, and therefore, the image appears mostly flat (5-6). During the last phase (77mm-102.6mm), the undetected body parts (limbs and mid-torso) are defined as the low-level elevation. They finally pass the layer (7-8). The elevation on the dorsal mid-torso is particularly low, and it needs further 7.4mm to be completely detected.

Distortion on images (Horizontal movement, x30°, y-70° – y70°)

This image is distorted by topography in a similar way to N5. The neck is particularly deformed by an elevated surface on the right to the shoulder; the convex topography pushes the outline of the chest inward and shortens the body to a great extent as the viewing angle increases (Figure 4.31). At this time, the neck appears elongated. Furthermore, the convex on the neck and head pushes these parts front, highlighting their presence. This distortion does not happen in the 2D simulation. This distortion occurs when the viewing angle is between y0° and y70°.

Figure 4.31: N7 on the 3D surface (left) and 2D surface (right) seen from y70°. The neck is particularly deformed by the raised surface which is located on the right to the shoulder. This topographic feature pushes the outline of the chest inward and forces the neck to stretch. On the other hand, such a distortion is absent in the image on the 2D surface where the body sustains its original appearance.

Meanwhile, when N7 is viewed from the left, significant distortion does not occur except the frontal limbs. There is an interval between the forelegs, but this space gradually narrows and finally disappears as the viewing angle decreases; only one leg appears to the viewers in the end. The cause of this unique distortion is that the right foreleg is located on the wall of the lower elevation than the other leg. As a viewing point moves to the left, the left leg overlaps the right one. This is most apparently perceived between y-70° and y-50°.

Horse (N8)

General description

An incomplete image of a horse facing left (Figure 4.32). Provided anterior sections is remarkable quality as N7. The horse also has a detailed mane, wherein six lines represent the hair (Barquin et al. 1998). The face and neck are fully coloured. Its cervical-dorsal line is depicted in a firm line, whereas ventral line appears somewhat obscured. The tip of the legs is visible, whereas the forearms are hard to confirm. N8 is located immediately right to N7. As the image faces to N7, it appears an intentional composition with a specific association between these images (Ibid). Although the posterior is not provided, the size of the horse is rather large (64 cm).

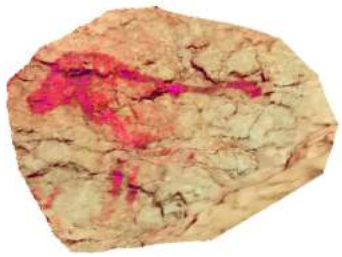

Figure 4.32: N8, incomplete image of a horse facing left (Hue/Saturation filter is applied). N8 is located on the centre of the Frieze, immediately right to N7. It is assumed that this image, together with N7, constitutes a unified theme.

Integration of natural lines

This wall contains countless natural lines which are utilised for N8's contour. For instance, an edge crossing horizontally on the face turns into a groove from the right end of the mane, and the dorsal line overlaps the groove (Figure 4.33). This groove vanishes at a certain point, but the dorsal line still extends to the further right along a convex surface below the outline.

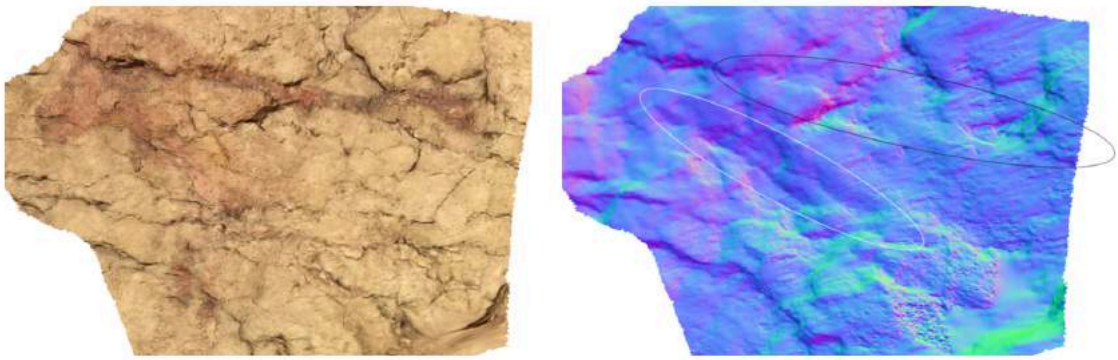

Figure 4.33: Examples of the integration. N8 (left) and its highlited topography (right). The dorsal line is integrated with a deep groove on its cervical area and then continues along an edge of a convex surface (see the black circle). The front neck and lower jaw are also outlined, following the curve of a valley line (see the white circle).

Additionally, the contour of the front neck is also superimposed on a crack line between rocks. This line extends semi-vertically to the upper left from the shoulder as it slightly curves on its way. The curved outline of the neck and lower jaw corresponds to this curvy line.

Topographic condition

Because the posterior body is absent, the entire thigh, tail and hind limb are not examined. The surface under N8 considerably undulates as deep concave and high convex surfaces appear alternately; it could be no flat areas are found in the examined region. Especially a dent on the dorsal mid-torso and ventral shoulder features such a dynamic wavy topography. The total depth is 84mm (the model is at 1/100 scale: Figure 4.34); the highest point corresponds to the frontal leg, while the lowest to the dorsal mid-torso. The range within which most of the body parts are defined their elevation level is between 24.1mm and 72mm (high: 24.1-40mm, medium: 40.1-56mm, and low: 56.1-72mm). Ranges between 0.1mm and 24mm and between 72.1mm and 84 are respectively higher and lower than the above range. There is a body part which is defined its elevation level between 0.1mm and 24mm, and therefore, N8 contains the extra high level.

Figure 4.34: N8 (1/100 scale) seen from the vertical position. The highest elevation is found on the frontal leg, while the lowest is on the dorsal mid-torso.

The surface is firstly detected at two spots of the frontal limb. The elevation of these surfaces is particularly high, and detection immediately spread to the other leg and then extends upward. As a result, the front limbs are mostly discerned by the depth of 24mm (see Figure 4.35, 1-3). Thus, the section is assessed as the extra high level. At 24mm, detection also begins at the head and ventral mid-torso, and these regions further extend during the next phase. The topography in the head continually passes the cross-section layer between 24.1mm and 40mm, covering the dorsal-central neck-shoulder. Consequently, the elevation of the anterior parts is high (4-6). Despite a noticeable

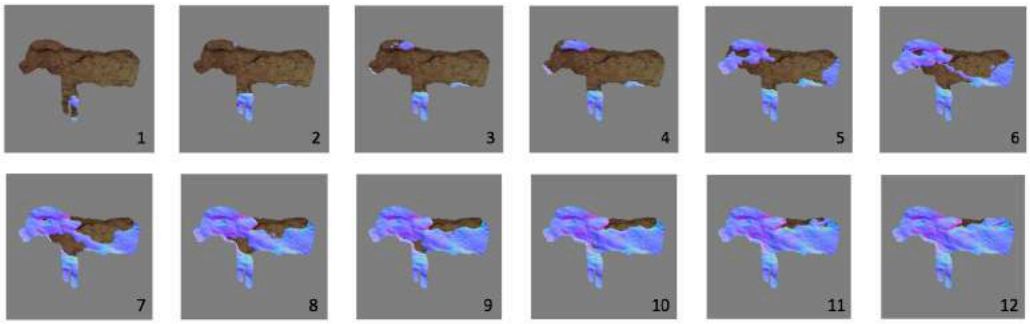

Figure 4.35: These 12 images illustrate the depth of N8. When the cross-section layer passes the surface of N8, the colour of the surface changes; dark regions denote lower elevation than coloured parts. Images 1-3 are for 0.1mm - 24mm, 4-6 for 24.1mm - 40mm, 7-9 for 40.1mm - 56mm, and 10-12 for 56.1mm - 72mm.

detection in the mid-torso, the extent is limited. However, these undetected regions also pass the layer within the range between 40.1mm and 56mm), and finally, the ventral-central mid-torso is assessed as medium. Simultaneously, the layer continues detecting the surface on the ventral neck-shoulder; this section is also located on the medium level (7-9). Meanwhile, the dorsal mid-torso is labelled as the low level. From 56.1mm, the area gradually narrows and mostly passes the cross-layer at 72mm (10-12). Although there is still undetected surface on its centre, the dorsal middle is fully detected by 84mm.

Distortion on images (Horizontal movement, X30°, Y-70° – Y70°)

When the viewpoint moves to the left, the neck becomes remarkably longer and thinner and extends semi-vertically (Figure 4.36). The elongated image still sustains its robustness, while in the 2D simulation the neck merely stretches. This distortion can be attributed to multiple factors. Firstly, as the viewing angle decreases, the concave dorsal mid-torso is gradually hidden by the convex neck. As a result, the dorsal line appears shortened. Secondly, the limbs appear sliding to the right as if they grow from the belly, not from the shoulder; at this time, the shoulder turns out to be a part of the neck. For this reason, the neck appears significantly longer. Meanwhile, the volume of the convex surface on the neck becomes more visible as viewing position moves to the left. Therefore, the neck maintains its robustness without any losses of its volume. This distortion most noticeably happens between y-70° and y-40°. Also, the neck appears moving up and down by this distortion. At the same time, the head also seems to shake because it shrinks inwards due to a small convex at its muzzle.

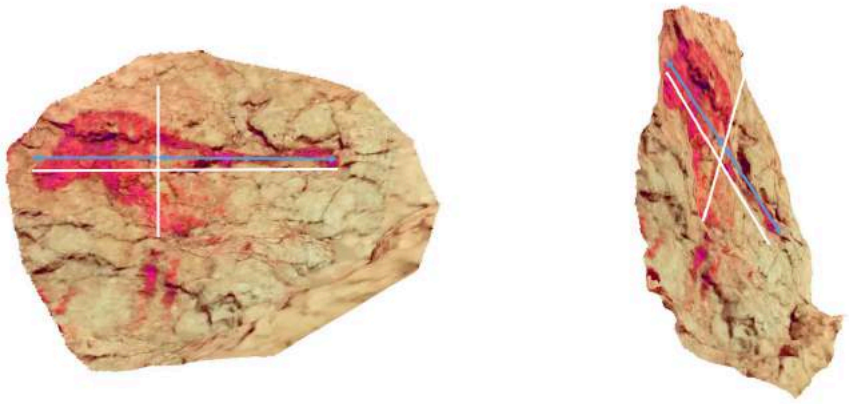

Figure 4.36: N8 seen from y0° (left) and y-70°(right). The body proportion between the anterior and posterior is noticeably disturbed by the topography as the viewing angle decreases.

Unknown quadruped animal (N12)

General description

An outline image of headless quadruped mammal, facing right (Figure 4.37). The ventral body is missing; only the cervical-dorsal line and front neck are outlined. The species for N12 is unidentifiable because the head is absent. The executed technique is overlapping dots (Barquin et al. 1998). The dorsal line is not drawn in a smooth curve. Especially at its middle, the contour turns to be zigzag. N12 is fixed to a high position but slightly lower than N1. This image appears together with another deer (N13). Despite the incomplete body, this is the second largest image in El Pendo (96 cm).

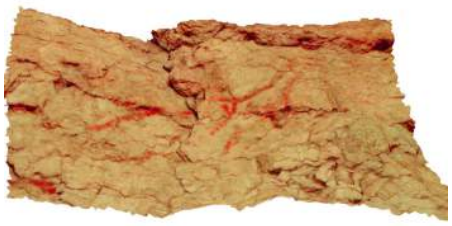

Figure 4.37: N12 (above), outline image of unknown quadruped animal facing right (Hue/Saturation filter is applied). The head and ventral side are missing. It is depicted immediately above N13.

Integration of natural lines

There are several grooves and edges on this wall, but these lines do not overlap with any of N12's sections except the dorsal line. The cervical line is superimposed on a fissure which forms between two convex in the area (Figure 4.38). Apart from this, there is also a possible overlap at the middle dorsal where the outline breaks due to an elevation gap generated between two different rocks. The part in which the contour is absent appears substituted by an edge of the rock on the right. Apart from these integrations, N12 does not borrow an assist from natural lines.

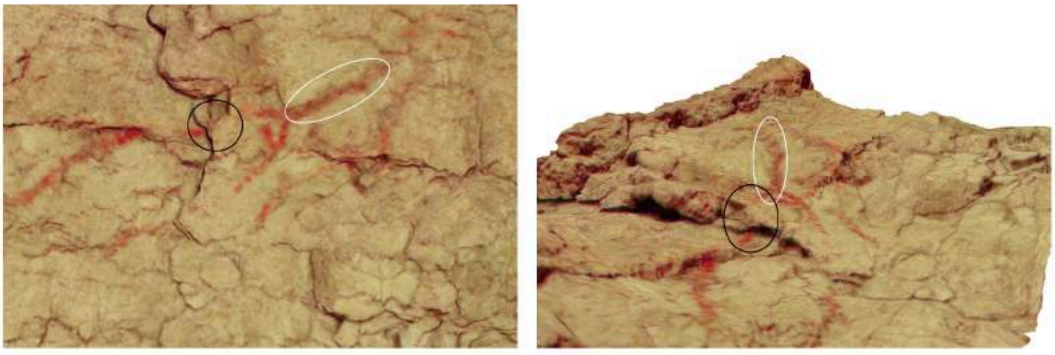

Figure 4.38: Examples of the integration in N12. The white circle shows that the valley between two convex is integrated into the cervical dorsal. On the other hand, the black circle indicates the possible integration; the part in which outline is absent appears to adopt the edge line of a rock, and this edge naturally merges into the dorsal line.

Topographic condition

As N12 is an incomplete image, the whole neck-shoulder, dorsal-central mid-torso and dorsal thigh have been analysed. The entire body fits in a sizeable plate-like concavity, although the wall undulates area to area: the surface protrudes on the neck and shoulder; a crack which is situated vertically on the centre of the long torso causes an elevational gap. The total depth is approximately 126mm (the model is at 1/40 scale: Figure 4.39). The highest point corresponds to the front neck, while the lowest to the dorsal mid-torso. All body parts are distributed within the above range (high: 0.1-43.8mm, medium: 43.9-87.7mm, and low: 87.8-126mm). There are no extra elevation levels in N12.

Figure 4.39: N12 (1/40 scale seen from the vertical direction). The highest elevation is found on the front neck, while the lowest is on the dorsal mid-torso.

The surface is firstly detected at a part of the ventral neck. The coloured area gradually extends as the cross-sectional layer proceeds, and the ventral neck-shoulder is defined its elevation level as high by 43.8mm (see Figure 4.40, 1-3). At this depth, the detection also begins at the edge of the thigh. Between 43.9mm and 87.7mm, detection further continues inward from the posterior and the anterior. The dorsal-central neck-shoulder and dorsal thigh belong to the medium elevation level (4-6). During the last phase (7-10), detection from the anterior stops at the centre of the torso where an elevational gap exists between two rocks (7). After this, detection continues only from the anterior, and the dorsal-central mid-torso is assessed as the low level by 126mm.

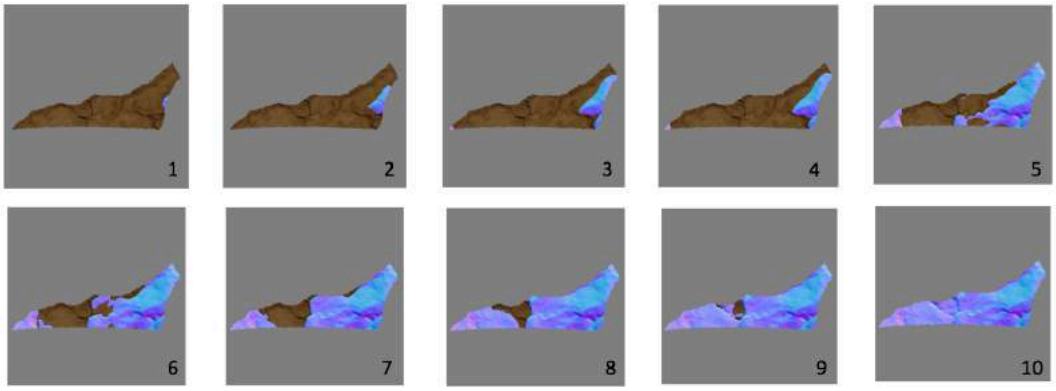

Figure 4.40: These ten images illustrate the depth of N12. When the cross-section layer passes the surface of N12, the colour of the surface changes; dark regions denote lower elevation than coloured parts. Images 1-3 are for 0.1mm - 43.8mm, 4-6 for 43.9mm - 87.7mm, and 7-10 for 87.8mm - 126mm.

Distortion on the image (Horizontal movement, x30°, y-70° to y60°)

Distortion does not appear when N12 is viewed from the left. However, a remarkable deformation occurs when a viewpoint is taken to the right. As the viewing angle increases, the width of the neck gradually goes narrower, and the contour of both front and cervical the neck overlap with each other in the end (Figure 4.41). This is because of the convex surface on the chest area: this swelling pushes the outline of the ventral neck-shoulder inward as was seen in N7. This distortion most noticeably happens between the range of y20° and y60°.

Figure 4.41: An example of distortion in N12. Above three images are N12 seen from y0°(left), y40°(centre) and y60° (right). The convex wall under the neck gradually narrows the neck as viewing angle increase, and finally both outlines of the front neck and cervical dorsal perfectly overlap at y60°.

Deer (N13)

General description

An outline red deer facing right (Figure 4.42). N13 is also an incomplete figure as only its head, neck and cervical-dorsal line are depicted. The image is also situated on a high position slightly below N12. It is executed by overlapping dots (Barquin et al. 1998). However, because these dots are not densely overlapping, N13's presence is somewhat weaker compared to N12. Even so, the V-shape ears are identifiable. This deer is the smallest of all examined images in El Pendo; the length is approximately 43cm (ibid).

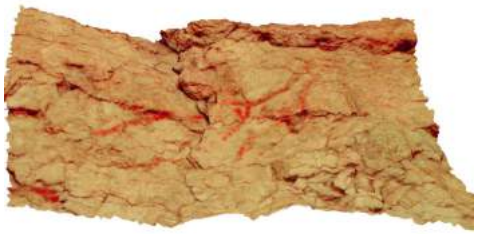

Figure 4.42: N13 (below), outline red deer facing right. The ventral side of the body is absent. It is placed immediately below N12.

Integration of natural lines

Despite its significantly limited sections, the outline of N13 overlaps with natural lines to a great extent. One of the examples is found in the face. The contour of the upper muzzle is drawn along a cliff edge created by a steep convex surface (Figure 4.43). Subsequently, the facial line sharply turns its course backwards, outlining the lower muzzle. The line from the part to the front neck is drawn along an edge of a rock. Another case is found at the right end of the dorsal line. This outline curves gently along an edge line of a rock fraction.

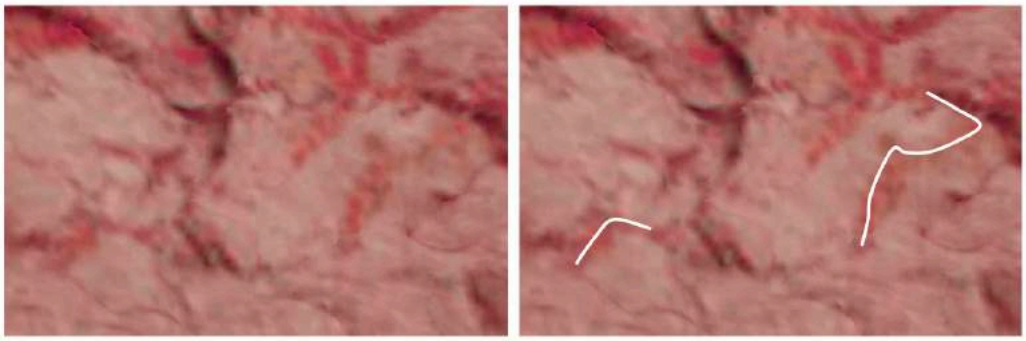

Figure 4.43: Examples of integration in N13. The rocky surface generates a large number of edges, grooves, and ridgelines. N13 maximises those lines in order to outline its body as the integration is found on the multiple locations: the facial area, front neck and posterior dorsal.

Topographic condition

As N13 is an incomplete image, the examined body sections are the head, dorsal neck-shoulder, dorsal mid-torso, and dorsal thigh. The total depth is approximately 39mm (the model is at 1/20 scale: Figure 4.44); the highest point corresponds to the muzzle, while the lowest to a part of the dorsal mid-torso. The range within which all body parts are defined their elevation level is limited between 14mm and 30.6mm (high: 14-19.5mm, medium: 19.6-25.1mm, low: 25.2-30.6mm). None of the significant parts of the body is fixed on the ranges between 0.1mm and13.9mm and between 30.7mm and 39mm. Therefore, there are no extra elevation levels in N13.

Figure 4.44: N13 (1/20 scale) seen from the vertical position. The highest elevation is found on the muzzle, while the lowest is on the dorsal mid-torso.

The surface is firstly detected at the tip of the muzzle. As the cross-section layer proceeds, the whole muzzle passes the layer by 11.1mm (see Figure 4.45, 1-2). At the

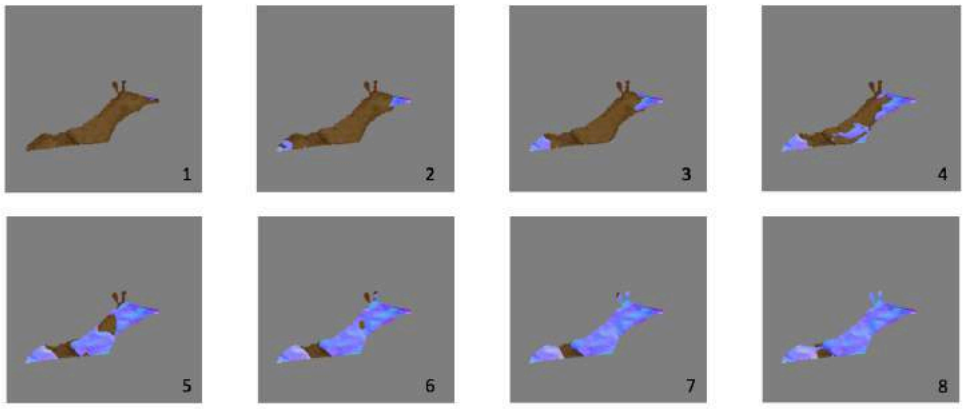

Figure 4.45: These eight images illustrate the depth of N13. When the cross-section layer passes the surface of N13, the colour of the surface changes; dark regions denote lower elevation than coloured parts. Images 1 and 2 are for 0.1mm - 13.9mm, 3 and 4 for 14mm - 19.5mm, 5 and 6 for 19.6mm - 25.1mm, and 7 and 8 for 25.2mm - 30.6mm.

same time, detection also begins from the thigh, and then the coloured area extends inward from both edges of N13; however, both thigh and head are not defined their elevation level within this range because the detection is limited. Nevertheless, the thigh is defined as high during the next phase: the detected area further extends and covers over half of the body section (14-19.5mm: 3-4). The anterior body (the head and neck) also passes the layer by 19.5mm, but the extent is still limited. Between 19.6mm and 25.1mm, these parts are finally assessed as the medium level (5-6). The elevation of the dorsal mid-torso is low as most of this part is fixed to the range between 25.2mm and 30.6mm (7-8).

Distortion on the image (Horizontal movement, x30°, y-70° – y60°)

If a viewing position is taken on the left, the body appears to be shrunk inwards considerably. As the 2D simulation does not generate a similar distortion, the detected distortion is attributed to an intervention of topography. This is because the convex thigh hides the concave mid-torso. So the size of the image seems significantly contracted; this phenomenon is most noticeable between y-70° and y-40°. This contracting body allows viewers to manipulate the appearance of N13 by moving within the above range.

Unknown quadrupedal animal (N14)

General description:

An image of quadrupedal mammal, facing right (Figure 4.46). The body is fully coloured in red, and so this figure still possesses its significant presence in the entire panel as N7 and N8. Although N14 does not have the head which makes it difficult to identify its species, it has the main body (neck-shoulder, mid-torso and thigh) and four robust limbs. The figure is located on the bottom of the central area of the frieze. The wall immediately under the image has been collapsing, and the bottom forms an edge which provides N14 with a horizontal axis; the animal appears walking on this edge line. The length of N14 is approximately 83 cm.

Figure 4.46: N14, image of a quadrupedal animal facing right. Despite its stunning presence, the species is not discernible due to the absence of its head.

Integration of natural lines

An uncountable number of grooves and edges exist on this panel, and N14 utilises some of those lines for its outline in multiple regions: the ventral line, dorsal line, buttock, and left hind leg. The most dynamic integration is found in the ventral line. The wall noticeably elevates in the area between the back leg and thigh, and the edge of this protuberance extends to the lower right from the point where the belly begins. The ventral line of N14 is superimposed on this edge line (Figure 4.47, left). Next, another salient integration is confirmed in the buttock. Although the contour from the dorsal to the buttock appears like a half square, such an angular shape already exists on the wall as an edge of a convex surface (Figure 4.47, right). The buttock overlaps on the edge of

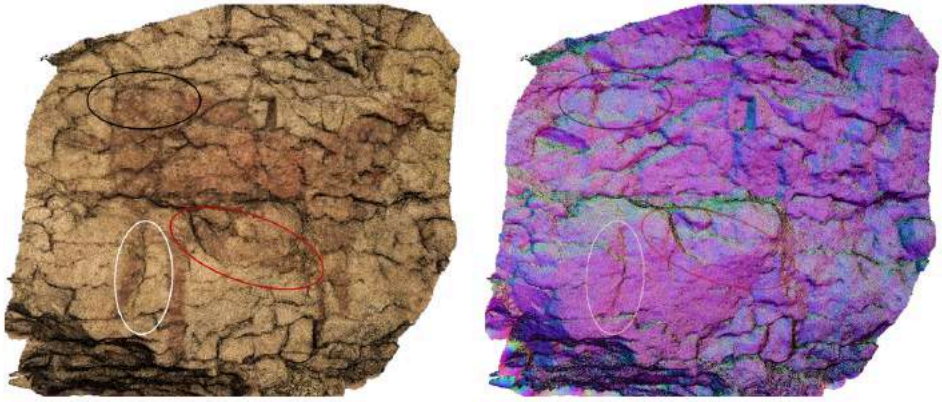

Figure 4.47: Examples of integration. N14(left) and its highlighted topography (right). The red circle on the images suggests the integrated section of the ventral line. Most of the belly is provided along the edge which lies horizontally. The black circle shows the contour of the buttock and the croup is exactly fixed to an edge of the wall of half-square shape. Meanwhile, one of the hind legs is drawn along a groove (see the white circle).

the convex wall. This edge line turns into a groove as it continues downward, sub-vertically traversing the left hind limb to the right. The left hind leg borrows this groove as a part of its outline. Moreover, natural lines are used in the dorsal line although a limited extent: from the middle dorsal to the neck, thin and short natural grooves overlap, replacing one after another. Thus, integration is confirmed in N14 to a significant degree. Given the dynamics of integrations seen in N14, pre-existing patterns on the panel assisted the ice-age artist in producing this image.

Topographic condition

The elevation in the ventral side characterises the topographic condition of this wall. The raised surface lies horizontally across the ventral body (especially the thigh and mid-torso) and forms a ridge, although the elevation lowers toward the shoulder area. Additionally, the surface consists of an innumerable fraction which generates an elevational gap by region. The total depth is 147mm (the model is at 1/50 scale: Figure 4.48); the highest point corresponds to the hind leg, while the lowest to the ventral neck. The range within which most of the body parts are defined their elevation level is between 54.5mm and 136.1mm (high: 54.5-81.7mm, medium: 81.8-108.9mm, and low: 109-136.1mm). Ranges between 0.1mm and 54.4mm and between 136.2mm and 144mm are respectively higher and lower than the above range. A body section belongs to the range between 0.1mm and 53.7mm, and there is the extra high level in N14, therefore.

Figure 4.48: N14 (1/50 scale) seen from the vertical position. The highest elevation is found on the hind leg, while the lowest is on the ventral neck.

The surface is first detected at a point on the left hind leg. As detection continues, the highlighted area entirely covers the left leg by 26.9mm (see Figure 4.49, 1-2); the right hind leg also begins passing the cross-section layer at the same time. The rear limb is mostly detected by 54.4mm, and hence it is assessed as the extra high (3).

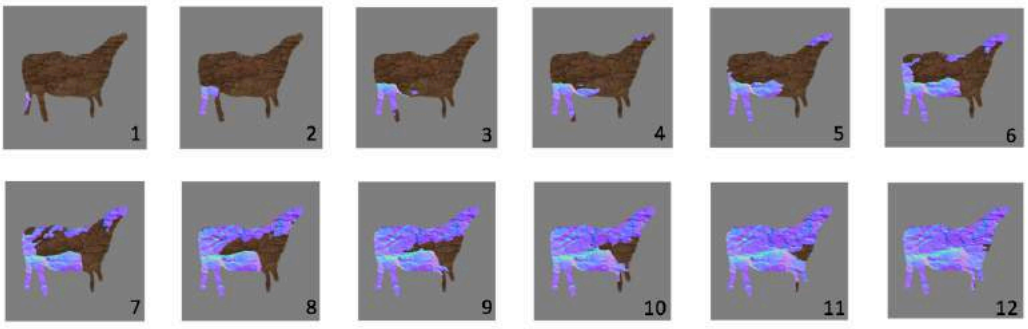

Figure 4.49: These 12 images illustrate the depth of N14. When the cross-section layer passes the surface of N14, the colour of the surface changes; dark regions denote lower elevation than coloured parts. Images1-3 are for 0.1mm - 54.4mm, 4-6 for 54.5mm - 81.7mm, 7-9 for 81.8mm - 108.9mm, and 10-12 for 109mm - 136.1mm.

Simultaneously, the coloured area, although limited, extends to both the ventral thigh and ventral mid-torso. The detection further continues based on these areas during the next phase (54.5-81.7mm). The region of the high elevation level gradually spreads upward and rightward, including most of the ventral thigh and ventral mid-torso (4-6). By the time, the surface has also passed at multiple regions (the ventral-central thigh, dorsal mid-torso, and dorsal neck-shoulder). However, the extent is not significant enough to define their elevation level. Between 81.8mm and 108.9mm, these sections are also assessed as medium (7-9). Accordingly, the undetected sections (the central mid-torso, central-ventral neck-shoulder, and frontal limb) are defined as the low elevation level. These undetected regions mostly pass the layer between 109 mm to 136.1mm (10-12). The ventral neck is the lowest part in N14, and it needs further 10.8mm to complete detection.

Distortion on images (Horizontal movement, x30°, y-70° to y70°)

Overall, a remarkable deformation is detected in the ventral side. The area continually appears to be moving side to side within the full range of the viewing angle (y-70° and y70°) due to the large convexity; by contrast, N14 on a 2D surface is never distorted in such a manner. Figure 4.50 is N14 viewed from three different points (y-70°, y0° and y70°). As the viewing angle decreases, the hind legs slide to the right, and when the viewing angle reaches y-70°, these legs appear to grows from the belly. At the same time, the shape of the thigh and mid-torso is deformed to be considerably thinner. This is an illusion caused by the sharply elevated surface in the posterior ventral: this raised wall overlaps the central thigh and middle part, generating a hidden area. As the hidden area constantly changes whenever the viewing position moves, the hind limbs are perceived as if sliding side to side. Additionally, between y-70° and y-50°, the forelimbs are also overlapped by this convex wall and go invisible.

Figure 4.50: N14 seen from y-70° (left), y0°(middle), and y70°(right). This shows significant distortion because of topographic features. Especially, the shape of the thigh and mid-torso is remarkably deformed because the position of the hind legs constantly slides side to side. Apart from distortion to these parts, the appearance of the neck and forelimbs also changes: the neck appears stretched when the image is viewed from right; the interval between forelimbs gradually narrows, and the right limb vanishes at y-70°.

On the contrary, once the viewpoint moves to the right, the hind legs then slides to the left significantly. At 70°, these limbs extend from the left edge of the thigh (see Figure 4.50). Simultaneously, the neck appears to stretch. As the case of N5 and N7, a convex surface is located on the right to the front neck, and the high wall pushes the contour of the under-neck upward and narrows the width. Hence, the neck is perceived longer than seen from the direct position (y0°). This distortion occurs within the range between y20° and y70°.

Deer (N16)

General description

An image of a red deer, facing left (Figure 4.51). All body sections are provided except the tail, although some parts are obscure (notably the head and foreleg). The body is fully coloured. The original colour is red but has altered into a somewhat brownish hue, especially in the thigh and back legs. N16 is one of the most visible images in El Pendo, with a strong presence occupying a visual space on the right of the whole panel, together with another deer (N17). It is executed with a simple line of dots and colour wash (Barquin et al. 1998). Its length is approximately 70 cm.

Figure 4.51: N16, image of a deer facing left. Although its head appears somewhat blurred due to decay, the deer still possesses strong presence.

Integration of natural lines

The fractured surface of the wall on which N16 was painted generates an inestimable number of grooves and edges. This image maximises those natural lines for its outline. Figure 4.52 illustrates the original shape of the surface: the dorsal and ventral line almost entirely overlap on a rock edge. The shape of the wall already contains the essential form of N16.

Apart from the above integrations, natural lines are also utilised for outlining other sections: muzzle's tip is superimposed on a crack, and rock edges are integrated into most of the buttock.

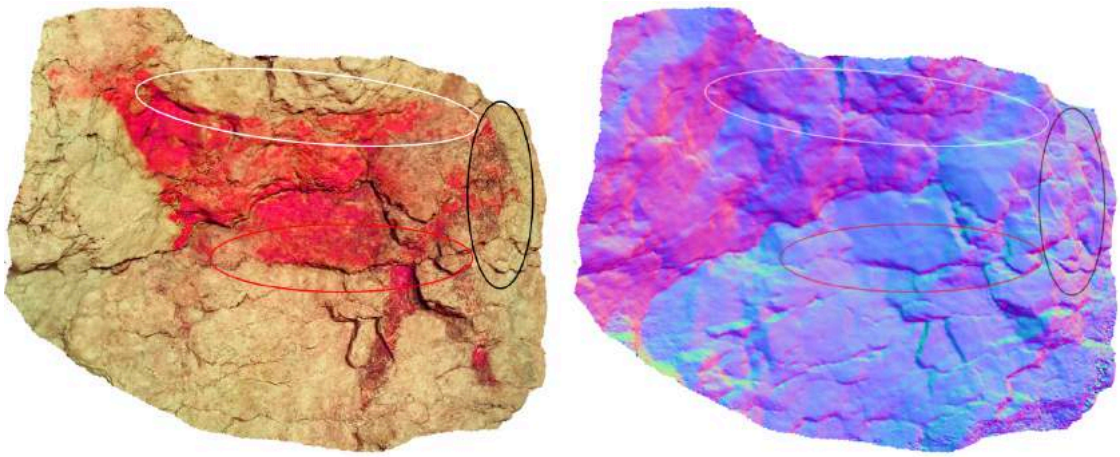

Figure 4.52: N16 (left) and its highlighted topography (right). Natural lines are integrated into most of the dorsal (see the white circle), buttock (see the black circle), and ventral line (see the red circle). As the wall itself already appears the basic form of N16, the artist took full advantage of this condition.

Topographic condition

N16 is depicted on a dynamically undulating wall. Overall, the topography is a large bowl-like concavity; additionally, the elevation is low on the ventral side. The face and the posterior is placed on the region where the elevation is noticeably high. The total depth is approximately 205mm (the model is at 1/30 scale: Figure 4.53). The range within which most of the body parts are defined their elevation level is between 93.7mm and 200.5mm (high: 93.7-129.2mm, medium: 129.3-164.9mm, and low: 165-200.5mm). Ranges between 0.1mm and 93.6mm and between 200.6mm and 205mm are respectively higher and lower than the above range. Two body sections are defined its elevation level between 0.1mm and 93.6mm, and therefore, there is the extra high level in N16.

Figure 4.53: N16 (1/30 scale) seen from the vertical position. The highest elevation is found on the hind leg, while the lowest is on the ventral mid-torso and frontal limb.

Detection begins from the hind legs. The detected area extends upward, involving the other back limb and ventral thigh by a depth of 93.6mm (see Figure 4.54, 1-3). These sections are assessed as the extra high elevation. As the cross-section layer proceeds from 93.7mm and 129.2mm, detection further continues upward from the ventral thigh, and the central thigh is assessed as the high level (4-6). The detected area also extends toward the ventral mid-torso; however, the extent is insufficient to define the elevation of the region. In the meantime, the face starts detected from its jaw at 102.5mm. The coloured area spreads inward and includes most of the head. Therefore, the elevation level of the head is also high. During the next phase (129.3mm and

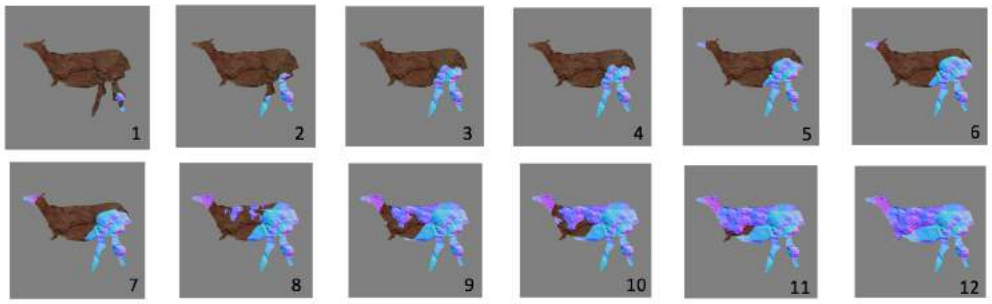

Figure 4.54: These 12 images illustrate the topographic depth of N16. When the cross-section layer passes the surface of N16, the colour of the surface changes; dark regions denote lower elevation than coloured parts. Images1-3 are for 0.1mm - 93.6mm, 4-6 for 93.7mm - 129.2mm, 7-9 for 129.3mm - 164.9mm, and 10-12 for 165mm - 200.5mm.

164.9mm), the detected area extends inward from both head and thigh. After a depth of 142.6mm, a surface on the dorsal mid-torso begins to be detected as the topography on the region is elevated. Consequently, the coloured area considerably expands by 164.9mm (7-9). Thus, the dorsal thigh and dorsal-central mid-torso are defined as the medium level. Between 165mm and 200.5mm, undetected areas further narrow, and finally, the remaining sections are defined as the low level (ventral mid-torso, entire neck-shoulder, and the frontal limb: 10-12). The elevation is particularly low in the frontal appendage and ventral mid-torso, although they are fully detected at a depth of 205mm.

Distortion on images (Horizontal movement, x30°, y-60° to y60°)

N16 is a subject to multiple distortions. If a viewpoint is set to the left, distortion occurs at three sections: the neck, head and the hind limbs. At first, the neck appears to be shrunk. This is because a convex surface on the left to the neck pushes the part upward, changes the direction, and narrows its width. This phenomenon is most likely perceived between y-30° and y-50°. The similar effect also happens to the head due to that topographic condition. As a result, N16 seems to shake its head and neck side to side, extending these sections vertically as the viewpoint moves toward the left (see Figure 4.55 left). In the 2D simulation, N16 is not deformed in such a manner. Furthermore, the hind limbs appear bent backwards as the viewing angle decreases from y0° to y-60°. The high elevation of the limbs is responsible for this bending.

Even when the viewpoint is taken on the right, N16 is significantly deformed. Figure 4.55 (right) illustrates an image viewed from the position of y60°. The proportion of N16 collapses, and the thigh sticks out from the central part of the body. The cause of this distortion is two different convex, one of which is located on the ventral thigh and the other is on the right hind leg. As the viewpoint moves to the right, these convex surfaces overlap the dorsal-central thigh and cause a significant contraction on the thigh.

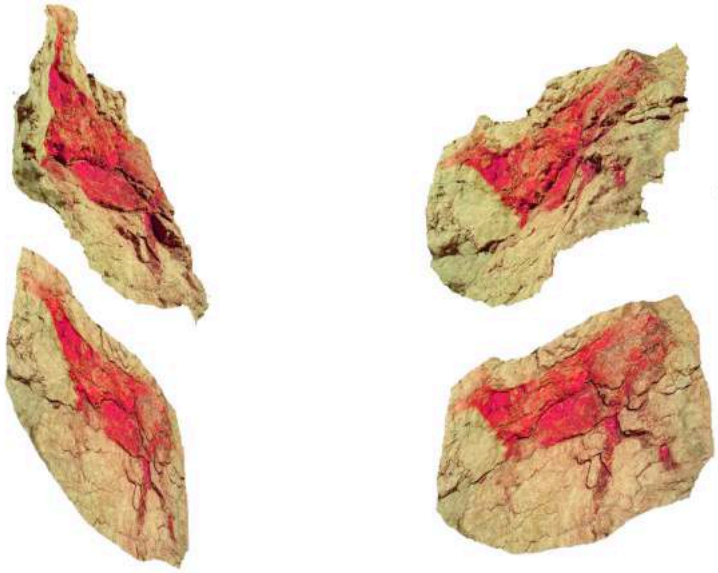

Figure 4.55: N16 on the 3D surface (above) and 2D surface (below) seen from y-60° (left) and y60° (right). The combination of the concave and convex surface distorts the deer dramatically as a viewpoint sifts side to side. In contrast, significant distortions do not occur on N16 on the 2D surface (below left and below right)).

In the distorting process, the image achieves a dynamism, specifically as if a deer is kicking the ground. This visual illusion occurs when the angles are set between y0° and y60°.

Deer (N17)

General description:

An image of a red deer, facing right (Figure 4.56). N17 is located on the rightmost of the frieze, immediately right to N16, approximately 30 cm away. This deer shares characteristics with N16; they are placed on the almost same height; the size is 68 cm which is equivalent to the other deer; all body parts except the tail are provided. N17 is fixed in a back-to-back position against N16 which forms a symmetrical composition. It is executed in colour-wash and simple line (Barquin et al. 1998). The image was originally painted in red (ibid.); however, the anterior body barely sustains red, and the posterior part is altered into a brownish hue.

Figure 4.56: N17, image of red deer facing right (Hue/Saturation filter is applied). This deer is located on the rightmost of the Frieze of Pictures. As it is fixed in back-to-back position against N16, these two images are depicted in a symmetrical composition.

Integration of natural lines

Even though there are numerous natural lines on this wall, N17 does not utilise any of these lines. The dorsal and ventral line do not overlap with any of edges that exist in the region. This is the only image in El Pendo cave with no observable integration among all examined images.

Topographic condition

N17 is painted on a dynamic topography; it is placed on an overall but acute concavity. The total depth is approximately 237mm (the model is at 1/60 scale: Figure 5.57). The highest point corresponds to the ear, while the lowest to the tip of the frontal limb. The range within which most of the body parts are defined their elevation level is between 0.1mm and 147.6mm (high: 0.1-49.2mm, medium: 49.3-98.4mm, and low: 98.5-147.6mm). A body section is defined its elevation level between 147.7mm and 237mm, and therefore, there is the extra low level in N17.

Figure 4.57: N17 (1/60 scale) seen from the vertical position. The highest elevation is found on the ear, while the lowest is on the frontal limb.

The surface is firstly detected at the right ear, and the area gradually extends to the other ear by 13.4mm. At this depth, detection also begins from the muzzle and thigh. These detected areas further spread, and the head and entire thigh almost fully pass the cross-section layer by 49.2mm (see Figure 4.58, 1-3). Accordingly, they are assessed as the high elevation level. Detection steadily continues inward from the above areas during the medium elevation level (49.3-98.4mm: 4-6), and the entire mid-torso is located in this elevation level. The expansion of the detection is slow from the head because the elevational gap in the neck-shoulder is acute; only the dorsal neck-shoulder passes the layer by 98.4mm. The remaining sections (the central-ventral neck-shoulder

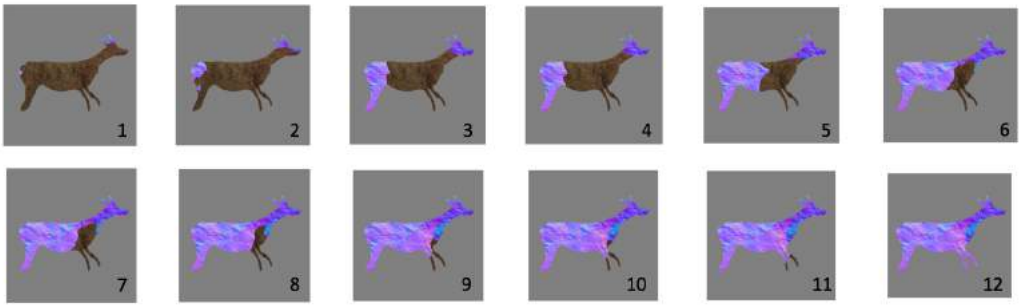

Figure 4.58: These 12 images illustrate the depth of N17. When the cross-section layer passes the surface of N17, the colour of the surface changes; dark regions denote lower elevation than coloured parts. Images 1-3 are for 0.1mm - 49.2mm, 4-6 for 49.3mm - 98.4mm, 7-9 for 98.5mm -147.6mm, and 10-12 for 147.7mm - 237mm.

and frontal limbs belong to the surface of a lower elevation. Notably, the elevation of the frontal legs is profoundly lower than the central-ventral neck-shoulder; while these areas in the neck are assessed as the low level by 147.6mm (7-9), the forelimbs need further 89.3mm to be fully detected (147.7mm and 237mm: 10-12). This deep level is defined as the extra low.

Distortion on images (Horizontal movement, x30°, y-80° to y50°)

Overall, N17 is distorted in all of its body parts. As the viewpoint shifts to the left, the mid-torso and thigh gradually become thinner. Once compared with N17 in the 2D simulation, the deformation is marked (Figure 4.59). This is because the dorsal area (lower elevation) is hidden by the ventral body (higher elevation) and goes unseen. This overlap takes place between y-80° and y-50°. At the same time, the interval between two forelimbs shortens, and the left limb overwraps on the other at y-80°. Meanwhile, the anterior part sustains a certain proportion because the massive uplift on the forefront body constantly displays the anterior side to the viewer on the left.

Figure 4.59: N17 on 3D surface (left) and 2D surface (right) seen from y-80°. The mid-torso and thigh appear thinner because the central area overlaps the dorsal region. The convex topography on the left frontal limb also overlaps on the other leg. Meanwhile, the anterior part sustains a certain proportion because the massive convex on the forefront body constantly displays the part towards the viewer on the left. These changes are never detected in the 2D simulation.

On the other hand, when a viewing position is taken to the right, the convex surface on the right of the chest hides the neck and replaces the outline of the neck's contour with its edge (at 50°: see Figure 4.60). As this edge overlaps the neck, the neck gradually appears thinner as a result. At this time, the contour of the chest which is depicted in the concave smoothly merges into this edge, so the outline of the section appears consistent. Consequently, only the neck seems to be deformed, as if N17 stretches its head upward. The edge hides the neck completely at y60°, and the head appears separated from the body. Additionally, the convex surface in the neck and head pushes these parts front once N17 is viewed from the right, and the image appears

Figure 4.60: N17 on the 3D surface (left) and 2D surface (right) seen from y50°. The combination of the concave and convex surface distorts the deer dramatically. Especially, the distortion on the neck is significant as it narrows its width. The hind leg also appears bent backwards. The extent of the topographic intervention is visualised once compared to N17 on the 2D surface.

shaking the head and neck side to side if the angle shifts between y30° and y50°. There is also another distortion: the hind leg is seen extending outwards as if a deer seems to be kicking the ground. This bending leg is noticeable especially when the viewpoint is set between y20° and y50°. In this way, the unique topographic condition interferes the appearance of N17 to a significant extent.

4.4 Results

Integration of natural lines

Integration of natural line with the depiction can be confirmed in 10 of the 11 analysed images (N1, N2, N4, N5, N7, N8, N12, N13, N14, N16). This number is considerably higher than that observed in Covalanas cave (11 out of 18 images). I attributed a high occurrence of integration to the condition of the surface of El Pendo's "Frieze of paintings". As the inestimably fractured wall creates a massive number of natural lines, the paintings in El Pendo maximise those lines. Figure 4.61 shows the number of integrations by body section. Among six sections, the most integrated part is the dorsal line (with ten images); that is, all images with integration contains the integrated dorsal line. Integration also likely happens in the ventral line, with nine images (N1, N2, N4, N5, N7, N8, N13, N14, and N16). The number for the dorsal and the ventral region are remarkably high compared to the other four parts; five integrations are found in the buttock (N2, N5, N7, N14, N16), and four in the head (N4,

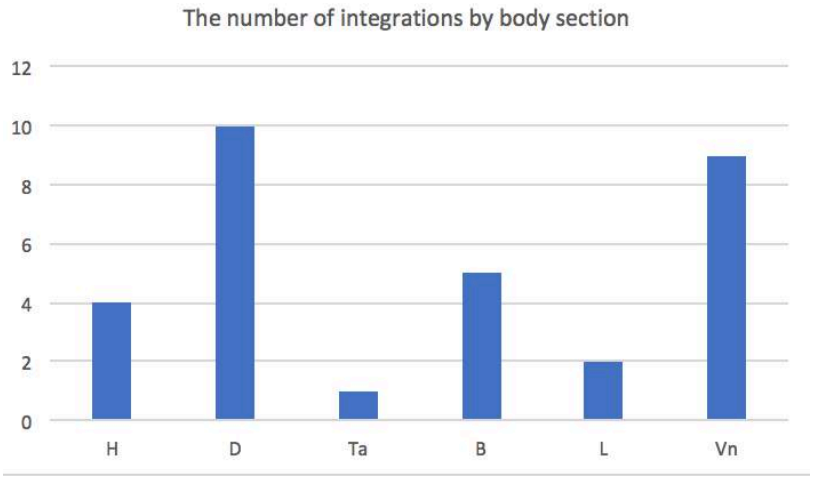

Figure 4.61: The number of images with integration by body part (H: Head, D: Dorsal, Ta: Tail, B: Buttock, L: Limbs, and V: Ventral). Integration mostly likely occurs on the dorsal line (10 images) and then ventral line (9). Especially, almost all images (10 out of 11 images) utilise natural lines for outlining the dorsal line. By contrast, limbs (2) and the tail (1) were not preferred sections for integration.

N8, N13, and N16). The leg and tail are least popular body part for integration as natural lines are used in the limb only twice (N4 and N14) and in the tail only once (N5).

Integration is significantly common in El Pendo cave, and the number of the image with plural integrations is also high. Figure 4.62 illustrates the number of images by the frequency of integration. Whereas there is only one image (N12) with a single integration, at least two integrated contours are confirmed in nine images; eight images contain more than three integrations (N2, N4, N5, N7, N8, N13, N14, N16). Thus, almost all images rely on natural lines to outline multiple sections.

Among images with plural integrations, a trend can also be detected in the combination of integrated sections. Figure 4.63 shows the frequency of the combination by body parts. It is clear that the all body parts except the tail co-occur with the other body parts at least once. Above all, the number of the combination of the dorsal and ventral line is noticeably high (nine images: N1, N2, N4, N5, N7, N8, N13, N14, and N16), but such a high co-occurrence is not surprising because the number of the integration into these parts is originally high. What should be noted is the relation between the head and buttock. Each of these sections marks 4-5 times of integration with either dorsal or ventral (buttock: N2, N5, N7, N14, and N16, head: N4, N8, N13, and N16). However, integration of the head-buttock combination occurs only once (N16) as if the palaeo-artist intended to avoid them occurring. Integration into these parts might be an additional element to integration into the dorsal and the ventral line. I will discuss this point further in Chapter 6.

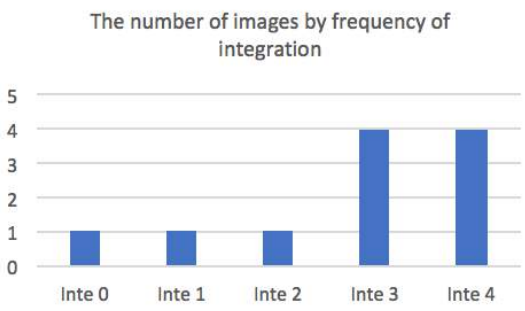

Figure 4.62: The number of images by the frequency of integration (Inte = Integration). In El Pendo cave, multiple integrations are a significantly common phenomenon as 9 images contain at least 2 integrated body parts. Particularly, the number of images with 3 integrated parts and 4 integrated parts are high (each case contains 4 images). This is attributable to the fractured wall surface where innumerable natural lines are available for integration.

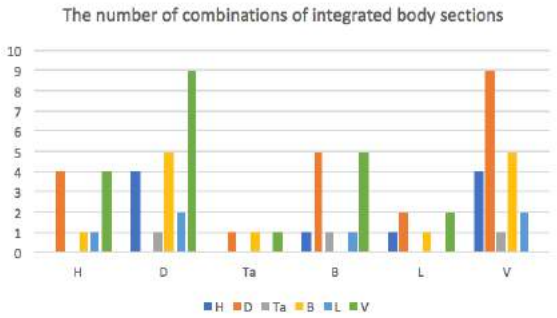

Figure 4.63: The number of combinations of integrated body sections. Despite the high value for the combination of the dorsal and ventral line (9 images), this result is understood given the high occurrence of integration for these body sections. Meanwhile, the result for the head and buttock is only once in spite of relatively high occurrences for them (4 and 5 images, respectively). That seems as if the palaeo-artist intended to avoid simultaneous integration on these two parts.

Topographic condition

Although all of the analysed topographic conditions are unique, a remarkable trend is confirmed. Figure 4.64 illustrates a correlation between body sections and their elevation level. According to Figure 4.64, there are six images whose head is assessed as the high level; that number is the highest regarding this elevation level. Meanwhile, the main body (the neck-shoulder, mid-torso, and thigh) is most likely paced on a medium-level surface. Moreover, the low elevation level tends to occur frequently in the mid-torso and the appendages. As for the extra levels, the number of detections itself is rare as it is limited to six times. However, except for one example in the ventral thigh, five times have been confirmed in the legs; this result is similar to the case of Covalanas where extra levels are also likely located on the limbs.

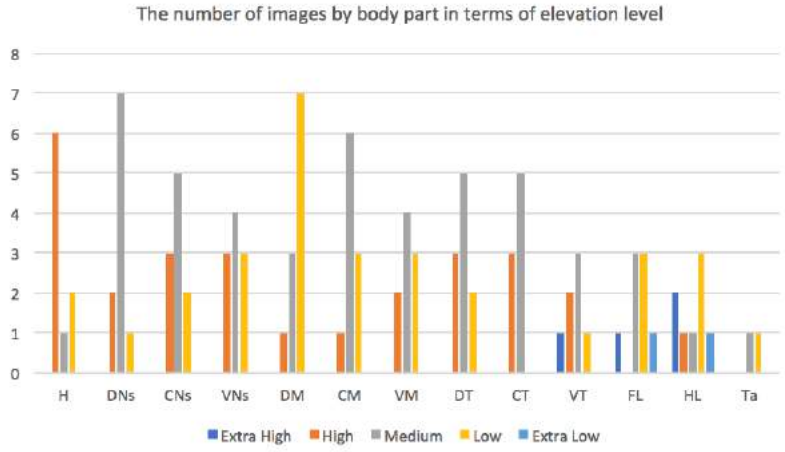

Figure 4.64: The number of images by body part regarding elevation level (H: Head, Ns: Neck-shoulder, M: Mid-torso, T: Thigh, FL: Front Leg, HL: Hind Leg, Ta: Tail. D, C, and V, refer to Dorsal, Central, and Ventral, respectively). Certain trends are visible in the graph: High elevation tends to be placed on the head (6 images); Medium level is more likely found on the main body (Ns: 7-4, M: 6-3, T: 5-3); the elevation for the mid-torso (7-3) and limbs are more likely low (FL: 4, and HL: 4); Extra elevation level is mostly allocated to limbs (FL: 3, and HL: 4). However, some images are not complete figure as the head, thigh, limbs or tails are missing, while all images contain the neck-shoulder and mid-torso. Therefore, this result is not obtained from images in the same condition.

Although the nine divisions of the main body are united, the overall trend remains almost the same (Figure 4.65). Figure4.66 demonstrates a generalised elevation level by body section, which is obtained based on the above-simplified data. In this graph, the elevation points directly reflect the degree of the elevation. According to this, the neck-shoulder tends to be located on a convex surface more than any other sections (35 points), followed by the thigh (33 points); the total points for the head is 31 points, while for the mid-torso is 30 points. It is even lower for the legs and the tail.

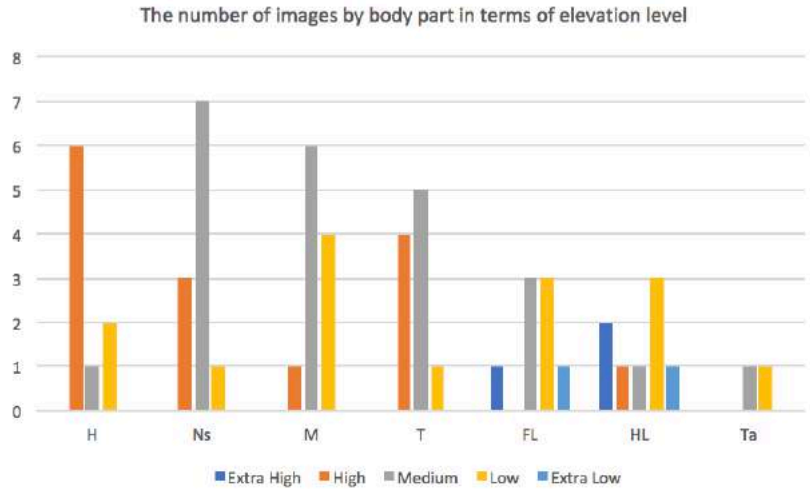

Figure 4.65: A simplified graph of the topographic condition for 11 images by body part (H: Head, Ns: Neck-shoulder, M: Mid-torso, T: Thigh, FL: Front Leg, HL: Hind Leg, Ta: Tail). Although the nine main body parts are integrated into the three parts (Ns, M, T), the result still reflects the trends seen in Figure 4.64.

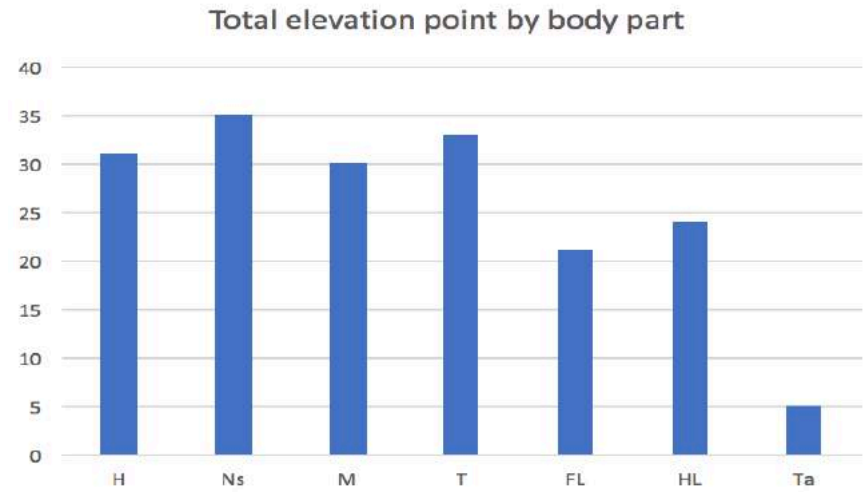

Figure 4.66: A graph of the total elevation point by body section (H: 31 points, Ns: 35, M: 30, T: 33, FL: 21, HL: 29, and Ta: 5). The elevation reflects high if the point is high, while the depth is deeper if the point is low.

However, this result does not accurately represent a general trend in topographic condition. Whereas all images are provided with the neck-shoulder and the mid-torso, the head or thigh is absent in some samples. Therefore, elevation points of those missing parts are not added to the result, and inevitably their points are lower. Among all analysed samples in El Pendo, seven images (N1, N2, N4, N5, N7, N16, and

N17) are complete if the absence of the tail is not taken into account: N8 has no thigh and hind leg; N12 lacks the head and both frontal and hind legs; legs are also absent in N13; the head is missing in N14. Remember, a prioritised element is the general shape of the surface from the head to the thigh as was mentioned in the second chapter. Therefore, I calculated the elevation point again, based on eight images with the head, neck-shoulder, mid-torso, and thigh (N1, N2, N4, N5, N7, N13, N16, and N17), thus the result properly reflects the data obtained from the same condition. Consequently, the result shows a different trend from the previous one; as illustrated in Figure 4.67, the head and thigh tend to be fixed at a position of higher elevation than the neck-shoulder

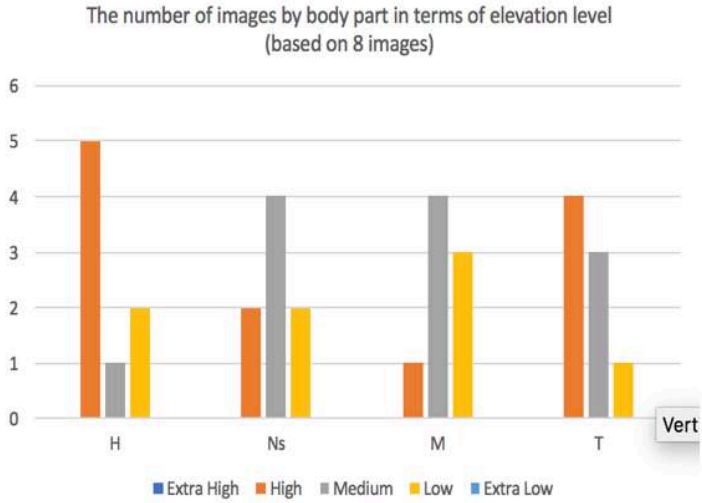

Figure 4.67: A simplified graph based on 8 images (H: Head, Ns: Neck-shoulder, M: Mid-torso, T: Thigh). Unlike the previous result, the values of Medium level for Neck-shoulder, Mid-torso, and Thigh remarkably drop (4, 4, and 3, respectively), but instead the value of High for Thigh increases (4).

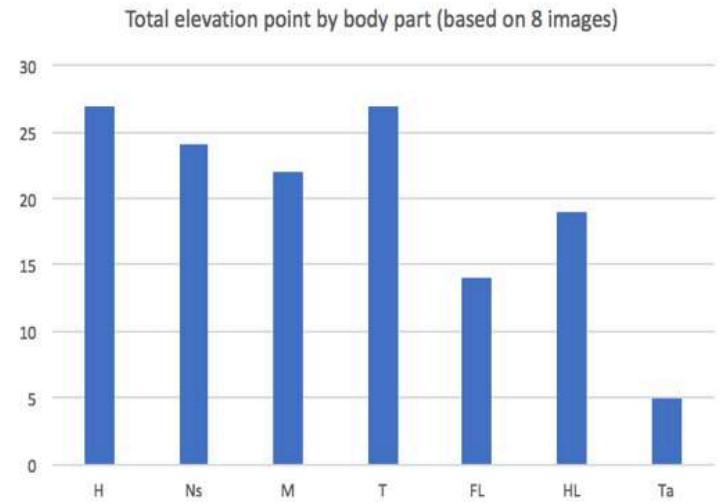

Figure 4.68: A graph of total elevation point by body part based on eight images (H: 27 points, Ns: 24, M: 22, T: 27, FL: 14, HL: 19, and Ta: 5). Unlike the previous result, points for Head and Thigh are higher than Neck-shoulder and Mid-torso. That means examined images are generally found on an overall concave. This result is the same as the case of Covalanas.

and the mid-torso. Figure 4.68 demonstrates the elevation points by body section. Compared to the previous result (see Figure 4.66), the score of the neck-shoulder decreased to 24 points, and the mid-torso marks 22 points. Instead, the head and thigh come higher than neck-shoulder and mid-torso as both sections achieve 27 points respectively. This result indicates that images in El Pendo tend to be depicted on overall concavities as was seen in Covalanas cave.

In total, five topographic patterns were detected based on the complete eight images: Overall concavity (P1), Overall slope (P2), Overall convexity (P3), Zigzag (P4), and Partial concavity (P5). Above all, P1 is the most popular type, with three images (N7, N16, and N17: see Figure 4.69), followed by P5 (two images: N2 and N13). On the other hand, the other types contain only one image respectively (P2: N1, P3: N4, P4: N5). If P1 and P5 are united, more than half of the images are associated with concave topography. This fact is reflected in the generalised data.

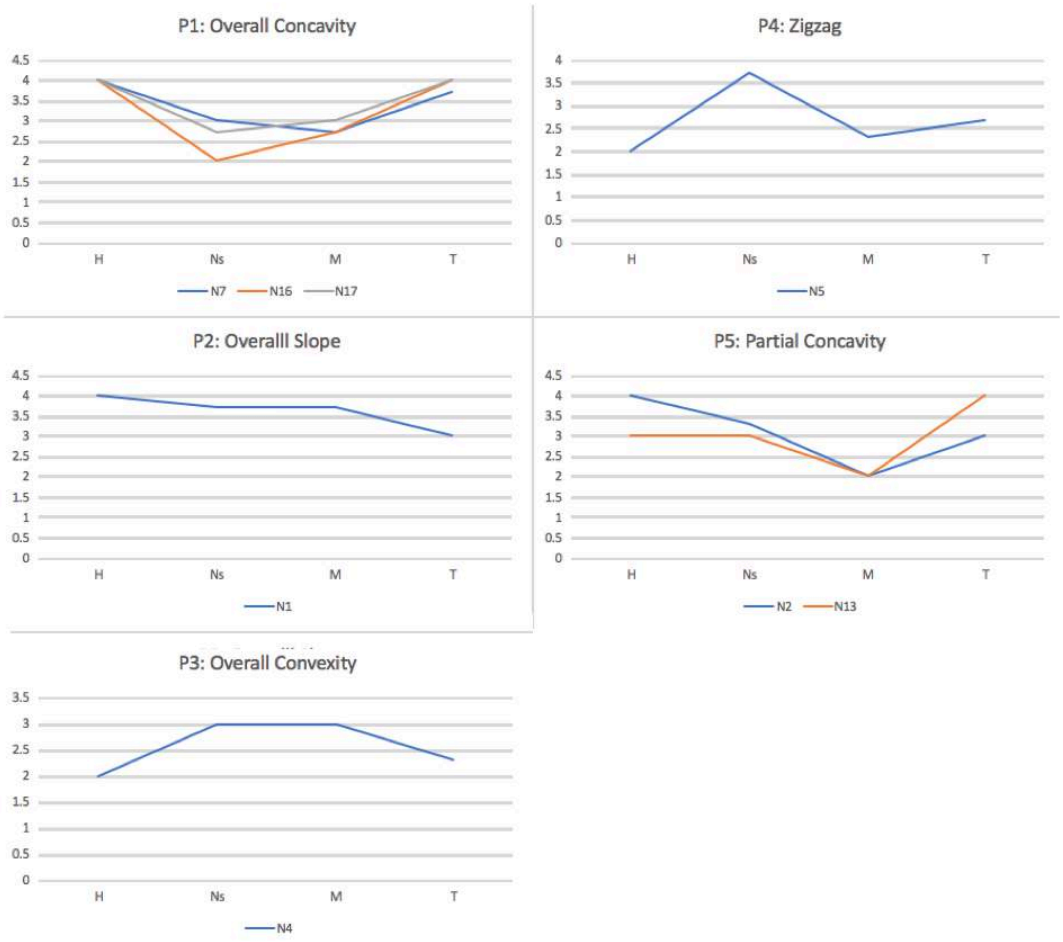

Figure 4.69: Numerically visualised topography patterns. 5 patterns are detected in El Pendo: Overall concavity (P1), Overall slope (P2), Overall convexity (P3), Zigzag (P4), and Partial concavity (P5). Above all, P1 is the most popular type, with 3 images (N7, N16, and N17), followed by P5 (N2 and N13). On the other hand, the other types contain only 1 image respectively (P2: N1, P3: N4, P4: N5).

Distortion on images

In El Pendo Cave, all pictorial samples are distorted. Figure 4.70 shows the number of images and the frequency of distortion on each. One distortion takes place in only three images (N1, N12, and N13), while distortion occurs at least more than twice in eight images (N2, N4, N5, N7, N8, N14, N16, N17). Remarkably, the number of images with more than three distortions is six, which accounts for more than half of all pictures (Dis3: N4 and N5, Dis4: N8, N14, N16, and Dis5: N17). Generally, these images change their shape considerably by viewing them from different viewpoints. Distortion is a profoundly common phenomenon in El Pendo.

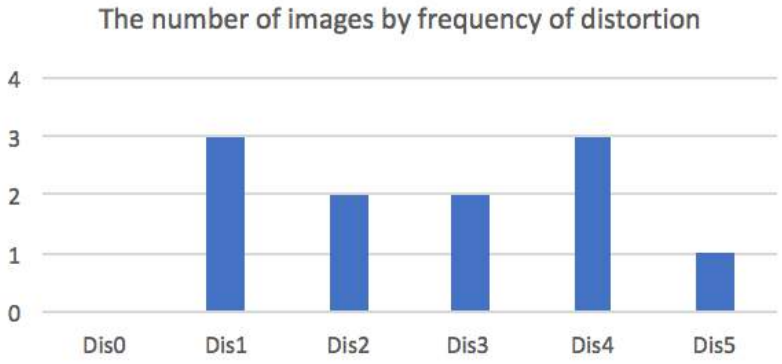

Figure 4.70: The number of images by the frequency of distortion (Dis = Distortion). All images are subject of distortion in El Pendo cave (Dis0: 0 image, Dis1: 3, Dis2: 2, Dis3: 2, Dis4: 3, and Dis5: 1). Multiple deformations are significantly common as 8 images contain at least 2 distorted body parts. This fact signifies the active role of the topography to distort images.

With regard to the relationship between distortion and body sections, some sections are more frequently deformed. Figure 4.71 illustrates the number of distortion by body part. Deformation most likely occurs at the neck-shoulder (10), which is followed by the leg (7) and head (6). On the contrary, the deformation is less likely

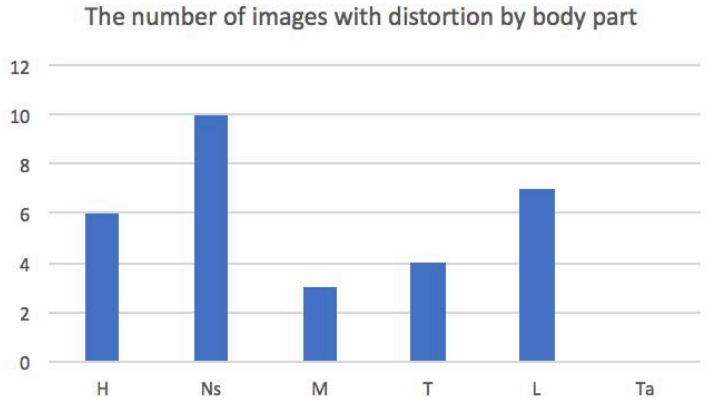

Figure 4.71: The number of images with distortion by body part (H: Head, Ns: Neck-shoulder, M: Mid-torso, T: Thigh, L: Limbs, and Ta: Tail). Distortion intensively occurs in the neck, with 10 images. The limbs are the second preferred section, with 7 images. The mid-torso has the lowest value as only 3 images contains distorted mid-torso.

confirmed in the thigh (4) and mid-torso (3). The tail is never deformed; this section is absent in almost all the images analysed.

This observation shows both similarity and dissimilarity to Covalanas. The neck-shoulder is the most frequently distorted section in both caves. However, in Covalanas the frequency of head and thigh distortion is also remarkably high, whereas in El Pendo deformation is more likely caused in the legs. As for the limb, its highly distortable nature was already noted in the previous chapter; although the low frequency of distortion on a limb in Covalanas, the ratio itself (the number of distortion on a leg/ the number of images with a leg) is higher than the head and thigh. In El Pendo, because there are only two images without limbs, the suggested potential of the limb is reflected in the result. Therefore, the reason for the limb's high occurrence of distortion is understandable.

Summary

This case study analysed 11 images of the Palaeolithic parietal art in El Pendo cave. Although the number of images is the smallest among the three case studies, notable trends were confirmed in all analysed data categories. Those trends are reminiscent of the result from Covalanas, though there are minor differences. The similar tendencies might imply the existence of a shared principle between the caves in terms of both image-making and image-viewing. I summarise below the essential points obtained from this case study:

- Integration is found in almost all images (10/11). Notably, there are eight images contain more than three integrations. Such a high frequency highlights the importance of integration as an essential artistic method in El Pendo cave. The reason for this high occurrence is attributable to the condition of the cave wall; the frieze contains a large number of fractures which generate countless natural lines (integration of natural lines).

- The most integrated section is the dorsal line (10 images), followed by the ventral line (eight images). On the other hand, integration into the buttock or head takes place as if by doing is an additional element to that into dorsal-ventral lines (integration of natural lines).

- Based on the eight complete images, the high elevation level tends to be found in the head (five images) and the thigh (four images). In contrast, the neck-shoulder and the

middle are more likely placed on the medium and low level. The extra-level surface (extra high and extra low) is located in the legs in almost all cases (topographic condition).

- Total elevation points are higher in the head and thigh than neck-shoulder and mid-torso. Therefore, images in El Pendo tends to located on overall concave surface (topographic condition).

- There are roughly five patterns in topographic condition (P1: overall concavity, P2: overall slope, P3: overall convexity, P4: zigzag, P5: Partial concavity). The most frequent type is overall concavity (topographic condition).

- Distortion was confirmed in all images. Notably, the number of images with more than two distorted sections is eight, which comprises more than 70% of the entire proportion (distortion on images).

- Distortion in the neck-shoulder almost always occurs. Legs are also frequently deformed. Meanwhile, distortion on the head and thigh is relatively rare, particularly in comparison to Covalanas (distortion on images).

These are the crucial observations from the collated data in this chapter. Detected trends show a significant similarity to Covalanas cave, and details on each point will be discussed in Chapter six once the data from all case study have been gathered. On the other hand, elements specific to El Pendo were also detected (such as a significantly high occurrence of integration and deformation), and topographic condition plays a decisive role defining those elements. Therefore, even though this is generally called "cave art", no two cases are perfectly identical. The topographic features utilised for the image-making and the following interactivity with cave art may well vary widely between cave sites. If so, the ways cave art was conceived, executed and viewed may well have been diverse in the Palaeolithic. Thus, a comparison between El Pendo and Covalanas reveals that the state of the cave wall will directly affect the degree of artistic interaction with it. I now move on to an analysis of images in El Castillo cave.

Chapter 5

Case Study 3: El Castillo cave

5.1 General Information

Site

El Castillo cave is one of the most significant caves in Palaeolithic Archaeology. Through its long inhabitation history beginning with the Mousterian and ending in the Middle ages (de Quiros et al. 2015), it preserves a large and diverse archaeological record. The finds of the Upper Palaeolithic in particular are so rich in quantity and diversity that archaeologists presume that this cave was one of the essential seasonal aggregation sites among the hunter-gatherers who settled in the Cantabrian region (Conkey 1980, Groenen 2012).

As well as the abundance of its archaeological record, the parietal art attests to the importance of El Castillo during the Upper Palaeolithic. The cave contains numerous engraved and painted figurative and non-figurative images both including a large number of hand stencils. Moreover, they cover almost all themes in cave art and techniques (e.g. outlining, multi-colouring, sculpturing, etc.). The preserved parietal art in this cave is, therefore, regarded as an "encyclopedia of Palaeolithic cave art" (García-Diez et al. 2015, 03). Such a large number of parietal art accords El Castillo cave public recognition, leading the site to the inscription as a UNESCO world heritage site in 2008. In addition to this, as the recent application of uranium series dating indicates a significantly older date for hand stencils than previously suspected (at least 37,290 BP: García-Diez et al. 2015).

El Castillo forms part of the karstic system of Monte Castillo, in Puente Viesgo, Cantabria, Northern Spain. Monte Castillo contains six other caves: El Oso, El Lago, La Flecha, Las Monedas, La Pasiega and Las Chimeneas. In addition to these, there are numerous small cavities, and all of them constitute the unique karstic system of the mountain (Foyo et al. 2009). The top of Monte Castillo reaches 355m above sea level, and the entrance of El Castillo cave is located at a point of 195 meters. The approximate length of the entire underground network is 760 m.

Monte Castillo is a conical hill which is easily accessible from the nearby Pas river (and its valley. Because this area contains abundant natural resources and is ecologically diverse, it is considered that Monte Castillo played a key strategic role in economic activities and food procurement of prehistoric population. The caves of Monte Castillo have yielded a significant variety of archaeological records which contribute to

the reconstruction Palaeolithic hunter-gatherer activity in the region (Garcia-Diez et al. 2015).

El Castillo cave is the largest cave in Monte Castillo, and consists of several sections. It has five main halls (named Room A, B, C, D and the 'Final Room'). The interior is divided into two parts (east and west); Room A-D are located in its eastern part, whereas the Final Room is in the west. In addition to these essential sections, a long corridor called Gallery of Discs connects the east and the west parts. Additionally, small chambers (Room of Tectiforms, Hands Gallery and Hands Ceiling) are situated in the north of Room A (Figure 5.1).

Room A is the widest hall in the cave (30m wide, 25m long, and 8m high). This room has an extended part (diverticulum) on its south side with a length of 28m and a width of 5m. In the centre of Room A, large stalagmitic pillars developed, occupying most of the space in the hall. A staircase for modern tourists is installed around the pillars. From this, visitors can reach other chambers to the north and Room B to the west. Room C is located on the west to Room B. The joint passage between these rooms is now paved for tourism as a tunnel under the stalagmitic wall. However, it is considered that in Palaeolithic time cave visitors used a narrow passage on the left of the stalagmitic wall or a small elevated chamber on the right of Room B to travel between these two rooms (Groenen et al. 2008). Room C leads to Room D. From the stairs in Room D, one can access to Gallery of discs which is a straight, long and narrow passage (approximately 75m long, 3m wide and 8-10m high) which connects Final Room. Final Room is space with a high ceiling, and there are numerous stalagmites along the south side. This part continues to the deepest section of El Castillo cave which consists of

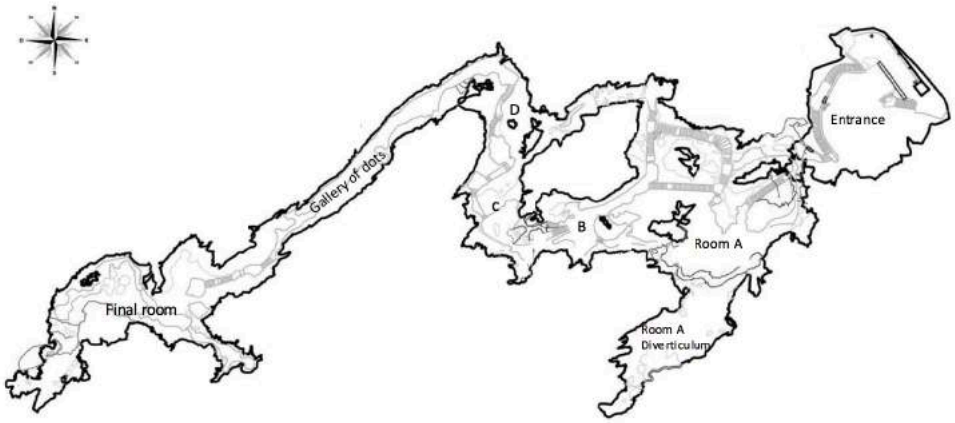

Figure 5.1: A site plan of El Castillo cave. The cave is the largest of the Monte Castillo caves, constituting five large halls called Room A, B, C, D and the final room. The interior is divided into East and West area; Room A-D are located in the east part, whereas the Final Room is in the west. These sections are connected by a long corridor called Gallery of Discs, and some other small chambers (Room of Tectiforms, Hands Gallery and Hands Ceiling) are situated in the north part of Room A.

further narrow passages and small rooms. Extra chambers in the north of Room A are areas of a low ceiling. Nevertheless, such areas lie nearly 30 m connecting Room A and Room D.

Previous research

El Castillo cave was discovered in 1903 by Hermillio Alcalde del Rio. Since then excavations have been conducted mostly in its entrance/daylight zone, which was used as a residential area from the late Lower to Upper Palaeolithic. A series of excavations have revealed 26 units of the stratigraphic sequence which reaches 21m thick. The archaeological record recovered from this is testimony to the frequent use over at least 150,000 years by Neanderthals and *Homo sapiens* (García-Diez et al. 2015). From the lowest level, Acheulian lithic tools have been discovered. The Mousterian level is the thickest part, which means a longer chronological sequence than the subsequent Upper Palaeolithic, and this level contained an abundance of tools associated with Neanderthals. With regard to the Upper Palaeolithic, the extraordinary number and diversity of artefacts (e.g. lithic tools, bone/antler items and portable art) from the Magdalenian sequence in particular, reveal that by this time at least, occupation was intensive. Among other artefacts, the late Magdalenian sequence yielded harpoons, sagaies and batons with an engraved figure of a stag, while the early Magdalenian layer preserved scapulae that have a design of a red deer. (García-Diez et al. 2015).

With regard to the parietal art in El Castillo, our knowledge mostly relies on intensive researches which have been performed by Marc Groenen and his colleagues since 2003 (e.g. Groenen 2006, 2007, 2012, Groenen et al. 2008, and Warzee et al. 2009). The outcomes of these researches have hitherto been the most comprehensive. Before these archaeologists, any formal analysis of the cave's pictorial samples had been absent since 1912 when H Alcalde del Rio, H. Breuil and L. Sierra published *Les cavernes de la région cantabrique,* which today is a classic reference for cave art research (Warzee et al. 2009). Groenen's and his colleagues' painstaking fieldwork have made a significant contribution to our understanding of El Castillo cave, shedding light on what previous archaeologists failed to record. Their work involved the use of modern equipment to digitally document the cave's art, allowing them to distinguish traces of artistic activity from the natural configuration of the cave's walls. By using digital recording and analysis, they were able to avoid a subjective judgement over the identification of images (see particularly Warzee et al. 2009). Consequence, the project has reported the ongoing discovery of a massive number of images; while 200 of engraved and painted graphics were confirmed at the time of H. Breuil, the number has now increased to over 2500. The animal figures account for some 42% of the total (Groenen 2012). Although the species of many images remain unidentified, the dominant animal motif is deer

(22.82%: Groenen et al. 2008). Equid is second (11.19%), and bison is third (8.05%). Figurative images in the cave are executed in a naturalistic way, as seen in other caves, depicted by dots or lines in yellow, red and black. Although most of the motifs are of animals, two images are hybrid of two different animals; I will return to these images later. After all these discoveries, Groenen's research project is still ongoing. Currently, it is examining traces of other anthropomorphic alterations in the cave environment, aiming to record a comprehensive symbolic significance of El Castillo cave (Groenen and Paillet 2014).

5.2 Examined images, locations, methodology

Selection of images

As noted above, about 2500 pictorial images are currently known in El Castillo. Because my interest is in figurative (animal) images, nearly 2000 of non-figurative images and negative hands could be eliminated from the list of samples to be studied. Thus, the total number is reduced to about 500. However, this number is still too large to provide each of those images with a detailed analysis and description. Considering the selection of samples, the most vital criteria are the *visibility* of pictures and the *accessibility* of their location.

As most of figurative graphics constitute engravings executed in thin lines, it is difficult to confirm their presence in the dark space or study their context in great detail. Also, images are occasionally placed where access is considerably hard. In such cases, data collection for 3D reconstruction could not be performed (e.g. a series of deer images is drawn on the east-side wall of Room D, but the wall is located on the height of several metres). Therefore, visibility and accessibility are vital elements in this case study. Based on these prioritised matters, I selected 25 images. These images maintain the most significant presence of all images in El Castillo cave and are located in easily-accessible locations. Furthermore, the total number is adequate for this study, taking account of the number of samples from other case studies (11 images in El Pendo and 18 in Covalanas). The following information details the selected samples and the regions where they are located. They derive from six areas of the cave (Figure 5.2); however, of 19 pictures are found in the north side of Room A. The information of each location is described below.

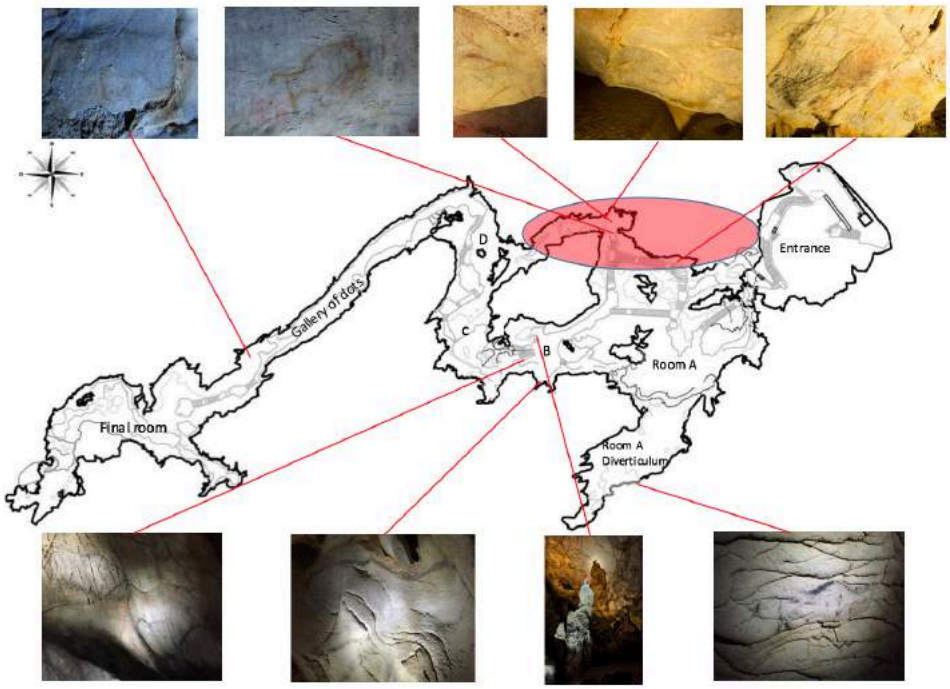

Figure 5.2: The images analysed here and their location. In total, 25 images were selected for the study, based on their visibility and accessibility. These samples are distributed in 6 different regions throughout the cave. However, the most of them (19 images) is located in the north side of Room A which is covered by the red oval over the cave plan.

Polychrome Panel

The polychrome panel is located on the north side of Room A. The area is considerably large, with a length of 550 cm and a height of 350 cm. Its topography is moderate on the right side, while significantly undulating on the left. The polychrome panel contains a large collection of well-preserved figurative images, and its density is the highest of all investigated areas in this case study; in total, 11 animal images are left on the panel. These pictures include five bison, three deer, two horses, and one unidentified quadruped. In this study, the above samples are treated as PB1-PB5 (Polychrome Bison 1-5), PD1-PD3 (Polychrome Deer 1-3), PH1-PH2 (Polychrome Horse1-2), and PU1 (Polychrome Unknown 1). Figure 5.3 shows the entire figure of the panel and the location of each sample. On this panel (especially on the left), at least six hand stencils and several signs are also visible in addition to the above images. Although they are not examined, these images contribute to the further concentration and consequently causes a somewhat chaotic appearance of the panel. Despite the name of the panel "polychrome", none of the animal images is depicted in three colours; mostly they are executed in single colour (black or red) or double (black and red, or black and yellow). The chronology of the examined images varies: PB1-PB4 date to the Magdalenian (Valladas et al. 2001), while the animals in red (PB5, PD1-PD3, PH1-PH2, PU1) are attributed to the pre-Magdalenian (Solutrean or earlier: Garcia-Diez et al. 2015).

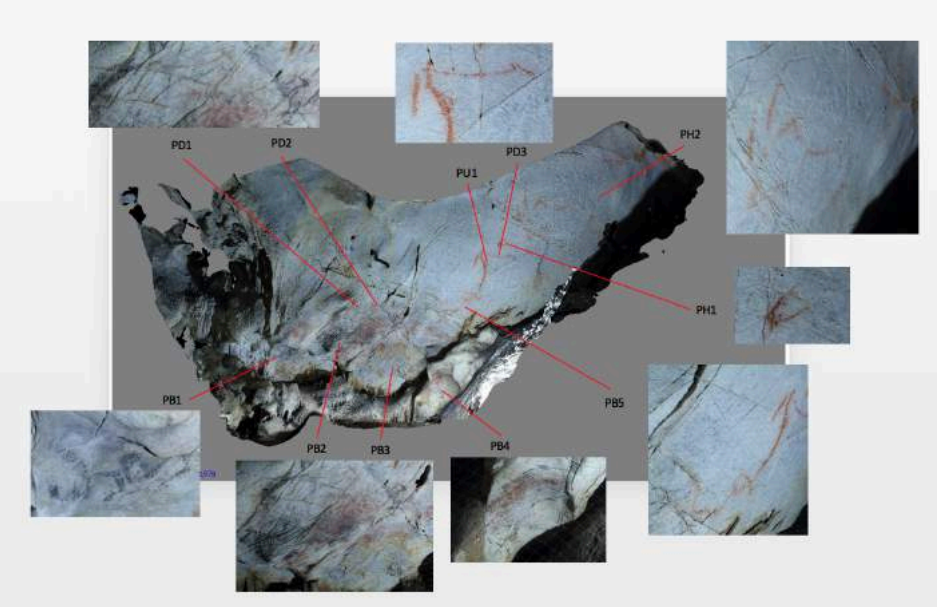

Figure 5.3: 11 images on Polychrome Panel. These images include five bison (PB1-PB5), three deer (PD1-PD3, two horses (PH1 and PH2), and one unknown quadruped animal (PU1). This panel contains the largest number of samples in this case study. The surface is smooth on the right side of the panel, while the wall severely undulates on the left.

The floor on the left part has been excavated approximately 50 cm, although the details for this excavation does not remain.

Diverticulum

Toward the south to Room A, there is an external hall called diverticulum. The region is quite broad (30m wide and 25 m long), although the ceiling (8m at the highest) gradually lowers its height as it approaches the far end of the hall. The image of an Aurochs is found on a wall of the south side. The appearance, although blurred in some parts, can be easily confirmed in naked eyes (Figure 5.4). This image is the only sample from the diverticulum and is treated as DA1 (Diverticulum Aurochs 1).

Figure 5.4: An image of Aurochs located in Diverticulum of Room A. Although the picture is somewhat blurred due to weather, the figure is visible to naked eyes. This Aurochs is treated as DA1.

The panel of hands

This is a confined hollow located at the west-end of Room A. The high ceiling of Room A lowers in the area, eventually becoming so low that adults must bend their bodies or crouch down in this area to proceed any further into the cave. The ceiling of hands is situated immediately before the entrance of the room of tectiforms and the gallery of hands. On this ceiling, a significant number of images is preserved (approx. 320: Groenen 2012). Most of them are non-figurative, but they include nine outlined bison, two engraved deer (Alcalde del Rio et al. 1911) and at least 40 hand stencils are placed on this single area (Garcia-Diez 2015). Given such a high density of graphics, the ceiling of hands is considered a crucial location of the artistic practice which took place in El Castillo. The pictures to be examined are five bison. It has been known that there are in total nine bison since the time of Alcalde del Rio et al. (1911). However, four images are hardly visible due to severe weathering even through a digital filter; among them, one vertical bison which was reported by Alcalde del Rio and his colleagues (Ibid) is completely absent. Therefore, this study focuses on the rest of the visible five images, treating them as CB1-CB5 (Ceiling Bison 1-5: see Figure 5.5). They are fixed within an approximate distance of 350 cm (from CB1 to CB5), although the length of the entire region is over 700 cm. The floor of this area was excavated, and the original level is supposed to be 30-40 cm higher than the present.

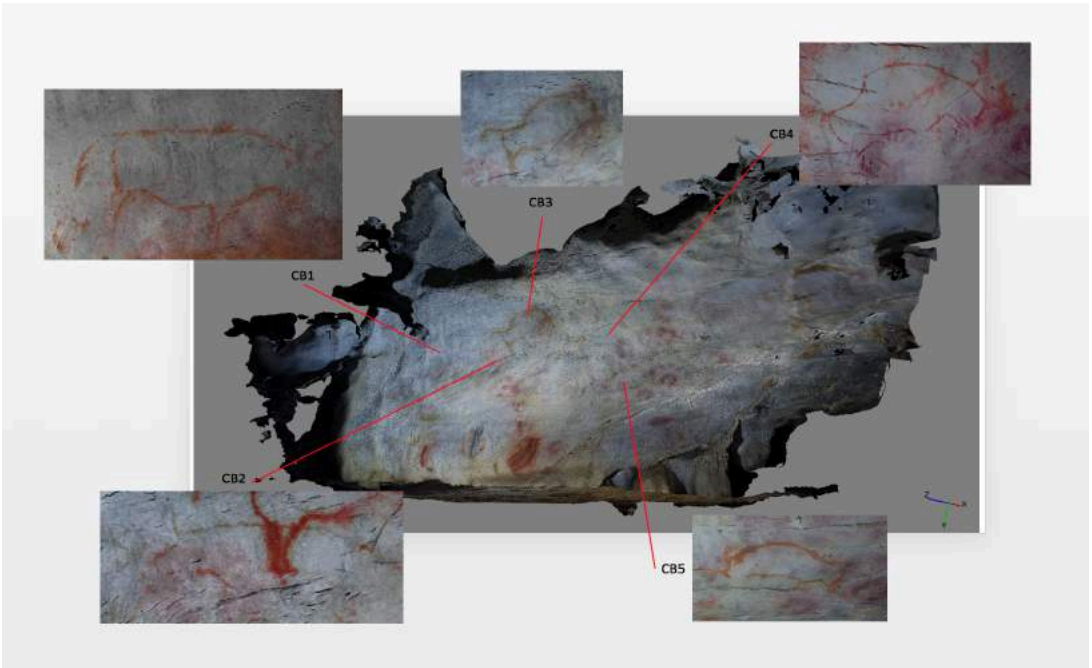

Figure 5.5: Five images on Ceiling of hands (CB1-CB5). This ceiling contains over 320 graphics and 40 hand stencils, which signifies the importance of this place for the practice of cave art in El Castillo.

The entrance of hands gallery

Proceeding further to the north from the ceiling of hands, cave visitors reach an intersection space which leads to the room of tectiforms and the gallery of hands. The location is only reachable for adults in a crouching posture as the height between the ground and ceiling is as low as 130cm. Furthermore, the shape of the ceiling occasionally forms a sharp convex, and therefore visitors continuously need to pay attention to the morphology of the ceiling so that they avoid injuries by hitting their head on the ceiling. There are three images in this intersection: two horses and a deer. They are treated as EH1-EH2 (Entrance Horse 1-2) and ED1 (Entrance Deer 1). However, these images are not fixed on a single panel but two separated walls: E-H1 is located on the wall of the north-end, whereas E-H2 and E-D1 are placed as a pair on one of the surfaces of the undulating ceiling (Figure 5.6). The latter panel is located on the halfway to the north-end from the ceiling of the hands, and the distance between EH1 and the pair of EH2-ED1are approximately 200 cm. No excavations have taken place in this area, and the ground therefore sustains its original shape which is flat.

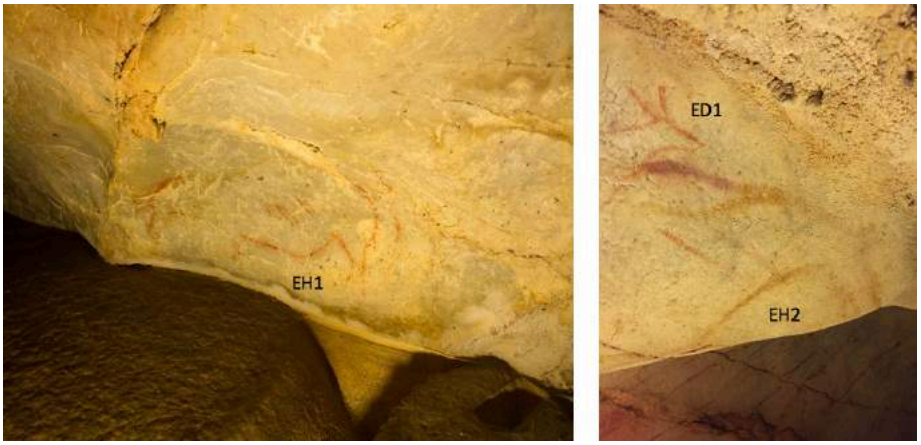

Figure 5.6: Two horses (EH1-EH2) and one deer (ED1) in Entrance of Hands Gallery. These images are fixed on different walls: EH1 is located on a wall of the north-end, whereas EH2 and ED1 are placed as a pair on an undulating ceiling. The distance between those panels is approximately 200 cm. EH1 is a complete figure, while the posterior is absent in EH2 and ED1.

Gallery of discs

Connecting Room D and Final Room, the gallery of discs is a straight, long passage with a length of approximately 75m, a width of 3m and height of 8-10m. This corridor preserves 420 images, the highest number of all of the cave's areas (Groenen 2012). The most noticeable marks are a large number of discs (or dots) on the passage's north-side wall and a picture of a mammoth at the east-end of the collider. This mammoth is to be examined in this case study (Figure

Figure 5.7: GM1, an image of a mammoth located on the wall in the west of the gallery of discs.

5.7), being treated as GM1 (Gallery Mammoth 1). The ground remains original as no excavations have been performed.

Room B

Room B is a wide hall, smaller than Room A. It is located at the centre of the cave between Room A and Room C. From this area, I selected four images to study: one anthropomorphic animal, two bison, and one unidentifiable quadruped (Figure 5.8). Those pictures are not located on a single panel but found in three different areas. As for the anthropomorph, this is considered as a hybrid image of a human and bison, widely known as the 'Man-Bison'. A cluster of large stalagmites has formed at the north of Room B, and this unrealistic creature is depicted on one of these columns. On the other hand, the figure of an unknown mammal is depicted on the south-side wall in the section. Two bison are found in a passage which connects Room B to Room C. This passage is located along a huge stalagmite wall between the two rooms, and it is considered that in the Palaeolithic time that this narrow corridor was used to travel from one room to the other (Groenen et al. 2014). Two bison are placed on the wall on the south along the passage. They are treated as BMB1 (B Man-Bison 1), BB1-BB2 (B- Bison 1-2), and BU1 (B Unknown 1). There is no trace of artificial modification on the ground around BMB1 and BU1, but the floor around BB1 andBB2 has been excavated 20-30 cm.

Figure 5.8: Four images in Room B. BMB1 is a hybrid image of human and bison. BU1 is an unknown quadruped mammal whose head is absent, and BB1 and BB2 are bison. These samples are collected from three different regions in Room B; BMB1 is located on a stalagmite pillar which forms at the north area; BU1 is placed on the wall on the south; BB1 and BB2 are fixed in the passage connecting Room B to Room C.

3D model

A 3D model was generated for each location in this case study. As for samples which are placed in the same area but on different walls, I produced a model of each wall. Consequently, nine models are reconstructed (one for Polychrome Panel, one for Ceiling of Hands, one for Gallery of Discs, one for Diverticulum, two for Entrance of Hands Gallery, and three for Room B). The total number of photographic data which was used for the reconstruction varies by model: 558 for Polychrome panel, 373 for

Ceiling of hands, 39 for Gallery of disks, 47 for Diverticulum, 66 for Entrance of Hands Gallery (EH1), 81 for Entrance of Hands Gallery (EH2 and ED1), 83 for Room B (BB1 and BB2), 81 for Room B (BMB1), and 58 for Room B (BU1). Figure 5.9 illustrates generated models and camera positions. As artificial electric lights were installed in some locations (Polychrome Panel, Ceiling of Hands, and Room B) which generates enough visibility for the photoshoot, I utilised those on-site lights. Otherwise, a flashlight was used.

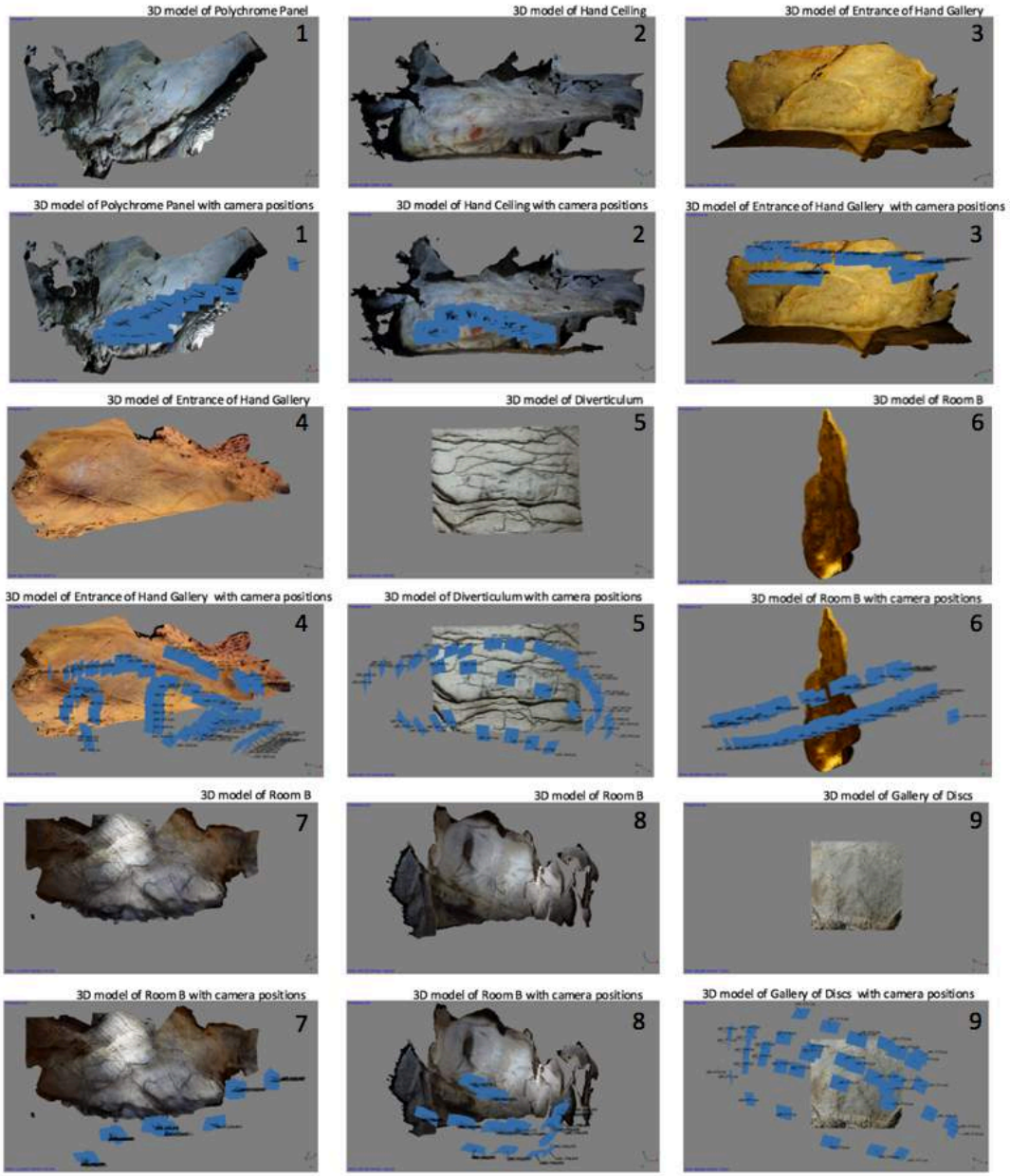

Figure 5.9: Nine reconstructed 3D models. Blue squares represent camera positions. The total number of photographic data for the reconstruction of each model is following: 558 for Polychrome panel (1), 373 for Ceiling of hands (2), 66 for Entrance of hands gallery (3: EH1), 81 for Entrance of hands gallery (4: EH2 and ED1), 47 for Diverticulum (5), 81 for Room B (6: BMB1), 83 for Room B (7: BB1 and BB2), and 58 for Room B (8: BU1), and 39 for Gallery of disks (9).

Generated models were scaled and assessed for their accuracy. Images which were arbitrarily selected to scale models are PB3, CB3, EH1, EH2, BMB1, BU1, BB1, GM1, and DA1. A physical measurement of these images was input to the same image on Meshlab, a 3D modeling software, to generate a scaled mode. As for the models with a single image, such as EH1, BMB1, BU1, GM1 and DA1, the physical measurement of the width of these images were used. The physical measurement of the width of BU1 was hard to obtain in the fieldwork because the ventral line does not appear clear, and therefore the actual measurement of the vertical length of the major convex part on the thigh of the animal was used to compare virtual measurement of the same part. The result is shown in Table 5.1 below.

Consequently, the difference between actual and virtual measurements for any images are within the range of ± 2.5 cm. As the result of the other caves, this range seems to be acceptable. Thus, the generated nine models are accurate enough to be used for pictorial analysis in this case study.

Motifs	Actual measurements (cm)	Virtual measurements (cm)	Difference (cm)	Difference (%)
PB1 (Bison)	60	59.42	0.58	0.1
PB2 (Bison)	123	122.87	0.13	0.1
PD1 (Deer)	51	50.47	0.53	1
PD2 (Deer)	43	43.92	0.92	2
PB3 (Bison)	116	116	0	0
PB4 (Bison)	56	54.79	1.11	2
PB5 (Bison)	90	92.02	2.02	2
PU1 (Unknown)	18	17.23	0.77	4
PD3 (Deer)	60	62.03	2.03	3
PH1 (Horse)	20	18.80	1.2	6
PH2 (Horse)	188	188.41	0.41	0.2
CB1 (Bison)	72	72.67	0.67	0.9
CB2 (Bison)	50	50.39	0.39	0.8
CB3 (Bison)	78	78	0	0
CB4 (Bison)	69	71.02	2.02	3
CB5 (Bison)	60	62.37	2.37	4
EH1 (Horse)	107 33 (width)	107 31.76 (width)	0 1.24	0 3
EH2 (Horse)	61	61	0	0
ED1 (Deer)	23	23.31	0.31	1
BMB1 (Man-Bison)	75 40 (width)	75 38.12(width)	0 1.88	0 5
BU1 (Unknown)	60 30 (width)	60 32.1 (width)	0 2.1	0 7
BB1 (Bison)	99	99	0	0
BB2 (Bison)	68	66.5	1.5	2
GM1 (Mammoth)	38 35 (width)	38 34.93 (width)	0 0.07	0 0.2
DA1 (Aurochs)	46 16 (width)	46 15.6 (width)	0 0.4	0 3

Table 5.1: Comparisons between physical measurements and virtual measurements. The error gap for all images is within the range of ± 2.5 cm. This fact indicates the high accuracy of the reconstructed 3D models.

Simulation

As well as for the other caves (Covalanas and El Pendo), I performed a simulation for this case study aiming to understand exactly how topography distorts images. The range of the rotation is summarised in Table 5.2. Most of the pictures on the Polychrome Panel fall into a narrow range. This is because a steep slope lies on the right side of the panel, which prevents viewers from moving freely around it. Also, each image is provided with a fixed angle in the X-axis. A fixed angle is determined based on an image's position; images on a higher position tend to be given a larger angle. The measurement of the height of all images obtained from the fieldwork was applied to the determination of the angle. In areas where the previous excavations modified their original floor, a fixed angle is decided based on the assumed original level of the ground. These settings were also applied to the 2D simulation.

Motifs	Horizontal rotation (Y-axis)	Fixed angle (X-axis)
PB1 (Bison)	70° (left limit: 0°, front: 0°, right limit: 70°)	0°
PB2 (Bison)	140° (-70°, 0°, 70°)	0°
PD1 (Deer)	130° (-60°, 0°, 70°)	0°
PD2 (Deer)	130° (-60°, 0°, 70°)	0°
PB3 (Bison)	60° (-60°, 0°, 0°)	0°
PB4 (Bison)	100° (-60°, 0°, 40°)	0°
PB5 (Bison)	70° (-70°, 0°, 0°)	10°
PU1 (Unknown)	60° (-80°, -20°, -20°)	20°
PD3 (Deer)	60° (-80°, -20°, -20°)	20°
PH1 (Horse)	60° (-80°, -20°, -20°)	20°
PH2 (Horse)	50° (-80°, -30°, -30°)	30°
CB1 (Bison)	140° (-70°, 0°, 70°)	0°
CB2 (Bison)	150° (-70°, 0°, 80°)	0°
CB3 (Bison)	150° (-80°, 0°, 70°)	10°
CB4 (Bison)	140° (-60°, 0°, 80°)	20°
CB5 (Bison)	140° (-70°, 0°, 70°)	20°
EH1 (Horse)	150° (-70°, 0°, 80°0	0°
EH2 (Horse)	140° (-70°, 0°, 70°)	20°
ED1 (Deer)	140° (-70°, 0°, 70°)	20°
RMB1 (Man-Bison)	150° (-80°, 0°, 70°)	0°
RU1 (Unknown)	80° (-40°, 0°, 40°)	20°
RB1 (Bison)	130° (-60°, 0°, 70°)	10°
RB2 (Bison)	130° (-60°, 0°, 70°)	10°
GM1 (Mammoth)	140° (-70°, 0°, 70°)	10°
DA1 (Aurochs)	160° (-80°, 0°, 80°)	20°

Table 5.2: Angle ranges of horizontal rotation for each image. Horizontal rotation simulates how the appearance of images changes when the viewer moves side to side. On the other hand, the fixed angle represents a degree at which a viewer looks up the image according to the height of the image. These ranges are decided based on the actual environmental setting.

Regarding BB1 and BB2, they are given the fixed angle of 10° despite their positioning at a low height (approximately 80 and 100 cm). That is due to the actual position where viewers stand; in fact, the nearest floor to these images is not on the passage itself but an elevated area which forms along the passage. This floor is over one meter higher than the passage where viewers, and therefore, the two bison must be looked up at from the passage. Similarly, fixed angles for CB4 and CB5, EH1 and ED1 are 20° even though their position is not high. This is because these image are fixed on a low ceiling under which one needs to move in a crouching posture, and therefore, viewers must look up at those images.

5.3 Analysis of Images

Bison (PB1)

General description

An outline bison, facing left (Figure 5.10). All body parts are drawn in a robust black line. The body of PB1 is distinctively different between its posterior and anterior. As for the posterior area, the appearance is mostly visible due to its well-preserved condition. The thick hind legs are dynamically bent at their hock, and the shape creates an impression as if the bison is powerfully kicking the ground. Hooves seem also be depicted. A long tail is present: because it is also dynamically depicted (wavy), this bison appears to wave its tail vigorously. The contour of the back legs partly extends to the inside of the image. This treatment achieves perspective; the left leg sets behind, while the other is on the front. Regarding the anterior body, the outline is somewhat ambiguous. Moreover, the image itself is depicted abstractly. Details of the face (eyes, nose and mouth) are missing. The front legs are also depicted vaguely. Above all, the most salient feature of PB1 is its unnaturalistic expression: one of the frontal limbs extends ahead further unnaturally and then turns its direction upwards; this unrealistically deformed leg disturbs the proportion of the whole body. PB1 is located on the leftmost of Polychrome panel. The length is 60 cm, and height is about 70 cm from the nearest floor.

Figure 5.10: PB1, outline bison facing left. While the image is clear in its posterior area, its anterior is somewhat ambiguous. PB1 contains an unnatural depiction: one of its frontal leg abnormally long and extends forward.

Integration of natural lines

The wall contains a number of natural grooves. Moreover, the noticeably undulating topography creates edges/ridges. PB1 is integrated with some of those natural lines in its dorsal line, buttock and tail. Firstly, a notable integration is found in the dorsal line. As the half of this image (posterior side) is located immediately beneath a sharp convexity, a dorsal line is drawn along the edge of this convex surface (see Figure 5.11). The other integrated sections are the bottom of the buttock and the tip of the tail. They are outlined along with grooves.

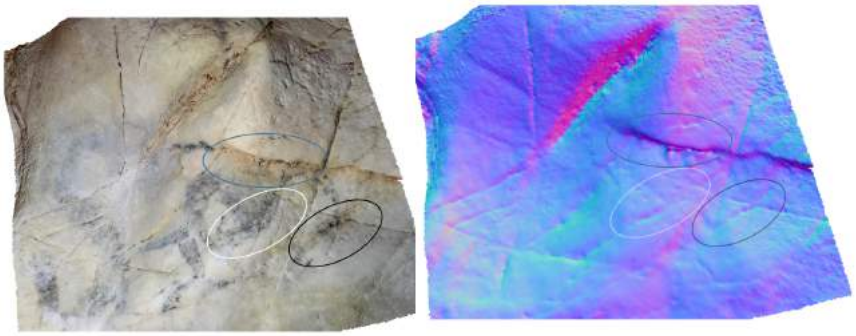

Figure 5.11: Examples of integration. The posterior dorsal line overlaps on the edge of a convex surface (see the blue circle). The buttock (see the white circle) and the tip of the tail (see the black circle) are also integrated with grooves.

Topographic condition

Overall, two topographic features characterise the wall behind PB1. There is a bowl-shaped concavity on the left side and a hill-like convex on the right. This bison is located on such an undulating medium, and therefore the elevation level differs by region; the extension on the frontal limb are excluded from the analysis. The total depth is 73.6mm (the model is at 1/40 scale: Figure 5.12). The tip of the frontal leg corresponds to the highest point, while a part of the central shoulder and the tail to the lowest. All body parts are defined at elevation levels at high (0.1-22.1mm, medium: 22.2-47.8mm, and low: 47.9-73.6mm), and there are no additional levels for this image.

Figure 5.12: PB1 (1/40 scale) seen from the vertical position. The highest elevation is found on the tip of the frontal leg, while the lowest is on the central shoulder and tail.

The surface is firstly detected at the tip of the frontal limb, and detection continues upward from this region. After a depth of 14.7mm, the hind limbs start passing the cross-section layer. As the detected area extends, the major part of both frontal and back legs are detected by 22.1mm (see Figure 5.13, 1-3). There is also a detected area on the croup; however, the extent is limited. In the medium level, the layer

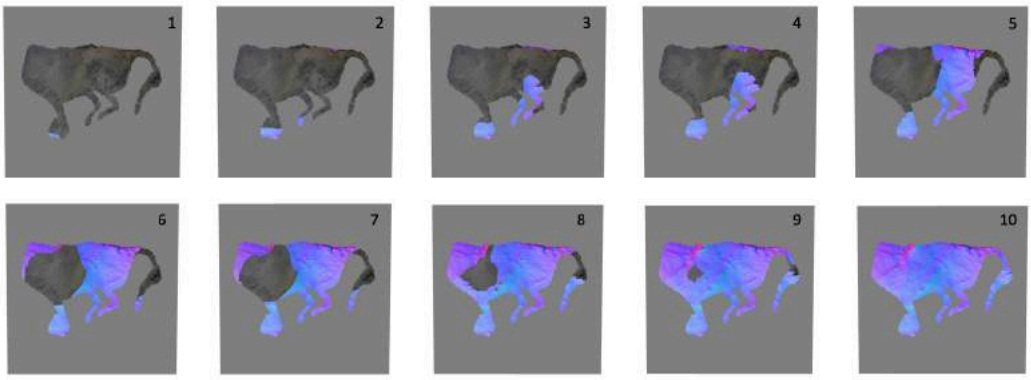

Figure 5.13: These ten images illustrate the depth of PB1. When the cross-section layer passes the surface of PB1, the colour of the surface changes; dark regions denote lower elevation than coloured parts. Images 1-3 are for 0.1mm - 22.1mm, 4-6 for 22.2mm - 47.8mm, and 7-10 for 47.9mm - 73.6mm.

captures the entire thigh (22.2-47.8mm: 4-6). The topography is also detected on the left edge of the head and the tip of the tail; however, the extent is insufficient to define their elevation level. The last phase (47.9-73.6mm: 7-10) is the low-level elevation: remained body parts are the head, whole neck-shoulder and whole mid-torso, and tail. The detection continues towards the centre of the anterior and a part of the tail as their elevation is the deepest. These areas finally pass the layer at a depth of 73.6mm.

Distortion on images (horizontal rotation, x0°, y0° to y70°)

Although the viewing position can only be taken to the right from the front, the appearance of PB1 is noticeably affected by its topographic condition. As noted above, the topography of this image consists of a concave and convex feature, and this set of the topography causes a noticeable contraction of PB1's body. As the viewing angle increases, the convex on the thigh gradually overlaps the concaved middle and shoulder, and finally, the body appears much shorter than the image on the 2D surface (Figure 5.14). In turn, the contracted mid-torso stretches to a remarkable degree as the viewing

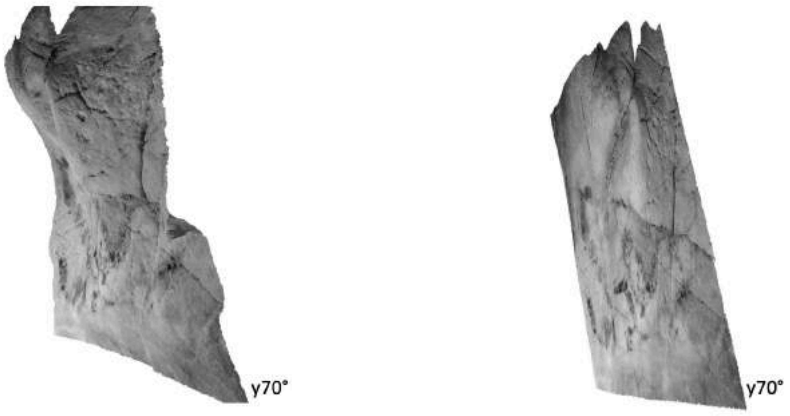

Figure 5.14: PB1 on the 3D surface (left) and 2D surface (right) seen from y70°. The length of the mid-torso on the 3D wall is significantly shortened because the convex thigh hides the part. Meanwhile, such deformation is absent in the 2D simulation.

position moves to the front. Apart from the contraction on the main body, no other distortion is confirmed. Despite that the curved tail is located on a convexity, the result is more or less the same between the 3D and 2D simulation.

Bison (PB2)

General description

An image of bison facing to the upper right (Figure 5.15). The whole body except the tail is depicted in black, although it is partly ambiguous due to weathering. Especially, the decay on the front neck and dorsal side is severe. However, the curve of the dorsal line is still visible, which allows viewers to grasp an overall figure of PB2; the image seems as if it rolls its body. The two hind legs and one foreleg are provided, with the hoof on the top of each limb. The head remains in good condition. The most significant feature of this image is an overlap with five other images (three hand stencils, PD1 and PD2). Such a high concentration of pictures makes PB2 appear considerably chaotic. Among these superimposed pictures, PB2 is the youngest (hand stencils are at least Gravettian, and two deer is pre-Magdalenian: see Garcia-Diez et al. 2015, while the bison is Magdalenian: see Valladas et al. 2001). That is the artist of PB2 intentionally depicted it over the hands and the two deer. The length of the image is 123 cm. Although it is located at a height of about 100 cm from the nearest floor, this floor is excavated about 50 cm.

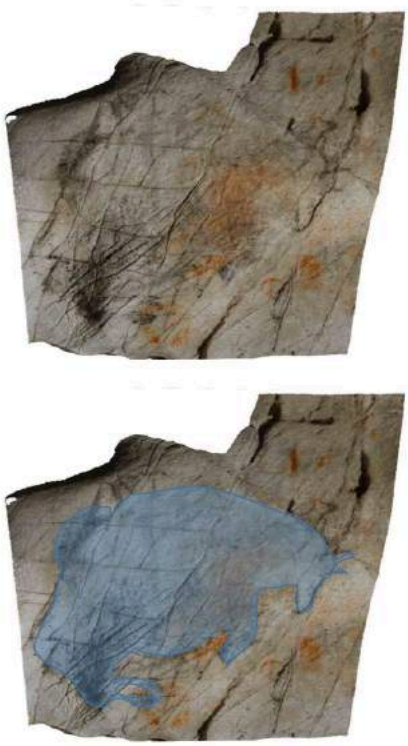

Figure 5.15: PB2, image of bison facing upper right. Despite that the face and limbs are relatively well conserved, most of the body parts appear unclear. Five images (three hand-stencils and two deer) are superimposed on PB2. Such a high density of images generates a chaotic impression.

Integration of natural lines

A significant number of natural lines are located on this surface. Although most of them are irrelevant to PB2, the contour of its head, frontal neck and dorsal line is integrated

with them. The most conspicuous integration is found in the head. The wall rises in the region where the head is depicted, and the head is outlined from its top to the mouth along with an edge of the convex surface (Figure 5.16). Furthermore, on the left of the mouth, there is a short but sharp ridge which in turn extends upper right. This ridge takes over an edge line and corresponds to the under-neck. Regarding the dorsal line, the contour is not fully substituted by the natural line, but integration occurs at three places intermittently. Firstly, the edge line which outlines the head further extends to the upper left, and this edge is utilised for the cervical dorsal. Next, two rounded outlines as two humps are depicted in the middle dorsal area, but one of the hump (on the right) is outlined along with a groove. Finally, the contour of the rump is drawn along the deep groove in that place.

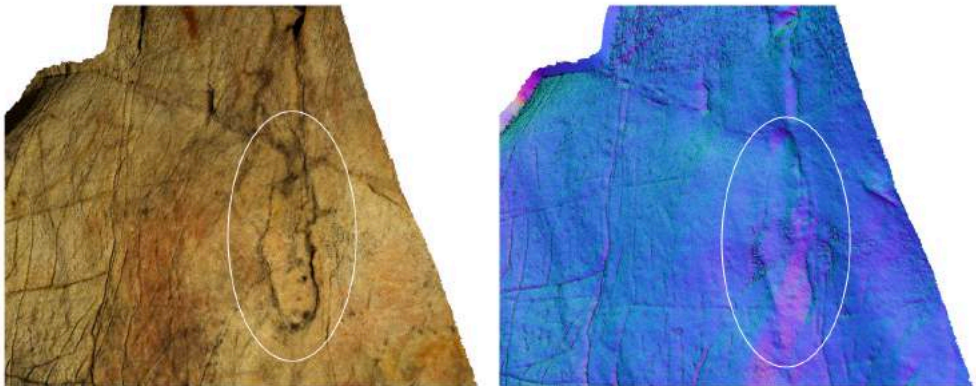

Figure 5.16: Examples of integration. The head is outlined by an edge (from its top to the muzzle) and by a ridge (from the muzzle to the jaw).

Topographic condition

This wall undulates and generates an elevational gap between regions. Particularly, convex areas, which are respectively located in the posterior dorsal, the posterior ventral and the head, is responsible for this waving topography; above all, the convex surface on the posterior ventral is noticeable. The total depth is approximately 116 mm (the model is at 1/10 scale: Figure 5.17). A part of the ventral thigh corresponds to the highest point, while the tip of the muzzle to the lowest. The range within which the elevation level of most body parts is defined is limited between 31mm and 77.3mm (high: 31-46.4mm, medium: 46.5-61.9mm, and low: 62-77.3mm). Although there are ranges outside of this (0.1-30.9mm and 77.4-116mm), none of the body parts is included in the higher elevation range, but the deepest range contains part of the hind limbs. Therefore, there is an extra-low level for this image.

Figure 5.17: PB2 (1/10 scale) seen from the vertical position. The highest elevation is found on the ventral thigh, while the lowest is on the tip of the muzzle.

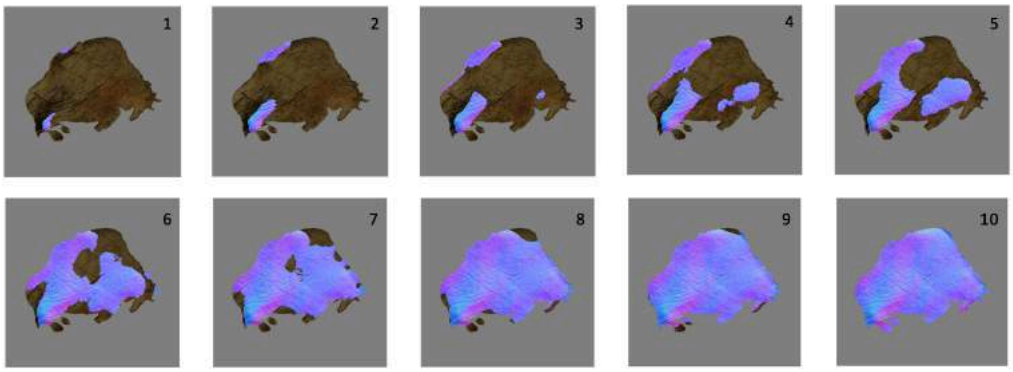

Figure 5.18: These ten images illustrate the depth of PB2. When the cross-section layer passes the surface of PB2, the colour of the surface changes; dark regions denote lower elevation than coloured parts. Images 1 and 2 are for 0.1mm - 30.9mm, 3 and 4 for 31mm and 46.4mm, 5 and 6 for 46.5mm - 61.9mm, 7 and 8 for 62mm - 77.3mm, and 9 and 10 for 77.4mm - 116mm.

The surface is first detected at the ventral thigh, and secondly at the dorsal mid-torso. Detection continues based on these areas between 0.1mm and 30.9mm, but the extent is considerably limited (see Figure 5.18, 1-2). As for the high level, the coloured areas extend; nevertheless, the extent is limited as only the ventral thigh belongs to this level (31-46.4mm: 3-4). Meanwhile, the detection also starts on the ventral neck-shoulder. As the cross-section layer proceeds, the detected regions noticeably expand during the next phase; the dorsal thigh, the dorsal-ventral mid-torso and central-ventral neck-shoulder are assessed as the medium elevation (46.5-61.9mm: 5-6). The head, dorsal neck-shoulder, central mid-torso, central thigh, and frontal leg are located in the low elevation level. (62-77.3mm: 7-8). However, the periphery of these low areas remain undetected as well as the hind limb, and they gradually pass the layer after 57.4mm, and all topography is completely assessed by 86mm (9-10).

Distortion on images (horizontal rotation, x0°, y-70° to y70°)

Despite the dynamic topography, a remarkable distortion is absent in PB2. In the 3D simulation, the appearance of the head and mid-torso seems to change as the viewing point shifts side to side; the face changes its direction, and the mid-torso is contracted. However, those distortions are also confirmed in the 2D simulation. Therefore, the cause of the distortion is simply the perspective, not topographic intervention. However, a clear distortion occurs in the hind limbs. As the viewing point moves to the left, the sizeable convex surface on the ventral thigh gradually hides the legs. Finally, these limbs go completely unseen at y-70° (Figure 5.19). Such a deformation does not occur in the image on a 2D surface. This distortion most likely appears within the range between y-70° and y-50°.

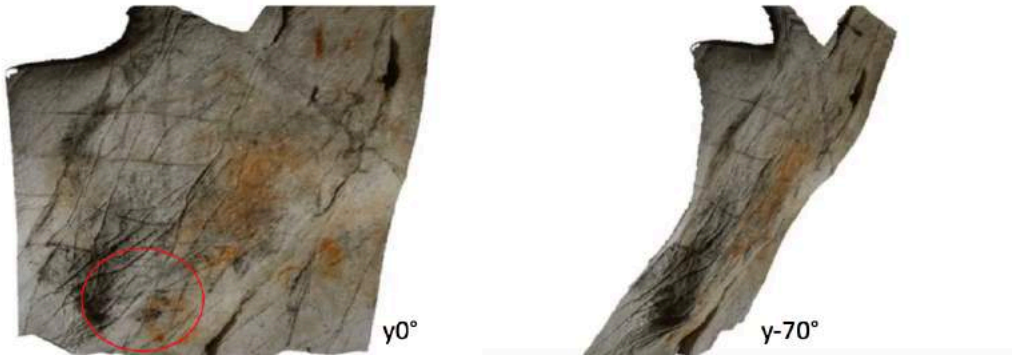

Figure 5.19: PB2 seen from y0°(left) and y-70° (right). While the hind limbs are visible when PB2 is viewed from y0° (the legs are in the red circle), the convex ventral thigh hides the makes the lim```bs unseen at y70°.

Bison (PB3)

General description

An image of bison facing to the upper right (Figure 5.20). Located on the lower right of PB2 (approx. 20cm away), PB3 is provided with the entire body except for the hind leg. However, due to the severe conservation condition, it is difficult for viewers to grasp the whole figure. Details of the head (eyes, nose, mouth and ears) are not depicted, whereas the boundary between the tail and the thigh is clearly visible. The contour on the anterior side appear to be connected by dots. The yellow colour, although weathered and therefore being unclear, are left on the torso, neck, and head. This colouring indicates that this bison was once depicted vividly in black and yellow. Two red hand stencils are overlapped by the mid-dorsal. Additionally, there is a hand stencil and a geometric sign in red on the same section. This image is 116 cm in length and located at a height of 70 cm from the nearest floor.

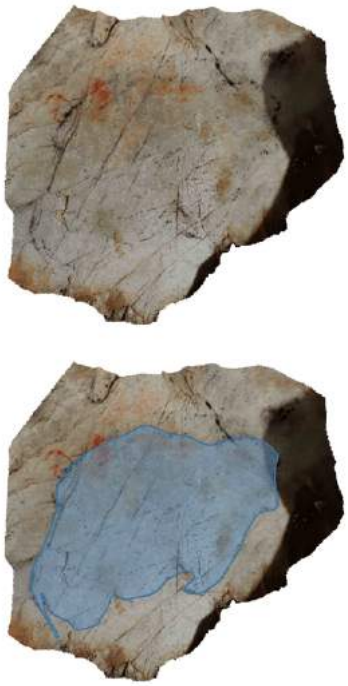

Figure 5.20: PB3, image of bison facing upper right (digital filter is applied). Most of the body parts are unclear due to severe decay. The yellow colour is visible on the anterior body. Also, a hand stencil and a geometric sign are superposed on the dorsal mid-torso.

Integration of natural lines

There are countless grooves, edges and ridges on this wall. These natural lines are distributed over the entire body of PB3, and integration is found in the dorsal line. In this case, the integration does not occur based on a single natural line but involves adjacent two different lines. At first, immediately on the left to the bison, the surface rises, and an edge forms along this convex. A part of the dorsal is outlined along this edge at its middle section (indicated in the black circle: see Figure 5.21). This edge then continues upwards and intersects with grooves extending from the right. A part of the cervical dorsal is outlined by a zigzag groove (indicated in the white circle: Figure 5.21).

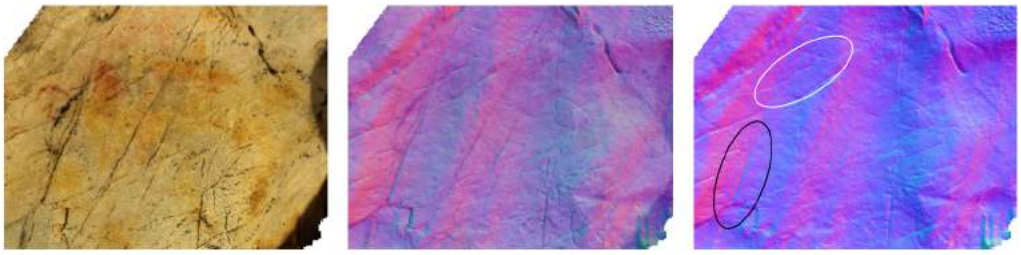

Figure 5.21: Examples of integration in PB3. The dorsal is integrated with an edge and a groove. On the left to the bison, the surface elevates and creates an edge which is partially used for the posterior dorsal (indicated in the black circle). Meanwhile, a zigzag groove is used for a part of the anterior dorsal line (shown in the white circle).

Topographic condition

PB3 is noticeably undulating. Two convex surfaces are located on the image, specifically on the ventral neck-shoulder and on the central mid-torso. As a result, the area between those elevated regions appears as a concavity. The total depth is approximately 105mm (the model is at 1/10 scale: Figure 5.22). A part of the ventral neck-shoulder corresponds to the highest point, while a part of the central neck-shoulder to the lowest. All body parts are defined their elevation level within the provided range (high:0.1-32.8mm, medium:32.9-65.6mm, and low: 65.7-105mm). Accordingly, there are no extra elevation levels in PB3.

Figure 5.22: PB3 (1/10 scale) seen from the vertical position. The highest elevation is found on the ventral neck-shoulder, while the lowest is on the central neck-shoulder.

The surface is firstly detected at a part of the ventral neck-shoulder. Detection continues based on this area, covering more than half of the region by the depth of 32.8mm (see Figure 5.23, 1-3). At the same time, the short hind limb is also defined as the high elevation level. A further detection occurs during the next phase: as well as the

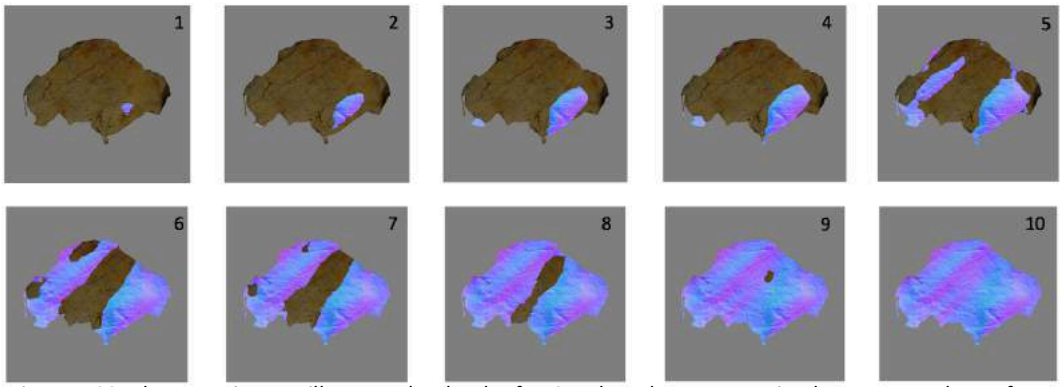

Figure 5.23: These ten images illustrate the depth of PB3. When the cross-section layer passes the surface of PB3, the colour of the surface changes; dark regions denote lower elevation than coloured parts. Images 1-3 are for 0.1mm - 32.8mm, 4-6 for 32.9 - 65.6mm, and 7-10 for 65.7mm - 105mm.

shoulder and the back leg, the surface passes the cross-sectional layer at multiple regions (the tail, the dorsal thigh, the dorsal-central middle, the dorsal neck, and the head), and detected areas expand from these sections. Consequently, by 65.6mm, the head, the central neck-shoulder, the front limb, the dorsal mid-torso, the central-ventral thigh, and the tail are assessed as the medium level (4-6). As the layer proceeds further, the dorsal thigh and the dorsal mid-torso are detected completely by 78.6mm (7), and thus central-ventral middle body, and the dorsal neck is left undetected. This swathe of undetected concave area gradually narrows and is finally defined as the low level (8-10).

Distortion on images (horizontal rotation, x0°, y-60° to y0°)

Because of the environmental restriction, the range of the viewing angle is considerably limited; viewers only can move to the left from the front. Nevertheless, PB3 is deformed by its topographic condition. As the viewing angle decreases, the image shows disproportion mainly in the middle of the dorsal side and the head. Regarding the middle part, the dorsal area appears moving upward, shortening its outline. This is because the convex surface on the middle section partly hides the area of the dorsal mid-torso when viewers see the image from the left. At this time, the thigh appears not distorted as it sustains a certain proportion due to the convex in the section even when the viewpoint changes (Figure 5.24). Therefore, the distortion on the middle dorsal is highlighted and becomes further perceptible because of that stable thigh. As for the head, the part appears noticeably smaller, seen from the left. This deformation takes place to a greater extent than in the 2D simulation. What is responsible for this distortion is the convex on the shoulder which hides the head.

Figure 5.24: PB3 seen from y0°(left) and y-60° (right). Distortion occurs on the dorsal mid-torso and head. As for the dorsal mid-torso, when viewers see the image from the left, the area appears moving upward, shortening its outline. This is because the convex surface on the body hides the mid-torso. Similarly, the distortion on the head is caused by the convex neck-shoulder: as the head is concealed by the neck-shoulder, the part appears contracted at y-60°.

Bison (PB4)

General description

An image of bison facing lower left (Figure 5.25). While its outline is drawn in black, the body (i.e. interior) of PB4 is painted in red. Since the contour has partially disappeared due to decay, it is not easy to confirm the whole figure of the image; Especially, it is hard to confirm the contours of the head, ventral and buttock. On the contrary, the limbs and the dorsal line are still visible. PB4 is provided all the body parts except the tail. Unlike the other images on Polychrome panel, this image is not located on the same wall; PB4 is drawn on an independent rock that forms immediately in front of Polychrome panel. Nevertheless, this bison shares the same artistic features and the chronology with the previous three bison. The length of the image is 60 cm, and it is located on a height of approximately 10 cm from the nearest floor.

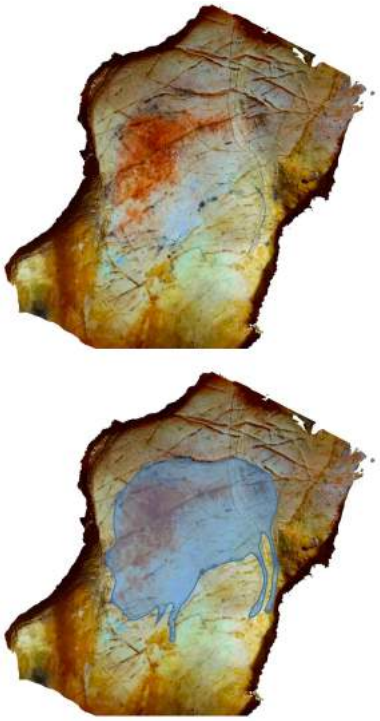

Figure 5.25: PB4, image of bison facing lower left (digital filter is applied). The outline of most of the body parts is unclear due to severe decay. However, the red colour is visible on the anterior body. PB4 is located on a rock in front of the polychrome panel.

The integration of natural lines

There are countless grooves on this wall. Moreover, numerous edge lines are also confirmed. PB4 is integrated with these natural lines in most of its body parts. Especially, the clearest use of natural lines is found in the dorsal line; in fact, the dorsal has two different ways of integration between the posterior and anterior. Concerning the posterior body, the wall slightly rises and creates an edge, and a groove forms along the edge. The posterior dorsal line is integrated with this groove; this integration partly includes the buttock too (Figure 5.26). Meanwhile, the cervical dorsal is located immediately under the upper edge of the rock. The cervical line, together with the head, is executed along with this edge. Apart from the dorsal line, integration is found in the ventral line. Although the ventral line is somewhat blurred, a thin groove is used for outlining the contour of the belly. Furthermore, in the region where the hind limbs are fixed, the wall steeply rises and creates a ridge line, and one of the legs is drawn along the ridge. Thus this image uses natural lines in almost all sections of its body.

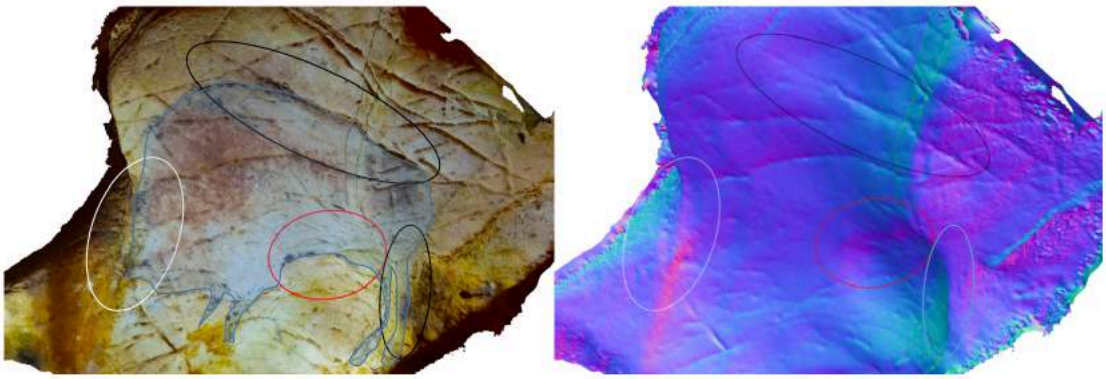

Figure 5.26: Examples of integration in PB4. Natural lines are utilised for the outline in five sections: grooves are used for the posterior dorsal, buttock and ventral, edges are used for the cervical dorsal and head. Also, a ridge is integrated into the hind limb.

Topographic condition

The rock surface is a large bowl-shaped concavity and its elevation significantly rises at both edges, and this is where the almost entire body of PB4 is placed. Therefore, the mid-torso corresponds to the bottom of the concaved wall. The total depth is approximately 280mm (the model is at 1/30 scale: Figure 5.27). The tip of the hind limbs corresponds to the highest point, while the central mid-torso to the lowest. The range within which most of the body parts are defined their elevation level is limited between 89.2mm and 280mm (high: 89.2-152.7mm, medium: 152.8-216.4mm,

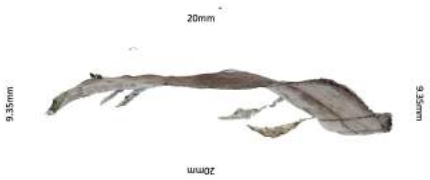

Figure 5.27: PB4 (1/30 scale) seen from the vertical position. The highest elevation is found on the hind limbs, while the lowest is on the central mid-torso.

and low: 216.5-280mm). There is a body part whose elevation level is assessed within the range between 0.1mm and 89.1mm, and this range is treated as the extra high.

The surface is first detected at the tip of the right-hind leg. The detected area continues only on this side of the leg until 50.9mm, but then the detection also begins on the other side of the hind leg. The cross-section layer touches the major area of the hind legs by 89.1mm (see Figure 5.28, 1-3); the hind limbs are therefore defined as the extra high. At this depth, a part of the central thigh also begins detected as the right edge of the overall concave forms as a sharp convex. During the next phase, the topography is detected based on this convex. The highlighted area extends between 89.2-152.7mm, and most of the central-ventral thigh are included in this region (4-6). Simultaneously, the detection starts on the left edge of the image. As the layer proceeds in the medium level, the detected surface expands inwards from both sides, but its extent is somewhat limited. The head, the frontal limbs, and the ventral thigh are located on this elevation level (152.8-216.4mm: 7-9). Thus, the entire neck-shoulder and mid-torso remain undetected, meaning that they are defined as the low elevation level. Nevertheless, an elevation gap is visible among these body parts, especially elevation is higher on the ventral than the dorsal; the ventral side is fully detected by 254.5mm, while the dorsal region is still undetected. Finally, the dorsal body passes the layer at a depth of 280mm (10-12).

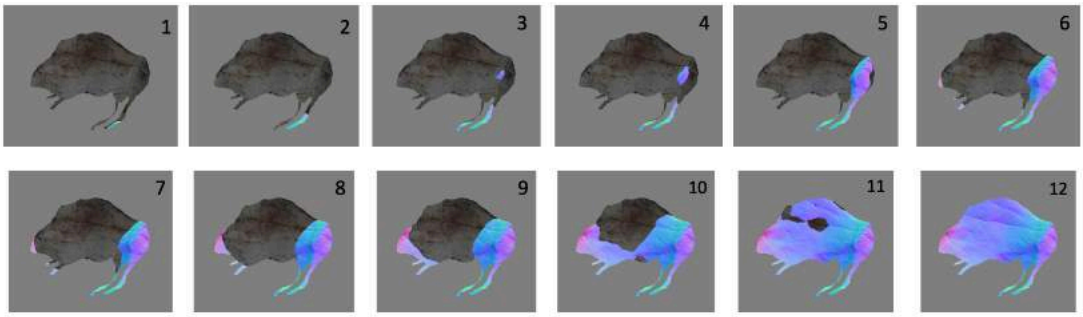

Figure 5.28: These 12 images illustrate the depth of PB4. When the cross-section layer passes the surface of PB4, the colour of the surface changes; dark regions denote lower elevation than coloured parts. Images 1-3 are for 0.1mm - 89.1mm, 4-6 for 89.2mm - 152.7mm, 7-9 for 152.8mm - 216.4mm, and 10-12 for 216.5mm - 280mm.

Distortion on images (horizontal rotation, x0°, y-60° to y40°)

PB4 constantly appears distorted by the topography. As distortion occurs almost in the entire body, the bison never has a fixed shape. Above all, the thigh is deformed most remarkably. The body section is located on a highly elevated surface, and the edge of that convexity become the outline of the buttock when the image is seen from left. At this time, the right edge of the thigh goes completely unseen (Figure 5.29); however, as soon as the viewing position moves to the right, the hidden area again appears in sight, and in turn, the sculptural quality of the thigh is highlighted. The appearance is

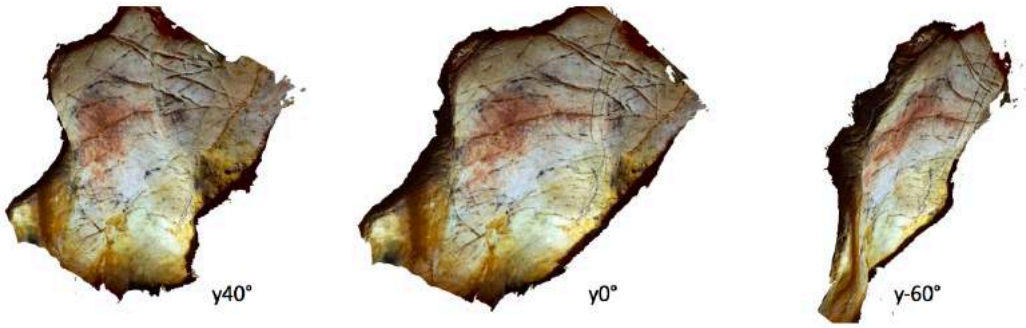

Figure 5.29PB4 seen from y40°(left), y0° (centre), and y-60° (right). Distortion occurs on multiple body parts: The thigh, hind limbs, mid-torso, neck-shoulder, and head. The convex posterior distorts the thigh and hind limbs; this convex hides the buttock area once PB4 is viewed from the left (y-60°), while two hind legs partly overlap each other viewed from the right. The mid-torso, neck-shoulder and head are located on outer-edges of overall concave, and these parts are also largely distorted by the topography.

significantly different between the images seen from left and right. Such a dissimilarity is not detected in the 2D simulation.

In addition to the thigh, the distortion on rear legs is also not ignorable. Viewers can see from the left that there is space between these limbs. However, that space gradually disappears as the viewing point moves to the right, and finally, these limbs appear almost overlapped (see figure 5.29). This is because the right-hind limb is depicted on the edge of the convex and this edge hides the space once the image is seen from the right. Simultaneously, the orientation of the other hind leg appears changing as it is fixed on a concave surface. The distortion on the posterior takes place within the full range of the viewing angle.

The unique topography of PB4 causes further deformation. As was mentioned earlier, the head, neck-shoulder, and the mid-torso are located on a bowl-like concave. This setting generates the unusual movement on these body part. For instance, the top of the dorsal area appears moving forward and backward (between y-60° and y-40°); the mid-torso contracts to a significant degree (between y-60° and y-40°); and the head and the neck appears enlarged (between y-60° and y-30°). These deformations are not confirmed if the image is depicted on a 2D medium.

Bison (PB5)

General description

An outline bison, fixed vertically and facing downward (Figure 5.30). The contour is drawn in red. The posterior body is missing. The face is depicted in detail which contains the eye, nose, mouth, and horn. The condition of the image is remarkably good. Above all, the red dorsal line remains vivid. The upper end of the dorsal line is shared with a contour of the face of an unknown herbivore (PU1). Moreover, the dorsal line crosses the dorsal line of PD3 as the buttock of PD3 is superimposed on PB5. The total length of the depicted part is 90 cm (from the mouth to the upper end of the dorsal line). It is fixed at a height of approx.180 cm from the floor where viewers can stand.

Figure 5.30: PB5, outline bison. This bison is incomplete as only limited sections (the head, cervical dorsal, and frontal) are provided. PB5 contains superimposition with two other images (PU1 and PD3) on its dorsal middle area.

Integration of natural lines

This wall contains a number of grooves and ridges. Especially numerous thin grooves run beneath PB5's chest and face, but nothing is integrated into their contours. However, PB5 is an image with conspicuous dynamic integrations. Groenen (2007) argues that this bison acquires a new body due to a ridge and a groove which depict the dorsal and ventral line respectively. As for the dorsal line, the red outline is drawn along a ridge. On the dorsal side, the wall surface rises, forming another ridge which extends toward the top of the panel. The ridge integrated into the dorsal line merges into this peak line, enlarging the body of PB5 (indicated by the red line: see Figure 5.31). About the ventral line, the red contour disappears at the lower jaw; however, a groove takes over the outline. At a point, this groove turns 90 degrees and further continues upward. Since the groove parallels to the dorsal line, it appears that this bison achieves an extended body (indicated by the blue line: Figure 5.31).

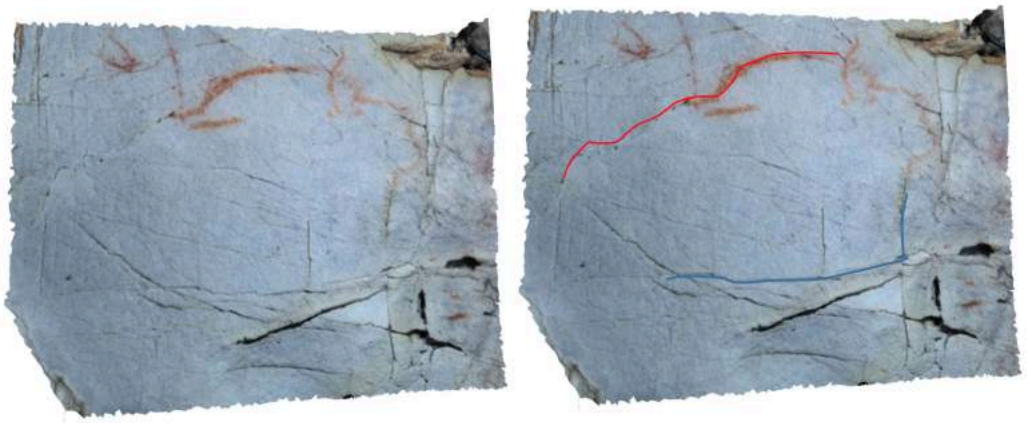

Figure 5.31: Examples of integration in PB5 (indicated by the red line and the black line). Ridges are utilised for the dorsal line, while grooves are substituted for the ventral line. Because these natural lines continue even after the contour disappear, the body of PB5 appears enlarged.

Topographic condition

As PB5 is an incomplete image, the limbs, tail, and the whole thigh were not analysed. This surface lacks topographic features except for the deep concavity on the ventral neck. The wall is more or less flat in most of the region, although the elevation is higher in the dorsal area. The depth is approximately 156mm (the model is at 1/200 scale: Figure 5.32); the highest point is found on the dorsal middle, while the ventral neck corresponds to the lowest. The range within which all body parts are defined their elevation level is considerably limited between 22.4mm and 55.7mm (high: 22.4-33.4mm, medium: 33.5-44.6mm, and low: 44.7-55.7mm). Because none of the major body sections is located on the ranges between 0.1mm and 22.3mm and between 55.8mm and 156mm, there are no extra elevation levels in PB5.

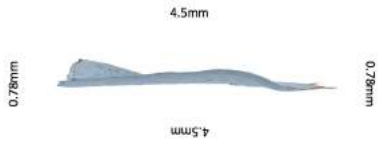

Figure 5.32: PB5 (1/200 scale) seen from the vertical position. The highest elevation is found on the dorsal mid-torso, while the lowest is on the ventral neck.

The surface is first detected at a part of the dorsal mid-torso. This detected area extends downward, involving the dorsal neck-shoulder. However, most of these sections remain undetected by a depth of the 22.3mm (see Figure 5.33, 1). The highlighted area extends sufficiently to define its elevation level when the cross-section layer proceeds until 33.4mm. Thus, the dorsal mid-torso and the dorsal neck-shoulder is assessed as the high level (2). At this depth, detection also begins in the ventral area, although the extent is limited. During the next phase, the detected regions spread

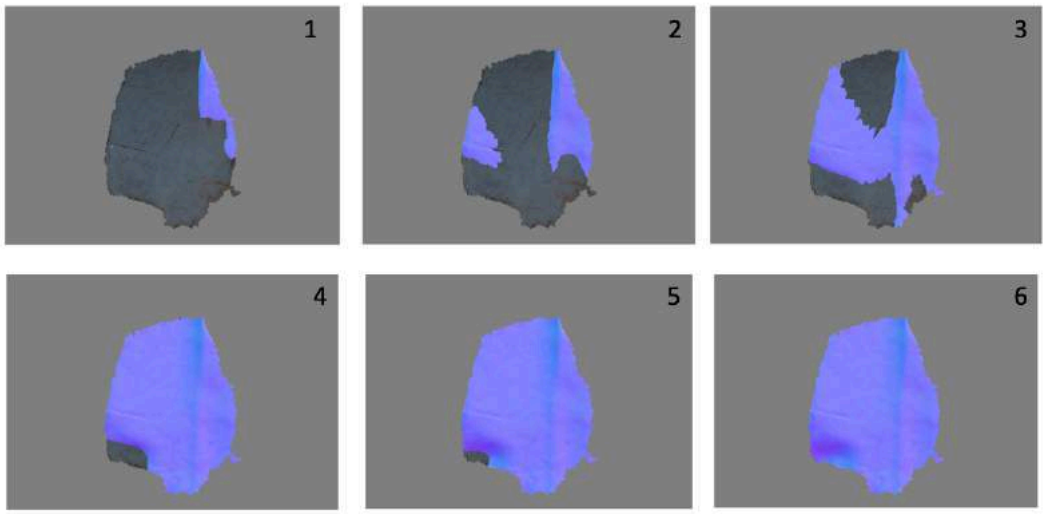

Figure 5.33: These six images illustrate the depth of PB5. When the cross-section layer passes the surface of PB5, the colour of the surface changes; dark regions denote lower elevation than coloured parts. Image 1 is for 0.1mm - 22.3mm, 2 for 22.4mm - 33.4mm, 3 for 33.5mm - 44.6mm, 4 for between 44.6mm - 55.7mm, and 5 and 6 for 55.8mm - 156mm.

dramatically and cover a significant part of the ventral mid-torso, and the central-ventral neck-shoulder (33.5-44.6mm: 3). Thus, these body sections are assessed as the medium level. Between 44.7mm and 55.7mm (4), the rest of the parts are also defined their elevation level as low, although there are still undetected regions. The concave surface on the ventral neck-shoulder is significantly deep as only the feature itself has a depth of almost 100mm. The area is fully detected by 156mm (5-6).

Distortion on images (horizontal rotation, x10°, y-70° to y0°)

The 3D simulation does not show any specific distortions, and the result is almost similar to that in the 2D simulation. Despite a few topographic features on the image, it seems they are not significant enough to generate the visual effect.

Red Deer (PD1)

General description

An outline red deer facing right (Figure 5.34). Even though the original colour is red, the pigment has been discoloured into somewhat yellowish due to decay. Only the anterior body is visible to the naked eye. However, the whole body except for the tail becomes apparent once a digital

Figure 5.34: PD1, outline red deer (digital filter is applied). Partly superimposed on PB2, the posterior body is somewhat ambiguous; however, PD1 contains the hind legs and thigh.

filter is applied; although the posterior has gone almost invisible, PD1 is provided with the robust hind legs and precisely outlined buttock and belly (see figures 5.34). Meanwhile, the eyes and mouth are not depicted on the face. PD1 is located in juxtaposition on the left to another red deer (PD2). Together with PD2, this deer is fixed in superimposition on the dorsal area of PB2. The length of PD1 is 44 cm, and it is located at a height of 140 cm from the nearest floor. However, this floor is dug down about 50 cm in a previous excavation.

Integration of natural lines

Numerous natural grooves are located on this wall. Those natural lines lie on the image horizontally and obliquely; however, none of them is integrated into the contour of PD1.

Topographic condition

There are not conspicuous topographic features on this wall, although it undulates to some extent. The total depth is approximately 28mm (the model is at 1/10 scale: Figure 5.35); the elevation is the highest at multiple regions (the frontal limb, under-neck, and dorsal thigh), while it becomes the lowest point is found at the ventral mid-torso. The range within which all body parts are defined their elevation level is between 0.1mm and 22.9mm (high: 0.1-7.6mm, medium: 7.7-15.3mm, and low: 15.4-22.9mm). None of the significant parts of the body is fixed on the outside of the above range (23-28mm), and therefore, there are no extra elevation levels.

Figure 5.35: PD1 (1/10 scale) seen from the vertical position. The highest elevation is found on the frontal limb, ventral neck, and dorsal thigh, while the lowest is on the ventral mid-torso.

The first_Detection occurs in three regions: the frontal leg, ventral neck, and dorsal thigh. Although the most area of the leg is detected and accordingly assessed as the high elevation by 2.5mm, the significant area of the central-ventral neck-shoulder is also detected and therefore defined as high by 7.6mm (see Figure 5.36, 1-2). On the other hand, expansion of the coloured area on the thigh is limited. Between 7.7mm and 15.3mm, the cross-section layer detects the almost entire anterior of PD1: the detection continues upward and inward, covering the face and the dorsal neck-shoulder (3-4). Simultaneously, the detected area extends from the right edge of the body, and consequently, it was revealed that the dorsal thigh and the hind leg are also located on the medium elevation level. The undetected area lies on the almost entire mid-torso and the central-ventral thigh as the surface forms concave in these regions. This concave

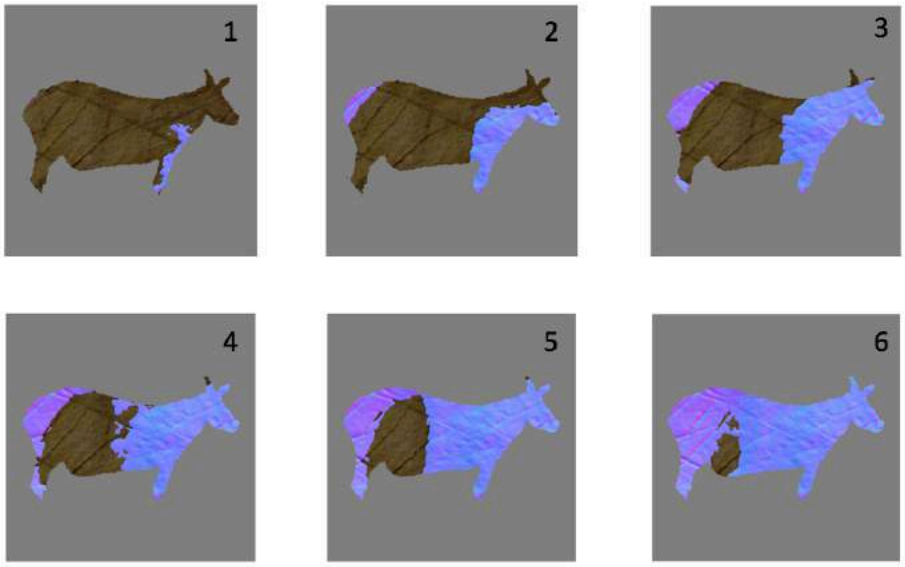

Figure 5.36: These six images illustrate the depth of PD1. When the cross-section layer passes the surface of PD1, the colour of the surface changes; dark regions denote lower elevation than coloured parts. Images 1 and 2 are for 0.1mm - 7.6mm, 3 and 4 for 7.7mm - 15.3mm, and 5 and 6 for 15.4mm and 22.9mm.

wall passes the cross-section layer, gradually narrowing the undetected area downward, and remained body parts are finally assessed as the low level by a depth of 22.9mm (5-6).

Distortion on images (horizontal rotation, x0°, y-60° to y70°)

The 3D simulation does not show any specific distortions on the appearance of PD1, and the result is almost similar to that in the 2D simulation. Despite a few topographic features on the image, it seems that they are not significant enough to generate the visual effect.

Red Deer (PD2)

General description

An outline red deer facing right (Figure 5.37). Even though PD2 was originally depicted in red, its colour has been altering into brownish or appears black in some parts (the muzzle and the chest). The figure is not well-preserved as the posterior side has become almost invisible to the naked eye. This deer possesses all body parts; however, its tail and limb are not confirmable. The head contains V-shaped ears but lacks eyes. It also has a forelimb. The ventral line vanishes after the frontal-neck because the red cloud of the negative hand is located on the belly; however, the invisible

posterior resurrects once a digital filter is applied. Placed immediately on the right to PD1, this image shares similarities with the previous deer: the body shape, the posture, the size, and the V-shaped ears. This deer is fixed in superimposition on PB2, slightly on the left to the head of the bison. The length is 38 cm, and it is located at a height of 140 cm from the nearest floor. However, this floor is dug down about 50 cm in a previous excavation.

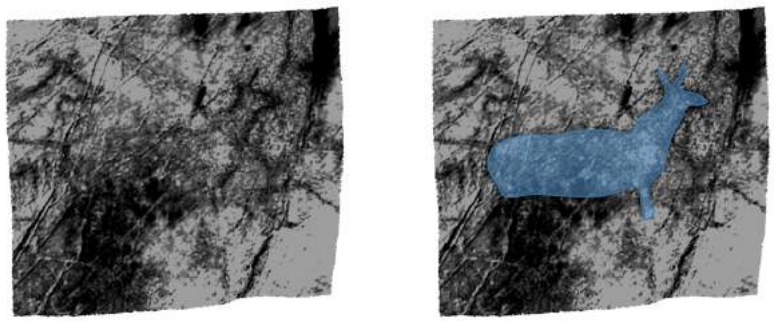

Figure 5.37: PD2, outline red deer (a digital filter is applied). Located immediately on the right to PD1 and partly superimposed on PB2, this image is considerably blurred due to severe decay. Especially, the ventral area is hardly confirmable even through a digital filter.

Integration of natural lines

Numerous small natural grooves run on this wall. Also, a noticeable deep groove which partly outlines the head of PB2 traverses the deer on its neck semi-vertically (from the lower left to the upper right). However, none of them is integrated into the contour of the deer except a groove on the buttock: at the left end of the image there is a vertical groove, and this line outlines the buttock.

Topographic condition

Unlike the previous deer, this wall contains a noticeable concave topography which forms a valley between two convex on the face and the posterior area. The total depth is approximately 28mm (the model is at 1/10 scale: Figure 5.38); while the highest points are found on the dorsal thigh and the tip of the ear, the lowest point is located on the tip of the frontal limb. The range within which all body parts are defined their elevation level is between 4.1mm and 22mm (high: 4.1-10mm. medium: 10.1-16mm, and low: 16.1-22mm). None of the significant parts of the body is fixed on the outside of the above range (0.1-4mm and 22.1-28mm), and there are no extra elevation levels, therefore.

Figure 5.38 PD2 (1/10 scale) seen from the vertical position. The highest elevation is found on the dorsal thigh and ear, while the lowest is on the frontal limb.

The surface is first detected at the ear, dorsal thigh, and then central mid-torso (0.1-4mm: see Figure 5.39, 1-2). However, the extent is limited as none of the body parts is defined their elevation level within this range. As the cross-section layer proceeds, these detected areas further extend and covers the head, entire thigh, and almost all mid-torso (4.1-10mm: 3-4). Thus, the whole posterior, constituting the majority of the body, is fixed to the high elevation level, and the surface appears almost flat in the region. During the next phase, the undetected surface narrows from the dorsal neck-shoulder to the central neck-shoulder. These parts are assessed as the medium level by 16mm (5-6). The ventral neck-shoulder and the frontal limb remain undetected: although the elevation on these sections is lower than any other regions, their surface almost fully passes the layer within the range between 16.1mm and 22mm (7-8). Accordingly, the limb and the ventral neck-shoulder are defined as the low level.

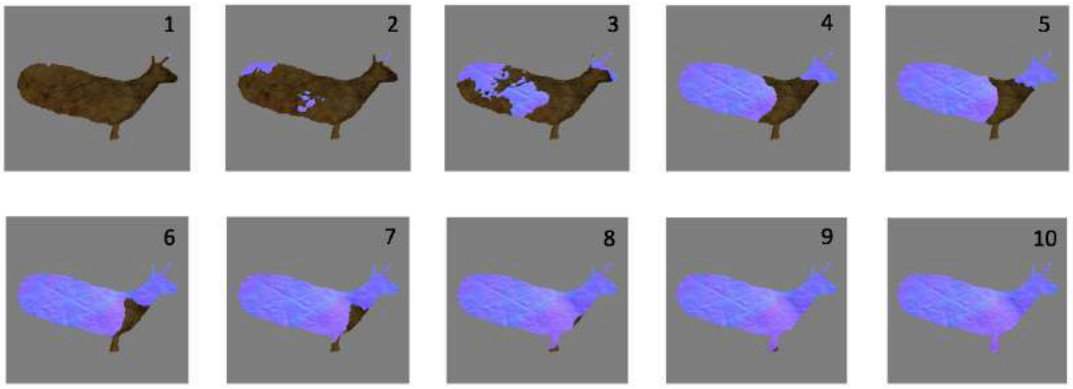

Figure 5.39: These 12 images illustrate the depth of PD2. When the cross-section layer passes the surface of PD2, the colour of the surface changes; dark regions denote lower elevation than coloured parts. Images 1 and 2 are for 0.1mm - 4mm, 3 and 4 for 4.1mm - 10mm, 5 and 6 for 10.1mm - 16mm, 7 and 8 for 16.1mm - 22mm, and 9 and 10 for 22.1mm - 28mm.

Distortion on images (horizontal rotation, x0°, y-60° to y70°)

The 3D simulation does not show any specific distortions on the appearance of PD2, and the result is almost similar to that in the 2D simulation. Despite a few topographic features on the image, it seems that they are not significant enough to generate the visual effect.

Deer (PD3)

General description

An outline red deer facing right (Figure 5.40). The colour of the contour is red. PD3 is an incomplete image, as the ventral body is absent. The head is outlined but only the upper muzzle and ears. The buttock is also drawn; however, it is considerably longer compared to the length of the dorsal line, and therefore the overall proportion is disturbed. The dorsal line of PD3 horizontally intersects at its croup the dorsal line of PB5. This figure is located immediately under PH1 (approx. 15cm). The posterior dorsal is used for the muzzle of PU1. The total length is about 45 cm, and the image is located at a height of about 200 cm from the floor where viewers can stand.

Figure 5.40: PD3, outline deer. The ventral line is absent. The dorsal line is also used for the muzzle of PU1. The buttock is disproportionally long. This buttock is drawn on the body of PB5.

Integration of natural lines:

There are countless grooves on this wall, but none of them is integrated into any sections of PD3. Therefore, the image is depicted independently from the natural line.

Topographic condition:

As this image is incomplete, the analysed body sections are the head, dorsal neck-shoulder, dorsal mid-torso and dorsal-central thigh. The total depth is 12mm (the model is at 1/200 scale: Figure 5.41); the highest point is located on the dorsal thigh, while the lowest point corresponds to the central thigh. The range within which all body parts are defined their elevation level is between 1.6mm and 10.5mm (high: 1.6-4.5mm, medium: 4.6-7.5, and low: 7.6-10.5mm). None of the major parts of the body is fixed on the outside of the above range (0.1-1.5mm and 10.6-12mm), and there are no extra elevation levels, therefore.

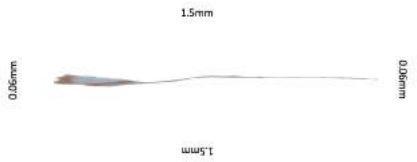

Figure 5.41: PD3 (1/200 scale) seen from the vertical position. The highest elevation is found on the dorsal thigh, while the lowest is on the central thigh.

The surface is first detected in a part of the dorsal thigh (0.1-1.5mm: see Figure 5.42, 1). This area extends from the point radially and covers the almost all dorsal thigh, defining its elevation as the high level (1.6-4.5mm: 2-3). During the next phase (4.6-7.5mm), the extent of the detection is limited as only the central thigh is assessed as the medium level. Despite that the surface of the muzzle passes the cross-section layer, the head remains mostly undetected (4-5). The anterior sections are finally assessed their elevation level as low by a depth of 10.5mm (6-7). At this time, there are still undetected areas on the neck, mid-torso, and the thigh. However, they also pass the layer by 12mm (8).

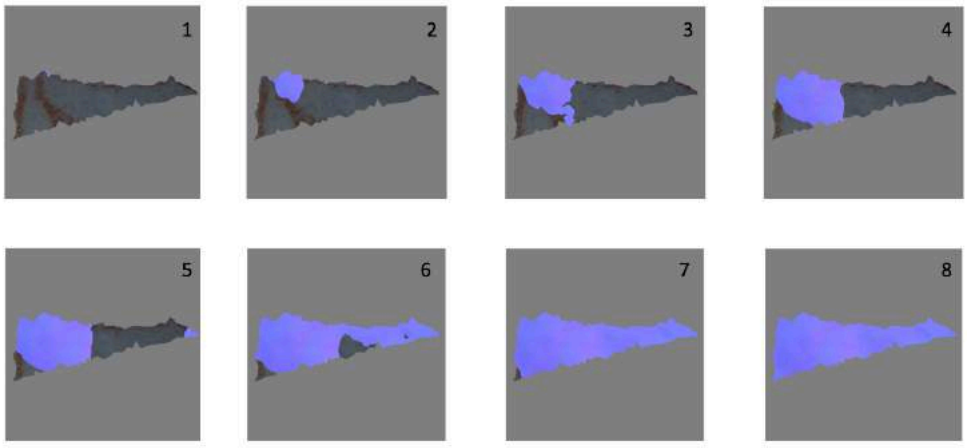

Figure 5.42: These eight images illustrate the depth of PD2. When the cross-section layer passes the surface of PD2, the colour of the surface changes; dark regions denote lower elevation than coloured parts. Image 1 is for 0.1mm - 1.5mm, 2 and 3 for 1.6mm - 4.5mm, 4 and 5 for between 4.6mm -7.5mm, 6 and 7 for 7.6mm-10.5mm, and 8 for 10.6mm - 12mm.

Distortion on images (horizontal rotation, x20°, y-80° to y-20°)

The 3D simulation does not demonstrate any remarkable distortions. There is also no detectable difference compared to the 2D simulation. This is because this wall is almost flat.

Unknown herbivore (PU1)

General description

An outline herbivore facing left (Figure 5.43). The contour is drawn in red. This herbivore is an incomplete image as only the head is provided; we cannot identify the depicted species due to the lack of information. PU1 shares its contour with two images. The upper side of the muzzle is shared with the dorsal line of the PD3, and the muzzle's tip overlaps the upper end of the dorsal line of PB5. The length is approximately 20cm, and it is located on at a height of 200 cm from the floor where viewers can stand.

Figure 5.43: PU1, outline image of an unidentifiable herbivore. Only the face is provided. PU1 shares its outline with PD3 and PB5: the line of the upper muzzle is also used for the dorsal line of PD3, while the tip of the muzzle is a part of the dorsal line of PB5.

Integration of natural lines

Even though this wall contains a large number of grooves, integration is absent in this figure. Therefore, PU1 is depicted independently from the natural line.

Topographic condition

This image contains only the face. Since such a limited body does not suit the analysis of the topography. In any case, there are no particular topographic features on this image. Although several small holes are located on the surface, they do not cause any irregularities on the surface. Furthermore, the total depth is significantly shallow (approx. 8mm), and hence the wall appears almost flat.

Distortion on images (horizontal rotation, x20°, y-80° to y-20°)

The 3D simulation does not demonstrate any remarkable distortions. Moreover, there is also no detectable difference compared to the 2D simulation. This is because the wall on which PU1 is depicted is almost flat.

Horse (PH1)

General description

An outline face of a horse facing left (Figure 5.44). Only the head is depicted. The contour is drawn in red. The face contains details such as the eye, nostrils and mouth. The contour of the frontal neck is also visible as it continues from the lower jaw; however, this outline is drawn only slightly. PH1 is located on the right side of the polychrome panel, under PH2 (approx. 24cm), and immediately

Figure 5.44 PH1, an outline face of a horse. Although the only facial part is provided, the face has the details (eye, mouth, nostril).

above PD3 (approx. 15cm). The length of the face is approximately 20 cm. This figure is fixed at a height of 220 cm from the floor.

Integration of natural lines

There are numerous grooves on this wall, and two of those natural lines overlap with the lower jaw. Those integrated grooves are not connected, but they are located on the almost same straight trajectry. Therefore, the two grooves are integrated with the single contour of the lower jaw (Figures 5.45). Apart from this example, no more integration is found. There are thin grooves on the outline of the nose, but they merely traverse the contour, and so it is difficult to consider it as an integration.

Figure 5.45: The example of integration in PH1. The lower part of the muzzle is drawn on two independent grooves.

Topographic condition

This image contains only the face. Since such a limited body does not suit the analysis of the topography. In any case, there are no particular topographic features on this image. Although several small holes are located on the surface, they do not cause any irregularities on the surface. Furthermore, the total depth is significantly shallow (approx. 8mm), and hence the wall appears almost flat.

Distortion on images (horizontal rotation, x20°, y-80° to y-20°)

The 3D simulation does not demonstrate any remarkable distortions. Moreover, there is also no detectable difference compared to the 2D simulation. This is because the wall on which PH1 is depicted is almost flat.

Horse (PH2)

General description:

An outline horse facing right (Figure 5.46). Although the whole body is provided in a red outline, the colour appears partly ambiguous. PH2 is not well-preserved on its dorsal side, especially the line from the rump to the buttock is almost invisible. Also, the contour of the anterior-ventral is under a severe decay, and only the foreleg is barely visible. Furthermore, the head is also unclear as pigments are left only on a limited part

of the muzzle. In contrast, the line from the belly to the hind limb and the buttock is clear. The thick, long tail is also visible. Four projectiles are depicted in purple on the belly and shoulders (three in the belly, and one in the shoulder). These projectiles have been associated with hunting magic (Groenen 2007 and 2012). The total length is 188 cm, and it is the largest image among all graphics in the El Castillo cave. The height of the location is 300 cm from the nearest floor.

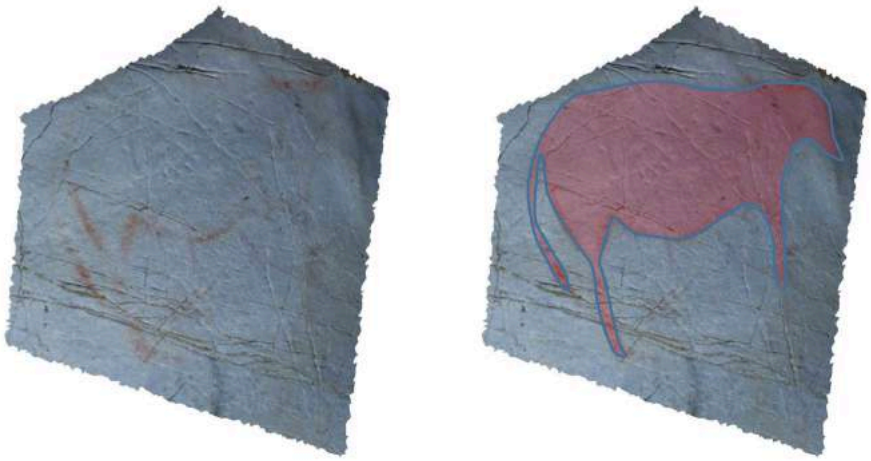

the largest figure of all samples in El Castillo (188cm). All body parts are provided. Because four projectiles are depicted on its body, PH2 is associated with a practice of the hunting magic.

Integration of natural lines:

Although there are several grooves on this wall, none of them is used for the contour. PH2 is depicted without any assists of the pre-existing pattern of the cave wall.

Topographic condition:

The area on which PH2 is located is mostly flat except the convex surface on the head. The shape of that convex wall is reminiscent of a long and thin face of a horse, and this feature is exactly placed from the forehead to the muzzle. Therefore, the horse's head achieves sculptural quality. The total depth is approximately 100mm (the model is at 1/400 scale: Figure 5.47). The highest points are located on the tail, head, and dorsal mid-torso, whereas the lowest point corresponds to the tip of the frontal limb. The body parts are distributed in four elevation levels within this range (high: 0.1-22.2mm, medium: 22.3-44.4mm, low: 44.5-66.7mm, and extra low: 66.8-100mm).

Figure 5.47: PH2 (1/400 scale) seen from the vertical position. The highest elevation is found on the tail, head, and dorsal mid-torso, while the lowest is on the frontal limb.

The surface is first detected at multiple regions (the head, dorsal mid-torso, and tail), and the detected area covers more than half of the head and tail by a depth of 22.2mm (see Figure 5.48, 1-2). The topography of the thigh also passes the cross-section layer at its buttock at this time; however, the extent is too limited to be assessed its elevation level. Between 22.3mm and 44.4mm, most of the body parts are defined. The detected area dramatically extends inward from the head and thigh. Consequently, the entire thigh, the whole mid-torso, and the dorsal neck-shoulder and the hind leg are assessed as the medium level (3-4). As the layer proceeds, the undetected area further narrows in the range between 44.5mm and 66.7mm (5-6). In the low elevation level, the central-ventral neck-shoulder is located, although the elevation of the central part is slightly higher than the ventral. The frontal leg remains entirely undetected and therefore that the region is located in the lowest elevation. The forelimb is disproportionally lower than the rest of the body parts and needs further 33.2mm (66.8-100mm) to be fully detected (7-8).

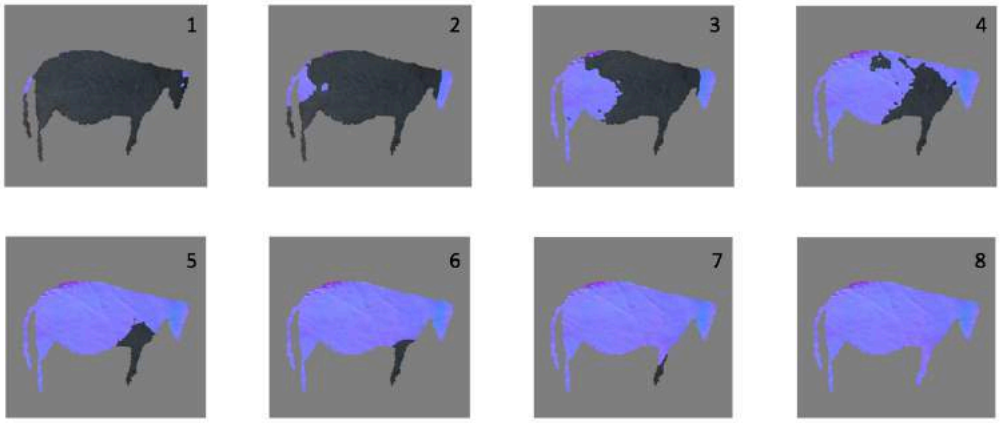

Figure 5.48: These eight images illustrate the depth of PH2. When the cross-section layer passes the surface of PH2, the colour of the surface changes; dark regions denote lower elevation than coloured parts. Images 1 and 2 are for 0.1mm - 22.2mm, 3 and 4 for 22.3mm - 44.4mm, 5 and 6 for 44.5mm - 66.7mm, and 7 and 8 for 66.8mm - 100mm.

Distortion on the image (horizontal rotation, x30°, y-80° to y-30°)

The 3D simulation does not demonstrate any remarkable distortions. There is also no detectable difference compared to the 2D simulation. This is because the wall of PH2 is almost flat.

Bison (CB1)

General description

An outline bison facing right (Figure 5.49). Its used colour is dark yellow. The image is subject of a severe decay and hardly distinguished from the panel without a digital filter. However, the CB1 is provided with all body sections. Regarding the head, the eye and the ear are absent, but the mouth is presented. This bison appears in a posture which keeps its neck low. CB1 has both frontal and hind leg, with one on each section. Below this image red pigments are left as smoke, and this area partially overlaps the front leg. This image is located immediately left to CB2 (approx. 15cm) as they face each other. The image's size is 72 cm, and it is depicted on an approximate height of 145 cm from the nearest floor.

Figure 5.49: CB1, outline bison facing right (digital filter is applied). Although the image is subject of severe decay, its entire body is meticulously drawn.

Integration of natural lines

There are numerous grooves on the region where CB1 is depicted, although almost all of them are thin and short. Despite those abundant natural lines, the overlap on the contour is rare as it only occurs on the buttock and tail. As for the buttock, there is a thin vertical groove, and almost entire buttock is drawn along the line (Figure 5.50). This line continues further downwards until the back leg, merging another groove. However, the contour of the leg is unclear so that the overlap is not confirmable. Meanwhile, the tip of the tail is also outlined along with a short groove (see Figure 5.50). Although there are three other grooves of similar size in proximity to the tail, the overlap only happens with this groove at the left edge of the contour.

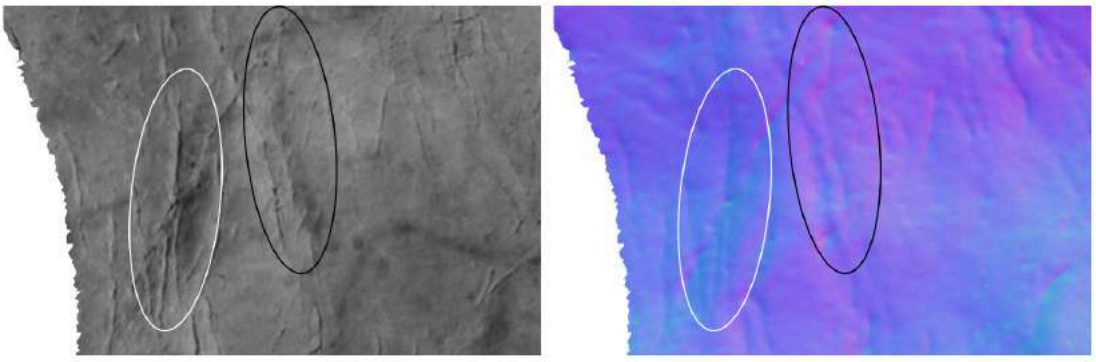

Figure 5.50: Examples of integration in CB1. A thin groove is utilised for the outline of the buttock (see the black circle). The tip of the tail is also drawn along a groove (see the white circle).

Topographic condition

Although the topography of CB1 is relatively moderate as no acute convex and concave features are located, this wall forms a bowl-like concave. The total depth of the image is approximately 73mm (the model is at 1/10 scale: Figure 5.51). The frontal leg corresponds to the highest point, while the central mid-torso to the lowest point. The range within which most of the body parts are defined their elevation level is limited between 34.4mm and 73mm (high: 34.5-47.2mm, medium: 47.3-60.1mm, and low: 60.2-73mm). A level outside this range is applied to the frontal leg (0.1-34.4mm). Because the major extent of the limb belongs to the range between 0.1mm and 34.4mm which is disproportionally large against the entire elevation range, the section is assessed as the extra high.

Figure 5.51 CB1 (1/10 scale) seen from the vertical position. The highest elevation is found on the tip of the frontal leg, while the lowest is on the central body.

Detection starts from the tip of the frontal leg. The detected area then extends upward, and over half of the section passes the cross-section layer by a depth of 34.4mm (see Figure 5.52, 1-2). At the same time, the tail, horn, ventral neck, and hindlimb are also partially detected their topography. During the next level (high), detected areas further extend inward from all edges of the examined surface and covers a number of sections: the head and back leg are fully detected; the majority of the tail and dorsal thigh also pass the cross-section layer (34.5-47.2mm: 3-4). As the layer proceeds, the regions of the medium elevation level are revealed. The coloured area extends further inward, and the central-ventral thigh, dorsal-ventral mid-torso, and dorsal-ventral neck-shoulder are fell in this elevation level (47.3-60.1mm: 5-6) Finally, only the central mid-torso and the central neck-shoulder remain undetected. These two areas are categorised as the low level and located between 60.2mm and 73mm (7-8).

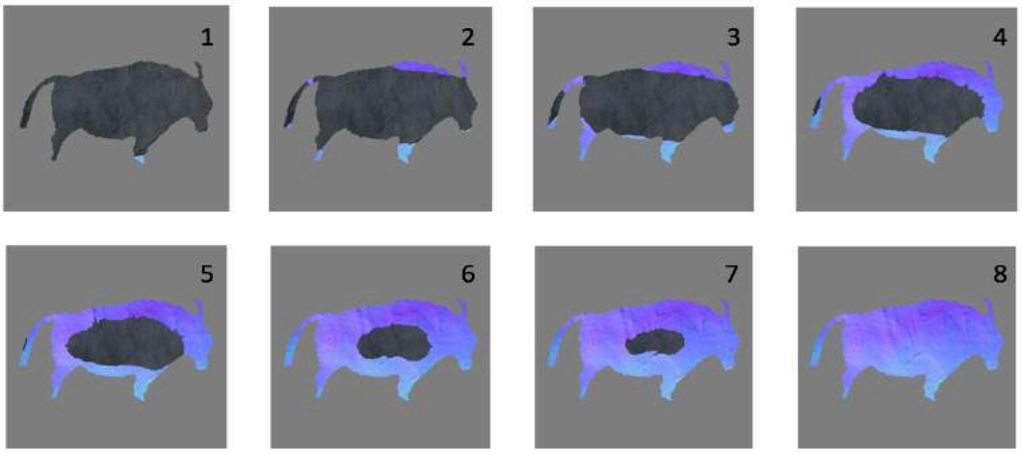

Figure 5.52: These ten images illustrate the depth of CB1. When the cross-section layer passes the surface of CB1, the colour of the surface changes; dark regions denote lower elevation than coloured parts. Images 1 and 2 are for 0.1mm - 34.4mm, 3 and 4 for 34.5mm - 47.2mm, 5 and 6 for 47.3mm - 60.1mm, and 7 and 8 for 60.2mm - 73mm.

The distortion on images (horizontal rotation, x0°, y-70° to y70°)

The 3D simulation demonstrates that noticeable distortion occurs to CB1. Although the region is mostly concave, the dorsal side is located on the outer edge of the topography whose elevation is slightly higher than the centre. Sections which are located on such an elevated surface (the head, neck, thigh) are remarkably deformed. Firstly, the shape of the head and the neck is constantly distorted. As the angle increases (toward y70°), the cervical dorsal area appears shorter, and simultaneously, the shape of the head seems more contracted. Therefore, the proportion of the bison at y70° is outstandingly different from that at y0° (Figure 5.53). This distortion is most likely perceived within the range between y30° and y70°.

Meanwhile, when the viewing position is taken on the left, the thigh also appears deformed: the dorsal side of the thigh is pulled upward (at y-70°). This deformation process is conspicuous when viewing position moves between y-70° and y-40°.

Apart from these body parts, the limbs seem to change their directions; although at y70° both frontal and hind leg appear extending slightly backwards, the frontal limb is gradually bent frontward as the viewpoint shift to the left. Same is true for the other leg: as the viewing angle decreases, the hind leg, in contrast to the frontal leg, appears bent further backwards. As a result, the interval between these legs is significantly widened.

Figure 5.53*:* CB1 seen from y-70°(left), y0° (centre), and y70° (right). Distortion occurs on the head, neck-shoulder, thigh, and limb: the cervical dorsal and head appears noticeably contracted as the angle increases to y70; the dorsal thigh is pulled upward as the viewing position moves to the left (y-70°); both frontal and back leg appear bending their directions between y-70°and y70°. The overall concave surface causes these distortions.

Bison (CB2)

General description

An outline bison facing left (Figure 5.54). The colour is dark yellow. The ventral body is absent. Because the image is under a severe deterioration which obscures the outline, its appearance is hardly recognisable. CB2 is outlined by a single thin stroke, although the line appears slightly wider in the upper muzzle and the frontal neck. The details in the face (the eye, the mouth, and ears) are absent. However, there is a line extending upward from the forehead, and this line might represent the horn. The dorsal line extends toward the right until it disappears after crossing two grooves. CB2 is overlapped with two other images: there is a hand-stencil on the neck; the hind leg of another bison (CB3) is located on the CB2's mid-torso. The image size is approximately 50cm, and it is located on a height of 153 cm from the nearest floor.

Figure 5.54: CB2, outline bison facing left (digital filter is applied). Due to severe conservation condition, the image is hardly recognisable to viewers. The ventral side is missing.

Integration of natural lines

There are numerous grooves on this region. Occasionally, edge lines are also present. These natural lines are distributed throughout the surface; however, integration is confirmed only in the posterior dorsal. There is an edge formed by a concave surface. The edge of the concave area runs horizontally and then turns downward. Along with this curve edge, the dorsal line is outlined: the cervical line corresponds to the horizontal edge, while the posterior dorsal is assigned to the vertical edge (Figure 5.55).

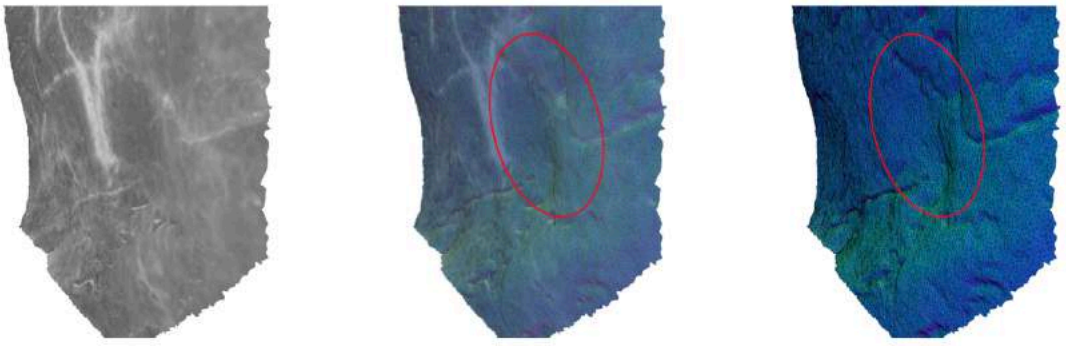

Figure 5.55: The example of integration in CB2. The dorsal line is drawn along the edge of a concave surface.

Topographic condition:

The topography of this bison is slightly undulating, forming elevational gaps. However, the wall is almost flat as the total depth is significantly shallow: 14mm (the model is at 1/10 scale: Figure 5.56). The highest points correspond to the tip of the horn and the central shoulder, while the lowest point is found on the ventral thigh. Since CB2 is an incomplete figure, the head, dorsal-central neck-shoulder, dorsal-central mid-torso, the dorsal thigh are subject to the analysis. All body parts are defined their elevation level within the range between level 0.1mm and 14mm (high: 0.1-4.7mm, medium: 4.8-9.3mm, low: 9.4-14mm).

Figure 5.56: CB2 (1/10 scale) seen from the vertical position. The highest elevation is found on the central shoulder and tip of the horn, while the lowest is on the ventral thigh.

Detection begins from the tip of the horn and the central shoulder. Detected areas further extend, and the predominant region of the central neck-shoulder belongs to the high elevation level (0.1-4.7mm: see Figure 5.57, 1-2). The entire horn passes the layer during this phase; however, the extent does not involve the half area of the face. Between 4.8mm and 9.3mm, almost all body parts are detected and assessed as the medium level. The sections which fall into this level are the head, dorsal neck-shoulder, dorsal-central mid-torso (3-4). As these parts are fixed within in considerably narrow range, the image appears almost flat. The rest of the undetected body (the dorsal thigh) is assessed as the low elevation level (9.4-14mm: 5-6). This section also entirely passes the cross-section layer by a depth of 14mm.

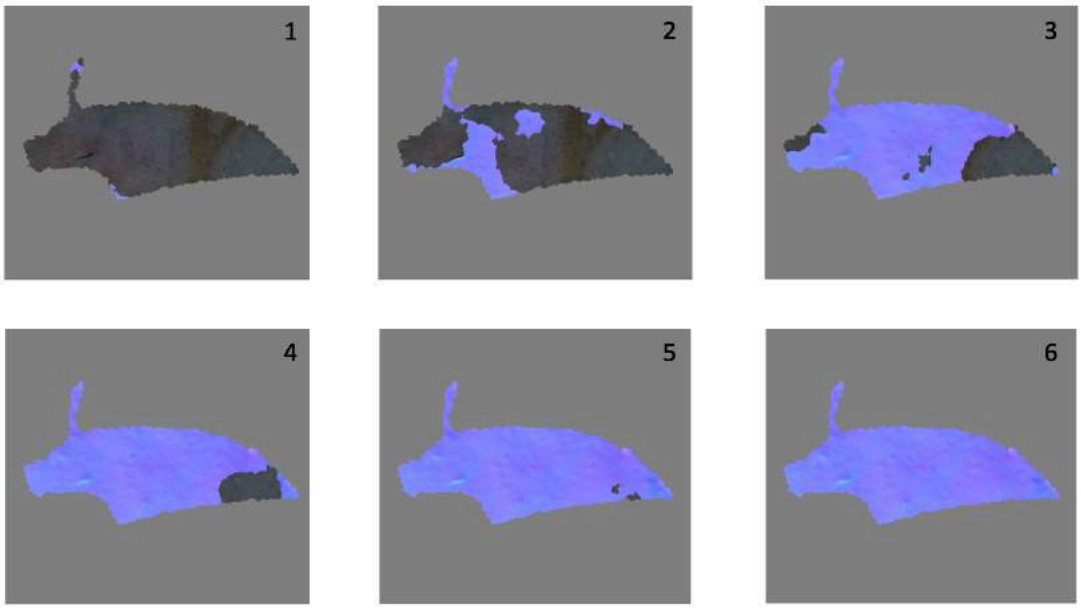

Figure 5.57: These six images illustrate the depth of CB2. When the cross-section layer passes the surface of CB2, the colour of the surface changes; dark regions denote lower elevation than coloured parts. Images 1 and 2 are for 0.1mm - 4.7mm, 3 and 4 for 4.8mm - 9.3mm, and 5 and 6 for 9.4mm - 14mm.

The distortion on images (horizontal rotation, x0°, y-70° to y80°)

Between CB2 in the 3D and 2D simulation, no remarkable differences in the appearance are discerned. It is because of its relatively flat surface and difficulty in distinguishing distortions on an incomplete body.

Bison (CB3)

General description

An outline bison facing right (Figure 5.58). The colour is red. CB3 is a complete image which is well-preserved as its red contour still possess the vividness. Although most of the body is drawn in a single thin line, the outline becomes somehow blurred on the head and frontal neck. The face is not given its details, but two curve lines are extending downward from the face. There is also a thick line which grows upward from the facial section, and the appears as a horn. The anterior-dorsal line is curvey, but it turns to be straight at the posterior and continues horizontally. The tail appears clearly from the thick base on the buttock, and it gradually narrows its width towards the tip. The two back legs are painted and partly superimposed on the CB2. The ventral line is also preserved mostly vivid; however, the section where the forelimb begins is slightly ambiguous. The image size is 78 cm, and it is located on a height of approximately 180 cm from the nearest floor.

Figure 5.58: CB3, outline bison facing right (digital filter is applied). Provided with the entire body, CB3 is in the best condition of all the other pictures on the ceiling. The outline becomes ambiguous in the anterior. There are lines which extend from the head.

Integration of natural lines

There is a large number of grooves here, while ridges and edges are absent. Although the size of the grooves differs, they are mainly thick and short. These natural lines are distributed throughout the region, and some are located on CB3. The use of the natural lines for outlines are confirmed on the posterior dorsal and the tail: the posterior dorsal is executed along a horizontal groove (Figure 5.59). This groove continues to the left, slightly rising upward. Along with this groove, the tail grows upward from the buttock, although the rest of the tail does not overlap the groove. Apart from these sections, the apparent superimposition is absent.

Figure 5.59 Examples of integration in CB3. A thin horizontal groove runs along the posterior dorsal line and the root of the tail (see the black circle).

Topographic condition

The topography for CB3 is relatively moderate because no acute convex and concave features are visible. However, this wall is not entirely flat. The total depth of CB3 is approximately 49mm (the model is at 1/10 scale: Figure 5.60). The tip of the tail corresponds to the highest point, whereas the central neck-shoulder to the lowest. All body parts are defined their elevation level within this range (high: 0.1-18.4mm, medium: 18.5-30.6mm, low: 30.7-49mm).

Figure 5.60: CB3 (1/10) scale seen from the vertical position. The highest elevation is found on the tail, while the lowest is on the central neck-shoulder.

The surface is first detected at the tip of the tail, and slightly after this first detection, a part of the ventral neck-shoulder also passes the cross-section layer. The surface of the high elevation extends from these areas, covering most of the frontal limb and the entire tail (0.1-18.4mm: see Figure 5.61, 1-3). Simultaneously the central thigh

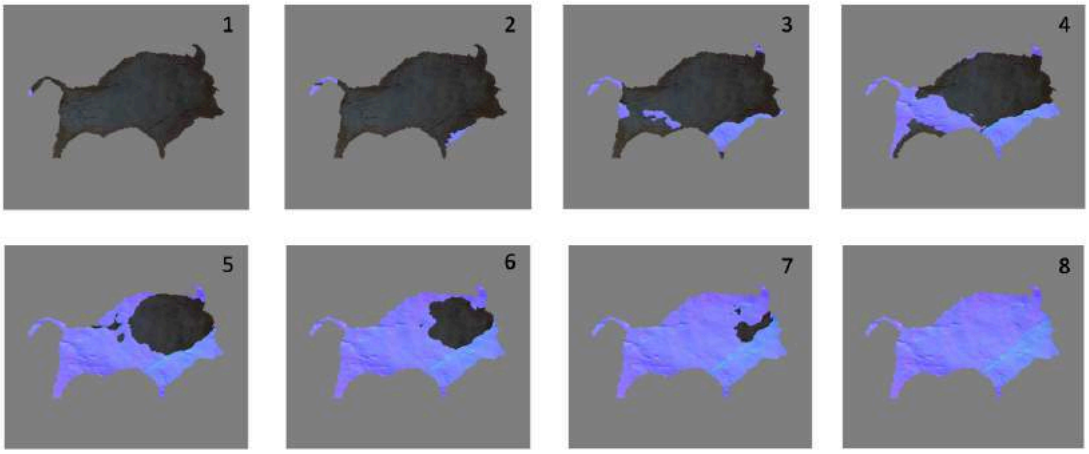

Figure 5.61: These eight images illustrate the depth of CB3. When the cross-section layer passes the surface of CB3, the colour of the surface changes; dark regions denote lower elevation than coloured parts. Images1-3 are for 0.1mm - 18.4mm, 4 and 5 for 18.5mm and 30.6mm, and 6-8 for 30.7mm - 49mm.

and mid-torso are also partially detected. As detection continues, it is revealed that the elevation is higher on the ventral side than dorsal. In the medium level, the almost all surfaces on the ventral side is first detected (18.5-24.5mm: 4), and then the highlighted area covers all posterior (24.6-30.6mm: 5). At this time, an elevation gap is visualised on the anterior body; there is a wide concave laying under the dorsal mid-torso, dorsal-central neck-shoulder, and forehead. These low sections finally pass the layer at the range between 30.7-49mm: 6-8).

The distortion on images (horizontal rotation, x10°, y-80° to y70°)

The 3D simulation shows that the appearance of CB3 is significantly distorted. As a fundamental transformation, the image merely appears flattened whenever seen from sides, according to the 2D simulation. In the actual setting, the image alters its appearance in a considerably complicated manner: as the view-position moves from the left to the right, the body gradually becomes flattened, but due to the convex on the anterior-ventral pushing the outline of that area upward, the head, the neck-shoulder, and the mid-torso becomes further thinner than seen in the 2D setting at y70° (Figure 5.62). The concave on the head which is hidden by this convex when viewed from the right also contributes to this deformation. Also, since the wall leans front and the image is located on a high position, CB3 appears rotating as viewers move towards the right; finally, the image seems in a vertical position at y70°.

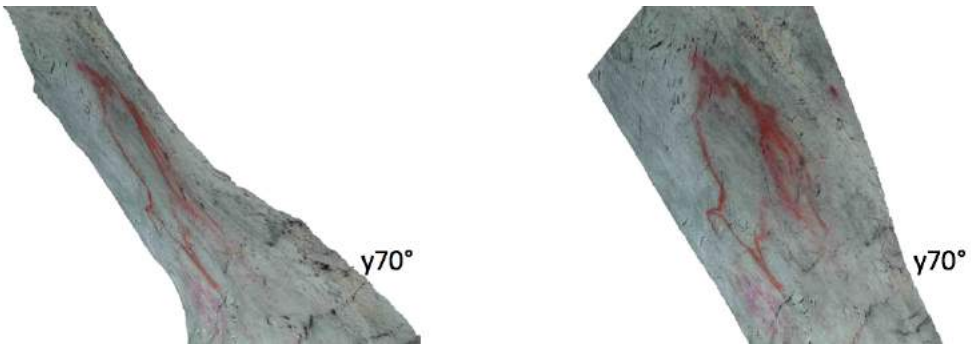

Figure 5.62: CB3 on the 3D surface (left) and 2D surface (right) seen from y70°. While the body is significantly contracted on the 3D surface, CB3 sustains its general proportion on the flat surface. This is because the wall is elevated in the ventral shoulder area.

Apart from the body, the hind leg is also distorted. As the viewing point shifts from the left, the limb which appears stretching backwards at y-80° starts gradually bending forward (y-80° to y-30°). After sustaining its shape unchanged between y-20°and y30°, again the leg starts stretching backwards from y40° to y70°. Thus, the limb demonstrates considerably irregular movement. This is attributed to the concave topography located along the front of the leg.

Bison (CB4)

General description

An outline bison facing right (Figure 5.63). Its colour is yellow. The picture is under weathering condition which blurs and weakens its presence. The bison is provided with all body parts including the tail in a schematic manner rather than realism. The face lacks the eye, mouth and ear but contains a horn. CB4 has only one leg: there is an abstract back limb. The frontal neck is depicted by three short oblique lines, leaving the outline of the part intermittent. CB4, although slightly, has an overlap with two hand-stencils: one is located on the belly as the tips of the fingers cross the ventral line; the other is on the frontal neck as the finger or cloud part is superimposed on this animal. The image size is 68 cm, and it is located on a height of 195 from the nearest floor.

Figure 5.63: CB4, outline bison facing right (digital filter is applied). The condition of the image is good. CB4 is depicted schematically, with three oblique lines portraying the frontal neck. Additionally, a superimposition with a hand-stencil is found on the belly and frontal neck.

Integration of natural lines

Overall, integration is not detected in CB4. There are a large number of grooves on the area where CB4 is depicted. Although the size of these differs, they are mostly thick, long, and therefore conspicuous. These natural grooves are distributed throughout the region. None of them, however, is utilised for the outline.

.

Topographic condition

The topography of this wall is noticeably undulating due to a wide concavity which lies in CB4's central mid-torso. Consequently, this feature defines the overall topographic condition of CB4. The total depth is approximately 66mm (the model is at 1/60 scale: Figure 5.64). The elevation level of all body parts are assessed within this range (high:0.1-23.3mm, medium: 23.4-46.6mm, and low: 46.7-66mm). The highest point corresponds to the tip of the hind leg, while the lowest to the central middle area.

Figure 5.64: CB4 (1/60 scale) seen from the vertical position. The highest elevation is found on the tip of the hind leg, while the lowest is on the central mid-torso.

The elevation is first detected at the tip of the tail and hind limb. As the detection on these areas extends, the surface of the head also starts passing the cross-section layer from its right end. By a depth of 23.3mm, the elevation of the entire head, tail, hind limb, and the major area of the ventral thigh are assessed as the high level (see Figure 5.65, 1-3). During the next phase (23.4-46.6mm), the detection continues inward from the above-detected areas. Most of the body parts (the dorsal-central thigh, ventral mid-torso, dorsal-ventral neck-shoulder, and frontal leg) are located on this range (4-6). Accordingly, the concave section in the central mid-torso remains undetected. That concave topography also involves the dorsal mid-torso and dorsal neck-shoulder at its peripheries, and therefore the elevation of these areas are lower than any other body parts. These sections also gradually pass the layer, and a part of the central mid-torso is finally detected (46.7-66mm: 7-9).

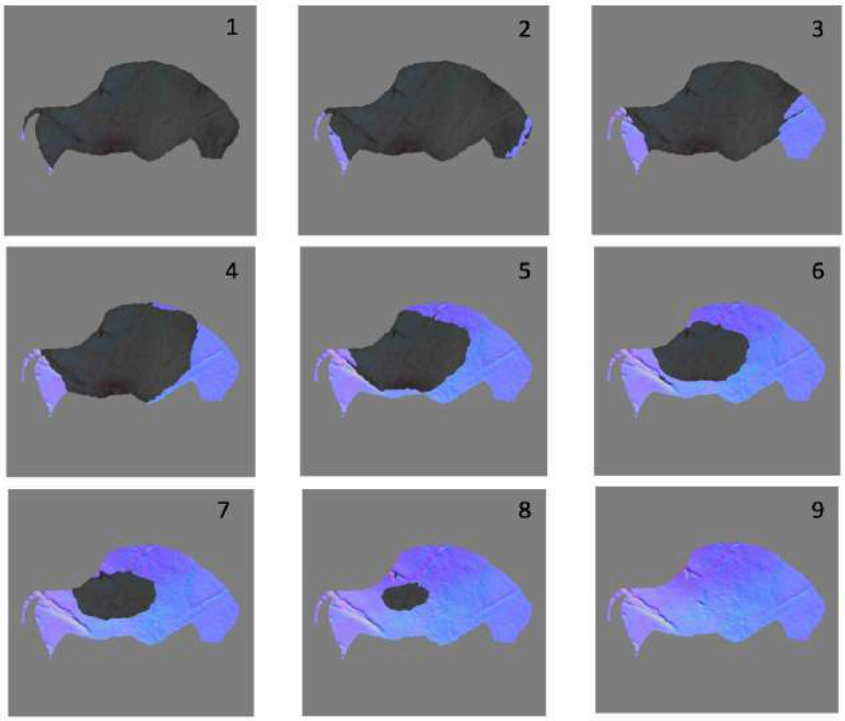

Figure 5.65These nine images illustrate the depth of CB4. When the cross-section layer passes the surface of CB4, the colour of the surface changes; dark regions denote lower elevation than coloured parts. Images1-3 are for 0.1mm - 23.3mm, 4-6 for 23.4mm - 46.6mm, and 7-9 for 46.7mm - 66mm.

The distortion on images (horizontal rotation, x20°, y-60° to y80°)

Despite the noticeable concave surface in the centre of the body, no distinguishable distortion is confirmed in the 3D simulation. Also, the result is almost identical to that of the 2D simulation. This distortion less body is due to the angle of the wall: the surface on which CB4 is located is almost a ceiling rather than a vertical wall.

Bison (CB5)

General description

An outline bison facing left, in yellow (Figure 5.66). CB5 contains all body sections except the front limb and is depicted in a schematic fashion as well as CB4. The condition is better than most of the other images on the ceiling of hands. From around the forehead, a curve line grows upward, which might represent a horn. Numerous red pigments are located on and around CB5. Some of them appear as signs (on the head, dorsal and buttock), and some might be a red cloud of a hand stencil (on the middle). The image size is 60cm and placed on an approximate height of 155 cm.

Figure 5.66: CB5, outline bison facing left (digital filter is applied). The condition of the image is relatively good. There are red pigments on CB5: some of them appear signs, while the red colour on the dorsal mid-torso might be a cloud part of a hand-stencil.

Integration of natural lines

There is a large number of natural grooves on the region where CB5 is depicted. The size of those grooves varies greatly from thin to significantly thick. These natural lines are distributed throughout the area, and some are located on the bison. None of them are integrated into the image's contour, however.

Topographic condition

There are no acute features; CB5 is mostly located on a calm convex surface (the thigh, mid-torso and neck-shoulder). The total depth of CB5 is approximately 20mm (the model is at 1/30 scale: Figure 5.67). The tip of the tail and a part of the mid-torso correspond to the highest point, while the dorsal neck to the lowest. All body parts are defined their elevation level within this range (high: 0.1-7.5mm, medium: 7.6-12.5mm, and low: 12.6-20mm).

Figure 5.67: CB5 (1/30 scale) seen from the vertical position. The highest elevation is found on the tip of the tail and central mid-torso, while the lowest is on the dorsal neck.

The surface is first detected at the tip of the tail and a part of the mid-torso, and then at the horn. These areas extend and cover the major area of the tail, dorsal-central thigh, and central mid-torso (0.1-7.5mm: see Figure 5.68, 1-2). As the cross-section layer proceeds, the elevation level reaches the medium. The area which passed the layer dramatically expands during this phase, including all body except the dorsal neck-shoulder (7.6-12.5mm: 3-4). Accordingly, since most of the body sections are located on the narrow medium level, CB5 appears relatively flat. The part remaining undetected is the dorsal neck, and this part fully passes the layer between 12.6mm and 20mm (5-6).

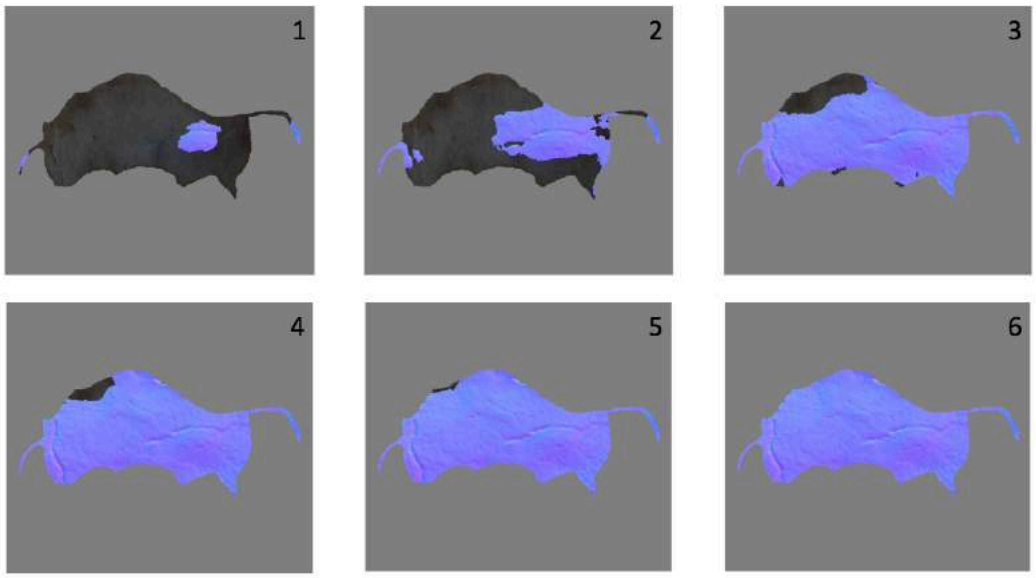

Figure 5.68: These six images illustrate the topographic depth of CB5. When the cross-section layer passes the surface of CB5, the colour of the surface changes; dark regions denote lower elevation than coloured parts. Images 1 and 2 are for 0.1mm - 7.5mm, 3 and 4 for 7.6mm - 12.5 mm, and 5 and 6 for 12.6mm - 20mm.

The distortion on images (horizontal rotation, x20°, y-70° to y70°)

The 3D simulation shows no remarkable transformation even though the bison is located on a convex wall. There are also no detectable differences in the comparative analysis. This is because the convex topography lies under CB5's body is too subtle to distort the image. Therefore, the images in both simulations appear more or less similar.

Horse (EH1)

General description

An outline image of a horse facing left (Figure 5.69). This has been interpreted as a hybrid image of a horse and an aurochs, because the ears appear to be relatively long and resemble horns of a bovid (see Groenen 2006, 2007 and 2012). Depicted in red,

EH1 is a complete figure. The condition of the image is sufficient enough for viewers to grasp the whole body easily. However, the outline is thin and faded at the dorsal and breast area, compared to other sections. Three signs (two V-shaped and one short line) are found in the centre of the body. These marks are interpreted as projectiles left in the image during the hunting magic ritual (Groenen, 2012). The total length of the image is as large as 107 cm, and it is located on a height of 17 cm (at the belly) from the nearby floor.

Figure 5.69: EH1, outline image of a horse facing left (digital filter is applied). According to Marc Groenen, this is a hybrid species of a horse and an aurochs because the ears are much longer and resemble the horns of a bovid.

Integration of natural lines

A large number of thin grooves exists on this wall, and EH1 is integrated from some of those lines. For example, the chest is not outlined by a distinct line, but a thin groove corresponds to the contour. Also, a groove is utilised for drafting the lower side of the muzzle. Moreover, the cervical-dorsal line overlaps a white, thin line.

Apart from these examples of the use of grooves, another integration also features this image. Above this horse, a thick ridge forms and runs diagonally to the lower right, and the posterior dorsal and the upper part of the buttock are outlined on this ridge. The significance of this integration becomes apparent once the picture is seen from the right side; from this viewing position, the ridge appears a half arch which substitutes the dorsal line. This curve naturally merges to the outline of the buttock and the hind leg (Figure 5.70).

Figure 5.70: A unique example of integration in EH1. A conspicuous ridge runs obliquely above the image (indicated in the black circle on the left picture)). On this ridge, the posterior dorsal and upper part of the buttock are outlined. Once viewed from the right, the ridge seems a half arch which turns to be a natural dorsal line (indicated in the black on the right picture), and this curve naturally merges to the outline of the buttock and hind leg.

Topographic condition

EH1 is located on a bowl-like concave wall; the surface elevates towards both right and left edge. The total depth is 95mm (the model is at 1/30 scale: Figure 5.71). The tip of the ear corresponds to the highest point, while a part of the central mid-torso to the lowest. The range within which all body parts are defined their elevation level is limited between 35.7mm and 89.1mm (high: 35.7-53.4mm, medium: 53.5-71.3mm, and low: 71.4-89.1mm). The ranges between 0.1mm and 35.6mm and between 89.2mm and 95mm do not define the elevation level of any body parts, and therefore there are no extra levels in EH1.

Figure 5.71: EH1 (1/30 scale) seen from the vertical position. The highest elevation is found on the tip of the ears, while the lowest is on the central mid-torso.

The surface is first detected at the tip of the right ear. Immediately after this initial detection, the wall also begins to pass the cross-section layer at the tip of the hind limb and then at the tail and dorsal thigh. These areas extend, although they fail to define none of the body parts by 35.6mm (see Figure 5.72, 1-2). During the next phase, the detection, although slowly, continues from the already-detected areas. The most extent of the hind leg and central thigh are located in this high elevation level (35.7-53.4mm: 3-4). Between 53.5mm and 71.3mm, the cross-section layer detects the surface of the left and the right edge. In the medium level, the head, dorsal neck-shoulder, dorsal mid-torso, dorsal-ventral thigh, and tail are allocated (5-6). The frontal leg and the central parts of the body are left still undetected: the limb, these sections are finally detected between 71.4mm and 89.1mm (7-8) and assessed as the low level. Although a tiny area on the central mid-torso remains undetected, this part finally passes the layer at a depth of 95mm.

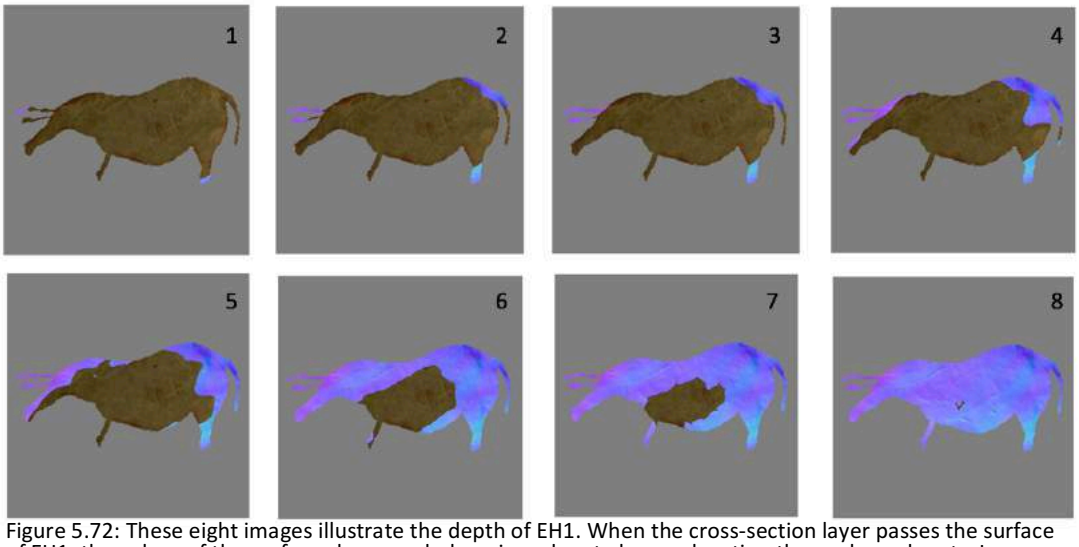

Figure 5.72: These eight images illustrate the depth of EH1. When the cross-section layer passes the surface of EH1, the colour of the surface changes; dark regions denote lower elevation than coloured parts. Images 1 and 2 are for 0.1mm - 35.6mm, 3 and 4 for 35.7mm - 53.4mm, 5 and 6 for 53.5mm - 71.3mm, and 7 and 8 for 71.4mm - 89.1mm.

Distortion on images (horizontal rotation, x0°, y-70° to y80°)

The simulation demonstrates that the appearance of EH1 is significantly different as the viewing angle moves from side to side. Basically, the anterior and the posterior side becomes enlarged alternately when the viewing position changes from left and right respectively. This deformation is not caused by perspective but by the wall's topographic condition. When the image is seen from the direct position (y0°), the shape of the wall appears flat and therefore so does the horse. Regarding the posterior, the reason for the transformation is attributed to the elevated ridge line which overlaps the contour of the croup: when EH1 is viewed from y80°, the ridge substituted for the dorsal line shortens the overall length of the horse itself and cause a disturbance of the overall proportion. For this reason, viewers perceive that the posterior is disproportionally large against the rest of the body as a result (see Figure 5.70). The distortion most likely occurs between y30° and y80°.

As for the anterior body, the wall elevates and leans front at the head and neck. This topographic condition magnifies the presence of these body sections once it is seen from the left (Figure 5.73). As well as the enlargement caused by the perspective, the head and neck appear elongated due to the convex and the surface's tilt itself; especially the muzzle seems to extend further forward. Therefore, the image is considerably distorted. This phenomenon is most visible when the viewing angle is between y-70° and y-30°.

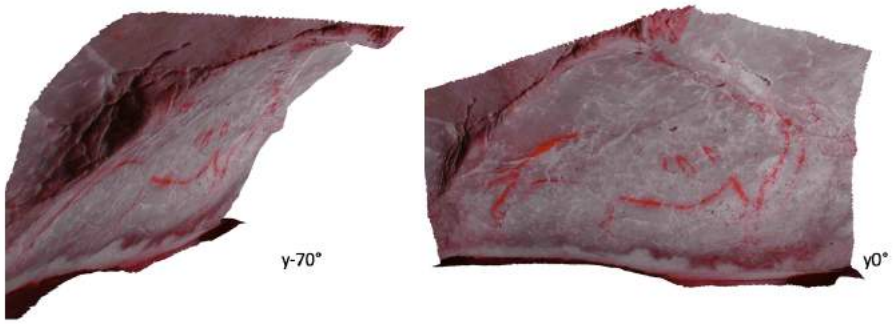

Figure 5.73: EH1 seen from y-70°(left), and y0° (right). The head and neck are significantly distorted when viewed from the left due to the convex topography on these body sections. The leaning wall also enhances the extent of the distortion.

Apart from these distortions, the hind leg is also noticeably deformed. The leg is located on an elevated area near the floor, and it appears straight when viewed from y0°. However, as the viewpoint moves to the right, the actual shape of the wall is gradually disclosed, and the limb appears significantly bent. This distortion is particularly salient between y0° and y80°.

Horse (EH2)

General description

An outline horse facing right (Figure 5.74). This image is drawn in yellow on a convex surface developed from a low ceiling. EH2 is an incomplete figure as the posterior body is missing. The muzzle is noticeably long. There are also ears, although they are unclear. The cervical-dorsal line is separated into two lines at a point, of which the upper contour is given in reddish colour. This red outline overlaps the ventral line of another image (ED1) at its edge, which is located just above this horse. Also, two red lines are left in parallel on the neck. Red pigment is also visible on the left side of the wall, but whether or not it is related to this image is unknown. The length is 61 cm, and the image is located on a height of about 120 cm from the floor.

Figure 5.74: EH2, outlined horse facing right. The image is provided only with the anterior body. Although the used colour is yellow, a part of the dorsal line appears red. Also, two parallel lines are left inward from the frontal neck.

Integration of natural lines

Several noticeable deep grooves run on this wall. Also, the convex develops as a wedge from the ceiling, and it forms a sharp ridge at its bottom. Although those grooves are not used for outlining EH2, the ridge is integrated into the ventral line; a part of the belly line partly overlaps the peak-line of the wedge. (Figure 5.75).

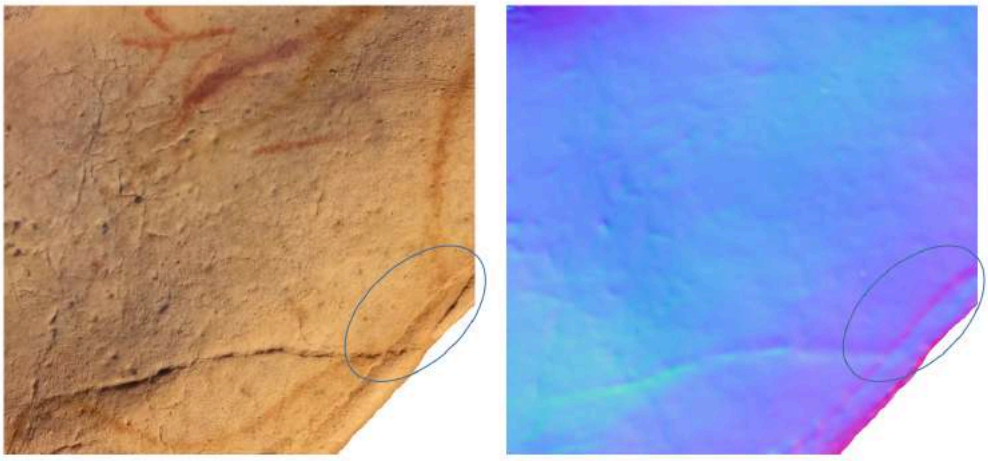

Figure 5.75: An example of integration in EH2. A ridgeline on the convex ceiling is used for a part of the ventral line.

Topographic condition:

Because EH2 is incomplete, the examined body parts are the head, the whole neck-shoulder and mid-torso. As mentioned earlier, the protruded ceiling shapes as a wedge, and therefore the wall curves sharply toward the tip. The total depth is approximately 129mm (the model is at 1/30 scale: Figure 5.76). A part of the ventral mid-torso corresponds to the highest point, while a part of the dorsal mid-mid-torso to the lowest. All body parts are defined their elevation level within a limited range between 24.3mm and 96.8mm (high: 24.3-48.4mm, medium: 48.5-72.6mm, and low: 72.7-96.8mm). The ranges outside of this range (0.1-24.2mm and 96.9-129mm) do not define the elevation level of any body parts, and therefore there are no extra elevation levels in EH2.

Figure 5.76: EH2 (1/30 scale) seen from the vertical position. The highest elevation is found on the ventral mid-torso, while the lowest is on the dorsal mid-torso.

The surface is first detected at the left edge of the ventral mid-torso. This detected region gradually extends as the cross-section layer proceeds between 0.1mm and 24.2mm (see figure 5.77, 1-2). However, but this area fails to define the elevation level of any sections. In the high-level elevation, the detection continues from the above area, but the surface also starts to pass the layer at the head and the neck. This high elevation topography constantly expands between 24.3mm and 48.4mm and covers the almost entire central-ventral side of the body (3-4). Therefore, the head, the central-ventral neck-shoulder and the ventral mid-torso are assessed as high. During the next phase (medium: 48.5-72.6mm), detection occurs on the dorsal side. The topography of the ventral neck and the central mid-torso mostly pass the layer (5-6); the detected region also expands to the ventral side. At this depth, the dorsal thigh remains undetected, meaning that the part is the lowest of EH2's body parts. The major area of the section is finally detected by the depth of 96.8mm (7-8).

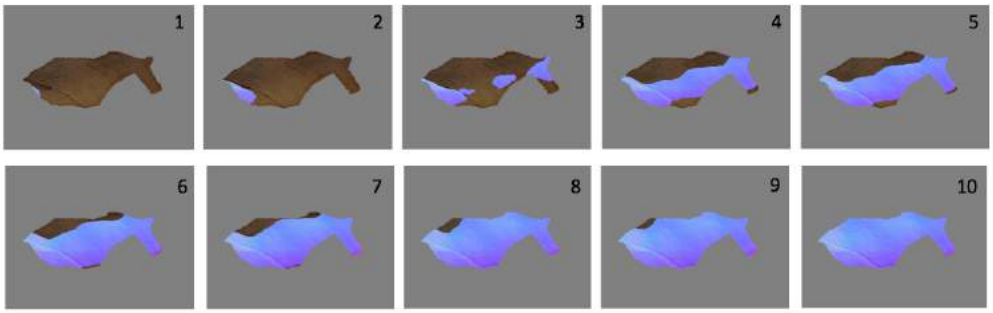

Figure 5.77: These ten images illustrate the topographic depth of EH2. When the cross-section layer passes the surface of EH2, the colour of the surface changes; dark regions denote lower elevation than coloured parts. Images 1 and 2 are for 0.1mm - 24.2mm, 3 and 4 for 24.3mm - 48.4mm, 5 and 6 for 48.5mm - 72.6mm, 7 and 8 for 72.7mm - 96.8mm, and 9 and 10 for 96.9mm - 129mm.

Distortion on images (horizontal rotation, x20°, y-70° to y70°)

EH2 is mostly flat, and therefore remarkable transformations are not discernible in most of the body parts. Although the mid-torso and neck-shoulder are continuously contracted and stretched as the viewing-point moves to the side to side, the overall appearance of EH2 is more or less similar to that in the 2D simulation. However, the muzzle which is located on the edge of the ceiling appears moving forward and backwards. This deformation is absent in the 2D simulation (Figure 5.78). This phenomenon is especially visible in the angle range between y-20° and y70°.

Figure 5.78: EH2 on the 3D surface (left) and 2D surface (right) seen from y70°. The muzzle appears considerably longer in the 3D simulation than in the 2D simulation.

Deer (ED1)

General Description

An outline red deer facing right (Figure 5.79). ED1 is incomplete as the posterior body is absent. The V-shaped ears are confirmable, although the face does not contain the eye, nose and mouth. The contour continues from the ear to the left but disappears at a point. The ventral line also is invisible at the frontal neck. This deer is located immediately above EH2, and the ventral line of ED1 and the dorsal line of EH2 partially superimpose. The length is about 25 cm, and the image is fixed on a height of approximately 123 cm above the nearest floor.

Figure 5.79: ED1, outline red deer facing right. This is an incomplete image as it only contains the anterior body. ED1 is located immediately above EH2.

Integration of natural Line

This image is placed on a wall where numerous small grooves exist. However, none of them is integrated into any sections of ED1 except for the muzzle: the outline of the muzzle discontinues between its lower and upper part, but a short and thin groove connects the discontinuity (Figure 5.80).

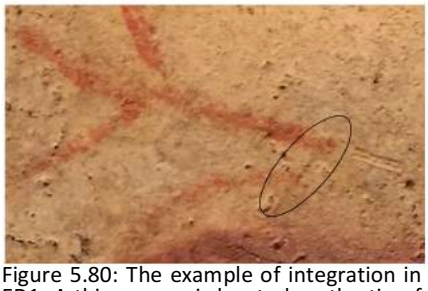

Figure 5.80: The example of integration in ED1. A thin groove is located on the tip of the muzzle connecting the upper and the lower jaw.

Topographic condition

Because ED1 is not a complete figure, the examined sections are the head, neck-shoulder, and dorsal mid-torso. The total depth is significantly shallow, with approximately 19mm (the model is at 1/50 scale: Figure 5.81). The tip of the ear corresponds to the highest point, whereas the muzzle and the dorsal mid-torso to the lowest. All body sections are defined their elevation level within in a range between 11.8mm and 16.1mm (high: 11.8-13.2mm, medium: 13.3-14.6mm, and low: 14.7-16.1mm). The depth outside of this range (0.1-11.7mm and 16.2-19mm) does not define the elevation level of any body parts, and therefore there are no extra elevation levels in this image.

Figure 5.81: ED1 (1/50 scale) seen from the vertical position. The highest elevation is found on the tip of the ears, while the lowest is on the muzzle and dorsal mid-torso.

The surface is first detected at the tip of the right ear, and this high area extends downward. In the meantime, the tip of the left ear also passes the cross-section layer, and then the entire ears are fully detected by a depth of 11.7mm (1-2: Figure 5.82). However, the detected area is not large enough to define the elevation level of the head. The most extent of ED1 passes the layer during the next phase: the detection occurs noticeably, defining the elevation level of the dorsal-central neck-shoulder as high (11.8-13.2mm: 3). In the medium level, the detection extends to the right and left, and consequently, the ventral neck-shoulder is fell into this level (4). The remained parts (the head and the dorsal mid-torso) are assessed their elevation as low within the range between 14.7mm and 16.1mm (5) These low body parts are partially left undetected; however, they are also entirely detected by19mm (6).

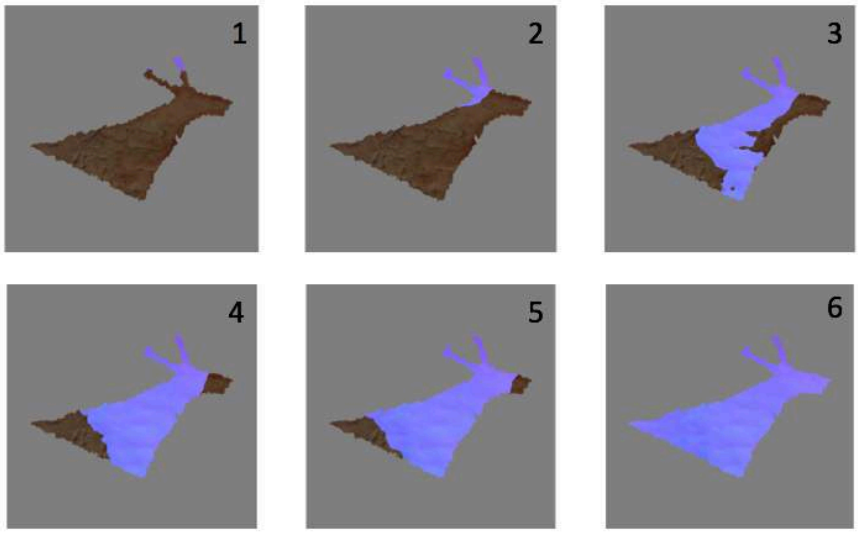

Figure 5.82: These six images illustrate the depth of ED1. When the cross-section layer passes the surface of ED1, the colour of the surface changes; dark regions denote lower elevation than coloured parts. Images1 and 2 are for 0.1mm - 11.7mm, 3 for 11.8mm - 13.2mm, 4 for 13.3mm - 14.6mm, 5 for 14.7mm -16.1mm, and 6 for 16.2mm - 19mm.

Distortion on images (horizontal rotation, x20°, y-70° to y70°)

Overall, significant distortions are not detected in the 3D simulation. The appearance of ED1 is also constantly identical, compared to that in the 2D simulation. This result can be attributed to the absence of the outstanding topographic feature on this wall; in fact, this surface is almost flat. Therefore, the topographic condition of the medium itself is identical to the 2D setting.

Aurochs (DA1)

General description

An outline aurochs facing right (Figure 5.83). depicted in black, DA1 is a complete figure. However, the appearance is somewhat ambiguous due to decay; especially it is difficult to identify the outline of the head and ventral anterior. According to Groenen (2007), the face contains ears, horns, eyes, and half-open mouth.

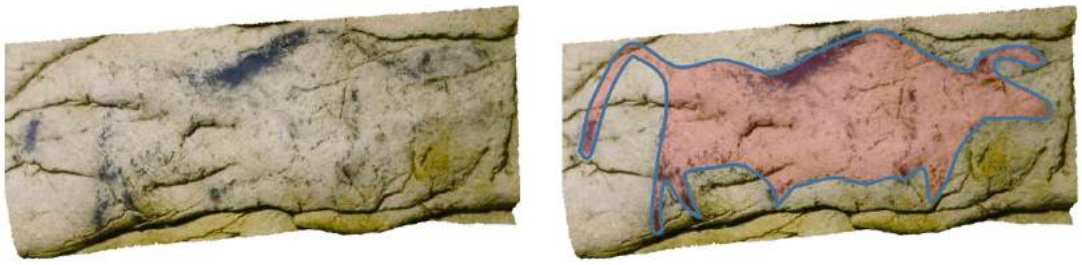

Figure 5.83: DA1, outline aurochs facing right. DA1 is under severe decay as the contour has gone somewhat unclear in some parts.

The dorsal line is drawn in a thick line. Although the tail is partly invisible, its tip is well-preserved so that viewers can grasp the shape of the entire tail. Thanks to the shape of the back legs and tail, DA1 acquires dynamism as if an aurochs is vigorously kicking the ground. The total length of this image is 46 cm, and it is fixed at the height of 197 cm from the nearest floor. However, the floor of this area was dug down 25 cm during an archaeological excavation.

Integration of natural lines

The relationship between the natural line on this wall and the DA1's outline is unique. This wall consists of deep grooves and edges; the presence of those lines are emphasised once the light generates shadows. When DA1 is viewed under illumination, the natural line highlighted by the shadow and the black contour of DA1 appear combined, and as a result, the image seems if lurking among such natural lines. Therefore, it is difficult to distinguish its existence from the background. However, there are only a few natural lines integrated into the image: edge lines respectively overlap on the forehead and the belly (Figure 5.84). Otherwise, no integration is discerned.

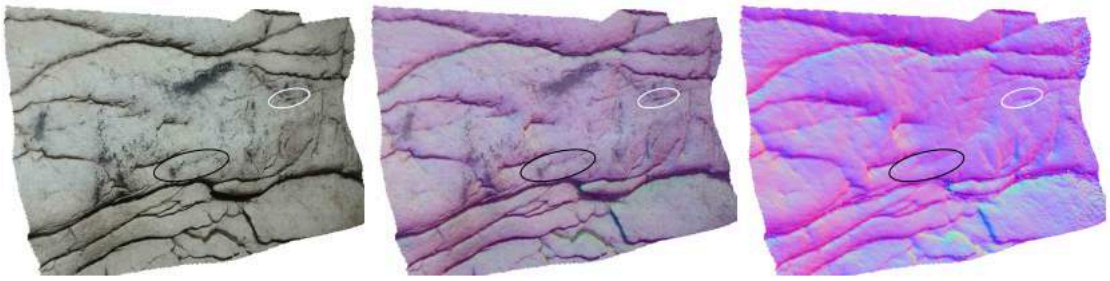

Figure 5.84: Examples of integration in CB2. The forehead is outlined along with a steep edge (as indicated by the white oval). The ventral line also partly corresponds to an edge line (the black oval).

Topographic condition

Even though this surface is finely corrugated, the topography is relatively mild. Especially, the wall is almost flat on the anterior side, although it forms a gentle convex on the ventral shoulder. The depth of DA1 is approximately 29mm (the model is at 1/100 scale: Figure 5.85). The tip of the hind limb corresponds to the highest point, while the central mid-torso to the lowest. Almost all body parts are defined their elevation level within in a range between 7.1 mm and 29mm (high: 7.4-14.5mm, medium: 14.6-21.8cm, low: 21.9-29mm). There is

Figure 5.85 DA1 (1/100 scale) seen from the vertical position. The highest elevation is found on the hind limb, while the lowest is on the central mid-torso.

also a body section located in the range between 0.1mm and 11.7mm, and therefore, this range is defined as the extra-high level).

The surface is first detected at the tip of the left hind limb. This elevated area extends upward, involving the other back leg, and the majority of this body section is detected by 7.3mm (Figure 5.86, 1-2). Thus, the hind limbs are assessed as the extra-high. At this time, the tip of the tail and a part of the dorsal thigh also passes the cross-section layer. The elevation for these posterior regions is the high level as detected areas further extend and cover the dorsal-ventral thigh by 14.5mm (3-4). Most of the body parts is located in the medium elevation level: as the detection continues from the posterior, the ventral neck-shoulder, central thigh, almost entire mid-torso, tail, and frontal leg are assessed as the medium level by 21.8mm (5-6). The body parts which remain undetected are therefore revealed: the head, the dorsal-central neck-shoulder. These anterior regions are finally assessed as the low level (21.9-29mm: 7-8). Due to the corrugated wall, there are still undetected areas on each middle section, but they also pass the layer by 29mm.

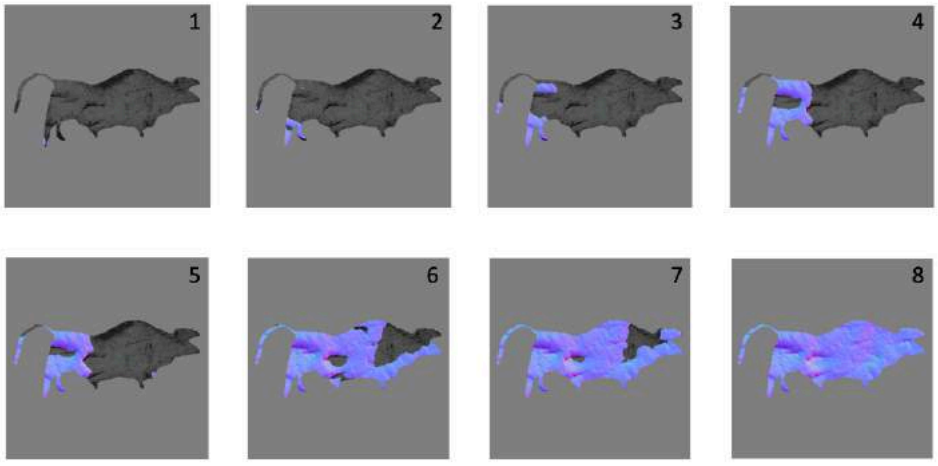

Figure 5.86: These eight images illustrate the topographic depth of DA1. When the cross-section layer passes the surface of DA1, the colour of the surface changes; dark regions denote lower elevation than coloured parts. Images1 and 2 are for 0.1mm - 7.3mm, 3 and 4 for 7.4mm - 14.5mm, 5 and 6 for 14.6mm - 21.8mm, and 7 and 8 for 21.9mm - 29mm.

Distortion on images (horizontal rotation, x10°, y-80° to y80°)

As for this aurochs, distortion cannot be confirmed due to the ambiguity of the outline; the unclear contour makes it difficult to identify deformed regions. Even regarding the visible area such as the thigh and dorsal, the 3D simulation does not demonstrate distinguishable distortions, compared to DA1 in the 2D simulation. This is because of the flat topography of the wall.

Anthropomorphic figure (BBM1)

General description

An anthropomorphic figure, generally known as the Bison-man because it possesses the anterior parts of a bison and the posterior of a human (Figure 5.87). BBM1 is vertically fixed on one of the stalagmite pillars in the room B. All body parts are provided, including the tale. The outline is thickly drawn in black; however, the concentration of small dents somewhat ambiguates the anterior ventral area. The artist of this figure also executed a remarkable engraving skill: the section from the pelvis to the feet is meticulously incised so that it represents a full detail of human legs (even one can distinguish the ankles). Additionally, a few black dots are left on BBM1. Bison-man has significant iconographic importance in European Upper Palaeolithic art because the theme frequently appears: such bison-man figures are commonly found from Franch caves (e.g. Chauvet, Trois-Freres, and La Gabillou). The presence of BBM1 indicates that the cultural significance of this theme is also shared in Spain (Groenen 2007). Bison-man is 75 cm long and located at the height of 94 cm (at its leg) from the nearest ground.

Figure 5.87: BBM1, image of a human-bison hybrid. Vertically fixed on a stalagmite pillar, all body parts are provided. As well as painting, the artist of BBM1 also executed a remarkable engraving skill on the feet.

Integration of natural lines

Grooves and ridges are absent on this stalagmite. However, the irregular surface generates edges, and BBM1 uses those edges dynamically for its contour. This figure is located on a convex surface whose entire outline already appears basic form of Bison-man (Figure 5.88). Therefore, the artist who created Bison-man simply outlined the

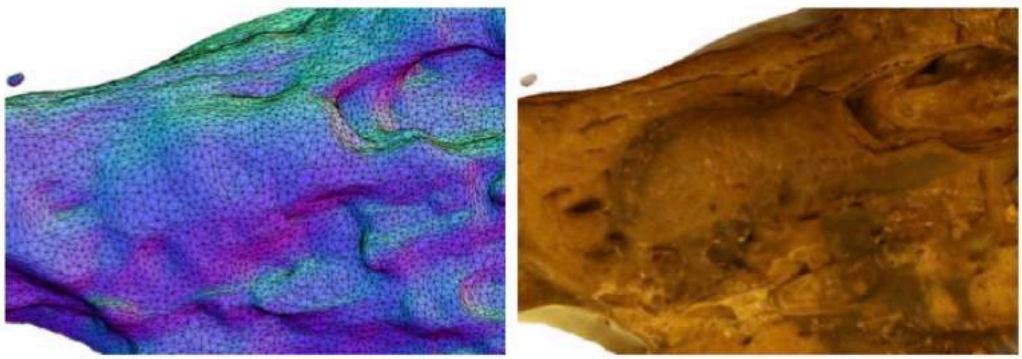

Figure 5.88: These two pictures represent BBM1 (right) and its topographic condition (left). Bison-man is located on a convex surface whose appearance is already reminiscent of its basic form. The contour is drawn along the edge of this elevated wall.

whole body of BBM1 along the edge of this convex surface. Also, there is a half arc edge at the bottom of the buttock and the right side of the hind feet. The tail is depicted along this edge line.

Topographic condition

The bison-man is located on a convex surface that developed on a stalagmite pillar. It possesses a sculptural quality. The total depth is 156mm (1/20 scale: Figure 5.89). The highest point is located in the central mid-torso, while the lowest point corresponds to the extended area of the head. All body parts are defined their elevation level within the range between 0 cm and 69.9cm (high: 0-23.4mm, medium: 23.5-46.8mm, low: 46.9mm-70.2mm). The extended part of the head is disproportionally deep, comprising more than half of the total depth, 85.7mm (70.3mm-156cm); however, this section fails to cover the major extent of the head. There is not the extra low level for BBM1, therefore.

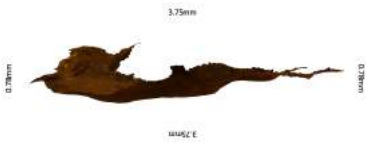

Figure 5.89: BBM1 (1/20 scale) seen from the vertical position. The highest elevation is found on the central mid-torso, while the lowest is on the head.

The high area begins at the central mid-torso, and detection continues upward and rightward from that torso. By a depth of 23.4mm, most of the central neck and central thigh pass the cross-section layer (Figure 5.90 1-3). The next level is the medium (23.5-46.8mm), and most of the body parts belong to this elevation level: the dorsal-central neck-shoulder, dorsal-ventral mid-torso, and the dorsal-ventral thigh (4-6). The detected areas further expand as the cross-section layer proceeds, and finally, the rest of the body parts (the head, ventral neck-shoulder, tail, and hind leg) are defined as the low-level elevation (46.9-70.2mm: 7-9). The head partly remains undetected, and this area passes the layer by the depth of 156mm (10-12).

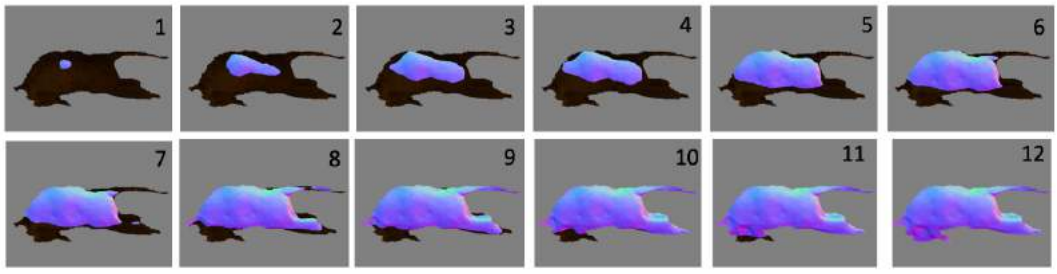

Figure 5.90: These 12 images illustrate the depth of BBM1. When the cross-section layer passes the surface of BBM1, the colour of the surface changes; dark regions denote lower elevation than coloured parts. Images 1-3 are for 0.1mm - 23.4mm, 4-6 for 23.5mm - 46.8mm, 7-9 for 46.9mm - 70.2mm, and 10-12 for 70.3mm - 156mm.

The distortion to images (horizontal rotation, x0°, y-80° to y70°)

The 3D simulation highlights a sculptural aspect of Bison-man. Seeing Bison-man from side to side, the image is not merely flattened unlike in the 2D simulation, but instead, it shows the ventral side and its back as if viewers walking around a sculpture. Particularly, Bison-man gradually reveals the other leg hidden behind the front leg when the angle increases from y-30°, and viewers can finally confirm the detail of the back thigh, two legs, and even ankles (at y60°).

Changing viewing angles also generates a distortion on the legs, although the main body (from the head to the thigh) remains unchanged. The legs extend straight downward when viewed from around the direct position, while they appear bending backwards as the viewing angle decreases (Figure 5.91). This is because of the convex on the calf and foot. This distortion seems noticeably animating the image once a viewer moves between y-70° and y0°.

Figure 5.91: BBM1 viewed from y0° (left) and y-70° (right). Because of its sculptural quality, the image appears considerably different as viewing angle changes. In particular, the distortion on the hind leg is noteworthy: when the viewpoint moves to the left, the limb gradually bends backwards. This change is due to the convex surface on the calf and feet. Because of this distortion, BBM1 constantly appears folding and stretching its hind legs within the angle range between y-70° and y0°.

Unidentifiable quadruped (BU1)

General description

An outline quadruped mammal facing right (Figure 5.92). BU1 is a headless figure, and therefore it is impossible to ascertain its specific identification. BU1 is located on the wall on the south of Room B where the ceiling becomes considerably low due to stalactites developing along the wall. This environmental condition forces viewers to crouch down to view the

Figure 5.92: BU1, outline quadruped mammals facing right. Entire body except the head is provided; because the neck is attached to a calcite plate which vertically develops from the wall, BU1 appears as if beheaded by the plate.

image. The contour is drawn in black. The tail is depicted as a thick and long arc. The dorsal line is also conspicuous. In contrast, the ventral line is somewhat unclear from the thigh and to the chest. In the place where the head should be attached, there is a thin calcite plate which develops vertically from the wall as if beheading the head. The total length of BU1 is approximately 60 cm, and it is fixed on a height of 135 cm from the nearest floor (the dorsal line from the floor).

Integration of natural lines

BU1 borrows natural lines in some of its sections. The most salient of these is the contour line of the buttock. As will be discussed in detail later, the thigh is placed on a large protuberance, and the buttock is outlined along the left edge of the convex surface (Figure 5.93). Furthermore, by viewing the image from the right, the edge of this protuberance gradually overlaps with the buttock and in the end becomes the contour of the buttock itself. Another integration sample is found in the ventral line. As three wavy grooves cross the image obliquely from the convex thigh to the lower right, and one of them appears overlapping with the ventral line (particularly blurred belly: see Figure 5.93). At this time, another one of these grooves appears the missing forelimb.

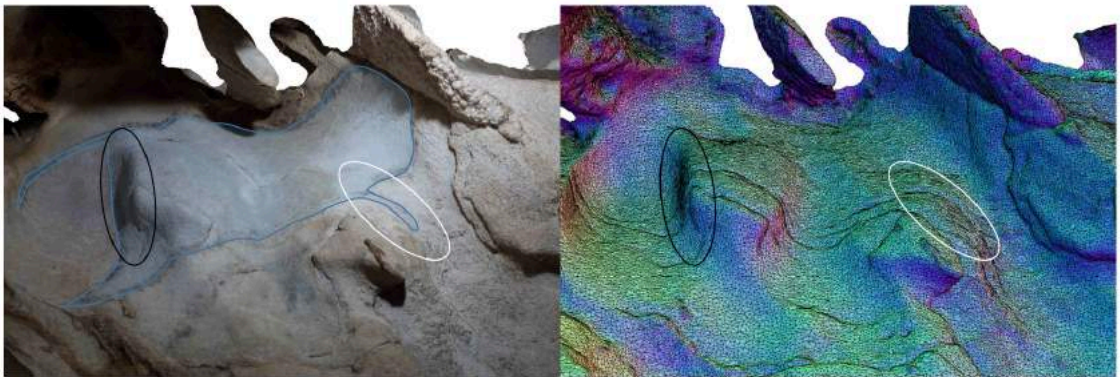

Figure 5.93: Examples of integration in BU1. An edge of a large convex surface is used for outlining the buttock (see the black circle), while a deep groove corresponds to the ventral line. This groove extends to the further right, as if depicting the missing forelimbs (see the white circle).

Topographic condition

The large convexity which corresponds to the thigh highlights the overall topography of this wall as its elevation is remarkably higher than any other regions except for the tail. The tail is placed on the area at which the surface sharply rises. The depth of BU1 is approximately 146mm (1/40 scale: Figure 5.94). The tail corresponds to the highest point, while the ventral neck to the lowest. Most of the body parts are defined their elevation level between 98mm and 146 mm (high: 98-114mm, medium: 105-130mm,

Figure 5.94: BU1 (1/40 scale) seen from the vertical position. The highest elevation is found on the tail, while the lowest is on the ventral neck.

low: 131-146mm). The tail, hind limb and entire thigh are located within the range between 0.1mm and 98mm. This range is treated as the extra-high level.

The surface is first detected at the tip of the tail. Immediately after the first detection, the convex on the thigh starts passing the cross-sectional layer, and the posterior part are almost entirely detected by 98mm (Figure 5.95, 1-3). The elevation of the right edge of the neck is also as high as these body sections; however, the area fails to involve the most extent of the neck. Meanwhile, the topography of the ventral mid-torso is detected in the next phase; the detection begins from a depth of 99mm, and most of this region passes the layer by 114mm (4-6). As the layer further proceeds, the detected area expands inward. Consequently, the central mid-torso, dorsal-central neck is categorised as the medium elevation (115-130mm: 7-9). At this time, undetected areas are the dorsal mid-torso and ventral neck, and they are fell into the low elevation level. Their surface is finally detected between 131-146mm (10-12).

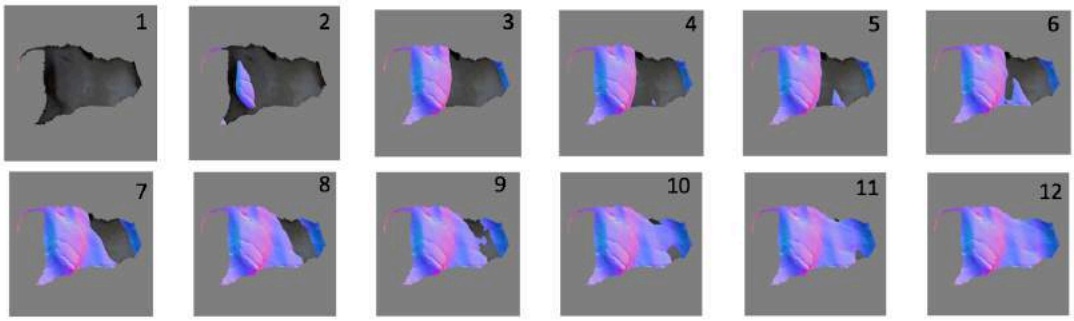

Figure 5.95: These 12 images illustrate the depth of BU1. When the cross-section layer passes the surface of BU1, the colour of the surface changes; dark regions denote lower elevation than coloured parts. Images 1-3 are for 0.1mm - 97mm, 4-6 for 98mm - 114mm, 7-9 for 105mm -130mm, and 10-12 for 131mm - 146mm.

The distortion on images (horizontal rotation, x20°, y-40° to y40°)

When the viewing position shifts, deformation takes place in the thigh. As was mentioned earlier, the buttock's contour overlaps with an edge of the convex surface (when the angle set between y30 and y40°: see Figure 5.96). However, the overlapping two lines are gradually detached as the angle decreases, emphasising the sculptural quality of the thigh, and finally, the back side of the convex surface comes in sight.

Figure 5.96: BU1 viewed from y-70° (left), y0° (centre), and y40° (right). The shape of the thigh significantly changes as the viewing position moves.

During this movement, the appearance of the thigh changes significantly, and BU1 on a 2D surface does not generate such deformation. Apart from this distortion, distortion is not notably visible within the narrow range of the viewing angle; interrupted by the low ceiling of stalactites, viewers can see only limited aspects of BU1.

Bison (BB1)

General description

An outline bison facing right (Figure 5.97). Being drawn in black, all body parts are provided; even the image contains a phallus-like section. Although the posterior is provided in a precise contour, the anterior part is somewhat obscure; especially, the outline of the forelimb and breast seems not clearly defined. The contour recovers its clarity at the head, although the facial elements (nose, eyes and mouth) are not depicted. The body length is 99 cm, and it is fixed at a height of about 80 cm from the nearest floor.

Figure 5.97: BB1, outline facing right. The image is well-preserved, although the outline is somewhat ambiguous at the anterior ventral.

Integration of natural lines

Several grooves and edges form on this wall, and some of those natural lines are integrated into BB1's contour. Figure 5.98 illustrates the original pattern of the wall, and the configuration already resembles to the basic form of a quadruped mammal. This fact allows us to quickly assume that the artist of BB1 mostly relied on the pre-existing pattern rather than his\her own imagination. According to Figure 5.98, the bison's dorsal line is superimposed on a deep groove. Under this groove, there is an edge line caused by an elevational gap which runs horizontally. Although this line extends from the right to the left, it suddenly changes its direction to the bottom at a point. This

Figure 5.98: BB1 (left) and highlighted topographic images (centre and right). The original pattern of the wall is already a reminiscent of BB1 as the dorsal, hind leg, and ventral line mostly relies on natural lines.

horizontal and vertical edge is also integrated into the contour of the ventral line (belly) and hind limb.

As well as these integrations, BB1 also contains an intriguing case of integration. The wall noticeably elevated on the right to the image; this rise generates an edge running diagonally. When the picture is viewed from the right, this edge overlaps the outline of the back head and neck (see Figure 5.101). The use of natural lines in this way attests the existence of the multiple view-points.

Topographic condition

BB1 is depicted on an overall concave surface. The thigh, head and neck-shoulder are provided on the outer edges of the bowl-like topography, and therefore their elevation is higher than the other sections. The total depth of BB1 is 208mm (the model is at 1/200 scale: see Figure 5.99). The hind leg corresponds to the highest point, while the ventral mid-torso as the lowest. However, the elevation level of all body parts is defined between 49mm and 195.8mm (high: 49-97.9mm, medium: 98-146.8mm, low: 146.9-195.8mm). A body part is located in the range between 0.1mm and 48.9mm, whereas no sections belong to the deepest level (195.9mm and 208mm. Therefore, there is the extra-high level in BB1.

Figure 5.99: BB1 (1/200 scale) seen from the vertical position. The highest elevation is found on the hind leg, while the lowest is on the ventral mid-torso.

The surface is first detected at the tip of the hind leg. The detected area continues to expand upwards and covers over half of the back limbs by 48.9mm (Figure 5.100, 1-3). Simultaneously, both edge of this overall concave wall (the head and buttock) also passes the cross-section layer, but the extent is limited. During the next level which is defined as the high elevation, the detected region further spread inward from both edges and covers the whole head, tail and the major section of the ventral thigh (49-97.9mm: 4-6). As the layer proceeds, the dorsal and the central thigh are assessed as the

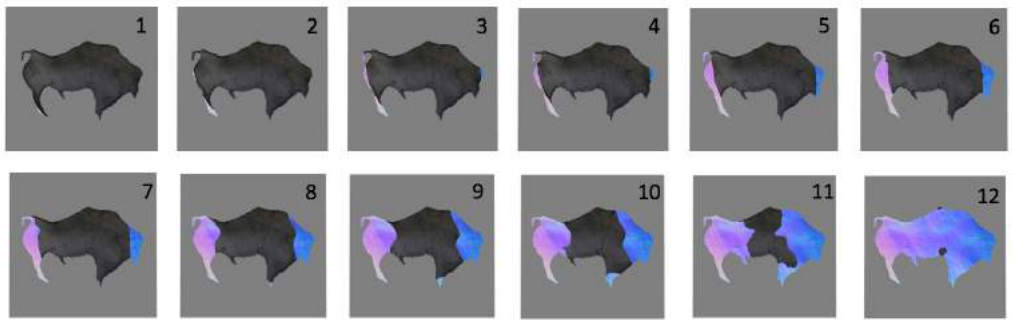

Figure 5.100: 100: These 12 images illustrate the depth of BB1. When the cross-section layer passes the surface of BB1, the colour of the surface changes; dark regions denote lower elevation than coloured parts. Images 1-3 are for 0.1mm - 48.9mm, 4-6 for 49mm - 97.9mm, 7-9 for 98mm - 146.8mm, and 10-12 for 146.9mm - 195.9mm.

medium level (98-146.8mm: 7-9). The neck also starts passing the layer; however, the extent is limited because the elevation gap between the face and neck is considerably large. The neck is defined as the low level as it is fully detected between 146.9 and 195.9mm (10-12). The entire mid-torso is also categorised as this level; although the elevation of the central mid-torso is slightly higher than the dorsal-ventral sides.

Distortion on images (horizontal rotation, x10°, y-60° to y70°)

As a viewing point moves from side to side, this wall significantly distorts BB1. The remarkable distortion occurs particularly in sections located on the outer edges and in both frontal and back limbs. First of all, the head and neck-shoulder are deformed when the viewing point moves to the right (from y0° to y70°); the elevated rims of the bowl-shaped concavity push those body parts upward. Consequently, BB1 appears as if shaking its head up and down and also side to side. In particular, the distortion is noticeably perceived when the viewpoint is between y10° and y40° (Figure 5.101). In the 2D simulation, this distortion is not detected as the head and neck merely appear enlarged when the viewing angle increases. This type of distortion is also confirmed in the thigh (between y-20° and y-60°) because the part is located on the other elevated edge of the topography.

Figure 5.101: BB1 on the 3D surface (left) and 2D surface (right), viewed from y60°. Pushed inward by the elevated surface, the anterior body appears significantly contracted. In contrast, BB1 on the 2D surface maintains its body proportion unchanged.

A significant distortion also happens to both front and hind limbs. Since they are depicted on an elevated area, their directions appear constantly changing as the viewpoint moves. Unlike the other distorted sections (head, neck-shoulder, and thigh), the deformation on the limbs is visible throughout all rotation process: although both legs appear bent forward at y-60°, they are bent backwards at y70°.

Bison (BB2)

General description

An outline bison facing right (Figure 5.102). The contour is drawn in black. Located on the immediate left (approx. 5cm) to BB1, BB2 seems as if following after the other bison. All the body parts are provided except for the tail. The image contains a robust face with details such as the eye, horn, and mouth. The foreleg is depicted considerably short; it grows only subtly from the ventral line. Compared to BB1, the presence of BB2 is weaker as the contour appear slightly pale which causes an ambiguity. The artist of this bison carefully prepared before carrying out image-making: the limestone surface behind BB2 was cleaned and finely abraded (Groenen et al. 2007). This artistic execution adds the whitish colour to the image. The length of the image is about 70 cm, and it is fixed at a height of 96 cm from the nearest floor.

Figure 5.102: BB2, outlined bison facing right. Located immediately on the left to BB1, all body parts are provided. As the wall behind the image is cleaned and abraded, it is considered that the artist of BB2 carefully prepared before carrying out the image-making.

Integration of natural lines

Integration is confirmed in the head and dorsal line. The groove which depicts the dorsal of BB1 diagonally crosses the head of BB2, and the horn is drawn along this groove (Figure 5.103). There is also an edge line extending obliquely to the left from the upper part of the head, and this line is integrated into the cervical dorsal line. Around a centre of the dorsal, this edge disappears, but instead, the dorsal line on the posterior is substituted by a ridge which forms along the peak of the convex surface. Apart from these examples, no regions borrow an assist of natural lines.

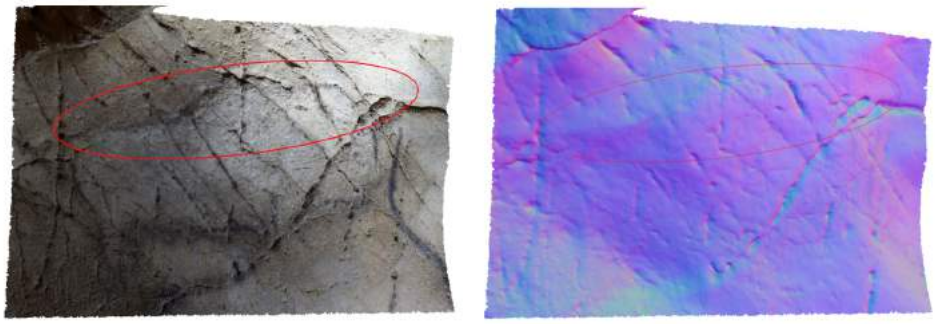

Figure 5.103: BB2 (left) and highlighted topographic images (right). The groove which is integrated into the dorsal line of BB1 obliquely crosses the head of BB2, and the horn is drawn along this groove. There is also an edge line extending obliquely to the left at the upper part of the head, and this line corresponds to the anterior dorsal line. This edge disappears at the centre of the dorsal area, but instead, a ridge which forms by the peak of the convex surface substitutes the posterior dorsal line (see the red circle).

Topographic condition

BB1 is located on an overall-convex wall. Especially, the surface profoundly elevates in the dorsal mid-torso, featuring the topographic condition of the image. The depth of BB2 is approximately 86mm (the model is at 1/200 scale: Figure 5.104). The dorsal mid-torso corresponds to the highest point, while the horn to the lowest. The range within which all body parts are defined their elevation level is limited between 0.1mm and 60.2 mm (high: 0.1-17.2mm, medium: 17.3-38.7mm, low: 38.8-60.2mm). None of the body parts is defined their elevation level within the range between 60.3mm and 86mm, and there is not the extra-low level in BB2, therefore.

Figure 5.104: BB2 (1/200 scale) seen from the vertical position. The highest elevation is found on the middle dorsal, while the lowest is on the horn.

Detection begins from the peak of the convex surface (the dorsal mid-torso. This area extends downwards, and the dorsal-central middle part passes the cross-section layer by17.2 mm (1-2: Figure 5.105). Simultaneously, the surface of the ventral mid-torso is also detected, although its extent is limited to the edge of the belly. During the medium-level elevation, the highlighted region further expands: firstly, the ventral mid-torso is fully detected, and then the whole neck-shoulder passes the layer (17.3-38.7mm: 3-5). The peripheries of the convex surface (the head, thigh, and hind leg) remain undetected. These parts are assessed as the low elevation: these body parts mostly passes the layer by the depth of 60.2mm (6-8). At this time, the horn and the left edge of the thigh have not been detected yet. It requires further 25.8 mm until they fully pass the layer.

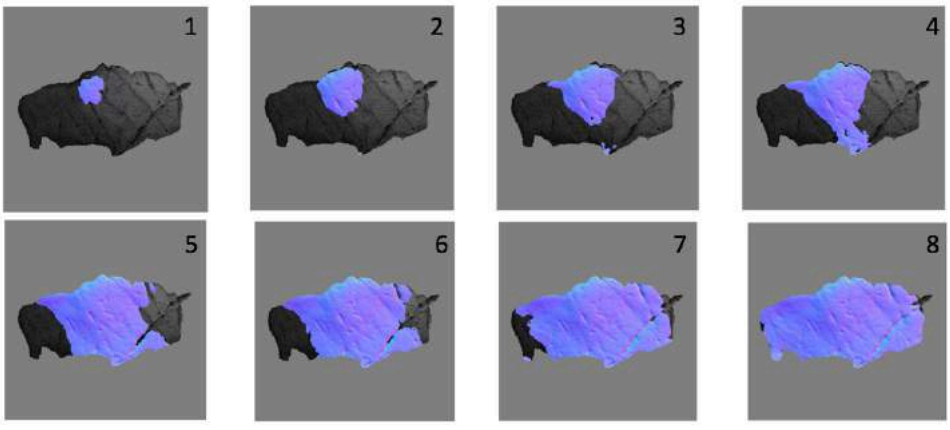

Figure 5.105: These eight images illustrate the depth of BB2. When the cross-section layer passes the surface of BB2, the colour of the surface changes; dark regions denote lower elevation than coloured parts. Images 1 and 2 are for 0.1mm - 17.2mm, 3-5 for 17.3mm - 38.7mm, and 6-8 for 38.8mm - 60.2mm.

The distortion on the image (horizontal rotation, x10°, y-60° to y70°)

Overall, the 3D simulation demonstrates a noticeable distortion. The large convex in the dorsal mid-torso is the cause of the distortion: due to its high elevation, the middle part hides the thigh when BB2 is viewed from the right. Consequently, that causes a contraction of BB2's body (at y70°: Figure 5.106); the anterior part appears far enlarged, while the posterior seems shrunk. This distortion is most remarkably confirmed within the angle range between y50° and y70°. The 2D simulation does not generate this result.

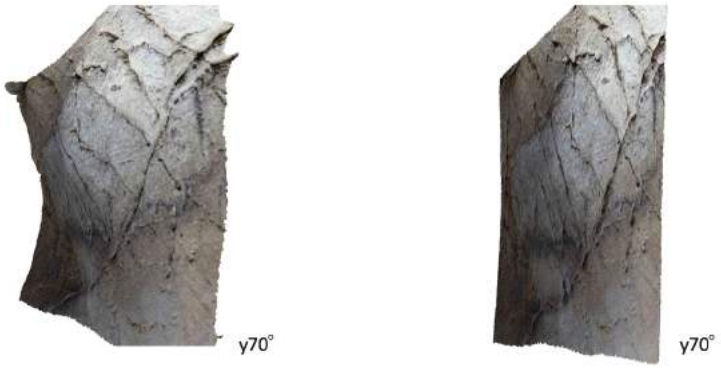

Figure 5.106: BB2 on the 3D surface (left) and 2D surface (right), viewed from y70°. The elevated wall on the mid-torso hides the thigh and causes a significant contraction. At the same time, the anterior part appears by far enlarged. Such a distortion is absent in BB2 on the 2D wall.

On the other hand, BB2 is not remarkably deformed, even though being viewed from the left. Since the elevation of the mid-torso is higher than the head and neck-shoulder, these sections also goes unseen by the middle area. However, the extent is somewhat limited as BB2 is more or less identical to one on a 2D surface. This is because the elevation gap between the mid-torso and neck-shoulder is smaller than the gap between the mid-torso and thigh. Therefore, the distortion is not significantly generated.

Mammoth (GM1)

General description

An outline mammoth facing left (Figure 5.107). All body parts are provided, including the tail. While GM1 appears unclear at the dorsal side, the ventral line is relatively easier for viewers to recognise. Such an ambiguous contour has been altered into a slightly darkish colour, but it was originally executed in red. This mammoth figure lacks details: both limbs are also roughly

Figure 5.107: GM1, outline mammoth facing left (digital filter is applied). It is originally executed in red, although the colour has altered into somewhat darker.

outlined; the face does not contain the eyes, mouth and ears. However, a thin long nose is attached. The tip of the nose is the most vivid part of this image, and its red colour is readily distinguishable. The length of the mammoth is 38 cm, and it is located at a height of 172 cm from the nearest floor.

Integration of natural lines

Overall, no integrations are detectable. Even though the body is drawn on a gently raised surface, but neither the dorsal nor ventral line is drawn along natural lines. The most salient natural line on this wall is a groove obliquely crossing the head. However, it is also irrelevant to the animal's contour.

Topographic condition

This wall gently elevates. Body parts except for the limbs are situated on this convex topography, which adds a 3D volume to the image. The total depth of GM1 is approximately 48mm (the model is 1/at100 scale: Figure 5.108). A part of the central mid-torso corresponds to the highest point, while the tip of the frontal leg to the lowest. Most of the sections are defined their elevation level within a significantly narrow range between 2.8mm and 10.7mm (high: 2.8-5.3mm, medium: 5.4-8mm, low: 8.1-10.7mm). The ranges outside of the above range (0.1-2.7mm and 10.8-48mm) are assigned to several area on the main body (0.1-10.6mm) and both frontal and hind limb (10.8-48mm). While the highest area covers the only limited extent, the entire legs are located in the deepest zone; therefore, there is the extra-low level in this mammoth.

Figure 5.108: GM1 (1/100 scale) seen from the vertical position. The highest elevation is found on the central mid-torso, while the lowest is on the tip of the frontal leg.

The surface is first detected at multiple regions: an area in the central mid-torso, ventral neck and dorsal thigh (0.1-2.7mm: see Figure 5.109, 1). However, because these areas are considerably limited, none of the body parts is defined their elevation level. During the high-level elevation, the detection continues from these detected regions. The most extent of the dorsal and central thigh passes the cross-section layer; consequently, these posterior sections are assessed as high (2.8-5.3mm: 2). The layer also detects a surface at the head and ventral-central neck-shoulder, but the areas are not large enough. In the medium level (5.4-8mm), most of the body parts are placed. The detected surface extends from the centre to the dorsal and ventral body, covering the head, central neck-shoulder, and entire mid-torso (3). As the layer proceeds further, the rest of the sections are also detected: the dorsal-ventral neck-shoulder and ventral thigh,

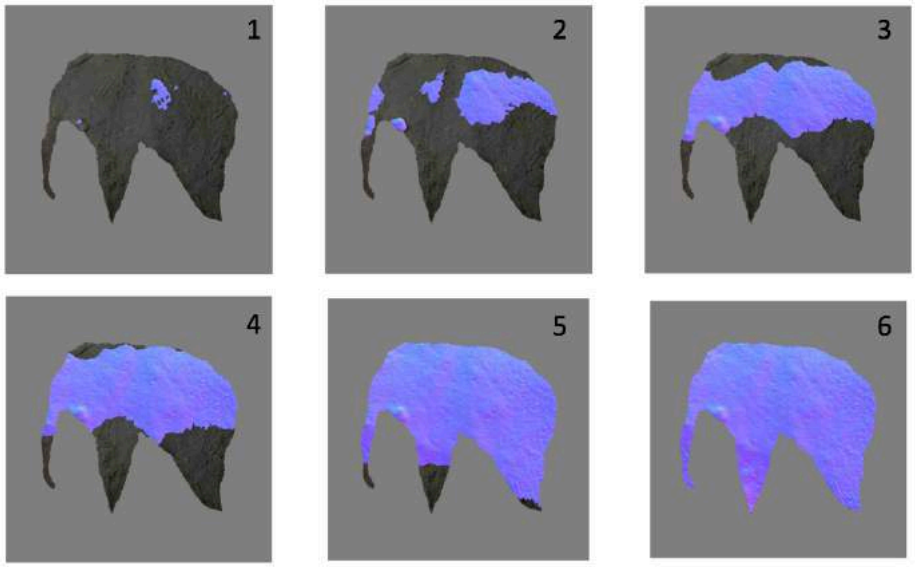

Figure 5.109: These six images illustrate the depth of GM1. When the cross-section layer passes the surface of GM1, the colour of the surface changes; dark regions denote lower elevation than coloured parts. Image 1 is for 0.1mm - 2.7mm, 2 for 2.8mm - 5.3mm, 3 for 5.4mm - 8mm, 4 for 8.1mm - 10.7mm, and 5 and 6 for 10.8mm - 48mm.

although not entirely, pass the layer between 8.1mm and 10.7mm (4). Their elevation level is defined as low, accordingly. Still, there are undetected body parts: the frontal and hind limbs, and nose. As detection continues extending downward on the appendages, and the back leg entirely passes the layer at a depth of 32mm, the nose at 42.7 mm, and finally, the frontal leg is fully detected at the 48mm. Although the nose does not affect the defined level of the head (medium), both limbs are assessed as the extra-low level (5-6).

Distortion on images (horizontal rotation, x10°, y-70° to y70°)

The 3D simulation does not demonstrate obvious distortions, which means the image appears more or less the same as that in the 2D simulation. The relatively flat surface is responsible for the absence of any noticeable deformations.

5.4 Results

Integration of natural lines

Among the 25 images analysed in El Castillo, 18 images contain clear examples of integration, accounting for over 70%, of the sample. Because of this, one might conclude that the use of natural lines must have been a fundamental method for image-making in this cave. Most notably, multiple integrations were present in 12 images, also highlighting the importance of this method. Figures 5.110 shows the number of images by the frequency of integration. Four figures have two integrations (CB1, CB3, BB2, PB5), whereas three integrations are found in five images (PB1, PB2, DA1, BU1, and BB1). Three pictures contain four or more integrated sections (four: EH1, five: PB4, and six: BMB1). Hence, the frequent use of natural lines is common in El Castillo. Such a high frequency is attributed to the characteristics of the wall. El Castillo is a complex cave consisting of several regions, and examined samples are taken from various areas in the cave. Since the condition of the surface differs significantly by area, the number of natural lines also differs by region. For example, natural lines are abundant on the left side of the Polychrome Panel, and images depicted on this surface contains integrated contour frequently; in this region, more than three integrations are found in three images (PB1, PB2 and PB4). In contrast, Panel of Hands is an area with fewer natural lines, and no image has more than three integrations. Therefore, the frequency of integration, as El Pendo cave, also reflects the condition of the wall even in El Castillo.

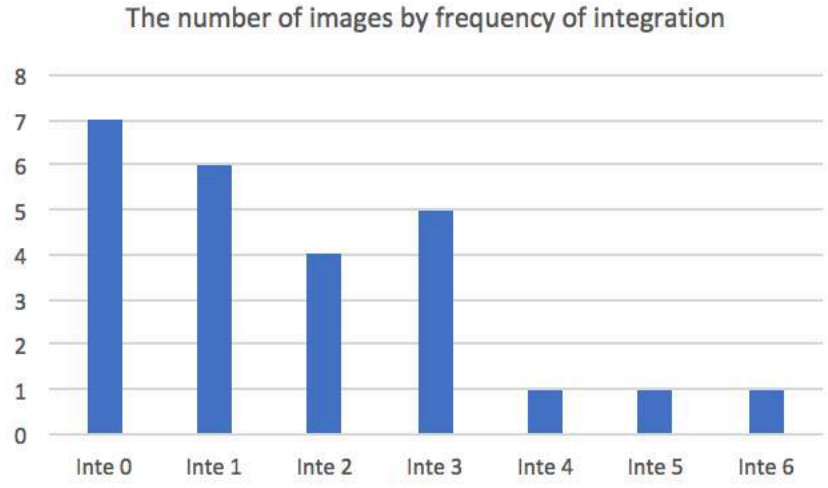

Figure 5.110: The number of images by the frequency of integration (Inte = Integration). In El Castillo cave, plural integrations occur in 12 images which accounts for nearly a half of all examined pictures (Inte 0: 7 images, Inte 1: 6, Inte 2: 4, and Inte 3: 5, Inte 4: 1, Inte 5: 1, and Inte 6: 1). Given this number, it can be said that integration is a common artistic method in the cave. Especially, the condition of the wall is responsible for the multiple integrations as images with more than 3 integrations are located on the wall where natural lines are abundant.

In total, 44 integrations were detected, and there was a particular trend in the relation between body parts and integration. Figure 5.111 demonstrates the number of integrations by body section. According to this graph, the use of natural lines was most likely found in the dorsal line (12), and then in the ventral line (9). Integrations were confirmed eight and seven times respectively in the head and buttock, while the tail and limb were the least integrated body parts (four times respectively). Although the number of integrations differs remarkably between the dorsal and ventral, this result is consistent with the case of the other two caves.

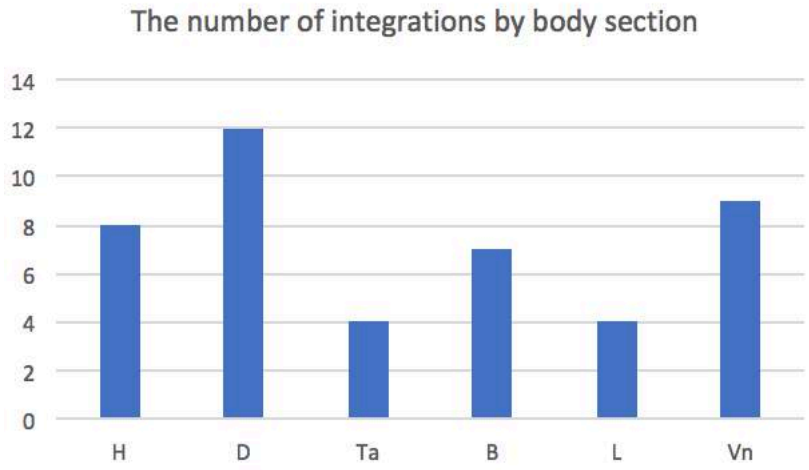

Figure 5.111: The number of integrations by body part (H: Head, D: Dorsal, Ta: Tail, B: Buttock, L: Limbs, and V: Ventral). Integration mostly likely occurs on the dorsal line and then ventral line (12 and 9 images, respectively). On the other hand, limbs (4) and the tail (4) are not preferred for integration. This result conforms to the other two caves.

Among images with more than two integrations, the most frequent combination is dorsal and ventral, with seven cases (see Figure 5.112). The second popular combination is head and dorsal (6), head and ventral (6), buttock and ventral (5), followed by the combination of ventral and limb (4), ventral and buttock (4). Hence, all of these frequent combinations include integration either into dorsal or ventral line. On

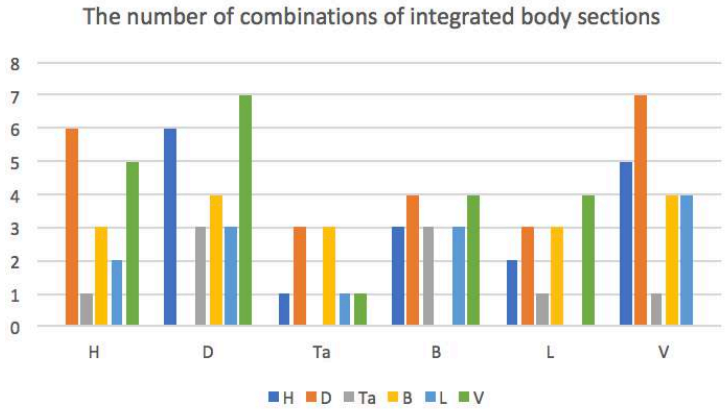

Figure 5.112: The frequency of combinations of body parts among images with multiple integrations. The combination of the dorsal and ventral line appears most frequently (7 images), and all the other frequent combinations also include integration either into the dorsal or ventral line (H-D: 6, H-V: 5, B-D: 4, and B-V: 4). This result reflects the general result of the predominant body section for integration.

the other hand, the head-buttock combination is relatively rare as they co-occur only three times, and lower values concentrate on combinations include tail and limbs. The above result reflects the general result of the predominant body section for integration.

Topographic condition

Regarding the topographic condition, the high elevation level tends to be located on the head (six images), thigh (six), hind limb (six) and tail (seven). The neck-shoulder and mid-torso are less likely depicted on this elevation level as only four and two images contain the parts in the high level, respectively. On the other hand, the medium level is confirmed mostly in the neck-shoulder, mid-torso, and thigh (between eight and eleven images), and the low level is most frequently found in the neck-shoulder (nine-ten images), head (nine), and mid-torso (seven - ten). The above result is illustrated in Figure 5.113 (above). The result remains almost the same in a simplified graph where

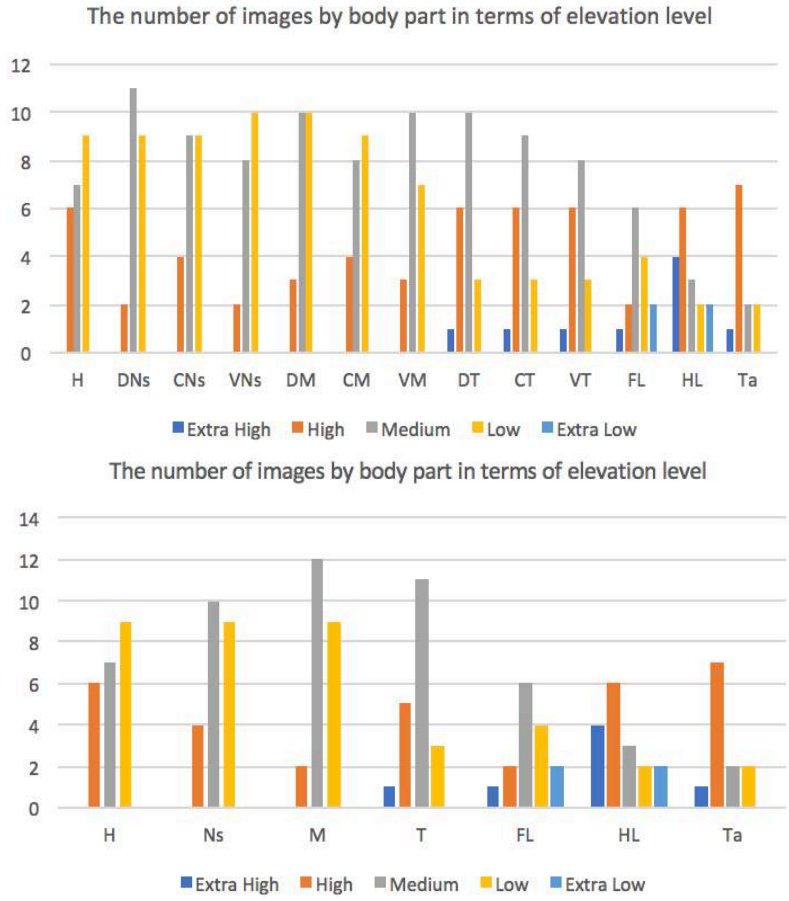

Figure 5.113: These two graphs show the number of images by body part regarding elevation level (H: Head, Ns: Neck-shoulder, M: Mid-torso, T: Thigh, FL: Front Leg, HL: Hind Leg, Ta: Tail. D, C, and V, refer to Dorsal, Central, and Ventral, respectively). The graph above includes sub-divisions in the neck-shoulder, mid-torso, thigh, while in the graph below those divisions are united. Nevertheless, these two graphs are almost identical. Unlike the other two caves where High level concentrates on the head and where Medium and Low levels are likely placed on the shoulder and mid-torso, the distribution of elevation levels is more complicated in El Castillo. On the other hand, Extra levels are exclusively located on the legs (FL: 3 images, and HL: 6) and tail (1) in all cases except 1 case on the thigh. In particular, the rate for the hind legs with Extra levels is high as 4 images contain the limb on Extra High and 2 images on Extra Low.

three divisions in the neck-shoulder, mid-torso, and thigh are respectively united (see Figure 5.113 below). This result shows a slightly different tendency, compared to the other case studies. In Covalanas and El Pendo cave, the high elevation concentrates on the head, and the medium and low levels are likely placed on the shoulder and mid-torso. Regarding the extra level, except the thigh where one image has extra high, all cases are located on the legs and the tail in El Castillo. In particular, the hind leg frequently appears in the extra levels; four images in the extra high, and two images in the extra low. This association between appendages and the extream levels is commonly seen in the other two cases studies.

Regarding the topographic condition between the head and thigh, however, we must take account of a fact: not all images are complete. The head and thigh are more likely missing than the neck-shoulder and mid-torso, and therefore, the above result was not obtained from the graphic samples of the same condition. One must be careful to treat this result because it does not equitably represent the situation of each body parts. For this reason, I focused on 19 complete images as was done in the previous case study. Figure 5.114 is a simplified graph which shows the relationship between elevation levels and body sections (legs and the tail are eliminated) based on the complete images. The values for the medium and low level grows in the neck-shoulder and mid-torso, although the thigh still has the highest value in the medium level. On the other hand, the value for the head in the low level is reduced. Overall, this result demonstrates a similar trend in Covalanas and El Pendo, although there are slight differences.

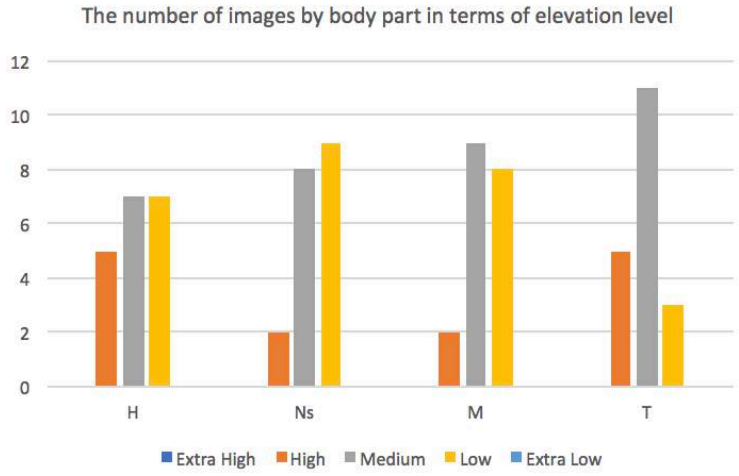

Figure 5.114: A simplified graph regarding the topographic condition by body part based on 19 images (H: Head, Ns: Neck-shoulder, M: Mid-torso, and T: Thigh). Values for Medium and Low level grow in the neck-shoulder (8 and 9 images, respectively) and mid-torso (8 and 7 images, respectively), although the thigh still has the highest value in Medium level (11). At the same time, the value for the head in Low level is reduced (7). In consequence, the result shows a similar trend to that in Covalanas and El Pendo.

Thus, the head and thigh tend to be found on a higher elevation, while the torso is apt to be placed on a lower elevation. This trend is also visible in the generalised

information of the topography. Figure 5.115 demonstrates the sum of elevation levels by body section. As a result, the elevation point is highest in the thigh (59 points), and then the head (55 points). Meanwhile, the mid-torso gains 51 points, and the neck-shoulder has 50 points. Thus, the head and thigh are more likely drawn on a higher elevation than the neck-shoulder and mid-torso. This fact is also compatible with the other case studies, although there is a slightly different element; in Covalanas and El Pendo, the mid-torso is most likely placed on a surface of the lowest elevation among the four body sections. Even so, the generalised topography forms the overall concave surface (P1), and all case studies show the same trend in this respect.

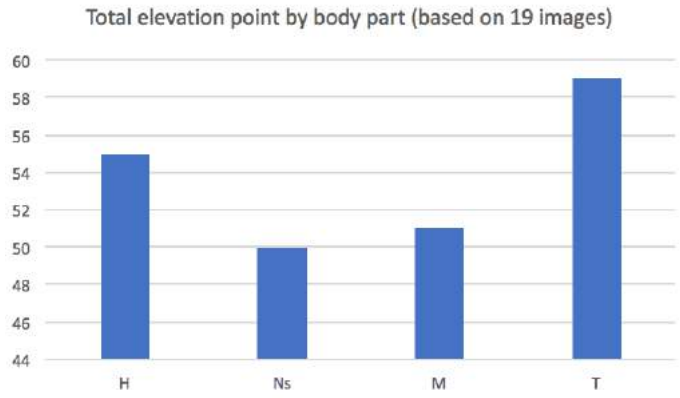

Figure 5.115: A graph of total elevation point by body part based on 19 images (H: 55 points, Ns: 50, M: 51, T: 59). Generally, the elevation of the head and thigh is higher than both Neck-shoulder and mid-torso, meaning that the general shape of the topography is overall concavity.

As for the topographic pattern, six patterns were detected based on the above 19 images. All of them have been already seen by the previous case studies (P1-P6). Among all topographic patterns, P1 (overall concave) and P5 (partial concave) are the most popular in El Castillo cave (see Figure 5.116), with five images respectively (P1: PB4, CB1, CB4, EH1 and BB1, and P5: PB3, PD2, PH2, CB5, and GM1). The next common pattern is P2 (overall slope) and P6 (partial slope), with three images respectively (P2: PB2, CB3, and DA1, and P6: PB1, PD3, and BBM1). Meanwhile, P3 (overall convex) and P4 (zigzag) are not a preferred shape; only two images (CB2 and BB2) and one image (PD1) respectively belong to these types. The predominance of the P1 conforms to the result from both Covalanas and El Pendo. P5 is also a highly common pattern in those caves. The number of images which is depicted on these concave types accounts for the majority of all pictorial samples; this fact is reflected in the general shape of topography.

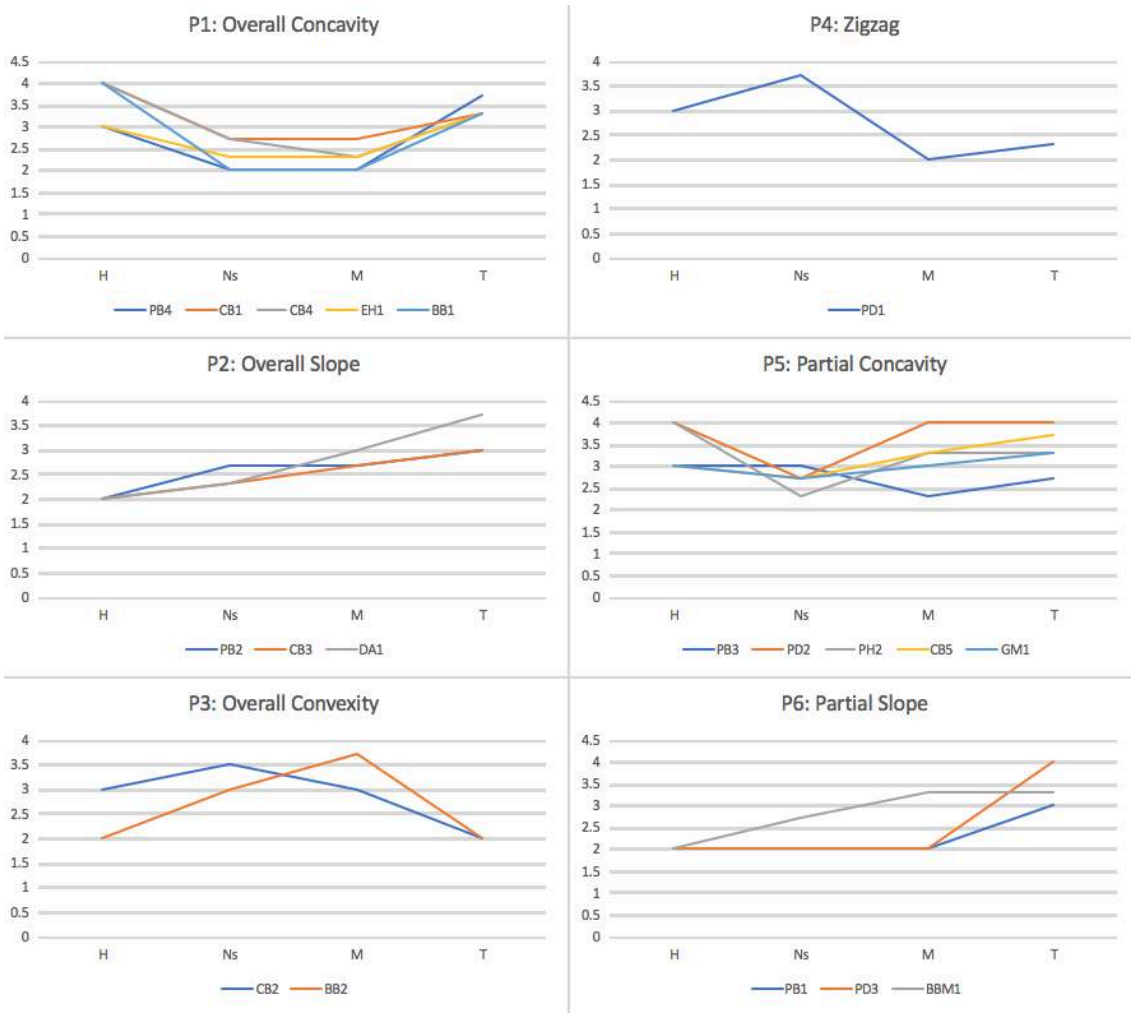

Figure 5.116: The numerically-visualised shapes of images. 6 patterns are detected from 19 images. The most common patterns of the topography are P1 and P5 as each pattern contains 5 images. The next common pattern is P2 and P6, with 3 images respectively. Meanwhile, P3 and P4 are not preferred patterns as only 2 images and 1 image belong to P3 and P4 respectively. The fact that concave surface is the predominant topographic type conforms to the general shape of topography.

Distortion on the images

Distortions are confirmed on 12 images (PB1, PB2, PB3, PB4, CB1, CB3, EH1, EH2, BMB 1, BU1, BB1, and BB2). This number suggests that obvious distortion is a relatively rare phenomenon, compared to the other cases. Figure 5.117 shows the number of images by the frequency of distortion. Six images contain only one distorted section (PB1, PB2 EH2, BMB1, BU1, and BB2), whereas in the remaining six images (PB3, PB4, CB1, CB3, EH1, and BB1) plural distortions are confirmed. Especially the number of images with four distorted body parts is high, with four images (CB 1, CB3, EH1, and BB1); otherwise, two distortions are found in PB3, whereas PB4 contains five distortions. Images with more than four distorted parts constantly change their appearance as the viewpoint moves, and the deforming process is highly noticeable.

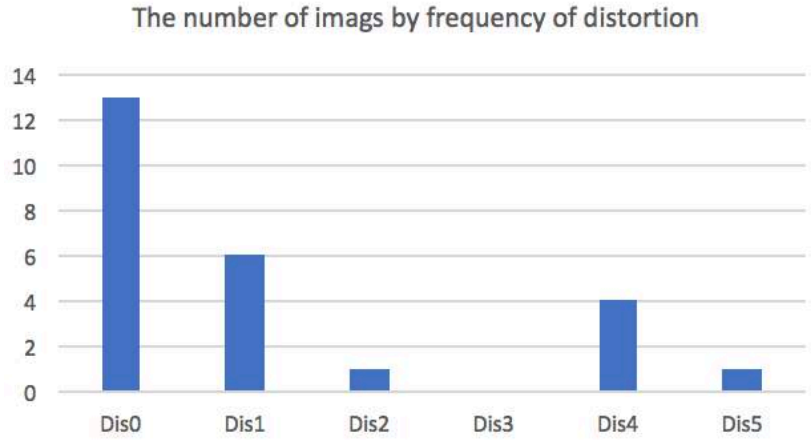

Figure 5.117: The number of images by the frequency of distortion (Dis = Distortion). 12 images are subject of distortion in El Castillo (Dis0: 13 image, Dis1: 6, Dis2: 1, Dis3: 0, Dis4: 4, and Dis5: 1) Overall, images with distinguishable distortion are relatively rare in the cave, compared to the other cases. Multiple distortions in a single image are also less common.

As for the relationship between body parts and distortion, the result demonstrates a somewhat different tendency from the other cases. Figure 5.118 illustrates the number of distortions by body section. Distortion occurs 29 times in total. The head and leg are the most popular parts as they contain seven distortions respectively. The thigh is also distorted frequently, with six images. On the other hand, topography less likely deforms the neck-shoulder and mid-torso as only five and four distortions are found in these sections respectively. The tail is never distorted, even though the region is provided with over a half of all images.

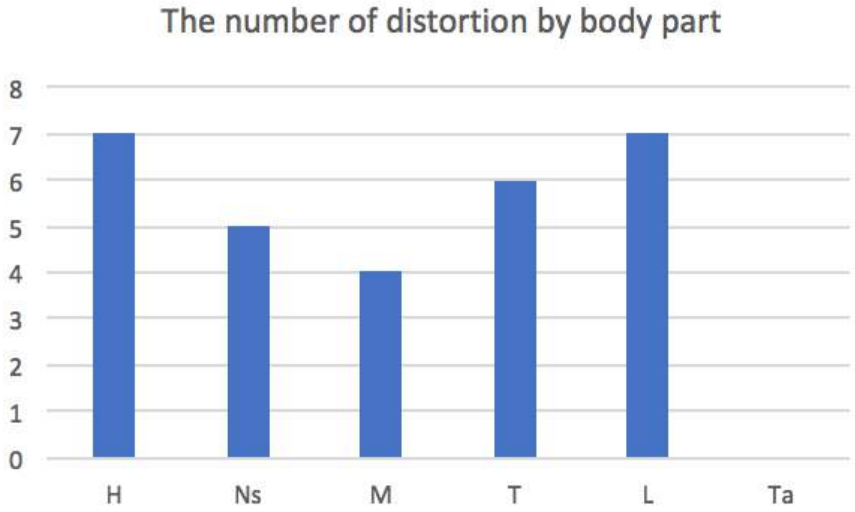

Figure 5.118: The number of distortion by body part (H: Head, Ns: Neck-shoulder, M: Mid-torso, T: Thigh, L: Leg and, Ta: Tail). Distortion most frequently occurs on the head (7 images) and the limb (7). Topography less likely deforms the neck-shoulder and middle part as only 5 and 4 distortions are found respectively.

In this case study, the high occurrence of distortion on the leg was confirmed, as was seen in El Pendo. Additionally, the low frequency in the mid-torso is also consistent with the result from the other studies. Meanwhile, the result for the neck-shoulder is less significant than Covalanas and El Pendo; instead, distortion on the head is outstanding. The reason for this result might be found in a difference in predominant motifs: in Covalanas and El Pendo, red deer account for the majority of whole pictorial samples, while the dominant theme in El Castillo is bison. Deer contains no noticeable separation of the neck from the head, whereas the head and neck of bison are closely attached. the nature of the latter's anatomy makes it hard to draw a clear boundary between them. Therefore, distortion on the neck becomes less noticeable than deer. This point will be discussed in the next chapter.

Summary

This case study examined a total of 25 pictures in El Castillo cave, with an aim of detecting any signs of interactivity in the production phase and post-production phase. Consequently, collated data demonstrates a significant trend in all analysed categories. In most cases, the result is coherent to that from the previous case studies, but some aspects are unique to El Castillo cave. As was noted in the previous chapter, the site-specific environmental condition is responsible for those unique aspects, and therefore characteristics of cave art differ by a cave. Points obtained from this case study are summarised here:

- 20 images integrate natural lines into their outline. Multiple integrations in particular are found in 12 images, which constitute almost half of whole sample from this cave. Therefore, one may conclude that the use of natural lines was a common technique for image-making in El Castillo (integration of natural lines).

- The most integrated body sections are the dorsal and ventral lines, although integrations in the dorsal occur more often than the ventral. This result is same as the other case studies (integration of natural lines).

- Based on 19 complete images, the high elevation level tends to be located in the head and thigh. The favoured location for the medium level is also the thigh, while the low level is most likely found in neck-shoulder. The extra levels (extra high and extra low) have been found only in the legs and the tail (topographic condition).

- The shape of the generalised wall is typically concave, as the elevation point of both neck-shoulder and mid-torso is lower than both head and thigh. This result is consistent with the other case studies (topographic condition).

- There are six patterns regarding the wall's shape. The most frequent topography types are overall concave (P1) and partial concave (P5) (topographic condition).

- Distortion was confirmed in 12 images, with the lowest rate of all three case studies. Images with more than two distorted parts are also rare (distortion on images).

- The most distorted body sections are the head and limb. On the other hand, the neck-shoulder and mid-torso are most unlikely distorted. The low frequency for the neck-shoulder does not conform to the results from Covalanas and El Pendo, and a difference in predominant motifs causes this dissimilarity (distortion on images).

These are the main elements obtained from this case study. As mentioned above, consistent trends were detected in all analysed categories in the three case studies. These trends suggest that specific universal principles might have existed in the Upper Palaeolithic regarding both image-making and image-viewing. On the other hand, minor differences were also confirmed. They are defined by the conditions of a medium's surface. Therefore, external environmental factors played a significant role in creating images since the wall of the different state leads to a different result. In this sense, image-making does not only rely on an artist's creativity, but also the medium itself actively intervenes. In the next chapter, this thesis will incorporate the data from all three case studies, and discuss what the data is informing. In so doing, the points which have been raised will also be referred to in further detail.

Chapter 6

General Results and Discussion

"You can keep as quiet as you like, but one of these days somebody is going to find you"

(Haruki Murakami, *1Q84*)

I have investigated a total of 54 animal pictures from three caves (Covalanas, El Pendo, and El Castillo) in Cantabria, Spain, focusing on interactivities of cave art during the production and post-production phases. The data were collected by fieldwork, and digitally analysed in terms of the concept of cave-installation art through the provision of concrete observations obtained from the actual setting of decorated caves. The data comprise three categories, each of which testifies a different type of interactivity: Integration of natural lines; topographic condition; and distortion on images. The core environmental factor which enables those interactivities is the condition of the cave surface. The medium's state allows humans to interact with the wall creatively. Although this study examined specific ways of both image-making and image-viewing, they are thus considered as *a particular reaction to an environmental constraint*. Such a mutual relationship between an actor and an artistic medium inevitably redraws our concept of cave art to an interconnection between environment, art, and human. That is the essence of the cave installation-art approach.

With regard to the analysis, photographic data are vital data. It was used to 3D document the images focused on in the thesis, including their topographic context. The photo data were firstly visualised as 3D models, using digital photogrammetry. Secondly, the generated models were inspected to detect factors along with a criterion set in each data category. Finally, resulting observations were analysed to discern any significant trends which may characterise interactivity. As a result, the analysis revealed substantial tendencies in all categories; significantly, they were universally seen among three case studies. These trends strongly suggest the existence of essential principles for both image-making and communicating visual-works; therefore, this study affirms a specific artistic intention involved in the interactive nature of Palaeolithic cave art. In this chapter, results from each case study will be united and then re-examined by category. At the same time, I also attempt to interpret detected trends based on facts.

6.1 Integration of natural lines:

General results

Statistical data were managed in terms of the following two aspects: the number of integrations in a single image and the frequency of integration by body part. The data were also sorted by label (Direct or Offset, Full or Partial). It is then further analysed from differing perspectives (the combination of integrated body sections, types of natural lines, the frequency of lone integration by body part, and so on). As a result, the analysis demonstrated a significant trend in this interaction category. Overall, integration must have been a fundamental method of image-making, at least in the studied three caves. Furthermore, the position and shape of natural lines might have been one of the most prioritised factors for Palaeo-artists. The data about a correlation between integration and body sections strongly suggest that the integration was not performed randomly, but there must have been a principle that the creators of cave art obeyed.

Integration was detected in 39 images, which accounts for 72% of the total (39/54 images). This proportion signifies integration as an essential method for image-making in Covalanas, El Pendo, and El Castillo. Furthermore, multiple (two or more) integrations occur in a single image in a remarkably high probability as the ratio constitutes almost half of the entire proportion (44%). The proportion of images with integration varies by site: 61% (11/18 images) in Covalanas, 91% (10/11) in El Pendo, and 72% (18/25) in El Castillo. No cave yielded a value under 60%, meaning that the use of natural lines occurs in significantly high frequency, especially in El Pendo.

The main factor which differentiates the ratio by site is the condition of the medium's surface. In El Pendo, the Frieze of Pictures is fractured and therefore contains a countless number of edges throughout the panel. For artists facing such a wall with abundant natural lines, drawing an image along pre-existing lines might be easier than avoiding any overlaps on them. On the other hand, noticeable natural lines are sparse on the wall in Covalanas. Such a condition contributes to the lowest occurrence of integration in the three caves. Given this, the more natural lines on the cave wall, the more the images tend to be integrated with those natural lines.

Nevertheless, Covalanas also reveals a particular desire for integration on the part of the Palaeo-artist: in the cave, the artist used considerably subtle edges and, although only one case (A1), a borderline which forms between smooth and porous surface. In any case, these natural lines are highly inconspicuous and require cave-careful observation on the part of explorers in order that they detect these features as a line in a poorly lit space. Accordingly, the artist/s of Covalanas must have put a great effort into seeking available natural lines. Thus, the artist attempted to use natural lines

even on a wall without noticeable configuration. Such an attempt reflects the significance of integration in cave art.

Breaking this down, integration occurs in six body sections, with a total of 92 examples. A trend seen in the data is consistent throughout the three case studies. Figure 6.1 illustrates the number of integrations by body part (H: Head, D: Dorsal, Ta: Tail, B: Buttock, L: Limb, V: Ventral), and integration is most frequently found in the dorsal line (30 examples) and the ventral (23). The buttock and the head respectively hold 15 and 13 examples, whereas integrations were much less common in the leg (6) and the tail (5). Because each case study demonstrates the dorsal-ventral line as the predominant section and the leg-tail as the most marginal part, the result reflects a sort of universality as if integration into the dorsal and ventral section was a fundamental principle of the image-production. The result of Chi-square test indicates that this numeric distribution is not random as the p-value is significant ($p=0.0029$: see Table 51 in Appendix). Therefore, the dominance of the integration in the dorsal and ventral line highly likely reflects an intention of Palaeolithic artists.

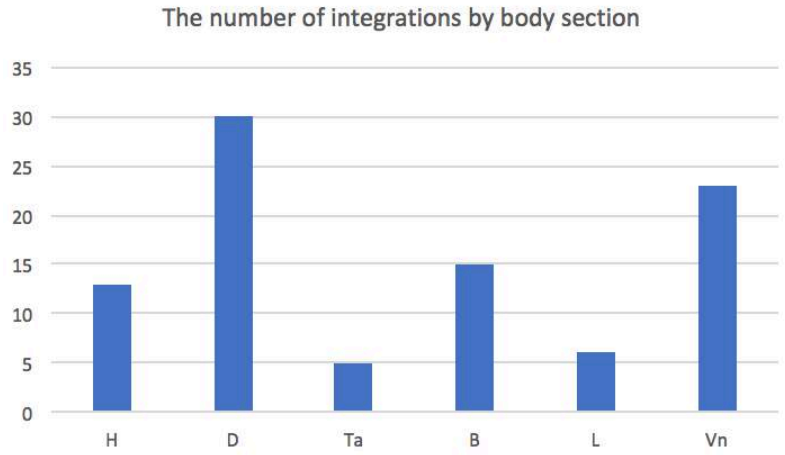

Figure 6.1: The number of integration by body part (H: Head, D: Dorsal, Ta: Tail, B: Buttock, L: Limbs, and V: Ventral). Integration most likely occurs on the dorsal line (30 images) and then ventral line (23). Buttock and Head are also relatively popular (15 and 13, respectively). On the other hand, the limbs (6) and tail (5) are not preferred parts for integration.

Benefits: integrations for outlining axis and edges

Indeed, utilising natural lines for the dorsal and ventral line must have offered significant benefit to Palaeo-artists. These outline sections are the axis which defines the basic shape of quadruped mammals, comprising the most substantial proportion in the entire body. Therefore, pre-existing patterns which already appear as an animal's axis must have been recognised as the blueprint of an overall animal figure before image-making. Because the distance between the dorsal and ventral lines (height) is shorter

than that between the head and buttock (length), finding available lines for the dorsal or ventral contour at first could provide a rough estimation of an image's shape. In other words, such lines are more "suggestive" for one to recognise them as animal figures, compared to lines available for the head and thigh. Although Hodgson and Pettitt (2018) briefly mention the intensive use of natural lines occurs on the cervico-dorsal line, the reason for this preference is found in such a suggestive nature of axis-like natural lines. Therefore, based on those suggestive shapes, Palaeolithic people could first "discover" animals in natural rocks and then visualised them by image-making (Gombrich 1960). Whether or not recognising animal shapes on the cave wall itself had a particular meaning is unknown (e.g. image-making as a culturally meaningful behaviour to summon animal spirits to the real world: Lewis-Williams 1997). Nonetheless, the dorsal-ventral integration must have provided artists with a practical benefit: in doing so, the ice-age artists could complete a figure easier by this method than integrating the head-buttock first.

This hypothesis appears validated, given that integration into both the dorsal and ventral area co-occurs at a considerably high frequency. Among 24 images with more than two integrated body sections, 18 images contain integration into both of these sections; this is the most frequent combination among all the other combinations (see Figure 6.2). Using natural lines for both the dorsal and ventral part simultaneously can define the shape of an image more than integration into either the dorsal or ventral. Therefore, by so doing can optimise the production process. I am not denying the existence of a meaning behind integrated animal representations in Upper Palaeolithic and its cultural significance which motivated artists to follow the integration method, but I am simply describing a benefit in the technique itself. Namely, for whatever the

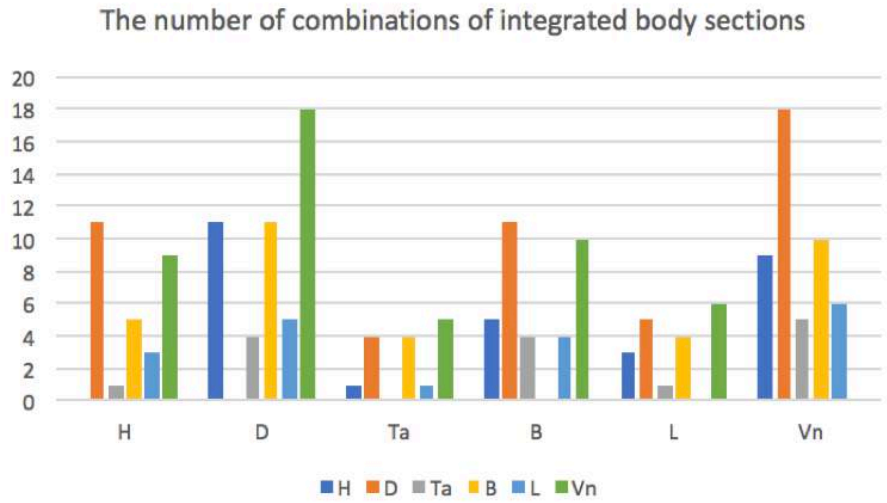

Figure 6.2: The frequency of simultaneous integration with other body parts (H: Head, D: Dorsal, Ta: Tail, B: Buttock, L: Limbs, and V: Ventral. The dorsal line and ventral line are the most popular combination (13). Integration into the head and buttock are in most case accompanied by that into the dorsal or ventral line (H-D: 10, H-V: 9, D-V: 14, BD: 11, and B-V: 9).

cultural reasons integration was practised, following this method also simultaneously allowed palaeo-artists to draw images easier as in any case finding torso-like natural patterns on the wall enabled them to grasp a rough overview of what they were going to depict. Hodgson and Pettitt (2018) attributes the origin of figurative art to the suggestive configuration of the medium. In another way, humans simply imitated natural ques at the dawn of figurative image-making rather than depicting what they observed in their life; Breuil (1905) also discuss this point based on the observation of children's paintings. If so, apart from the meaning of the activity, using natural lines as suggestive-axis were highly beneficial condition for the early stage of artists to "copy" animals and make them visible on a surface because such pre-existing shapes assisted to complete image-making. Of course, I do not mean the artists in the examined three caves were incapable of depicting figurative images without the help of suggestive ques. Given the general fact that images without integration also exists in cave art, Palaeolithic people were skilled artists. The reason why artists painted images with/without integration is not understandable to us, but probably they might have reflected a different mode of tradition and meaning. If natural shapes were a crucial element for humans to invent animal representations and to fix them on a medium, probably particular meanings were also attached to the activity itself through the enculturation process, and integration might have become a meaningful tradition; the meaning is not visible to us, however. Seeing integration at least from the practical aspects, thus, the reason for the intensive integration into the dorsal-ventral is understandable.

As for integration as an enhancing method for image-making, the statistics regarding the extent of integration also supports the above view. Full integration far more frequently occurs in the dorsal and ventral line than in the other body sections. Large integration occurs in the dorsal area 21 times and in the ventral 15, while partial integration is found only nine times in the dorsal and six times in the ventral (see Figure 6.3). In the other body parts, the difference between full and partial integration is not remarkable, but the number of partial integration is noticeably high in the head. The predominance of full integration in the dorsal and ventral section is almost consistent in the three case studies, apart from one case in Covalanas where partial integration occurs one time more than full integration in the ventral line. Statistic test also yielded the significant result ($p=0.03421$: see Table 51 in Appendix), denying the coincidental distribution; full integration in the dorsal and ventral line is likely intentional. Considering the benefit of integration into the dorsal-ventral area, it is not difficult to understand what this result suggests. Namely, the use of a longer line can determine the more detailed shape of an animal image. One can imagine a complete form of images better with natural lines which are available for full dorsal-ventral integration in

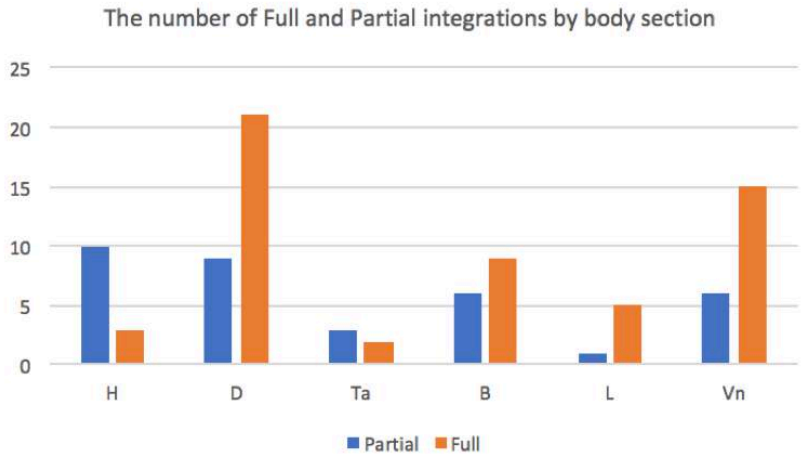

Figure 6.3: The number of full and partial integration by body section ((H: Head, D: Dorsal, Ta: Tail, B: Buttock, L: Limbs, and V: Ventral). Large integration mostly occurs in the dorsal (21 times) and ventral area (15 times). This result might reflect an optimised way of image-making: the use of longer natural lines can determine the more detailed shape of an animal image. One can better imagine a complete form of images in advance of image-making with natural lines which are available for full dorsal or\and ventral integration.

advance of image-making (e.g. B1, N2, N16, BB1) than lines for partial integration (e.g. A5, A8, CB3). Therefore, one can consider that full integration into the axis of the animal body is the most optimised method.

On the other hand, integration into the head and buttock seems to have had a different purpose. Although integration into these sections could also happen alone (head: two times, and buttock: one time), their frequent co-occurrence with integration into the dorsal-ventral line suggests another particular function. As shown in Figure 6.2, a combination of integrated sections involving the head, dorsal, buttock, and ventral occurs rather frequently (H-D: 11, H-V: 9, D-V: 18, BD: 11, and B-V: 10). Taking account of this data and the low frequency of lone integration into the head (two) or buttock (one), integration into these areas are in most case accompanied by that into the dorsal or ventral line. This observation informs us of another aspect of the artistic method. As noted earlier, dorsal-ventral lines form the essential axis for determining the primary form of a mammal's body, and so the artists could obtain a rough draft of an image by applying natural lines for these sections. The data suggest that this was the priority in integration. If so, the integration into the head and buttock must have been less critical, but by doing so further enhances the image-making. That is, natural lines seen as the outline of the head and buttock provide draft images with another "edge", and consequently, the artists could gain a better overview as the size and the shape of the image is further determined. Hence, the artists were able to hold a more concrete vision of a complete picture in advance of the production by selecting natural lines for the axis (dorsal and ventral) and edge (head and buttock) at the same time.

The benefit is ascribed to a unique function of the human cognitive system. Even if the contour of a figure is fragmented, we can recognise what it is because our cognitive system automatically complements fragmented information and restores the subject into its original figure (Snodgrass and Feenans 1990, Snodgrass and Kinjo 1998). The view of such a human's cognitive ability is also already discussed by Hodgson (e.g. 2000, 2003, 2006, and 2008) regarding cave art as we saw in Chapter 1. According to Snodgrass and Freemans (1990), the efficiency of the restoration of the lost subject depends on the number of visual cues (Figure 6.4). This fact suggests that the more cues for outlining, the less the artists needed to rely on their imagination. From this perspective, applying multiple integrations will be a significant aid during the production, although there were prioritised body sections; available natural lines for the head and buttock might have been an additional visual cue to the central axis (the dorsal and ventral contour). This explanation is also able to elucidate why integration hardly takes place on the legs and the tail. Namely, these appendages are peripheral, not an essential element that determines the fundamental form of mammals.

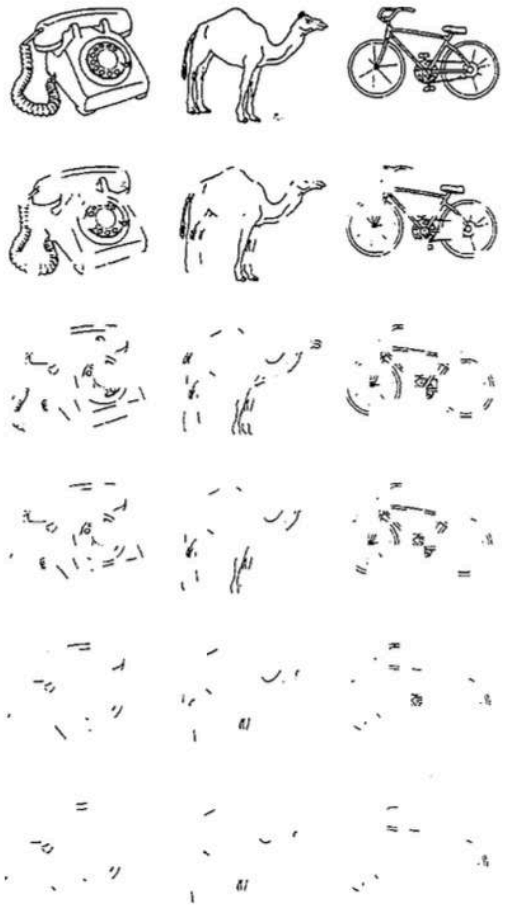

Figure 6.4: Different levels of fragmentation of images. When subjects have more visual cues, the perception will be easier. (After Snodgrass and Feenan 1990).

In any case, depicting an image on a surface where its draft figure had already existed would dramatically reduce the risk of representational failure. As suggested by recent research into a spatial organisation of cave art (notably Pastoors and Weniger 2011; Gittins and Pettitt 2017), producing cave art must have been a communal activity involving preparation of pigments, provisioning, and careful planning. It seems logical, therefore, that the reduction of the risk of representation failure by integration must have been consciously advantageous; but, as discussed above, this benefit does not deny cultural accounts which drove palaeo-people to combine natural lines and images' outlines. They coexist together.

Additionally, image-making according to these principles determines the size of image. In particular, images with multiple integrations, the width and length are already provided by natural patterns. If walls with available lines for both axis and edge were the ideal condition for image-making, the location of images was also naturally determined at the same time.

Thus, the data suggest two leading roles in the use of natural lines. While integration into the dorsal-ventral line worked as the axis, outlining the head and buttock along natural lines provided the axis with edges so that images' shape and size were further determined. These principles and their benefits denote the significance in the cave-human interaction; Ice-age artists who entered into these caves might have sought the above specific conditions of the cave wall then transformed them into animal pictures. The process of seeking proper locations for image-making might have involved painstaking effort in a dark environment of caves.

Integration and environmental variants

Natural lines were fundamental elements that palaeo-artists clearly took into account. Integration must have been one of the essential steps in the production of cave art. Even so, the three caves examined cannot be characterised in the same way. Each cave yielded a unique situation which testifies how a particular environmental setting had an impact on the artists' decision-making. As was argued above, the frequency of integration in El Pendo is the highest: 31 integrations were detected from the set of 11 images. The probability of integration, therefore, is also high because the average number of integration per image is approximately 2.84. In such a case, lone integration scarcely takes place as only one time is confirmed in the dorsal line (N12). On the other hand, Covalanas shows the lowest density (17 total integrations/ 18 total images = approx. 0.94 integrations per image), and lone integration occurs eight times. Importantly, these solitary cases are found in the dorsal and ventral line (dorsal: 4, ventral: 2). What this fact implies is that the artist in Covalanas only applied an axis-focused integration, following the above-discussed priority in body sections. As the natural lines in the cave are not as abundant as in El Pendo, the artist might have focused on searching available lines for the dorsal and ventral. Therefore, the priority and the artist's intention (or behaviour) is more visible to us in Covalanas than El Pendo. Meanwhile, the result of El Castillo is not as straightforward as these caves. Even though the probability of integration is moderate compared to Covalanas and El Pendo (44 total integrations/ 25 total images = approx. 1.76 integrations per image), the presence of lone integration by body part is somewhat random (Head: 2, Dorsal: 2, Tail: 0, Buttock: 1, Limb: 0, Ventral:

1). Such randomness might be attributed to the cave's particular conditions: El Castillo consists of multiple sections unlike the other two caves, and the condition of the wall surface largely differs by area. Furthermore, the chronology of images is also inconsistent, and so there might have been a variation in the mode of integration as well. For these reasons, the result for El Castillo might be reflecting a wide variety in the pattern of integration. In this way, each cave offers a unique possibility of integration, depending on its environmental condition (Covalanas: Essential; El Pendo: Abundant, El Castillo: Various). "Essential" means an essential extent of integration. In the above discussion, axis-focused integration was defined as the most functional aid of image-making. The case of Covalanas highlights this most beneficial way of the use of natural lines despite the lowest frequency of the total number of integrations among the three caves, and the pattern is coherent. Accordingly, integration in the cave is considered as an essential use. "Abundant" refers to the frequency of integration. While "Essential" concerns axis-focused integration, natural lines are frequently used for both axis and side-edges of a single image. Such mixed integration is coherent in El Pendo, and therefore, the total number of integrations in each image is high. In El Castillo, different patterns (axis-focused, mixed, and edge-focused where integration occurs only on the head and/or buttock) exist, and there is a lack of cohesion. Thus, the way of integration observed in El Castillo more varies than the other two caves. In any case, integration can be an informant to measure how much an environmental factor defines the cave-artists' action (e.g. Covalanas is more artist-based, while El Pendo is more environmental-based).

The environmental condition also affects the type of available natural lines. Five types of natural lines were detected here: Groove, Edge, Ridge, Border and Valley line. Edge is the most popular type (46 cases: Figure 6.5), Groove is applied in 35 cases, whereas Ridgeline is the third in preference (10 cases). These three types were detected in all the case studies. Contrastingly, Border and Valley were not a universal line-type as each of them are found from a single cave (Border: Covalanas, Valley: El Pendo). The detected samples of these lines are somewhat limited (Border: 1, Valley: 4). These types can be considered as site-specific examples which are defined by the different morphological condition of caves.

Even though Edge is the predominant type, it does not immediately claim its universality because the dominant type differs by cave: for example, grooves are most frequently used in El Castillo, while the use of edges is most commonly seen in El Pendo. With regard to El Castillo, the intensive use of grooves might be due to the abundance of salient grooves in the cave. Therefore, Palaeolithic artists in El Castillo took advantage of such a condition of the cave wall. By contrast, fractured surface of "the Frieze of Pictures" in El Pendo generates an uncountable number of edges as mentioned above,

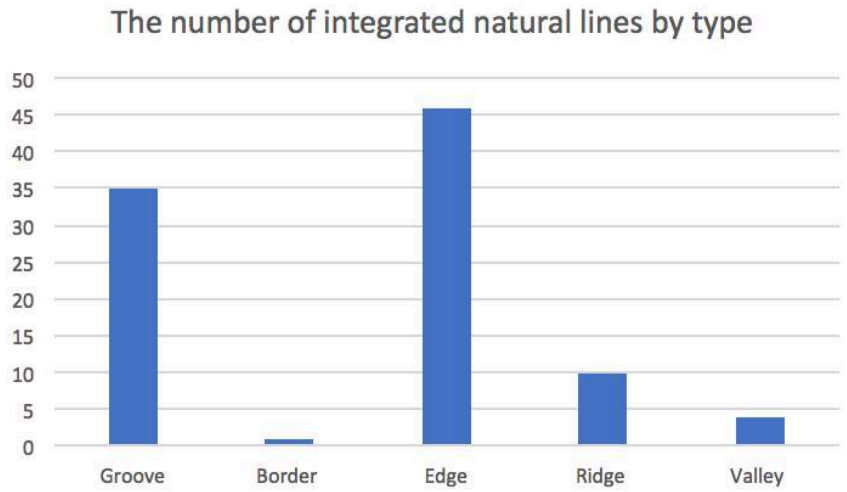

Figure 6.5: The number of integrated natural lines by type. Edges are the most popular type of integration (46 cases). Grooves are applied for the outline in 35 cases, whereas the ridgeline is the third popular type (10 cases). Border (1 case in Covalanas) and valley lines (3 cases in El Pendo) were detected not as a universal type but as a site-specific example.

but other types of natural lines are mostly absent. Therefore, almost all integration relies on edge lines. In Covalanas where outstanding natural lines are not abundant, artists most frequently used ambiguous edges which are generated by a subtle elevation gap. Given these facts, at least based on these three caves, Palaeo-artists did not have a preference concerning the use of specific type, but instead, they merely utilised everything that appears as a line. Thus, the use of particular type of lines does not represent a preference but an artists' response to an environmental constraint. Even so, the effort to maximise the pre-existing elements is commonly visible in all three caves.

Integration for another purpose

Apart from outlining, natural lines are occasionally utilised for another purpose. For example, there are cases where natural lines are used for designing the inside the body (e.g. Covalanas: A3 and D1, El Pendo: N7). Those images with internal patterns achieve a far more detailed quality than figures only with the contour. Another unique case is those with off-set integration. In total, 15 cases of this type of integration are confirmed; the extent is especially remarkable in C1, B4, N5. Although, the purpose of offset integration applied to these three images remains unknown, it is possible to make an assumption based on previous research. For instance, N5 appears as if superimposed on another image of the similar form because of the contour of the rock used for offset integration. Even though the wall's shape had an apparent influence on the shape of the image's frontal neck and dorsal line, no overlap is made with the actual outline as if the

artist deliberately avoided direct integration. This case is reminiscent of another interactivity where animation effects can be induced by movement of light sources as is discussed by Azema and Reviere (2012). By changing the position of the light and shadow, viewers can manipulate the appearance and disappearance of the actual contour of N5 as the original edge of the rock merges into the partly disappeared frontal-cervical neck. As a result, N5 might appear shaking its head and neck up and down (see Figure 4.23). The similar animation effect can potentially be confirmed in B4 and C1. If it is a case, even how to utilise natural lines can be an indication of interactivity during the post-production phase.

6.2. Topographic conditions:

General results

In this category, this thesis examined the topographic condition of 54 images. The image was first divided into seven sections (head, neck-shoulder, mid-torso, thigh, front leg, back leg, and tail), and then the neck-shoulder, mid-torso, and thigh were provided with further subdivisions (dorsal, central, ventral). Thus, each image was split into 13 divisions. After the elevation level of these 13 divisions was evaluated based on five levels (Extra High, High, Medium, Low, Extra Low), the subdivisions in the main body were united again by obtaining the average value of elevation for each section. This average value was determined by rounding decimals. The topographic data, so assessed, was explored statistically in order to detect any specific tendencies in the use of topography. The result from each case study was consistent, as it suggested a correlation between elevation levels and body sections of the images. This fact indicates the careful selection of specific morphology of cave wall for image-making. Also, all topographic data was integrated and quantified to generate a generalised version of the topographic condition for each case study. The topographic situation of each image was also visualised and classified. As this visualisation especially focuses on the body from the head to the thigh, images lacking any of the parts in the main body were excluded from the final verification; finally, a total of 45 images (Covalanas: 18, El Pendo: 8, El Castillo: 19) remained as subjects. As a result, this study detected six types of topographic pattern. Below is both description of the general outcome and discussion about the possible explanation for discerned trends.

The three case studies showed the same trend, which is also reflected in the combined statistics, therefore. Figure 6.6 illustrates the distribution of each body section

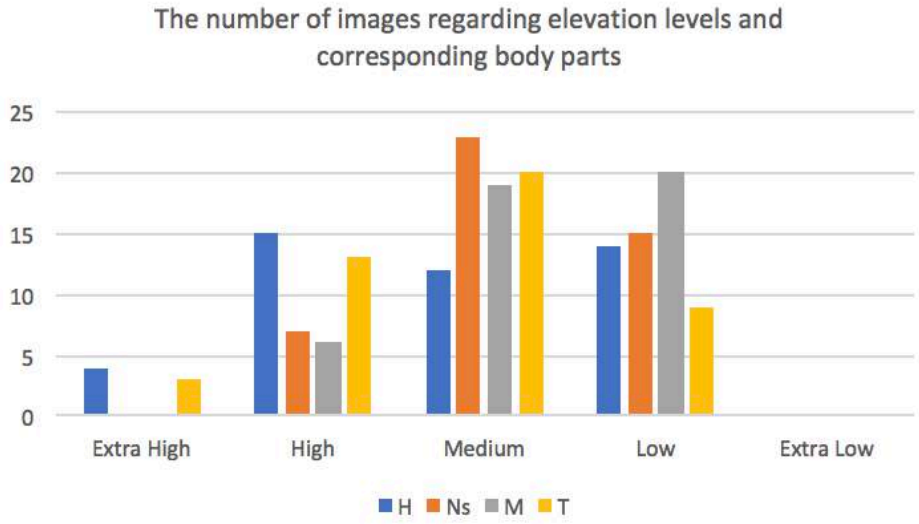

Figure 6.6: The number of images regarding elevation levels and corresponding body parts, based on 45 images (H: Head, Ns: Neck-shoulder, M: Mid-torso, and T: Thigh. Limbs and Tail are eliminated). There is a clear tendency as the head and thigh are more frequently placed on a higher elevation (19 images and 16 images, respectively) than the neck-shoulder and middle part (7 and 6, respectively).

(head, neck, mid-torso, thigh) by elevation level. As is seen from this graph, the head and thigh are more frequently placed on the wall of higher elevation than the neck-shoulder and middle part. This correspondence highly likely reflects the deliberate selection of the palaeo-artists due to the significant result of Chi-square ($p=0.0057$: see Table 52 in Appendix). Figure 6.7 shows a generalised topographic condition; namely, the sum of the elevation points by body section. The chart clearly illustrates that images are most likely depicted on an overall-concave surface. Also, clear features appear even in the leg and tail. Figure 6.8 demonstrates the distribution of elevation levels by body section (this figure involves all 54 images). According to this graph, these sections tend to be located on Extra levels at a much higher frequency than the rest of the body parts

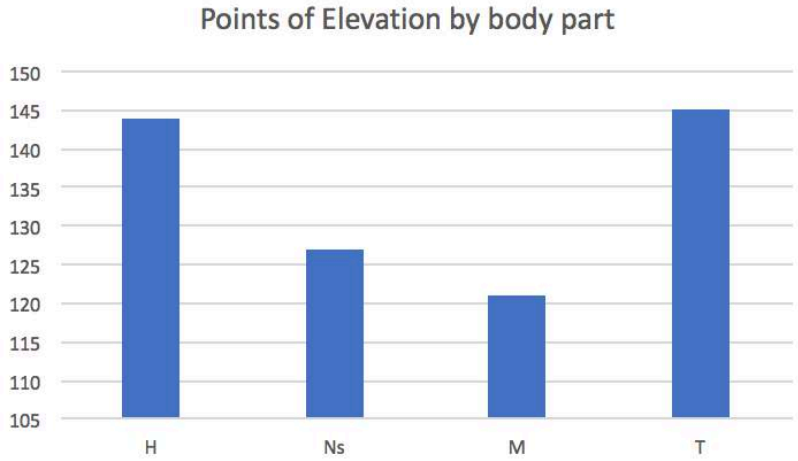

Figure 6.7: The generalised model of the topographic condition (H: 144, Ns: 127, M: 121, and T: 145). Higher points denote higher elevation. Based on the topographic data of 45 images, the general topography in the three studied caves is overall concavity.

(18 images). As will be described later, above locational arrangement might not be a coincidence, but it might reflect a particular preference of Palaeolithic artists. I performed Chi-square test to see whether or not this relation between limbs and the extreme elevation levels is obtained by chance. As a result, the test rejects the null hypothesis and strongly suggests the preferential use of the extra levels for legs (p=2.68E-14: see Table 53 Appendix).

The generalised topographic condition is indeed compatible with reality. In the case studies, the topography of each image was expressed as a line graph based on elevation level of the head, neck-shoulder, mid-torso and thigh so that the shape of the line graph directly represents the topographic condition. These graphs were subsequently classified by common features and revealed six topographic patterns (Figure 6.9); P1 (overall concavity), P2 (overall slope), P3 (overall convexity), P4 (zigzag), P5 (partial concavity), P6 (partial slope). P1 is the predominant topographic pattern (13 images), followed by P5 (10 images); P5 topography also contains a concave feature. This number accounts for over half of the total, which is significantly higher than the rest of the types (P2: 7, P3: 5, P4: 5, and P6: 5). That reality conforms to the generalised topographic condition (overall concave). To test significance of this result, I united the value for P1 and P5 as concavity and P2 and P6 as slope type because by doing so enable to assess the probability of association between four types of topography (Concavity, Slope, Convexity, and Zigzag). Consequently, the null hypothesis (there is no preferential use of specific topography) is rejected (p=0.00024: see Table 54 in Appendix). Therefore, it is highly likely that Palaeo-artists intentionally seek concave surface to fix images.

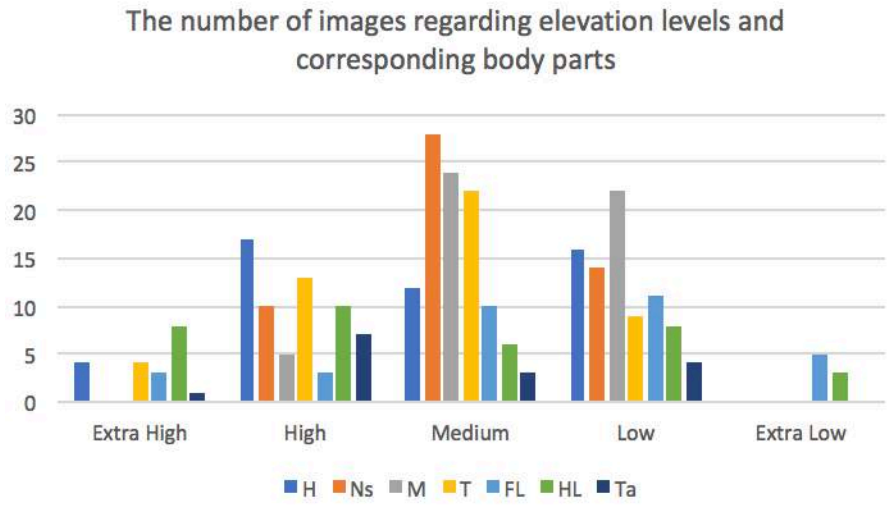

Figure 6.8: The number of images regarding elevation levels and corresponding body parts, based on 54 images (H: Head, Ns: Neck-shoulder, M: Mid-torso, T: Thigh, FL: Front Leg, HL: Hind Leg, and Ta: Tail). The legs tend to be located on Extra elevation levels at a much higher frequency (19 images) than the rest of the body parts (H:4, Ns:0, M:0, T: 3, and Ta: 1).

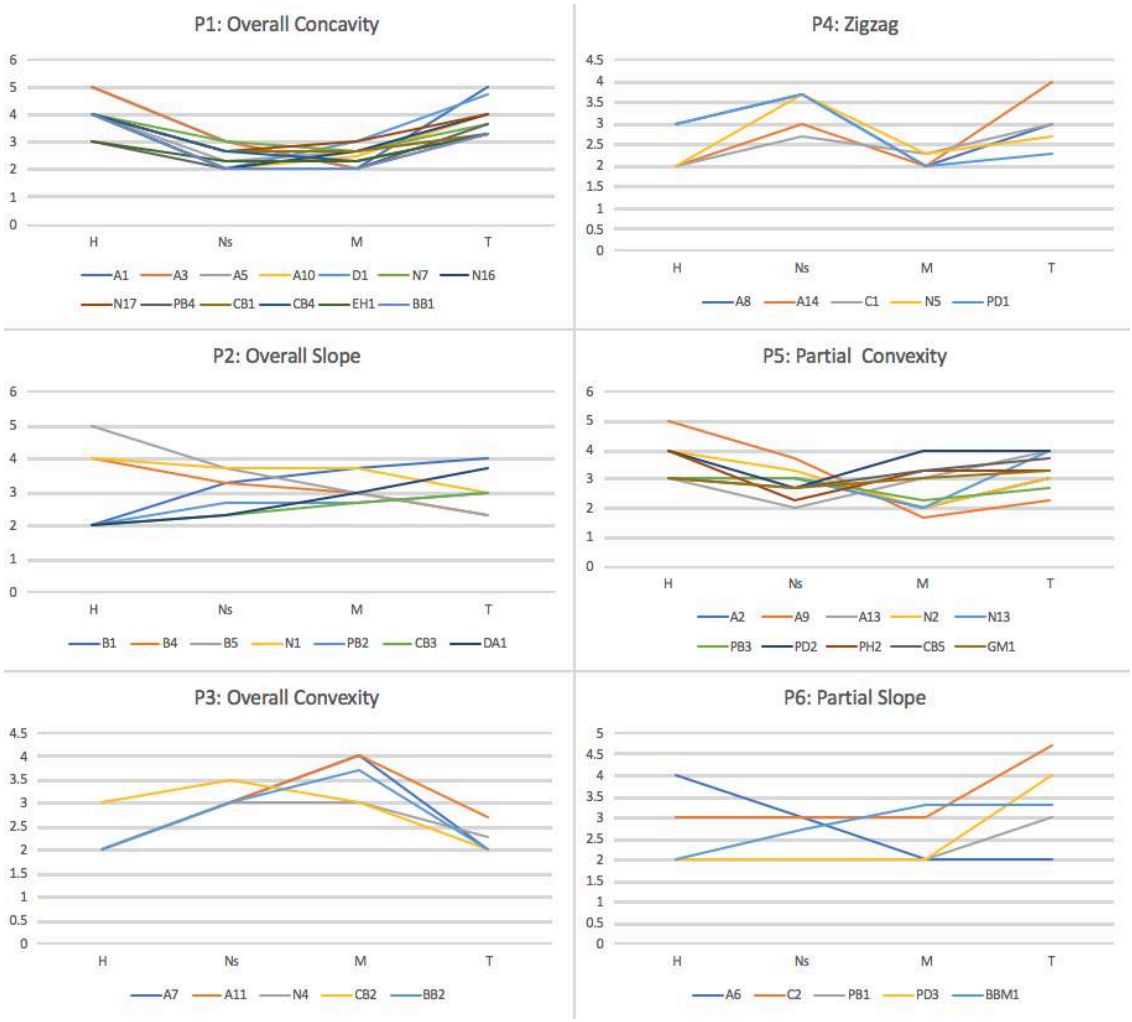

Figure 6.9: Briefly visualised topographic condition of images. Six patterns are detected from 45 images. The most common pattern is P1, with 13 images. The next common pattern is P5 (ten images) and then P2 (seven images). Meanwhile, P3, P4 and P6 contain five images respectively. Thus, the surface with a concave feature is the predominant topographic type. This fact conforms to the general shape of the topography seen in Figure 6.7.

The predominant use of overall concavity: four advantages

The frequent use of the overall concave topography might not be a mere coincidence but reflect an intentional selection by Palaeo-artists. To discuss the intention, reviewing the feature of this particular topography is necessary. The bottom of the overall concave is relatively flat compared to its outer edges. This fact is demonstrated in the generalised model: where the head, neck-shoulder, mid-torso, and thigh are respectively given elevation points (144, 127, 122, and 145: see figure 6.7). As these values directly represent the degree of elevation, the higher the value denotes the higher elevation level. The gap is 17 between the head and neck shoulder, five between the neck-shoulder and mid-torso, and 23 between the mid-torso and thigh. Therefore, the elevation gap between the neck-shoulder and mid-torso is the lowest, meaning that the topography of this adjacent area is closer to flat than the others.

Such a feature is advantageous for viewing images. Generally, when a viewer sees an image on a flat surface from the front, the image, although limited extent, is inevitably distorted at its both sides. Due to the imbalance in the distance between a viewpoint and the image's centre and between the view position and image's edges, the centre appears more massive than the sides (Ahn et al. 2014: Figure 6.10). In contrast, when viewers stand in front of an image on a moderately concaved surface, the imbalance is cleared as the topography adds a distance between the viewpoint and the centre. Consequently, viewers can recognise a less distorted image (Ibid.). This benefit is particularly significant in the cave's dark environment. The Inside of caves is space where darkness permanently rules, and for travelling in such a dark area, the use of artificial lights is essential. As was mentioned before, the available light sources in upper Palaeolithic were limited (hearths, torches and stone lamps (see Pettitt 2016;Pettitt et al. 2017): Especially, the use of stone lamps must have enhanced activity in caves as they are one of the major inventions in Upper Palaeolithic (Lewis-Williams 2002), although it might have been used for outside of caves (de Beaune 2004). However, the visibility obtained by the lamps must have been considerably limited within the range of 4m diameter (Pastoor and Weniger 2011); namely, the visible range is the only 2m radius. In such a dark environment, viewers must view images within such a close range to capture them in a clear vision. As for viewing a flat surface, the closer viewing-distance causes more noticeable distortion as the inequality in the distance between the three points (viewpoint, edges and centre) grows larger than when viewed from a distance (Figure 6.11). Therefore, depicting images on overall concave surfaces is a beneficial way to mitigate distortion in a dark environment.

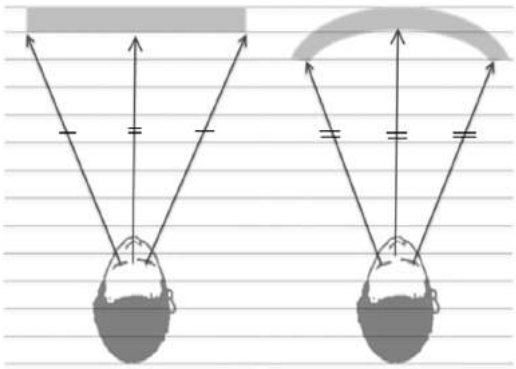

Figure 6.10: A merit of using an overall concave surface. When a viewer sees an image on a flat surface from the front, the image, although limited extent, is inevitably distorted at its both sides; due to the imbalance in the distance between the viewpoint, the centre of the surface, and the edges of the surface, the centre area appears larger than the sides. In contrast, when images on a moderate concave surface are viewed, the imbalance is cleared as the topography forms a distance between the viewpoint and the centre, and, as a result, viewers can experience less distorted images.

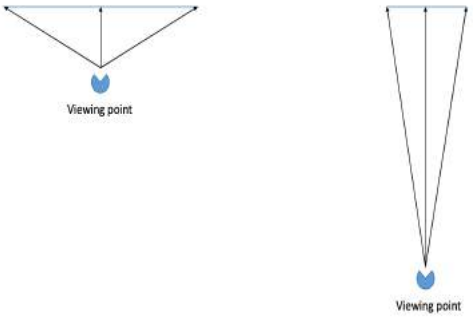

Figure 6.11: A different degree of distortion caused by viewing from different distances. Closer viewing-distance causes more noticeable distortion as the inequality in the distance between the viewpoint, the edges of the wall and the centre is larger than a distant viewpoint.

To confirm whether or not this benefit is applicable to 13 images of P1 type, I performed further analysis on each of these images. First, I set a viewing point of three different distances at the direct position (200cm, 100cm, and 50cm), and in this stage, images are considered as a flat surface. The second procedure is to obtain the distance between the viewpoints to both edges based on the length of the picture, and the viewing distances. Third, I added the depth to each viewing distances by image to acquire the actual distance between the viewpoints and the concaved bottom. Finally, gaps in distance between viewpoint-edge and viewpoint-centre (flat) and between viewpoint-edge and viewpoint-centre (concave) are compared. If the gap is closer to 0, the distance is more equalised, and distortion is more mitigated, therefore. The smaller gap in the concave cases means that concave surface eases the distortion, and it is considered that the image is applicable to the benefit of using concave surface. Table 6.1-6.3 show the results. When the viewing distance is set 200cm, distortion is cleared only in two images (N7 and EH1: see Table 6.1); however, further six images (A1, A10, D1, CB1, CB4, and BB1) mitigate their distortion if viewing position is set at 100 cm (Table 6.2); and distortion is also eased on A3, A5, and N16 when view position is located at the distance of 50cm (Table 6.3). Thus, a total of 11 images is subjected to the benefit within the viewing range of 200-50cm. Accordingly, viewers can see images without distortion as they adjust the viewing distance within this range. The significance of this benefit will be highlighted by comparing to the case of the overall convexity. Figure 6.12 illustrates a difference in a viewer's experience between viewing an image on an overall concavity and overall convexity from the same distance; the size of the two topographies is the same. Unlike the concavity which equalises the distance of viewpoint-centre (A-c) and that of viewpoint-edges (A-a and A-b), the overall convexity emphasises the inequality in the distance between viewpoint-centre (B-f) and viewpoint edge (B-d and B-e) because the centre of the topography is located closer to the viewer. In the case of the convex wall, the image appears noticeably distorted as the

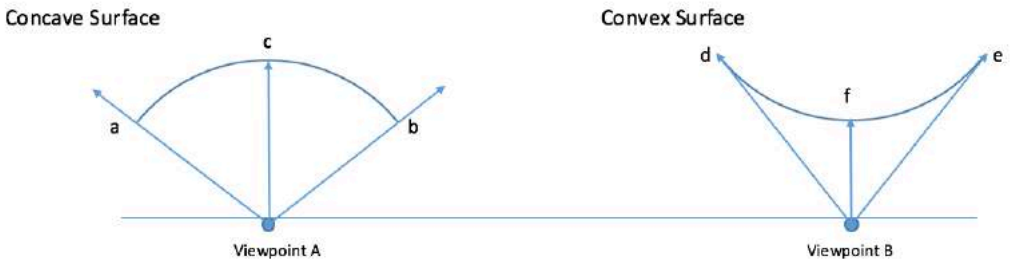

Figure 6.12: Illustration of viewing an image on an overall concavity (left) and overall convexity (right) from the same distance. The concavity equalises the distance of viewpoint-centre (A-c) and that of viewpoint-edges (A-a and A-b), while the convexity emphasises the inequality in the distance between viewpoint-centre (B-f) and viewpoint edge (B-d and B-e). Therefore, the image on the convexity appears noticeably distorted.

central area is perceived disproportionally large. Of course, this idea remains theoretical. However, Upper Palaeolithic is the period where the vast possibility of visual expression was explored (see Bahn 2016), and therefore, there would be no surprise even if palaeo-artists found the overall concave surface as a useful medium to optimise viewers experience.

Another advantage of the use of the concavity is also understandable by comparing it to the convexity because these contrasting topographic patterns define the viewing-range differently. Figure 6.13 shows the concave and convex surface and their viewing-range where viewers can see an image without unseen areas; both the viewing distance and the size of the topographies are same. Concerning the convex surface, as soon as the viewer moves to the left (Viewpoint D), the right edge of the image (d) goes unseen as the convex surface (d') hides the region, and therefore, the viewer fails to see the entire image. Similarly, from Viewpoint F, the left edge of the image (c) is not visible because of the topography (c'). In contrast, a viewer can see a whole image as for a concavity without topographic overlap from a wider viewing-range as no topographic features obstacle the viewer's sight (see concave surface in Figure 6.13). In short, too see the entire figure on the concavity, viewers can select a viewpoint from a broader range, whereas viewers of convexity have to stay around the front area; even so, images on a convex wall always appear more deformed than the case of the concavity. These facts can explain the dominance of the concavity and the rare use of the convexity: namely, concave walls are preferred to the convexity due to its capability to provide viewers with better viewing experience and wider choices of positioning.

At the same time, this wide viewing range potentially allows to accommodate multiple viewers. If images on an overall concavity more likely appear without unseen regions even when being viewed from different angles, multiple persons simultaneously standing different positions can potentially perceive images of relatively-similar shape. In other words, such a condition provides multiple viewers with better shared-vision. In the cave art study, whether or not images were meant to

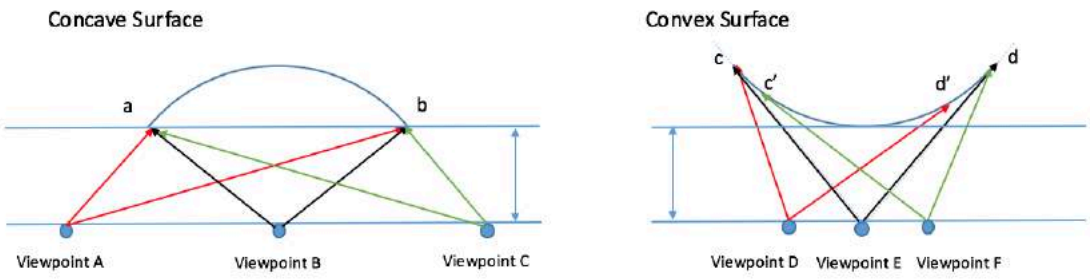

Figure 6.13: Illustration of viewing an image on an overall concavity (left) and overall convexity (right). The image on the concavity can be viewed from a much wider viewing range than one on the convexity. It means that the viewers can select a viewpoint from a broader range to see images on a concavity without unseen areas, whereas viewers have to stay around the front area in the case of the convexity. This wide viewing range potentially allows accommodating multiple viewers.

be viewed is one of the essential discussions (see Bahn 2003 and 2011), and it is argued that some images were publicly seen as cave's interior is modified to obtain a better visibility (e.g. Candamo and Cougnac cave: Bahn 2011, 351). Meanwhile, not all images are depicted for viewing, and some are believed to be 'private' due to their hardly-accessible locations (e.g. extremely narrow corridors: Fronsac, La Pasiega, high shafts: Bernifal, isolated chambers: Le CombelIbid, Ibid). However, given the possible capacity of the concave surface and its dominant use, it is presumable that at least images on the overall concavity in the three caves were not private and meant to be publicly viewed; therefore, naturally, viewers might have also seen the adjacent pictures of these concave images. The rare usage of convexity and its disadvantage for viewing purpose also reinforce this presumption.

The last merit is attributed to a rather practical purpose. The use of overall concave walls might have heightened the noticeability of images in the caves' environment and reduced a risk that viewers pass by without being aware of images' existence. Since the surface of P1 type elevates from the centre to both sides, the elevated edges are more likely to face viewers when images are viewed either from the left or right (Figure 6.14). Therefore, viewers can notice images easier on the wall of this type. This merit is particularly significant, taking account of the situation where images can be unnoticed because of the low visibility of caves. In contrast, in the case of other topography types (including a flat surface), this bilateralism is lost, or images appear more distorted. For this reason, the probability for viewers to miss images increases. Considering this advantage and the former, the use of overall-concave surface is understandable. Of course, it cannot be ruled out that predominance of P1 type is coincidental due to its not-decisive number. However, given the cases where images are located on the cases, especially dynamic concavity (e.g. A1, A3, N16, N17, PB4, and BB1), it is also hard to see the randomness in the selection of the medium's shape. Therefore, those advantages can refer to the purposeful use of this specific topography. Apart from these benefits, there is another possibility. I will discuss that benefit in association with viewing interaction in the next section.

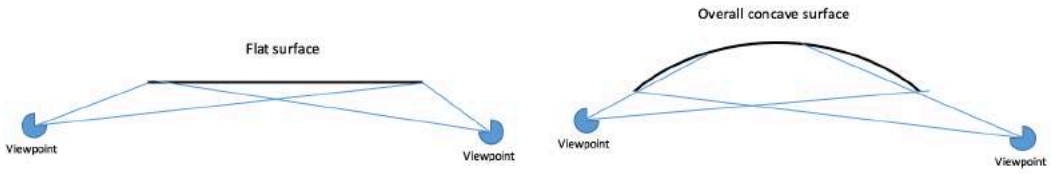

Figure 6.14: Another merit of using P1 topography. Since both edges of overall concave surface elevate, these edges are more likely to face viewers when images are viewed from sides. On the other hand, an acute angle forms between the surface and a viewer in the case of the flat surface because the wall does not face viewers standing on sides. The use of the overall concave might have had merit to reduce a chance that images were unnoticed.

	Size (cm)	Depth (cm)	Distance to flat bottom (cm)	Distance to edges (cm)	Distance to concave bottom (cm)	Distance gap (edge-flat bottom) (cm)	Distance gap (edge-concave bottom) (cm)	If concave surface mitigates distortion (Yes\ Not)
A1								
A3	74	14.6	200	203	214.6	-3	11.6	N
A5								
A10								
D1	64	7.8	200	203	207.8	-3	4.8	N
N7	125	10.9	200	210	210.9	-10	0.9	Y
N16	70	20.5	200	203	220.5	-3	17.5	N
N17	68	23.7	200	203	223.7	-3	20.7	N
PB4	60	28	200	202	228	-2	26	N
CB1	72	7.3	200	203	207.3	-3	4.3	N
CB4	68	6.6	200	203	206.6	-3	3.6	N
EH1	107	9.5	200	207	209.5	-7	-2.5	Y
BB1	99	20.2	200	206	220.2	-6	14.2	N

Table 6.1: Whether or not the concave surface mitigates the distortion when viewers see images from the distance of 200cm. Only N7 and EH1 appear less distorted in this setting (A1, A5 and A10 are eliminated because the minimum viewing distance for them is around 1m due to environmental restriction.

A1	**106**	**20.3**	**100**	**113**	**120.3**	**-13**	**7.3**	**Y**
A3	74	14.6	100	107	114.6	-7	7.6	N
A5	43	3.2	100	102	103.2	-2	12	N
A10	84	4.4	100	108	104.4	-8	-3.6	Y
D1	64	7.8	100	105	107.8	-5	2.8	Y
N7	125	10.9	100	118	110.9	-18	-7.1	Y
N16	70	20.5	100	106	120.5	-6	14.5	N
N17	68	23.7	100	106	123.7	-6	17.7	N
PB4	60	28	100	104	128	-4	24	N
CB1	72	7.3	100	106	107.3	-6	1.3	Y
CB4	68	6.6	100	106	106.6	-6	0.6	Y
EH1	107	9.5	100	113	109.5	-13	-3.5	Y
BB1	99	20.2	100	112	120.2	-12	7.8	Y

Table 6.2: When viewers see images from the distance of 100cm. In addition to N7 and EH1, six images (A1, A10, D1, CB1, CB4, and BB1) become less distorted.

A1	**106**	**20.3**	**50**	**72.9**	**70.3**	**-22.9**	**-2.6**	**Y**
A3	74	14.6	50	62.2	64.6	-12.2	2.4	Y
A5	43	3.2	50	54.4	53.2	-4.4	-1.2	Y
A10	84	4.4	50	65.3	54.4	-15.3	-10.9	Y
D1	64	7.8	50	59.4	57.8	-9.4	-1.6	Y
N7	125	10.9	50	80	60.9	-30	-19.1	Y
N16	70	20.5	50	61.6	70.5	-11.6	8.9	Y
N17	68	23.7	50	60.5	73.7	-10.5	13.7	N
PB4	60	28	50	58.3	78	-8.3	19.7	N
CB1	72	7.3	50	61.6	57.3	-11.6	-4.3	Y
CB4	68	6.6	50	60.5	56.6	-10.5	-3.9	Y
EH1	107	9.5	50	73.2	59.5	-23.2	-13.7	Y
BB1	99	20.2	50	70.4	70.2	-20.4	-0.2	Y

Table 6.3: When viewers see images from the distance of 50cm. Distortion is also eased on A3, A5, and N16. Thus, a total of 11 images is subjected to the benefit of using overall concave within the viewing range of 200-50cm. Accordingly, viewers can see images without distortion as they adjust the viewing distance within this range.

In any case, accepting the deliberate choice of a particular topography can also elucidate the reason for a strong correlation between leg-tail and extra elevation levels. Namely, placing the main body on a specific topographic condition might have been the priority, and the topography of marginal area had a low priority, and hence not much attention to the topography for the appendages was paid. If it is a case, the probability that these parts are located on Extra elevation levels naturally increases. Thus, the reason why these parts are more likely placed such extra levels can also be explained by the high priority of the main body. However, the correlation between Extra levels and the appendages can also be addressed by the notion of the deliberate distortion on these parts. In that case, even the arrangement of Extra levels to legs-limbs might have been intentional. This point will also be discussed later.

Topography as sculptural quality

The use of the topography is not only attributed to the reasons discussed above. Aside from the concave surface, undulating surfaces are utilised for another purpose: a further expression of naturalism. More specifically, by assigning topographic features on specific body parts, 2D images achieve sculptural quality (Leroi-Gourhan 1965, and Bahn 2016). BBM1 in El Castillo epitomises such sculptural images: although BBM1 is classified as P6, the subtle undulation of the body (neck-shoulder, mid-torso, thigh) is reminiscent of a real mammal once its topography is carefully examined. At the same time, the undulation on the hind leg corresponds to the way how human legs appear. Also, since the entire body of BBM1 is located on a slight convex whose elevation especially rises from the mid-torso to the thigh, for viewers, the Bison-man no longer appears as a 2D image but as a relief. There are other unique samples for such a sculptural painting are also found in other cases. C2, N16, PB2, and BU1, for example, contain a large convex on their thigh, and the body part is noticeably elevated as a result of such a particular arrangement. Accordingly, the elevation of the thigh appears the rise of muscle. As for BB1, the entire posterior is slightly elevated from the wall, and therefore, the image seems a hybrid figure of a relief and an image. In this way, topography can also be an element to add 3D volume to a plain image.

Location of images

Considering the probability in which available natural lines and topographic patterns met the purpose of the artists, it seems that not so many locations are available for art in the caves despite the abundant space available in their interior. Therefore, places to depict images are naturally defined or, if not entirely, at least further limited. If there are preferred topography and ideal natural lines for integration at the same time, such locations might be more special than elsewhere, and images depicted after all the elements meet artists' consideration become significantly specific to their location. If so, there is no mystery even if images were associated with same specialness which such a location might have been given. In any case, images were not placed at random, but rather a locational arrangement must have involved a significant degree of discretion. As far as inferring from the data, not only natural lines but also the topography must have been carefully observed by ice-age artists. Given this, cave art is not a product of the ability of the artists alone. Rather, the dynamic interaction between the human and the cave contributes to the production of the Palaeolithic parietal art.

6.3. Distortion on images:

General result

The discussion in this section focuses on human-medium interaction in the post-production phase. As noted in the Chapter two, researchers such as Boado and Romeo (1993), Groenen (2000), Azema and Revere (2012), and Sakamoto (2014) argued the interactive nature of cave art. Cave art involves viewers' deliberate bodily engagement, which facilitates manipulating the appearance of images (see Table 2.1 in the second chapter). In this category, I examined interactivity by which viewers experience constant modification of images' appearance; images on a non-flat medium are distorted by the undulation of the medium itself when being viewed from a different angle. Therefore, they never possess a fixed shape. However, that fact does not immediately indicate the existence of the deliberate interaction because distortion might merely represent a consequence of depicting images on such an undulating surface. Hence, it is essential to discern any signs of the intentional use of distortion, and that is the purpose of the analysis in this section.

Among a total of 54 pictorial samples, distortion was confirmed in 33 images. As this number accounts for 61% of the whole, deformations are relatively frequent

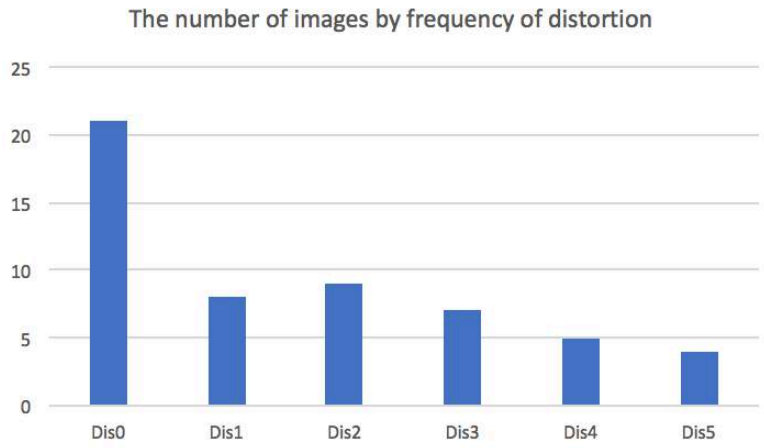

Figure 6.15: The number of images by the frequency of distortion (Dis = Distortion). A total of 33 images are distorted in the three caves, which accounts for 61% of the whole samples. Particularly, the number of images with more than two distorted body parts is 25 (Dis2: 9, Dis3: 7, Dis4: 5, and Dis6: 4), nearly 50% of all, and the appearance of these images are subjected to a remarkable deformation.

phenomena in Covalanas, El Pendo, and El Castillo (Figure 6.15). Particularly, the number of images with more than two distorted body parts is 25, which comprises nearly 50% of all, and the appearance of these images noticeably deformed. However, the ratio is not consistent among the three caves: in Covalanas distortion occurs in 11 images out of 18 (61%); in El Pendo nearly all images are deformed (10/11 images: 91%); but El Castillo distortion is least likely, with 12 images out of 25 (12/25 images: 48%). This inconsistency might be attributed to how images are distributed in each cave. In Covalanas and El Pendo, images are depicted on a single panel or at least adjacent areas whose topographic condition is homogenous. If the surface within a particular area sustains undulation of the similar degree which is sufficient to cause distortion, all images distributed in the area are also distortable in the same degree. On the other hand, in El Castillo collected graphic samples are located in several distant regions where the condition of the wall noticeably varies, and some walls are significantly featureless. Such a lack of consistency in topography, therefore, is reflected in the result.

With regard to the correlation between body sections and distortion, three caves demonstrated a meaningful trend. As illustrated in Figure 6.16, distortions mostly occurred on the head (22 cases), neck-shoulder (20), and legs (18), whereas the thigh (15) and mid-torso (12) were less frequently deformed. Meanwhile, no distortion was found on the tail. Although the result represents a general trend, the value for legs and neck-shoulder varies by cave. For instance, in Covalanas only four cases of deformation have been confirmed on legs, while in the other caves the part is highly subjected to deformation. The reason can be ascertained to the fact that legs are absent in the majority of images in Covalanas. Additionally, the inconsistency for the neck-shoulder is particularly noteworthy because the result depends on the dominant motif in each cave.

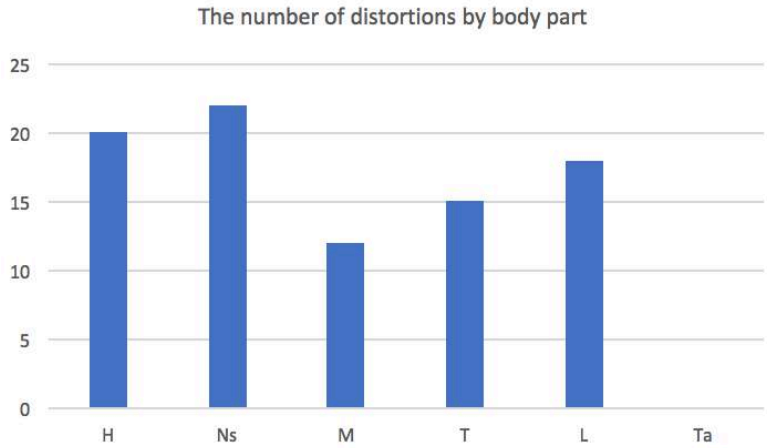

Figure 6.16: The number of distortions by body part (H: Head, Ns: Neck-shoulder, M: Mid-torso, T: Thigh, L: Limbs, and Ta: Tail). Distortions mostly occur on the head (20 cases), neck-shoulder (22), and legs (18). On the other hand, the thigh (15) and mid-torso (12) were less frequently deformed. Meanwhile, no distortion was found on the tail.

In El Castillo where bison is the most frequent motif, the frequency of distortion for the neck-shoulder was the third lowest, while the section is most likely distorted in Covalanas and El Pendo where red deer is by far dominant motif. This is because bison contains much less of a clear boundary between the head and neck than do the deer, and the distortion on the neck-shoulder in Bison is not as clearly confirmable as in deer. For this reason, the unclear boundary between the head and neck makes the perception of the distortion difficult, resulting in the low frequency in El Castillo. On the other hand, the value for the head and mid-torso are consistent in all case studies; the head is likely distorted in the three caves, whereas the middle part mostly remains undistorted. Overall, the trend is not conspicuous. The gap in the value for each body section shows no significant difference except the tail. Even so, the result of the chi-square test ($p=0.0055$) rejected the null hypothesis (there is no correlation between distortion and specific body parts: see Table 55 in Appendix). Therefore, that numerical distribution is not obtained by chance. Indeed, the head, neck (except the case of bison), mid-torso, and legs - if all images in Covalanas had been complete – exhibit a certain level of consistency: while the head, neck and legs are commonly distorted in the three case studies, the mid-torso tends to be static.

The data and cautious treatment

To interpret the above results, associating the data with the actions of real animals may be fruitful. The head, neck and legs are the most moving /dynamic body parts in living quadruped mammals, whereas the movement of the torso and the thigh is less conspicuous. For example, quadrupeds regularly swing their head and neck

either vertically or horizontally as they intake diet and collect information of surroundings. The legs also continuously appear in motion whenever mammals travel. The movement in the main body (shoulder, mid-torso, thigh), by contrast, is relatively static, unless animals take a substantial action such as kick and looking backwards, each of which involves the contraction of the thigh and the mid-torso. Thus, interpreting the result based on animal actions seems compatible with what is visible in the data. In addition, the process of deformation can be perceived as an animation by viewers moving within a certain range, and in some cases images actually appear as if they shake their head and neck (e.g. A1, B4, N4, N17, etc.) or in some cases images stretch and shrink their neck (e.g. B5, N5, N7, N14, etc.). Similarly, the orientation of legs noticeably changes in many images (e.g. A9, B5, N4, CB1, BB1, etc.). Based on this correspondence, one might assume a particular purpose of cave art shared among the ice-age artists; namely, cave art, if not all cases, represents an artistic attempt to produce animated images as if real animals.

However, this interpretation requires caution of a significant degree. In this analysis, I determined the presence/absence of deformation based on the distortion on the contour. In that case, the smaller the outlined area, the more noticeable the deformation. Therefore, viewers are inevitably apt to notice the distortion on the head, neck, and legs rather than the torso (shoulder, mid-torso, thigh). This principle has already been mentioned earlier; deformation on the thin neck of red deer is readily noticeable in Covalanas and El Pendo, whereas the thick neck of bison is hardly deformed as in the case of El Castillo. Accordingly, the result might only represent such a principle, and that correspondence might be irrelevant to an artistic intention. Therefore, this data will immediately prove deliberate interactivity concerning distortion.

Two fundamental elements for viewing interaction

Are there any detectable signs of a deliberate interaction? Or more directly, what can be considered as such signs? To discuss "signs", first of all, we must clarify the fundamental elements of the analysed viewing-interaction. Those elements are two types of awareness: the awareness of the plurality of the viewpoint and the awareness of distortion itself. Unless the existence of these two elements is logically affirmed, the premise of this viewing-interaction itself will collapse.

'Viewpoint' in cave art has been often discussed by various researchers. Although several studies dealing with the issue from a different perspective (e.g. the plurality of horizontal axis [Boado and Romero 1993]; Anamorphosis[Groenen 2000];

Shared gaze [Geneste 2004]), anamorphosis is a subject which is directly related to the issue of multiple viewpoints. A number of researches have detected anamorphic images from different regions (Lascaux cave: Aujoulat 1985, and Surre 1992: Cougnac cave: Lorblanchet 1984, Groenen 2000, Tito Bustillo: Aujoulat 1985: Reseau Clastres: Clottes and Simonnet 1990). Above all, the most famous example is the red cow depicted on a corner of the ceiling in the Axial gallery of Lascaux. This cow appears to viewers in proper proportion when they look up at the cow from the frontal position, while the harmony is gradually disturbed as the viewpoint elevates and approaches to the actual height at which the artist worked (Surre 1992). Another example, anamorphic herbivore in Cognac, requires further action. Even though this image is fixed on a wall at the height of standing viewers, it appears deformed when viewed from this height. However, the herbivore achieves the proper form when viewers crouch down and look up (Groenen 2000). Thus, the presence of anamorphosis in cave art supports the notion that the ideal viewpoint was shared between artists and viewers (Gittins and Pettitt 2017), and viewing such images naturally involved the awareness of different viewpoints. Accordingly, it seems safe to argue the special awareness of plural viewpoints in cave art.

Apart from Anamorphic images, indicators of such an awareness have also been confirmed in this research. For example, B4 (Covalanas), EH1 and BB1 (El Castillo) are images where natural lines are unusually integrated into their outline. Despite their normal appearance when being viewed from the direct position, natural lines which exist irrespectively around or on the images turn into a part of their outline once a viewpoint moves to a side (Figure 6.17). Especially regarding B4 and EH1, in both cases,

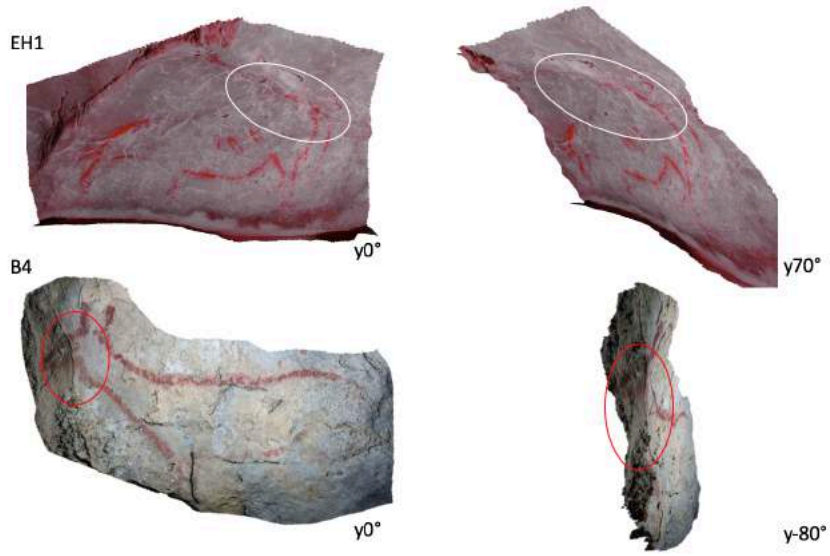

Figure 6.17: Examples of unusual integration (EH1 and B4). Despite their normal appearance when being viewed from the direct position, natural lines which exist irrespectively around/on the images (see circled areas) turn into a part of the outline once viewpoint moves to a side. These lines can be an obstacle for viewers, and potentially the artists could have avoided this composition if they had aimed them to view only from the front.

ridges are located on a particular position (face: B4, Croup: EH1) where these lines can be an obstacle for viewing, and potentially the artists for these images could have avoided this composition if they had aimed them to view only from the front. Considering the reason for such arrangements and the fact that these lines perfectly overlap on the contour once seen from a specific position, it seems more reasonable to presume that these compositions were deliberately arranged. Furthermore, a deer in Covalanas, which is not examined in this thesis due to difficulty in accessibility, also represents the plurality of viewpoint: the deer located in the narrow area behind the panel for B1 and B4-5 shows itself only when it is looked up from the main passage (Pizzato 2013). This example also testifies the special attention of palaeolithic humans to the viewpoint.

In addition to the plurality of viewpoints, the awareness of the deformation must be discussed. Because samples of anamorphic images have been reported from both French and Spanish caves, the notion of anamorphosis and its principle were widely shared among communities in the Franco-Cantabrian region. This principle denotes mutual agreements between artists and viewers about a proper proportion and a viewing position. Regarding this point, Groenen (2000) states that examining anamorphosis will 'allow us to find the ideal position for an observer' (104). The 'ideal position' is, in fact, a crucial keyword: if the "ideal position" was shared as a 'community of gazes' (Geneste et al. 2004, 74), the opposite notion, namely, "non-ideal position " was also necessarily recognised at the same time. That is, assessing the ideal viewing point requires a clear awareness to determine whether or not an image's proportion is ideal. Without the awareness of the binary opposition of the proper and non-proper proportion, it is impossible to find such a perfect viewpoint.

Viewers in Upper Palaeolithic surely saw deformed images. In all images examined in the three case studies, the proper proportion is obtained when viewing the image from the front, while the degree of deformation increases as the viewpoint moves to sides; in this sense, the "ideal viewpoint" for all images is located in front of them. However, viewers are not always able to start viewing images from the front. Due to environmental conditions, in most cases, viewers must start seeing images from a side. In Covalanas, for example, images are fixed on both sides of the wall of the narrow passage. Viewers, who travel in that corridor, perceive images from their edge except for B4 and A3 which are located at the corner of the bending path. In other words, viewers firstly recognise an image in its deformed state; secondly their appearance changes into a proper shape as the viewer proceeds; lastly, they appear deformed again when the viewer leaves the front area. This deformation process repeats whenever viewers encounter a new image except for B4 and A3. Also, same is true for El Pendo where all examined images are located on a panel of approximately 8m width.

Considering such a wide area and visual space with limited illumination, viewers must move along the wall from the one end to the other to view all images. Therefore, as in Covalanas, firstly images enter into a viewer's sight from the deformed state, secondly change into a proper proportion, and finally, they appear deformed again. Such experience cannot be entirely applied to El Castillo where spatial conditions significantly diverse. For instance, as Polychrome Panel is located at a corner of the cave wall on the north side of Room A, the perception begins with the frontal view of images. CB3 and EH1 also show its frontal view firstly because these images are fixed to face the viewer travelling on the way. However, there are also examples which viewers start to recognise from their edge. Since BB1 and BB2 are located on a side wall in a passage connecting the room B and C, they are perceived from the left side of their body. Same is true for GM1: viewers who proceed the Gallery of Discs will begin to recognise GM1 from its edge. Hence, as for images in a particular spatial condition, viewing must start from the side of images. In such cases, Palaeo-viewers must have experienced images in a deformed state.

For the reason noted above, it is hard to deny the existence of the viewers' awareness of the distortion. Moreover, due to the unique luminary condition of the cave's environment, the attention of viewers to deformation is further enhanced. In the interior of caves where the light level is considerably limited, everything appears ambiguous (Pettitt 2016; Pettitt et al. 2017). Therefore, the detail of the morphology of the cave surface, although depending on the viewing distance, is also significantly lost. In such a condition, viewers perceive images on the ambiguous surface; especially red images appear conspicuously floating from their medium. If so, viewers experience the effect of deformation to a significant extent. In addition, remember that cave's environment is a favoured situation for experiencing motions: our brain is more sensitive to recognise movements than shapes because the speed of processing information of motion is faster than that of shape (Dobrez 2013). Also, in dark spaces where the amount of visual information is significantly reduced, the brain creates false vision because it attempts to process the same amount of information as in well-illuminated environment (Moyes 2012, and Moyes et al. 2017). Given these facts, in caves, humans more likely perceive distortion on images as an illusion as if viewing motion pictures. The combination of such environmental constraints and features of our cognitive system, accordingly, also reinforce the fact that viewers were well aware of the dynamism of deformation.

Thus, viewers in Upper Palaeolithic must have been aware of the plurality of viewpoints and distortion of images. Therefore, it is difficult to consider that they were ignorant about the deforming process in the head, neck, and legs. These arguments are the premise of this viewing-interaction. Remember that the issue is whether or not the

nature of distortion is intentionally embedded in a viewer-art relation. These two types of awareness enable us to hypothesise the existence of the viewing action, but they do not evidence to prove the intentional use of distortion as a part of the interaction. Even so, considering them with other factors, if not entirely, might allow us to point out a glimpse of the intention. Those factors are found in the selection of specific topographic condition.

A sign of intentionality: limbs and Extra-elevation levels

The primary element of artists' intention might be found in the relation between limbs and their topographic condition. In the previous section, it was noted that the legs were far more likely located at Extra-elevation levels than the other body parts; 18 images contain their limbs either on extra-low or extra-high wall. Meanwhile, four images include their thigh on Extra levels, and there are three images with their head on the highly concave\convex surface. In contrast, Extra levels are not found on the neck-shoulder and mid-torso in these case studies. In the previous section, I attributed the reason for such a high correspondence between limbs and extra levels to the lower priority in the selection of topography; topographic condition for legs was less paid attention. However, this explanation is not plausible enough. Even if the palaeolithic artists failed to pay attention to the topography of the legs, limbs did not necessarily correspond to Extra levels; the result of chi-square test (<0.05) also supports an intentional selection of Extra levels to limbs. Therefore, since the number for limbs (18 images) seems outstanding in comparison with that for the other sections, one can naturally assume intentionality for this arrangement of the topography.

The enigmatic relation between limbs and Extra levels is understandable once deliberate distortion is taken into account because allocating a body part on such a remarkably convex\concave surface is an ideal way to cause distortion. Limbs are the narrowest outlined area, of which viewers most likely perceive a deformation. Once such a limited section is allocated to a highly undulating topography, the degree of distortion becomes by far conspicuous. This fact is reflected in N14, N16, B5, PB4, CB1, and BB1 where the elevation gap largely changes the direction of legs. As viewers move side to side while viewing these images, they experience images' legs constantly bending forward and backwards. Given the distortable nature of the limb and such dynamism of distortion, the high rate of the correspondence between the limb and Extra levels might reflect a specific will of the palaeolithic artists. Concisely, the arrangement can be a method for maximising distortion-related interaction.

A sign of intentionality: overall concavity

To consider the intentionality in an alternate way, examining a correlation between topography types and distortion provides us with useful insights. In the previous section, I argued that the most popular topography type was Overall concave (P1) and that there were two benefits from using the pattern. First, the curved surface mitigates the distortion when viewed from the direct position. Second, the use of overall concave maximises the chance that viewers notice paintings even in the dark environment; images on this topography were more likely captured in sight when seen from a side because one of the elevated edges always faces viewers. This topography, in fact, also features viewer engagement and potentially testifies the intentional use of distortion. Figure 6.18 shows the correlation between topographic types and the number of images with distortion on the main body (the head, neck-shoulder, mid-torso, and thigh). P1 contains the highest ratio, with 92% (12/13 images), followed by Overall slope(P3), with 60% (3/5 images); values for the rest of topography types are between 30% and 57%. Given the fact that the total number of P1 images is almost three times higher than P3, the high ratio of P1 is significant. This significance is clearly visualised if the number of distortions per single image is also taken into account. Figure 6.19 shows the number of images and the total number of detected distortion (without values for limbs) by topography type. The value for P1 is outstanding with a total of 35 distortions, while P2 and P5 contain only eight distortions respectively. Based on this data, the average number of distortion per single image of P1 type is approximately 2.9 (35 distortions/ 13 images), whereas the average number for the rest types are less than 1.1 (P2: 1.1, P3: 1, P4: 0.6, P5: 0.8, P6: 0.4, and N\A: 0.8, see line graph Figure 6.19).

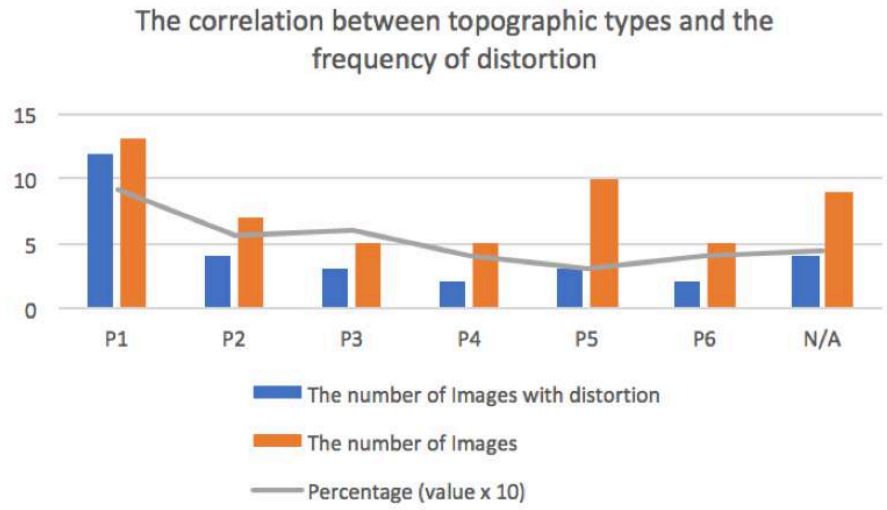

Figure 6.18: The correlation between topography types and the frequency of distortion. Distortion most frequently occurs to images on P1 (92 per cent: 12/13). However, the ratio for other topography type is between 60 and 30 percent.

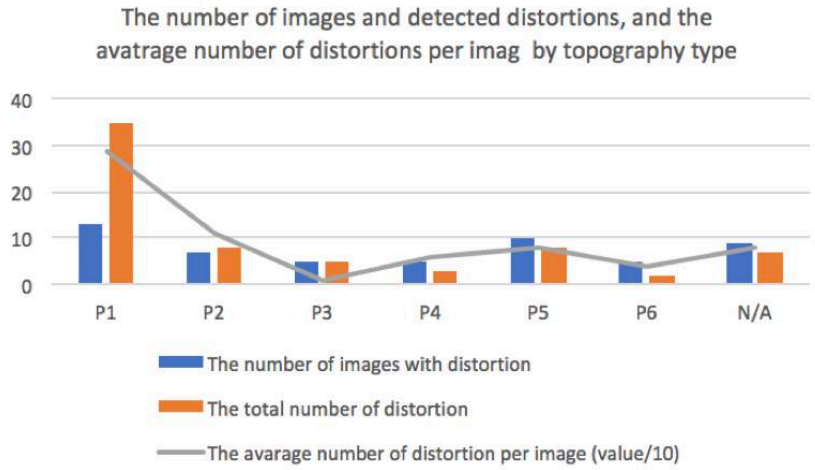

Figure 6.19: The number of images, detected distortions, and the average number of distortion per image by topography type. The number of distortion for P1 images are significantly higher than images of other topography types. In average, almost three distortions are detected from each image of P1 (see the line graph), while values for the other types are less than 1.1.

Accordingly, P1 type is more associable with topographic intervention on images' appearance. The significance of this statistical data (the total number of distortions by topography type) is tested by Chi-square test, and obtained p-value is remarkably small (p=3.19456E-15: see Table 56 in Appendix).

The reason for this conspicuously high frequency might be attributed to the symmetric shape of overall concavity. Figure 6.20 illustrates the mechanism of how different viewing angles distorts images on P1 topography. In theory, when the viewpoint is set in the direct position, both ends of the image are equally captured in sight (A). However, once the viewpoint moves to the left, that equality collapses, and the body part depicted on the left side will be distorted remarkably due to the interference by the elevated surface(B). On the other hand, since the body part which is drawn on the right area of the wall faces the viewer, the degree of deformation is kept to a minimum, and the appearance is maintained and still similar to what is perceived

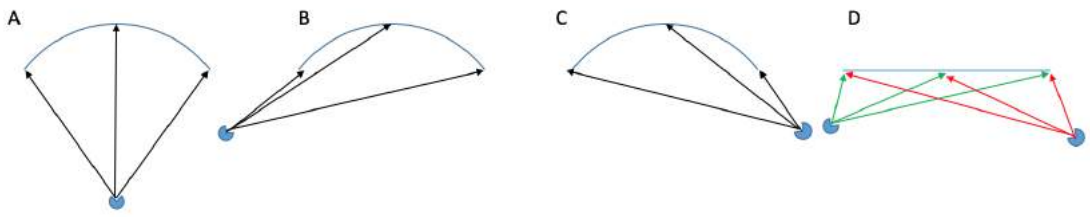

Figure 6.20: These images show a mechanism of how viewing from different positions distorts images on an overall concave surface. When viewing point is taken in front of the wall, both edges of an image are equally captured in sight (A). However, once the viewpoint moves to the left, that balance collapses, and the body part depicted on the left side will be distorted remarkably due to the interference by the elevated surface. On the other hand, since the body part is drawn on the right area of the wall faces the viewer, the part maintains its original shape (B). Similarly, when the viewpoint is taken on the right, the image deforms greatly on the right side, while the left side sustains a relatively stable shape (C). If the image were placed on a flat surface, the opposite edge would always fail to face a viewer standing either on the left or right. Therefore, an acute angle would form between the viewpoint and the surface, and images would appear shrunk at the opposite side to the viewer (D).

when it is viewed from the front. Similarly, when the viewpoint is taken on the right, the image deforms significantly on the right side of the concave surface, while the left part of the image sustains a relatively stable shape (C). If the image were placed on a flat surface, the opposite edge would not face a viewer standing either on the left or right. Therefore, an acute angle would form between the viewpoint and the surface, and as a result, the image would always appear shrunk at the opposite side to the viewer (D). By this mechanism, images on the overall concave surface tend to contain three deformed body parts (the head, neck-shoulder, and thigh). According to the above example, the head and neck-shoulder appear significantly distorted when viewers stand on the left, while the thigh is deformed when viewers move to the right. Therefore, the average number of distortion per image becomes naturally high. Indeed, this distortion model is applicable to the most of P1 images (A1, D1, N16, N17, PB4, CB1, EH1, BB1: 8/13 images).

On the other hand, other topography types are fundamentally less associable with distortion. Theoretically, in asymmetric topography types (P2, P5, and P6), a topographic feature is located on one side of images. In such a condition, distortion is also one-sided (e.g. P2: B4, B5, N1, CB3; P5: N2; P6: C2). As for P3 (overall convex), a convex feature lies on the neck-shoulder and mid-torso on which distortion is least likely noticeable because the outlined area is wider than the other body parts. Accordingly, distortion tends to be detected on the head and\or thigh (e.g. A7, A11, CB2, and BB2). In any case, the detection occurs in lower probability than P1. Irregular topography type is zigzag (P4). This type potentially generates a contraction of torso area when it is viewed from sides. Therefore, distortion should intensively happen in the neck-shoulder and mid-torso area. However, in this study, none of the P4 images shows this type of distortion. Of course, the topographic pattern is not the only determinant of absence\presence of distortion because deformation takes account of multiple factors (e.g. the depth of topography, the height of the image's location, the degree of wall's inclination). Hence, I must insist that images are not always deformed in the specific ways described above. However, at least most of the images of P1 are distorted as was indicated in the distortion model, and the data suggests the most substantial connection to distortion.

Overall concavity is thus associable to an ideal cause of dynamic distortion. Further to this, considering the above distortion model of P1 type allows us to discuss a specific manner of intentional distortion. In situation B (Figure 6.20), viewers experience distortion on the anterior side, while sustaining the shape of the posterior constant. In this regard, viewers by themselves can produce more perceptible and meaningful animation on the head and the neck. Figure 6.21 demonstrates a model which applies the above mechanism to A1 (Covalanas). Since A1 is located on an overall

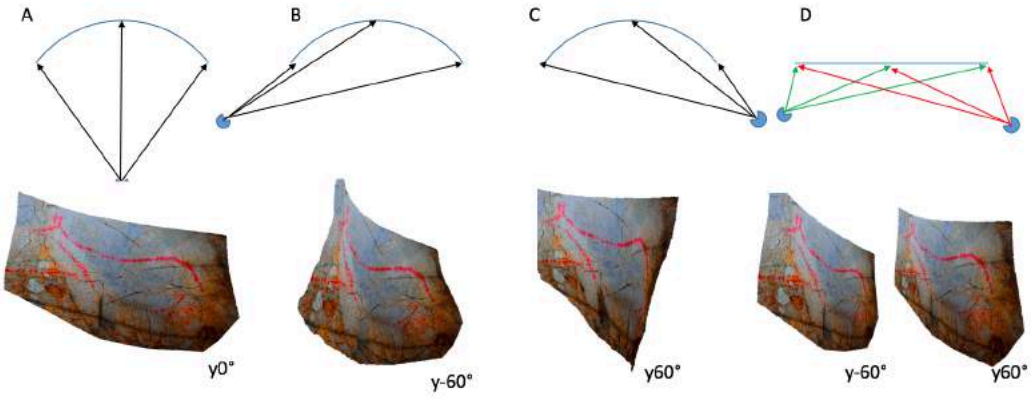

Figure 6.21: Mechanism of how A1 (Covalanas) is deformed by viewing different viewpoints. Since A1 is located on an overall concave surface, the head and neck-shoulder maintain their original shape even if the viewpoint moves to the right (y60°), while the thigh is deformed largely. In contrast, once the viewpoint moves to the left (y-60°), the thigh recovers its original shape, whereas the head and neck are deformed to a great extent. This phenomenon is unique to the overall concave surface and does not occur on a flat medium.

concave surface, the head and neck-shoulder maintain their original shape even if the viewpoint moves to the right (y60°), while the thigh is mainly deformed. Once the viewpoint moves to the left (y-60°), the thigh recovers its original shape, whereas the head and neck are in turn deformed to a great extent. Such a unique feature potentially enables viewers to cause distortion purposefully only on the head and neck by moving between y0° and y-60° as the deformation process is perceived as if deer shaking its head and neck side to side (Figure 6.22). Viewers' attention to this shaking will be further heightened if the dim light only illuminates the anterior and in turn send the posterior unseen. In this way, viewers can manipulate A1's shape, adding a meaningful motion to the image.

This way of interaction can also involve multiple images. In Convalanas, A3 and A5, both of which are drawn on an overall concave wall, are located as they face each other; A3 is on the right, while A5 on the left. Since A3 is located at the corner of the aisle, it first appears in front of a viewer who has travelled in the cave; there is no distortion on the image at the beginning of viewing. If the viewer watches A5 from the front of A3, the neck of A5 should appear raised upward. As the

Figure 6.22: Viewers can deliberately change the appearance of the head and neck of A1 by moving between y0° and y-60°. The deformation process is perceived as an animation as if deer shaking its head side to side.

viewer moves to the front of A5, the raised neck gradually sets downward. Similarly, when A3 is viewed from the front of A5, its neck and head should appear lifted, and as the viewer returns to the front of A3 again, these parts are stretched downward. Hence, a deliberate interaction is also possible even moving between two images.

Thus, the predominant use of overall concavity is also explained from the perspective of the deliberate distortion. Although the various merits of P1 topography have been considered, those merits do not necessarily contradict each other. The overall concave reduces distortion on the centre area when images are viewed from the front position, and the topography also increases images' noticeability. Moreover, the concave wall could be a vital medium for viewers to interact with images deliberately. The more advantages in a particular type of topography, the more chance of utilising it. Therefore, co-existing multiple benefits on different purposes might have led this topography to the most predominant type.

Data and possible interpretation

So far, we have confirmed two types of awareness; one which concerns the plurality of viewpoint, and another that denotes the perception of the deformed state of images. These two points are fundamental conditions for the discussion on whether or not deliberate distortion existed in Palaeolithic time. Subsequently, I argued two possible signs of the intended use of distortion. The intentionality might be reflected in the selection of specific topographic condition (allocating Extra levels to limbs and selecting overall concave surface) as these settings maximise the extent of distortion. Verifying whether or not these signs indicate the truth is impossible, given the nature of an open question. Even so, at least this study can suggest that the distortion was a crucial element in the examined three caves.

Of course, not all images are associated with distortion. Some images are located on a considerably flat surface and do not involve any salient deformations, or some might have been produced as a sculpture. In this case, probably images were depicted as merely visual information or related to other interactivity such as seeking images from the configuration of the surface (e.g. DA1). Otherwise, images are highly deformed. Their appearance is freely manipulated by viewers, and the process of deformation is indeed perceived as animation while viewers move from a viewpoint to another viewpoint. Given the rationales discussed, it seems safe to argue that some images, if not all, are highly interactive.

The arguments raised in this discussion enable us to interpret the data in a meaningful way. At the beginning of this section, I referred to a correspondence

between the predominantly distorted sections (head, neck, and limbs) and the most moving parts of real animals. Regarding this point, I also argued that this correspondence alone could not testify the artists' intentionality because it might have merely represented a unique nature of distortion; that is, the narrower outlined areas cause more noticeable distortion. However, the "awarenesses" and the rationales for the intentionality infer a meaningful link between those corresponding factors. Remember the hypothesis posed earlier: the examined viewing-action, namely, deliberately distorting images, could be a method to transform static animal figures into animated images as if real animals. Indeed, in some cases, deformation appears as if animals are shaking its head and neck. Similarly, the constantly-bending legs could be interpreted in relation to the animal's locomotion. Importantly, in the discussions by Watchel (1993) and Azema and Rivere (2012), animation in these body parts was also the reason why those authors interpreted cave art as cinema (see Figure 2.6b-c in Chapter 2). Essentially, the data is irrelevant to whether or not palaeo-viewers associated animation with the motion of real animals. However, if the notion of plural viewpoints and that of ideal-non-ideal proportion of images were widely shared as a norm of the cave-art tradition, and if the palaeo-artists deliberately selected a specific topography to add animation effects to the particular body sections (the head, neck, and limbs), the purpose of causing distortion can be attributed to a will to reconstruct the motion of real animals.

If we interpret the data in this way and admit intentional use of distortion, we can discuss the cause of distortion from the broader point of view. Placing images on a high position epitomises this alternative method; images are significantly deformed by being viewed from a lower side. For example, in El Pendo, Palaeo-viewers must have looked up all images from the bottom. Images on a high position are subjected to severe distortion regardless of their topographic condition, and that is applied for even images on a 2D surface (Figure 6.23: see 2d x-30° y70°). Above all, deformation in the neck and head is noticeable as these parts more likely appear stretched upward: for instance, the neck of N7 is considerably elongated, so its original shape is no longer identical when the image is viewed from the lower right (Figure 6.23: see 3d x-30° y70°). The appearance is also noticeably different from that seen from y70° of the same height on which the image is placed (Figure 6.23: see 3d x0° y70°). In addition to that effect, topographic intervention to N7 is also intensified by viewing from the bottom; the neck appears stretched further because the outline of the neck and the chest is pushed inward by the convex surface located under the neck. On the other hand, the image appears in an almost proper proportion, being viewed from the front (Figure 6.23: see x-30° y0°). Accordingly, viewers perceive the expansion and contraction of the neck as dynamic

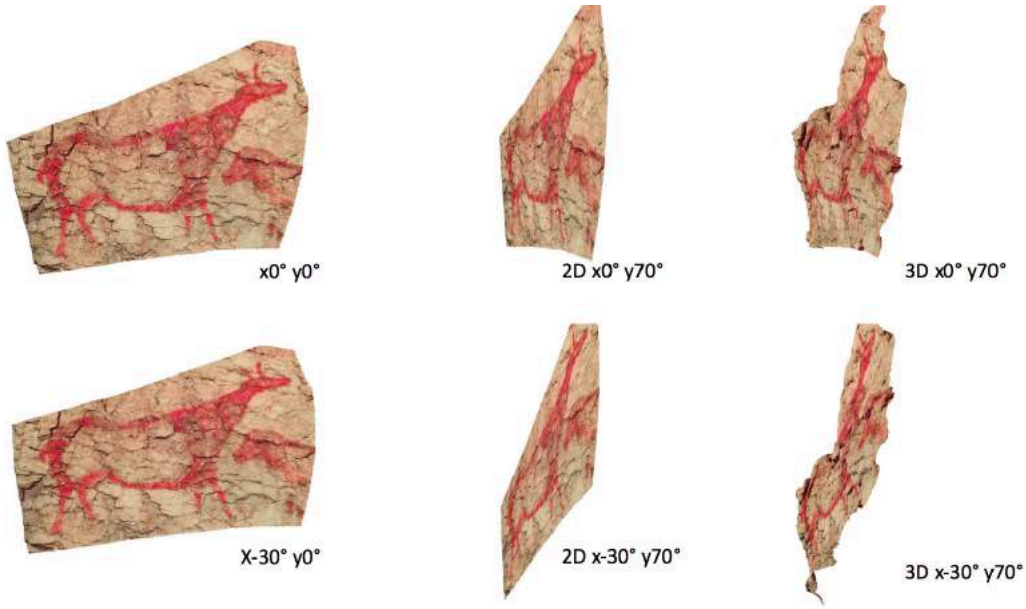

Figure 6.23: An example of distortion caused by placing an image on a high position (e.g. N7 in El Pendo). N7, even on a 2D surface, appears largely deformed when it is viewed from lower right (x-30°, y70°), and the extent is conspicuous compared to the same image seen from the same height. The neck appears to expand and contract in motion as viewers move between the front (y0°) and right (y70°), and viewers potentially can manipulate the shape of N7.

animation by moving between the front (y0°) and the right (y70°). As a result, they can manipulate the shape of N7. Thus, placing an image on a high location is an enhancer of distortion. Because of this principle, the overall composition of the panel in El Pendo constantly changes when viewers move. Other images on the frieze, apart from N7, therefore, always appear different as if the panel never hold a fixed viewpoint.

Thus, locating images at a high position can be associated with the deliberate use of deformation, and, in fact, this interpretation can also address another issue. Geneste (2004) mentions that in cave art images are frequently placed at high positions. This placing seems an enigma to the modern art theory where visual works are displayed at a height between a viewer's eyes and shoulder as the ideal position which allows viewers to keep their posture in a comfortable standing position and to concentrate on appreciating artworks (Meecham and Sheldon 2013). However, such a modern norm is not applicable to Palaeolithic parietal works, and therefore this issue has been puzzling archaeologists. The reason for the placing images on a high location or anywhere viewers must look up to capture images can be understood as a way to maximise the awareness towards the animation and cause interactivity once you accept the deliberate use of distortion. Of course, to fully address this issue from the perspective of this viewing interaction, we need more examples and consideration about the environmental context (e.g. whether or not viewers can move around in the location). However, at least the three caves studied in this thesis suggest a way to approach the issue.

Considering the discussion above, we have to admit that the interpretations above are suggestive of a possibility of viewing-interaction, not indicative of an absolute truth. We can never prove whether or not viewing-interaction existed in the way we have seen so far. However, simultaneously, this possibility cannot also be eliminated because of the nature of an open question; as was mentioned in Chapter 1, because no written document is available in prehistory, any examination on any issues cannot lead us to the absolute correct answer, but instead, we can propose at least a reliable possibility (Renfrew and Bahn 1991). It is only possible for us to infer meaningful information from the facts obtained and elucidate the possible figures of the past as logically as possible. Although there is such a limitation, the proposed interpretation accompanied with the above-logical arguments seems to secure its validity.

6.4 Cave art as installation art

Based on all arguments discussed in this chapter, it seems safe to claim that some of the art of Covalanas, El Pendo, and El Castillo functioned as installation art. Although the examined interactive medium is limited to the cave wall, we have learned how essentially the cave surface "affords" both image-making and image-viewing. In the first place, the reason why Palaeolithic humans entered into a cave is ultimately unknown (Pettitt 2016). In any case, palaeolithic humans repeatedly visited caves' deep interior and enculturated their activity, and practised the tradition of cave art. Considering the theory of cave-installation art as we saw in Chapter 2, this art tradition is inseparable from multisensory novelties of its environment, and the same is true for the three caves examined. Palaeo-artists, standing in a dark area of these caves and facing the wall, sought specific patterns and conditions to give birth to animal figures for a particular purpose. Subsequently, Palaeo-viewers, walking in a dark corridor of these caves while facing the images, might have caused animation by their own. Still, regardless of the phase of interaction, environmental components such as darkness, silence, the topography of floor etc. regularly "affords" bodily engagement and immersive experience.

Earlier, I hypothesised a purpose of artists of these caves as 'reconstructing real animals'. Once it is considered from a wider sensorial context, this hypothesis involves the overall sense of reality. We live in a multisensory world, and sense of reality is built by information collected by multiple senses (Levent and Pacual-Leone 2013). Therefore, caves' multisensory environment also continually provides a sense of reality (Sakamoto 2014). Considering such a commitment of our senses to the environment, the reconstruction of real animals might have denoted the reconstruction of an artificial

reality. In this way, an essential function of cave art can be argued from the perspective of installation art, and an old question - why caves were selected as a place for art? – is also provided with an explanation.

It is generally believed that cave art represents the cosmology of Upper Palaeolithic society as depicted images can be a record of the symbolic system (see Leroi-Gourhan 1968, Sauvet and Wlodarczyk 2008, Bahn 2016). Although selected motifs differ by the region in Franco-Cantabria (Sauvet and Wlodarczyk 2008), a particular narrative related to the depiction must have existed. Regarding El Pendo and Covalanas, deer is by far dominant motif, and therefore there might have been a cosmological narrative related to this particular species.

On the other hand, El Castillo, unlike these two caves, the variation of depicted motifs is noticeably wide, even including anthropomorphic images, and their chronology varies from Solutrian to pre-Magdalenian (Garcia-Diez et al. 2015). Given the difference in theme and chronological inconsistency in the set of dictions, it seems harder to assume about the narrative in El Castillo. However, once the 'narrative' is taken into consideration, we can deduce that cave art must have functioned as a place to experience the cosmological narrative. The crucial point is how the cosmology was experienced, and this cannot be separated from the nature of installation art.

As a method to experience cosmology, one of the most notable ways is shamanic trance. In shamanism, by entering a shamanic trance, the shaman's spirit is released from his body and travels the spiritual world of sky and underground (Eliade 1964). However, cave art is fundamentally different from such an inner journey of a shaman due to the actuality of caves. The cosmological narrative of Upper Palaeolithic cave art has tangible space which literally stimulates human's multiple senses in an unusual way. Therefore, even though such an inner trip of a shaman evokes vivid, dynamic experience, it is fundamentally different from actual multisensory interaction between humans and cave art. Caves can be external cosmological space, unlike that in one's mind. Therefore, although in shamanism the experience of cosmological travel is limited to shamans, in the case of cave art is potentially open to anyone who enters into caves. It is likely that only a handful of people were permitted to enter caves, especially, narrow caves such as Covalanas, but what I stress is the actuality of the space which provides anyone with a potential cosmological experience.

Cave art might have been a narrative space which sees its completion when participants were installed into the cosmology. Another way, one's own body and senses enter into a scene of the ancient narrative and experience the cosmological journey during which one can manipulate and interfere with the cosmological space with a firm sense of reality. Accordingly, if animal figures appear in motion when viewers move, such space also achieves further reality as if the static images actually

exist alive in a part of the real world. To experience the cosmology, humans in Palaeolithic time must have selected caves' environment because its spatial features concern aspects of both the art and the humans. For the externalised cosmological space to be another world to the real world, multisensorial novelties of caves' environment must have been necessary. As mentioned above, Watchel (1993) and Azema and Rivere (2012) interpret cave art as cinematic. They reached this view through observing limited elements of cave art (for example, Watchel refers to lighting condition, and Azema and Rivere studied superimposed images). However, their interpretation remains insufficient unless whole factors related to the environmental components are taken into account. Given multisensorial aspects of caves and its interactive nature, cave art is not cinematic, but rather involving full body experience. In this sense, cave art is interactive installation art as decorated caves and its environmental elements surround participants and allow them to communicate with space.

In the >40,000 years of Upper Palaeolithic cave art culture, it can be the case that palaeolithic humans gradually associated art and cosmology with a cave, exploring the space, interacting with the environment and expanding their perception for affordance. In consequence, exploiting the novel properties and transforming cave into a space for art, Palaeolithic humans produced external cosmological space. The case studies of Covalanas, El Pendo, and El Castillo, suggests such trace of enculturation, and attest the nature of cave-installation art.

Conclusion

Beginning with the notion of 'cave art as an installation art', I have explored in this thesis the interactive nature of cave art. As described in Chapter 2, the idea of cave-installation art originated in the theory of installation art and affordance. These theories emphasise the significance of the cave's environment in the creative process as a mediator of human action. Such a perspective allows us to draw a meaningful link between the novel properties of the cave's environment and the characteristics of the Palaeolithic process of art creation and viewing. In caves, humans are constantly stimulated with multisensorial elements and come under strong psychological encouragement to interact with the environment. As a result, they become embodied in cave art, and viewers, therefore, stop being simply a passive receiver of visual information and transform into active participants. Such viewers' active participation is the core of the theory of cave-installation art. Thus, the approach combining both the notion of installation art and affordance theory introduces a new perspective to some 150 years of research into Palaeolithic art. More importantly, the approaches to cave-installation art can elucidate at least part of the reasons why humans left visual works in such enigmatic spaces; the deep interior of caves. If we ignore these environmental factors we will never be able to address that most basic enigma regarding cave art, that it is by its very nature a clear and visible form of communication, but that it is so difficult for archaeologists in the present world to understand it. Here lies the essential benefit of the cave-installation approach.

Based on this theoretical framework, and through focusing on the action-reaction relationship between humans and their environmental context, I examined formally three types of interaction: the integration of natural lines into images; the background topographic conditions of these images; and manner and effects of distortion on them. These interactivities yield concrete information about how humans in Palaeolithic time communicated with their artistic medium (the cave wall) during image-making, and how the images they depicted encouraged viewers towards further interaction as an image-viewing activity. In this thesis, it has been suggested that these interactions, mediated by the cave wall, seem to have been prioritised more than interactivities of any other kind (e.g. the use of light and auditory conditions). They seem to have acted as an essential. Each of the elements examined is intrinsically unique, so that previous research has highlighted them as a remarkable feature of Palaeolithic cave art, albeit in undefined and formally undemonstrated ways. Additionally, studying them is relatively straightforward because of the recordable nature of visual information, compared to interactions mediated by other environmental constraints. Exploring these aspects, therefore, was a fundamental and vitally important way of

providing the theory of 'cave art as an installation art' with an empirical foundation. By undertaking this, the research lead to the further development of the theory, the purpose of this thesis.

In the three case studies (Covalanas, El Pendo, and El Castillo cave), I analysed a total of 54 animal images. The photographic data for 3D documentation were collected for each image through first-hand recording in the caves concerned. The resulting 3D models were digitally investigated according to specific criteria in terms of interaction categories. Although each of these caves is of course topographically and socio-culturally unique, the results obtained demonstrate a significant degree of consistency between them in most aspects. This consistency suggests that specific regulations regarding both production and post-production phases of cave art were in existence here, reflecting shared notions between humans in Upper Palaeolithic and therefore in terms of their intentionality. The use of cave wall for image-making was, therefore, not randomly practiced; instead, artists' must, at least to a degree, have followed a rule aimed at the optimisation of production/effect of art. Additionally, the selection of particular topography could well denote artists' expectation about how images were to be viewed. I summarise here the main discoveries of the thesis.

- Integration must have been one of the essential methods for the production of cave art in the three caves, as approaching 75% of the examined images demonstrate it. The more noticeable and obvious natural lines the cave wall contains, the more likely it is that integration occurred.

- Natural lines were most likely used to outline the dorsal and ventral sections of animal images, and it is most likely that the two co-occur. Integration of the head and buttock are the next likely elements to be integrated, and in almost all cases, integration of the head and buttock is accompanied by that of the dorsal and/or ventral line. This observation is consistent among the three caves studied. The consistency may well suggest that a fundamental rule was determining this particular artistic method. Since the dorsal and ventral areas comprise the essential axis and most substantial proportion of the quadrupeds depicted, the artists could draft the overall size and shape of images through the integration of natural lines into these body parts. by contrast, integration of the head and buttock may have been a practical means to provide the axis of the depiction with an additional edge. Finding a location with such natural lines, therefore, determined the overall dimension of the images in advance of their production; by so doing, the artists may have been able to reduce the chance of failure of image-making.

- Even though integration is a common phenomenon in the three caves studied, differences in the physical medium (the cave wall) stimulated different behaviours in the artists. El Pendo represents an 'environmental-based' case because the artists of this cave seem to have relied more on the cave's natural lines than their own imagination. This was presumably dictated by the abundance of natural lines in the cave. By contrast, Covalanas is 'human-based' as integration mainly occurred only in an essential manner (integration of the images' axial elements); here, the limited number of natural lines in the cave forced (or freed up) the use of the artist's imagination. El Castillo is a more complicated case. The way of integration is not coherent here; unlike the other two caves lone integration also often took place with an edge (head or buttock). This is because of the variety of condition of the cave's walls. These three contrasting results highlight above all the significance of the physical environment (i.e. the medium's pre-existing condition) to image-making. The production of cave art is, therefore, not only determined by aspect human-focused 'artistic' aspect.

- In the three case studies, there is no universal trend in the way that specific types of natural lines (e.g. grooves, edges, and ridges) were used. Palaeo-artists may have integrated any type of lines.

- A clear trend is detected in the relation between topographic condition and body parts. The elevation level for the head and thigh tend to be higher than that for the neck-shoulder and middle section. Meanwhile, legs are most likely allocated to the wall of extra elevations levels (Extra high and Extra low). This is unlikely to be coincidental.

- There are, in total, six types of basic topography (overall concave, overall slope, overall convex, zigzag, partial concave, and partial slope). The most common of these is overall concave, followed by partial concave. While concavities are the most commonly integrated shape of the walls, convexities are not preferred. This result is also universally seen among the three caves. This generalised topographic pattern also demonstrates the predominant use overall of concave surfaces.

- In terms of the possible benefits to using overall concave media, three possibilities are considered. The first is to maximise the noticeability of images

in a dark space, as one of the images' elevated edges will constantly face viewers standing to one side. The second merit is to offer an optimum viewing experience to viewers standing directly in front of the image, by mitigating distortion. Finally, the overall concave pattern causes multiple distortions to images, which enhances viewers' participation in the post-production phase. These three benefits are compatible with each other, and this compatibility may be responsible for the predominant use of overall concave backgrounds.

- The reason for intensive use of extra elevation levels for the legs is understandable once one admits the deliberate use of distortion in order to affect viewing-interaction. Otherwise, the result might only represent a 'lower priority' of legs' among artists.

- Topography was also utilised in order to add 3D volume to images. Noticeable convex surfaces were occasionally used for the shoulder and thigh. In such cases, the artists may have aimed to express the volume of the muscles. Such figures achieve better realism and appear more 'sculptural' than 2D images.

- Given these observations on integration and topographic condition, is is clear that the location of images was not determined randomly. As some locations were ideal with regard to both integration and topography, the artists may have actively sought such ideal surfaces in order to depict images. Accordingly, the specific placing of images may have been determined by the topographic condition and availability of natural lines for integration. Selected locations, therefore, may have been special and achieved a specific meaning.

- Remarkable distortions were confirmed in more than half of the examined images. The frequency was exceptionally high in El Pendo and Covalanas, where entire images were located on a single panel or panels in an adjacent area. However, we cannot claim that all images are interactive, because images without any detectable distortion were also found. In such cases, images appear only as visual information, or they were depicted for an unknown purpose.

- Deformation processes appear to have been used as a form of animation by viewers. The dark interior of caves is one of the ideal locations for experiencing motion, due to the human cognitive capacity. This animation was presumably deliberately and conspicuously perceived.

- The most frequently deformed body parts are the head, neck, and limbs; whereas the shoulder, mid-torso, thigh are mostly static. Sections where distortion occurs, however, differ slightly according to the anatomical characteristics of the depicted motifs. Motifs with the distinguishable neck (e.g. hind and caprid) are more likely deformed at their neck than those without a clear distinction between head and neck (e.g. bison). Given this, the narrower the outlined part of the image is, the more distortion is noticeable.

- Considering the prevailing examples of anamorphosis in cave art, and examples detected in samples from Covalanas and El Castillo where natural lines were integrated in an unusual fashion, both Palaeolithic artists and viewers in must have shared the notion of the plurality of viewpoints. Accordingly, they must have been aware whether or not images were in proper proportion of not.

- Certain topographic conditions (limbs on Extra elevation levels and the predominant use of overall concavity) may attest the deliberate use of distortion. Those conditions are most likely to cause noticeable and dynamic distortion on the head, neck and limbs. In particular, viewers can animate images on the overall concave surface as if animals were shaking their head and neck. These facts reinforce the notion of intentional interaction with images in the post-production phase.

- Locating images in high places also causes a dynamic distortion. Attributing such a method of deliberate placement so as to cause deliberate distortion explains one reason why many cave art images are sometimes found in otherwise unnecessarily high positions.

- The body parts which are most frequently deformed (head, neck, and limbs) correspond to the sections of real animals that are most often in motion. Based on this fact and other points regarding the distortion of these images, at least among the three studied caves, we may hypothesise that Palaeolithic artists deliberately embedded distortions into images, so that when viewers moved around these, static images could be transformed into moving figures as if they were alive. If such animal depictions represent a cosmological narrative of Upper Palaeolithic society, cave art could be interpreted as an externalised interactive device where anyone can experience the cosmology in a multisensorial way by being installed into the narrative.

The conclusions summarised above elucidate the specific nature of artistic interactions mediated by the cave wall. Although the interactions I have examined are only concerned with the condition of the physical medium, the observations presented here allow us to establish a firm foundation for the theory of 'cave art as installation art'. This argument requires us to reconsider our notion of what cave art was, and how it functioned. Cave-installation art defines that the cave environment was itself an artistic device, and the results of this study now provide a concrete set of examples of the interactions that were a fundamental element of image-making. They demonstrate that the medium was not used randomly and passively, and suggest instead the existence of a well-established non-random and active methodology for creating 'art'. This certainly adds to the impression as to how much thought and labour went into optimising the production process of animal figures; image-making must have been preceded by the careful observation and selection of specific parts of the cave wall. Those complete animal figures were also used for further interaction – this possibility was also reinforced based on from the observations of the case studies. Accordingly, the theory of cave –installation art also demonstrates examples of interactivity in the post-production (i.e. viewing) phase. The results listed above should form part of the criteria that future study of cave art could address.

Needless to say, there are many elements of the cave art repertoire that remain to be studied. in order to enrich this theory with further objective details, we must also look into the relationship between humans and other multisensory properties; the effect of light on interaction, for example, and its impact on both image-making and image-viewing. Methodologies to approach these points and criteria for their assessment will also need to be established only by developing methodologies to apply in the field can one hope to add empirical evidence to the theory. By so doing, these will lead us to a more comprehensive understanding of the interactive, multisensorial, and site-specific nature of cave-installation art. Obviously one cannot generalize from the three case-studies here that these are universal phenomena. How chronologically and geographically variable are they, for example? After everything, I have to admit that there is still a very long way to go. I hope, though, that this study has taken a crucial first step to understanding the interactive nature of cave art.

Appendix

List of Data Tables (Covalanas):

	H	D	Ta	B	L	V
A1	0	0	0	0	0	1(D, F)
A2	0	0	0	0	0	0
A3	0	1(D, F)	0	0	0	0
A5	0	1(D, P)	0	0	0	0
A6	0	0	0	0	0	0
A7	0	0	0	0	0	0
A8	0	0	0	1(D, P)	0	1(D, F)
A9	0	0	0	0	0	1(D, P)
A10	0	0	0	0	0	0
A11	0	0	0	0	0	0
A13	0	0	0	0	0	0
A14	0	1(D, F)	0	0	0	0
B1	1(O, P)	1(D, F)	0	1(D, F)	0	0
B4	0	1(O, P)	0	0	0	1(O, P)
B5	0	1(D, F)	0	0	0	0
C1	0	1(O, F)	0	0	0	1(D, F)
C2	0	1(O, P)	0	1(D, F)	0	0
D1	0	0	0	0	0	0

Table 1: Integration and location by image. '0' refers to absence of integration, while '1' means presence. D: Direct integration, O: Offset integration, F: full integration, P: Partial integration. (H: Head, D: Dorsal, Ta: Tail, B: Buttock, L: Limbs, and V: Ventral).

	Images
Inte 0	7
Inte 1	6
Inte 2	4
Inte 3	1

Table 2: The number of images by frequency of integration. This table was used to generate Figure 3.88.

	Integration	Direct	Offset	Full	Partial
H	1	0	1	0	1
D	8	5	3	5	3
Ta	0	0	0	0	0
B	3	3	0	2	1
L	0	0	0	0	0
V	5	4	1	3	2

Table 3: The number of integrations by body part and type of integration. This table was used to generate Figure 3.88.

	H	D	Ta	B	L	V
H		1	0	1	0	0
D	1			2		2
Ta	0	0		0	0	0
B	1	2				1
L	0	0	0	0		0
V	0	2	0	1	0	

Table 4: Combinations of body sections among images with multiple integrations. This table was used to generate Figure 3.90.

	H	DNs	CNs	VNs	DM	CM	VM	DT	CT	VT	FL	HL	Ta
A1	5	3	3	3	2	2	2	5	5	5	0	0	0
A2	3	3	3	3	2	2	2	3	3	3	0	0	0
A3	5	3	3	3	2	2	2	4	3	3	1	3	0
A5	4	3	2	2	3	3	2	3	3	4	2	5	0
A6	4	3	3	0	2	2	0	2	2	0	0	0	0
A7	2	3	0	0	4	0	0	2	0	0	0	0	0
A8	3	3	4	4	2	2	2	3	3	3	0	2	0
A9	5	4	4	3	2	2	2	3	2	2	4	3	0
A10	4	2	2	0	3	2	0	4	4	0	0	0	0
A11	2	3	3	3	4	4	4	2	3	3	0	4	2
A13	3	2	0	0	3	0	0	4	0	0	0	0	0
A14	2	3	0	0	2	0	0	4	0	0	0	0	0
B1	2	4	3	3	3	4	4	4	4	4	2	5	0
B4	4	3	3	4	2	3	4	2	2	3	5	4	0
B5	5	4	3	4	3	3	3	2	2	3	1	2	0
C1	2	2	3	3	2	2	3	2	3	4	0	5	0
C2	3	3	3	3	3	3	3	5	4	4	0	2	0
D1	4	2	2	2	3	3	3	4	5	4	3	0	0

Table 5: Topographic condition of each image by body section (H: Head, Ns: Neck-shoulder, M: Mid torso, T: Thigh, L: Limbs, Ta: Tail.) Ns, M and T contains further divisions (D: Dorsal, C: Centre, V: Ventral). Legs are also divided into two parts (F: Front, H: Hind). Elevation levels are presented in a numeric value (Extra High: 5, High: 4, Medium: 3, Low: 2, Extra low: 1, N/A: 0).

	H	Ns	M	T	FL	HL	Ta
A1	5	3	2	5	0	0	0
A2	3	3	2	3	0	0	0
A3	5	3	2	3.3	1	3	0
A5	4	2.3	2.7	3.3	2	5	0
A6	4	3	2	2	0	0	0
A7	2	3	4	2	0	0	0
A8	3	3.7	2	3	0	2	0
A9	5	3.7	1.7	2.3	4	3	0
A10	4	2	2.5	4	0	0	0
A11	2	3	4	2.7	0	4	2
A13	3	2	3	4	0	0	0
A14	2	3	2	4	0	0	0
B1	2	3.3	3.7	4	2	5	0
B4	4	3.3	3	2.3	5	4	0
B5	5	3.7	3	2.3	1	2	0
C1	2	2.7	2.3	3	0	5	0
C2	3	3	3	4.7	0	2	0
D1	4	2	3	4.7	3	0	0

	H	Ns	M	T	FL	HL	Ta
A1	5	3	2	5	0	0	0
A2	3	3	2	3	0	0	0
A3	5	3	2	3	1	3	0
A5	4	2	3	3	2	4	0
A6	4	3	2	2	0	0	0
A7	2	3	4	2	0	0	0
A8	3	4	2	3	0	2	0
A9	5	4	2	2	4	3	0
A10	4	2	2	4	0	0	0
A11	2	3	4	3	0	4	2
A13	3	2	3	4	0	0	0
A14	2	3	2	4	0	0	0
B1	2	3	4	4	2	5	0
B4	4	3	3	2	5	4	0
B5	5	4	3	2	1	2	0
C1	2	3	2	3	0	5	0
C2	3	3	3	5	0	2	0
D1	4	2	3	5	3	0	0

Table 6 (left) and Table 7 (right): These are simplified version of Table 5 as divisions in Ns, M, T are united. Values for these united sections represent an average value (Table 6), but values with decimals are rounded in Table 7. Table 6 was used to generate Figure 3.95.

	EHigh	High	Med	Low	ELow
H	4	5	4	5	0
DNs	0	3	11	4	0
CNs	0	2	10	3	0
VNs	0	3	8	2	0
DM	0	2	7	9	0
CM	0	2	5	8	0
VM	0	3	4	5	1
DT	2	6	4	6	0
CT	2	3	6	4	0
VT	1	5	6	1	0
FL	1	1	1	2	2
HL	2	3	2	3	0
Ta	0	0	0	1	0

	EHigh	High	Med	Low	ELow
H	4	5	4	5	0
Ns	0	3	11	4	0
M	0	3	6	9	0
T	3	4	6	5	0
FL	1	1	1	2	2
HL	2	3	2	3	0
Ta	0	0	0	1	0

Table 8 (left) and Table 9 (right): These two tables represent the frequency of elevation levels by body section. Table 8 are obtained based on Table 5, while Table 9 are obtained based on Table 7. Table 8 was used to generate Figure 3.91, and Table 9 was used to generate Figure 3.93.

	Elevation Points
H	62
Ns	53
M	48
T	59
FL	18
HL	34
Ta	2

Table 10: Sum of elevation points by body section. Higher number directly reflects a higher elevation. Points were calculated based Table 9. Table 10 was used to generate Figure 3.94.

	H	Ns	M	T	L	Ta
A1	1	1	0	1	0	0
A2	0	0	0	0	0	0
A3	1	1	1	1	0	0
A5	1	1	0	1	1	0
A6	0	1	0	0	0	0
A7	0	0	0	0	0	0
A8	0	0	1	1	1	0
A9	1	1	1	1	1	0
A10	0	1	0	0	0	0
A11	1	1	0	1	1	0
A13	1	0	0	0	0	0
A14	0	0	0	0	0	0
B1	0	0	0	0	1	0
B4	1	1	0	0	0	0
B5	1	1	1	0	1	0
C1	1	1	0	0	0	0
C2	0	0	0	1	1	0
D1	1	1	0	1	0	0

Table 11: Presence\absence of distortion and its location by image. '0' refers to absence, while '1' means presence. (H: Head, D: Dorsal, Ta: Tail, B: Buttock, L: Limbs, and V: Ventral).

	Images
Dis 0	3
Dis 1	3
Dis 2	3
Dis 3	5
Dis 4	3
Dis 5	1

	Distortion
H	10
Ns	11
M	5
T	8
L	7
Ta	0

Table 12 (left): The number of images by frequency of distortion. This table was used to generate Figure 3.96.

Table 13 (right): The number of distortion by body part. This table was used to generate Figure 3.97.

List of Data Tables (El Pendo):

	H	D	Ta	B	L	V
N1	0	1(O, F)	0	0	0	1(D, P)
N2	0	1(D, F)	0	1(D, F)	0	1(D, F)
N4	1(D, P)	1(D, F)	0	0	1(D, P)	1(D, F)
N5	0	1(D, O, F)	1(D, O, F)	1(D, P)	0	1(O, F)
N7	0	1(D, F)	0	1(D, F)	0	1(D, F)
N8	1(D, P)	1(D, F)	0	0	0	1(D, F)
N12	0	1(D, P)	0	0	0	0
N13	1(D, F)	1(D, P)	0	0	0	1(D, P)
N14	0	1(D, P)	0	1(D, F)	1(D, F)	1(D, F)
N16	1(D, P)	1(D, P)	0	1(D, F)	0	1(D, F)
N17	0	0	0	0	0	0

Table 14: Integration and location by image. '0' refers to absence of integration, while '1' means presence. D: Direct integration, O: Offset integration, F: full integration, P:partial integration. (H: Head, D: Dorsal, Ta: Tail, B: Buttock, L: Limbs, and V: Ventral).

	Images
Inte 0	1
Inte 1	1
Inte 2	1
Inte 3	4
Inte 4	4

Table 15: The number of images by frequency of integration. This table was used to generate Figure 4.65.

	Integration	D	O	F	P
H	4	4	0	1	3
D	10	9	2	7	3
Ta	1	1	1	1	0
B	5	5	0	4	1
L	2	2	0	1	1
V	8	8	1	7	2

Table 16: The number of integrations by body part and type of integration. This table was used to generate Figure 4.64.

	H	D	Ta	B	L	V
H		4	0	1	1	4
D	4		1	5	2	9
Ta	0	1		1	0	1
B	1	5	1		1	5
L	1	2	0	1		2
V	4	9	1	5	2	

Table 17: Combinations of body sections among images with multiple integrations. This table was used to generate Figure 466.

	H	DNs	CNs	VNs	DM	CM	VM	DT	CT	VT	FL	HL	Ta
N1	4	4	4	3	4	4	3	3	3	3	0	2	0
N2	4	3	3	4	2	2	2	3	3	3	3	3	0
N4	2	3	3	3	2	3	4	2	3	2	3	1	0
N5	2	3	4	4	2	3	2	2	3	3	3	2	2
N7	4	3	3	3	2	3	3	4	4	3	2	2	3
N8	4	4	4	3	2	3	3	0	0	0	5	0	0
N12	0	3	3	4	2	2	0	3	0	0	0	0	0
N13	3	3	0	0	2	0	0	4	0	0	0	0	0
N14	0	3	3	2	3	2	4	3	3	4	2	5	0
N16	4	2	2	2	3	3	2	3	4	5	2	5	0
N17	4	3	2	2	3	3	3	4	4	4	1	4	0

Table 18: Topographic condition of each image by body section (H: Head, Ns: Neck-shoulder, M: Mid torso, T: Thigh, L: Limbs, Ta: Tail.) Ns, M and T contains further divisions (D: Dorsal, C: Centre, V: Ventral). Legs are also divided into two parts (F: Front, H: Hind). Elevation levels are presented in numeric value (Extra High: 5, High: 4, Medium: 3, Low: 2, Extra low: 1, N/A: 0).

	H	Ns	M	T	FL	HL	Ta
N1	4	3.7	3.7	3	0	2	0
N2	4	3.3	2	3	3	3	0
N4	2	3	3	2.3	3	1	0
N5	2	3.7	2.3	2.7	3	2	2
N7	4	3	2.7	3.7	2	2	3
N8	4	3.7	2.7	0	5	0	0
N12	0	3.3	2	3	0	0	0
N13	3	3	2	4	0	0	0
N14	0	2.7	3	3.3	2	5	0
N16	4	2	2.7	4	2	5	0
N17	4	2.3	3	4	1	4	0

	H	Ns	M	T	FL	HL	Ta
N1	4	4	4	3	0	2	0
N2	4	3	2	3	3	3	0
N4	2	3	3	2	3	1	0
N5	2	4	2	3	2	2	2
N7	4	3	3	4	2	2	3
N8	4	4	3	0	5	0	0
N12	0	3	2	3	0	0	0
N13	3	3	2	4	0	0	0
N14	0	3	3	3	2	5	0
N16	4	2	3	4	2	5	0
N17	4	2	3	4	1	4	0

Table 19 (left) and Table 20 (right): These are simplified version of Table 18 as divisions in Ns, M, T are united. Values for these united sections represent an average value (Table 19), but values with decimals are rounded in Table 20. Table 19 was used to generate Figure 4.73.

	EHigh	High	Med	Low	ELow
H	0	6	1	2	0
DNs	0	2	7	1	0
CNs	0	3	5	2	0
VNs	0	3	4	3	0
DM	0	1	3	7	0
CM	0	1	6	3	0
VM	0	2	4	3	0
DT	0	3	5	2	0
CT	0	3	5	0	0
VT	1	2	3	1	0
FL	1	0	3	3	1
HL	2	1	1	3	1
Ta	0	0	1	1	0

	EHigh	High	Med	Low	ELow
H	0	6	1	2	0
Ns	0	3	7	1	0
M	0	1	6	4	0
T	0	4	5	1	0
FL	1	0	3	3	1
HL	2	1	1	3	1
Ta	0	0	1	1	0

Table 21 (left) and Table 22 (right): These two tables represent the frequency of elevation levels by body section. Table 21 are obtained based on Table 18, while Table 22 are obtained based on Table 20. Table 21 was used for Figure 4.68, and Table 22 was used to generate Figure 4.69.

	Elevation Points
H	31
Ns	35
M	30
T	33
FL	21
HL	24
Ta	5

Table 23: Sum of elevation points by body section. Higher number directly reflects a higher elevation. Points were calculated based Table 22. Table 23 was used to generate Figure 4.70.

	EHigh	High	Medium	Low	ELow	Elevation Points
H	0	5	1	2	0	27
Ns	0	2	4	2	0	24
M	0	1	4	3	0	22
T	0	4	3	1	0	27
FL	0	0	3	2	1	14
HL	1	1	1	3	1	19
Ta	0	0	1	1	0	5

Table 24: The frequency of elevation levels (left) and the sum of elevation points by body section (right). This table is generated based on 8 images which contain all of H, Ns, M and T. This table was used to generate Figure 4.71 and Figure 4.72.

	H	Ns	M	T	L	Ta
N1	0	1	0	0	0	0
N2	1	1	0	0	0	0
N4	1	1	0	0	1	0
N5	1	1	0	0	1	0
N7	0	1	0	0	1	0
N8	1	1	1	0	1	0
N12	0	1	0	0	0	0
N13	0	0	0	1	0	0
N14	0	1	1	1	1	0
N16	1	1	0	1	1	0
N17	1	1	1	1	1	0

Table 25: Presence\absence of distortion and its location by image. '0' refers to absence, while '1' means presence. (H: Head, Ns: Neck-shoulder, M: Mid Torso, T: Thigh, L: limbs, Ta: Tail).

	Images			Distortion
Dis 0	0		**H**	6
Dis 1	3		**Ns**	10
Dis 2	2		**M**	3
Dis 3	2		**T**	4
Dis 4	3		**L**	7
Dis 5	1		**Ta**	0

Table 26 (left): The number of images by frequency of distortion. This table was used to generate Figure 4.74.

Table 27 (right): The number of distortion by body part. This table was used to generate Figure 4.75.

List of Data Tables (El Castillo):

	H	D	Ta	B	L	V
PB1	0	1(D, F)	1(D, P)	1(D, P)	0	0
PB2	1(D, F)	1(D, F)	0	0	0	1(D, P)
PB3	0	1(O, F)	0	0	0	0
PB4	1(D, P)	1(D, F)	0	1(D, P)	1(D, F)	1(D, P)
PD1	0	0	0	0	0	0
PD2	0	0	0	1(D, P)	0	0
PB5	0	1(D, F)	0	0	0	1(D, F)
PD3	0	0	0	0	0	0
PU1	0	0	0	0	0	0
PH1	1(D, P)	0	0	0	0	0
PH2	0	0	0	0	0	0
CB1	0	0	1(D, P)	1(D, F)	0	0
CB2	0	1(D, F)	0	0	0	0
CB3	0	1(D, P)	1(D, P)	0	0	0
CB4	0	0	0	0	0	0
CB5	0	0	0	0	0	0
EH1	1(D, P)	1(D, P)	0	1(D, P)	0	1(D, P)
EH2	0	0	0	0	0	1(D, P)
ED1	1(D, P)	0	0	0	0	0
BMB1	1(D, F)	1(D, F)	1(D, F)	1(D, F)	1(D, F)	1(D, F)
BU1	0	0	0	1(O, F)	1(O, F)	1(D, F)
BB1	0	1(D, F)	0	0	1(D, F)	1(D, F)
BB2	1(D, P)	1(D, F)	0	0	0	0
GM1	0	0	0	0	0	0
DA1	1(D, P)	1(O, P)	0	0	0	1(D, F)

Table 28: Integration and location by image. '0' refers to absence of integration, while '1' means presence. D: Direct integration, O: Offset integration, F: full integration, P: Partial integration .(H: Head, D: Dorsal, Ta: Tail, B: Buttock, L: Limbs, and V: Ventral).

	Images
Inte 0	7
Inte 1	6
Inte 2	4
Inte 3	5
Inte 4	1
Inte 5-6	2

	Integration	D	O	F	P
H	8	8		6	2
D	12	10	2	9	3
Ta	4	4		1	3
B	7	6	1	3	4
L	4	3	1	4	0
V	9	9	0	5	4

Table 29 (left) and Table 30(right): The number of images by frequency of integration (Table 29), and The number of integrations by body part (Table 30). These tables were used to generate Figure 5.110 and Figure 5.111.

	H	D	Ta	B	L	V
H		6	1	3	2	5
D	6		3	4	3	7
Ta	1	3		3	1	1
B	3	4	3		3	4
L	2	3	1	3		4
V	5	7	1	4	4	

Table 31: Combinations of body sections among images with multiple integrations. This table was used to generate Figure 5.112.

	H	DNs	CNs	VNs	DM	CM	VM	DT	CT	VT	FL	HL	Ta
PB1	2	2	2	2	2	2	2	3	3	3	4	4	2
PB2	2	2	3	2	3	3	2	3	2	4	2	1	0
PB3	3	2	3	4	3	2	2	2	3	3	3	4	3
PB4	3	2	2	2	2	2	2	3	4	4	3	5	0
PD1	3	3	4	4	2	2	2	3	2	2	3	4	0
PD2	4	3	3	2	4	4	4	4	4	4	2	0	0
PB5	2	4	3	3	4	2	3	0	0	0	0	0	0
PD3	2	2	0	0	2	0	0	4	3	0	0	0	0
PU1	0	0	0	0	0	0	0	0	0	0	0	0	0
PH1	0	0	0	0	0	0	0	0	0	0	0	0	0
PH2	4	3	2	2	3	3	3	3	3	3	1	3	4
CB1	4	3	2	3	3	2	3	4	3	3	5	4	4
CB2	3	3	4	0	3	3	0	2	0	0	0	0	0
CB3	2	2	2	3	2	3	3	3	3	3	4	3	4
CB4	4	3	2	3	2	2	3	3	3	4	3	4	4
CB5	3	2	3	3	3	4	3	4	4	3	3	3	4
EH1	3	3	2	2	3	2	2	3	4	3	2	4	3
EH2	4	3	4	4	2	3	4	0	0	0	0	0	0
ED1	2	4	4	3	2	0	0	0	0	0	0	0	0
BMB1	2	3	3	2	3	4	3	3	4	3	0	2	2
BU1	0	3	3	2	2	3	4	5	5	5	0	5	5
BB1	4	2	2	2	2	2	2	3	3	4	2	5	4
BB2	2	3	3	3	4	4	3	2	2	2	0	2	0
GM1	3	3	3	2	3	3	3	4	4	2	1	1	0
DA1	2	2	2	3	3	3	3	4	3	4	3	5	4

Table 32: Topographic condition of each image by body section (H: Head, Ns: Neck-shoulder, M: Mid torso, T: Thigh, L: Limbs, Ta: Tail.) Ns, M and T contains further divisions (D: Dorsal, C: Centre, V: Ventral). Legs are also divided into two parts (F: Front, H: Hind). Elevation levels are presented in numeric value (Extra High: 5, High: 4, Medium: 3, Low: 2, Extra low: 1, N/A: 0).

	H	Ns	M	T	FL	HL	Ta
PB1	2	2	2	3	4	4	2
PB2	2	2.3	2.7	3	2	1	0
PB3	3	3	2.3	2.7	3	4	3
PB4	3	2	2	3.7	3	5	0
PD1	3	3.7	2	2.3	3	4	0
PD2	4	2.7	4	4	2	0	0
PB5	2	3.3	3	0	0	0	0
PD3	2	2	2	4	0	0	0
PU1	0	0	0	0	0	0	0
PH1	0	0	0	0	0	0	0
PH2	4	2.3	3.3	3.3	1	3	4
CB1	4	2.7	2.7	3.3	5	4	4
CB2	3	3.5	3	2	0	0	0
CB3	2	2.3	2.7	3	4	3	4
CB4	4	2.7	2.3	3.3	3	4	4
CB5	3	2.7	3.3	3.7	3	3	4
EH1	3	2.3	2.3	3.3	2	4	3
EH2	4	3.7	3	0	0	0	0
ED1	2	3.7	2	0	0	0	0
BMB1	2	2.7	3.3	3.3	0	2	2
BU1	0	2.7	3	5	0	5	5
BB1	4	2	2	3.3	2	5	4
BB2	2	3	3.7	2	0	2	0
GM1	3	2.7	3	3.3	1	1	0
DA1	2	2.3	3	3.7	3	5	4

	H	Ns	M	T	FL	HL	Ta
PB1	2	2	2	3	4	4	2
PB2	2	2	3	3	2	1	0
PB3	3	3	2	3	3	4	3
PB4	3	2	2	4	3	5	0
PD1	3	4	2	2	3	4	0
PD2	4	3	4	4	2	0	0
PB5	2	3	3	0	0	0	0
PD3	2	2	2	4	0	0	0
PU1	0	0	0	0	0	0	0
PH1	0	0	0	0	0	0	0
PH2	4	2	3	3	1	3	4
CB1	4	3	3	3	5	4	4
CB2	3	4	3	2	0	0	0
CB3	2	2	3	3	4	3	4
CB4	4	3	2	3	3	4	4
CB5	3	3	3	4	3	3	4
EH1	3	2	2	3	2	4	3
EH2	4	4	3	0	0	0	0
ED1	2	4	2	0	0	0	0
BMB1	2	3	3	3	0	2	2
BU1	0	3	3	5	0	5	5
BB1	4	2	2	3	2	5	4
BB2	2	3	4	2	0	2	0
GM1	3	3	3	3	1	1	0
DA1	2	2	3	4	3	5	4

Table 33 (left) and Table 34 (right): These are simplified version of Table 32 as divisions in Ns, M, T are united. Values for these united sections represent an average value (Table 19), but values with decimals are rounded in Table 34. Table 33 was used to generate Figure 5.116.

	EHigh	High	Med	Low	ELow
H	0	6	7	9	0
DNs	0	2	11	9	0
CNs	0	4	9	9	0
VNs	0	2	8	10	0
DM	0	3	10	10	0
CM	0	4	8	9	0
VM	0	3	10	7	0
DT	1	6	10	3	0
CT	1	6	9	3	0
VT	1	6	8	3	0
FL	1	2	6	4	2
HL	4	6	3	2	2
Ta	1	7	2	2	0

	EHigh	High	Med	Low	ELow	Points
H	0	6	7	9	0	63
Ns	0	4	10	9	0	64
M	0	2	12	9	0	62
T	1	5	11	3	0	64
FL	1	2	6	4	2	41
HL	4	6	3	2	2	59
Ta	1	7	2	2	0	43

Table 35 (left) and Table 36 (right): These two tables represent the frequency of elevation levels by body section. Table 36 also denote the sum of the elevation points. Table 35 are obtained based on Table 32, while Table 22 are obtained based on Table 34. These tables were used to generate Figure 5.113.

	EHigh	High	Medium	Low	ELow	Elevation Points
H	0	5	7	7	0	55
Ns	0	2	8	9	0	50
M	0	2	9	8	0	51
T	0	5	11	3	0	59
FL	1	2	6	4	2	41
HL	3	6	2	2	2	51
Ta	1	7	2	2	0	43

Table 37: The frequency of elevation levels (left) and the sum of elevation points by body section (right). This table is generated based on 19 images which contain all of H, Ns, M and T. This table was used to generate Figure 5.114 and Figure 5.115.

	H	Ns	M	T	L	Ta
PB1	0	0	1	0	0	0
PB2	1	0	0	0	1	0
PB3	1	0	1	0	0	0
PB4	1	1	1	1	1	0
PD1	1	1	1	1	1	0
PD2	1	1	0	0	1	0
PB5	0	0	0	0	0	0
PD3	0	0	0	0	0	0
PU1	0	0	0	0	0	0
PH1	0	0	0	0	0	0
PH2	0	0	0	0	0	0
CB1	1	1	0	1	1	0
CB2	0	0	0	0	0	0
CB3	1	1	1	0	1	0
CB4	0	0	0	0	0	0
CB5	0	0	0	0	0	0
EH1	1	1	0	1	1	0
EH2	1	0	0	0	0	0
ED1	0	0	0	0	0	0
BMB1	0	0	0	0	1	0
BU1	0	0	0	1	0	0
BB1	1	1	0	0	1	0
BB2	0	0	0	1	0	0
GM1	0	0	0	0	0	0
DA1	0	0	0	0	0	0

Table 38: Presence\absence of distortion and its location by image. '0' refers to absence, while '1' means presence. (H: Head, Ns: Neck-shoulder, M: Mid Torso, T: Thigh, L: limbs, Ta: Tail).

	Images
Dis 0	11
Dis 1	5
Dis 2	2
Dis 3	2
Dis 4	3
Dis 5	2

Table 39 (left): The number of images by frequency of distortion. This table was used to generate Figure 5.117.

	Distortion
H	10
Ns	7
M	5
T	6
L	9
Ta	0

Table 40 (right): The number of distortion by body part. This table was used to generate Figure 5.118.

List of Data Tables (Covalanas, El Pendo, El Castillo):

	Covalanas	El Pendo	El Castillo		Total
Inte0	7	1	7		15
Inte1	8	1	6		15
Inte2	2	1	5		8
Inte3	1	5	4		10
Inte4	0	3	1		4
Inte5	0	0	1		1
Inte6	0	0	1		1

Table 41: The number of images by frequency of integration. Results from all case studies are listed in this table.

	Covalanas	El Pendo	El Castillo	Total		D	O	F	P
H	1	4	8	13		12	1	3	10
D	8	10	12	30		24	7	21	9
Ta	0	1	4	5		5	1	2	3
B	3	5	7	15		14	1	9	6
L	0	2	4	6		5	1	5	1
V	5	9	9	23		21	2	15	6

Table 42: The number of integrations by body part and type of integration. Results from all case studies are listed in this table. This table was used to generate Figure 6.1 and Figure 6.3

	H	D	Ta	B	L	V
H		11	1	5	3	9
D	11		4	11	5	18
Ta	1	4		4	1	5
B	5	11	4		4	10
L	3	5	1	4		6
V	9	18	5	10	6	

Table 43: Combinations of body sections among images with multiple integrations. This table was used to generate Figure 6.2.

	Covalanas	El Pendo	El Castillo		Total
Groove	3	7	25		35
Border	1	0	0		1
Edge	8	19	19		46
Ridge	3	1	6		10
Valley	0	4	0		4

Table 44: The number of integrations by type of natural lines. Results from all case studies are listed. This table is used to generate Figure 6.4.

	EHigh	High	Medium	Low	ELow		Elevation Points
H	4	15	12	14	0		144
Ns	0	7	23	15	0		127
M	0	6	19	20	0		121
T	3	13	20	9	0		145

Table 45: The frequency of elevation levels (left) and the sum of elevation points by body section (right). This table is generated based on 45 images which contain all of H, Ns, M and T. This table was used to generate Figure 6.6 and Figure 6.7

	EHigh	High	Med	Low	ELow
H	4	17	12	16	0
Ns	0	10	28	14	0
M	0	5	24	22	0
T	4	13	22	9	0
FL	3	3	10	11	5
HL	8	10	6	8	3
Ta	1	7	3	4	0

Table 46: The frequency of elevation levels by body sections. A total of 54 images are considered in this table. This table was used to generate Figure 6.8.

	Covalanas	El Pendo	El Castillo		Total
P1	5	3	5		13
P2	3	1	3		7
P3	2	1	2		5
P4	3	1	1		5
P5	3	2	5		10
P6	2	0	3		5

Table 47: The number of images by topography type. Results from the three case studies are listed.

	Covalanas	El Pendo	El Castillo		Total
Dis0	7	1	13		21
Dis1	0	2	6		8
Dis2	6	2	1		9
Dis3	4	3	0		7
Dis4	0	1	4		5
Dis5	1	2	1		4

Table 48: The number of images by frequency of distortion. Results from the three case studies are listed. This table was use to generate Figure 6.13.

	Covalanas	El Pendo	El Castillo		Total
H	7	6	7		20
Ns	8	9	5		22
M	4	4	4		12
T	6	3	6		15
L	4	7	7		18
Ta	0	0	0		0

Table 49: The number of distortion by body section. Results from the three case studies are listed. This table was use to generate Figure 6.14.

	Images	Images with distortion	Percentage	Distortion	Average
P1	13	12	92	35	2.9
P2	7	4	57	8	1.1
P3	5	3	60	5	1
P4	5	2	40	3	0.6
P5	10	3	30	8	0.8
P6	5	2	4	2	4
N/A	9	4	4.4	7	8

Table 50: Values for five categories by topography type (Image and Images with distortion: the number, percentage: Images with distortion/ Images, Distortion: the total number of detected distortions, Average: Distortion/ Images). Results from the three case studies are considered. This table was used to generate Figure 6.16 and Figure 6.17.

	Presence (Expected value)	Absence (Expected Value)	Total
H	13 (17.671)	37 (32.129)	50
D	28 (18.024)	23 (32.976)	51
Ta	5 (5.301)	10 (9.699)	15
B	15 (16.964)	33 (31.036)	48
L	6 (17.783)	33 (25.127)	39
V	21 (16.257)	25 (29.743)	46
Total	88	161	249

Table 51: The number of presence and absence of integrations by body section. This table is used for Chi-square test (p303).

	Partial	Full	Total

	(Expected value)	(Expected Value)	
H	10 (5.056)	3 (7.944)	13
D	9 (11.667)	21 (18.333)	30
Ta	3 (1.944)	2 (3.056)	5
B	6 (5.833)	9 (9.167)	16
L	9 (2.333)	5 (3.667)	6
V	6 (8.1667)	15 (12.833)	21
Total	35	55	90

Table 52: The number of partial and full integration by body part. This table is used for Chi-square test (p305).

	Extra high + High (Expected Value)	Medium (Expected Value)	Low (Expected Value)	Total
H	19 (12)	12 (18.5)	14 (14.5)	45
Ns	7 (12)	23 (18.5)	15 (14.5)	45
M	6 (12)	19 (18.5)	20 (14.5)	45
T	16 (12)	20 (18.5)	9 (14.5)	45
Total	48	74	58	180

Table 53: The number of images regarding elevation levels and corresponding body parts. This table is used for Chi-square test (p312).

	Extra levels (Expected value)	Not Extra levels (Expected Value)	Total
H	4 (5.401574803)	45 (43.5984252)	49
Ns	0 (5.732283465)	52 (46.26771654)	52
M	0 (5.732283465)	52 (46.26771654)	52
T	4 (5.291338583)	44 (42.70866142)	48
L	19 (4.188976378)	19 (33.81102362)	38
Ta	1 (1.653543307)	14 (13.34645669)	15
Total	28	226	254

Table 54: The number of images regarding extra elevation levels and corresponding body parts. This table is used for Chi-square test (p313).

	Number of Images	Expected Value
Concavity (P1 + P5)	23	11.25
Slope (P2 + P6)	12	11.25
Convexity (P3)	5	11.25
Zigzag (P4)	5	11.25
Total	45	45

Table 55: The number of images by type of topography. This table is used for Chi-square test (p313).

	Presence (Expected value)	Absence (Expected Value)	Total
H	20 (18.61572052)	29 (30.38427948)	49
Ns	22 (19.75545852)	30 (32.24454148)	52
M	12 (19.75545852)	40 (32.24454148)	52
T	15 (18.23580786)	33 (29.76419214)	48
L	18 (10.63755459)	10 (17.36244541)	28
Total	87	142	229

Table 55: The number of presence and absence of distortion by body section. This table is used for Chi-square test (p323)

	Total number of distortions	Expected Value
P1	35	9.714285714
P2	8	9.714285714
P3	5	9.714285714
P4	3	9.714285714
P5	8	9.714285714
P6	2	9.714285714
N/A	7	9.714285714
Total	68	68

Table 56: The total number of distortions by topography type. This table is used for Chi-square test (p330)

References:

Abadía, O. M. (2006). 'Art, crafts and Paleolithic art', *Journal of Social Archaeology*, *6*(1), pp119-141.

Aglioti, S. M., and Pazzaglia, M. (2011). 'Sounds and scents in (social) action', *Trends in cognitive sciences*, Vol.15, No.2, pp47-55.

Ahn, S.H., Jin, B., Kwon, S. and Yun, M.H. (2014). 'A research on curved display comparing to flat display regarding posture, tilt angle, focusing area and satisfaction', *대한인간공학회지*, 33(3), pp.191-202.

Alcalde del Río, H., Breuil, H. and Sierra, L. (1911). Les cavernes de la région cantabrique. *Impr. Chêne, Monaco ([IPH, Peintures et gravures murales des cavernes paléolithiques, 1], 265 p., 258 fig.)*.

Alland, A. (1983). *Playing with Form*: *Children Draw in Six Cultures*. New York: Columbia University Press.

Anderson, H. (2013). 'A Distinguishing Skill Art, Language, and Complex Cognition', *Journal of Consciousness Studies*, *20*(3-4), pp6-32.

Apellániz, J.M., (1978). 'Análisis e interpretación de Ekain', *Munibe*, 30, pp.110-150.

Arakawa, S. and Madeline, G. (2002). *Architectural body*. University of Alabama Press.

Arias, P. (2009). 'Rites in the dark? An evaluation of the current evidence for ritual areas at Magdalenian cave sites', *World Archaeology*. 41(2), pp262–294.

Arias, P and Ontañón, R. (2012). 'La Galma [Spain]: Long term human activity in a karst system', In Bergsvik, K. A and Skeates, R. (eds.) *Cave in Context, The cultural significance of Caves and Rock shelters in Europe,* pp101-117. Oxford: Oxbow.

Arnott, S. R. and Alain, C. (2014). 'A brain guide to Sound Galleries', In Levent, N. and Pascual-Leone, A. (eds.) *The Multisensory Museum: Cross-disciplinary Perspectives on Touch, Sound, Smell, Memory, and Space*, pp85-108. Rowman & Littlefield.

Ascher, R. (1961). 'Analogy in archaeological interpretation', *Southwestern journal of anthropology*, pp317-325.

Aujoulat, N., (1985). 'Analyse d'une oeuvre pariétale paléolithique anamorphosée in XXXX anniversaire', *Préhistoire Ariégeoise. Bulletin de la Société Préhistorique de l'Ariège Tarascon-sur-Ariège*, *40*, pp.185-193.

Aujoulat, N. (2005). *The splendour of Lascaux: rediscovering the greatest treasure of prehistoric art*. Thames & Hudson.

Azema, M. and Rivere, F. (2012). 'Animation in Palaeolithic art: a pre-echo of cinema', *Antiquity*, 86(332), pp316-324.

Bacci, F and Pavani, F. (2014). '"First Hand," Not " First Eye" Knowledge: Bodily Experience in Museum', In Levent, N. and Pascual-Leone, A. (eds.) *The Multisensory Museum: Cross-disciplinary Perspectives on Touch, Sound, Smell, Memory, and Space*, pp17-28. Rowman & Littlefield.

Bahn, P.G., (1995). 'Cave art without the caves', *Antiquity*, *69*(263), pp.231-237.

Bahn, P. G. (2003). Location, location: What can the positioning of cave and rock art reveal about Ice Age motivations? In Pastoors, A., and Weniger, G. C. (eds.), Ho¨hlenkunst und Raum: Archa¨ologische und architektonische Perspektiven, Jan van der Most, Du¨sseldorf, pp. 11–20.

Bahn, P.G., (2007). *Cave art: A guide to the decorated ice age caves of Europe*. frances lincoln ltd.

Bahn, P. G. (2011). Religion and ritual in the Upper Palaeolithic. In T. Insoll (Ed.), The Oxford handbook of the archaeology ofritual and religion (pp. 344–357). Oxford: Oxford University Press.

Bahn, P. G., (2016). *Images of the Ice Ag*: Oxford, Oxford University Press.

Bahn, P. G. and Vertut, J. (1997). *Journey Through The Ice Age,* Great Britain: Weidenfeld and Nicolson.

Bahn, P. G., and Helvenston P. A. (2002). *Desperately seeking Trance Plants: Testing the "Three Stages of Trance" Model,* New York: RJ Communications LLC.

Baptista, A. M. (2009). *O paradigma perdido: o Vale do Côa ea arte paleolítica de ar livre em Portugal*. Edições Afrontamento.

Barquin, R.M., Gonzalez, J.S., Laguna, A.J.G. and Luque, C.G. (1998). 'New Palaeolithic cave art in cueva de El Pendo, Cantabrian region, Spain', *Rock Art Research,* 15*(2),* pp89-97.

Barquin, R.M., (2001). 'Las manifestaciones rupestres paleoliticas', In Sainz, C.G. and Llamosas, C.S.M. (eds.), *Las cuevas del desfiladero: Arte rupestre paleolítico en el valle del río Carranza (Cantabria-Vizcaya)*. Santander: Universidad de Cantabria. pp175-203.

Barquin, R.M., (2003).'El conjunto rupestre paleolitico de la cueva de El Pendo (Escobedo de Camargo)' *La Arqueología de la Bahía de Santander*, 1, pp227-249.

Batarda Fernandes, A., Reis, M., Escudero Remirez, C. and Vázquez Marcos, C., (2017). 'Integration of natural stone features and conservation of the Upper Palaeolithic Côa Valley and Siega Verde open-air rock-art', *Time and Mind*, 10(3), pp.293-319.

Bednarik, R. G. (2008). 'Children as Pleistocene artists', *Rock Art Research,* 25(2), pp173-182.

Beltran, A (1998) 'Introduction', In Ramos, P. A., Múzquiz Pérez-Seoane, M., and Beltrán Martâinez, A. (eds.) *The Cave of Altamira*, pp8-16. Barcelona: Lunwerg Editores.

Bicho, N., Carvalho, A. F., González-Sainz, C., Sanchidrián, J. L., Villaverde, V., and Straus, L. G. (2007). 'The Upper Paleolithic Rock Art of Iberia', *Journal of Archaeological Method and Theory*, 14(1), 81-151.

Binford, L. R. (1967). 'Smudge pits and hide smoking: the use of analogy in archaeological reasoning', *American Antiquity*, pp1-12.

Bintliff, J. (1991). 'Post-modernism, rhetoric and scholasticism at TAG: the current state of British archaeological theory', *Antiquity*, 65(247), pp274-278.

Bishop, C. (2005). *Installation art*. London: Tate Publishing.

Bischoff, J., Díez, M.G., Morales, M.R.G. and Sharp, W. (2012). 'Aplicación del método de series de Uranio al grafismo rupestre de estilo paleolítico: el caso de la cavidad de Covalanas (Ramales de la Victoria, Cantabria)', *Veleia*, 20, pp143-150.

Boado, F. C., and Romero, R. P. (1993). 'Art, time and thought: a formal study comparing palaeolithic and postglacial art', *World archaeology*, 25(2), pp187-203.

Breuil, H., 1905. L'art à ses débuts. *Revue de philosophie*.

Breuil, H. and Windels, F. (1952). *Quatre cents siècles d'art pariétal: les cavernes ornées de l'âge du renne*. Centre d'études et de documentation préhistoriques.

Carballo, J. (1960). *Investigaciónes Prehistóricas II*. Santander: Diputación Provincial.

Carballo, J. and Echegaray, J.G. (1952). 'Algunos objetos inéditos de la cueva de El Pend', *Empúries: revista de món clàssic i antiguitat tardana*, 14, pp37-48.

Chandler, J.H. and Fryer, J.G. (2005). *Recording aboriginal rock art using cheap digital cameras and digital photogrammetry*, CIPA 2005 International Symposium, 26 September -01 October 2005, Torino, Italy.

Chodoronek, M., (2015). The Use and Application of Photogrammetry for the In-field Documentation of Archaeological Features: Three Case Studies from the Great Plains and Southeastern Alaska. *Unpublished Master's Thesis*, Department of Anthropology, Lincoln. University of Nebraska, 99pp.

Classen, E., and Zimmermann, A. (2003). Ra¨ umliche Statistik, soziale Netzwerkanalyse und Raumversta¨ndnis. In Pastoors, A., and Weniger, G. C. (eds.), Ho¨hlenkunst und Raum: Archa¨ologische und architektonische Perspektiven, Jan van der Most, Du¨sseldorf, pp. 91–104.

Clottes, J. (1993). 'Contexte archéologique interne', In: *L'art pariétal Paléolithique*. Techniques et méthodes d'étude. CTHS, Paris, pp. 49–58.

Clottes, J. (2005). 'Forward', In Heyd, T. and Clegg, J. (eds.). *Aesthetics and Rock Art,* Ashgate, Hampshire, ppxix-xxv.

Clottes, J., Rouzaud, F., and Wahl, L. (1984). 'Grotte de Fontanet' In Leroi-Gourhan, A. (eds.), *L'Art des cavernes. Atlas des grottes ornées paléolithiques françaises. Imprimerie Nationa*le, Paris, pp433–437.

Clottes, J. and Simonnet, R., (1990). 'Retour au Réseau Clastres (Niaux, Ariège)', *Préhistoire Ariégeoise*, *45*, pp.51-139.

Clottes, J. and Lewis-Williams, J. D. (1998). *The Shamans of Prehistory: Trance and Magic in The Painted Caves*. Harry N Abrams.

Clottes, J., Courtin, J., Vanrell, L. (2005). *Cosquer redécouvert*. Seuil, Paris.

Codispoti, M., & De Cesarei, A. (2007). 'Arousal and attention: Picture size and emotional reactions', *Psychophysiology*, 44(5), pp680-686.

Costall, A. (2006). 'On Being the Right Size: Affordances and the Meaning of Scale', In Lock, G. and Molyneaux, B. L (eds.), *Confronting Scale in Archaeology: Issues of Theory and Practice*, pp15-26. New York: Springer Science + Business Media, LLC.

Conkey, M. W. (1987). 'New Approaches in the Search for Meaning? A Review of Research in "Paleolithic Art', *Journal of Field Archaeology*, 14(4), pp413-430.

Conkey, M. W. (2001). 'Hunting for images, gathering up meanings: art for life in hunting-gathering societies', In Panter-Brick, C., Layton, R. H and Rowley-Conwy. P (eds), *Hunter-gatherers: An Interdisciplinary Perspective*, pp267-291, Cambridge University Press.

Conkey, M. W. (2010). 'Images without words: the construction of prehistoric imaginaries for definitions of 'us'', *Journal of Visual Culture*, 9(3), pp272-283.

Conkey, M. W., Beltrán, A., Clark, G. A., Echegaray, J. G., Guenther, M. G., Hahn, J., and Valoch, K. (1980). 'The Identification of Prehistoric Hunter-Gatherer Aggregation Sites: The Case of Altamira [and Comments and Reply]', *Current Anthropology*, pp609-630.

Daniel, G. E. (1950). *A hundred years of archaeology*. G. Duckworth.

Darvill, T. (2002). *Oxford Concise Dictionary of Archaeology*, NewYork: Oxford University Press.

De Beaune, S. (1987). 'Palaeolithic lamps and their specialization: a hypothesis', *Current Anthropology*, 28(4), pp569-577.

De Beaune, S. (2004). 'Un atelier magdalénien de sculpture de la stéatite au Rocher de la Caille (Loire)', In, Lejeune, M., and Welté, A.C. (eds.), *L'art du paléolitique*, pp177–186. Liège: ERAUL.

De Cesarei, A., & Codispoti, M. (2006). 'When does size not matter? Effects of stimulus size on affective modulation', *Psychophysiology*, 43(2), pp207-215.

Delannoy, J.J., Geneste, J.M., David, B., Katherine, M. and Gunn, R.G. (2012). 'Apports de la géomorphologie dans l'aménagement et la construction sociale de sites préhistoriques. Exemples de la grotte Chauvet-Pont-d'Arc (France) et de Nawarla Gabarnmang (Australie)', *PALEO. Revue d'archéologie préhistorique*, (23), pp.85-104.

Delluc, B. and Delluc, G. (2009). 'Eye and vision in Palaeolithic art', In Bahn, P. (eds.) *An Enquiring Mind: Studies in Honor of Alexander Marchack.* pp77-97. Oxford: Oxbow and Cambridge MA: American School of Prehistoric Research Monograph Series.

De Quirós, F.B., Maíllo-Fernández, J.M., Castaños, P. and Neira, A. (2015). 'The Gravettian of El Castillo revisited (Cantabria, Spain)', *Quaternary International*, *359*, pp.462-478.

Dobrez, L. (2013). 'The Perception of Depicted Motion', *Arts*, 2(4), pp383-446.

Duday, H. and Garcia, M.A. (1983). 'Les empreintes de l'Homme préhistorique. La grotte du Pech-Merle à Cabrerets (Lot): une relecture significative des traces de pieds humains', *Bulletin de la Société préhistorique française*, pp.208-215.

Dutton, D. (2009). *The art instinct: beauty, pleasure, & human evolution*. Oxford University Press.

Eliade, M (1964) *Shamanism: Archaic Technics of Ecstasy,* New York: Bollingen Foundation.

Ewing, E. (1997). 'Preliminary Report on Crack Feature Incorporation from the Franco-Cantabrian Regions of France and Spain', *American Indian Rock-art* 23: pp147-160.

Ferrier, C., Debard, E., Kervazo, B., Brodard, A., Guibert, P., Baffier, D., Feruglio, F., Gély, B., Geneste, J.M., Maksud, F. (2014). 'Les parois chauffées de la grotte Chauvet-Pont d'Arc (Ardèche, France): caractérisation et chronologie', *Paléo* 25, pp59–78.

Fogelin, L. (2007). 'Inference to the best explanation: a common and effective form of archaeological reasoning', *American Antiquity*, *72*(4), pp.603-626.

Foyo, A., Sanchez, M.A., Tomillo, C. and Iriarte, E. (2009). 'El Castillo Mountain prehistoric caves (Cantabria, North of Spain). Structural geology, karstic development and prehistoric art manifestations', *World Heritage*, UNESCO 2008.

Gamble, C. (1982). 'Interaction and alliance in Palaeolithic society', *Man*, pp92-107.

Garate, D., Bourrillon, R., Rios-Garaizar, J. (2012). 'La grotte ornée paléolithique d'Etxeberri (Camou-Cihige, Pyrénées-Atlantiques): datation du context archéologique de la «salle des Peintures', *Bulletin de la Société Préhistorique Française* 109(4), pp637–650.

Garcia-Diez, M. and Torre, J.E. (2007). 'Los dibujos rojos de estilo paleolítico de la Cueva de La Haza (Ramales de la Victoria, Cantabria): estudio monográfico', *Munibe Antropologia-Arkeologia*, 58, pp.177-222.

García Díez, M., González Morales, M.R. and Straus, L.G. (2012). 'El grafismo rupestre paleolítico de la cueva de El Mirón (Ramales de la Victoria, Cantabria, España): una propuesta para su datación estratigráfica', *Trabajos de Prehistoria,* 69, pp21-36.

García Díez, M. and Ochoa Fraile, B. (2012). 'Implicaciones en la secuenciación cronológica rupestre del grafismo figurativo mueble gravetiense peninsular', *Veleia*, 29: pp359-372.

García-Diez, M., Garrido, D., Hoffmann, D.L., Pettitt, P.B., Pike, A.W. and Zilhão, J., (2015). 'The chronology of hand stencils in European Palaeolithic rock art: Implications of new U-series results from El Castillo Cave (Cantabria, Spain)(advance online)', *Journal of Anthropological Sciences*, *93*, pp.1-18.

García-Mondéjar, J. (1990). 'The Aptian–Albian carbonate episode of the Basque–Cantabrian Basin (northern Spain): general characteristics, controls and evolution', *Carbonate platforms—facies, sequence and evolution, London, International Association of Sedimentologist, Special Publication*, *9*, pp.257-290.

Geneste, J. M., Hordé, T., Tanet, C., and Dagen, P. (2004). *Lascaux, a Work of Memory*. Fanlac.

Gibson, J. J. (1979). *The ecological approach to visual perception*. Psychology Press.

Gittins, R. and Pettitt, P. (2017). 'Is Palaeolithic cave art consistent with costly signalling theory? Lascaux as a test case', *World Archaeology*, *49*(4), pp.466-490.

Groenen, M. (2000). *Sombra y luz en el arte Paleolitico.* Barcelona: Ariel

Groenen, M. (2006). 'La grotte d'El Castillo (Puente Viesgo, Cantabrie, Espagne)', *L'Archéologie à l'Université Libre de Bruxelles (2001-2005). Matériaux pour une histoire des milieux et des pratiques humaines*: pp153-161.

Groenen, M. (2007). 'Voir l'image préhistorique: bilan des travaux dans la grotte ornée d'El Castillo (Cantabrie, Espagne)', In *Un siècle de construction du discours scientifique en préhistoire:... Aux conceptions d'aujourd'hui* (pp. 307-321). Société préhistorique française.

Gröenen, M. (2012). 'Recorridos por la cueva de El Castillo. En busca de la mirada del Paleolítico', *En busca de la mirada del Paleolítico, 1*, pp.372-393.

Groenen, M., Groenen, M.C., Del Moral, J.M.C. and Echegaray, J.G. (2008). 'Bilan de sept années de recherche dans la grotte ornée d'El Castillo (Cantabrie, Espagne)', *Nous*.

Groenen, M. and Paillet, P.P. (2014). 'Présences humaines dans la grotte ornée d'El Castillo (Cantabrie, Espagne): dépôts, prélèvements et traces de passage', In *Les arts de la préhistoire: micro-analyses, mises en contexte et conservation.: Actes du Colloque" Micro-analyses et datations de l'art préhistorique dans son contexte archéologique"., 1* (pp. 195-210). Musée national de Préhistoire, Paleo.

Gombrich, E.H. (1960). Art and Illusion. London: Phaidon.

Halverson, J. (1992). 'The first pictures: perceptual foundations of Paleolithic art', *Perception*, *21*(3), pp389-404.

Hodder, I. (1986). *Reading the past: current approaches to interpretation in archaeology*. Cambridge University Press.

Hodgson, D. (2000). 'Shamanism, Phosphenes, and Early Art: An Alternative Synthesis1', *Current anthropology*, *41*(5), pp866-873.

Hodgson, D. (2003). 'The Biological Foundations of Upper Palaeolithic Art: Stimulus, Percept and Representational Imperatives', *Rock Art Research,* 20(1), pp3-22.

Hodgson, D. (2006). 'Altered states of consciousness and Palaeoart: an Alternative Neurovisual Explanation' *Cambridge Archaeological Journal,* 16(1), pp27-37.

Hodgson, D. and Pettitt, P. (2018). 'The Origins of Iconic Depictions: A Falsifiable Model Derived from the Visual Science of Palaeolithic Cave Art and World Rock Art', *Cambridge Archaeological Journal*, *28*(4), pp.591-612.

Hoffmann, D.L., Standish, C.D., García-Diez, M., Pettitt, P.B., Milton, J.A., Zilhão, J., Alcolea-González, J.J., Cantalejo-Duarte, P., Collado, H., De Balbín, R. and Lorblanchet, M. (2018). 'U-Th dating of carbonate crusts reveals Neandertal origin of Iberian cave art', *Science*, *359*(6378), pp.912-915.

Hoyos Gómez, M. and Laville, H. (2009). Nuevas aportaciones sobre la estratigrafía y sedimentología de los depósitos del Paleolítico Superior de la Cueva de El Pendo (Santander): sus implicaciones.

Humphrey, N. (1998). 'Cave art, autism, and the evolution of the human mind', *Cambridge Archaeological Journal*, *8*(02), pp165-191.

Jacucci, G., Spagnolli, A., Chalambalakis, A., Morrison, A., Liikkanen, L., Roveda, S., & Bertoncini, M. (2009). 'Bodily explorations in space: Social experience of a multimodal art installation', In *Proceedings of the INTERACT 09 conference.* Lecture notes in computer science, 50(27), pp. 62-75, Springer Berlin Heidelberg.

Jochim, M. (1983). `Palaeolithic cave art in ecological perspective', In Bailey G (eds.), *Hunter-gatherer economy in prehistory*, pp212-219, Cambridge University Press.

Katz, D. and Friess, M. (2014). 'Technical note: 3D from standard digital photography of human crania—a preliminary assessment. *American journal of physical anthropology'*, 154(1), pp.152-158.

Keane, J. (2013). 'Initiating Change: Architecting the Body-Environment with Arakawa and Gins', *Architectural Design*, 83(1), pp76-83.

Kersten, T.P. and Lindstaedt, M. (2012). 'Image-based low-cost systems for automatic 3D recording and modelling of archaeological finds and objects', In *Euro-Mediterranean Conference* (pp. 1-10). Springer Berlin Heidelberg.

Koutsoudis, A., Vidmar, B. and Arnaoutoglou, F. (2013). 'Performance evaluation of a multi-image 3D reconstruction software on a low-feature artefact', *Journal of Archaeological Science*, 40(12), pp.4450-4456.

Lahlou, S. (2008) 'Cognitive technologies, social science and the three-layered leopardskin of change', *Social science information*, 47(3), pp227-251.

Laming, A. (1959). *Lascaux: Paintings and engravings* (Vol. 419). [Harmondsworth, Middlesex; Baltimore, Md.]: Penguin Books.

Layton, R. (1991). 'Figure, motif and symbol in the hunter-gatherer rock art of Europe and Australia', In Bahn, P and Rosenfeld (eds.) *Rock art and prehistory,* pp23-38 Oxford: Oxbow Monographs.

Layton, R. (1992). 'Ethnographic analogy and the two archaeological paradigms', In Goldsmith, S (eds.) *Ancient images, Ancient Thought: the Archaeology of Identity,* pp211-221. Calgary: Archaeological Association, University of Calgary.

Layton, R. (2000). 'Shamanism, Totemism and Rock art: *Les Chamanes de la Prehistoire* in the Context of Rock art research', *Cambridge Archaeological Journa,* 10(1), pp169-86.

Lerma, J.L., Navarro, S., Cabrelles, M. and Villaverde, V. (2010). 'Terrestrial laser scanning and close range photogrammetry for 3D archaeological documentation: the Upper Palaeolithic Cave of Parpalló as a case study', *Journal of Archaeological Science*, 37(3), pp.499-507.

Leroi-Gourhan, A. (1968a). *The Art of Prehistroric Man in Western Europe*, London: Thames and Hudson.

Leroi-Gourhan, A. (1968b). The evolution of Paleolithic art. *Scientific American*, *218*, pp58-70.

Leroi-Gourhan. A, (1986). 'The religion of the caves: Magic or metaphysics?', translated by A. Michelson, *October*, 37, pp7-17.

Leroi-Gourhan, A. (1992). *L'art Pariétal: Langage da la Préhistoire*. Grenoble: Jérome Millon.

Levent, N and Pascual-Leone, A. (2014). 'Introduction', In Levent, N. and Pascual-Leone, A. (eds.), *The Multisensory Museum: Cross-disciplinary Perspectives on Touch, Sound, Smell, Memory, and Space*, ppxiii-xxvi. Rowman & Littlefield.

Lewis-Williams, J. D. and Dowson, T. A. (1988). 'Signs of All Times: Entoptic Phenomena in Upper Palaeolithic Art', *Current Anthropology*, 29, 2, pp201-245.

Lewis-Williams, J.D., 1997. Harnessing the brain: vision and shamanism in Upper Palaeolithic Western Europe. *Beyond art: Pleistocene image and symbol*, *23*, pp.321-342.

Lewis-williams, J. D. (2002). *The Mind in the Cave: Consciousness and the Origins of Art*, London: Thames & Hudson Ltd.

Lorblanchet, M. (1984). 'Nouvelles découvertes d'art pariétal paléolithique en Quercy', *L'art pariétal paléolithique. Actes des Colloques de la direction du Patrimoine, Périgueux-Le Thot*, pp.79-105.

Maestu, I.B. (1994). 'Arte mueble del Paleolítico cantábrico: una visión de síntesis en 1994', *Complutum*, 5, pp.45-80

Maidagán, D.G. (2010). 'Las ciervas punteadas en las cuevas del Paleolítico: una expresión pictórica propia de la cornisa cantábrica', *Munibe. Suplemento*, 33, pp.1-454.

Mateos, L.O. (1982). 'Arpones inéditos del Magdaleniense de la cueva de" El Pendo"(Santander)', *Boletín del Seminario de Estudios de Arte y Arqueología: BSAA*, 48, pp.73-84.

McCarthy, J. and Benjamin, J. (2014). 'Multi-image photogrammetry for underwater archaeological site recording: An accessible, diver-based approach', *Journal of maritime archaeology*, *9*(1), pp.95-114.

Mithen, S. J. (1988). 'Looking and Learning: Upper Palaeolithic Art and Information Gathering', *World Archaeology*, 19(3), pp297-327.

Mithen, S. J. (1999). *The prehistory of the mind: The cognitive origins of art, religion and science*. London: Thames and Hudson.

Medina-Alcaide, M.A., Sanchidrián, J.L., Zapata, L. (2015). 'Lighting the dark: Wood charcoal analysis from Cueva de Nerja (Málaga, Spain) as a tool to explore the context of Paleolithic rock art', *C.R. Palevol*, 14(5), pp411–422.

Medina-Alcaide, M.Á., Garate-Maidagan, D., Ruiz-Redondo, A. and Sanchidrián-Torti, J.L. (2018). 'Beyond art: The internal archaeological context in Paleolithic decorated caves', *Journal of Anthropological Archaeology*, 49, pp.114-128.

Meecham, P., and Sheldon, J. (2013). *Modern art: a critical introduction*. Routledge.

Moure Romanillo, A., Morales, M.G. and Sainz, C.G. (1990). 'Las pinturas rupestres paleolíticas de la cueva de Covalanas (Ramales de la Victoria, Cantabria)', *Trabajos de Prehistoria*, *47*, p.9-38.

Moure Romanillo, A.M., Sainz, C.G. and Morales, M.R.G. (1991). *Las cuevas de Ramales de la Victoria, Cantabria: arte rupestre paleolítico en las cuevas de Covalanas y La Haza* (5). Ed. Universidad de Cantabria.

Morales, M.R.G. and Straus, L.G. (2000). 'La Cueva del Mirón (Ramales de la Victoria, Cantabria): excavaciones 1996-1999', *Trabajos de Prehistoria*, 57(1), pp.121-133.

Morris, N. J. (2011). 'Night walking: darkness and sensory perception in a night-time landscape installation', *cultural geographies*, 18(3), pp315-342.

Moyes, H. (2012). *Sacred darkness: A global perspective on the ritual use of caves*. University Press of Colorado.

Moyes, Holley, Lilly Rigoli, Stephanie Huette, Daniel Montello, Teenie Matlock and Michael Spivey. (2017). 'Darkness and the Imagination: The Role of Environment in the Development of Spiritual Belief', In Papadopoulos. G., and Moyes. H. (eds.), *The Oxford Handbook of the Archaeology of Light*, (Oxford Handbooks Online.) Oxford: Oxford University Press.

Nabil, M. and Saleh, F. (2014). '3D reconstruction from images for museum artefacts: A comparative study', In *Virtual Systems & Multimedia (VSMM), 2014 International Conference on* (pp. 257-260). IEEE.

Ochoa, B. and García-Diez, M. (2015). 'Chronology of western Pyrenean Paleolithic cave art: A critical examination', *Quaternary International*, 364, pp.272-282.

Ogawa, M. (2005). 'Integration in Franco-Cantabrian Parietal Art: A Case Study of Font-de-Gaume Cave, France', In T. Heyd, and J. Clegg (eds.), *Aesthetics and Rock Art*, Aldershot, UK: Ashgate, pp117-129.

Orians, G. H., and Heerwagen, J. H. (1992). 'Evolved responses to landscapes', In Barkow, J. H., Cosmides, L., and Tooby, J. (eds.). *The adapted mind: Evolutionary psychology and the generation of culture*, pp. 555–579. New York: Oxford University Press,

Palacio-Perez, E (2010) 'Cave art and the theory of art: the origins of the religious interpretation of Palaeolithic graphic expression', *Oxford Journal of Archaeology*, 29(1), pp1-14.

Pastoors, A., and Weniger, G. C. (2011). 'Cave art in context: Methods for the analysis of the spatial organization of cave sites', *Journal of Archaeological Research*, 19(4), pp377-400.

Petchkovsky, L. (2008). Some Preliminary Reflections on the Biological Substrate of Meaning-Making. In *The Uses of subjective experience. Proceedings of the Conference 'The Uses of Subjective Experience: A Weekend of Conversations between ANZSJA Analysts and Academics who Work with Jung's Ideas,* pp20-21.

Pettitt, P. (2014) 'The European Upper Palaeolithic', *The Oxford Handbook of the Archaeology and Anthropology of Hunter-Gatherers*, pp279-309.

Pettitt, P. B (2016). 'Darkness visible. Shadows art and the ritual experience of caves in Upper Palaeolithic Europe', In Dowd. M. and Hensey. R. (eds), *The archaeology of darkness*, Oxford: Oxbow, pp11-23.

Pettitt, P., T. Sakamoto and S. Lelushko, (2017). 'Light, human evolution, and the Palaeolithic', In Papadopoulos. G., and Moyes. H. (ed.), *The Oxford Handbook of the Archaeology of Light*, (Oxford Handbooks Online.) Oxford: Oxford University Press. DOI: 10.1093/oxfordhb/9780198788218.013.1

Pettitt, P., Castillejo, A. M., Arias, P., Peredo, R. O., and Harrison, R. (2014). 'New views on old hands: the context of stencils in El Castillo and La Garma caves (Cantabria, Spain)', *Antiquity*, 88(339), pp47-63.

Pfeiffer, J. E. (1982). *The creative explosion. An inquiry into the origins of art and religion.* New York: Harper and Row.

Pike-Tay, A., Valdés, V.C. and de Quirós, F.B. (1999). 'Seasonal variations of the Middle–Upper Paleolithic transition at El Castillo, Cueva Morın and El Pendo (Cantabria, Spain)', *Journal of Human Evolution*, 36(3), pp.283-317.

Pizzato, M. (2013). 'Cave Rituals and the Brain's Theatre", In *Theatre Symposium* (Vol. 21, No. 1, pp 116-136). The University of Alabama Press.

Plisson, H. and Zotkina, L.V. (2015). 'From 2D to 3D at macro-and microscopic scale in rock art studies", *Digital Applications in Archaeology and Cultural Heritage*, *2*(2), pp.102-119.

Porter, S.T., Roussel, M. and Soressi, M. (2016). 'A Simple Photogrammetry Rig for the Reliable Creation of 3D Artifact Models in the Field Lithic Examples from the Early Upper Paleolithic Sequence of Les Cottés (France)', *Advances in Archaeological Practice*, 4(1), pp.71-86.

Ramos, P. A., Múzquiz Pérez-Seoane, M., and Beltrán Martâinez, A. (1999). *The Cave of Altamira*. Barcelona: Lunwerg Editores.

Ran, F. (2009). *A history of installation art and the development of new art forms: technology and the hermeneutics of time and space in modern and postmodern art from cubism to installation*. New York: Peter Lang.

Reinach, S. (1903). *L'art et la magie a propos des peintures et des gravures de l'age du renne*. L'Anthropologie, 14, pp257-266.

Reiss, J. H. (1999). *From margin to center: the spaces of installation art*. MIT Press.

Renfrew, C., and Bahn, P. G. (1991). *Archaeology: theories, methods and practice* (Vol. 2). London: Thames and Hudson.

Reznikoff, I. (1995) 'On the sound dimension of prehistoric painted caves and rocks', In Tarasti, E (eds.), *Musical Signification: Essays in the Semiotic Theory and Analysis of Music*, pp541-557. Berlin, New York: Mouton de Gruyter.

Reznikoff, I. (2008). 'Sound resonance in prehistoric times: A study of Paleolithic painted caves and rocks', *Journal of the Acoustical Society of America*, 123(5), 3603. doi: 10.1121/1.2934773.

Reznikoff, I. (2014) 'On the Sound Related to Painted Caves and Rocks', In Ikaheimo, J., Salmi, A. K. and Aikas, T (eds.), *Sounds Like Theory 12 Nordic Theoretical Archaeological Group Meeting in Oulu 25. -28.4. 2012, Monographs of the Archaeological Society of Finland 2*, pp101-109.

Rivero, O., Fano, M.A., G_arate, D. (2014). 'Relationships between recent Magdalenian societies in Cantabrian Spain, through the technical and formal analysis of frontal representations of ibex', In Otte, M., Le Brun-Ricalens, F. (eds.), *Modes of contact and mobility during the Eurasian Palaeolithic. Actes du Colloque international de la commission 8* (Pal_eolithique sup_erieur) de l'UISPP, Universite de Liege, 28-31 mai 2012. Luxembourg, CNRA. Universit_e de Li_ege, Li_ege, pp. 589-600.

Sabloff, J (2013). 'Processual archaeology', In Renfrew, C., and Bahn, P. (eds.), *Archaeology: the key concepts*. Routledge.

Sakamoto, T. (2014). *Upper Palaeolithic Cave Art as Multisensory Interactive Installation Art: Analysis of Human-Art-Environment triad* (Unpublished Master Dissertation). Durham University, Durham, UK.

Sauvet, G. and Wlodarczyk, A (2008). 'Towards a Formal Grammar of the European Palaeolithic Cave Art', *Rock Art Research*, 25(2), pp165-172.

Sauvet, G., Layton, R., Lenssen-Erz, T., Taçon, P. and Wlodarczyk, A. (2009). 'Thinking with animals in Upper Palaeolithic rock art', *Cambridge Archaeological Journal*, 19(3), pp319-336.

Schenk, T. (2005). 'Introduction to photogrammetry'. *The Ohio State University, Columbus*.

Segal, E. M (1994) 'Archaeology and cognitive science', in Renfrew, C., and Zubrow, E. B. (eds.), *The ancient mind: elements of cognitive archaeology*, pp22-28. Cambridge: Cambridge University Press.

Sharpe, K., and Van Gelder, L. (2006a). 'The study of finger flutings', *Cambridge Archaeological Journal*, 16(03), pp281-295.

Sharpe, K., and Van Gelder, L. (2006b). 'Evidence for cave marking by Palaeolithic children', *Antiquity*, 80(310), pp937-947.

Shiner, L. (2001). *The invention of art: a cultural history*. University of Chicago Press.

Sieveking, A. (1991). 'Palaeolithic Art and Archaeology: The Mobiliary Evidence', *Proceedings of the prehistoric Society,* 57(1), pp33-50.

Snodgrass, J.G. and Feenan, K. (1990). 'Priming effects in picture fragment completion: Support for perceptual closure hypothesis', *Journal of Experimental Psychology: General* 119, pp276–98.

Snodgrass, J.G. and Kinjo, H. (1998). 'On the generality of the perceptual closure effect', *Journal of Experimental Psychology: Learning, Memory, and Cognition,* 24(3), pp645– 58.

Snow, D. R. (2013). 'Sexual Dimorphism in European Upper Palaeolithic Cave Art', *American Antiquity*, 78(4), pp746-761.

Sontag, S. (1969). 'The aesthetics of silence', In Sontag, S. (eds.), *Styles of radical will*, pp3-34. New York: Farrar, Strauss and Giroux.

Steinkamp, J. (2001). 'My Only Sunshine: Installation Art Experiments with Light, Space, Sound and Motion' *Leonardo*, 39(2), pp109-112.

Straus, L. G. (1976). 'The Upper Paleolithic. Cave Site of Altamira (Santander, Spain)', *Quaternaria. Storia Naturale e Culturale del Quaternario*, *19*, pp135-148.

Straus L. G. (1987). 'The paleolithic cave art of Vasco-Cantabrian Spain', *Oxford Journal of Archaeology*, *6*(2), pp149-163.

Straus, L. G. (1990). 'Underground archaeology: perspectives on caves and rockshelters', *Archaeological method and theory*, pp255-304.

Straus, L. G. (2009). 'Observations on Upper Paleolithic art, old problems and new directions', *Zephyrvs*, 34-35, pp71-80.

Straus, L.G., Morales, M.R.G., Martínez, M.Á.F. and García-Gelabert, M.P. (2002). 'Last glacial human settlement in eastern Cantabria (Northern Spain)', *Journal of Archaeological Science*, 29(12), pp1403-1414.

Surre, Y. (1992). 'L'anamorphose dans l'art pariétal: mythe ou réalité?', *Préhistoire Ariégeoise*, 47, pp.95-104.

Till, R. (2014). 'Sound archaeology: terminology, Palaeolithic cave art and the soundscape', *World Archaeology*, 46(3), pp292-304.

Topper, D. (2000). 'On anamorphosis: Setting some things straight', *Leonardo*, 33(2), pp115-124.

Trigger, B. G. (1989). *A history of archaeological thought*. Cambridge University Press.

Ucko, P. J., and Rosenfeld, A. (1967). *Palaeolithic cave art*. McGraw-Hill.

Valladas, H., Tisnerat-Laborde, N., Cachier, H., Arnold, M., De Quiros, F.B., Cabrera-Valdes, V., Clottes, J., Courtin, J., Fortea-Pérez, J.J., Gonzales-Sainz, C. and Moure-Romanillo, A. (2001). 'Radiocarbon AMS dates for Paleolithic cave paintings', *Radiocarbon*, 43(2; VOL B), pp.977-986.

Van Gelder, L., and Sharpe, K. (2009). 'Women and girls as Upper Palaeolithic cave 'artists': deciphering the sexes of finger fluters in Rouffignac Cave', *Oxford journal of Archaeology*, 28(4), pp323-333.

VanPool, C. S., and VanPool, T. L. (1999). 'The scientific nature of postprocessualism', *American antiquity*, pp33-53.

Vialou, D. (1998). *Our Prehistoric Past: Art and Civilization*. Thames and Hudson.

Wachtel, E. (1993). The first picture show: cinematic aspects of cave art. *LEONARDO* 26(2), pp135-140.

Waltham, T. (1974). *Caves*. New York, Crown publishers Inc.

Warzée, N., Groenen, M., Rosoux, J., Debeir, O., Ercek, R., Reichling, C., Vergnieux, R. and Delevoie, C., (2009). 'Numérisation 3D de la grotte d'El Castillo (Puente Viesgo)', In *Actes du colloque Virtual Retrospect 2007* (pp. 221-229). Ausonius.

Welker, W. (2016). 'First Palaeolithic rock art in Germany: engravings on Hunsrück slate', *Antiquity*, 90(349), pp.32-47.

Westoby, M.J., Brasington, J., Glasser, N.F., Hambrey, M.J. and Reynolds, J.M., (2012). 'Structure-from-Motion'photogrammetry: A low-cost, effective tool for geoscience applications', *Geomorphology*, 179, pp.300-314

White, R. (2003). *Prehistoric Art: the symbolic journey of humankind.* New York: Harry N. Abrams, Inc.

Woodmansee, M. (1996). *The author, art, and the market: Rereading the history of aesthetics*. Columbia University Press.